



UNIVERSITÀ
DEGLI STUDI
DI PADOVA

PhD in MOLECULAR SCIENCES
PHARMACEUTICAL CURRICULUM
CICLE XXXII
Department of Chemistry
University of Padova

Design and synthesis of novel chemical entities with anticancer activity

Head of the PhD Program: Prof. Leonard Prins

Supervisor: Prof. Giuseppe Zagotto

PhD Candidate: Enrico Zanforlin

Index

ABSTRACT	1
1 INTRODUCTION	3
1.1 CELLULAR HOMEOSTASIS AND SIGNALLING	5
1.2 KINASES AND PHOSPHATASES.....	6
1.2.1 KINASES	6
1.2.2 PHOSPHATASES	7
1.3 PROTEIN PHOSPHATASE 2A (PP2A).....	9
1.3.1 PP2A: Structure.....	10
1.3.1.1 PP2Ac: Catalytic subunit.....	11
1.3.1.2 PP2A _A : Scaffold subunit.....	12
1.3.1.3 PP2A _B : Regulatory subunit.....	13
1.3.2 PP2A: Regulation.....	15
1.3.2.1 PP2A and post translational modifications	15
1.3.2.1 PP2A and physiological modulators	17
1.3.3 PP2A: Function.....	20
1.3.3.1 PP2A and cellular homeostasis.....	20
1.3.3.2 PP2A and cancer	22
1.3.4 PP2A: Small molecule modulators	25
1.3.4.1 PP2A inhibitors	25
1.3.4.2 PP2A activators.....	27
1.4 SRC HOMOLOGY REGION 2 DOMAIN-CONTAINING PHOSPHATASE-1 (SHP-1).....	35
1.4.1 SHP-1: Structure	36
1.4.2 SHP-1: Regulation	37
1.4.3 SHP-1: Function.....	41
1.4.3.1 SHP-1 and Cellular Homeostasis.....	41

1.4.3.2 SHP-1 and cancer.....	42
1.4.4 SHP-1: Small molecule modulators.....	43
1.5 CASEIN KINASE 2 (CK2).....	47
1.5.1 CK2: Structure.....	47
1.5.1.1 CK2: CK2 α and CK2 α^1	48
1.5.1.2 CK2: CK2 β	50
1.5.2 CK2: Regulation.....	52
1.5.3 CK2: Function.....	53
1.5.3.1 CK2 and cellular homeostasis.....	53
1.5.3.2 CK2 and cancer.....	54
1.5.4 CK2: Small molecule modulators.....	54
2 AIM OF THE THESIS.....	57
3 RATIONALE AND RESULTS.....	61
3.1 PP2A: Rationale and Results.....	63
3.1.1 Synthesis of PP2A activators.....	63
3.1.1.1 Fingolimod analogues.....	63
3.1.1.2 Chimeric compounds of ApoE deriving peptides and Fingolimod analogues.....	80
3.1.1.2 Chimeric compounds deriving from TD-19 and CC11 chemical structures and attempt of synthesis of chimeric compounds deriving from TGI1002 and CC11 molecular scaffolds.....	90
3.1.2 Pharmacokinetic and Pharmacodynamic studies on the lead compound CC11.....	99
3.1.2.1 Pharmacokinetic profiling of CC11.....	100
3.1.2.2 Identification of the CC11's biological target.....	104
3.1.2.3 Development of new fluorometric tools for the detection of phosphatase activity and super-resolution microscopy.....	119
3.2 SHP-1: Rationale and Results.....	147
3.3 CK2: Rationale and Results.....	157

4 CONCLUSIONS	171
5 MATERIALS AND METHODS.....	175
5.1 ABBREVIATIONS	177
5.2 CONSUMABLES	181
5.3 INSTRUMENTS.....	182
5.4 PP2A methods	183
5.4.1 Synthesis of PP2A activators.....	183
5.4.1.1 Synthetic scheme of the first class of Fingolimod analogues	183
5.4.1.2 Synthetic scheme of the second class of Fingolimod analogues	201
5.4.1.3 Synthetic scheme of the third class of Fingolimod analogues.....	213
5.4.1.4 Synthetic scheme of the Chimeric compounds ApoE-Fingolimod analogues.....	217
5.4.1.5 Synthetic scheme of the Chimeric compounds TGI1002-CC11.....	235
5.4.1.6 Synthetic scheme of the Chimeric compounds TD-19-CC11	241
5.4.2 Synthesis of the resins for affinity chromatography.....	247
5.4.3 Synthesis of the photoactivatable probes.....	249
5.4.4 Synthesis of the fluorescent FRET probes	273
5.4.5 Biological experiments.....	295
5.4.5.1 Pharmacokinetic profiling of CC11.....	295
5.4.5.2 Spectroscopic behaviour of the photoactivatable probes	296
5.4.5.3 Biological experiments with the FRET fluorescent probe.....	297
5.5 SHP-1 methods.....	301
5.5.1 Synthesis of SC-43 analogues.....	301
5.5.2 Biological experiments.....	323
5.5.3 Docking studies.....	325
5.6 CK2 methods	327
5.6.1 Synthesis of the SRPIN803 analogues	327
5.6.2 Crystallographic and biological assays on SRPIN803 derivatives	339

6 INDEX OF THE FIGURES.....	343
7 REFERENCES	353

ABSTRACT

Currently, the canonical approach for the treatment of most of the malignancies is based on kinase inhibitors, in particular Tyrosine-Kinase Inhibitors (TKIs). Despite the great results obtained with the introduction in clinic of the first TKIs (e.g. Imatinib), the scientific community had to face soon with the limitations that these molecules bring with them. They present severe adverse effects, for their reduced selectivity between healthy and tumor cells. Furthermore, these drugs are prone to lead to the onset of resistances in patients. This last aspect causes the failing of the therapy and the recrudescence of the pathology. For these reasons, with the aim to explore other therapeutic options, that do not present the same limitations previously mentioned, this work has been focused on the development of new classes of anticancer molecules. For doing this, new molecular scaffolds have been synthesized, having as therapeutic targets enzymes that do not include Tyrosine Kinases. This research has led to the development of three different lines of research.

The first project has been focused on the synthesis of new activators of a well-known oncosuppressor: the serine/threonine phosphatase PP2A. An important part of this project has been based also on the study of the pharmacokinetic profile of these new molecules in animal models and the development of new fluorescent tools useful for the detection of the enzymatic activity of the desired phosphatase and the determination of the effective mechanism of action of the new synthesized compounds in whole cell lysates.

The second research branch has been based on the development of new molecules that are able to reactivate another important oncosuppressor, that is present in the downstream cascade of PP2A, the tyrosine phosphatase SHP-1.

Both these new approaches present several advantages and innovations if compared with the classical TKIs. Indeed, in several kind of malignancies, PP2A and SHP-1 are strongly downregulated and the possibility to reconstitute a physiological level of their activity in the tumor cells can induce apoptosis in cancerous cells without affecting the healthy ones. This is possible because in the normal cells the activity of these phosphatases is already at a basal level and for this reason these cells are not affected by the new molecules, granting a certain degree of selectivity between tumour and healthy cells. Furthermore, this approach seemed to be extremely promising also for avoiding the onset of resistances. This due to the fact that this pharmacological approach is effective also on tumor stem cells, that are usually insensitive to the classical treatments.

The third research line has been focused on the development of new molecules able to inhibit a serine/threonine kinase: CK2. CK2 is overexpressed in almost all known malignancies. It plays a crucial role in the control of the cell fate and in the mechanisms of resistances to the drug induced apoptosis. The development of new CK2 inhibitors is gaining interest in the last decade. This is due to the fact that this enzyme is a valid therapeutic option because it is the downstream effector of all the

principal oncogenic pathways present within the cell. Counteracting the overexpression of this kinase is not only promising for its therapeutic efficacy but also for the intrinsic reduced risk of inducing the onset of resistances.

1 INTRODUCTION

1.1 CELLULAR HOMEOSTASIS AND SIGNALLING

Cellular homeostasis is a complex and concerted sequence of events that aims to maintain a right balance between proapoptotic and proliferative signals and a physiological function of the cells.^[1-7] When this equilibrium is maintained the organism is fully functional and no pathological alterations are manifested. In case of disequilibrium of the cellular homeostasis we can assist to the onset of a pathological state.^[8,9] This picture is particularly true if we take in to account a peculiar pathological state like cancer is. In tumor cells, there is a strong upregulation of the proliferative signals and this leads to an uncontrolled replication and undifferentiation of the cancerous cells.^[4,10,11] Normally, in the healthy cells this delicate balance is granted by a wide number of processes and mechanisms. One of these, that is widely accepted by the scientific community as one of the principal systems that control the cell fate, is the phosphorylation state of the cellular proteins.^[12-17] The phosphorylation of the amino acid side chains of the proteins is a common phenomenon that is widely used by the cell for conveying different signals, in particular, to this kind of communication is entrusted the transmission of all the apoptotic or antiapoptotic impulses.^[18]

The degree of phosphorylation is controlled by two different classes of enzymes: kinases and phosphatases. Kinases introduce a phosphate group onto an aminoacidic side chain. Vice versa, phosphatases have the opposite task of removing the phosphate group introduced by the kinases.^[19] The introduction of a phosphate group on an aminoacidic side chain perturbs the morphology and the local electrostatic properties of the protein to which belong the modified amino acid, and this induce a deep alteration of the physiological functions of the modified protein altering also its activity profile. Usually kinases are considered proto-oncoproteins and an over activation of these enzymes is usually correlated with the onset of several pathologies, in particular cancer.^[20,21] As counterpart, phosphatases are considered as oncosuppressor proteins and in several kind of malignancies there is a strong downregulation of this class of enzymes.^[8,11,13,17,19,22-25] From a pharmacological point of view appears evident that these two categories of enzymes are extremely appealing for the development of new selective anticancer drugs. Indeed, after the identification of the variation that caused the onset of the pathology, acting on the modulation of this altered parameter it is possible to treat the disease and to repriminate the physiological state of the organism without affecting, or at least limiting the toxic effects for the healthy cells.^[4,15,18,21,26-32]

In the next session a brief description and classification will be introduced of the two classes of enzymes previously mentioned, kinases and phosphatases, and their implication in the development of anticancer therapies.

1.2 KINASES AND PHOSPHATASES

1.2.1 KINASES

Kinases are crucial enzymes that are involved in an enormous variety of process, fundamentals for maintaining a right cellular homeostasis. This kind of enzymes transfer a phosphoryl group, from a substrate enriched in phosphate moieties such as ATP or sometimes GTP, to nucleophilic groups present on the side chains of the amino acids following the scheme reported below.^[21]



This family of enzymes is deputed to the phosphorylation of the side chains of the amino acids, but not all the 20 amino acids synthesized by our organism can be phosphorylated by the protein kinases. The side chain, for being modified, has to present a nucleophile that is able to react with the anhydride bond of the nucleosides triphosphate. For this reason, actually, 9 different sites of phosphorylation have been identified:

1. the OH group of serine, threonine and tyrosine, through the formation of a phosphoester bond;^[11,27]
2. the carboxylic portion of aspartic acid and glutamic acid, obtaining a mixed anhydride linkage;^[28,33]
3. the nitrogen atoms of histidine (both the nitrogen atoms), lysine and arginine, forming phosphoramidate bonds.^[8,15,21]

Not all these residues present the same abundance in the phosphoproteomic profile of the cell; indeed, serine, threonine and tyrosine constitute almost the totality of the phosphoresidues. Proteomic analysis of 6600 phosphorylation sites on 2244 human proteins revealed that phosphoserine (pSer), phosphothreonine (pThr), and phosphotyrosine (pTyr) account for 86.4%, 11.8%, and 1.8%, respectively, of the phosphorylated amino acids.^[21]

Based on which kind of amino acids can be recognised by the enzymes, kinases can be divided in two different macroscopic classes:

- serine/threonine kinases (PSKs), which phosphorylate alkyl alcohols (PSKs);^[34]
- tyrosine kinases (PTKs), which can phosphorylate phenols.^[27,30,35]

Currently 518 different kinases are known; 385 enzymes are serine/threonine kinases, 90 are tyrosine kinases and other 43 members are tyrosine kinase like proteins.^[21]

Considering their abundances, and being the first class of enzymes whose abnormal activity has been directly linked with the onset of an oncologic pathology (e.g. Bcr-Abl in Chronic Myeloid Leukaemia), protein kinases, and in particular PTKs, have been widely studied and utilized for the development of targeted anticancer therapy.^[2,5,21,30,31,36-42] Despite the great results obtained with the introduction in clinic of the first selective tyrosine kinase inhibitors (TKIs) and the constant development of new ones, the scientific community had to face soon with the onset of resistances

and the severe side effects that these drugs bring with them.^[5,6,30,43–47] For these reasons nowadays the common efforts are focused on reducing these limitations, improving the efficacy of the actual strategies with the development of more effective analogues or combinations of known drugs, and the development of new therapeutic strategies that do not seem to present the same drawbacks showed by the canonical kinase inhibitors.^[30,45,48–50] This last option can be achieved focusing on other and probably more promising targets. For what concern the panorama of the kinases, a lot of interest has been showed in the last decade for CK2,^[21,51–53] a serine/threonine kinase, that has been subject of investigation for this thesis and it will be presented in detail in a dedicated chapter. The others possible targets that can rebalance the phosphoproteomic profile are the phosphatases.^[4,8,15,16,26] This last topic will be discussed in detail in the following paragraph, focusing on two principal enzymes, that have been deeply investigated during this thesis: PP2A and SHP-1.

1.2.2 PHOSPHATASES

Phosphatases are responsible of switching off all the signals and pathways activated by the kinases. Indeed, phosphatases remove phosphate groups from the side chain of the amino acidic residues granting a right balance between phosphorylated and unphosphorylated states of the protein.^[8,12,16,19,54,55] Despite their great importance in the control of the cellular homeostasis, phosphatases are represented by fewer enzymes compared to protein kinases. Indeed, there are only 107 putative protein Tyr phosphatases (PTPs) and far fewer protein Ser/Thr phosphatases (PSPs) (~30).^[8,16,23] Whereas the numbers of PTKs and PTPs roughly match each other, the number of catalytic subunits of PSPs is an order of magnitude lower than that of PSKs. This incongruity between PTPs and PSPs will be explained better in the next chapters of this thesis. In first, approximation, it can be assumed that PSPs make up for the reduced number of enzymes with a much more complex structural organization that allows them to dephosphorylate a wider plethora of substrates.^[56]

Phosphatases can be divided in three different families based on the nature of their substrate:

- a) tyrosine phosphatases (PTPs);
- b) serine/threonine phosphatases (PSPs);
- c) dual specific phosphatases (DSPs).

Each family can be further catalogued considering a structural point of view.

PTPs can be divided in to four different categories: the classes I, II and III Cys-based PTPs and the Aspartic based phosphatases. SHP-1, one of the target presented in this thesis, belongs to the class I of Cys-based PTPs. All the phosphatases that belong to these categories are constituted by a single filament, which include a catalytic site and one or more regulatory subunits.^[16]

For what concern PSPs, they can be divided in three different classes^[8,17]:

- I. The Metal-dependent Protein Phosphatases (PPM),
- II. The FCP phosphatase,
- III. The PhosphoProtein Phosphatases (PPP).

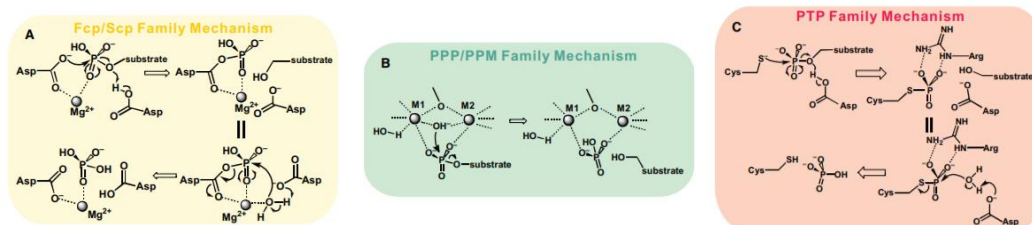


Figure 1. Catalytic mechanisms of different classes of phosphatases. **A.** Fcp/Scp class. Within the active site a single ion of Mg^{2+} is present. It is coordinate by the Dx Dx(T/V) motif and together exert the phosphatase activity. **B.** PPP and PPM classes. Two divalent cations are coordinated within the active site to mediate the phosphate transfer without forming an intermediate. **C.** PTPs, which are metal-independent Cys- based phosphatases, an active site cysteine serves as the nucleophile which attacks the phosphate group, forming a phosphocysteine intermediate.

PPMs are a subtype of PSPs that require a divalent metal cation for their enzymatic activity.^[17] Usually these enzymes present Mg^{2+} within their active site but they can incorporate also Mn^{2+} ions. In a physiological environment the concentration of Mg^{2+} ions is higher than the concentration of Mn^{2+} but in some *in vitro* experiments this last ion overpass the concentration of Mg^{2+} and this causes the exchange of the two ions. This substitution is often tolerated but, in many cases, this could lead to a non physiological behaviour of the enzyme losing the selectivity for its substrates or even, it modifies the selectivity for the aminoacidic side chains, switching from serine/threonine to Tyr residues. PPMs are composed by a single aminoacidic filament and they do not present regulatory subunits, instead they have additional domains and conserved sequence motifs that could drive the selectivity and substrate specificity of this class of enzymes.^[17,24,57]

FCP phosphatase is classified as Aspartate-based phosphatase and only a little is known about it.^[8]

PPPs constitute the much more important and complex class of phosphatases of the whole organism.^[8,24,29] To this class of phosphatases belong some of the most important and studied enzymes, crucial for the homeostasis of the cell, like: PP2A, PP1, PP2B (commonly known as calcineurin), PP4, PP5, PP6, and PP7. PPPs are not constituted by a single filament of amino acids, but instead they are composed by a catalytic subunit that needs, for its function, other regulatory subunits. These guarantee a certain degree of selectivity in terms of substrates and cellular localisation. Emblematic is the case of PP2A that will be illustrated in the next chapter. As PPMs also PPPs require the presence of metal ions within the active sites for the activation of a water molecule, fundamental for the dephosphorylation process.^[13,17]

Phosphatases are increasing their interest in the scientific community as anticancer targets for their central role in the regulation of the cellular homeostasis. In this thesis

the attention will be focused on two different types of phosphatases: PP2A and SHP-1.^[24,26,29,58]

1.3 PROTEIN PHOSPHATASE 2A (PP2A)

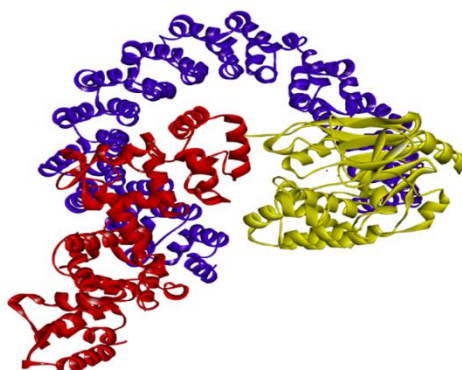


*Figure 2. Heterotrimeric structure of PP2A [PDB: 2IAE]. The catalytic subunit is reported in **yellow**, the regulatory one is coloured in **red** and the scaffold subunit in **blue**.*

PP2A is a serine/threonine phosphatase that is widely expressed within the organism and indeed it represents the 1% of all the protein synthesized in a cell.^[32] The majority of the phosphatase activity on serine and threonine residues is mediated by this enzyme. PP2A is also a phosphatase that is evolutionary conserved, and it is present in almost all the eukaryotes with an amino acid sequence that present a degree of homology between the different species of around 78-93%.^[57] This unique abundance and conservation during the evolutionary process is explained by the fact that PP2A is a crucial enzyme, that is involved in the control of the cellular homeostasis at different levels. It regulates the metabolism of the cell, tuning the activity of the enzymes involved in glycolysis, lipid metabolism and catecholamine synthesis. PP2A finely controls also the cell fate acting as a promoter of the apoptosis. It is involved in different signal pathways like PI3K/Akt, RAF, Mek and cdc2 kinase.^[24,55] This enzyme presents a complex architecture; indeed, it is not constituted by a single amino acid filament, but it requires for its activity a catalytic subunit, a scaffold subunit and for gaining a certain degree of selectivity in terms of substrates, spatial and temporal localisation, a regulatory subunit.^[14,59] Within the cell PP2A can be present in two different forms: a dimeric structure, constituted by the catalytic and structural subunits together; and a heterotrimeric form where, apart the two structures previously mentioned, it is included a regulatory subunit.^[14]

1.3.1 PP2A: Structure

PP2A presents a complex structure, three different subunits contribute to its activity:

1. PP2A_A, the scaffold subunit;
2. PP2A_B, the regulatory subunit;
3. PP2A_C, the catalytic subunit;

Each of these structures presents different isoforms, and this render this mosaic much more complex (Table 1).

	Gene name	Aliases (isoforms)
A subunit		
PP2A_A	PPP2R1A	PR65 α (A α)
	PPP2R1B	PR65 β (A β)
B subunits		
PP2A_B	PPP2R2A	B55 α , PR55 α (B α)
	PPP2R2B	B55 β , PR55 β (B β)
	PPP2R2C	B55 γ , PR55 γ 1 (B γ)
	PPP2R2D	B55 δ , PR55 δ (B δ)
PP2A_{B'}	PPP2R5A	B56 α , PR61 α (B' α)
	PPP2R5B	B56 β , PR61 β (B' β)
	PPP2R5C	B56 γ , PR61 γ (B' γ 1, B' γ 2, B' γ 3)
	PPP2R5D	B56 δ , PR61 δ (B' δ)
	PPP2R5E	B56 ϵ , PR61 ϵ (B' ϵ)
PP2A_{B''}	PPP2R3A	B130, PR130 (B'' α 1);
	PPP2R3B	B72, PR72 (B'' α 2)
	PPP2R3C	PR48 (B'' β 1, B'' β 2) G5PR (B'' γ)
PP2A_{B'''}	STRN, STRN3	PR110, PR93
C subunit		
PP2A_C	PPP2CA	PP2A α (C α)
	PPP2CB	PP2A β (C β)

Table 1. Different isoforms that constitute each subunit.^[18]

Thanks to this complex architecture, PP2A is able to face and overcome the fact that the number of serine/treonine phosphatases it is one order of magnitude less than that

one of the respective kinases. Considering the possibility of combining different isoforms together, Nature obtained with just two catalytic domains and a combinatorial approach, a plethora of active enzymes that presents a different selectivity and cellular localisation. Indeed, it has been demonstrated that in our organism nearly 100 PP2A holoenzymes can be found.^[60]

1.3.1.1 PP2Ac: Catalytic subunit

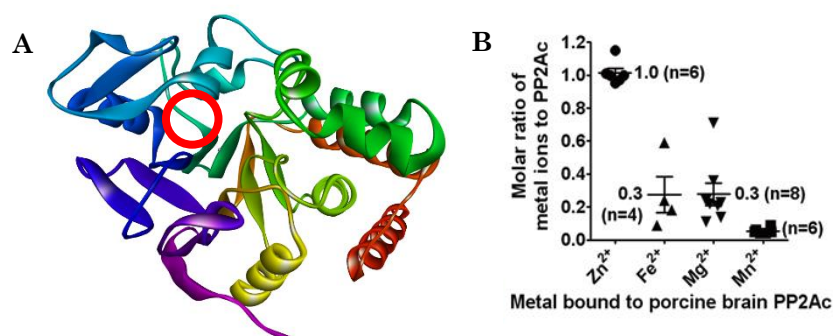


Figure 3. **A.** Crystal structure [PDB: 3FGA] of the catalytic subunit, isoform α , the red circle highlights the active site. **B.** Molar ratio of metal ion species vs PP2Ac in porcine brain.

PP2Ac is the catalytic subunit of PP2A. It has a globular shape and it is constituted by 309 amino acids reaching a molecular weight of 37 KDa.^[14,59] Within the cell PP2Ac is present in two different isoforms: α and β . They are encoded by two different genes (PPP2CA and PPP2CB), which are constituted by six introns and seven exons.^[12,57] The 2-6 exons encode for structures that are involved in substrate binding and catalysis, while exons 1 and 7 generate structures that are involved in the regulation of the enzymatic activity.^[57] The active site of PP2Ac comprises protein loops connected to two central β -sheets. Six highly conserved residues on these loops, Asp 57, His 59, Asp 85, Asn 117, His 167, and His 241, stably chelate two catalytic metal ions, which are common to all PPP family serine/threonine phosphatases.^[57] These ions are fundamental for the activity of PP2A, even the loss of one cation leads to a dramatic decrease of the functionality of the enzyme.^[61,62] The phosphatase cleavage is deputed to the catalytic triad constituted by Arg 89, His 118 and Arg 214.^[62] Despite their great homology in the amino acid sequence (97%), the two isoforms present different characteristics in terms of cellular localisation and levels of expression. C α is mainly present in the plasma membrane and its expression level is higher than C β .^[29] Probably this is due to its stronger promoter activity as well as due to differences in the rate of mRNA turnover. C β is predominantly localized in the cytoplasm. It has been demonstrated in several animal models that the two isoforms are not able to compensate the absence or the unbalanced activity of the other catalytic subunit. Indeed, it has been shown that a complete deletion of the C α does not allow the survival of embryos of mouse over the day 6.^[8] Also the N terminal region of the two isoforms is not conserved, indeed there is a discrepancy of eight amino acids and this lead to the conclusion that this part of the structure is not involved in the catalytic process. Instead, the C terminal portion of both subunits is identical, having a peculiar sequence: ³⁰⁴TPDYEL³⁰⁹. This region is involved in all the processes that control the

interactions between the catalytic subunit and the regulatory and scaffold ones.^[57] The previously mentioned sequence is also subject to different posttranslational modifications that regulate the phosphatase activity of the whole complex.

1.3.1.2 PP2A_A: Scaffold subunit

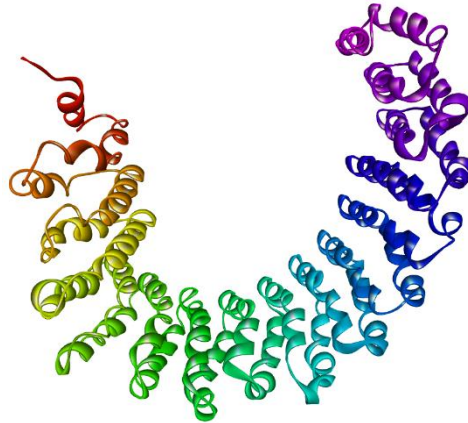


Figure 4. Crystal structure [PDB: 2IAE] of the structural subunit, isoform α .

The structural subunit PP2A_A serves as a scaffold for harbouring the catalytic and regulatory subunits. Its horseshoe shape allows a correct orientation of the two hosted structures. Thanks to this structural conformation, the regulatory and catalytic subunits can correctly interact one to each other and this allows the dephosphorylation of the different targets of PP2A.^[8,59,63] The A subunit is constituted by 15 repetitions of a 39 amino acid HEAT sequence (Huntington/elongation/A-subunit/TOR).^[59] Each repeat is formed by two antiparallel α -helices, connected by inter and intra loops. The catalytic subunit binds to 11–15 repeats and the regulatory subunit binds to 1–10 repeats of the HEAT sequence.^[14] The whole structure is characterised by a high degree of flexibility, this allows to PP2A_A to adapt to the different complexes of PP2A, like heterotrimer or dimer, and to the different regulatory and catalytic subunits present within the cell.^[8] PP2A_A has a molecular weight of 65 KDa, and from this comes the other name of this structure that is PR65, where 65 stands for the weight.^[12] This subunit, as the catalytic one, is expressed by the cells in two different isoforms: α and β . As previously seen for PP2A_C, also in this case the two isoforms are not interchangeable, and it has been demonstrated that one can not overcome the absence of the other one, even if they share an 86% of the aminoacidic sequence.^[57] In the 90% of the cases, the PP2A complexes present the PP2A_A α subunit which is predominantly expressed in all the mature cells accounting for the 0.1% of all the proteins.^[8] The β isoform seems to be majorly expressed during the first phases of the embryonic development, while during the maturation its concentration decreases and that one of the α isoform increases.^[54] Higher levels of the β subunit can be found in testis, suggesting a predominant role of this isoform during the spermatogenesis. Both the isoforms are prevalently present in the cytoplasm.^[32]

1.3.1.3 PP2A_B: Regulatory subunit

The group that includes all the regulatory subunits is the most complex and variegated of all the other structures presented till now. All the members of this class are united by the fact that they intervene on the heterotrimeric complex of PP2A modulating not only the selectivity of the phosphatase in terms of substrate, but they guarantee the specificity of the cellular localisation and also of tissue expression.^[3] Indeed, apart their ability to recognise different targets, all the regulatory subunits present a different distribution during various developmental stages and in diverse tissues. Currently, 15 different genes that encode for a different regulatory subunit have been discovered.^[14] These heterogeneous structures have been catalogued into four different families: B (commonly known as B55/PR55), B^I (B56/PR61), B^{II} (PR48/PR72/PR130), B^{III} (PR93/PR110).^[10,14,29] As already mentioned for the scaffold subunit, also in this case the numbers that follow the acronym PR stand for their approximate molecular weight.

B family (B55/PR55)

The B family is constituted by four isoforms (α , β , γ and δ).^[57] Each subtype is encoded by a different gene and presents a different amino acid sequence. They are united by the presence of a five degenerate WD-40 repeats.^[57] A WD-40 repeat is a conserved sequence, composed by approximately 40 amino acids, that terminates typically with a couple of tryptophan-aspartate.^[24,57] These repeats are necessary for mediating the interaction of the heterotrimeric holoenzyme with the target protein. The different isoforms of the B family present a different tissue distribution, indeed, while PR55 α and PR55 δ have a wide-spread tissue distribution, PR55 β and PR55 γ are highly enriched in brain.^[14,55,60] These subtypes present a significant difference also for what concern their temporal distribution. It has been demonstrated that the levels of PR55 β decrease after birth while those of PR55 γ contrary increase. The expression of the α subunit remains almost constant during all the development.^[18]

B^I family (B56/PR61)

Five different isoforms belong to the B^I (B56/PR61) family: α , β , γ , δ and ϵ .^[57] All these structures share an 80% of homology in the sequence, despite their different N- and C- terminals.^[24] Thanks to this similarity all the isoforms present some common features. First, they can be directly phosphorylated, which alter their functionality, and secondly, they are characterised by a predominant organization in alpha helices. Furthermore, they can directly bind to the core enzyme and enhance the reaction rate.^[14] Each isoform presents a different tissue and cellular distribution, that is due to the differences in the N- and C-terminal regions. The subtypes α , β and ϵ are exclusively expressed in the cytoplasm while B56 γ is predominantly expressed within the nucleus.^[18,29] B56 δ can be found in both the cytoplasm and nucleus. For what concern the tissue distribution, the α and γ subunits are expressed at high level in heart and skeletal muscle, while the β and δ subtypes can be found at higher concentrations within the brain.^[60] Several studies have shown that B56 presents different states of phosphorylation, sequence alignment and intracellular localization confirming its importance in the control of the cellular homeostasis.^[14,64]

B^{II} family (PR48/PR72/PR130)

This family present different components, not all the literature agrees for what concern the different isoforms that constitute this heterogeneous ensemble. PR72 and PR130 are commonly accepted as members of the B^{II} family.^[3,10,60,65] They present a significant sequence difference just in the N-terminal region. This high degree of homology highlights their common origin, it seems indeed, that they originated from the same progenitor gene after a process of alternative splicing. These subtypes present a different tissue distribution. PR130 is uniformly expressed in all the tissues, with a higher level in the heart and muscle. These body regions are also the only localizations for the PR72 subunit.^[8,57,66] PR72 presents a peculiarity, for facilitating its interaction with the scaffold subunit, it requires the binding of calcium in two EFX domains, present in its protein structure, and this leads to a conformational change that allow the formation of the heterotrimeric complex of PP2A.^[57] Other two isoforms have been identified belonging to this family: PR48 and PR59.^[29,55,57,67] Both these subtypes do not have a high degree of homology with the other members of the family. Despite this, it has been demonstrated that the PR48 and PR59 isoforms are united by the fact that in case of their overexpression there is an arrest of the cell replication at the G₁ phase.^[24]

B^{III} family (PR93/PR110)

The B^{III} family constitutes the last group of regulatory subunits. It is composed by two different isoforms: PR93 and PR110.^[8,18,29,55,57] The members of this family belong to the category of the calmodulin binding proteins (CaM).^[57] They interact with the dimeric PP2A, thanks to the presence of some 40-WD repeats as in the PR55 family, making the new complex sensible to the calcium signalling. These proteins also require ATP and Mg²⁺ for their activation.^[12]

1.3.2 PP2A: Regulation

PP2A's activity is modulated at different levels. Firstly, the holoenzyme, and in particular the catalytic subunit is subjected to post translational modifications that finely tune the phosphatase activity of PP2A. Subsequently, this enzyme is controlled by a series of accessory proteins that can increase or inhibit its function.^[3,60]

1.3.2.1 PP2A and post translational modifications

PP2A is subjected to two different kind of post translational modifications that alter its activity and also the affinity of the core structure with certain kind of B subunits. These modifications are: methylation and phosphorylation.^[10,60,68]



Figure 5. Crystal Structure of the catalytic subunit of PP2A (yellow) and LCMT-1 (orange) [PDB: 3P71]

The first important post translational modification is methylation. PP2A can be carboxymethylated at the level of its last amino acid of the catalytic subunits: Leu 309.^[10,57,69] Two different kind of enzymes are involved in the control of the methylation state of the C subunit: LCMT1 (Leucine Carboxyl MethylTransferase-I) and PME-1 (PP2A MethylEsterase-1).^[10,15,18,61,70] LCMT1 is deputed to the transfer of a methyl group from its co-factor SAM (S-adenosyl methionine) to Leu 309 of the catalytic subunit, principally in the cytoplasm.^[71] This transformation leads to the activation of the enzyme and in particular, it increases the affinity of the core dimer of PP2A with different regulatory subunits.^[60] The introduction of this methyl group is a fundamental step for the assembly of the heterotrimeric structure only *in vivo*, indeed, it has been demonstrated that *in vitro* this modification is not necessary.^[14,57] Not all the B subunits increase their affinity with the dimeric PP2A after methylation. It has been demonstrated that PR55 requires a methylated catalytic subunit for the formation of the fully active holoenzyme, while for PR72 and PR61 methylation is not essential.^[8,14,57]

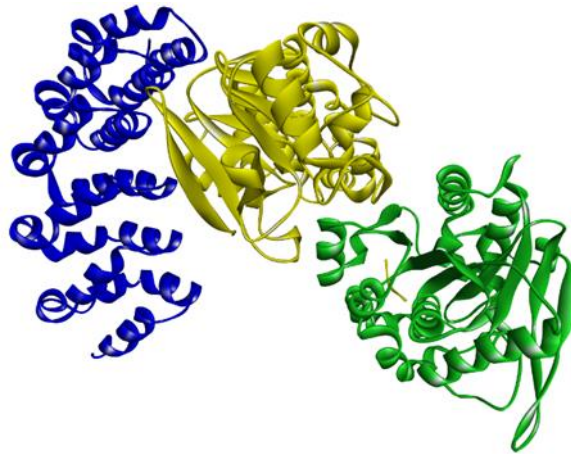


Figure 6. Crystal structure of the core enzyme PP2A (catalytic subunit in **yellow** and scaffold in **blue**) and PME-1 in **green** [PDB: 3C5W].

The other player that control the level of methylation of the catalytic subunits of PP2A is PME-1. PME-1 is a lipase-like methyl esterase prevalently expressed within the nucleus.^[10,60,72] This enzyme reverts the action of LCMT1 removing the methyl group from Leu 309 disactivating PP2A.^[8,57] Contrarily to the LCMT1 action, the demethylation mediated by PME-1 is not completely revertible.^[24] This is due to the fact that this enzyme does not remove only the methyl group, but it alters also the structure of the C subunit, denaturing its active site and leading to the loss of the two metal ions coordinated by PP2Ac.^[57] PME-1 rearranges also its catalytic triad composed by Ser 156, Asp 181 and His 349.^[8] Indeed, the side chain of His 349 is moved away from its functional position of 8 Å. Another macroscopic effect of the interaction between PME-1 and PP2Ac is that even the active pocket of the methyl esterase becomes bigger hosting the C-terminal tail of the C subunit for the dephosphorylation.^[61] Furthermore, the association of PME-1 and PP2Ac has the effect of stabilizing this complex, reducing the degradation rate of PP2Ac, forming in this way a pool of catalytic subunits readily available for the reactivation.^[61] The formation of a reservoir of PP2A is an event mediated also by another accessory protein: PTPA (Serine/threonine-protein phosphatase 2A activator).^[61,62] This protein exerts also a chaperone function on PP2A leading to the correct folding of the catalytic pocket of PP2Ac.^[62] PTPA presents a peptidyl-prolyl cis/trans isomerase activity that acts on the residue Pro 109 of the catalytic subunit of PP2A. Several studies have supposed that this could be the trigger that induce the reactivation of PP2Ac.^[61]

The C subunit of PP2A is also subjected to phosphorylation. It can occur at two different residues: Tyr 307 and Thr 304.^[8,73] Also, in this case, these modifications aim to modulate principally the interaction of the dimeric core of PP2A with different B subunits. Phosphorylation at Tyr 307 is mediated by pp60^{v-src} and pp56^{lck} kinases, EGFR and insulin receptor.^[55] This modification inhibits the methylation of Leu 309 and it favours the phosphorylation at Thr 304.^[55] This last phosphorylation does not influence the methylation state of the C subunit but, as for Tyr 307, it regulates the interaction with specific B subunits.^[55] In particular, phosphorylation at both sites blocks the interaction with PR55. Phosphorylation of Y307 prevents assembly of the holoenzyme with PR61/B^Iαβγε subunits, but not with the B^Iδ, PR72/B^{II} or PR70/B^{II}

subunits. The phosphorylation of these amino acids can be reverted by auto dephosphorylation mediated by PP2A.^[55]

1.3.2.1 PP2A and physiological modulators

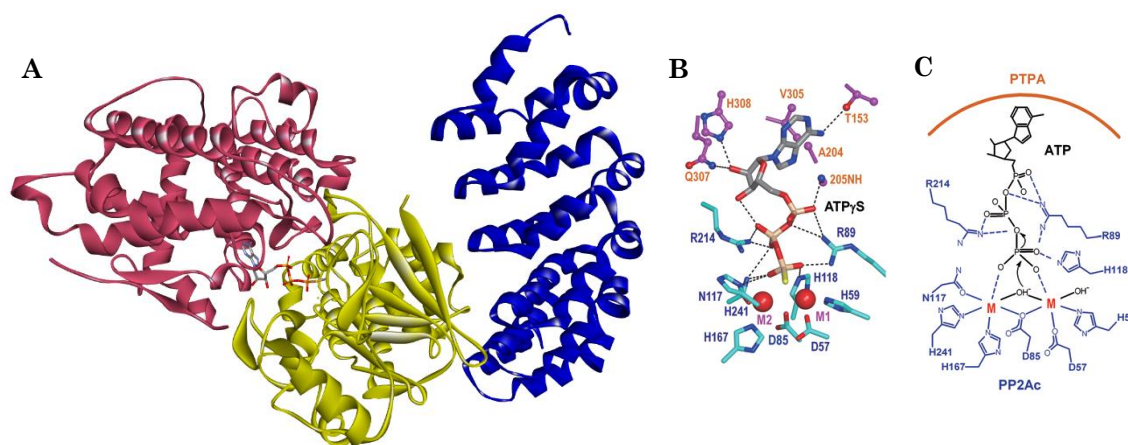


Figure 7. **A.** Crystal structure of PTPA (**red**) and the core structure of PP2A (catalytic subunit in **yellow** and scaffold subunit in **blue**) [PDB: 4LAC]. **B.** A close-up view of the combined ATP-binding pocket of the PP2A-PTPA complex bound to ATPyS. Residues from PTPA and PP2Ac are in ball-and-stick and cylinder, and colored magenta and cyan, respectively. ATPyS is shown in cylinder and colored by atom type. Catalytic metal ions are indicated by red spheres. The black dashed lines indicate H-bonds. **C.** Illustration of dual octahedral metal ion chelation at the PP2Ac active site by ATP γ phosphate and six metal ion-chelating residues with proposed mechanism of ATP hydrolysis.

One of the most important and well-studied physiological modulators of PP2A is PTPA.^[62] As highlighted in the previous paragraph, this protein is fundamental for guaranteeing a correct activation of the catalytic subunit of PP2A.^[61] PTPA stabilizes the protein folding of the apo-PP2Ac and allows its activation.^[62] This last action is a concerted mechanism that interplays PTPA, PP2A and an ATP molecule. ATP orientates its phosphoryl groups within the active site of the C subunit and there they facilitate the coordination in the catalytic pocket of two metal ions, that are fundamental for the phosphatase activity.^[62] This combined and controlled coordination exerts also a selection on the nature of the chelated metal ions. Indeed, the support given by the ATP molecule and PTPA promotes preferentially the coordination of a Zn^{2+} and a Mg^{2+} ions.^[61] This gives to the catalytic subunit the right substrate selectivity among phosphorylated serine or threonine. PTPA with these concerted events rearrange the active site of PP2Ac stabilizing its active conformation.^[74] This event renders the C subunit much more prone to be methylated by LCMT1 favouring again its right activation.^[60]

Another important modulator of PP2A is the α_4 protein. This structure interacts with the metal free and partially unfolded PP2Ac stabilizing it and preventing the protease degradation of this subunit.^[62] This accessory protein interacts specifically with the unfolded C structure, indeed α_4 is not only able to generate interactions with external surface of PP2Ac but also with a peculiar structure present in the unfolded state, such as a helix-loop switch situated near the active site. The α_4 -PP2Ac complex is a source of readily available catalytic subunits.^[62]

All the protein structures presented till here in this paragraph are prone to activate or at least stabilize the catalytic subunit and consequently, they sustain the phosphatase activity of PP2A. Within the cell other modulators are present that are able to selectively inhibit PP2A.

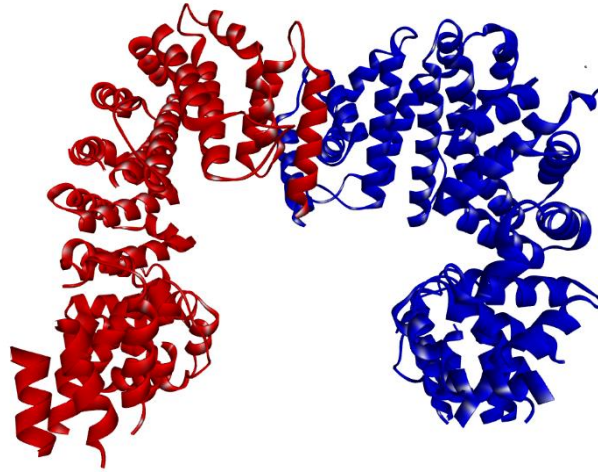


Figure 8. Crystal structure of the N-terminal region of CIP2A [PDB: 5UFL]

Among these, for sure CIP2A (Cancerous Inhibitor of Protein phosphatase 2A) is one of the most interesting. It has been widely studied during the last decade and it has been shown that its overexpression is recurrent in several malignancies. This pathological situation induces a deep inhibition of the PP2A activity and consequently to an over activation of all the antiapoptotic and proliferative signals mediated by the well-known cascades modulated by: c-MYC, Akt and E2F1.^[64,64,66,75-77] Only recently, some steps forward have been done with the aim to clearly understand which are the structural bases that modulate the inhibition of PP2A by CIP2A. Wang and co-workers have demonstrated that CIP2A tends to form homodimers for increasing its stability.^[64,64] This organisation is also useful for the inhibition of PP2A, indeed, with this configuration CIP2A can directly interact with the holoenzymes that present the B56 α and B56 γ subunits, inhibiting drastically their activity.^[64]

Another inhibitor that is worthy to consider is ANP32A (acidic nuclear phosphoprotein 32 kDa A) or I1PP2A (PP2A inhibitor 1): it has been found that this type of protein can bind sphingosine and inhibit PP2A consequently.^[15,18,29,60,63] From a functional point of view, this can affect cell proliferation, but striking evidences are still lacking, and this protein is still a matter of study.

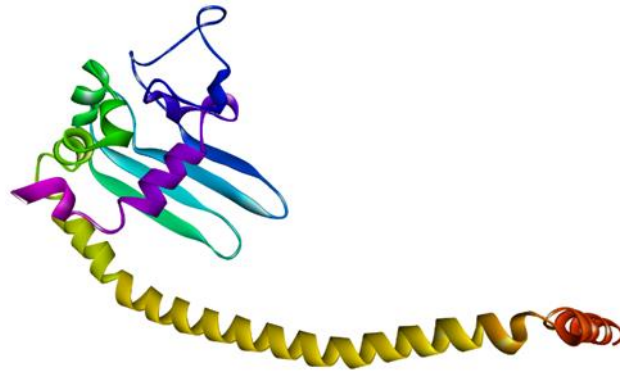


Figure 9. Crystal structure of SET protein, monomer edited with Swiss-Model from the PDB 2E50.

Considering all the physiological modulators of PP2A the most studied is SET (Suvar3-9, Enhancer of zeste, Trithorax), also known as I2PP2A.^[60,73,78] SET is a protein constituted by a single filament of 277 amino acids with an apparent molecular weight of 39KDa.^[79] It presents a globular N-terminal domain and a long alpha helix as C-terminal.^[3,15,80] It is expressed in several tissues and it localizes principally within the nucleus where it blocks the DNase activity and the histone acetylation.^[81] This last process is mediated by the acidic C-terminal that can tightly interact with the histones.^[79,81] SET is able to inhibit PP2A in a low nanomolar range and it is one of the most potent and selective inhibitors of this phosphatase.^[3,73] The structural mechanism by which SET interacts and inhibits PP2A is not clear yet. There is just one crystal structure of an incomplete SET dimer in the Protein Data Bank.^[81] Currently, few notions are available for understanding the mechanism of inhibition of PP2A mediated by SET. It is known that for its action I2PP2A has not to be dimerized, but it has to be phosphorylated, by PI3Ky and Cdk1, at two serine residues (Ser 7 and 9).^[82,83] SET interacts directly with the catalytic subunit of PP2A through its N-globular terminal.^[57] It has been shown also that the two fragments (i.e. N- and C-terminal fragments) obtained by the proteolytic cleavage mediated by granzyme A are able to inhibit potently PP2Ac.^[57] SET is found overexpressed in a plethora of cancers: CML and Ph1-ALL (both BCR/ABL driven leukemias), Wilms tumors, lung cancers, AML, B-cell non-Hodgkin lymphoma, B-CLL.^[57] SET gene was also found to be fused with the nucleoporin NU214 (CAN) in t(6;9) acute undifferentiated non-lymphocytic leukaemia, probably as a consequence of a chromosomal translocation.^[18,70] SET is also stabilized by another accessory protein that prevents its proteolytic degradation: SETBP1 (SET binding protein 1). In certain malignancies the overexpression of this protein leads to increased level of SET with consequent decreased PP2A activity.^[18,60,70,84]

1.3.3 PP2A: Function

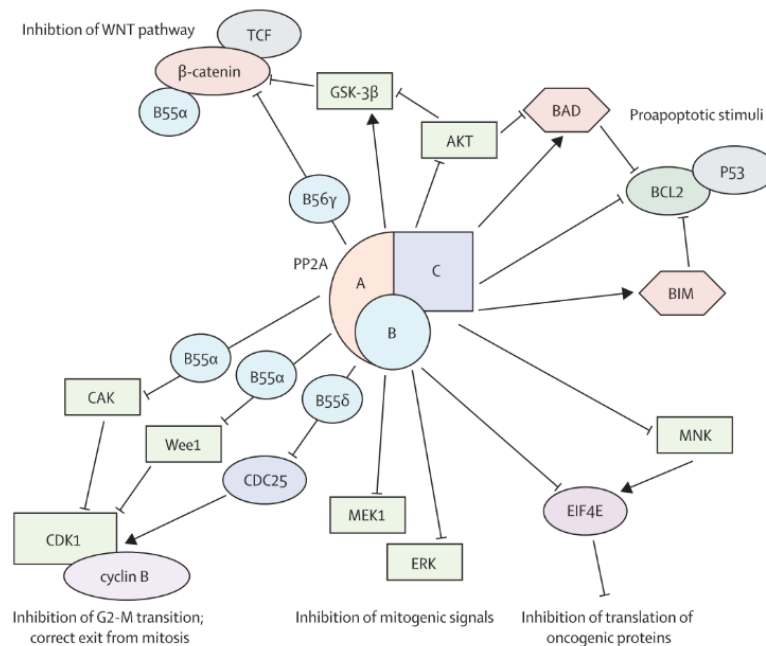


Figure 10. Schematic representation of the PP2A's network of pathways. The figure shows the many levels at which PP2A affects the normal physiology of cells.

Considering the large number of possible combinations of PP2A holoenzymes and their involvement in a multitude of processes that span from DNA replication to induction of apoptosis; seems to be interesting and useful, for understanding the importance of this enzyme in the control of the cellular homeostasis, to investigate in a deeper way the principal processes in which PP2A is involved. For this reason, in the next paragraphs the main pathways controlled by PP2A will be present.

1.3.3.1 PP2A and cellular homeostasis

The different complexes of PP2A are involved in various physiological processes. Their main action is to counteract and balance the activity of the kinases, thus almost all their effects are mediated by a direct dephosphorylation of a phosphor-serine or a phosphor-threonine.^[10]

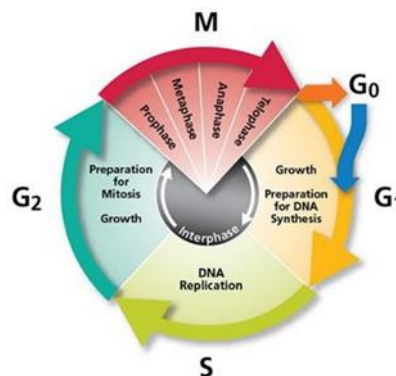


Figure 11. Schematic representation of the cell cycle

One of the principal roles that PP2A covers is the control of the cell cycle progression. Indeed, this phosphatase is directly involved in the regulation of the G₁-S transition. The B56γ-PP2A complex accumulates within the nucleus and it plays a critical role in the control of the phosphorylation state of another tumour suppressor protein: Retinoblastoma (Rb). This protein is inactivated by hyperphosphorylation mediated by CDKs, and when this happens, the progression through the cell cycle from the G₁ to S phase is allowed.^[8,10,14,57] PP2A competes to the same site of interaction between Rb and the CDKs blocking physically the phosphorylation and also it acts directly on the Rb, dephosphorylating it. This action reactivates the Rb blocking the G₁-S transition.^[55,57] PP2A tunes also the G₂-M transition. This action is mediated by the B55α-PP2A complex. This holoenzyme inhibits the maturation of promoting factors like CDK1 and Cyclin B through the direct dephosphorylation of CDK-activating kinase and Wee1 kinase.^[18,55] The complex B55α-PP2A regulates also the mitotic spindle breakdown, chromatin condensation and post mitotic reassembling of the nuclear envelope and Golgi apparatus.^[18,24,55] PP2A is also involved in the exit from mitosis. B56δ-PP2A directly dephosphorylate the CDC25 phosphatase inactivating it. This leads to an augmented level of phosphorylation for what concern CDK1 that becomes inactive.^[13]

PP2A is also responsible of the negative regulation of the cell survival and proliferation. It plays its fundamental role switching off the most important pathways deputed to the vehiculation of all the proliferative and antiapoptotic signals of the cell. Through direct dephosphorylation PP2A inactivates MEK1 and ERK family of kinases.^[11] It decreases the stability and functionality of transcription factors such as c-MYC and STAT5.^[11,57,79] PP2A suppress also the translation of oncogenes such as MCL1 and c-MYC through direct and indirect (via inhibition of MNK1,2 kinases) dephosphorylation of EIF4E.^[18]

The main target of PP2A is the induction of apoptosis through the inhibition of the PI3K/Akt pathway.^[11,19] Akt is one of the main oncogenic proteins, its overactivation is present in several malignancies and this leads to an uncontrolled cell proliferation. In its active form Akt is phosphorylated in two different residues: the Thr 308 and the Ser 473.^[3,24,57] The B55-PP2A complex is directly involved in the dephosphorylation of the Thr 308 residue and this leads to the inactivation of Akt.^[3,24,57]

PP2A modulates also the WNT signal pathway, that is involved in the embryonic development, cell growth, stem cell survival and self-renewal.^[60] The complexes B56γ and B55α are responsible for the direct dephosphorylation of the β-catenin, which is one of the main effectors of the WNT pathways.^[57] This dephosphorylation leads to the inactivation of the protein and consequently to its degradation. The directly interaction between PP2A and β-catenin is not the only mechanism by which the WNT cascade is inhibited. Indeed, the direct dephosphorylation and deactivation of Akt leads to the consequent activation of another enzyme: GSK-3β.^[29,57] This kinase inactivates the β-catenin concurring to the complete inhibition of the WNT signal.

Another important role of PP2A is to activate pro apoptotic stimuli like BAD and BIM and to block antiapoptotic effectors like BCL2-P53 complex.^[10,57] BAD and BIM are

reactivated through a direct dephosphorylation. BCL2 is activated by a phosphorylation at the Ser 70 residue.^[10] This leads to the breakdown of the BCL2-P53 complex having a proliferative effect. B56-PP2A complex directly dephosphorylate BCL2 at the activating residue, inhibiting the dissociation of the BCL2-P53 complex and consequently inducing the apoptosis.^[57]

Considering the different pathways in which PP2A is involved, it is not surprising that this phosphatase is also deputed to the maintaining of the cell adhesion and to the control of the cytoskeleton dynamics. PP2A co-localise with β 1-integrine and modulates the FAK (Focal Adhesion Kinase) complex.^[57] When there is a strong downregulation of the PP2A activity, we can assist to an upregulation of the FAK/Src/paxillin cascade, through hyperphosphorylation of the FAK complex.^[24] This leads to the disorganization of the focal adhesion sites and to an increased cell migration. The main consequence of this dysregulation is an increment of the cell motility, invasiveness and loss of cell polarity that is the first feature for having metastatic cells.^[18]

1.3.3.2 PP2A and cancer

	Change	Disease
Subunits		
PP2A ³⁴	Decreased expression, increased phosphorylation, decreased methylation	Alzheimer's disease
PR65 ^{18,34-39}	Decreased expression, loss of heterozygosity, deletion, point mutations	Alzheimer's disease; lung, colorectal, breast, ovarian, cervical, endometrial, and stomach cancer; bladder carcinoma, hepatocellular carcinoma, glioma, melanoma, B-CLL, AML
B55 α ^{34,40-42}	Decreased expression	Alzheimer's disease, AML, breast cancer
B56 α ^{37,42,43}	Decreased expression	Melanoma, AML
B56 γ ^{42,43}	Decreased expression	Melanoma, AML
B56 δ ⁴²	Decreased expression	AML
Binding partners		
ANP32A (I1PP2A) ³⁴	Increased expression	Alzheimer's disease
SET (I2PP2A) ^{34,34,44-48}	Increased expression, increased activity	Alzheimer's disease, CML, AML, Ph+ ALL, T-cell ALL, B-cell CLL, B-cell NHL, polycythemia vera
CIP2A ^{30-22,35,49-53}	Increased expression	Hepatocellular carcinoma; breast, colorectal, ovarian, cervical, prostate, lung, and head and neck cancer; CML, AML
SETBP1 ^{54,55}	Increased expression	T-cell ALL, AML
B-CLL=B-cell chronic lymphocytic leukaemia. AML=acute myeloid leukaemia. CML=chronic myeloid leukaemia. Ph=Philadelphia chromosome. ALL=acute lymphoblastic leukaemia. NHL=non-Hodgkin lymphoma.		

Table 2. Correlations between alterations in PP2A subunits or its binding proteins and different types of pathologies.

Till now we have defined PP2A as an onco-suppressor enzyme. This definition has been confirmed in principle by two different experimental evidences. The administration to healthy cells of two well-known PP2A inhibitors, okadaic acid and the SV40 small t antigen (a transforming viral antigen), transforms these cells into cancerous ones.^[9,79] These results confirm the general principle that a drastic reduction of the PP2A activity leads to the onset of several pathologies and the majority of these are neoplasms. The mosaic of subunits and regulators that concur to

an optimal activity of this fundamental enzyme is so complicated that each single protein structure, if altered in the conformation, expression or activity, can lead to the onset of a malignancy. Sablina and colleagues, with their work, have evidenced how the absence of expression of different PP2A's subunits can induce the onset of cancer.^[18,70] In their studies, these researchers utilized small hairpin RNA (shRNA) for blocking the expression of B56 α , B56 γ , PR72–PR130 and PTPA. The single knocking down of each protein led to a cellular phenotype that is strongly similar to that one observed after the administration of the SV40 small t antigen.^[18] More precisely, inhibiting the expression of B56 α , PR72–PR130 and PTPA increased the expression of c-MYC.^[85] The concomitant inhibition of the B56 γ and PTPA induced a cancerous phenotype characterised by an augmented phosphorylation level of Akt, and consequently an increased activity of this protein. Subsequently, it has been observed an elevated β -catenin dependent transcription.^[85] The phenotype that presented much more drastic changes compared the healthy one is when the PTPA expression is inhibited. In this case the absence of this protein leads to a diminished assembly of the holoenzyme.^[57,62] This is due to the fact that the catalytic subunit is not correctly assembled and structured and this leads to a reduction in the methylation at its C-terminal. All these effects concur to a reduced affinity between the catalytic and scaffold subunits, reducing the possibility of forming a functional enzyme.^[57,62]

Much more information has been obtained analysing the different profiles of protein expression in different cancers. It has been observed that there is a reduced level of B56 α and B56 γ in several melanomas.^[18] In this kind of malignancies, and in particular in their metastasis, the reduced PP2A activity is correlated with an augmented expression of c-MYC which subsequently leads to an increased phosphorylation of paxillin. This phenotype is responsible of the reduced number of focal adhesions present in this kind of cells. The expression of B56 α is strongly reduced also in Acute Myeloid Leukaemia (AML), with consequent aberrant activation of Akt, and in a set of luminal B breast cancers.^[18]

Also the scaffold subunit presents some significant alterations in several neoplasms. Mutations of the PR65 β isoform have been detected in 15% of lung tumours, 6% of lung tumor derived cell lines, 15% of primary colorectal carcinomas and in 13% of breast cancers.^[11] Aberrant transcripts of this isoform of scaffold subunit have been found in 29% of hepatocellular carcinomas.^[29] Loss of heterozygosity at the PR65 β locus (11q23) have been detected in breast, ovarian, cervix, stomach and bladder carcinomas and in melanoma.^[18] This isoform presents also gene deletion or alternative splicing in aggressive β -Cell lymphocytic leukaemia (β -CLL). This condition leads to increased values of phosphorylated RalA, a multifunctional GTPase involved in a variety of cellular processes including gene expression, cell migration, cell proliferation, oncogenic transformation and membrane trafficking, that becomes constitutively active.^[57] There are many other mutations at the expense of the scaffold subunits that result in a reduced affinity between the A and C or the A and B subunits, generating a reduced level of PP2A activity. For what concern specifically the PR65 α isoform, high frequencies of mutations and deletions have been spotted in lung cancers and in the 32% of uterine serous carcinomas.^[18] A significant reduction of the

expression level of this isoform of the scaffold subunit has been observed also in 43% of human gliomas, with a tenfold decrement, and in HEK293 cells, where the expression of PR65 α is reduced of 50%.^[57]

Interestingly, till now only few malignancies present altered levels of the catalytic subunit. To date there are no known alterations correlated to gene that encodes for the β isoform. Lower levels of expression compared to the physiological ones of the α isoform have been found in patients with AML or prostate cancer.^[57]

The loss of function of PP2A is not only correlated to abnormalities on the expression of the subunits that compose the enzymatic heterotrimer, but it can be linked also to anomalous overexpression of its physiological inhibitors present within the cell: CIP2A, SET and SETBP1.

Increased levels of CIP2A have been underlined in several neoplasms such as: hepatocellular carcinoma, triple negative breast cancer, head and neck squamous-cell carcinoma, colorectal cancer, serous ovarian cancer, non-small-cell lung cancer, prostate cancer, CML, and AML.^[4,57] The overexpression of this protein has as a consequence the stabilization of c-MYC, that is no more dephosphorylated at Ser 62, and the complete reactivation of the PI3K/Akt pathway.^[18,29,57,60,70,85]

Another physiological inhibitor of PP2A that is constitutively overexpressed in a series of cancers is SET (e.g. in BCR-ABL1-positive leukaemias such as CML-CP, CML-BC and Phpositive B-ALL, in AML, in primary B-CLL cells and in B-cell non-Hodgkin lymphoma cell lines).^[57] This kind of alteration is particularly recurrent in several kind of leukaemia and this configure SET as a leukaemogenic protein.^[18] The inhibition of the PP2A activity it is not the only mechanism of action of SET. This factor is able to suppress the DNase activity of the tumor suppressor NDKA (NM23-H1), to increase the AP-1 activity and to activate the MAPK signalling.^[18] Furthermore, SET is able to modulate the activity of PP2A exploiting also another mechanism. In CD34+ progenitors from myeloproliferative disorders associated with the Val617Phe mutation of JAK2 (JAK2-V617F), such as polycythaemia vera, SET is constitutively phosphorylated at the Ser 9 residue.^[18] This is due to the mutation of JAK2, that leads to the overactivation of PI3K γ kinase that phosphorylate SET at the serine residue.^[18] The augmented levels of phosphorylated SET are correlated with its accumulation within the cytoplasm. There SET prevents the activation of PP2A mediated by NOS2-peroxynitrite.^[18]

Another factor that is overexpressed in certain kind of malignancies and that negatively modulate the activity of PP2A is SETBP1 (SET Binding Protein).^[84] It is a SET interacting protein and incremented levels of its expression have been observed in 27.6% of patients with AML. SETBP1 interacts with SET preventing its degradation mediated by the proteases. This leads to incremented levels of SET and consequently to an augmented formation of the inactive complex SETBP1-SET-PP2A.^[18,60,70,84]

1.3.4 PP2A: Small molecule modulators

During the last decades a lot of efforts have been done by the scientific community with the aim to isolate and identify small molecules, natural or not, that are able to modulate the phosphatase activity of PP2A.

1.3.4.1 PP2A inhibitors

Inhibitors	Inhibition of PP1 IC ₅₀ (nM)	Inhibition of PP2A IC ₅₀ (nM)
Okadaic acid class		
Okadaic acid	3.4 ^a	0.07 ^b
Calyculin A	0.3 ^a	0.13 ^b
Microcystin-LR	0.1 ^a	0.10 ^b
Endogenous		
SET/I ₂ ^{PP2A}		2.0 ^c

a The catalytic subunit of PP1 was isolated from rabbit skeletal muscle.

b That of PP2A was isolated from human erythrocytes.

c PP2A was isolated from bovine kidney cytosol.

Table 3. Inhibition of protein phosphatase 1 and 2A.

Several compounds have been identified as PP2A inhibitors. Usually these molecules are catalogued as tumor promoter, indeed it is commonly accepted that being PP2A an oncosuppressor, its inactivation has as primary consequence the onset of a cancerous disease. The first evidence of this assumption has been investigated in concomitance of the discovery of a potent and selective inhibitor of PP2A: the Okadaic Acid (OA).^[9] This is a natural compound isolated from the black sponge *Halichondria okadai*.^[9,65] OA is able to inhibit PP2A interacting directly with the catalytic subunit of PP2A.

Other natural products have been isolated that are able to block the phosphatase activity of PP2A. These are:

- Dinophysistoxin-1 (or 35-methyl OA), extracted from the mussel *Mytilus edulis*;
- Calyculin A, isolated from the marine sponge *Discodermia calyx*;
- Microcystin-LR, produced by the blue-green algae *Cyanobacteria*;
- Nodularin, also isolated from the blue-green algae *Cyanobacteria*.

All these compounds are unified by the fact that they inhibit PP2A directly interacting with its catalytic subunit.^[9,10,17,55,65,67]

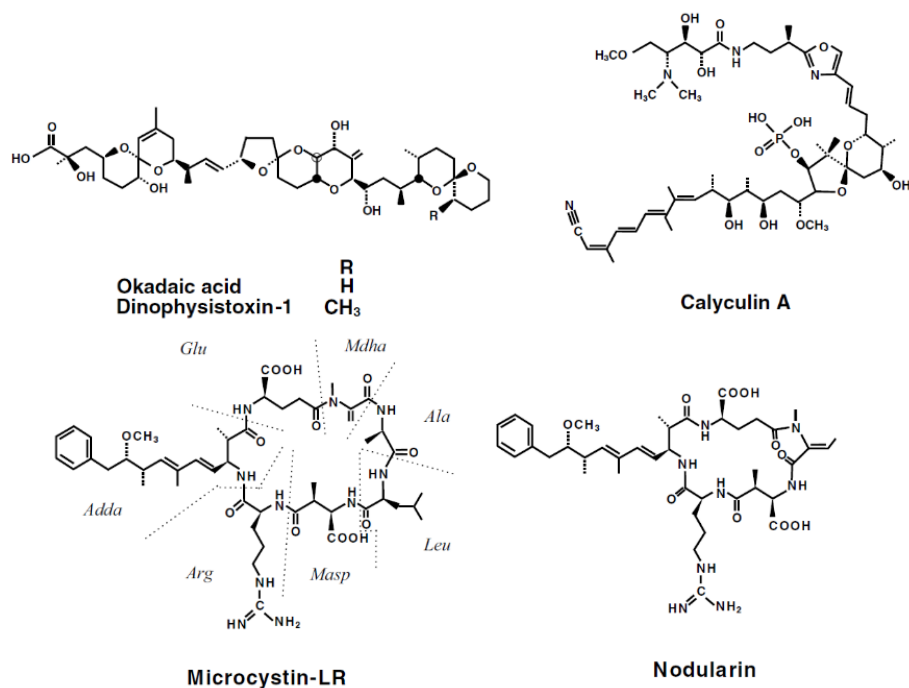


Figure 12. Molecular scaffold of the principal PP2A inhibitors.

In more recent years, cantharidin (isolated from *Lytta vesicatoria* beetles) and its derivatives LB100 and LB102 have shown to be able to inhibit PP2A, also in this case interacting directly with the catalytic subunit.^[3,86] Both of these molecules displayed significant effects when co-administered to classical anti-tumor drugs in several forms of cancer (LB100 showed its effects on hepatocellular carcinoma, while LB102 on glioblastoma, neuroblastoma, and stem cell-derived aggressive sarcoma); indeed, their inhibitor activity towards PP2A alters cancer cell signalling leading them to skip cell cycle checkpoints, fact that makes the cell more vulnerable towards external factors as anti-tumor drugs.^[3,86]

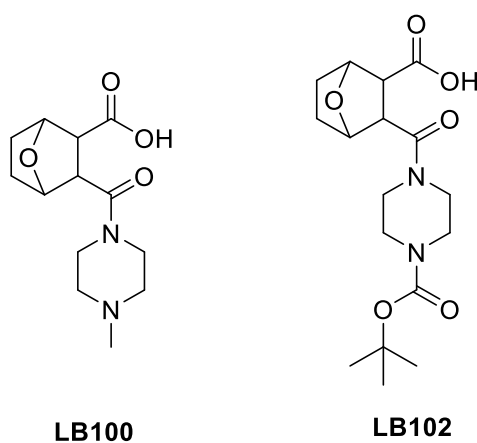


Figure 13. Molecular structure of two cantharidin derivatives: LB100 and LB102.

1.3.4.2 PP2A activators

Considering the role of PP2A in the control of cellular homeostasis and in particular its principal feature of oncosuppressor, it seems evident that a lot of studies and researches have been conducted with the common effort of finding a potent and effective candidate that is able to reprimarily the physiological functionality of PP2A in those pathological conditions where its phosphatase activity is strongly downregulated. This is an optimal therapeutic strategy, especially in the anticancer therapy. Indeed, the possibility to restore the PP2A activity in those cancerous cells where it has been silenced present several advantages:

1. This kind of therapeutic option does not present the same side effects of the canonical approach with TKIs, indeed this kind of pharmacological approach aims to increase the activity of an enzyme within the tumor cells that is already physiologically elevated in the healthy ones. In these healthy cells is difficult to increase the PP2A's activity, which remains almost untouched, and this allows to reduce the risk of off targets effects.^[8,10,18,60,67,70]
2. This strategy has been demonstrated effective also in cancerous stem cells, that are the main reservoir of resistances in cancer.^[77]
3. The utilize of PP2A activators could be effective also in those types of cancers that are resistant to the common pharmacological approaches.^[15,17,29]

Recently different compounds have been identified as PP2A activators. It is behind the scope of this brief introduction to give a detailed description of all the discovered molecules. Instead, in this paragraph the most interesting, recent and promising compounds will be introduced, and it will be focused the attention of the reader on the different approaches that can be exploited with the aim of reactivate PP2A within the cancerous cells.

Direct targeting of PP2A.

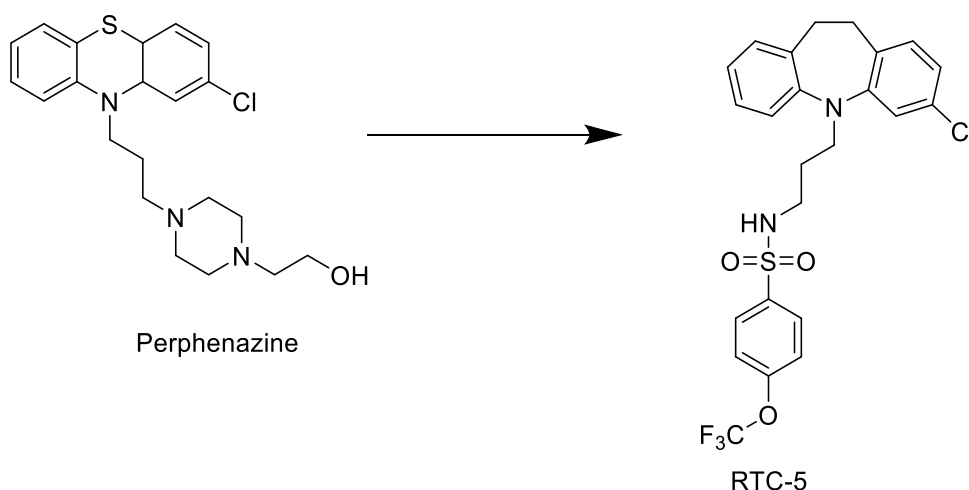


Figure 14. Chemical structure of Perphenazine and lead compound belonging to SMAPs category.

During the last years, several molecules have been discovered to be able to reactivate PP2A in cancerous cells directly interacting with the enzyme. The most famous case is that one of the Phenothiazines.^[3,60] This class of molecules are used traditionally as potent dopamine receptor antagonist for the treatment of psychiatric disorders, but it has been demonstrated that they show also an antitumor effect.^[87] Gutierrez et. al. have elucidated the mechanism of action of these molecules, demonstrating that they induce the apoptosis increasing the activity of PP2A.^[4,88] The lead compound of this class of molecules is perphenazine, which induces apoptosis in T-All cells through the inhibition of the pathway mediated by c-MYC and reducing the amount of phosphorylated Akt within the cells.^[88] Affinity chromatography experiments evidenced that the pharmacological target of this compound is PP2A. Considering the potent extrapyramidal and anti-cholinergic side effects that an anticancer therapy with these compounds could give, new analogues have been developed that decouple the CNS pharmacology from the antiproliferative properties of this drug class. The new class of compounds is called SMAPs (SMall Activator of PP2A) and they abolished the activity on the CNS removing the basic amine linked to the tricyclic system.^[87] These reengineered tricyclic compounds exert their pharmacological action interacting directly with the PP2A_A subunit and inducing a conformational change that reactivates PP2A.^[87] It has been demonstrated that in lung cancer models they can reduce the levels of phosphorylated ERK inducing apoptosis.^[87]

Targeting PP2A inhibitors

For achieving the reactivation of PP2A, another exploitable option is that one of inhibiting the inhibitors of PP2A. This concept seems more a play on words, but it is a fascinating approach that is leading to promising results.

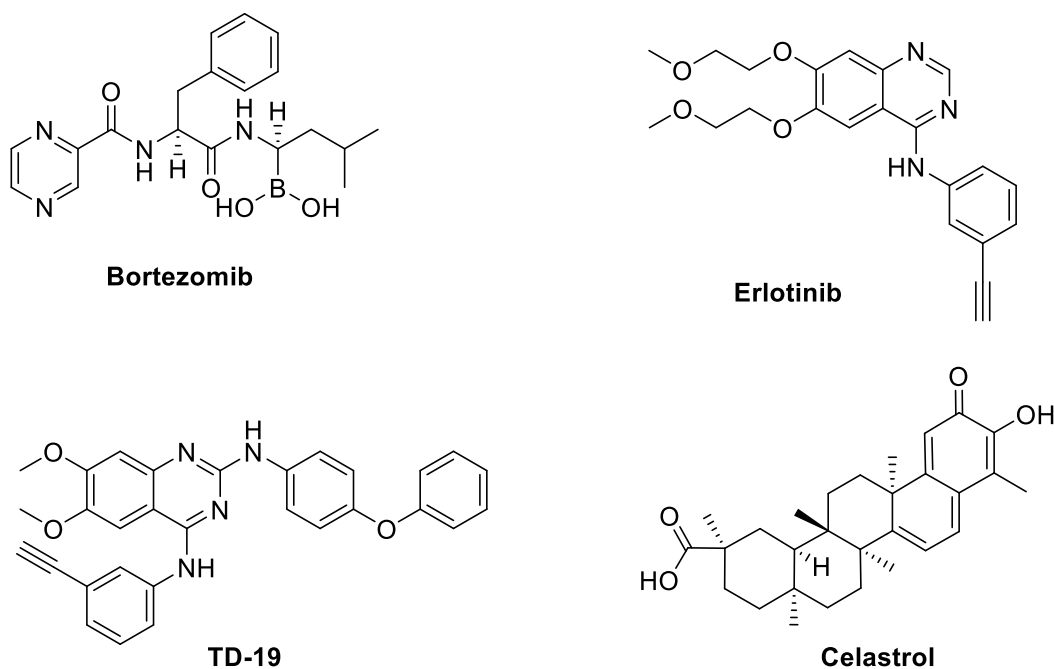


Figure 15. Chemical structure of the compounds active on CIP2A.

The first druggable PP2A's inhibitor is CIP2A. A lot of efforts have been done with the aim to discover small molecules able to remove the inhibition of PP2A mediated by CIP2A. The first evidence of the efficacy of this kind of approach has been obtained with Bortezomib (Velcade), an FDA approved proteasomal inhibitor utilized in multiple myeloma and mantle cell lymphomas.^[15,77] It has been demonstrated that this compound has a secondary effect, it is able to reduce the expression of CIP2A in hepatocellular carcinoma, head and neck squamous cell carcinoma, triple negative breast cancer and other various leukaemia.^[77] This reduction is induced at a transcriptional level and induces a strong decrease of phosphorylated Akt levels. Another molecule active on CIP2A is Erlotinib (Tarceva), an FDA approved EGFR kinase inhibitor for EGFR mutant Non-Small Cell Lung Cancer (NSCLC).^[27,40,89] It is able to reduce the expression of CIP2A. Some derivatives of this drug have been made with the aim of enhancing this effect on CIP2A expression. TD-19 is one of the most promising being much more cytotoxic than Erlotinib. Also in this case the reduction of CIP2A activity is mediated by a reduced expression of this protein.^[89] Indeed, these active compounds are able to diminish the expression of ELK-1, consequently this factor is less effective in binding the CIP2A gene promoter reducing the expression of this PP2A inhibitor.^[89]

Another mechanism of action is assigned to the active molecule: Celestrol. This compound is extracted from the traditional Chinese medicinal herb *Tripterygium wilfordii*. It has been demonstrated that this compound shows anticancer properties reducing the inhibitory activity mediated by CIP2A. Celestrol is able to bind directly to CIP2A and this facilitates its binding to the accessory protein CHIP, the ubiquitin E3 ligase that drives CIP2A to the proteasomal degradation.^[15,29,66,77]

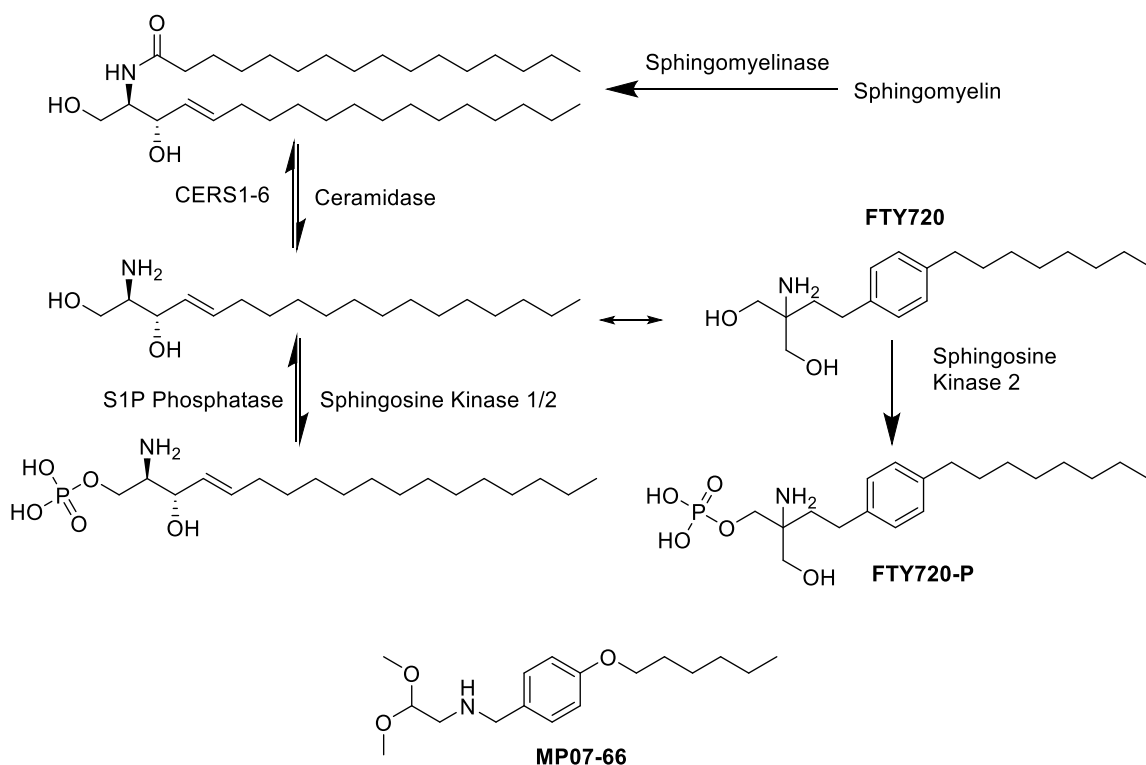


Figure 16. Mechanism of action of FTY720 and molecular scaffold of one of the non phosphorylatable derivatives synthesized in our laboratory.

The other pharmacological approach for targeting a PP2A inhibitor is to tackle the action of SET. This is the more studied and explored field in the matter of PP2A's activation and on this the majority of this PhD thesis has been focused on. The first evidences, that was possible to reprimarize the activity of PP2A inhibiting its physiological inhibitor SET, have been obtained with a class of natural compounds physiologically presents within our organism: Ceramides.^[15,29,67,73,78,79,90] This class of sphingolipids are constituted by a sphingosine backbone that has been N-acylated with a fatty acid of different lengths.^[78,91,92] Ceramides are able to activate PP2A binding directly with SET and preventing its interaction with the phosphatase.^[79] SET presents a binding pocket that is able to recognise only D-ceramides. Unfortunately, these molecules are not suitable for pharmaceutical aims because they are metabolically unstable and easily degradable.^[32] The natural development of this class of molecules have been discovered later. Nagahara et. al. demonstrated that FTY720 (fingolimod, Gilenya, Novartis), a synthetic sphingosine (myriocin) analogue, was able to induce apoptosis in HL-60RG and Jurkat cells increasing the activity of PP2A.^[78,93] FTY720 is an approved drug for the treatment of the multiple sclerosis.^[17,32,43,48,66,67,70,80,90,92-96] When administered, it is internalized within the cell and phosphorylated by SphK2 (Sphingosine Kinase 2). After its modification FTY720-P is excreted by the cell and it exert its autocrine/paracrine action binding with the Sphingosine-1-Phosphate Receptor-1 (S1PR1).^[94] After binding with S1PR1 the receptor is internalized and degraded and this leads to the immune suppression that is fundamental for treating such an auto-immune disease like multiple-sclerosis is.^[94] The unphosphorylated fraction of the drug is that one that exerts the antitumor effect.

FTY is able to induce apoptosis, inhibiting the Akt and ERK pathways.^[32,93] It has been demonstrated that FTY720 is able to directly interact with SET and this explains its secondary pharmacological effect.

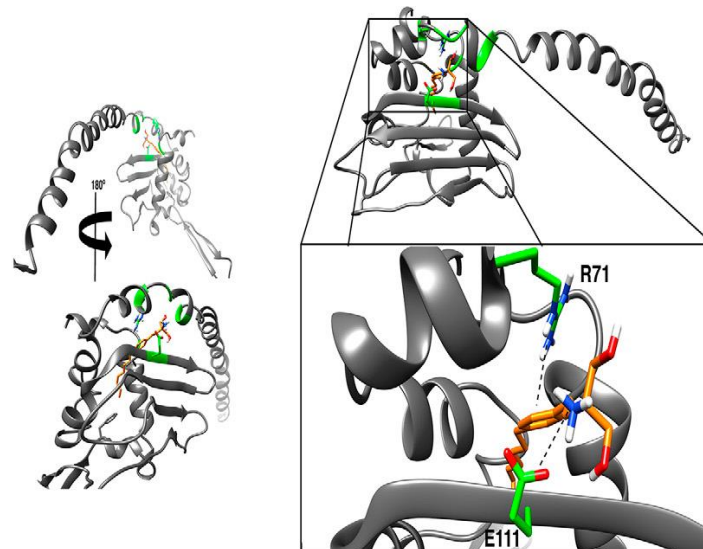


Figure 17. Model of FTY720 bound SET resulted from NMR-based analysis.

De Palma and colleagues have performed an accurate NMR-based characterization of the FTY720-SET complex and they have identified the pattern of interactions that interplay between FTY720 and SET.^[73] The active pocket that harbour FTY720 is exactly the same that host ceramides. Several analogues of Fingolimod have been synthesized with the aim to maintain and enhance the anticancer properties of these compounds and at the same time avoiding the immunosuppressant effect.^[32,96] A lot of research has been done in this laboratory before and during this PhD for pursuing this goal. The principal idea that led the design of our compounds and of those coming from other labs is to remove from the molecular scaffold any phosphorylatable moiety, avoiding in this way the immunomodulative action.

Compound	Sequence
COG133	LRVRLASHLRKLRKRL
COG1410	AS(Aib)LRKL(Aib)KRL*
COG112	RQIKIWFQNRMRKWKK-C-LRVRLASHLRKLRKRL
COG445	RQIKIWFQNRMRKWKK-C-LRVRLASHLRKLRKRL
(disulfide linked COG112)	
	RQIKIWFQNRMRKWKK-C-LRVRLASHLRKLRKRL
OP449 (previously COG449)	RQIKIWFQNRMRKWKK-C-LRVRLASHLRKLRKRL
(BMOE** linked COG112)	<bmoe>
	RQIKIWFQNRMRKWKK-C-LRVRLASHLRKLRKRL

* Aib = aminoisobutyric acid ** BMOE = bismaleimidoethane

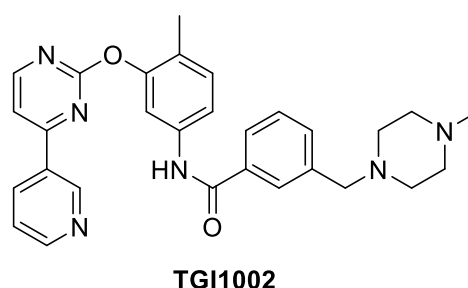
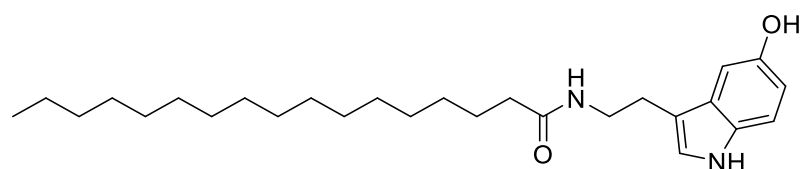


Figure 18. Sequence of the principal ApoE mimetics and chemical structure of TGI1002

FTY720 analogues are not the only compounds able to inhibit SET. ApoE mimetic peptides compose another class of PP2A activators.^[15,67] These compounds have been classified first as anti-inflammatory agents for their ability to reduce the activation of NF- κ B resulting in reduced phosphorylation of I- κ B. Successive studies have shown that the anti-inflammatory effects of the ApoE mimetics were not mediated by the

interaction with the ApoE receptor.^[15] One of the most promising and effective members of this class is OP449.^[60,67,80,84] This peptide is composed by the residues deputed to the direct interaction with SET (133-149 of ApoE) fused with the cell-penetrating antennapedia peptide. This compound interacts with the C-terminal region of SET, breaking the SET-PP2A complex, increasing the phosphatase activity.^[84] OP449 has shown anticancer activity in preclinical studies on AML, breast cancer and pancreatic cancer.^[84] Another molecule, that has shown to inhibit selectively SET, is the Imatinib derivative: TGI1002.^[15,80] This compound is the result of a screening whose aim was to identify a new molecule that could overcome the resistances induced by TKIs in CML. TGI1002 is able to break the PP2A-SET complex repriming the activity of PP2A and showing the ability to induce apoptosis in *in vivo* models of CML.^[15,80]

Targeting post translational modifications



eicosanoyl-5-hydroxytryptamide (EHT)

Figure 19. Chemical structure of EHT.

It has been elucidated in the previous paragraphs that the methylation of the residue Leu 309 is a fundamental process for granting the physiological activity of PP2A. Consequently, it seems evident that the possibility of increasing or repriming the methylation state of PP2A_C could be an interesting pharmacological approach in the research of new PP2A activators. Till now, there are not known strategies for enhancing the activity of LCMT1, while, there are two molecules that are able to block the demethylation mediated by PME-1. These compounds are eicosanoyl-5-hydroxytryptamide (EHT) and a novel class of aza- β -lactams called ABLs.^{[15,67][15,67]} These last compounds inhibit like EHT the active site of PME-1 but in a covalently way.

Other mechanisms of action

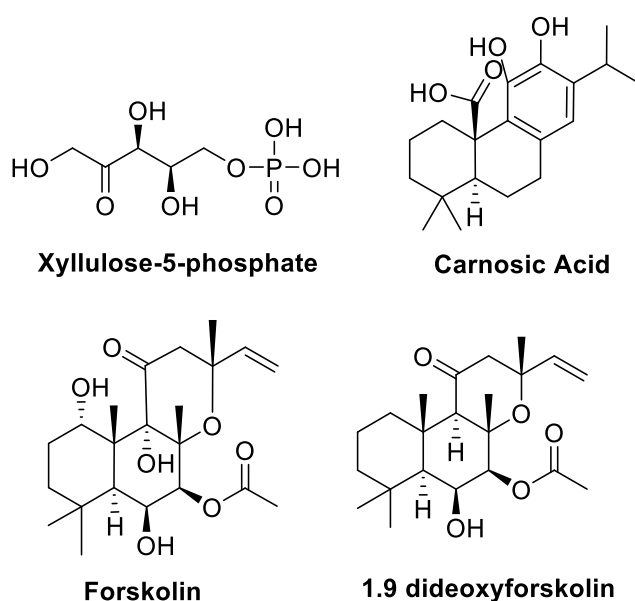


Figure 20. Chemical structure of different PP2A activators.

In the portfolio of PP2A activators there are some compounds that have shown their efficacy, but their mechanisms of action and their targets are not actually known. Xylulose-5-phosphate, a nucleotide precursor produced by the pentose phosphate pathway is able to increase the activity of PP2A.^[15,29] Carnosic acid, isolated from *Rosmarinus officinalis*, is another member of this class that inhibits the Akt pathway in a PP2A dependent manner.^[15,18,29,57,70] Forskolin, extracted from the roots of *Coleus forskohlii*, is an adenylate cyclase activator that increases the cAMP levels within the cell.^[10,75,89] It is able to activate PP2A in an unknown way that does not involve the overproduction of cAMP, considering that its analogue (1,9 dideoxyforskolin) is able to reprimarize the activity of PP2A without affecting the cAMP levels.^[10,15,18,67,75]

1.4 SRC HOMOLOGY REGION 2 DOMAIN-CONTAINING PHOSPHATASE-1 (SHP-1)

SHP-1, also known as PTN6 (Tyrosine-protein phosphatase non-receptor type 6), is a tyrosine phosphatase (PTP) which belongs to the category of the non receptor like protein tyrosine phosphatases (nrPTPs).^[26,97,98] All the members of this class of phosphatases are constituted by one catalytic domain directly linked to accessory modules. These subunits drive the selectivity for the substrates, and they are directly involved in the control of phosphatase activity. SHP-1 is one of the two cytosolic nrPTPs that presents two SH2 (Src Homology 2) domains in tandem, the other one is its close homologous SHP-2.^[16,23] These two SH2 accessory domains are fundamental for the fine tuning of the phosphatase activity of SHP-1. Indeed, as it will be explained in a much more detailed way in the next paragraph, these structures are responsible of the autoinhibitory mechanism of the phosphatase and also of the recruitment of the proper substrates of the enzyme.^[22,97] SHP-1 is mainly expressed in epithelial and hematopoietic cells and there it exerts a negative control on all the proliferative pathways of these kind of cells.^[23,26,99,100] Despite its presence in both the cell lines, the level of SHP-1 expression in epithelial cells is significantly lower compared to that one of the hematopoietic ones.^[22,98]

There are at least three different isoforms of SHP-1 that exerts slightly different effects on the control of the cellular homeostasis:^[23]

- A hematopoietic cell specific isoform constituted by 595 amino acids (67.5 KDa);
- A non-hematopoietic cell isoform, that is obtained from other different initiation sites, in this type of SHP-1 only 3 amino acids vary in the N-terminal region of the protein (67.5 KDa);
- One isoform of 70 KDa, called SHP-1L, which is longer of 66 amino acids in the C-terminal tail compared to the other isoforms. This is due to an alternative splicing mechanism that leads to a reading frame shift of the SHP-1 gene. This isoform lacks a Tyr in the C terminal, which is usually a phosphorylation site, but it presents a proline rich motif that is a potential site of binding for SH3 (Src Homology 3) present in other proteins.

This enzyme it has been proposed as a candidate tumour suppressor in Lymphoma, leukaemia and other cancers. Furthermore, it has been demonstrated that SHP-1 acts synergically with PP2A in the control of the cellular homeostasis.^[58]

1.4.1 SHP-1: Structure

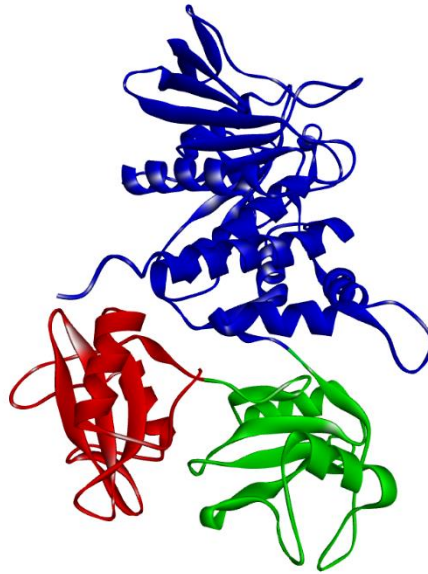


Figure 21. Crystal structure of the full length SHP-1 in its active conformation_[PDB: 3PS5]. The catalytic domain is highlighted in **blue**, in **green** the C-SH2 and in **red** the N-SH2.

Differently from PP2A, SHP-1 is a single filament protein that presents all the regulatory and catalytic subunits covalently bounded one to each other.^[23] This phosphatase is composed, starting from the N-terminus of the aminoacidic chain, by two SH2 domains in tandem, a catalytic domain and a C-terminal tail that is intrinsically unfolded but that exerts a fundamental role in the control of the phosphatase activity.^[22,97] SHP-1 is encoded by a gene located on chromosome 12p13 and it consists of 17 exons and two different promoters.^[101] The first promoter is situated 7 Kb before the second one and it is principally exploited in non-hematopoietic cells. The second one instead, is preferentially utilized by hematopoietic cells.^[98] The N-SH2 domain is encoded by exons 3-4, the C-SH2 by exons 5-6 and the catalytic domain by the exons 8-10. The SH2 domains are complex structures that are able to directly interact with phosphorylated residues of tyrosine and through this interaction they drive the substrate selectivity of the whole enzyme.^[98] Furthermore, their important role within the SHP-1 structure is not only related to the control of the substrate selectivity but also they are directly involved in the inhibition of the enzymatic activity.^[22,97] Indeed, these domains are extremely flexible and they can assume different conformations, one of these is able to inhibit SHP-1 through a direct interaction of the first SH2 domain (N-SH2) with the catalytic pocket of the enzyme. Structurally the two SH2 structures present the same organisation. They are composed by a central four-stranded β - sheet with one α -helix on each side. The N-SH2 is constituted by the 1-108 amino acids, while the C-SH2 by the 116-208 amino acids.^[22,97]

There are two peptide bridges that connects the N-SH2 to the C-SH2 (109-115 aa) and this last one to the catalytic domain (209-231 aa). These structures are intrinsically unfolded and it seems that they are not directly involved in any mechanism of control of the enzymatic activity of SHP-1.^[22,97]

The catalytic domain is formed by the 270-532 amino acids. Its structure is composed by a highly twisted ten-stranded β -sheet flanked by four α -helices in the convex side, and by two α -helices and one β -hairpin in the concave one. Its catalytic site presents the characteristic motif of the PTPs which is composed by the aminoacidic sequence (H/V)C(X₅)R(S/T).^[22] In this case the catalytic cysteine is the Cys 455 and the arginine that counterbalance the negative charge of the phosphate group of the phosphotyrosine is the residue 459.^[23] In the catalytic cleft an aspartic residue (Asp 421) is present which acts as a proton donor and proton acceptor during the phases of product's release.^[102] The catalytic pocket is surrounded by positively charged amino acids which electrostatically drive the target residue within the cleft for its dephosphorylation (Thr 349, Pro 418, Arg 495, Val 499 and Asn 303).^[22] The enzymatic activity is also modulated by the flexibility of the WPD motif, to which Asp 421 belongs. SHP-1 presents a consensus sequence for the substrate to dephosphorylate which is composed by the following aminoacidic sequence: (D/E)X(L/I/V)X₁₋₂pYXX(L/I/V). The substrate specificity is conferred by the β 5-loop- β 6 and α 5-loop- α 6 regions.^[103]

The last 60 amino acids of the C-terminal are heavily involved in the control of the SHP-1 activity and in signalling pathways.^[23]

1.4.2 SHP-1: Regulation

The mechanism of regulation of the enzymatic activity of SHP-1 is much less complex compared to that one of PP2A. Almost all the rearrangements that finely tune the degree of activation of this phosphatase are done by a regulatory portion of the enzyme itself.^[22,97] SHP-1 responds to the external stimuli just through the phosphorylation of some specific residues within the last 60 amino acids of the C-terminus or through the direct interaction with other effectors or substrates through its two SH2 domains.^[23] Constitutively, SHP-1 in its inactive conformation, is present in the cytosol. When, some signalling pathways, that are prone to activate SHP-1, are triggered, SHP-1 is recruited to the membrane-bound inhibitory receptors, through its SH2 domains. These SH2 subunits directly interact with the phosphorylated tyrosine residues of this plasma membrane structure. These phosphor-tyrosines are part of a protein structure, recognised by SHP-1, called Immune receptor Tyrosine-based Inhibitory Motifs (ITIMs) which are present on different inhibitory receptors such as: KIR, CD22, CD72, CD5, Fc γ RIIB, p70-NKB1.^[22,26] The recognition between the SH2 motifs and the phosphorylated residues triggers some conformational rearrangements that lead to the reactivation of SHP-1.^[104]

This is not the only mechanism of activation of SHP-1, indeed, it can be activated through phosphorylation of some specific tyrosine residues on the C-Tail or by acidic phospholipids.^[23]

Currently, there are not mechanistical experimental evidences about the processes that lead to the autoinhibition or activation of the enzyme. The available data, obtained with crystal structure analysis and with *in-vitro* and *in-vivo* experiments, underlined which are the structural characteristics of the two active and inactive isoforms and which are the post translational modifications that alter the SHP-1

activity. Nonetheless, these results do not fully explain which are the causes or the mechanisms that drive the transition between these two states.^[22,97] For this reason, in this chapter only the descriptions of the autoinhibited and active structures and the elucidation of the post translational modifications that alter the phosphatase activity will be presented.



*Figure 22. Crystal structure of SHP-1 in its inhibited conformation_[PDB: 2B30]. The catalytic domain is highlighted in **blue**, in **green** the C-SH2 and in **red** the N-SH2.*

Starting from the analysis of its inactive conformation, SHP-1 shows that the inhibition of its activity is mediated by a direct interaction between the N-SH2 domain and the catalytic pocket of the enzyme.^[97] In this conformation the N β ₄ and N β ₅ motifs of the N-SH2 penetrate within the catalytic site inhibiting it sterically. The interaction with the charged residues of the catalytic cleft is mediated by the NSGDF sequence of N-SH2.^[105] Indeed, in the crystal structure of the autoinhibited form, several interactions have been detected between the previously mentioned structures. The nature of the interactions are different: there is a salt bridge between Asp 61 and Lys 362, a π - π interaction between Phe 62 and Tyr 278 and a series of hydrogen bond between Asn 58-Gln 502, Ser 59-His 422 and Gly 60-Gln 506.^[97] The C-SH2 in this conformation does not interact with anyone of the two structures, but it seems to play a critical role in the activation of the enzyme.^[97] Indeed, despite both the SH2 domains expose their recognising pocket to the solvent, the C-SH2 structure, being not involved in any intramolecular interaction, is much more flexible and much more prone to explore the surrounding environment looking for a possible interactor.^[101,103] This first interaction between a phospho-tyrosine and C-SH2 leads to a conformational rearrangement that perturbs also the interaction between N-SH2 and the catalytic domain. After this step, N-SH2 is able to recognise a new interactor that presents a phospho-tyrosine, losing the autoinhibitory organisation and gaining a fully active conformation.^[23] This mechanism has been supported by the experimental evidence that SHP-1 without the C-SH2 is much less prone to be activated than a wild type enzyme.^[23] Nonetheless, N-SH2 is crucial for the inhibition of the phosphatase activity and its removal from the catalytic cleft is fundamental for the activation of SHP-1 and

a direct binding of a substrate to N-SH2 can activate directly SHP-1 bypassing C-SH2.^[106]

Recently, a crystal structure of the complete SHP-1 enzyme has been obtained in its fully active conformation. In this organisation, the reciprocal orientation of the three domain is dramatically changed compared to the autoinhibited isoform. C-SH2 is rotated of 110° and it directly interacts with N-SH2 stabilizing this active conformation.^[22] Also N-SH2 is moved away from the catalytic pocket and it is localised in a diametral opposite position compare to the inactive form. A new set of interactions is generated:

1. Between the C-SH2 and N-SH2 an hydrogen bond is generated (Met 1-His114) and a network of salt bridges between Arg 7/Glu 137 and Asp 144 is formed;
2. Between the N-SH2 and the peptide linker that connect C-SH2 to the catalytic domain there is the formation of new hydrogen bonds (Asn 101-Asn 219, Asp 104-Asn 219/Asp 222)
3. Between the N-SH2 and the catalytic domain new hydrogen bonds have been generated such as that one between Arg 21 and Asp 479, mediated by a water molecule, and between Asn 101 and Asp 479.

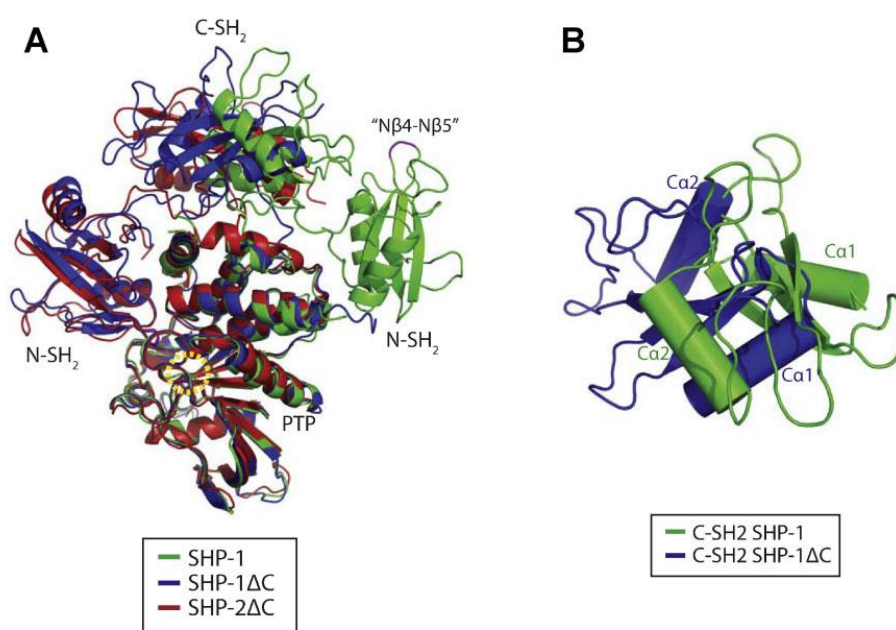


Figure 23. Structural comparisons of SHP-1 with the tail-truncated SHP-1 and SHP-2. A: Structural comparison of SHP-1 (green) with tail-truncated SHP-1 (blue) and SHP-2 (red). The yellow dashed circle shows the position of the active site. The Nb4-Nb5 hairpin loops are coloured magenta. The Nb4-Nb5 loop in SHP-1 is quoted because we use this name from tail-truncated SHP-1 regardless of the differences between their secondary structures. The N-SH₂ domains of the tail-truncated SHP-1 and SHP-2 are located on the left side of the PTP domain but shifted to the right side in the current SHP-1 structure, resulting in the exposure of the active site. B: The conformational change between the C-SH₂ domains in SHP-1 (green) and tail-truncated SHP-1 (blue) structures. The C-SH₂ domain of the intact protein is rotated anticlockwise by about 110° relative to the truncated protein as revealed from the superposition of their PTP domains.

Another crucial structure for the regulation of the phosphatase activity of SHP-1 is its C-terminal fragment composed by the last 60 amino acids of the aminoacidic sequence.^[23] It has been demonstrated that a deletion of the last 35 amino acids of the sequence leads to the obtainment of an enzyme with an enhanced activity, contrarily, the complete elimination of the all 60 amino acids leads to the obtainment of an enzyme normally active.^[23] In this tuning mechanism five different kind of processes are involved:

1. Phosphorylation of tyrosine residues;
2. Phosphorylation of serine residues;
3. Interactions with membrane lipids;
4. Lipid raft localization;
5. Interaction with Proline-rich domain interactors.

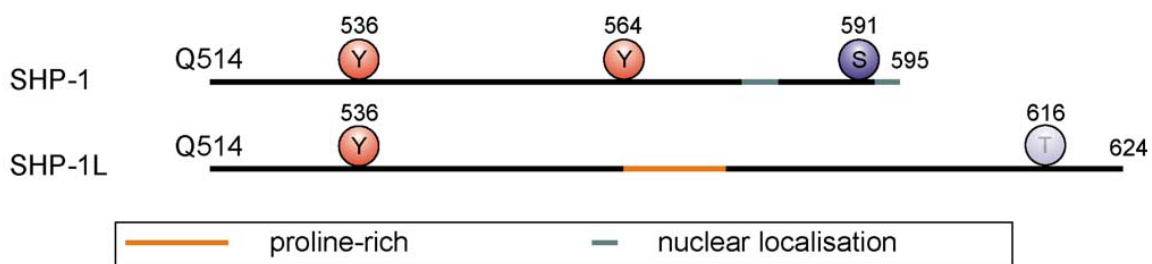


Figure 24. Schematic representation of the C-terminal tail of the two SHP-1 principal isoforms.

The phosphorylation of tyrosine residues is useful for two reasons, first of all the phosphor-tyrosines can recruit different accessory proteins exploiting their SH2 domains like Grb2 and SHIP, then these phosphor-residues can directly modulate the activity of the enzyme. SHP-1 is phosphorylated at Tyr 536 and at Tyr 564.^[107] It is phosphorylated in these sites by Lyn and LCK kinase. Phosphorylation of tyrosine 536 activates SHP-1 and allows the recruitment of other effectors such as Grb2.^[26,104,107] It has been demonstrated that the replacement of Tyr 536 or Tyr 536 and 564 with phenylalanine induces a significant reduction of the phosphatase activity. This residue (T536) is able to interact directly with the N-SH2 switching the enzyme from an inactive configuration to an active one. The phosphate group on Tyr 536 is rapidly cleaved by a mechanism of autodephosphorylation.^[23] The phosphorylation at the residue Tyr 564 leads to a modest increment in the phosphatase activity. It principally binds to the C-SH2 subunit of SHP-1. In the SHP-1L isoform this residue is substituted with a proline rich motif.^[23]

The phosphorylation of serine residues refers just at one amino acid: Ser 591.^[23,107,108] This residue is principally phosphorylated by PKC and this posttranslational modification leads to a decrement of the phosphatase activity. The mechanism by which this modification inhibits the activity of SHP-1 is not well understood but it seems that this phosphor residue could act as an anchor site for protein inhibitors of the phosphatase. SHP-1L lacks of the Ser 591, this residue is substituted by a Thr, that could exert a similar effect on the enzyme, but this isoform is constitutively more active than the other ones.^[23]

The C-terminal tail exerts a modulatory effect on SHP-1 because it drives also the subcellular localization of this enzyme. Through this terminal structure SHP-1 can interact directly with the plasma membrane and localize in proximity to receptor Tyrosine Kinases that it has to antagonise. This is mediated by a direct interaction of this peculiar structure of SHP-1 with phosphatidic acid and PIP3 present within the membrane.^[23,26,109]

The very last part of the C-terminus is able to induce the localisation within the nucleus of SHP-1 in non-hematopoietic cells. Indeed, while in hematopoietic cells SHP-1 is predominantly present in the cytoplasm, probably due to its phosphorylation at Ser 591, in the other cell types, this enzyme can be internalized within the nucleus, regulating positively the transcription of genes of mitogen-activated pathways and of early response genes.^[23] The Nuclear Localisation Sequences (NLS) are expressed in the N-terminal region, within the first 14 amino acids with the sequence KVKK, and in the C-terminal region with a KRK motif.^[107] This last one is the dominant one and for this reason, the strong phosphorylation at the adjacent residue Ser 591 in hematopoietic cells can mask this NLS avoiding its nuclear internalization. SHP-1L does not present the KRK motif and this could be explained by the fact that this isoform exerts different functions in different tissues compared to the others.^[110] This particular isoform does not present Tyr 564 but a proline rich motif. This part of the protein is constituted by 10 amino acids, prevalently hydrophobic and enriched in Leu and Pro (PVPGPPVLSP).^[23] The sequence of this portion of the enzyme is quite similar to the consensus sequence recognised by the SH3 domains of Src and Lyn kinases (PLPPLXP).^[23] This kind of structure could, through the interaction with different SH3 domains of various proteins, modulate the activity of SHP-1 and of its interactors.

1.4.3 SHP-1: Function.

1.4.3.1 SHP-1 and Cellular Homeostasis

SHP-1 is a phosphatase primary involved in the negative modulation of all the intracellular signalling mediated by transmembrane receptors: growth factor receptors with an intrinsic tyrosine kinase activity (e.g. CKT, CSF-1, TrKA and EGF), cytokine receptors (e.g. Epo-R, IFN α / β -R, IL-3R and IL-2R) and receptors involved in the immune response such as the T-Cell Receptor (TCR) complex and CD5.^[107] It binds, as previously mentioned, to inhibitory receptors through its SH2 domains and there it activates itself starting to dephosphorylate downstream signal molecules.^[22,26] SHP-1 is able to directly bind and inactivate JAK and STAT mediating an antiapoptotic effect. One example of this strong connection between this phosphatase and the proliferative cascade could be found in mutated cells that present an altered ITIM at the level of the erythropoietin receptor. In this cell line there is a strong downregulation of the activity of SHP-1 and consequently an increased activity of the JAK/STAT pathway.^[111]

SHP-1 is also involved in the control of the phosphorylation state of an important oncogenic transcription factor, STAT3, that regulates cell growth and survival by modulating the expression of target genes. STAT3 is constitutively active in many

cancers including liver, lung, head and neck, prostate, and breast cancers as well as myeloma and leukaemia. This phosphatase reduces the amount of phospho-STAT3 reducing its dimerization and consequently its activity.^[26,106,107,111–114]

SHP-1 acts synergistically with PP2A enhancing the respective activities. This has been demonstrated in Chronic Lymphocytic Leukaemia (CLL) cell lines where, reactivating the activity of one of the two phosphatases, also the other one resulted to be reactivated. In these cell lines, both PP2A and SHP-1 are normally expressed but their activity is strongly downregulated for the overactivation of a Src tyrosine kinase member: Lyn.^[58] This kinase activates the β -cell receptor through phosphorylation of its cytosolic portion, and inactivates PP2A phosphorylating it at the Tyr 307 residue, enhancing the binding of PP2A with its inhibitor SET. Furthermore, Lyn splits SHP-1 in two distinct populations: one active pool segregated at the plasma membrane, directly bound to CD5, and one group, constitutively inactive, localized in the cytosol and phosphorylated at Ser 591.^[58] It has been demonstrated that after reactivation of PP2A with small molecules also SHP-1 is reactivated through direct dephosphorylation of Ser 591 by PP2A. Also in case of selective reactivation of SHP-1, PP2A is dephosphorylated by SHP-1 at Tyr 307 reactivating its activity.^[58]

SHP-1 is fundamental for the maturation of the hematopoietic cells. Mouse moth-eaten (me/me) and moth-eaten viable mice (me^v/me^v) models, that present mutations of the gene SHP-1, show multiple severe abnormalities such as: neutrophilia, lymphopenia, splenomegaly and/or elevated serum immunoglobulins, severe combined immunodeficiency and systemic autoimmunity due to dysregulation of leukocyte development. This confirms the hypothesis that SHP-1 is an important oncosuppressor in several kind of malignancies.^[107]

1.4.3.2 SHP-1 and cancer

SHP-1 is deputed to the control of the phospho-tyrosines' levels in lymphocytes, counteracting the activity of the tyrosine kinases. A severe dysfunction of SHP-1 can cause abnormal growing and lead to oncogenesis in several kind of tissues.^[98,101,111,113] In lymphocytes, this condition is particularly dramatic and it leads to the onset of lymphomas, leukaemia and other related pathologies. Extensive studies on SHP-1 protein and SHP-1 mRNA revealed a reduced or abolished expression of SHP-1 in most cancer cell lines and tissues. The restoration of physiological levels of SHP-1 protein and activity is emerging as new therapeutic option in several malignancies, especially in lymphomas and leukaemia. Indeed, reactivating the right balance of SHP-1 activity can induce apoptosis in cancerous cells.^[26,98,113]

In Burkitt's lymphomas (B Cell-lymphomas) the level of expression or activity of this phosphatase is 1 till 3 order of magnitude reduced in those pathologies that do not present Epstein Barr Virus (EBV) infection, in those that present EBV the reduction of the expression is around 95%.^[115] Also in T-cell lymphomas there is a strong downregulation of SHP-1 activity and or expression. Ten of the fourteen different kind of T-cell lymphomas present this phenotype; of the remaining four, three present a

reduced effect of SHP-1 because they overexpress IL-5. In this case there is an over activation of the JAK/STAT pathway that overcome the limits imposed by SHP-1.^[26]

In several kind of leukaemia there is also a strong downregulation of SHP-1, in particular in T-CLL (T-Cell Lymphoid Leukaemia), CML (Chronic Myelogenous Leukaemia) and some kind of B-ALL (Acute B Lymphoblastic Leukemia) and MM (Multiple Myeloma).^[108,111]

In leukaemia and lymphomas, the downregulation of SHP-1 expression is principally due to two distinct mechanisms:

- A reduced expression of the mRNA, due to mutation of the gene or methylation of the promoter;
- Post transcriptional regulation of protein synthesis.^[98]

In other kind of cancers, the expression of SHP-1 is not as linear as in those malignancies that involve hematopoietic cells.

Breast cancers present a deep dysregulation of the phospho-proteomic profile that does not really match with the alterations of SHP-1 expression in this kind of malignancies. Indeed, six over ten different ER negative cell lines present a reduced expression of SHP-1, while in the complex, 58% (42/72) of primary breast cancer tissues have a 2 to 12-fold increase in SHP-1 mRNA expression.^[99]

Ovarian cancers are catalogued in to three different types: epithelial, germ and stromal. Considering that 90% of the ovarian cancers are epithelial and that SHP-1 is fundamental for the development of epithelial cells, it has been taken immediately in to account the possibility of a connection between the levels of SHP-1 expression and the manifestation of this kind of pathology. Contrarily to what was expected, in seven over eight ovarian cancers cell lines there was a 1.8 to 4.4 increase of the SHP-1 expression and this has become a clear indication of ovarian cancer.^[98]

In prostate cancer, it has been demonstrated that inducing an increase in the expression of SHP-1 in tumoral cells the proliferation is strongly reduced ameliorating the overall prognosis.^[98]

After all these considerations, it appears evident that the scientific community has increased the efforts for the development of a new class of molecules that can modulate the activity of SHP-1 in those kinds of malignancies that present an altered expression of this enzyme, in particular in lymphomas and leukaemia.^[26]

1.4.4 SHP-1: Small molecule modulators

During the last decade, a lot of efforts have been done with the aim to exploit SHP-1 as a target for the anticancer therapy. Currently, there are two different currents of thought: one is focused on the development of new SHP-1 inhibitors for counteracting those kinds of tumours where this phosphatase is strongly upregulated, and then another line of thought that aims to develop new SHP-1 agonists with the purpose of repriming a right phosphatase activity of SHP-1 in those malignancies where it is deeply downregulated.

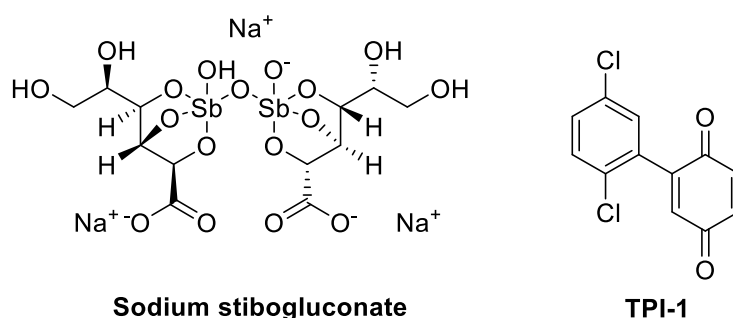


Figure 25. Chemical structure of the two principal SHP-1 inhibitors.

Currently, there are few SHP-1 antagonist available, and despite some of them gave promising results during the preclinical studies, they showed their inefficacy during the first clinical trials. One of the most investigated is Sodium stibogluconate, a potent inhibitor of SHP-1.^[116] This compound entered in clinical phase I for the treatment of malignant melanoma, without obtaining any results. Originally, this molecule has been developed for the treatment of leishmania but the Taolin's research group in 2001, has demonstrated that Sodium stibogluconate was a potent inhibitor of several PTPs, such as: SHP-1, SHP-2 and PTP1B.^[116] In particular this compound was able to reduce the activity of SHP-1 of the 99% at 10 μ g/mL, that is the therapeutic dosage for the treatment of leishmania. The same research group, several years later, developed a new series of selective SHP-1 inhibitors, with the aim of gaining a significant increment of IFN- γ in B16 melanoma tumours. This research project led to the development of TPI-1, a potent (low nM) and selective inhibitor of SHP-1.^[26,101,117] This compound showed a significant decrement of the tumour mass in *in vivo* mouse models, but it was not effective on isolated B16 melanoma cell lines. The same results have been obtained using different derivatives of the lead compound TIP-1 on other tumour models, such as K1735 melanoma tumours and MC-26 colon cancer tumours in mice.^[26,101,117] Also in these cases the pharmacological results were observable just *in vivo* and not *in vitro*, confirming the hypothesis that this kind of approach leads to the development of anti-tumour agents which act via an immune mechanism and not directly affecting the viability of the cancerous cells.^[117]

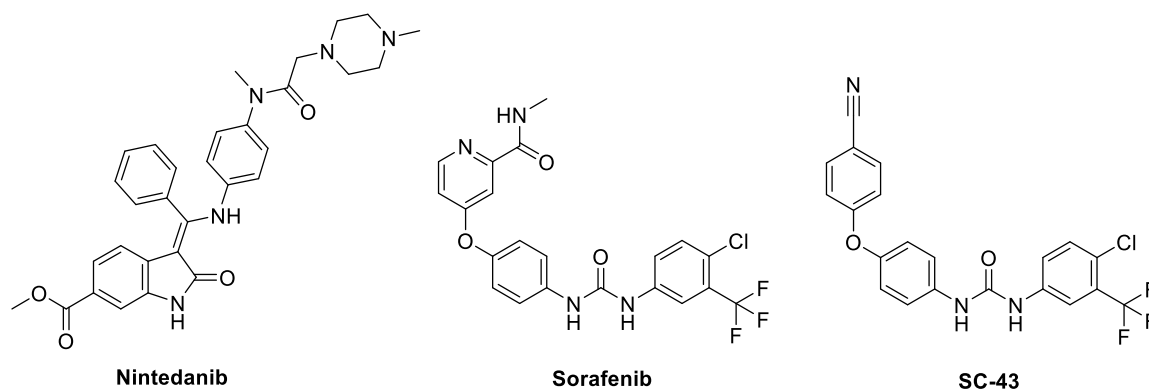


Figure 26. Chemical structure of the principal SHP-1 agonists.

The other pharmacological approach is the development of new anticancer drugs that are able to reactivate SHP-1 in those malignancies where its expression and activity are strongly downregulated.

One of the first molecules that showed this kind of behaviour has been Nintedanib.^[99] This compound is a tyrosine kinase inhibitor used for the treatment of idiopathic pulmonary fibrosis and non-small cell lung cancer. It inhibits the vascular Endothelial Growth Factor Receptor (EGFR), the Fibroblast Growth Factor Receptor (FGFR) and of the Platelet Derived Growth Factor Receptor (PDGFR).^[21,58] It has been shown that in two kind of cancer models, CLL and triple negative breast cancer, this small molecule was able to exert an antitumor effect without affecting the previously mentioned targets. The two distinct studies demonstrated that Nintedanib was able to directly activate SHP-1 exerting in this way its antitumor effect.^[58,99]

Another example of compound that activates directly SHP-1 as a side effect is Sorafenib.^[100,102,107,108,118–120] This compound is a common anticancer drug, currently used in clinic for the treatment of renal carcinoma and hepatocellular carcinoma. It targets two tyrosine kinases: c-Raf and b-Raf. Chen and co-workers observed that in different cell lines of hepatocellular carcinoma, medulloblastoma and esophageal carcinoma, Sorafenib was able to significantly reduce the levels of pSTAT3, exerting in this way its antitumor effect.^[102] Studies have shown that this result was not correlated with the inhibition of b-Raf or c-Raf, but instead it was due to the direct activation of SHP-1. These results paved the way for the development of Sorafenib analogues that maintain their activity on SHP-1 but that do not affect Raf kinases.^[108] From this project line, several compounds have been developed, and the most promising one is SC-43 which is almost effective as Sorafenib in the inhibition of cell growth of PLC5 cells at 10 μ M.^[100,102,107,108,118–120]

1.5 CASEIN KINASE 2 (CK2)

Casein Kinase 2, also known as CK2, is a messenger-independent protein serine/threonine kinase ubiquitously expressed in all the cells of the human organism and well conserved between the different species.^[20,33,51–53,121] It is involved in a myriad of cellular pathways; indeed, it is responsible of the phosphorylation of almost 160 different substrates.^[52] Principally this kinase is responsible for the maintenance of the cell viability and promotion of cell growth.^[51] Within the cell this phosphatase is organised prevalently in tetrameric complexes constituted by two regulatory subunits (CK2 β) and two catalytic structures (CK2 α and CK2 α^1).^[52] In the Human body there is just one isoform of regulatory subunit and two catalytic ones. Usually this tetrameric complex is considered the active form of CK2, but several experimental evidences confirmed the general hypothesis that also the two catalytic isoforms by themselves can exert the kinase activity.^[33,52] Another peculiarity of this enzyme, that is really rare among all the other kinases, is its ability to use both ATP or GTP as phosphate donors during the phosphorylation of the substrates.^[52] CK2 preferentially phosphorylate ser/thr that are in close proximity to acidic amino acid residues. It presents a consensus sequence that is typical Ser-XX-Acidic_amino acid(Glu, Asp, pSer and pTyr).^[52] This discriminant is also subject to some exceptions, indeed, there are some CK2 substrates that do not present the typical consensus sequence, and there are other proteins that contain the previously mentioned aminoacidic sequence that are not phosphorylated by CK2.^[122]

Despite CK2 has been identified as a ser/thr kinase, it has been shown that in some cases it is also able to phosphorylate tyrosine residues.^[52]

1.5.1 CK2: Structure

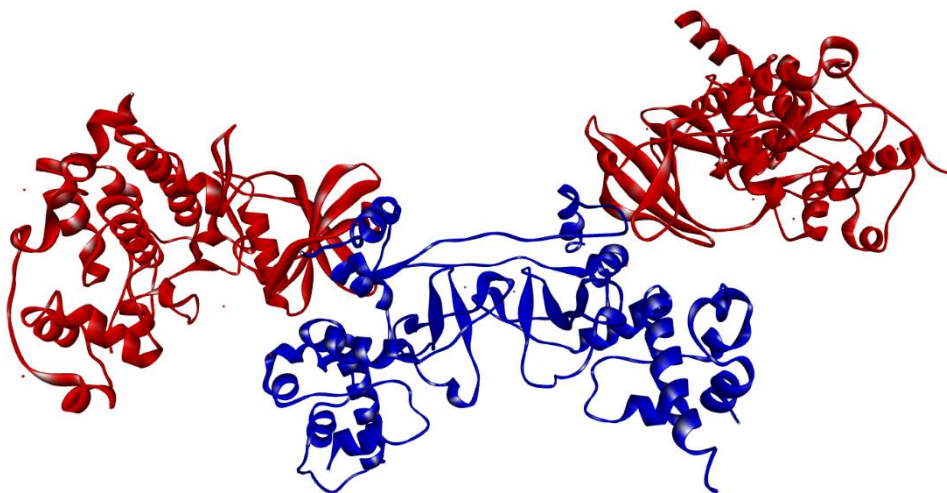


Figure 27. Crystal structure of the tetrameric form of CK2[PDB: 1JWH]. The catalytic domains are represented in red while the regulatory ones are shown in blue.

CK2, as already mentioned, in its most representative active conformation is constituted by a tetrameric complex formed by two catalytic and two regulatory subunits.^[51,52,121] The shape of this enzymatic architecture resembles that one of a

butterfly, indeed, the “wings” are constituted by the two different catalytic domains and the two regulatory ones form the “body”.^[121] The network of interactions between the different subunits is quite complex, and it will be further explained in the next paragraphs that analyse each single structure. For a general overview, it is interesting to note that in the tetrameric form of CK2, the two catalytic domains do not interact one with each other, instead, each alpha subunit generates an intricate network of interactions with both of the two regulatory domains.^[52] Furthermore, it has to be underlined that considering the existence of two different isoforms of the catalytic subunit (CK2 α and CK2 α^I), the stoichiometry of the tetramer can present different configurations: $\alpha_2\beta_2$, $\alpha^I_2\beta_2$ or $\alpha^I\alpha\beta_2$.^[51]

1.5.1.1 CK2: CK2 α and CK2 α^I



Figure 28. Crystal structure of the CK2 α subunit in the presence of an ATP mimicking molecule [PDB: 1JWH].

CK2 α and CK2 α^I are monofilament subunits that exerts the enzymatic activity of CK2.^[123] They are constituted by 391 amino acids reaching a molecular weight of 45 KDa.^[124] The two isoforms of the catalytic domain present a high degree of homology, but they are expressed by two different genes. Within the two catalytic domains they share a 90% of their sequence, evidencing their similar enzymatic activity.^[52,124] In the C-terminal region instead, they are not correlated one to each other and this discrepancy is well conserved between the species. For what concern the three-dimensional organisation of the two catalytic isoforms, both present a bilobal architecture that is typical of the catalytic core of almost all the eukaryotic kinases.^[125] The alpha subunits present a β -sheet rich N-terminal domain, an α -helical rich C-terminal domain and the active site that is situated between the two lobes.^[123,125] From an in-depth analysis of the available crystal structures of CK2 α , in its tetrameric and monomeric form, it appears evident that in both the conditions the three-dimensional organisation of the catalytic subunits is almost identical, confirming the fact that also in the monomeric form the alpha subunits are enzymatically active.^[125] This hypothesis has been confirmed by the fact that a CK2 substrate like calmodulin is

phosphorylated by the two monomeric catalytic subunits but not by the tetramer.^[52,122,123] The two alpha subunits, in the tetrameric complex, do not interact one to each other, but each catalytic structure interrelates, through their N-terminal lobe, with both the beta-subunits. The interactions are generated with the central core of one regulatory domain and with the C-terminal tail of the other.^[123-125] From an analysis of the total surface of interaction between the two regulatory subunits and the catalytic one, resulted evident that the stronger interaction in terms of higher contact surface is furnished by the C-terminal tail.^[123-125] A peculiarity of the tetrameric enzyme is that, contrarily to the regulatory subunits that are frozen in a fixed position, the two catalytic structures are quite flexible and can adapt their shape to different environmental conditions.^[123,126]

As illustrated till now, the two different isoforms, from a structural point of view are extremely similar and they can be discussed as a unique structure. For what concern their functionality, each one of them covers a specific set of functions within the cell. CK2 α and CK2 α^l present a different expression during the cell cycle, a different cellular localization and different substrates.^[52] It has been shown in mouse models that the α subunit is not able to fully compensate the absence of the α^l isoform, indeed, the mutant mice were viable, but the male offspring was sterile.^[52] In case of the deletion of both the isoforms the embryos can not survive, highlighting the crucial importance of CK2 in the maintenance of the cell viability.^[127,128] Considering what it has been exposed during this brief discussion, it seems evident that the two isoforms present significant differences in the substrate selectivity. One of the most evident examples of this heterogeneity is represented by PP2A, which interacts just with CK2 α . This contact is mediated by a specific aminoacidic sequence (HEHRKL) present only on the CK2 α isoform. This short amino acid chain closely resembles the consensus sequence of the simian virus 40 (HENRKL), a small antigen that recognises selectively PP2A.^[52] There are other examples of proteins that present a selectivity for one of the two catalytic isoforms. As an example, CKIP-1 (CK2 Interacting Protein 1) and Pin1, Prolyl isomerase 1, interact selectively with CK2 α during different phases of the cell cycle.^[52,128]

1.5.1.2 CK2: CK2 β



Figure 29. Crystal structure of the dimer constituted by two regulatory subunits [PDB: 1JWH].

CK2 β is the regulatory subunit of CK2. It is expressed in a single isoform, constituted by 215 amino acids, whose sequence is almost identical in all the species, confirming the crucial importance that this structure had in the evolution.^[51,121,126,128] From a structural point of view, CK2 β can be divided in a body, that includes an α -helical rich N-terminal domain and a Zn²⁺ containing domain, on one hand and a C-terminal tail on the other one. The Zinc finger is deputed to the complexation of a zinc ion. It constitutes the site of interaction between the two different β subunits in the tetrameric form of CK2.^[126] For the formation of the functional oligomeric structure of CK2, a fundamental role is played also by the C-terminal tail of the regulatory subunit.^[125] Indeed, this structure point out, away from the body of the β subunit, exploring the external environment with a highly conserved β -hairpin loop and then it organizes itself in an unfolded structure. This part of the regulatory subunit mediates the principal interactions with the body of the other β -subunit and with one of the two alpha subunits of the tetramer.^[125]

From a functional point of view, the CK2 β subunit present a complex scenario. Indeed, this structure not only modulates the activity of CK2 and manage the substrate selectivity of the whole enzyme exploiting different portions of its protein structure, but it has been demonstrated that this subunit presents several physiological functions in the cell that are not mediated by the interaction with CK2 α or CK2 α^I .^[125]

At the N-terminal region, CK2 β presents an auto-phosphorylation site that includes Ser 2, Ser 3 and Ser 4.^[126,129] The mechanism of auto-phosphorylation, after an accurate analysis of the crystal structures of the tetrameric complex, seems to be mediated by an intermolecular mechanism, and not an intramolecular, that involves higher degree of organisation of the tetrameric structures in more complex domains. The auto-phosphorylation domain is fundamental for regulating the enzymatic activity of CK2. Indeed, in its phosphorylated form, it loses its ability to bind directly to its acidic sequence of amino acids masking its inhibitory activity.^[126,129]

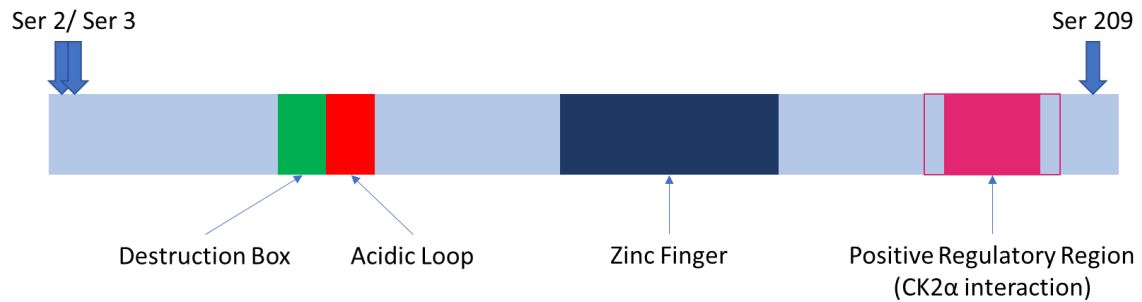


Figure 30. Schematic representation of the key regulation regions within the aminoacidic sequence of CK2 β .

CK2 β is phosphorylated at the residue Ser 209 in a cell cycle dependent manner by p34^{cdc2}. This posttranslational modification modulates the set of substrates that can be phosphorylated by the tetramer.^[130]

The regulatory subunit of CK2 includes a 10 amino acids sequence that resembles the destruction box that confers mitosis specific degradation to cyclin B. This sequence determines protein's susceptibility to ubiquitination and subsequently it drives to the proteolytic degradation CK2. This structure, in a concerted mechanism with the other structures of CK2, modulates the stability of the tetrameric structure and mediate its degradation.^[52,126]

In the structure of CK2 β is included a short sequence of acidic amino acids. This small fragment includes all the amino acids comprised between residue 55 and residue 64. The sequence (DLEPDEELED) resembles that one of the substrates of CK2 and it acts autoinhibiting CK2 in an intermolecular way.^[52,126] It binds to the basic cluster present on the catalytic subunit of CK2 encoded by the amino acids 74-80 (KKKKKR) inhibiting its activity.^[52] It has been demonstrated that masking the negative charge of this region of CK2 β through modifications of the aminoacidic sequence or through the administration of polyamines, the *in vitro* activity of CK2 is significantly augmented.^[52,126]

Another fundamental structure of CK2 β is the zinc finger sited in the middle of the aminoacidic sequence.^[126] This peculiar structure, that mediates the dimerization of the two β subunits, is constituted by four cysteines (Cys 109, 114, 137 and 140). Mutations at the residues 109 and 114 disrupt the zinc finger and the dimerization process.^[126] Considering that the formation of the dimer of CK2 β is fundamental for the formation of the tetramer, the disassembling of this core structure does not allow the maturation of a fully functional CK2. Facing with the importance that the formation of this dimeric structure has in the formation of the tetramer, it should not surprise that CK2 β is expressed at higher levels compared to the two others catalytic subunits and that the dimer tends to form also without the presence of any CK α or CK2 α ^I.^[52]

The C-terminal domain, as already mention, interact with CK α ^I stabilizing it and increasing the overall enzymatic activity.^[21,121,125] It has been demonstrated that synthetic peptides that cover the C-terminal aminoacidic sequence of the β subunit (181-203) are able to stabilize and increase the activity of the catalytic subunits.^[52]

Considering all the different portions and regulatory units included within the aminoacidic sequence of CK2 β , this subunit modulates the enzymatic activity of CK2 with a plethora of different mechanisms:

1. It furnishes the scaffold for the organisation of the tetrameric complex;
2. It enhances the catalytic activity and stability;
3. It modulates the substrate selectivity of CK2, furnishing a docking platform for the recruitment of CK2 substrates or potential regulators (e.g. of substrates: Nopp140, p53, Fas-associated factor 1 (FAF-1), topoisomerase II) (e.g. of regulators: FGF-2 (Fibroblast Growth Factor 2)).^[52,122]

Furthermore, CK2 β is also able to exert different functions by itself, indeed, there are regions within the cell where CK2 β is localized alone without any catalytic subunit. For example, the regulatory subunit is able to interact directly with c-Mos, inhibiting it, or with A-Raf protein kinases.^[122,126,127,130] There is also a debate regarding the ability of this structure to modulate the cell proliferation. Indeed, in the adipocytes, an overexpression of CK2 β blocks the cell proliferation, causing a G₂ delay or a G₂/M arrest. In other cell lines, an analogous overexpression does not significantly affect the cell viability. Why different cell lines are differently sensible to the overexpression of CK2 β is still not known.^[128]

1.5.2 CK2: Regulation

CK2 is a constitutively active enzyme involved in a multitude of pathways.^[126] Considering the heterogeneity of the tasks that this enzyme has to manage, it seems evident that different control mechanisms finely tune its activity in different cell lines and in different stages of the cell cycle.^[128] The regulation of this kinase is based on three different mechanisms:

1. Regulated expression and assembly;
2. Covalent modifications;
3. Regulatory interactions with protein and/or non protein molecules.

Regarding the assembly of CK2, CK2 β is the main player. As previously illustrated, it modulates the catalytic activity, the formation of the tetramer and the substrate selectivity. Furthermore, with its destruction box it mediates the ubiquitination and proteasomal degradation of the whole complex. For what concern the expression, CK2 varies its levels within the cell in function of the proliferation rate. Higher proliferation rates correlate with a higher expression of CK2.^[52,124,127,128]

CK2 is variously covalently modified in all its subunits, especially by phosphorylation. Despite these elements, it seems evident that these modifications do not alter significantly the activity of the enzyme, but rather they modify the selectivity profile and the stability of the kinase.^[51,126,127]

Taking in to account the possibility that CK2 could be modulated by the interaction with endogenous small molecules, several experimental evidences have demonstrated that is not the case. Indeed, CK2 is defined as a messenger independent kinase because it has not to interact with any small molecule for its activation or

modulation.^[130] The principal mechanism of regulation of CK2 is mediated by protein-protein interactions. Some proteins, like FGF-1, FGF-2, Hsp 90 and Cdc37 alter and stabilize its activity.^[51,52,121,122,131] Other regulators, such as FAF-1 and CKIP-1, target CK2 to specific site or structures within the cell. Pin1 interacts with CK2 when it is phosphorylated at its catalytic subunit and it prevents the phosphorylation of the Thr 1342 residue on topoisomerase II α .^[51,52,122,126,128,130] Chromatin transcriptional elongation factor (FACT), composed by hSpt16 e SSRP1, facilitates the phosphorylation of Ser 399 on p53. Considering the ability of CK2 to interact with different protein and substrates, it explains why this kinase is so heavily involved in the control of the cellular homeostasis.^[51,52,121,126]

1.5.3 CK2: Function

1.5.3.1 CK2 and cellular homeostasis

CK2 has a great variety of functions and substrates within the cell and this is mirrored by the fact that also its cellular localisation is heterogenous. Indeed, CK2 can be found in the nucleus, cytoplasm, in the inner and outer plasma membrane and in different organelles, such as Golgi Endothelial Reticulum (ER) and ribosomes.^[52] The fundamental role of this kinase in sustaining the viability of the cell is confirmed also by the fact that it is involved in the cellular transformation and in the carcinogenesis. Its substrates are:

- Proto-oncogene products such as c-Myc, c-Myb and c-Jun;^[51,52,122]
- Tumour-suppressor gene products like: p53 and BRCA 1 (BRCA1 Breast Cancer susceptibility gene 1);^[52,122]
- Transcriptional regulators (Max, Cut, PU.1/IRF4 (Interferon Regulatory Factor 4));^[52]
- Component of the canonical Wnt pathway.^[52,122,127]

CK2 is directly involved during the G₀/G₁, G₁/S and G₂/M transition. During mitosis, CK2 is involved in the control of the mitotic spindle and centrosomes and it is heavily phosphorylated in all its subunit demonstrating its mutational regulation during the cell cycle. During this phase of the cell cycle p34^{cdc2}, cdc34 and topoisomerase II are the targets of CK2.^[127,128]

CK2 has a fundamental role also in the prevention and blockade of the apoptosis cascade. Substantially with its kinase activity, CK2 is able to stabilize different proteins from the caspase's dependent proteolysis inhibiting the apoptosis.^[132] This mechanism of prevention of the caspase's cleavage is due to the fact that both caspases and CK2 have consensus sequences that are highly similar one to each other. One example of this action, that configure CK2 as one of the principal oncogenic proteins of the cell, is the prevention of the caspase's cleavage of ARC and BID.^[33,51,52,122] When these two proteins are phosphorylated by CK2, they maintain their antiapoptotic effect. pARC penetrates within the mitochondria and blocks caspase 8, while pBID is not degraded by caspase 8.^[33,121,122] In case of dephosphorylation of both the proteins at the CK2 site, ARC is no more able to penetrate within the mitochondria and it can not inhibit caspase 8. This protease is released in the cytosol, where it cuts BID in two

portions, one of which penetrate within the mitochondria provoking the release of Cyt C and consequently the apoptosis.^[33,121,122]

1.5.3.2 CK2 and cancer

CK2 is overactivated in almost all the known types of cancer. It is the terminal effector of a multitude of different antiapoptotic and proliferative pathways and the reasons why its activity is incremented can lie in different mechanisms: from genetic alterations of the CK2 genes, to an overactivation of all the pathways of which it is a downstream effector.^[51] It is involved in the inhibition of the apoptosis, modulation of signalling pathways, DNA damage response and cell cycle regulation.^[20,52,53,121] It has a positive and enhancing action on cell proliferation and growth, cell survival, and it induces changes in the cellular morphology, cell transformation and angiogenesis.^[51] CK2 regulates also the cascades of the Wnt signalling, Hedgehog signalling, Jak/STAT, NF-κB and PTEN/PI3K/Akt-PKB.^[51,121]

The involvement of CK2 in such a high plethora of different oncogenic pathways and its key function in the inhibition of the apoptosis, render this kinase a gold target for the development of a new anticancer therapy.

1.5.4 CK2: Small molecule modulators

During the last decades a lot of efforts have been done with the aim to develop a potent and selective CK2 inhibitor able to furnish a new pharmacological tool for the treatment of several malignancies. Currently, a lot of different molecular scaffolds have been developed and it is far behind the scope of this introduction to illustrate in a detailed way all the progresses reached in this field. Considering that the majority of the investigated compounds are classical kinase inhibitors that directly interact with the ATP binding pocket of the enzyme blocking the entrance of its natural substrate, only two distinct molecules, that belong to this class, will be presented.

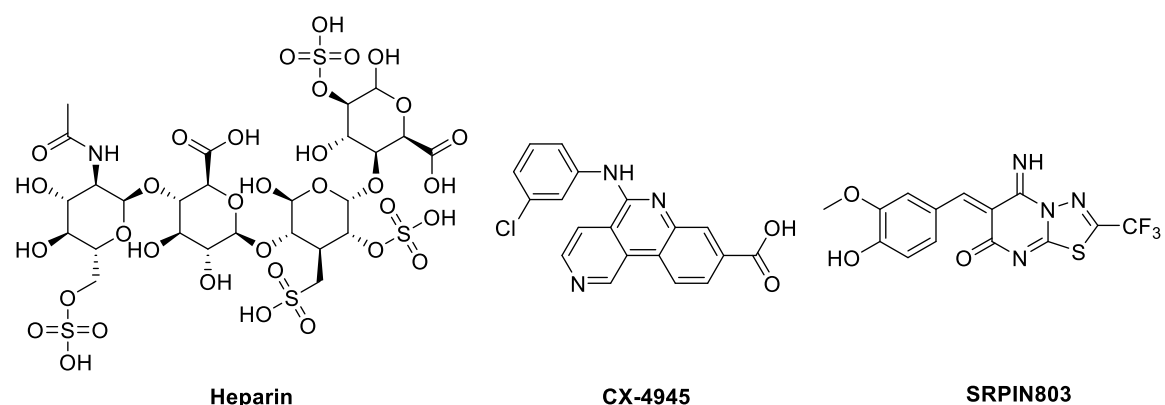


Figure 31. Chemical structure of the compounds presented in this paragraph.

Before to mention these compounds, that are important for the economy of this thesis, two other small molecules will be illustrated, because they can modulate the activity of CK2 in a non-ATP competing way.

It has been demonstrated that heparin, a negatively charged glycosaminoglycan, is able to inhibit CK2 in *in vitro* experiments.^[52,127] This small molecule mimics the regulatory activity of the acidic sequence presents on the β subunit that is able to reduce the activity of the catalytic domains.

The other special class of compounds are polyamines. This heterogeneous class of molecules is able to activate CK2 masking the previously mentioned acidic sequence of the β subunit and consequently polyamines are able to reactivate the CK2 kinase activity.^[52,127]

Focusing on the class of CK2 inhibitors that compete with ATP in the active pocket of the enzyme, the most well-known CK2 inhibitor is CX-4945, also known as Silmitasertib.^[131] This compound was developed by Cylene Pharmaceuticals of San Diego (California), after a campaign for the identification of new selective and potent PARP inhibitors. It is an ATP competitor resulted to be extremely selective for CK2 among all the other kinases and very potent, with an $IC_{50} \approx 1nM$. It has been the first CK2 inhibitor to reach the clinical trials in 2010, and in 2017 it has been defined by FDA as orphan drug for advanced cholangiocarcinoma. It is still in clinical trials for the treatment of other kinds of cancers.^[131]

SRPIN-803 is the last compound presented in this paragraph. This molecule has been developed by Mooroka and co-workers.^[133] It is a selective dual inhibitor of CK2 and SRPK1 (Serine Arginine Protein Kinase 1) able to block the synthesis of VEGF and consequently inhibiting the angiogenesis. It has been developed with the aim of attenuating the pathological angiogenesis observed in macular degeneration. This compound is the result of a virtual screening/synthetic approach focused on the optimization of another dual inhibitor, synthesized by Mooroka and colleagues: SRPIN340. SRPIN803 has an IC_{50} for CK2 of 203 nM. Also in this case, the molecule is designed as an ATP competitor, but currently there are no crystal structures that show the pattern of interactions that this compound generates with the ATP pocket of CK2.^[133]

2 AIM OF THE THESIS

The aim of this PhD thesis has been the development of new anticancer drug candidates that could represent an innovative therapeutic approach for the treatment of several malignancies, in particular some specific kind of leukaemia like LGLL (Large Granular Lymphocyte Leukaemia), CLL (Chronic Lymphocytic Leukaemia) and T-cell leukaemia. This goal has been pursued choosing two different approaches.

The first one has been focused on the development of new small molecule activators of two innovative targets like PP2A and SHP-1, that have been demonstrated to be strongly downregulated in several malignancies and whose reactivation has shown preliminary promising results in preclinical studies. This kind of approach is an innovation in the anticancer pharmacology because currently the actual antitumoral strategies are focused on the use of tyrosine kinase inhibitors, for the rebalancing of the phosphoproteomic profile. This classical strategy has brought ineluctable benefits to a multitude of patients, but its limitations are coming out, in particular the onset of resistances and of severe side effects are limiting the efficacy of these drugs. The idea of rebalancing the phosphorylation profile of the cell, trying to reactivate some silenced phosphatases like PP2A and SHP-1, could be a promising alternative way for treating patients that do not respond to the classical therapies or that become resistant to TKIs. These targets, if properly reactivated, are able to induce apoptosis in cancerous cells, also in those resistant to classical TKIs. This approach has shown to be promising also in targeting the stem cancer cells which are not affected by the conventional chemotherapy, representing the principal reservoir for the recrudescence of the pathology. During this three-years work, several PP2A and SHP-1 activators have been synthesized, with the aim to develop a selective and potent agonist for these two strategic targets.

For what concern PP2A, further studies have been conducted using a lead compound as model. These investigations aimed to determine the pharmacokinetic profile of the candidate drug and the univocal identification of its target protein. Furthermore, thanks to a placement in the laboratory of professor Rivera-Fuentes (ETH, Switzerland) new fluorometric tools have been developed with the aim to design a new experimental setup for the determination of the phosphatase activity *in vitro*. This new protocol is suitable for performing screening of compounds, on isolated enzymes or whole cell lysates. The synthesized fluorescent probes could help also in the identification of the cellular localization of the target phosphatases in living cells exploiting the super-resolution microscopy technique.

The second pharmacological approach has been focused on the development of new chemical entities able to modulate the activity of a different target that could be exploited for overcoming the aroused resistances to TKIs. Considering this important goal, CK2 presented the right profile. Indeed, being this kinase the downstream effector of different proliferative cascades, the inhibition of this key point could tackle the resistances that arise in all the enzymes that precede CK2 in the pathway. For this reason, another line of research, pursued during this PhD, has been based on the development of a new class of specific inhibitors of CK2. In this case the innovation has been the design of a new molecular scaffold able to act selectively on the CK2 kinase, trying to reduce the off-targets and consequently the possible side effects.

3 RATIONALE AND RESULTS

3.1 PP2A: Rationale and Results

In this paragraph all the rationale approaches and results regarding each project that has PP2A as main target will be presented and discussed. For simplicity and a better understanding of the whole research line, the different topics will be grouped in two main categories:

- Synthesis of PP2A activators;
- Pharmacokinetic and Pharmacodynamic studies on the lead compound CC11.

Each category will be further subdivided in different small topics united by a common rational approach or main goal.

3.1.1 Synthesis of PP2A activators

In this paragraph the synthesis of different classes of new PP2A activator candidates will be illustrated. The paragraph will be divided in three parts, mirroring the different rationales that led to the development of the general molecular scaffold of each class. In each part, the model that inspired the general chemical structure and the adopted synthetic pathway will be illustrated, focusing on the peculiarities and the problematics encountered in each category. The reader is also informed that in all the paragraph there will not be presented any biological data because this information is strictly confidential for patent reasons.

3.1.1.1 Fingolimod analogues

The first class of molecules synthesized during this PhD has been a series on Fingolimod analogues, a well-known activator of PP2A. This research line is the logic continuation of the work that has been done in this lab before this PhD.^[32] The general idea of this project, and of the previous research, is the synthesis of Fingolimod analogues that could maintain their ability to positively modulate PP2A but that do not present any immunomodulatory behaviour. For doing this, the chemical structure of Fingolimod has been slightly modified with the aim to remove all the phosphorylatable functional groups. Indeed, Fingolimod exerts its immunomodulatory effects acting directly on S1PR1 in its phosphorylated form, while the unphosphorylated fraction is the responsible of the antitumoral effect and the dissociation of the PP2A/SET complex.

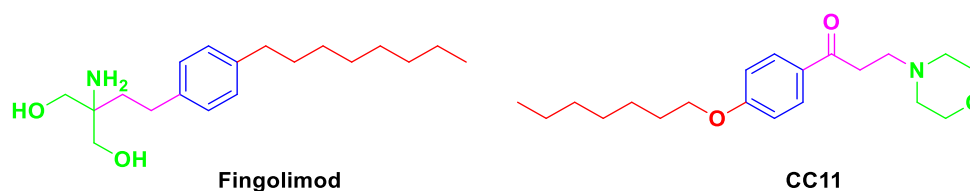


Figure 32. Comparison of the two chemical structures of Fingolimod and the lead compound that has been used as a model for the synthesis of the new analogues and for all the other studies.

As can be seen in figure 32, the general structure of Fingolimod has been maintained while all the phosphorylatable hydroxyl groups have been removed with the aim to avoid any immunomodulatory effects.

In the lead compound (CC11), developed by the previous PhD student Valeria Pavan, it has been maintained:

- a hydrophobic chain, represented in red, that mimic that one of Fingolimod;
- a para-substituted phenyl ring (in blue);
- a short spacer (in purple);
- a polar head (in green).

CC11 has shown to reactivate PP2A in B-CLL cells and in vivo models by dissociating the PP2A/SET complex, but without any immunosuppressive effect. From preliminary results, based on fluorescent assays and NMR experiments, this compound seems to be able to break down the PP2A/SET complex interacting just with SET, as demonstrated also for Fingolimod.

The logic prosecution of this project, that has been conducted during this PhD, has been the modification of the molecular scaffold of CC11 with the aim to develop a SAR that could help us in the synthesis of new active compounds much more potent and effective than the lead compound.

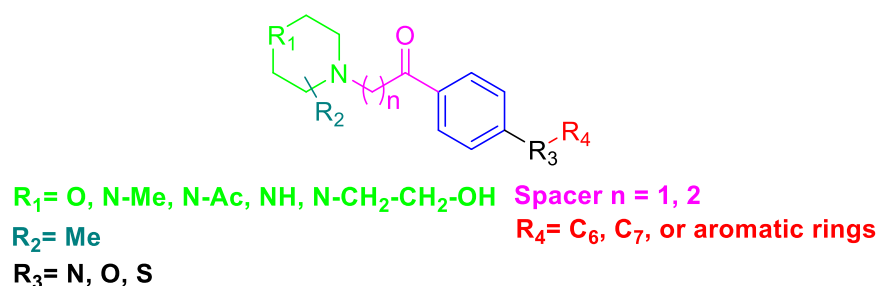


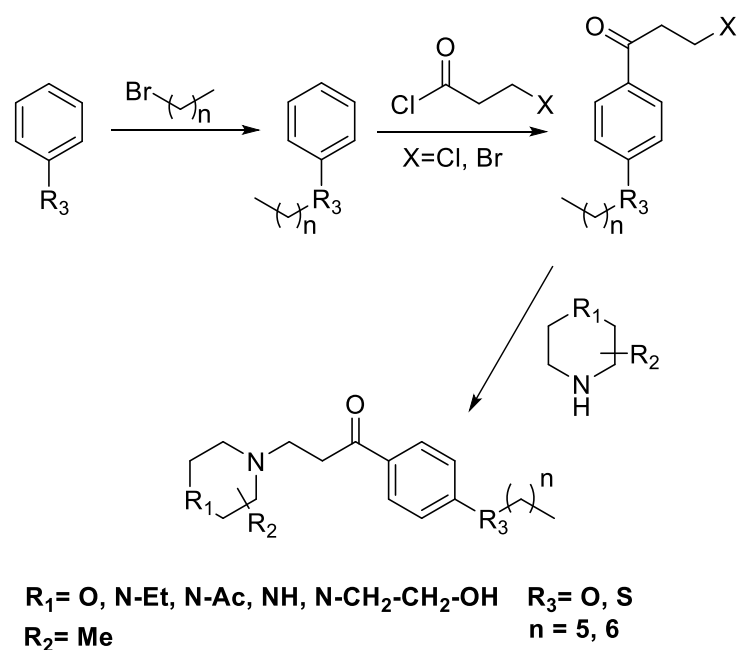
Figure 33. Pharmacophoric structure of the Fingolimod analogues synthesized during this PhD.

For developing an appropriate SAR of this class of compounds, almost all the different components of the pharmacophoric structure of CC11 have been varied. The alkyl, hydrophobic chain has been modified in length and it has been substituted with different aromatic rings. The linker atom R₃ that connect the hydrophobic tail to the aromatic ring has been varied, introducing other heteroatoms such as nitrogen, oxygen and sulphur. The para substituted aromatic ring is the only structural determinant that has not been modified. The spacer that connect the phenyl ring to the polar head has been changed varying its length. Finally, also different polar heads have been installed on this position. The different substituents vary the basicity, the hydrophilicity and the steric hindrance of this part of the molecule. Below all the adopted synthetic pathways will be illustrated.

First class of Fingolimod analogues

The first group of synthesized compounds aimed to explore principally the polar head of the pharmacophoric structure. In this case the R₃ substituents are only oxygen and sulphur, while the alkyl chain has been modified just in length. The substituents that have been introduced in the polar portion of the molecule have been chosen with the goal to explore the three-dimensional space that surrounds these molecules in their site of actions and its electrostatic properties. First, different hydrophobic substituents have been installed in different portions of the cyclohexylamine ring. These

modifications could be useful for the identification new hydrophobic pockets in close proximity to this part of the molecule that could increase the affinity and the potency of the new compounds. Secondly, also the basicity and hydrophilicity of the R_1 substituent have been varied. Indeed, the original oxygen atom has been varied with a methylene group, a NH, N-acetyl, N-ethyl, N-ethyl hydroxy substituents. The methylene group explored the possibility that in this region, more hydrophobic interactions are required. The other nitrogen-based substituent increased the basicity of the polar head and they confer a much stronger positive charge to the molecule; indeed, these substitutions, a part the n-acetyl one, introduce in the molecular scaffold a piperazine ring, that is much more basic and protonable of a morpholine or a piperidine ring. This modification aimed to verify if in this position, positively chargeable groups are well accepted by the active site of the target protein. The introduction, on the new nitrogen atom of different substituent has the goal to explore the space around this new functional group.



Scheme 1. Synthetic pathway adopted for the synthesis of this first class of PP2A activators.

The synthetic procedure illustrated in scheme 1 is quite simple and straightforward, characterised by discrete yields. The first step is a nucleophilic substitution between an alkyl halide, that acts as electrophile, and a phenol or thiophenol ring that acts as nucleophile ($\text{S}_{\text{N}}2$ Williamson etherification). For increasing the rate and the yield of this step, a strong base such as NaOH or KOH has been used in the reaction mixture with the same equivalents of the aromatic rings. This base has been used because thiophenol and in particular phenol, are weak acids. The aromatic ring acts as a modest electron withdrawing group and increases the acidity of the hydroxyl group. Furthermore, the formed alcoholate specie generated by the deprotonation is further stabilized because the negative charged localised on the oxygen atom can be delocalised within the π -system. The alcoholate and thiolate groups that are formed in situ with the base present a stronger nucleophile behaviour than the neutral compounds and this facilitates the proceeding of the reaction. In some cases, for

increasing the rate of the reaction an in-situ Finkelstein reaction has been performed. This reaction consists in the nucleophilic substitution of the halogen present at one terminal of the alkyl chain with iodine. This substitution is advantageous because iodide is the best leaving group, in a nucleophilic substitution reaction, compared to all the other halogens and it increases the formation's rate of the final desired ether. The reason why iodide is the best leaving group between halogens resides in two main characteristics:

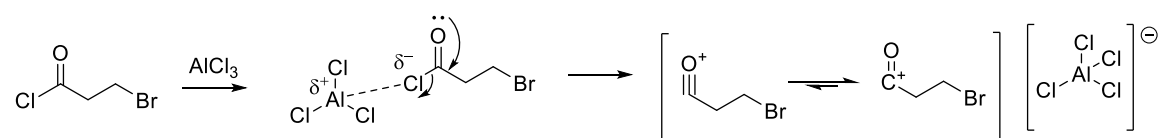
- iodide presents the lower pK_a, of the conjugate acid HX, and so is much more able to stabilize the negative charge in solution when it is free by the reaction;
- C-I bond has the lower strength, so it is easier to break than all the other C-X bonds.

Halide (X)	Strength of C-X bond, kJ mol ⁻¹	pK _a of HX
fluorine	118	+3
chlorine	81	-7
bromine	67	-9
iodine	54	-10

Table 4. Comparison among halides as leaving groups.

Despite iodide is a better leaving group compared to the other halides its in-situ introduction on the alkyl chain has been allowed, exploiting the different solubilities that the inorganic salts of the halides have in organic solvents. For the Finkelstein reaction acetone has been chosen as solvent. NaI is soluble in this solvent and furnish the I⁻ atoms necessary for performing the halide exchange. The sodium iodide is soluble in acetone because the carbonyl groups of this solvent coordinate the Na⁺ in solution and this coordination process creates a cavity with the two methyl branches of the acetone that has the right dimension for hosting I⁻. When the halide is switched, the new formed NaX salt is not soluble in acetone, because the anion species does not fit in the cavity, and precipitates, shifting the equilibrium versus the complete halide substitution.

The second synthetic step is an electrophilic aromatic substitution (Friedel-Crafts reaction) between the aryl ether, synthesized in the previous step, and an acyl-halide that acts as electrophile. In this reaction aluminium trichloride, a Lewis acid, has been introduced for activating the electrophile for the reaction.



Scheme 2. Scheme of activation of the acyl-halide and the formation of the reactive species acylium ion.

As shown in scheme 2 the Lewis acid activates the acyl-halide forming the active species: the acylium ion. This carbocation is a strong electrophile and rapidly reacts

with the aryether. In this case the aromatic ring reacts as nucleophile. This is allowed because the ether or thioether portions, located on the aromatic ring, are electron donating groups that consequently enrich the phenyl ring with their unpaired electrons favouring the electrophilic addition reaction. These electron donating groups orientate the reaction in para and ortho positions for resonance reasons illustrated in figure 34.

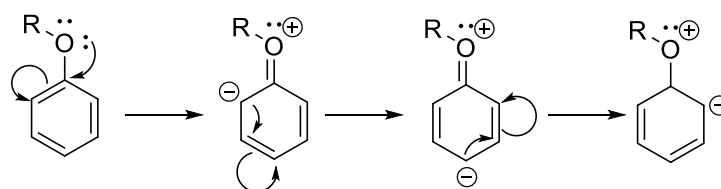


Figure 34. Ortho-para orientation in phenyl-ethers.

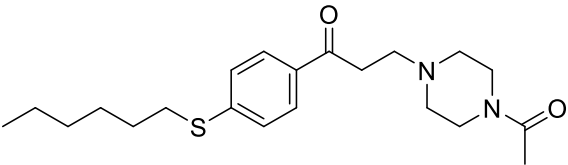
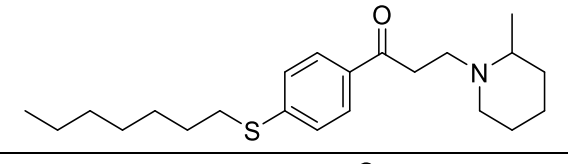
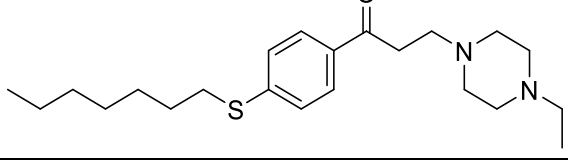
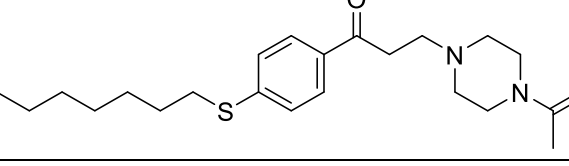
This reaction presents the intrinsic risk to give as final products both the ortho and para substituted aromatic rings. This never happened because the ortho product is disadvantaged in its formation. This position is strongly sterically hindered by the alkyl chains present on the oxygen or sulphur atoms and this prevents the side reaction.

The last step of the synthesis is again a nucleophile substitution. This reaction is much easier than the first one because a secondary amine has been used as nucleophile. This functional group is a better nucleophile than phenol or thiophenol.

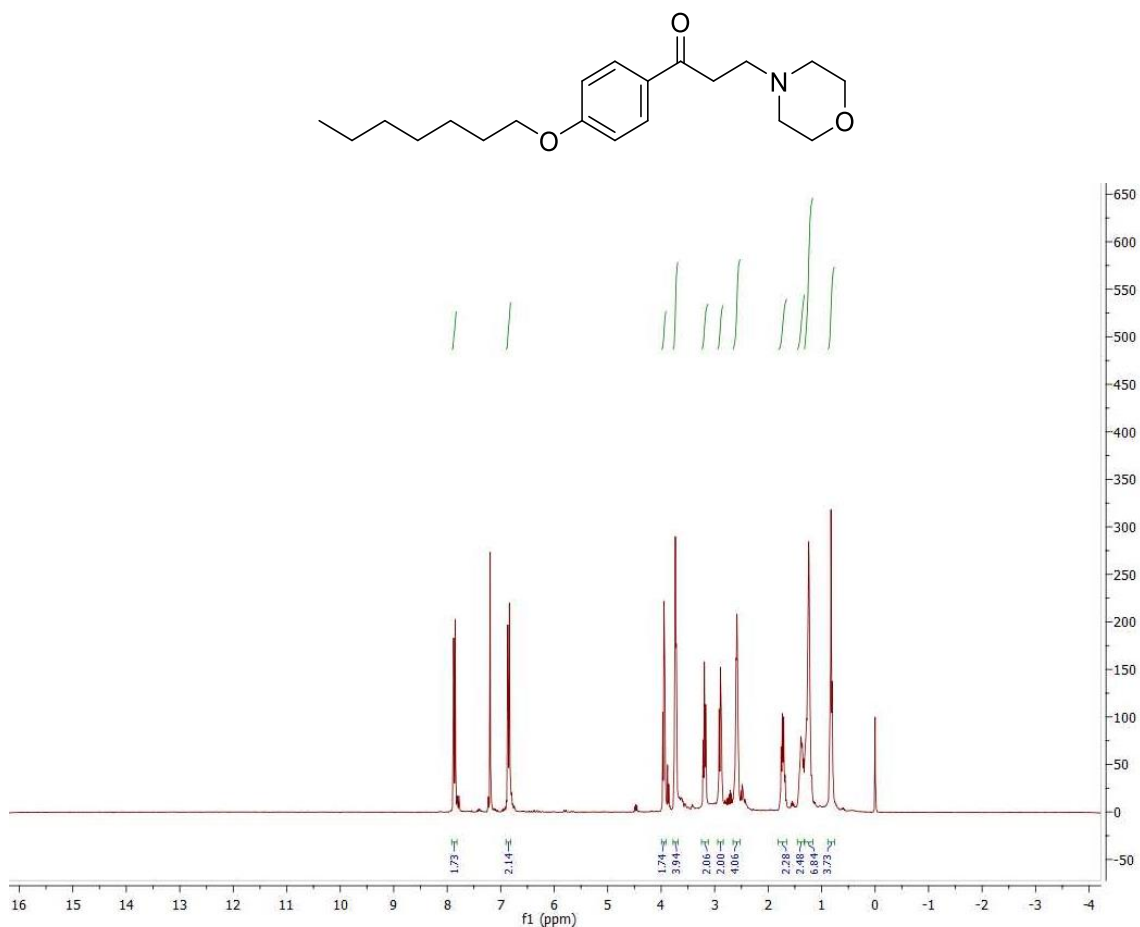
In the following table, all the synthesized compounds, obtained with this synthetic pathway, are shown.

Number of the compound	Chemical structure	IUPAC name
FAI-01		1-(4-(hexyloxy)phenyl)-3-morpholinopropan-1-one
FAI-02		1-(4-(hexyloxy)phenyl)-3-(piperidin-1-yl)propan-1-one
FAI-03		1-(4-(hexyloxy)phenyl)-3-(2-methylpiperidin-1-yl)propan-1-one
FAI-04		3-(4-ethylpiperazin-1-yl)-1-(4-(hexyloxy)phenyl)propan-1-one

FAI-05		3-(4-acetylpiperazin-1-yl)-1-(4-(hexyloxy)phenyl)propan-1-one
FAI-06		1-(4-(heptyloxy)phenyl)-3-morpholinopropan-1-one
FAI-07		1-(4-(heptyloxy)phenyl)-3-(piperidin-1-yl)propan-1-one
FAI-08		1-(4-(heptyloxy)phenyl)-3-(2-methylpiperidin-1-yl)propan-1-one
FAI-09		3-(4-ethylpiperazin-1-yl)-1-(4-(heptyloxy)phenyl)propan-1-one
FAI-10		3-(4-acetylpiperazin-1-yl)-1-(4-(heptyloxy)phenyl)propan-1-one
FAI-11		1-(4-(hexyloxy)phenyl)-3-(piperazin-1-yl)propan-1-one
FAI-12		1-(4-(hexyloxy)phenyl)-3-(4-(2-hydroxyethyl)piperazin-1-yl)propan-1-one
FAI-13		1-(4-(hexylthio)phenyl)-3-(2-methylpiperidin-1-yl)propane-1-one
FAI-14		3-(4-ethylpiperazin-1-yl)-1-(4-(hexylthio)phenyl)propan-1-one

FAI-15		3-(4-acetylpiperazin-1-yl)-1-(4-(heptylthio)phenyl)propan-1-one
FAI-16		1-(4-(heptylthio)phenyl)-3-(2-methylpiperidin-1-yl)propane-1-one
FAI-17		3-(4-ethylpiperazin-1-yl)-1-(4-(heptylthio)phenyl)propan-1-one
FAI-18		3-(4-acetylpiperazin-1-yl)-1-(4-(heptylthio)phenyl)propan-1-one

Example of NMR characterisation

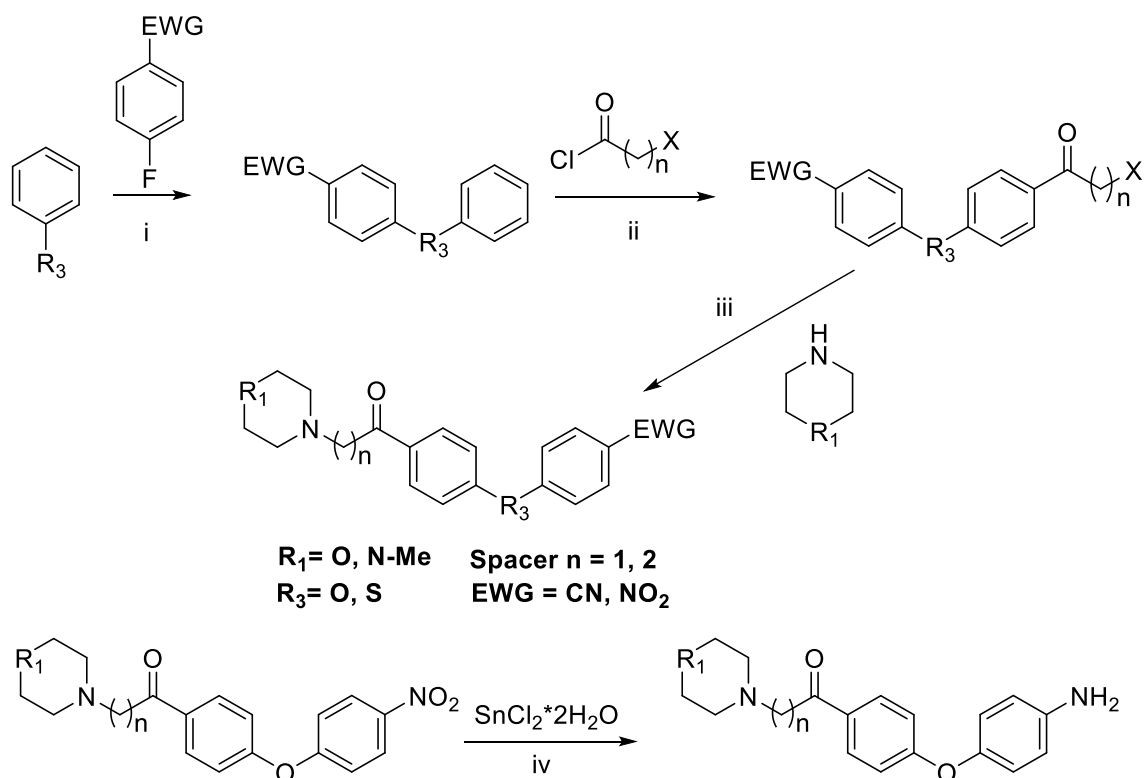


¹H NMR (400 MHz, CDCl₃)

Second class of Fingolimod analogues

This second class of Fingolimod analogues introduces a substantial modification in the pharmacophoric structure of all the compounds synthesized till now. The alkyl tail, that is present in Fingolimod and CC11, is substituted with a series of aromatic rings. This strategy aims to understand if this long alkyl chain is fundamental for the interaction with the protein target and consequently for the activity of the compounds. The substitution with an aromatic ring of such a flexible and hydrophobic moiety could present several advantages. Firstly, this modification could confer to the structure much more rigidity, reducing the number of rotatable bonds of the molecule. It has been demonstrated that for having a promising drug candidate the number of rotatable bonds should be tightly controlled. This is particularly true if we take into account the possibility of administering a small molecule orally. In this case, Veber's rules impose as a maximum limit of 10 rotatable bonds per molecule. CC11, our lead compound, presents 11 rotatable bonds, so for further development of the chemical structure of this model molecule, especially trying to develop a drug candidate that could be orally available, the reduction of the number of rotatable bonds could be desirable. Furthermore, considering the efficacy in activating PP2A this substitution could be advantageous. The network of interactions that a small molecule generates with its target is extremely specific and this allows the molecule to explore just a few conformations for exerting its desired effect. In such a flexible molecule, like CC11 is, the number of conformers that can be generated is really high but only one or few of these can interact with its target. Considered from this point of view the interaction between CC11 and the protein is entropically disfavoured and consequently the energy gain of the whole interaction process is invalidated by this. The reduction of the number of conformers should favour the contact between the small molecule and the target reducing the entropic cost. The only risk of applying such a stiffening protocol is to block the molecule in a conformation that is not able to recognise the desired biomolecule, in this case all the entropic gain would be lost. The last feature that could configure the substitution of an alkyl chain with an aromatic ring as an advantage is the fact that the aromatic rings are able to generate much more interactions compared to a hydrophobic and saturated alkyl chain. Apart from the Van der Waals forces generated in both cases an aromatic ring can generate π - π interactions, π -cations interactions and other useful forces that could stabilize the interaction of the new compounds with the target. Also in this case the introduction of stronger forces could be a disadvantage because in case of repulsion, this would reduce the affinity.

The inserted aromatic rings present also other functional groups that act as hydrogen bond acceptor and in one case also as hydrogen bond donors that could generate favourable interactions with the target.



Scheme 3. Synthetic pathway of the biarilic Fingolimod analogues.

The first reaction of the new synthetic protocol is a nucleophilic aromatic substitution. The reactants involved in this reaction are phenol or thiophenol and a fluorinated aromatic compound, substituted in para position to the halogen with an electron withdrawing group (EWG). The arrangement of the two different substituent groups on the phenyl ring is the key determinant that allows the completion of the reaction. Indeed, the electron withdrawing group, present on the aromatic ring, decreases the electron density of the conjugated system and this is due to its electronic properties. This electron deficiency is manifested with temporary partial charges delocalized on the aromatic ring preferentially in ortho and para positions. When in the ortho position to an EWG is located a halogen atom, the nucleophilic aromatic substitution can happen (Figure 35).

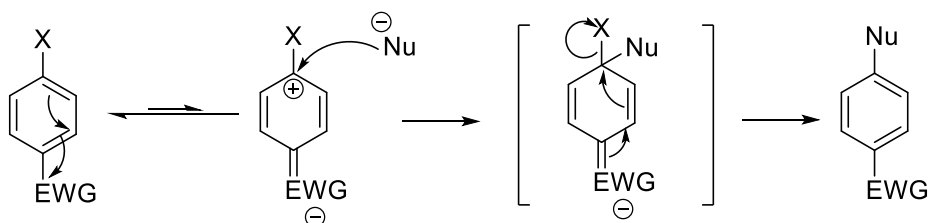


Figure 35. Mechanism of reaction of the nucleophilic aromatic reaction. For commodity it has been used a negatively charged nucleophile, but the same mechanism is followed by a non charged nucleophile.

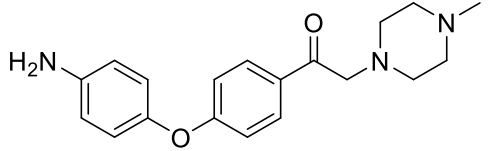
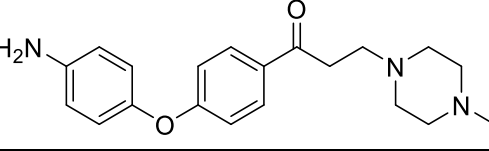
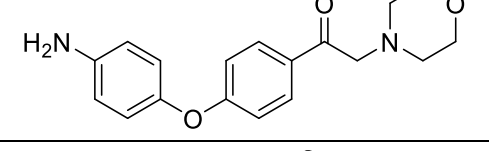
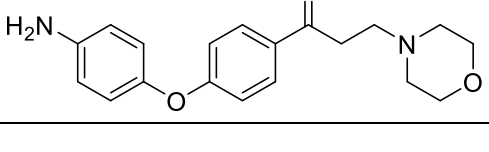
In this case respect to the first step of the previous synthetic pathway DMF has been used as solvent because a higher temperature was necessary for leading to completion the reaction. Instead of a nucleophile base that could interfere with the reaction, due

to the high temperature, potassium carbonate has been preferred. The second step of the synthetic pathway was a Friedel-Crafts reaction as before. In this case there are two aromatic rings that could react, but this is avoided because the electron withdrawing group on one reduces the reactivity of that aromatic ring giving just one final product. Unfortunately, when the thioethers have been used for this kind reaction, no products have been obtained and for this reason all the final compound do not present any sulphur atom in position R₃. The reason of this unsuccess has not been completely understood. For what concern the ether phenones, the last synthetic step has been a nucleophilic substitution as in the previous case.

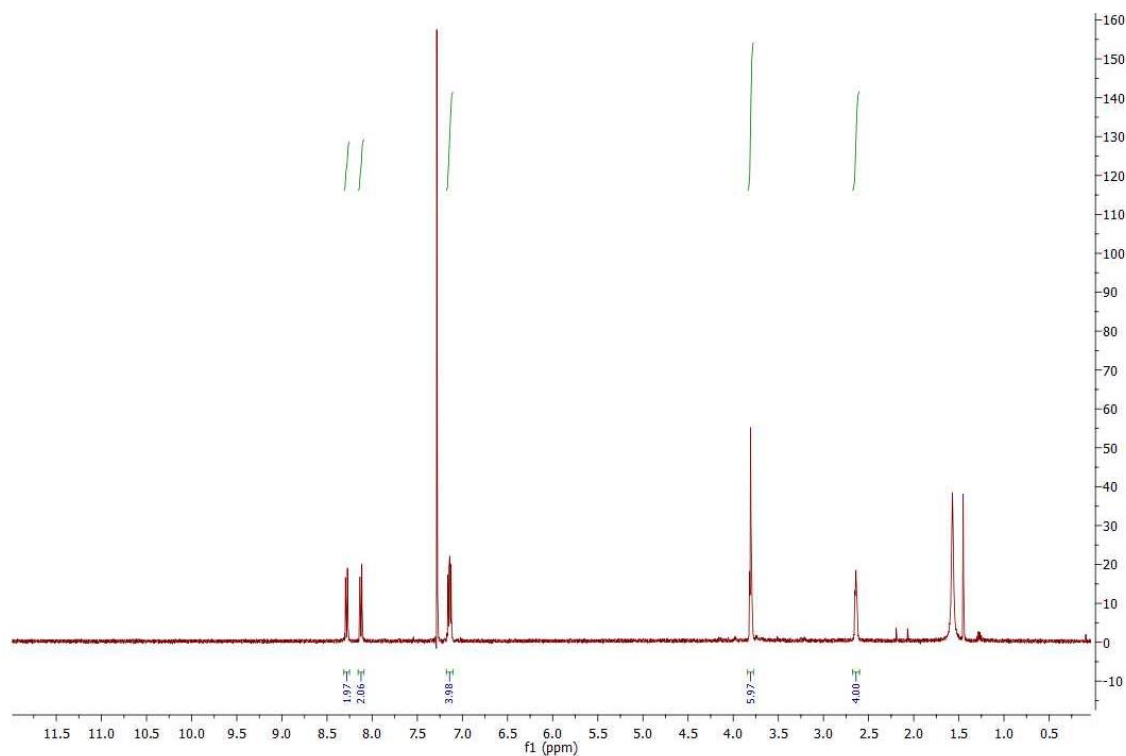
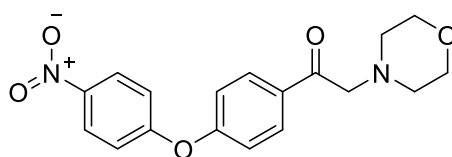
The introduced EWGs present just hydrogen bond acceptors; with the aim to explore if in this position hydrogen bond donors are more prone to interact with the therapeutic target, the nitro group of some compounds have been reduced obtaining the amino derivatives. The reductive step has been done as last step because otherwise, the introduction of a nucleophile within the molecular structure before one of the two last steps could alter the reactivity of the all mixture. Indeed, the acyl halide could react with the aniline ring forming an amide bond and the alkyl halide in a analogous manner could generates a secondary arylamine. The difficulty of doing the reduction as last step is to choose a reducing agent that does not reduce also the ketone present on the molecule. For this reason, SnCl₂*2H₂O has been used.

In the following table, all the synthesized compounds, obtained with this synthetic pathway, are shown.

Number of the compound	Chemical structure	IUPAC name
AFA-01		3-morpholino-1-(4-(4-nitrophenoxy)phenyl)propan-1-one
AFA-02		2-morpholino-1-(4-(4-nitrophenoxy)phenyl)ethan-1-one
AFA-03		3-(4-methylpiperazin-1-yl)-1-(4-(4-nitrophenoxy)phenyl)propan-1-one
AFA-04		2-(4-methylpiperazin-1-yl)-1-(4-(4-nitrophenoxy)phenyl)ethan-1-one
AFA-05		4-(4-(3-morpholinopropanoyl)phenoxy)benzonitrile

AFA-06		1-(4-(4-aminophenoxy)phenyl)-2-(4-methylpiperazin-1-yl)ethan-1-one
AFA-07		1-(4-(4-aminophenoxy)phenyl)-3-(4-methylpiperazin-1-yl)propan-1-one
AFA-08		1-(4-(4-aminophenoxy)phenyl)-2-morpholinoethan-1-one
AFA-09		1-(4-(4-aminophenoxy)phenyl)-3-morpholinopropan-1-one

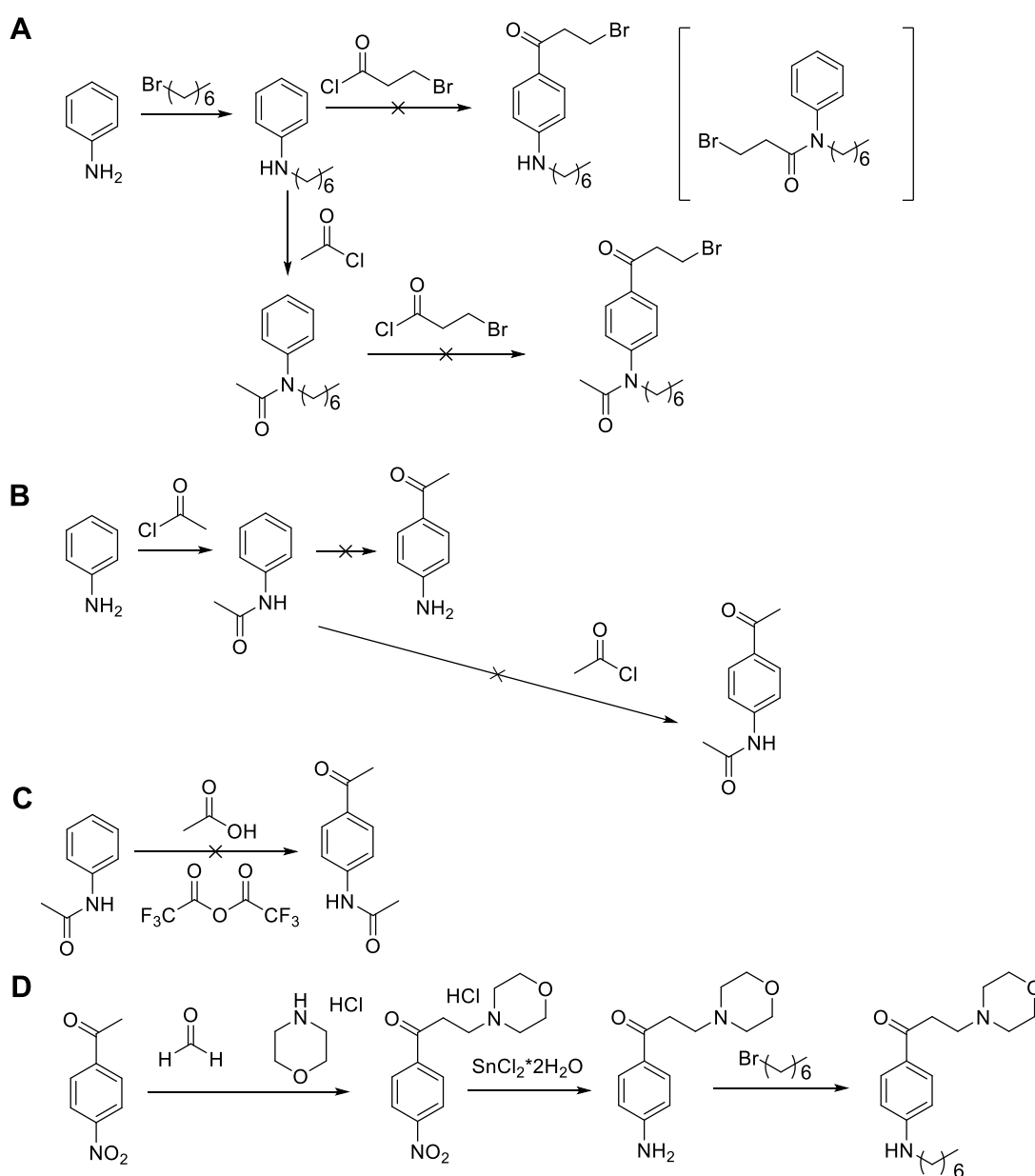
Example of NMR characterisation



¹H NMR (400 MHz, CDCl₃)

Third class of Fingolimod analogues

The aim of this part of the project was to explore the R_3 substituent that connect the hydrophobic portion of the molecule to the phenyl ring. In this class of compounds a hydrogen bond donor have been introduced in the molecular scaffold in the R_3 position. This has been done choosing a nitrogen atom instead of the classical oxygen or sulphur ones. This substitution introduces in the molecular scaffold a secondary ammine that could generate favourable hydrogen bonds with the target through this new functional group. The synthetic protocol for introducing such small modification needed a lot of attempts for optimising it. Indeed, this switch altered not only potentially the way of interaction with the therapeutic target but also the reactivity of the aromatic ring that has to be para-substituted. The optimisation process of the synthetic pathway has been illustrated in the next scheme.



Scheme 4. Optimization process of the synthetic protocol for the obtainment of a compound with a nitrogen atom in position R_3 .

As it is visible in scheme 4 a lot of efforts have been done with the aim to obtain a compound that presents a hydrogen bond donor in position R₃. The first synthetic attempt (A) tried to follow the same procedure of the previous classes of compounds. In this case the first nucleophilic substitution happened but it required much higher temperatures. This is due to the fact that in this primary ammine the nucleophilic behaviour, typical of this functional group, is strongly downregulated and quenched by the attached aromatic ring which delocalize the unpaired electrons of the nitrogen within the conjugated system of the ring. After the obtainment of this synthon, the Friedel-Crafts acylation have been tried. Unfortunately, this reaction does not lead to the obtainment of the desired compound. Indeed, this synthetic step led to the obtainment of the amide of the secondary amine in modest quantities. This is due to two different reasons. First, aniline rings can not undergo Friedel-Crafts reaction because the nitrogen atom, although it is considered a strong activator of the aromatic ring that allows para and ortho substitutions, in this case it complexes the aluminium as a Lewis base. Nitrogen involves its unpaired electrons for doing this and consequently the activation of the aromatic ring is reduced blocking the para substitutions. The small percentage of aniline rings that are not involved in the complexation of the Lewis acid are better nucleophile than the para position of the aromatic ring and they promote the amide bond formation. With the aim to avoid this side reaction and with the intent to reduce the complexation capacity of the aniline ring, an amide with acetyl chloride of the secondary amine have been done. Also in this case the Friedel-Crafts reaction does not happen and this was due probably to the fact that the amide bond still coordinates the aluminium ion. Another explanation could be that the amide itself reduces the activation of the aromatic ring because the unpaired electrons of the nitrogen atom are now delocalized also on the amidic bond reducing their delocalization within the aromatic ring.

In the second synthetic approach a new idea has been tried. In this case a Fries type rearrangement have been adopted for the transformation of the acetanilide in the para-aminoacetophenone. Fries rearrangement is a typical reaction that have been widely studied for phenolic esters, but during the last decade, several successful attempts have been done also with anilides. Historically the reaction is catalysed by Brønsted or Lewis acids such as HF, AlCl₃, BF₃, TiCl₄ or SnCl₄. The acids are used in excess of the stoichiometric amount, especially the Lewis acids, since they form complexes with both the starting materials and products.

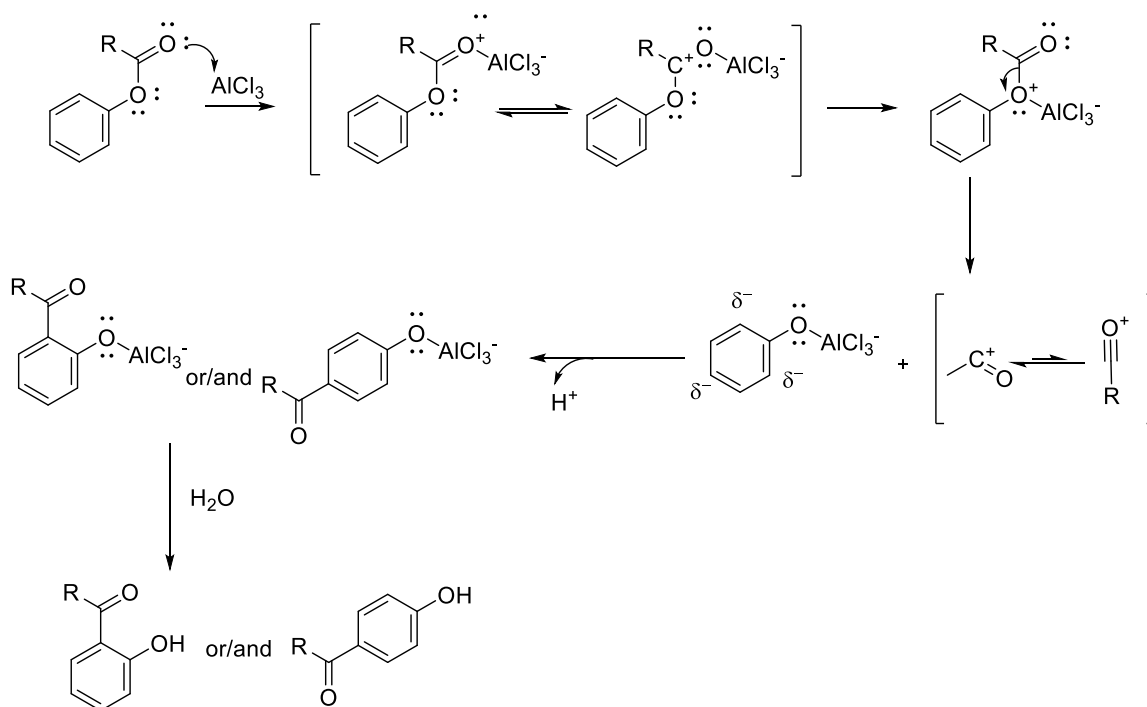


Figure 36. Reaction mechanism of Fries rearrangement. A similar mechanism is adopted also in case of the use of strong acids.

Considering that the complexation of the aniline intermediate strongly disfavours the acylation of the aromatic ring other mechanisms of reaction have been developed for anilides during last years and these have been tried for the obtainment of the para-aminoacetophenone. The use of strong acids instead of Lewis acids have been demonstrated effective for these types of substrate. Unfortunately, in this case this protocol does not lead to the obtainment of the desired compound. It has been shown that also UV irradiation can favour the Fries rearrangement.^[134]

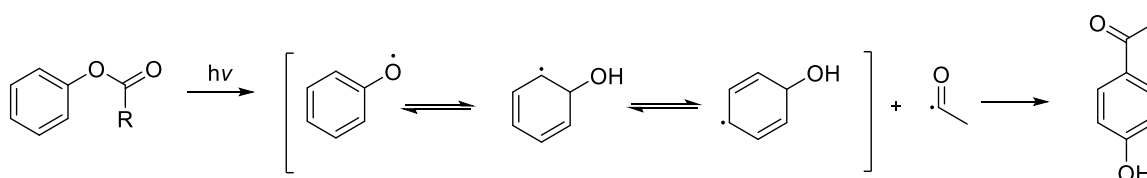


Figure 37. Reaction mechanism of the Fries rearrangement under UV irradiation.

Also in this case, after illumination with a TLC lamp at 254nm, no traces of the desired compound have been revealed.

Pathway C presents another possible solution for the obtainment of the para-aminoacetophenone synthon. It has been demonstrated by Corby et. al. that Friedel-Crafts acylation can be conducted in Lewis acid free environment.^[134] This is a desirable condition for avoiding the deactivation of the aromatic ring. This procedure provides the utilize of trifluoroacetic anhydride and phosphoric acid as activating agents and catalyst respectively, for the acylating agent that in this case is acetic acid. This mixture forms in-situ complex mixed anhydrides that super activates the acylating acid favouring the acylation of the aromatic ring. For avoiding the formation of the amide bond, the aniline has been already reacted with acetyl chloride. Also in

this case the desired compound have not been obtained. The reason of this unsuccess could be that the strong acidic environment tends, despite the amide bond, to slightly protonate the nitrogen atom increasing the deactivation of the aromatic ring.

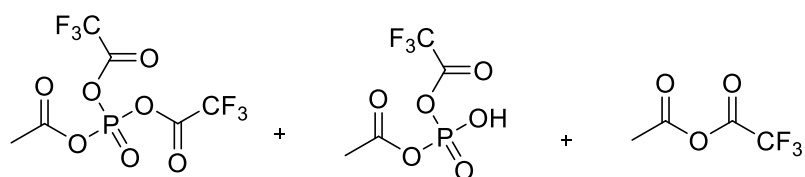


Figure 38. Chemical structure of the mixed anhydrides formed during the reaction.

The last synthetic protocol has been the successful one. In this case the aniline ring has been abandoned and substituted with the 4-nitroacetophenone synthon. The first synthetic step was a Mannich reaction that led successfully to the obtainment of the desired propyl spacer and the morpholine polar head. For this reaction 1.5 equivalents of paraformaldehyde and morpholinium chloride were used and the reaction has been conducted in microwave, reducing the time requested for its completion. Considering that this reaction is an equilibrium, the full conversion of the 4-nitroacetophenone is difficultly achievable, but fortunately the desired compound is isolated selectively through precipitation, rendering the non full conversion not a problem. The mechanism of reaction is illustrated in the following picture.

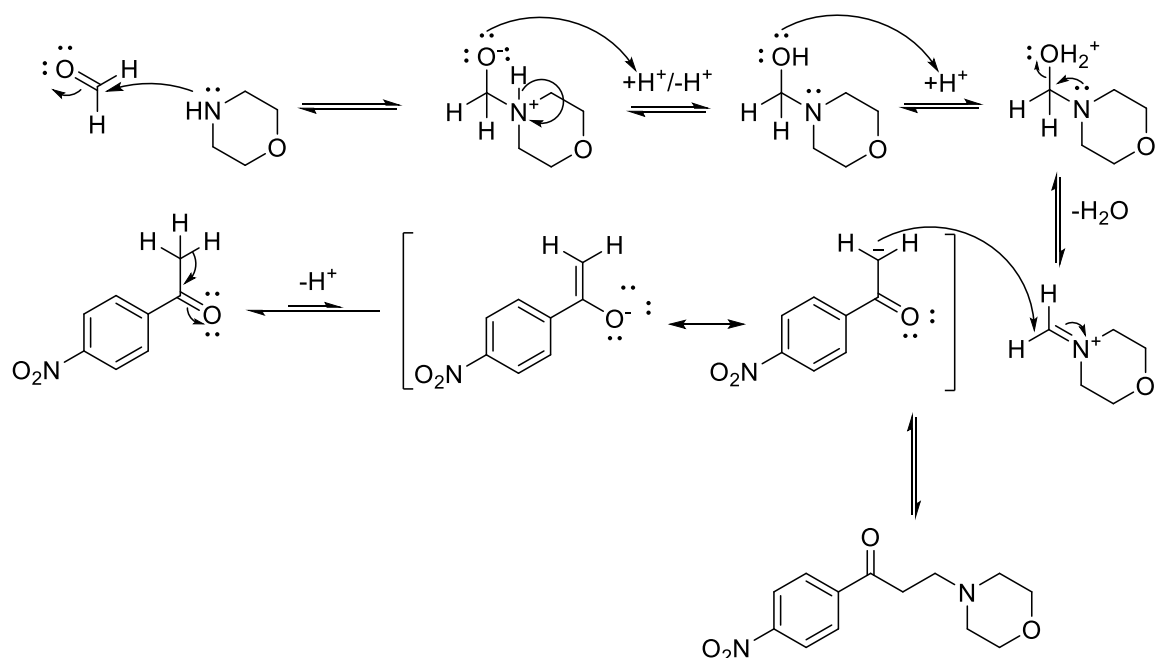


Figure 39. Reaction mechanism of the Mannich reaction.

The following step has been a selective reduction conducted with $\text{SnCl}_2 \cdot 2\text{H}_2\text{O}$, and this passage did not present particular difficulties. The last procedure for introducing the desired alkyl tail on the aniline ring has been particularly problematic. First, the nitrogen atom is attached to an aromatic ring and it has in para position a carbonyl group. Both the groups reduce the nucleophilicity of the primary amine through electronic mechanisms that involve the conjugated system of the phenyl moiety and the higher electronegativity of the carbonyl function. Furthermore, the carbonyl in

para position increase the delocalization of the unpaired electron pair of the nitrogen atom for resonance reasons (Figure 40).

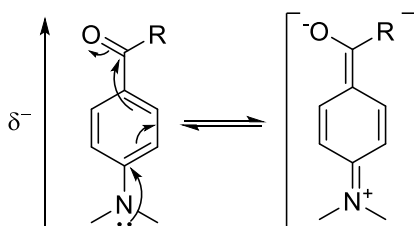


Figure 40. Delocalization mechanism of the unpaired electrons of the nitrogen atom.

All these conditions significantly reduce the nucleophilicity of the aniline ring consequently reducing the reactivity of the system. Another problematic encountered in this last step is the weakness of this Mannich base. Indeed, as previously mentioned the formation of the propyl spacing group with the morpholine nucleus at one end and the para-nitroacetophenone at the other (Mannich base) is an equilibrium process and it can be reverted generating the starting materials. This degradation process is pH sensible. It has been demonstrated that these Mannich bases have a maximum of stability around pH 2 and they start to degrade faster if the pH is altered at lower or higher values.^[135] In these experiments it is evident that higher pH leads to faster degradation rates. This is a problem for the obtainment of the final compound, because usually nucleophilic substitutions require the use of a base for buffering the release of acid that intervene during the reaction, and consequently leading to completion the process. In this case it was not possible to pursue this strategy because with the use of triethylamine or sodium carbonate the Mannich base started to degrade at fast rates. It has been observed that even the samples used for TLC start to degrade spontaneously and rapidly in DCM solutions. This never happened also with the final compounds previously synthesized that present the Mannich base portion. Probably, the resonance forms generated by this synthon increase the degradation rate. For overcoming this problem, the reaction has been buffered with Na_2HPO_4 and NaH_2PO_4 , moreover, silica gel for TLC have been used as catalyst. Indeed, in several paper it has been demonstrated that the silanols group of silica can activate the alkylating agent and temporarily adsorb and coordinate amines. These two groups are in close contact one to each other favouring the reaction. This kind of approach allowed the formation of the final compound that has been purified through silica gel.

This molecule presented several problems also during the phases of solvent evaporation and storage. Indeed, this compound had never reached the solid state, it is a viscous amorphous solid and it tends to become red during storage showing its propension to degrade. Probably it reacts giving a β elimination product as shown in figure 41.

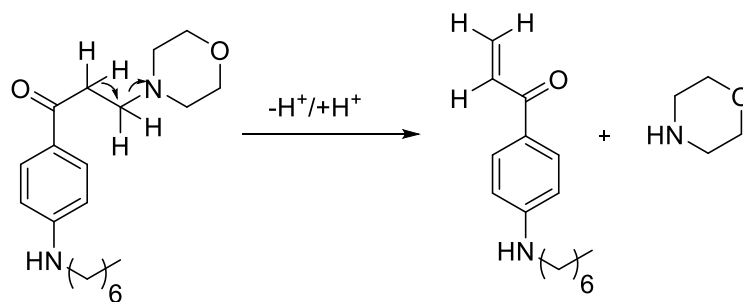
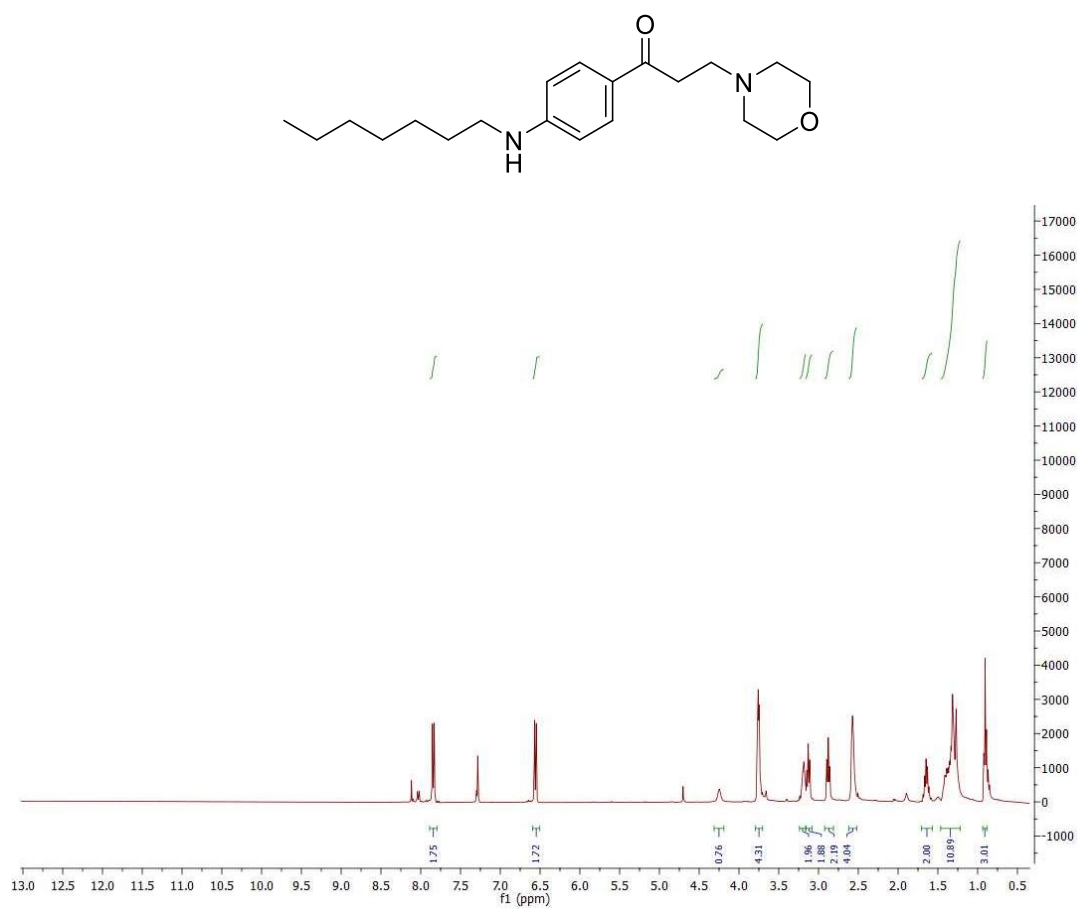


Figure 41. Supposed degradation mechanism of the isolated compound.

The synthesized compound is reported below.

Number of the compound	Chemical structure	IUPAC name
FA-A1		1-(4-(heptylamino)phenyl)-3-morpholinopropan-1-one

Example of NMR characterisation



^1H NMR (400 MHz, CDCl_3)

3.1.1.2 Chimeric compounds of ApoE deriving peptides and Fingolimod analogues

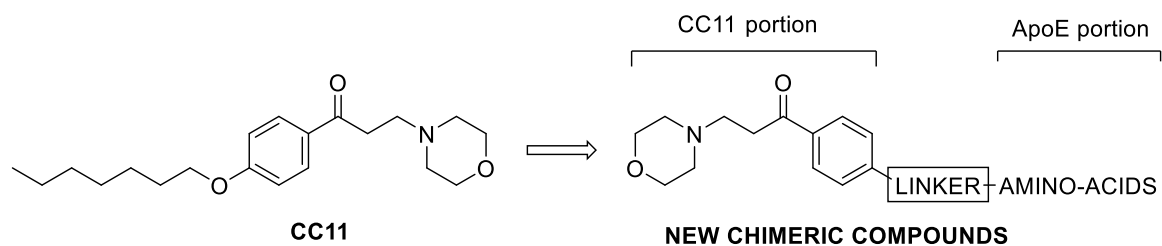


Figure 42. General molecular scaffold of the new chimeric compounds.

The second category presented in this paragraph includes a series of compounds whose molecular structure derives from a fusion of some features of the already shown classes of fingolimod analogues with small peptide chains. This idea was derived by two different hypotheses. The first thought has been to substitute the long hydrophobic alkyl chain of CC11 and Fingolimod with a much more hydrophilic structure like an amino acid tail is. The introduction of new functionalities that could generate a larger number of interactions with the protein target could also increase the potency of the derived compounds. The second idea was to introduce in the chemical structure of this class of molecules not just general and randomised sequences of amino acids but instead short peptides whose sequence is derived from the amino acid chains that have shown to be able to disrupt the PP2A/SET complex reactivating the phosphatase. This modification should produce a synergic effect obtaining a chimeric compound that should present both the positive characteristics of the original compounds. For this reason, the library of small peptide ApoE derivatives, synthesized by Vitek and colleagues, has been analysed and took as a model. From this study a short sequence of four amino acids has been used for the synthesis of the chimeric compounds (LRKL). The chosen tetrad of amino acids represents the core of all the ApoE mimetics and in some of them it is repeated almost identical in other portions of the peptide. Considering that the adopted sequence is highly symmetric also the scrambled sequence has been synthesized (LKRL). This modification aims to understand if the key determinant for the interaction with the target enzyme is the sequence itself or the global positive charge of the amino acids. Indeed, the C-terminal portion of SET, the identified target of Fingolimod and of ApoE derivatives, presents an amino acid sequence enriched in negatively charged amino acids and this could be the preferential site of interaction of this positively charged amino acid tetrad.

The complex part of this project has been the identification of a suitable linker between the CC11-derived portion of the molecule and the ApoE one. Indeed, the first idea has been to exploit the 1-(4-aminophenyl)-3-morpholinopropan-1-one compound, whose synthesis have been presented in the previous pages, and attaching to the aniline portion of the molecule the carboxylic group of one amino acid, in this case a Boc-glycine. This strategy exploits for the synthesis of the amide bond the in-situ formation

of the activated carboxylic acids using for this goal TBTU and triethylamine (TEA).

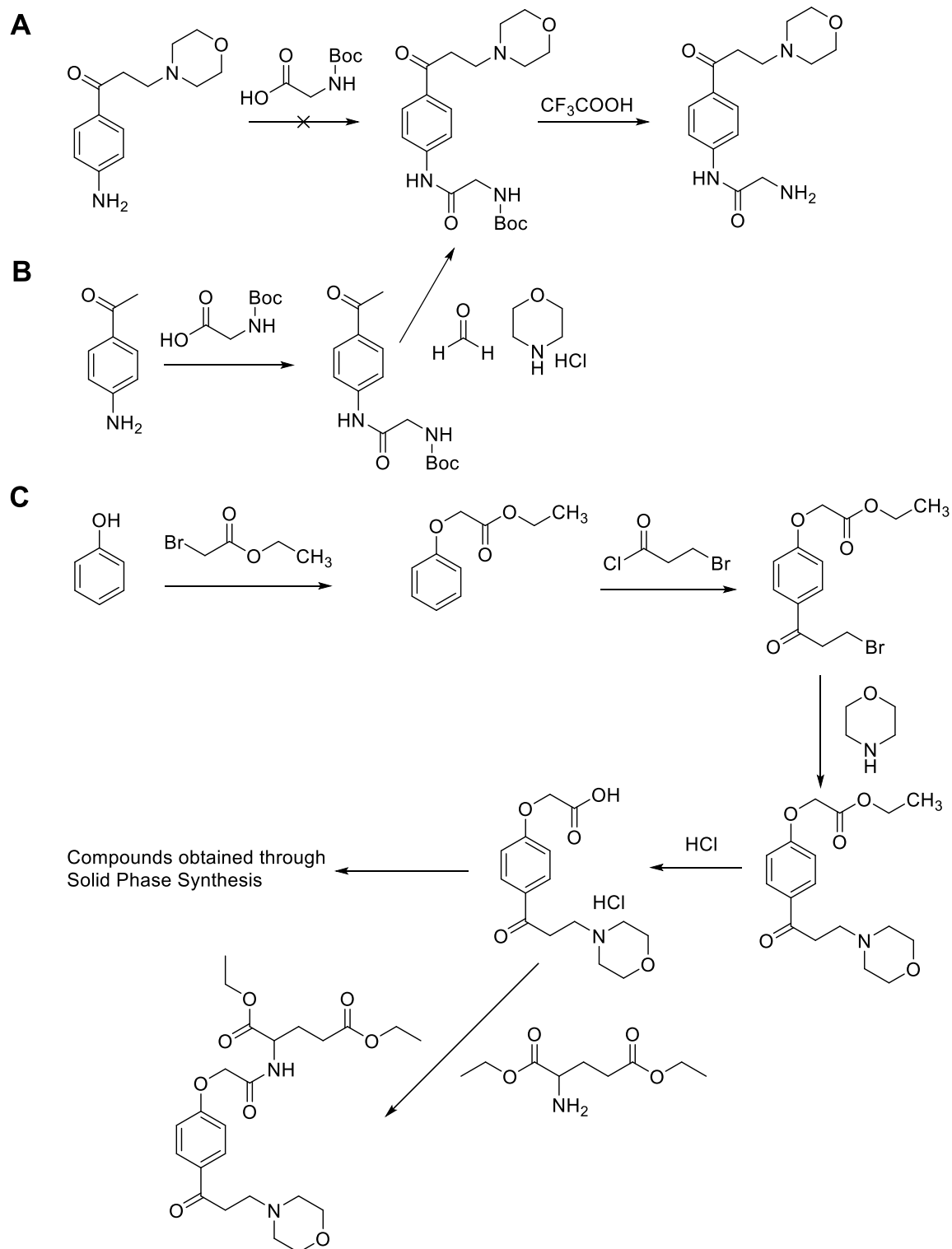


Figure 43. Synthetic protocol adopted for the synthesis of the chimeric ApoE/Fingolimod analogues.

As in the previous case, the starting material was not stable in the basic environment and degraded fast not allowing the isolation of the desired compound. For this reason, the second synthetic protocol used the para-aminoacetophenone as starting material. In this case the use of TBTU and TEA had the desired effect of obtaining the amide

bond between the Boc-glycine and the para-aminoacetophenone. The following step has been the Mannich reaction and subsequently the removal of the Boc protecting group from the molecule has been performed using trifluoroacetic acid. The isolated compound should be used for the attachment of the other amino acids using the free amino group of the glycine. It has been preferred to introduce a glycine as spacer between the amino acid chain and the phenyl ring for facilitating the coupling reactions between the two portions of the molecule, and consequently increase the yields of the adopted convergent strategy. Indeed, considering the instability of the 1-(4-aminophenyl)-3-morpholinopropan-1-one group and its poor reactivity, it seemed preferable to introduce a much more reactive functional group as the alkyl primary amine of the glycine. Also in this case the purified compound was not stable during storage and it presented poor physical-chemical properties, indeed it has been impossible to obtain a stable solid but the final compound was a viscous amorphous solid difficultly manageable.

Consequently, facing with the problematics encountered during the synthesis of the anilino derivatives, it has been decided to return to the original phenolic scaffold that has shown much better physical-chemical properties. Synthetic pathway C utilizes phenol as starting material. The first step of reaction has been a nucleophilic substitution between phenol and ethyl 2-bromoacetate. The reaction did not present any problems and the obtained molecule has been utilized for the following step.

The second step is catalogued as a Friedel-Crafts acylation of the phenolic ether. Also in this case there were not any complications and the same happened during the subsequent step, where the morpholine polar head has been introduced in the molecular scaffold. The last step of the synthetic protocol, that led to the obtainment of the desired synthon useful for the synthesis of different amino acid derivatives, required a bit of reasoning. Indeed, usually for breaking an ester bond an alkaline environment is preferred because it gives better results and yields. In this case it is not possible to adopt such a protocol because, even if the phenolic-based Mannich bases are much more stable compared to the aniline ones, the propyl spacer could be easily disrupted generating the acetophenone derivative. For this reason, an acidic hydrolysis has been preferred, which preserve majorly the stability of the synthesized compound. This kind of reasoning revealed to be right and led to the obtainment of the desired synthon. Subsequently, the synthesized compound has been utilized in two different synthetic approaches:

- In-solution peptide synthesis;
- Solid phase synthesis.

The first strategy has been adopted for monitoring the stability of the compound during the phases of amide coupling, for checking the robustness of the process and the degree of purity of the final compound. For the in-solution peptide synthesis TBTU and TEA have been used and a glutamic acid di-ethyl ester has been chosen as coupling amino acid. Figure 44 illustrates the general mechanism of reaction of the TBTU mediated amide coupling.

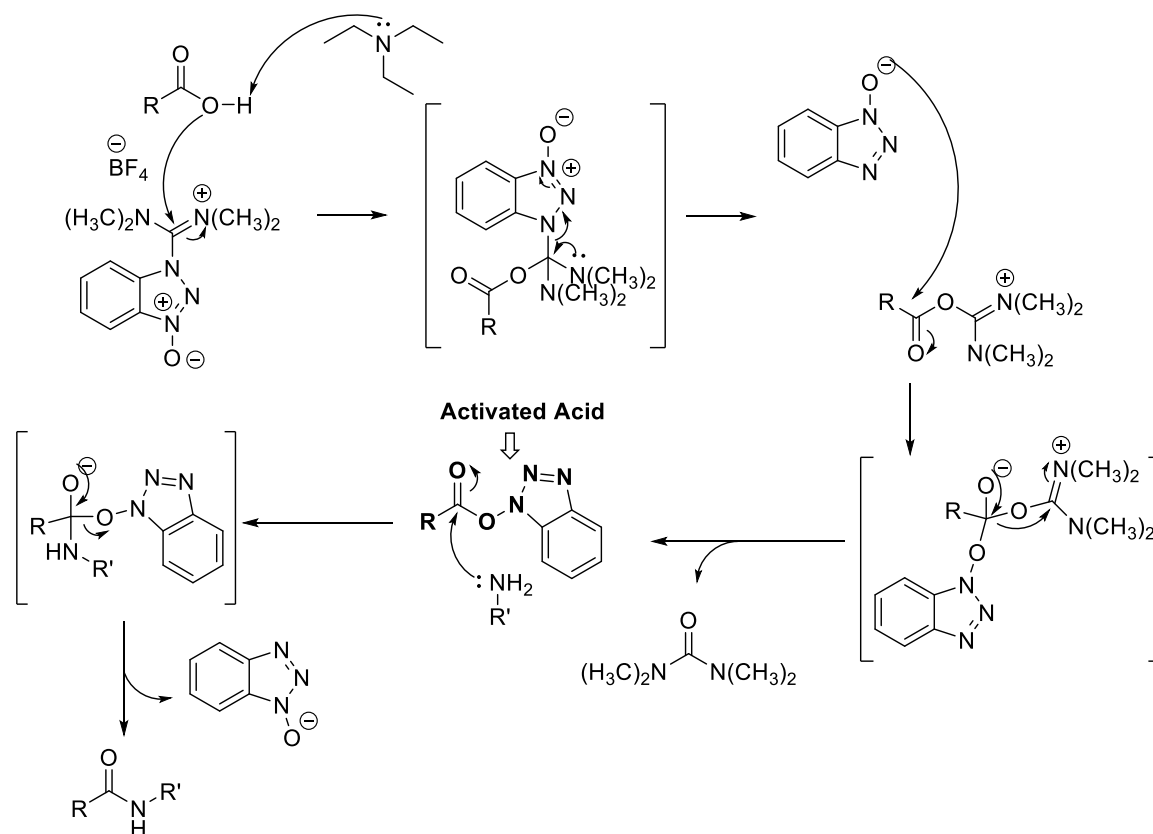


Figure 44. Reaction mechanism of the TBTU mediated amide coupling.

The first passage consists of the deprotonation of the carboxylic acid by TEA, then through electrostatic forces, the carboxylate reacts with the uronium portion of the TBTU molecule through a substitution mechanism that resembles that of a nucleophilic substitution. This leads to the formation of a 1H-benzo[d][1,2,3]triazol-1-olate and a uronium derivative of the carboxylic acid. These two intermediates are too unstable and remain in close proximity one to each other for electrostatic interactions. This facilitates the second step of the reaction where the 1H-benzo[d][1,2,3]triazol-1-olate reacts with the uronium centre of the other intermediate obtaining the HOBt ester, which is the activated form of the carboxylic acid, and as by-product a molecule of tetramethyl urea. The HOBt ester undergoes amino lysis with the primary amine of an amino acid obtaining in this way the desired amide bond.

This test reaction has shown no critical issues leading to the obtainment of the final compound with good yields. For this reason, a second synthetic strategy has been adopted: the Solid phase peptide synthesis. This kind of synthesis has been developed for the sequential synthesis of peptides using a solid support for the elongation of the amino acid chain. All the reactants necessary for the elongation are added in solution while the elongating peptide is covalently attached to a solid phase, that usually is constituted by resin beads which are able to swell and increase the overall exposed surface in the solvent of the reaction. This swelling allows to the elongating peptide to behave like if it is in solution. This kind of approach has several advantages:

- The isolation of the product or the intermediates, from the contaminants present in solution is much easier than the in-solution approach. Indeed, it is necessary just to filter the insoluble resin and wash it thoroughly.
- This particular feature allows to use a large excess of all the soluble reactants, and consequently this increases the yields and it reduces the time required for the completion of the reaction.

At the same time the solid phase peptide synthesis presents also some drawbacks:

- It is not possible to check the identity of the elongating structure till it is attached to the resin. It is necessary to detach the peptide for analysing it and understand if its sequence is correct or not.
- For the previously mentioned reason, this approach is not suitable for performing explorative reactions, especially if there is the suspect that there could be some side reactions that could impact the final outcome of the reaction.

For this last reason, it was not possible to directly adopt a solid phase peptide synthesis approach with our phenolic-derived Mannich base.

With this kind of synthetic approach, several peptide derivatives have been obtained. Some of these are just explorative, for experimenting different chains and for testing the solid phase peptide synthesis with our synthon, and others present the desired tetrad. All the obtained compounds share two common features: they have as N-terminal the synthon previously synthesized and as C-terminal a glycine amino acid. This last characteristic derives by the fact that the resin used for the synthesis was a Wang resin decorated with an Fmoc-glycine amino acid residue. The choice of using an already functionalized resin was imposed by the fact that these commercially available resins are well characterised, and it is already known their loading. This facilitates all the following reaction procedures. Furthermore, the step of resin loading is usually the longest and most laborious, so for time consuming reason and considering that this resin was already available in our laboratory, it has been preferred to a functionalizing it. This decision has been supported also by the fact that these first peptide-derivatives are merely explorative for testing the general idea. Considering that an extra glycine residue does not introduces dramatic changes in the final sequence, this compromise has been accepted. In case of success of this strategy, a more rigorous approach will be adopted.

The solid phase peptide synthesis is a simple synthetic strategy and it is composed by several steps that are repeated for each attached amino acid residue of the peptide (Figure 45).

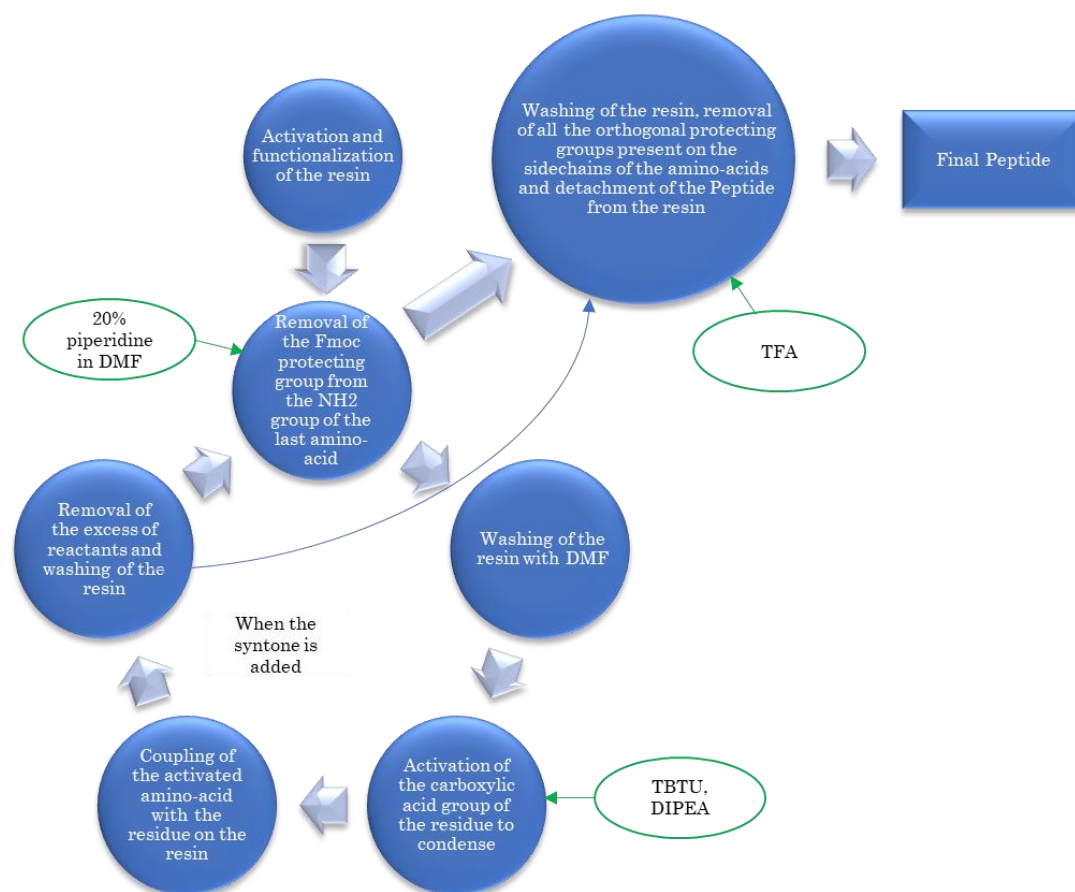


Figure 45. Representative scheme of the synthetic pathway adopted during the solid phase peptide synthesis.

The first step of this process has been the removal of the Fmoc protecting group from the α -amino group of the amino acid. This step is repeated for each amino acid added to the chain; it is skipped when the synthesized synthon is introduced at the N-terminal of the peptide because it does not present amino groups that can form an amidic bond. This is also the reason why the elongation of the amino acid chain is blocked. The protection of the α -amino group is fundamental for avoiding the attachment of more than one amino acid per time, indeed, if the amino group was not protected, once the amino acid is installed on the peptide it could immediately react with another residue altering the amino acid sequence. Fmoc is used as protecting group because its removal is obtained in basic condition (20% piperidine in DMF) and it does not affect the linkage of the peptide to the resin that is acid labile. After freeing the amino terminal group, the resin is washed for removing all the reactants in excess and the obtained by-products; then the α -carboxylic acid of the following Fmoc protected amino acid is activated with TBTU and N,N-diisopropylethylamine as base. The subsequent step is a coupling reaction between the activated carboxylic acid of the new amino acid and the N-terminal of the peptide anchored to the resin. After this step the resin is newly washed and the whole process is repeated. After this, when the previously synthesized synthon is reacted with the peptide and the resin is thoroughly washed, all the orthogonal protecting groups, localized on the functional groups of the amino acid side chains, are removed. These protecting groups are fundamental during

the peptide synthesis, indeed, they mask the nucleophile sites present on the amino acid side chains and in this way, they prevent side reactions. If this does not happen the addition of the activated carboxylic acid could react with the alpha amino group of the amino acid backbone or with the side chain of the amino acids making impossible to control the elongation process. During this solid phase peptide synthesis several protecting groups that are orthogonal to Fmoc have been used: Boc group for the ϵ -NH₂ of the lysine's side chain, Mtr and Pbf for the guanidine portion of Arginine's side chain. These protecting groups are stable to basic environment and, as for the linkage between the peptide and the resin, they are acid labile. For this reason, the removal of the orthogonal protecting groups and the detachment of the peptide from the resin are done contemporarily using TFA/H₂O. Then the resin is filtered from the TFA solution which contains the final peptide. The desired molecule is finally precipitated as TFA salt after the addition to the TFA solution of diethyl ether.

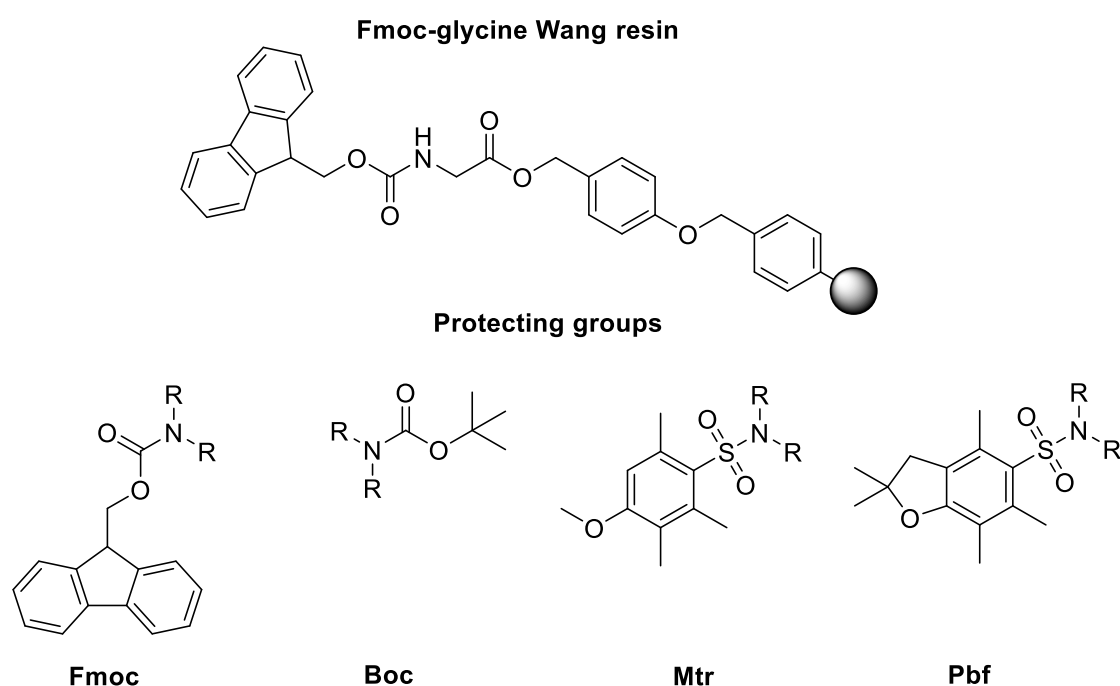


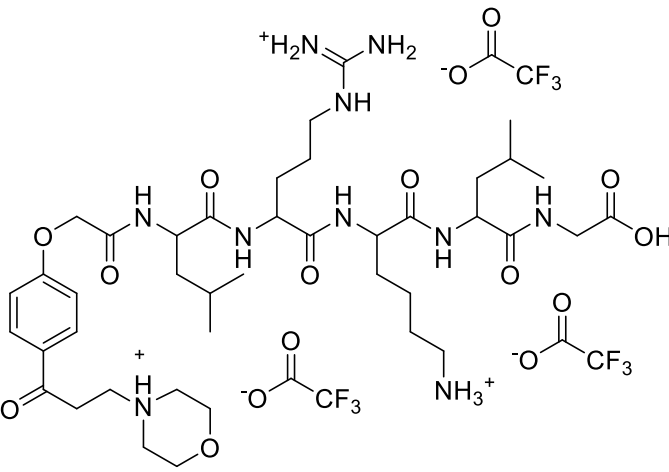
Figure 46. Chemical structure of the Fmoc-glycine Wang resin and of all the protecting groups used during the solid phase synthesis.

The whole process is robust and reproducible for all the synthesized compounds leading to the obtainment of several molecules. The only note that has to be done regards the choice of the protecting group of the guanidine portion of Arginine. The first attempt of synthesis of the desired sequence LKRL included as protecting group a Mtr group. This protecting moiety was not easily removed by the cleavage in TFA and a lot of time was necessary for its removal. This could be a problem considering that the Mannich bases are instable also in strong acidic environments, and so it was not optimal to leave the final compound in TFA for such a long time. For this reason, another protecting group has been used: Pbf. Pbf was much easier to remove compared to Mtr. The first peptides that still present the Mtr protecting group have been conserved because this additional functional group could have some beneficial effects for the interaction with the pharmacological target.

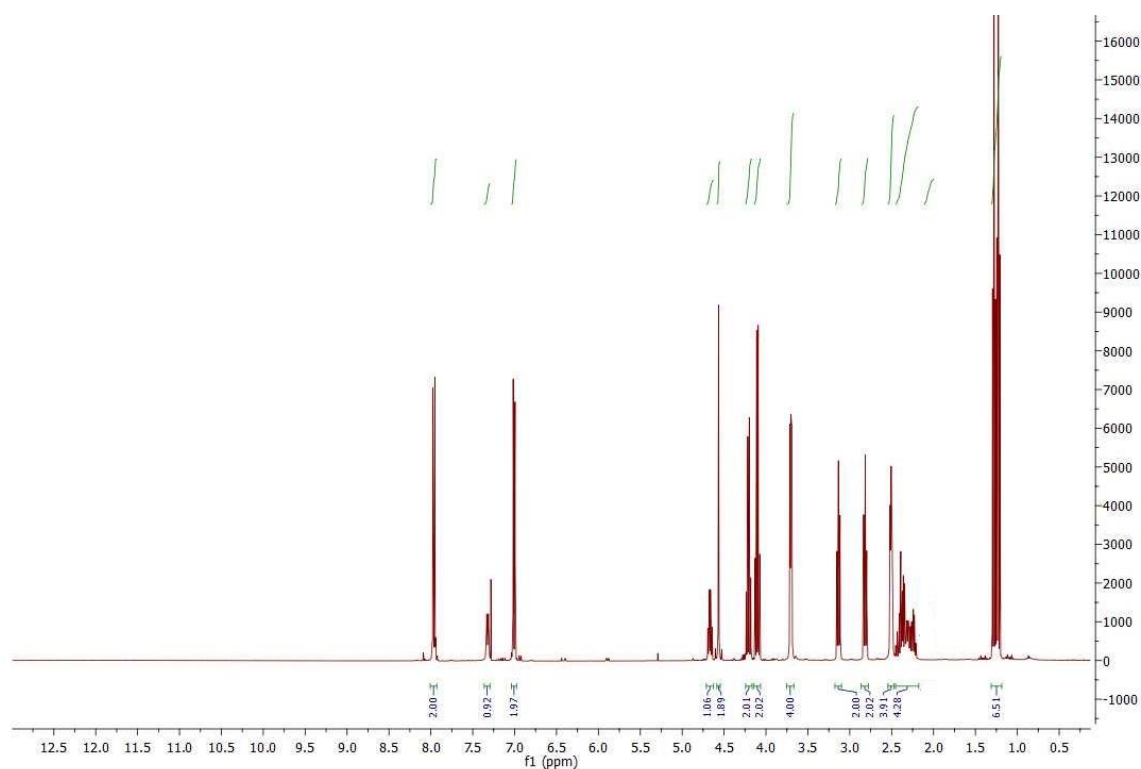
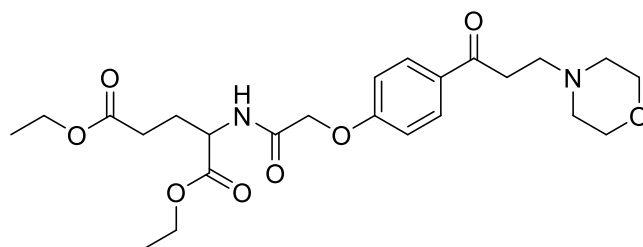
The following table reports all the synthesized compounds of this class.

Number	Chemical structure	IUPAC
AEFA-01		2-amino-N-(4-(3-morpholinopropanoyl)phenyl)acetamide
AEFA-02		4-(3-(4-(carboxymethoxy)phenyl)-3-oxopropyl)morpholin-4-ium chloride
AEFA-03		diethyl (2-(4-(3-morpholinopropanoyl)phenoxy)acetyl)glutamate
AEFA-04		4-(3-(4-(2-((carboxymethyl)amino)-2-oxoethoxy)phenyl)-3-oxopropyl)morpholin-4-ium 2,2,2-trifluoroacetate
AEFA-05		4-(3-(4-(2-((1-((1-((carboxymethyl)amino)-3-methyl-1-oxopentan-2-yl)amino)-3-methyl-1-oxobutan-2-yl)amino)-2-oxoethoxy)phenyl)-3-oxopropyl)morpholin-4-ium 2,2,2-trifluoroacetate

<p>AEFA-06</p>		<p>4-(3-(4-((10-(4-ammoniobutyl)-1-carboxy-4,13-diisobutyl-7-(3-(3-((4-methoxy-2,3,6-trimethylphenyl)sulfonyl)guanidino)propyl)-3,6,9,12,15-pentaoxo-2,5,8,11,14-pentaazahexadecan-16-yl)oxy)phenyl)-3-oxopropyl)morpholin-4-ium 2,2,2-trifluoroacetate</p>
<p>AEFA-07</p>		<p>4-(3-(4-((7-(4-ammoniobutyl)-1-carboxy-4,13-diisobutyl-10-(3-(3-((4-methoxy-2,3,6-trimethylphenyl)sulfonyl)guanidino)propyl)-3,6,9,12,15-pentaoxo-2,5,8,11,14-pentaazahexadecan-16-yl)oxy)phenyl)-3-oxopropyl)morpholin-4-ium 2,2,2-trifluoroacetate</p>
<p>AEFA-08</p>		<p>4-(3-(4-((7-(3-((amino(iminio)methyl)amino)propyl)-10-(4-ammoniobutyl)-1-carboxy-4,13-diisobutyl-3,6,9,12,15-pentaoxo-2,5,8,11,14-pentaazahexadecan-16-yl)oxy)phenyl)-3-oxopropyl)morpholin-4-ium 2,2,2-trifluoroacetate</p>

<p>AEFA-09</p>		<p>4-(3-(4-((10-(3-((amino(iminio)methyl)amino)propyl)-7-(4-ammoniobutyl)-1-carboxy-4,13-diisobutyl-3,6,9,12,15-pentaoxo-2,5,8,11,14-pentaazahexadecan-16-yl)oxy)phenyl)-3-oxopropyl)morpholin-4-ium 2,2,2-trifluoroacetate</p>
----------------	--	---

Example of NMR characterisation



¹H NMR (400 MHz, CDCl₃)

3.1.1.2 Chimeric compounds deriving from TD-19 and CC11 chemical structures and attempt of synthesis of chimeric compounds deriving from TGI1002 and CC11 molecular scaffolds.

This part of the project has been focused on the development of chimeric compounds that present structural determinants coming from different molecules that are able to reactivate PP2A. In this paragraph two different project lines of chimeric structures will be presented. Just one of these has led to the obtainment of the desired molecules, while the other one has never produced the desired results. This unsuccess is due to the fact that there was not enough time for optimizing the synthetic route, but a plausible synthetic solution has been thought for a future development.

For the different origin of their chemical structure and for the different outcomes, the two classes will be presented separately.

TGI1002-CC11 chimeric compounds: Attempt of Synthesis

This first class of compounds has been thought with the aim to develop a chimeric structure that could combine the efficacy of two molecules whose activity is to breakdown the PP2A/SET complex. The two structures considered for this project are CC11 and TGI1002. The analysis of the two pharmacophores is shown in figure 47. The two hydrophobic regions of the different molecules are underlined with a red circle. While CC11 presents the classical alkyl chain, TGI1002 includes a pyrimidine core substituted in position 2 and 4. The position 2 is functionalized with a 3-aminophenolic aromatic ring, that despite its meta substitution pattern could resemble the para substituted phenolic ring of CC11. Position 4 presents a C-C bond that connect the pyrimidine core to a pyridine ring. Considering that, as already mentioned, the reduction of the flexibility of CC11 and the introduction of new functionalities, able to generate hydrogen bonds and other kind of interactions, could increase the potency of CC11 analogues, the hydrophobic tail of TGI1002 has been taken as model. The 2,4 substituted pyrimidine core has been adopted. Position 2 has been linked with the para substituted aromatic ring of CC11, while for synthetic simplicity position 4 has been functionalized with a 3-trifluoromethyl aniline that take the place of the basic pyridine ring. The hydrophilic portion of both the starting materials present a basic group, in one case is a N-methyl piperazine and in the other a morpholine ring. In this region a carbonyl group is present in both cases, in one structure it is part of an amide and on the other one of a ketone. In each one of the two structures the carbonyl group is separated from the basic ring with a hydrophobic spacer. All these features have been conserved also in the chimeric structure that present the classical propyl spacer and the morpholine moiety of CC11.

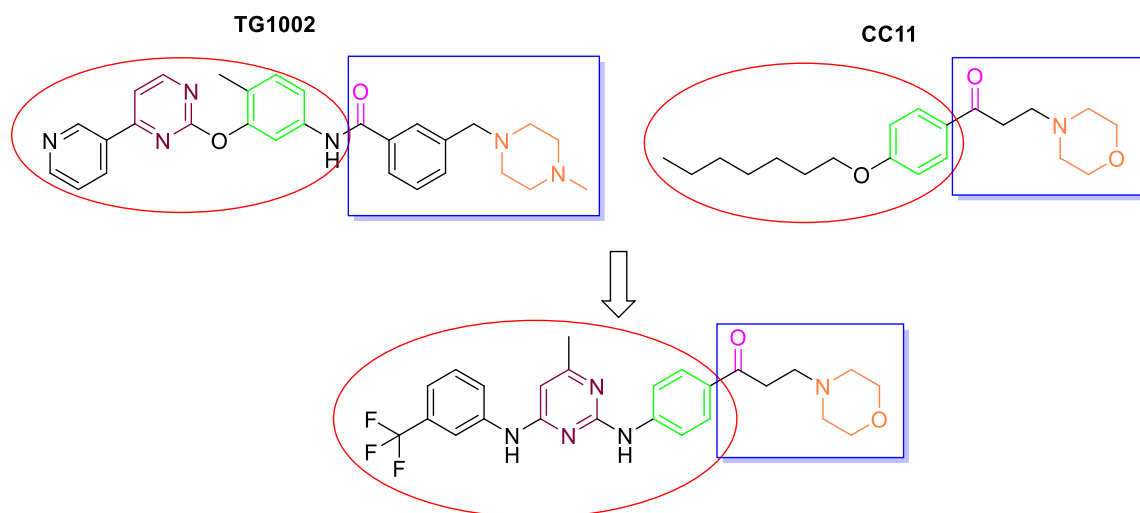
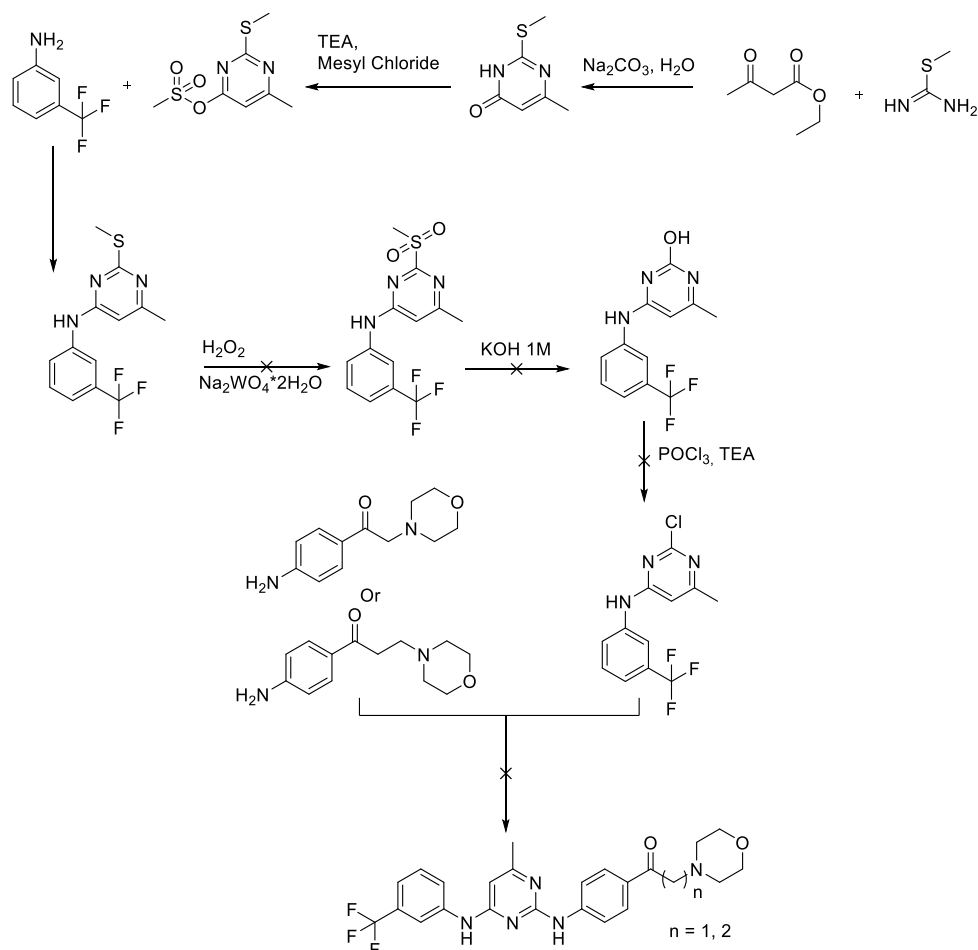


Figure 47. Pharmacophoric analysis of the molecular scaffolds of CC11 and TGI1002. With a red circle the hydrophobic portion of the two molecules is highlighted while the basic and polar moiety is underlined with a blue box. The key determinants of the structure that are conserved also in the chimeric molecule are evidenced with different colours.

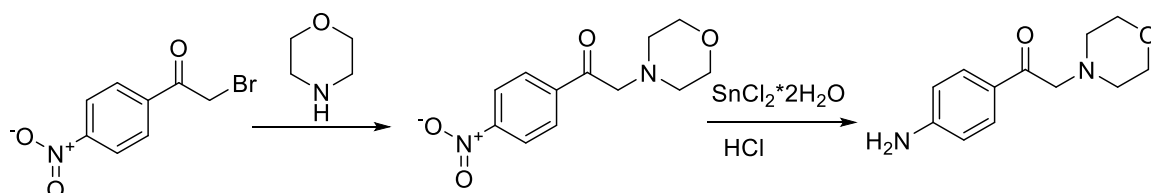


Scheme 5. Attempt of synthesis of TGI1002-CC11 chimeric compounds.

In the chimeric structure it has been thought to adopt as para substituted aromatic ring an aminoacetophenone structure instead of a phenolic one. This is due just to the

fact that this synthon was already available from the synthesis of the amino-based Fingolimod analogues.

Considering the instability of the amino-based Mannich bases it has been used an analogous synthon that includes instead of a propyl spacer an acetyl one. In this way it should not be possible to observe the degradation of the compound.



Scheme 6. Synthesis of 1-(4-aminophenyl)-2-morpholinoethan-1-one synthon.

The synthesis of 1-(4-aminophenyl)-2-morpholinoethan-1-one synthon is straightforward and resembles that one of the analogous molecule with a propyl spacer. In this case the first step includes a nucleophilic substitution between the starting material 2-bromo-1-(4-nitrophenyl)ethan-1-one and a slight excess of morpholine. The following step comprehends the selective reduction of the nitro group obtaining the desired compound.

The synthetic route designed for obtaining the final compound is quite long and complex. The first step consists in the synthesis of the pyrimidinone core; a β -dicarbonyl compound such as ethyl acetoacetate is cyclised with a N–C–N compound, in this case S-methyl isothiourrea (Figure 48). Differently from the pyrimidine ring of TGI1002, that was substituted in position 2 and 4, the synthesized one presents also a methyl group in position 6. This modification is due just to synthetic reasons, indeed in our laboratory it was readily available for the synthesis of the pyrimidine ring the ethyl acetoacetate. It could be possible that this extra functional group could alter the potency of the final compound, also in a negative way, but considering the complexity of the structure it seemed an acceptable compromise for testing this idea.

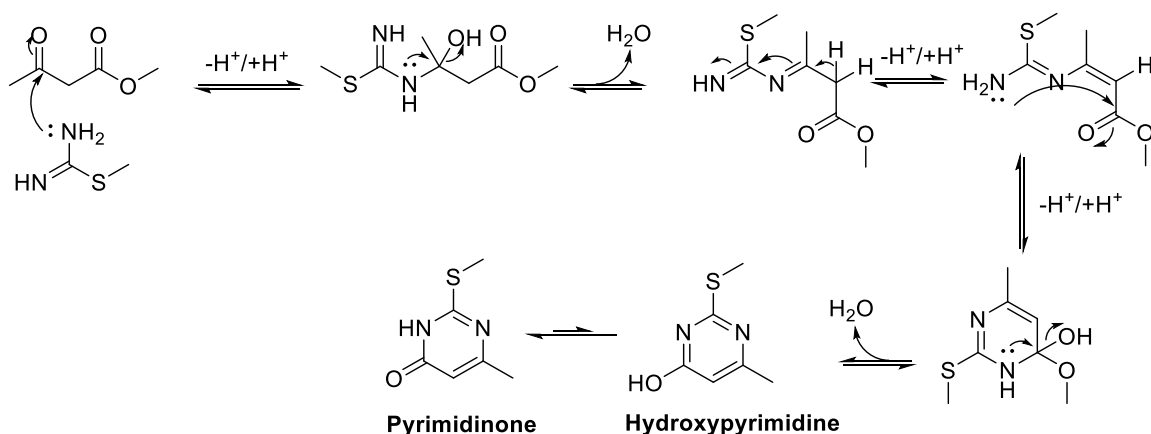


Figure 48. Reaction mechanism for the obtention of the pyrimidone ring.

The pyrimidone ring, the tautomer of the hydroxypyrimidine, has been synthesized with a thioether in position 2. This functional group is stable in this form and this allows to selectively activate for the nucleophilic substitution the oxygen atom present

in position 4 excluding in this way the possibility of side reactions in position 2. The thioether moiety can be activated and removed after oxidation and formation of the relative sulfone as will be illustrated further in this paragraph. Considering that position 2 is for the moment chemically inert to any kind of nucleophilic substitution, the hydroxyl portion present in position 4 can be easily manipulated for proceeding in the synthetic route.

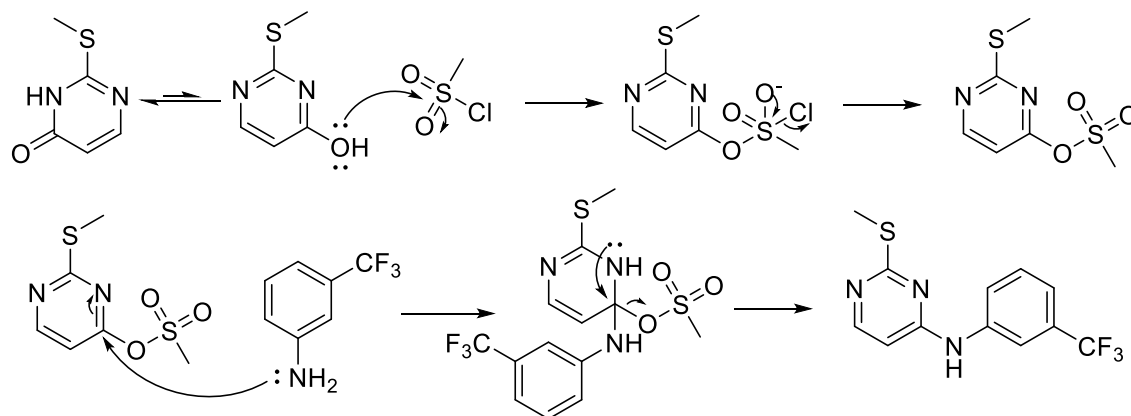


Figure 49. Reaction mechanisms for the synthesis of 2-(methylthio)pyrimidin-4-yl methanesulfonate and 2-(methylthio)-N-(3-(trifluoromethyl)phenyl)pyrimidin-4-amine.

The alcoholic group is not prone to undergo a nucleophilic substitution with the aniline derivative that has to be installed in that position. For this reason, the hydroxyl functional group has been transformed in a good leaving group reacting it with methane sulphonyl chloride. The reaction is a nucleophile substitution where the hydroxyl group of the pyrimidine ring acts as a nucleophile and the sulphonyl chloride as electrophile. This reaction generates a sulfonate ester that is the reactive species which allows the introduction of the 3-trifluoromethyl aniline on the pyrimidine ring. This functionalization reaction is a nucleophilic substitution and the leaving group in this case is the methane sulfonic acid. Both these synthetic steps are easy to do and allow to obtain the final desired synthon with good yields.

In the following synthetic step has been tried the oxidation of the methyl thioether for allowing the successive nucleophilic substitution and the introduction of a hydroxyl group in position 2. The oxidation process has been conducted using as oxidants hydrogen peroxide and sodium tungstate. The oxidation of the sulphur atom generates a pyrimidyl sulfone, which is a good leaving group and can be substituted in basic conditions (NaOH_{aq} 1M) with a hydroxyl group. Unfortunately, the oxidation step did not lead to the obtainment of the desired compound and the synthesis of this class of compounds has been stopped here.

For overcoming this limitation could be a good strategy to start the synthesis with the desired pyrimidine ring already functionalised in 2 and 4 with two chlorine atoms. That one in position 4 would be easily substituted by the desired aniline while for what concern position 2 further considerations have to be made. The conjugation of the aminoacetophenone rings with 2-chloro-6-methyl-N-(3-(trifluoromethyl)phenyl)pyrimidin-4-amine presents two drawbacks: the first one could be that the aminoacetophenone ring is not a good nucleophile for this reaction

for all the reasons elucidated in the previous paragraph. Another fact that could influence negatively the reaction is that the position 2 of the pyrimidine ring is not such a good nucleophile because the vicinal positions are two nitrogen atoms that with their unpaired electrons could quench the electrophilic behaviour of position 2. This condition is aggravated by the fact that in position 4 there is a nitrogen atom which could enrich the pyrimidine ring with its unpaired electrons quenching much more the reaction. For overcoming these limitations and for increasing the electrophilic behaviour of position 2 it could be a possibility to add a catalytic amount of concentrated HCl in the reaction mixture. In this way being the pyrimidine much more basic compared to the para aminoacetophenone group, it can be easily protonated. The protonation of one of the nitrogen atoms in position 1 or 3 transforms an electron donating group in a really efficient electron withdrawing group increasing in this way the electrophilicity of position 2.

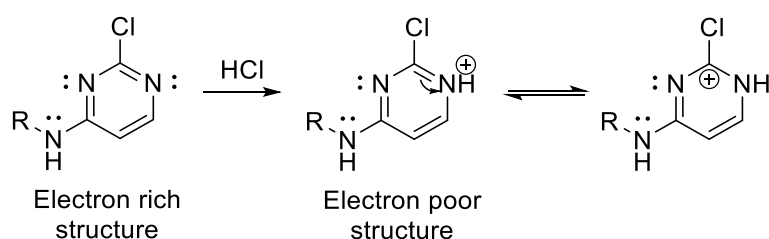


Figure 50. Proposed mechanism for the enhancing of the pyrimidine's electrophilic character mediated by the catalytic HCl.

This kind of strategy could help to overcome the synthetic problematics that could be encountered in this step and leading to the obtainment of the desired final compounds.

TD-19-CC11 chimeric compounds

As for the previous chimeric compounds, also in this case the designed molecular scaffold of the new compounds aims to conjugate the structural determinants that contribute to the efficacy of the original molecules in a unique scaffold. This molecular structure should maintain all, or at least the majority of, the benefits that the two starting compounds present, obtaining more potent and effective molecules. For this project two activators of PP2A have been chosen: CC11 and TD-19. Differently from the previous research line, this project tries to merge two structures that acts with two different mechanisms. Indeed, while CC11 reactivates PP2A disassembling the PP2A/SET complex, TD-19 acts downregulating the expression of CIP2A. The development of a chimeric compound that can interfere with both these PP2A inhibitors could be a great advantage. The new molecule could be effective in cancerous pathologies where SET or CIP2A are over expressed, separately or contemporarily. This kind of approach could be effective also for reducing the risk of resistances' onset. Indeed, tackling two of the principal mechanisms of PP2A's inhibition is difficult to assist to the enhancement of a third pathway that can overcome both these blocks.

Also in this case the design of the new chimeric structure started from the pharmacophoric analysis of the two starting molecules. Subsequently, a merging procedure has been adopted where the principal functional groups and molecular

structures of the two original compounds have been conjugated together in an unique structure (Figure 51). The new molecular structure presents a polar region that is derived from CC11 and includes the morpholine ring, the propyl spacer and the para amino substituted phenone group. TD-19 does not present merely hydrophilic portions and this could be one of the reasons why it does not interfere with the PP2A/SET. For this motive, it could be that the new compound continues to interact with PP2A/SET even if the alkyl chain has been substituted. The substitution has been performed with the quinazoline portion of TD-19. This structure resembles that one of TGI1002 and consequently it shouldn't affect the efficacy of the new compound's interaction with SET. The quinazoline portion is the core structure of TD-19 and it is reasonable to think that this could be the key determinant that mediates the downregulation of the CIP2A expression. For this reason, its introduction in the molecular scaffold of the new chimeric compounds should maintain the efficacy on CIP2A. The only modification that has been done to the quinazoline moiety has been the substitution of the alkyne group with a trifluoromethyl one.

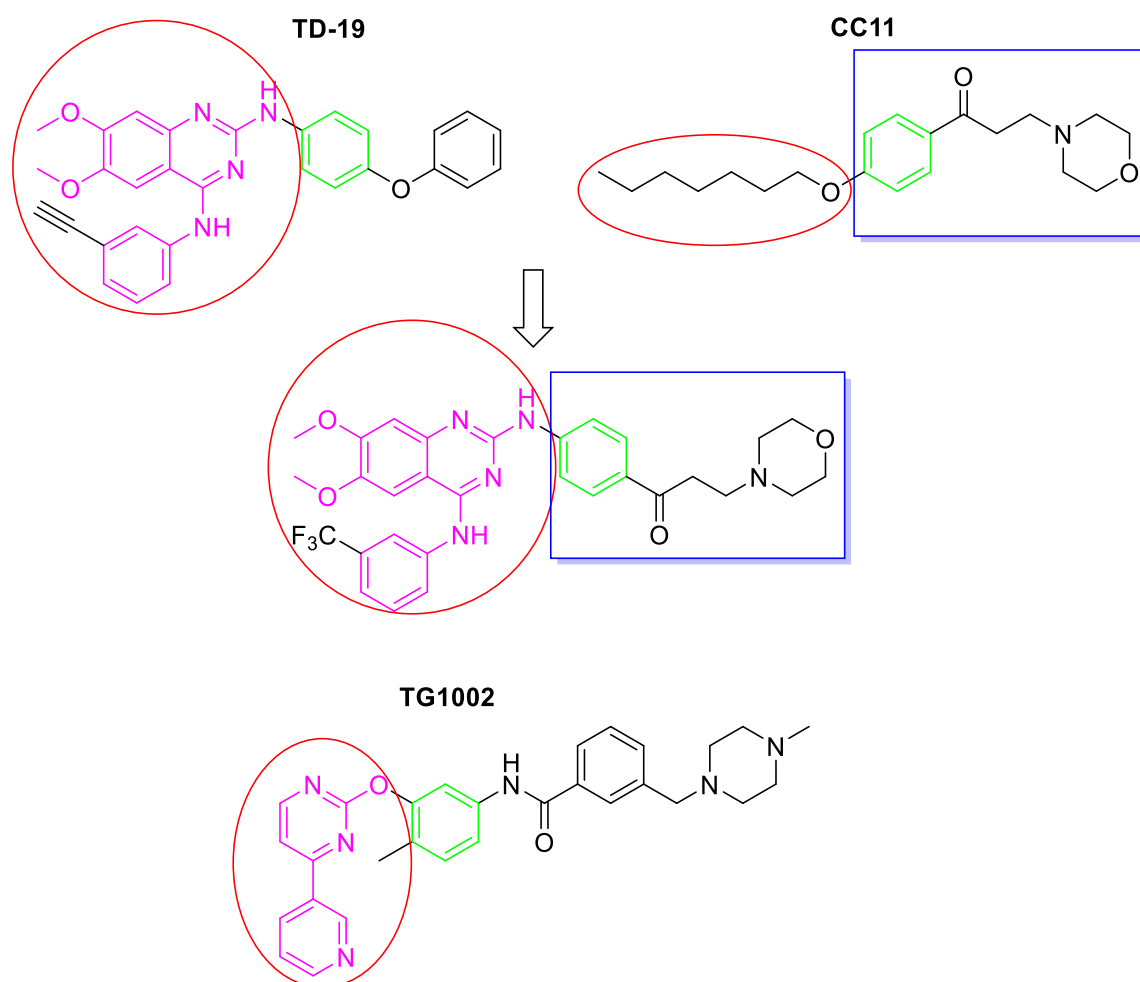
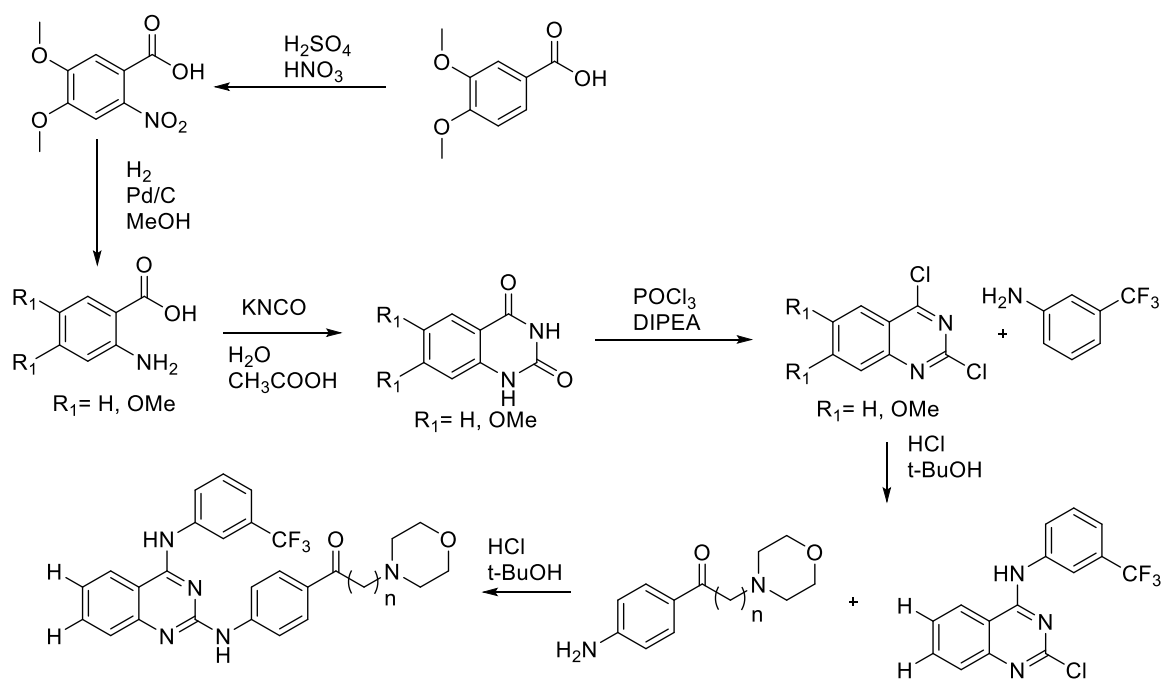


Figure 51. Pharmacophoric analysis of the molecular scaffolds of CC11 and TD-19. With a red circle the hydrophobic portion of the two molecules is highlighted while the basic and polar moiety of CC11 is underlined with a blue box. The key determinants of the structure that are conserved also in the chimeric molecule are evidenced with different colours.

With the aim to optimize the synthetic route of this new class of compounds the synthesis of analogues compounds that do not present the hydroxymethyl ether portions has been performed. After this, the synthesis of the desired compounds have been started but not finished for time reasons. It has been preferred to start with the synthesis of the analogues because the synthesis of the hydroxymethyl ethers ones requires two extra steps which were easy to perform, but the purification procedures were quite long and complexes.



Scheme 7. Synthetic pathway for the obtainment of the desired TD-19-CC11 chimeric compounds. The synthesis of the hydroxymethyl ether analogues has been stopped at the level of the 1,4-dichloroquinazolinone synthon.

The first extra step consists of an electrophilic aromatic substitution that leads to the nitration of veratric acid in position 5, with concentrated sulphuric and nitric acids. In this reaction the reactive species is the nitronium ion (NO_2^+). This ion is generated in situ for the presence of concentrated sulphuric acid which acts as dehydrating agent. Veratric acids has an aromatic ring that is enriched in electron density by the two hydroxymethyl units, and this activate the system for reacting with the nitronium ion. The phenyl structure is functionalized also with a carboxylic acid, which is a deactivating group that reduces the electron density of the system quenching its reactivity. The balance between the two opposite effects allows in any case the nitration of the compound. This functionalization could occur in all positions. Position 5 is preferred because is the only one that presents in para an activating agent, and this condition strongly favours the reaction.

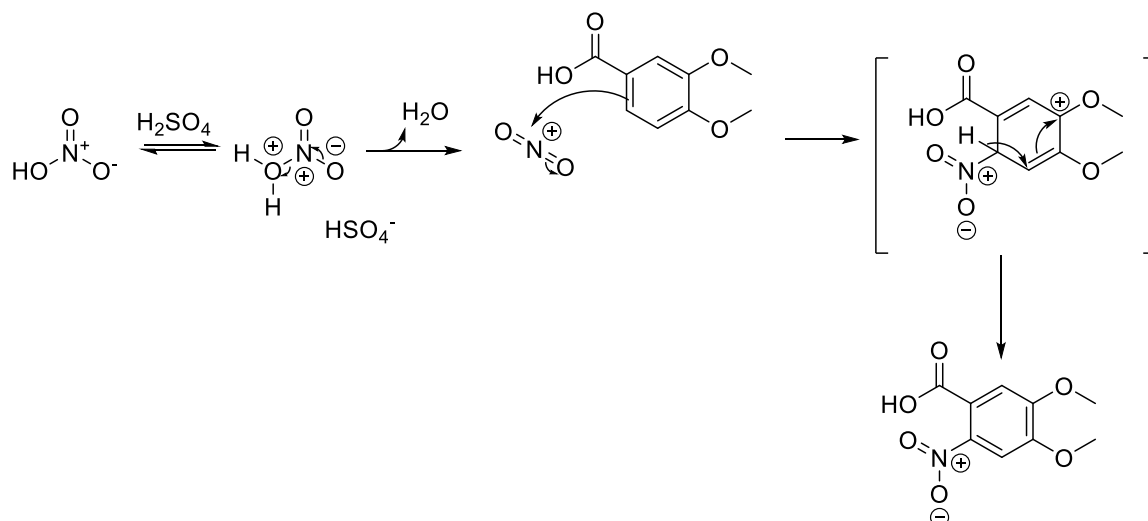


Figure 52. Reaction mechanism for nitration of veratric acid.

Subsequently, it has been performed the reduction of the nitro group obtaining the ortho amino benzoic acid derivative. From this point the synthetic strategies of both the molecular scaffold are identical. The first common step is the synthesis of the quinazoline core. The starting materials are the ortho aminobenzoic acids and potassium cyanate (KCNO), which have been reacted in acidic water ($\text{H}_2\text{O} + \text{CH}_3\text{COOH}$). The KCNO reacts first with the amine of the aromatic ring forming the respective urea functions, subsequently, catalysed by the acidic environment and favoured by the close proximity of the two reactive centres, there is the closing of the ring and the formation of the quinazolinone synthon.

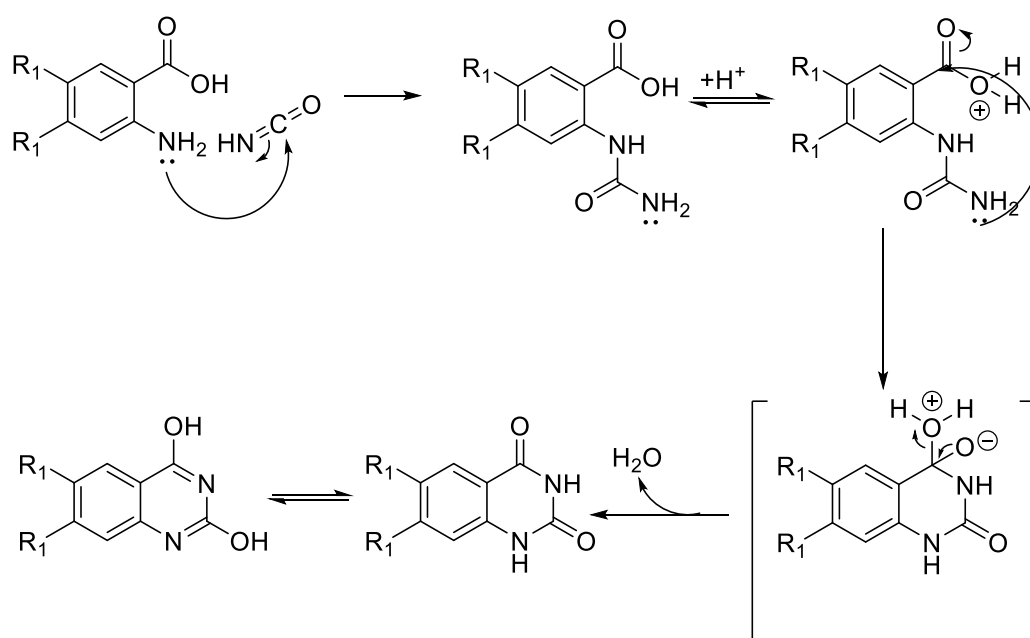


Figure 53. Reaction mechanism for the synthesis of the quinazoline-2,4-dione core.

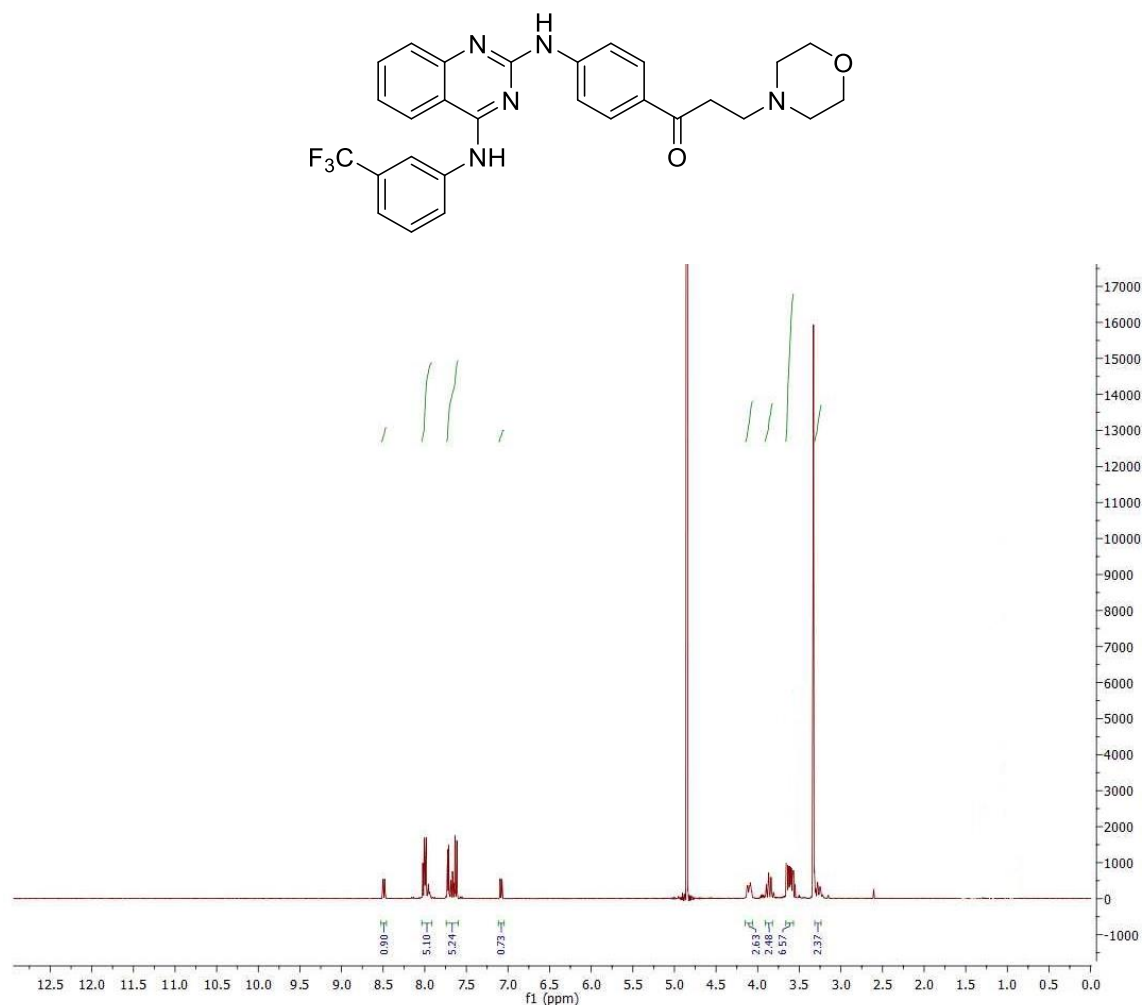
The following step has been the chlorination of the two hydroxyl groups. This reaction is fundamental for performing the nucleophilic substitution of the following steps. Phosphorus oxychloride has been used for this step, in presence of an organic base

(DIPEA). After this, the synthetic route proceeded with the first nucleophilic substitution. The two reactants that have to be condensed together are the 2,4-dichloroquinazoline and the 3-trifluoromethylaniline. For performing this reaction, a catalytic amount of concentrated hydrochloric acid has been utilized. Considering that the quinazoline core presents two different sites that can be prone to undergo nucleophilic substitution, position 2 and 4, it could be that the reaction conditions would lead to the obtainment of a mixture of products. This never happened because the two different positions are very different in terms of reactivity, one to each other. Position 2 is surrounded by two Nitrogen atoms with their unpaired electrons, and this reduces considerably its reactivity. The chlorine atom in position 4 is much more prone to be substituted because it is in close proximity with just one nitrogen atom and on the other side it is near to the phenyl ring, that with its conjugated system acts as a bland electron withdrawing group, activating a little bit this position. In this way it has been obtained the 2-chloro-4-aminoquinazoline that has been further reacted with the aminophenones synthons obtaining the final desired compounds.

The final synthesized compounds have been reported in the following table.

Number	Chemical structure	IUPAC
		3-morpholino-1-(4-((4-((3-(trifluoromethyl)phenyl)amino)quinazolin-2-yl)amino)phenyl)propan-1-one
		2-morpholino-1-(4-((4-((3-(trifluoromethyl)phenyl)amino)quinazolin-2-yl)amino)phenyl)ethan-1-one

Example of NMR characterisation



¹H NMR (400 MHz, MeOD)

3.1.2 Pharmacokinetic and Pharmacodynamic studies on the lead compound CC11

During this PhD several studies have been performed with the aim to understand the pharmacokinetic profile of the lead compound CC11 in a mouse model, after intraperitoneal injection. In particular we focused on determining the blood concentration during time after single dose and the tissue's distribution and accumulation after chronic treatment. Further studies have been performed with the aim to univocally identify the biological target of this class of compounds. This has been pursued with two different approaches. The first one consisted in the development of resins, variously functionalized with our pharmacophore, for performing affinity chromatography experiments. The other project has been focused on the synthesis of CC11 analogues functionalised with a photoactivatable fluorescent moiety that can covalently bind to the biological target after administration in live cells. The fluorescent tag allows to isolate and easily identify the biological target after western blot. Another research line has led to the development of new fluorometric

tools that can be used for the detection and quantification of the phosphatase activity even in complex matrices. One of these molecules could be used also for performing super-resolution microscopy in living cells, potentially allowing to identify the principal site of dephosphorylation within the cell of several phosphatases.

As for the treatise of the previous topic about PP2A activators, also this paragraph will be subdivided in different parts, and each one focused on a different topic.

3.1.2.1 Pharmacokinetic profiling of CC11

During previous studies, performed in the laboratory of Prof. Brunati, CC11 has been able to significantly reduce the count of cancerous lymphocytes in the majority of the treated B-CLL mouse models. For this reason, considering CC11 a valid compound that could prosecute on the route of drug development, a pharmacokinetic profiling has been conducted on healthy mice. This is an obligatory step for the prosecution with in vivo experiments, because it is necessary to assess the real bioavailability that this compound has in a living organism. As first parameter, the blood concentration has been assayed over time after intraperitoneal administration. These analyses determine the effective concentration that this molecule reaches in circle, and this reflects the amount of drug that can be directly absorbed by the cancerous cells in each district of the body.

The blood concentration of CC11 has been quantified using LC/MS experiments at 0, 1, 2, 4, 6, 24, 48 hours from an intraperitoneal injection of 20 mg/Kg of CC11. The protocol of analysis will be fully elucidated within the experimental part and it adopts an internal standard for the determination of the CC11's concentration. Each point of the analysis was obtained by a triplicate of samples applying the proper statistical protocol for the management of the data.

Before to perform the real experiment, a preliminary one has been done with the aim to determine the percentage of recovery obtainable with the adopted protocol.

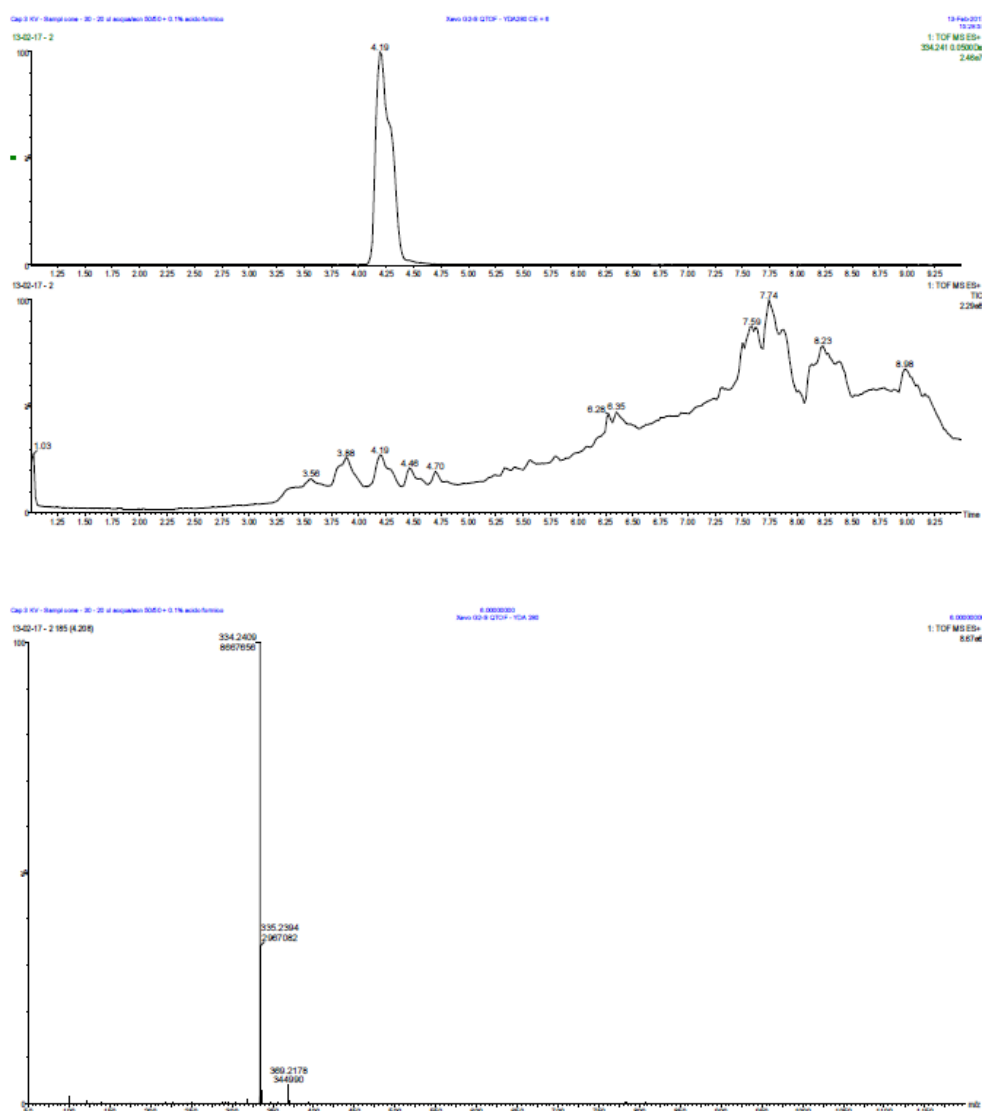


Figure 54. Blood sample added with 5 μ L of 50000 ppb solution of CC11 analysed through LC/MS. The lower part is the m/z ratio of CC11, the middle one is the TIC LC-MS chromatogram and the upper one the isolated peak of CC11.

For this experiment an uncontaminated blood sample was taken and then spiked with a standard solution of CC11, reaching a total concentration of the analyte within the sample of 0,5 μ g/mL. The percentage of recovery was estimated to be 60%.

For what concern the analysis of the blood samples a concentration profile has been obtained, it presents a maximum peak around the 9 hours of 1 μ g/mL and then a gradual decrease for the remaining time (Figure 55).

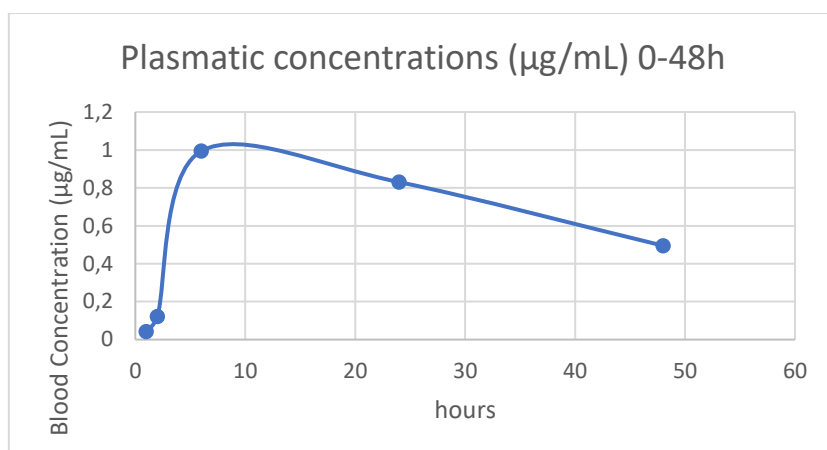


Figure 55. Blood concentration of CC11 from 0 to 48 hours after administration (all the shown data are the average value of the three experiments).

After that, other analyses have been performed with the aim to understand how the profile of distribution is, in particular which is the organ of election that shows the higher concentration of the compound after a chronic treatment. This experiment has been performed injecting daily two couples of mice with two different doses of compound for a week. One couple was treated with a high dose (H) of the molecule (40 mg/Kg) and the other one with a low dose (L) (20 mg/Kg). After one week of treatment the mice were sacrificed and biological samples were collected, in particular: blood, kidneys, brain, liver, heart and spleen. Blood apart, all the other organs have been homogenised and then extracted using an appropriate protocol that will be illustrated in the experimental part. Also in this case an internal standard has been utilized for determining the concentration of CC11.

All the samples were analysed with an LC/MS technique like that one used for the analysis of blood. All the obtained results are shown in Table 5.

Sample	Blood	Liver	Kidney	Heart	Brain	Spleen
H1	1.0951	0.0022	0.0039	0.0015	0.0007	0.0028
H2	0.6113	0.0010	0.0031	0.0033	0.0005	0.0049
L1	0.5056	0.0004	0.0032	0.0012	0.0013	0.0007
L2	0.7720	0.007	0.0009	0.0030	0.0009	0.0015
units	µg/mL	µg/mg tex	µg/mg tex	µg/mg tex	µg/mg tex	µg/mg tex

Table 5. Concentration of CC11 in several organs and in the blood. The concentration in the blood is expressed in µg/mL and the concentration of the analyte in the organs is reported in µg of CC11 versus mg of tissue analysed

As evidenced by the different analyses, this compound is preferentially accumulated within the liver, kidney and spleen, while the higher concentration has been found in blood.

These last analyses have evidenced a problem that was not revealed during the previous experiments on blood. Based on the lower response encountered during LC-MS experiments, it has been supposed that CC11 could be adsorbed on the surface of the plastic vials that have been used, leading to a drastic reduction of the detected

signal, not only that one of the analyte but also that one of the internal standard. This was confirmed by a series of experiments, comparing the utilise of plastic materials versus glass ones. As shown in the table and figures below the mass spectrums obtained with glass material were better than those ones derived from plastic materials and also the concentration was better maintained in glass vials respect to the plastic ones.

Concentration (μM)	Concentration after 1 night in glass (μM)	Decrease (%)	Concentration after 15 minutes in plastic (μM)	Decrease (%)	Concentration after 1 night in plastic (μM)	Decrease (%)
5	4.2	-16	3.7	-26	3.7	-26
1	0.95	-5	0.61	-39	0.58	-42
0.5	0.48	-4	0.46	-8	0.47	-6
average		-8		-24		-25

Table 6. Comparison between plastic vials and glass vials in the maintaining of the concentration

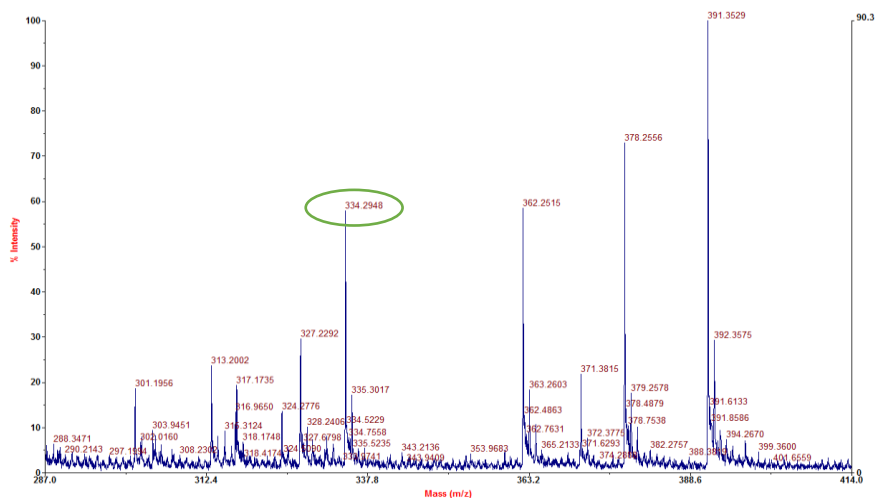


Figure 56. Mass spectrum of the analyte in plastic vials.

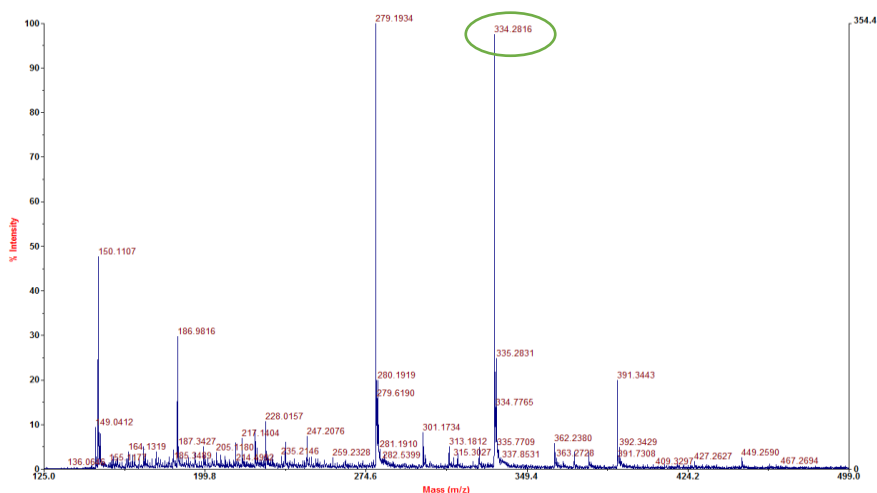


Figure 57. Mass spectrum of the analyte in glass vials.

For this reason, all these data have to be considered as preliminary results and can give us an approximative, but realistic idea of the pharmacokinetic profile of CC11. Unfortunately, it was not possible to reproduce these experiments because there were not available mice. Nonetheless, it is still desirable to repeat these analyses whenever new animal models could be available again for confirming the observed trend and these preliminary results.

3.1.2.2 Identification of the CC11's biological target

Another important question that has been affronted during this PhD was: Which is the real biological target of our class of compounds represented by CC11? Preliminary results on this topic have been obtained by the former PhD student. With waterLOGSY NMR studies and fluorescence experiments, it has been demonstrated that CC11 can bind to isolated SET confirming the general behaviour, encountered also in Fingolimod, that these compounds dissociate the PP2A/SET complex interacting directly with SET. On the other hand, these results can not be considered exhaustive because the binding affinity of CC11 for SET has been tested on a simple matrix and it could be possible that the recorded signals derive from nonspecific interactions. For this reason, a new research line has been started with the aim to identify the pharmacological target/targets of CC11 using a complex matrix like a whole cell lysate or even in living cells. This goal has been pursued following two different approaches:

1. The development of resin supports, covalently grafted with CC11 analogues, for performing affinity chromatography experiments;
2. The development of CC11 derivatives, tagged with a small photoactivatable fluorophore that can label covalently the biological target of CC11.

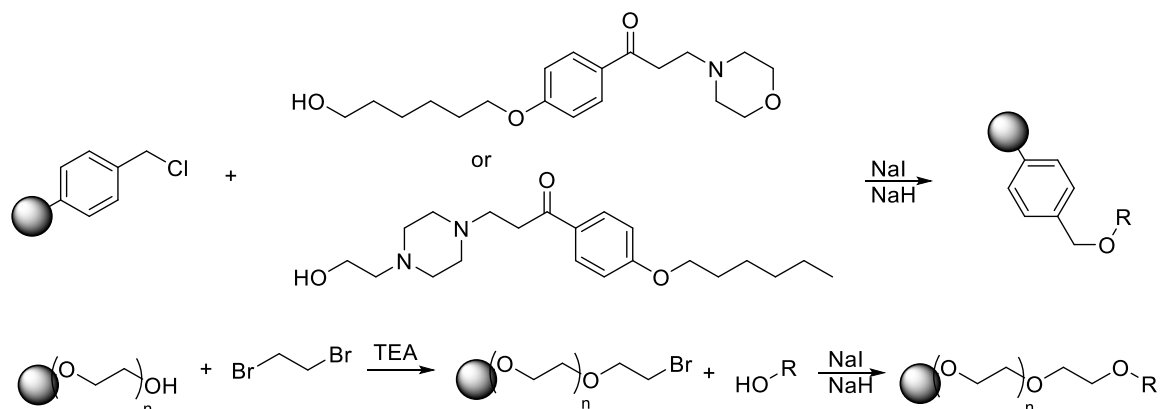
Both these projects will be presented in two separated paragraphs elucidating the rationales and the synthetic strategies adopted.

Affinity chromatography

The affinity chromatography technique is widely adopted nowadays with different aims: the identification of biological targets for small molecules, the protein purification, the screening of compounds and the detection of interactions between biological macromolecules. The principle of functioning is similar to the conventional chromatography. The solid phase is variously decorated with different subunits and functionalities, that could be small molecules but even big macromolecules such as protein, DNA or RNA. These pending groups have different degrees of affinity for the solutes present in the mobile phase. Obviously, the composition of the mobile phase varies in relation to the composition of the solid phase. This means that in all the cases the adopted solvent is a physiological water buffer that maintains the folded state of the biological macromolecules and reproduces a local environment that is much more similar to the physiological one in terms of pH and ionic strength. For what concern the analytes added to the mobile phase, their nature depends from the kind of pendants present on the resin. Considering the functionalization of the resin with biological macromolecules, the mobile phase can include small molecules, or complex matrices like whole cell lysates. In the first case it is possible to perform even a virtual screening of compounds, checking which one is able to interact with that specific biological target. In the second case, this approach is useful for identifying the pattern of interactions that the grafted macromolecule generates within the cell. In case that the solid phase is functionalized with small molecules, the mobile phase can be added with a mixture of biological macromolecules, even including complex matrices like whole cell lysates. That or those biological macromolecules that are eluted as last ones during these experiments, are those that are more affine to the stationary phase and consequently to the small molecule attached to it. For this reason, they can be considered as valid candidates for being the pharmacological target of the pendant small molecule. These macromolecules are further analysed with mass spectrometry experiments for their identification. This is what has been thought to be done for the identification of the possible biological targets of CC11 and for confirming or not the preliminary results obtained with the isolated SET^[136].

For the synthesis of the solid support two different kind of resins have been chose: Merrifield and Tentagel. We choose these two types of supports because they are readily available and are easy functionable. Furthermore they present a significant difference in their chemical structure, the Merrifield resin has the point of attachment that is directly located on the surface of the resin, while the Tentagel one has a PEG spacer that allows to the pendants to be majorly solvated and it resembles much more the physiological conditions. Typically, these supports are decorated through an ester bond that is acid labile and easy removed for obtaining the desired final compound. In our case it is not desirable that the CC11 substrate is removed from the resin by chemical hydrolysis or enzymatic one. For this reason, a stable linkage has been researched. The idea of inserting an amine in the molecular scaffold of CC11 was a good compromise from a synthetic point of view because the amino groups are good nucleophiles and the functionalization of the resin would be straightforward. Despite this is a desirable aspect, the introduction of a secondary amine on the molecular scaffold of CC11 could alter the pattern of interactions that this small molecule can generate and thus leading to the loss of the affinity for its target. For preserving the structural integrity of CC11 an ether bond has been chosen. The first idea of

functionalisation was based on the formation of the alcoholate with NaH in THF and then its reaction with the resin. This did not happen and for this reason a Finkelstein reaction has been proposed using KI as a halogen exchanger but maintaining at the same time the formation of the alcoholate. The ether linkage has been thought to be introduced in two different portions of the molecule, one on the polar head and one at the end of the alkyl chain. This solution has been designed with the goal to identify which part of the molecule can be modified without affecting the efficacy of the compound. For testing this idea, firstly two resins have been obtained exploiting the hydroxy ethyl piperazine portion of the molecule and grafting the two kind of resins: the Merrifield and the Tentagel.



Scheme 8. Synthesis of the different resins.

To determinate the degree of functionalisation of these resins, at preliminary level, it has been adopted a rough but well reported technique based on the protonation of all the amines present on the resin with a solution of concentrated HCl and THF (50/50%). After this the resin has been thoroughly washed with THF, MeOH and DCM for removing the excess of HCl. Finally, several washes with a solution of TEA and DCM (1/9) have been done. The resulting solution of these washes has been evaporated obtaining a solid residue composed by $\text{HN}(\text{Et})_3\text{Cl}$. This has been weighed and this reflects the degree of functionalisation of the resin.^[137]

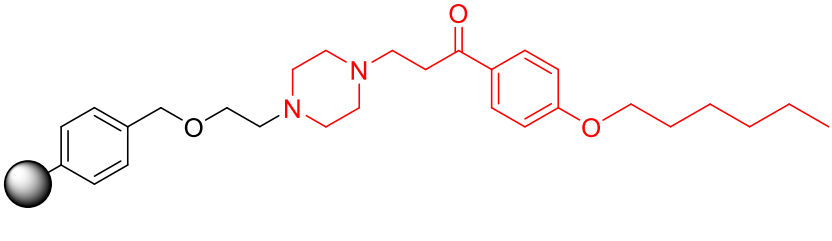
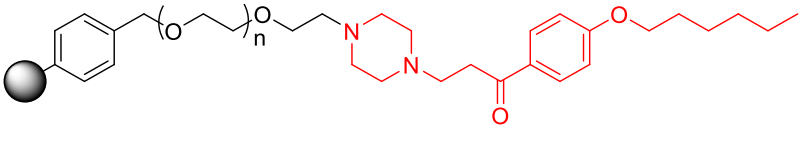
In this way it has been assumed that the degree of functionalisation of the Merrifield resin is 0.56 mmol of compound over g of resin, and that one of Tentagel is 80 $\mu\text{mol/g}$.

After the synthesis part, these resins have been tested on biological samples. The first test has been performed using purified SET as model of protein that can interact with our molecules. This protein has been chosen as first, and not a whole cell lysate, because it is a simpler matrix than a lysate and also because the preliminary tests underlined the ability of CC11 to interact with SET. For this experiment, all the resins have been poured in an aqueous phosphate buffer and the protein solution has been filtered through the resins.

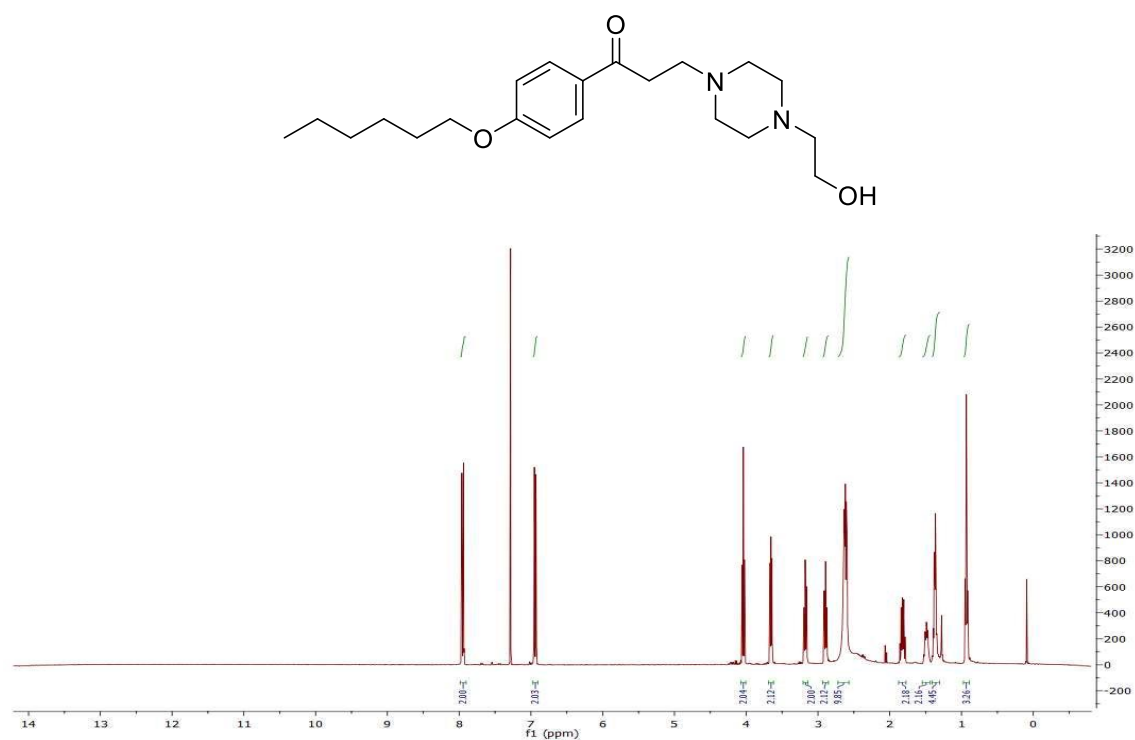
Unfortunately, the synthesized resins turned out to be not effective because they are too much hydrophobic and consequently, they are not able to swell in water. The resins have to swell in the buffer solution, because this increments significantly the surface exposed to the solvent. As a consequence of this, the number of exposed pendants is higher and this increases significantly the possibility to generate favourable

interactions between CC11 and SET. Despite the high loaded resins, they are not able to swell enough and therefore they do not expose a sufficient number of CC11 residues. Consequently, the interaction between SET and CC11 does not happen and the protein is not retained by the resin. Considering the failure of these solid supports, the synthesis of the other ones, functionalised on the hydrophobic tail of CC11, has been abandoned. This project could be improved exploiting new resins, much more hydrophilic, that can swell better in water.

Below, all the synthesized resins are illustrated, and their loading is reported.

Resin Type	Chemical structure	Loading (mmol/g of resin)
Merrifield		0.56
Tentagel		0.08

Example of NMR characterisation



^1H NMR (400 MHz, CDCl_3)

Photoactivatable probes

Another possibility for the univocal identification of the CC11's biological target is represented by the fluorescent labelling of the complex CC11/target. For doing this the molecular scaffold of CC11 has to be modified inserting two new functionalities:

- a fluorescent tag, that can label the compound,
- a functional group that can covalently bind the target macromolecule and consequently label it with the fluorescent tag attached to CC11.

This kind of approach is extremely useful because the modified pharmacophore can be used directly on living cells, testing it in the real physiological environment, where CC11 acts. Consequently, the risk of biases due to alteration of the environment are excluded. After the covalent labelling, the cells can be lysed, and the proteins separated through western blot. At this point the fluorescent bands represent the biological targets of CC11. Each band can be further analysed; it can be proteolytically cleaved, and then analysed in LC-MS. From the results of these analyses it is possible to identify the protein and to delimitate the site of interaction of CC11 within the protein structure. This is feasible because the compound is covalently attached to an amino acid residue that is close to the site of interaction, consequently those peptides that present a molecular weight different from the theorized one and whose difference is exactly that one of the fluorescent complex, this configures them as the plausible site of action of CC11.

For developing such fluorescent probes, the inserted modifications have to be done in positions of the molecular structure that are not fundamental for the affinity of the compound to the target. In this way it is reduced the risk of altering significantly the activity of the molecule. Furthermore, for the same reasons, the fluorescent tag and the covalent linker have to be small enough for not interfering during the interaction with the target.

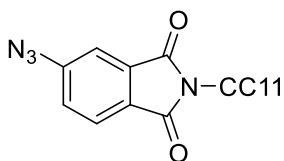


Figure 58. Molecular structure of the fluorescent photoactivatable synthon.

Considering all these parameters, an azido phthalimide group has been chosen and installed in different positions of the molecular structure of CC11. This structure embodies itself all the characteristics that a photoactivatable fluorescent probe should have:

- It is relatively small, especially compared with all the other fluorophores commercially available, such as rhodamines, fluorescein and others;
- It is able to bind covalently with the target protein;

Furthermore, this small molecule is non-fluorescent in the azido form but when it is irradiated at 365 nm, it photo-reacts through its aryl-azido portion and it forms a covalent bond with the side chain of different amino acids, especially those that

present a nucleophile, and it becomes fluorescent. This process exploits the photoactivation properties of the aryl-azido group. This functionality after irradiation at 365 nm releases a nitrogen molecule and this leads to the formation of the nitrene group, a strong electrophile, extremely reactive. Nitrene has six electrons on the valence shell, one covalent bond and four non-bonded electrons. The missing of two electrons for completing its valence level is what renders nitrene an extremely reactive functional group, able to react even with weak nucleophiles. This is what happens with the side chains of the amino acids in close proximity to CC11. This process covalently bonds the compound to the target, but it transforms also the phthalimide portion in a fluorescent molecule. This is due to the fact that the planar starting molecule presents functional groups that have all an electron withdrawing behaviour. This condition, despite the planarity of the structure, does not allow the fluorescent emission, but it favours a non radiative decay after irradiation. Subsequently to the formation of the nitrene group and the reaction with a nucleophile, the azido moiety is transformed in an amine group that is an electron donating group. This generates an electron push-pull system between the two parts of the molecule rendering, in combination with the planarity, fluorescent the final compound. In this way the target protein is covalently and fluorescently tagged.

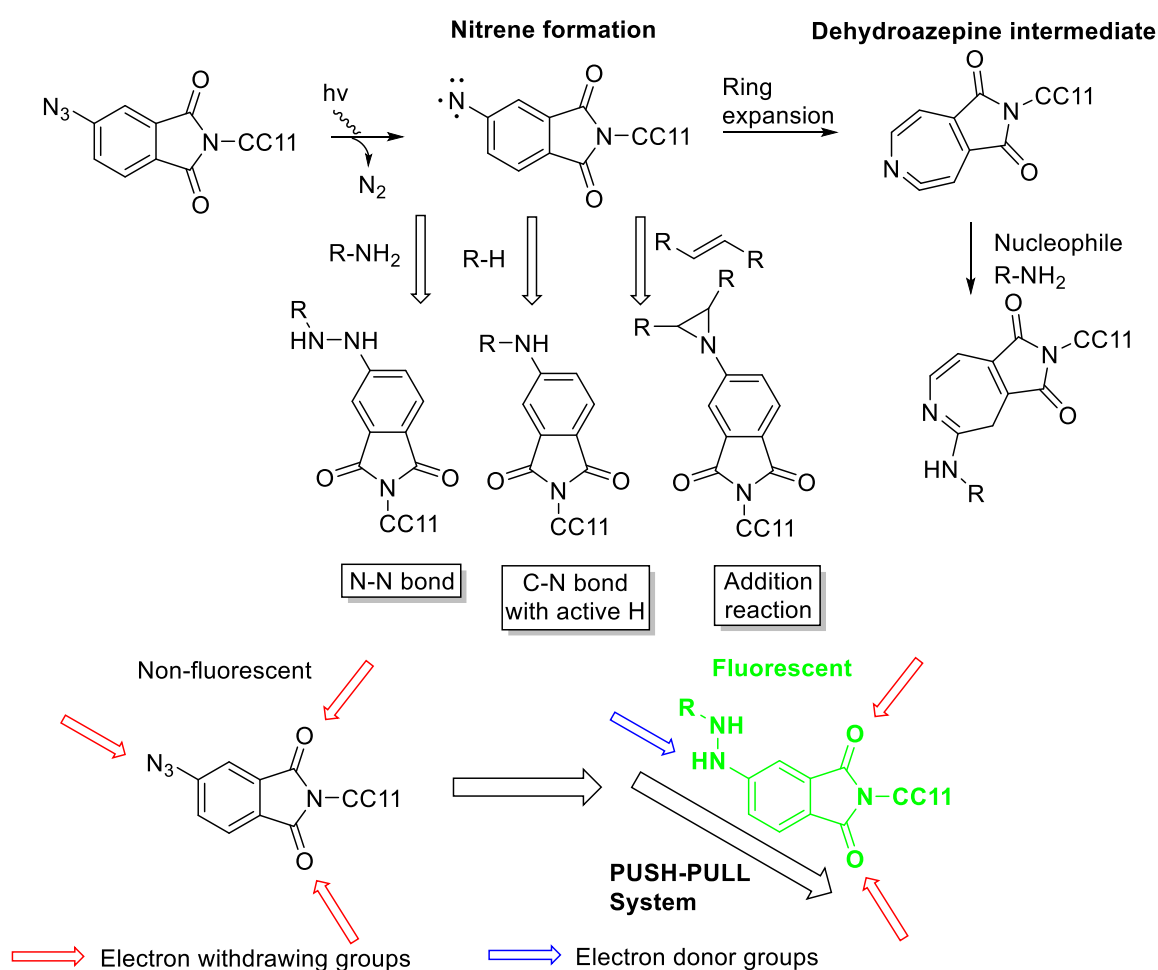
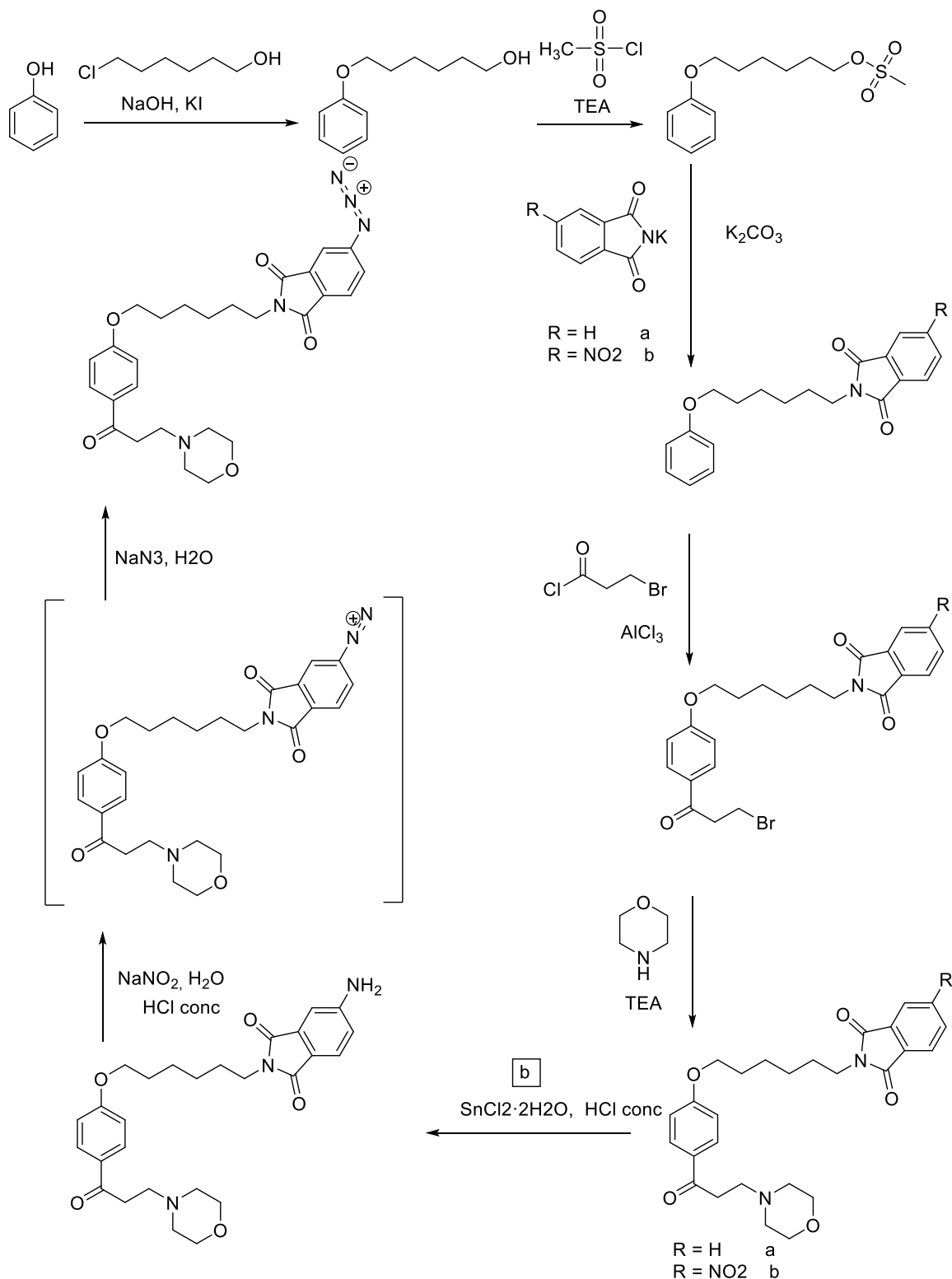


Figure 59. Mechanism of photoactivation of the azido phthalimide portion and of fluorescence of the photoactivated compound.

Also in this case it is important to understand where to install the photoactivatable portion within the molecular scaffold of CC11. The aromatic ring represents the core of the whole structure and for this reason is logic to think that any drastic modification of this crucial portion could alter also the affinity of the whole construct for the original targets. The modification of the peripheric positions of the molecule could reduce the risk of altering the nature of the compound. For this reason, the azido phthalimide has been introduced at the level of the polar head and on the alkyl chain. It has been synthesized also the analogous modified at the alkyl without the azido group for testing if this small group is able by itself to affect the activity of the conjugated CC11-azido phthalimide. For evaluating if these compounds preserve the ability of reactivating PP2A, they will be tested also as CC11 analogues.

The insertion of the phthalimide moiety in two different points of the CC11's structure required the development of two distinct synthetic pathways which are reported below (Scheme 9 and Scheme 10).



Scheme 9. Synthetic route for the synthesis of photoactivatable probes functionalised on the alkyl chain.

Scheme 9 illustrates the synthetic route adopted for the synthesis of the molecules functionalised on the alkyl chain. For the obtainment of these two compounds a linear synthesis has been adopted, starting with the formation of the phenolic ether through nucleophilic substitution with 6-chlorohexanol. The following step has been the

transformation of the hydroxyl group of the previous synthon in a good leaving group like methane sulfonate ester is. This new functionality has been exploited for performing a nucleophilic substitution with a phthalimide or nitro phthalimide function. This is the synthetic step where the two final compounds, the real azido probe and the analogous compound without the photoactivatable moiety, have been separated. In both cases the following step was a Friedel-Crafts reaction with bromopropionyl chloride. Despite, the molecular structure of the reactive compound presents two aromatic rings, the phthalimide one is strongly deactivated by the presence of two carbonyl groups, and in one case also for a nitro functionality, and for this reason the obtained final compound is just the para substituted phenone. After this step the morpholine polar head has been introduced on the propyl spacer obtaining the final compound without the azido portion. The nitrated molecule is the precursor of the final probe and more steps are necessary for its obtainment. The following one has been the selective reduction of the nitro compound for obtaining the amino derivative. This step has been performed with $\text{SnCl}_2 \cdot 2\text{H}_2\text{O}$. Subsequently this synthon has been reacted in an acidic aqueous environment with sodium nitrite obtaining as reaction intermediate the diazonium salt. This compound has not been isolated but it was reacted immediately with sodium azide. This two-step reaction leads to the obtainment of the desired final compound. All these last procedures, especially the workup have been made under dark condition preventing the compound from the accidental photoactivation.

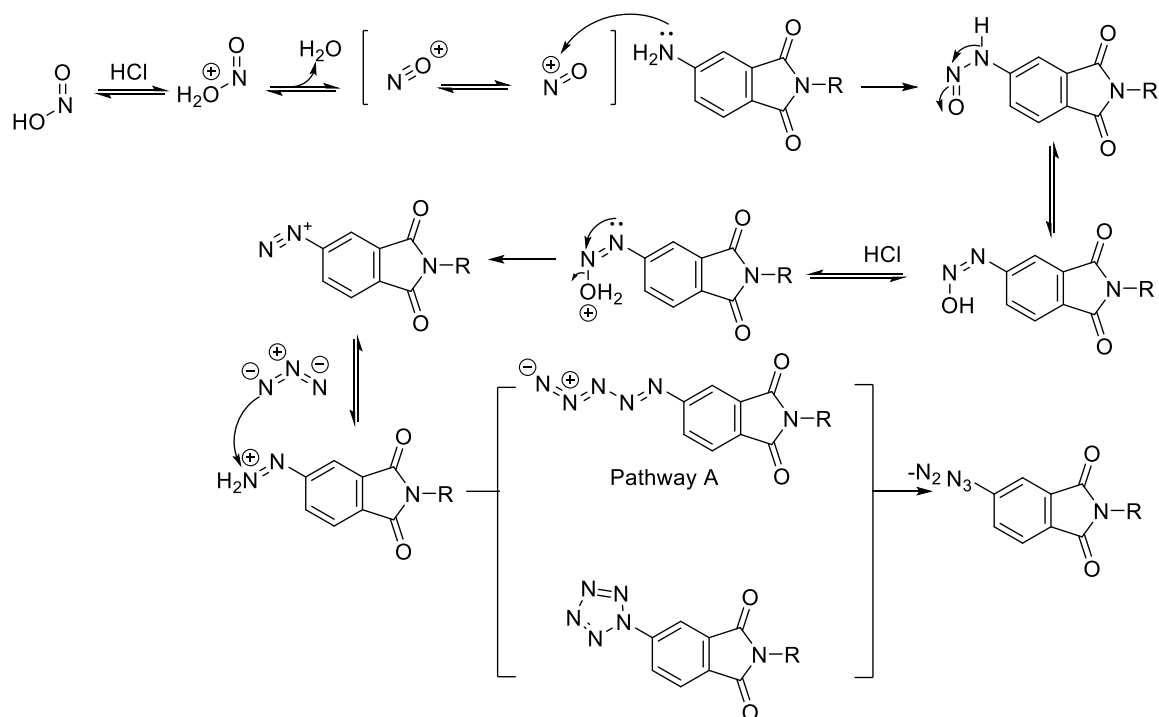
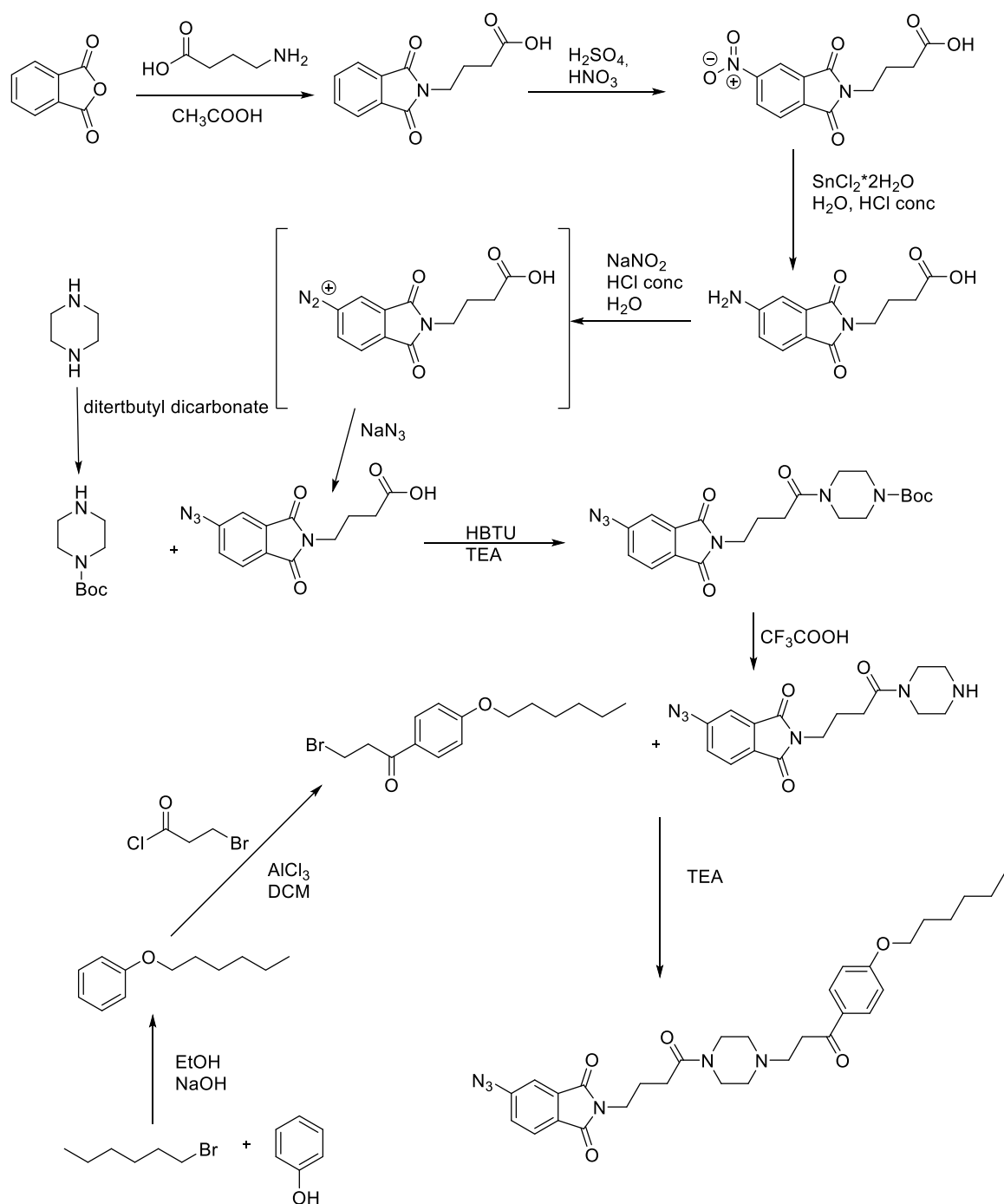


Figure 60. Mechanism of reaction of the azido phthalimide portion.



Scheme 10. Synthetic route for the synthesis of photoactivatable probes functionalised on the polar head.

The synthesis of the probe functionalized on the polar head required much more synthetic attempts and a more accurate design. For the synthesis of the previous structures, the azido phthalimide portion has been directly inserted as last element of the hydrophobic tail. This has been thought as a practical solution, considering that all the conjectures made till now, have evidenced how this part of the molecule is the more ductile and permissible to modifications. This is not the case of the polar head, that presents the higher density of possible interactions. Any modification in this region could affect significantly the pharmacodynamic profile of the compound and for this reason is not possible to functionalized directly this portion with the

photoactivatable fluorophore, but instead it is necessary to introduce a spacer that could reduce the steric hindrance caused by the azido phthalimide group. As spacer a butyl group has been chosen. Scheme 10 illustrates the synthetic pathway adopted for this kind of molecule. In this case the synthetic strategy adopted a convergent protocol, in this way the synthetic process required less time and the overall yield resulted to be higher. Two different structures of the final compound have been synthesized in parallel: the azido phthalimide group functionalized with the desired polar head and the hydrophobic core of CC11.

For what concern the obtainment of the photoactivatable moiety, the first step has been the synthesis of the phthalimide ring. This reaction has been performed with phthalic anhydride and GABA (gamma aminobutyric acid) in acetic acid as solvent (Figure 61).

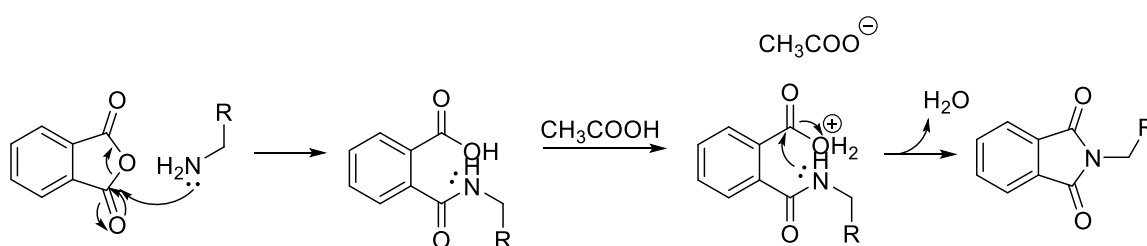


Figure 61. Mechanism of reaction for the synthesis of the 4-(1,3-dioxoisindolin-2-yl)butanoic acid.

The following step has been the nitration of the phthalimide ring in position 4 and then its reaction, in the subsequent passage, with tin chloride obtaining the amino derivative. This has been the synthon that led to the obtainment of the azido phthalimide portion using the same synthetic strategy previously illustrated (Figure 60). After the obtainment of the 4-(5-azido-1,3-dioxoisindolin-2-yl)butanoic acid the synthetic route planned to introduce on this synthon the polar head that is present on the molecular scaffold of CC11. For this aim was not possible to utilise a morpholine moiety because we needed to functional the hexyl ring in two positions and this is not allowed by this kind of substituent, for this reason piperazine has been chosen. The presence of two reactive nitrogen atoms allows the attachment of the azido phthalimide portion and the propyl spacer of the CC11 scaffold. Unfortunately, the presence of two nucleophiles is also the limit of exploiting piperazine in nucleophilic substitutions. The conjugation step between piperazine and the 4-(1,3-dioxoisindolin-2-yl)butanoic acid synthon is constituted by the formation of an amidic bond between one of the nitrogen atoms of piperazine and the carboxylic acid of the GABA spacer mediated by HBTU. The intrinsic risk of this reaction is to obtain as side product the difunctionalized piperazine, that is useless for our purposes. Usually for obtaining the mono substitution two different strategies are adopted:

- Use a large excess of piperazine, that is easily removed with aqueous washes during the workup procedures. In this way statistically, it is much more probable that a new piperazine ring reacts with a new activated acid molecule than the same piperazine reacts twice;

- Protect one of the two nitrogen atoms with a Boc protecting group. This procedure necessitates an equivalent of Boc-piperazine for the reaction and the workup procedures are facilitated because less aqueous washes are required. The only drawback of this strategy is that two extra synthetic steps are necessary: the protection and deprotection reactions.

Considering the length of the adopted synthetic route and the photo instability of the azido compound was desirable to avoid extra steps and for this reason the first synthetic approach has been tried. Another aspect that contributed to this kind of choice has been the fact that piperazine is much cheaper compared to the Boc protected one and so it can be used in large excess. Unfortunately, also with four equivalents of piperazine the only formed compound was the di-adduct. The principal hypothesis that has been made for explaining this behaviour is that being planar and rich of heteroatoms and electronic currents, the phthalimido compounds tend to organize themselves, even in solution, in stacked structures exploiting the π - π stacking. In this way once one the GABA spacer reacts with one piperazine, despite the global concentration of free piperazine is higher, the local concentration of reacted piperazine is able to overcome that one of the unreacted hexylamine ring leading to the exclusive obtainment of the difunctionalized structure. This is just a hypothesis and it needs to be confirmed but it could explain the anomalous behaviour of this reaction. Considering the failures of this first synthetic approach the second one has been adopted. First, Boc piperazine has been synthesized using di-tertbutyl carbonate for introducing the Boc protecting group. It has been used this kind of protecting group because it is stable in basic environment, a condition encountered in all the following steps, and for this reason is much more useful compared all the other ones. Furthermore, its cleavage is extremely fast and easy to workup. After the protection step the Boc piperazine was reacted with the carboxylic acid of the GABA spacer through a classical amidic coupling mediated by HBTU and TEA. The following step was the deprotection of the Boc-piperazine using trifluoroacetic acid as deprotecting agent, obtaining the 5-azido-2-(4-oxo-4-(piperazin-1-yl)butyl)isoindoline-1,3-dione compound.

Together with the synthesis of the azido phthalimide synthon, the hydrophobic core of CC11 has been obtained. The adopted synthetic strategy is the same of the other Fingolimod analogues presented in this thesis. The final coupling between the two synthons has followed the same procedure adopted for the insertion of the morpholine ring on CC11's structure. In this way the final probe, functionalized on the piperazine ring, has been obtained.

This kind of photoactivatable fluorophore has been already adopted for the same purposes by Yamaguchi et. al.^[138] In their paper, they highlighted the propensity of this kind of probe to selectively label just the target protein of the small compound to which the azido phthalimide is attached. During their research they illustrated the capacity of the azido phthalimide probe, upon photoirradiation, to form aniline derivatives and how the different substituents present on this new nitrogen atom can modulate the photophysical properties of the probe.

During this PhD research project, the UV-vis and fluorescence spectra of the azido phthalimide synthon before and after irradiation at 365 nm has been analysed. As preliminary result it has been assayed also the effective ability of this compound to interact and form a covalent bond with an excess of nucleophiles in solutions.

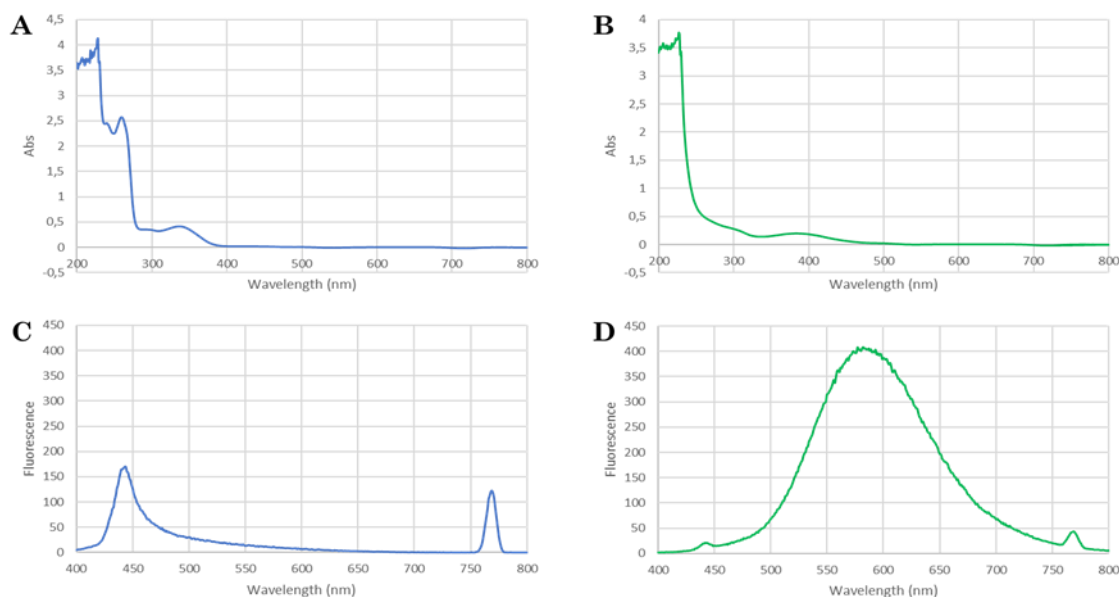


Figure 62. UV-vis and fluorescence spectra of the of the azido phthalimide synthon before and after one hour of irradiation at 365 nm in a PBS buffer solution at a concentration of 100 μ M. A and C are respectively the UV-vis and fluorescence spectra of the compound after irradiation. B and D are respectively the UV-vis and fluorescence spectra of the compound before irradiation.

For what concern the spectroscopic properties of the azido phthalimide synthon, they have been assessed measuring the UV-vis and fluorescence spectra before and after one hour of irradiation at 365 nm, that is the required wavelength for observing the photoreaction. The obtained spectra are reported in figure 62. Analysing the absorption spectra, it is possible to observe a red-shift of the maximum peak of absorption, in the visible region, after irradiation. Before the photo transformation the maximum peak of this region was at 350 nm while after it shifted at 384 nm. The bathochromic effect could be due to the presence in the photoactivated compound of an aniline ring that is a much more electron rich functionality compared to the azide one, and this leads to a decrement of the energetic HOMO-LUMO gap of the structure. Between the two considered spectra there is another significant difference. There is the disappearance of the peak at 261 nm after irradiation, this could be due to the fact that the compound, subsequently to the photolysis, does not present anymore the phenyl azido functionality that was responsible of this absorption. Taking in consideration the fluorescence spectra, it is possible to observe that after photo activation the phthalimide synthon become fluorescent, with a maximum of fluorescence at 588 nm. These experiments confirm the propensity of the synthesized probe to photo react generating fluorescent species useful for our purposes.

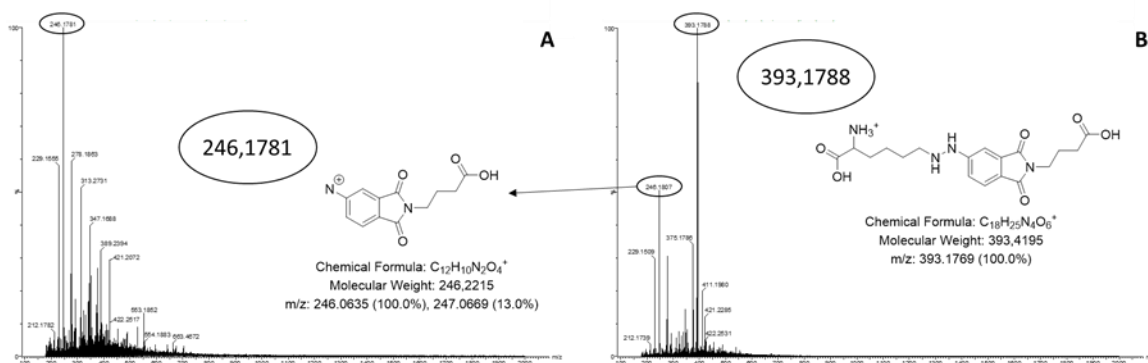


Figure 63. Mass spectra of the non irradiated (A) and irradiated (B) samples. The molecular structure of the principal peaks of the two spectra are reported.

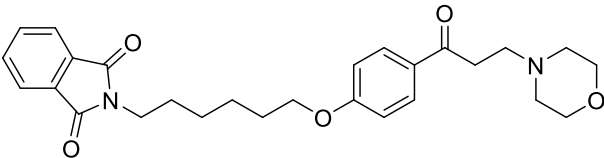
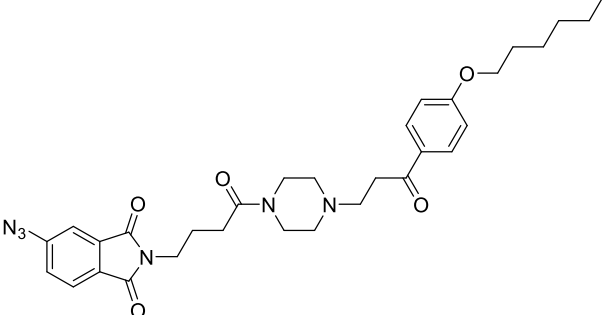
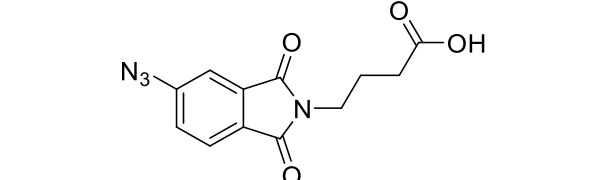
The capacity of the 4-(5-azido-1,3-dioxoisindolin-2-yl)butanoic acid to form covalent bonds with nucleophiles have been tested. To a 100 μ M solution of the synthesized compound in PBS, lysine hydrochloride has been added reaching a final concentration of 10 mM. The mixture has been irradiated for 20 min at 365 nm and then a sample of the irradiated solution and of the non irradiated one have been analysed through mass spectrometry. The analyses aim to observe if the irradiation of the compound has formed new species in the presence of strong nucleophile. For doing this the instrument has been setup with a cut-off of 200 m/z avoiding the saturation of the signal due to the high concentration of the lysine.

The spectrum of the non irradiated sample shows just one principal peak that has been identified as the radical cation of the nitrene intermediate (Figure 63A). Indeed, Abramovitch and colleagues, in 1971, has demonstrated that the high temperature of the ionisation source of a mass spectrometer can lead to the thermolysis of the aryl azides obtaining as principal ionized species the radical cation.^[139] After irradiation, the sample revealed another principal peak whose theorized molecular structure has been reported in figure 63B. Further characterisation studies were necessary for confirming the exact structure of the obtained compound; indeed it could be that the reactive point of the lysine is the α amino group, but this was not the goal of this experiment. Our aim was to demonstrate that the new azido phthalimide linker, despite the small structural differences compared to the molecular scaffold of Yamaguchi et. al. was able to form covalent bonds with an excess of nucleophiles, showing in this way its goodness as photoactivatable probe.

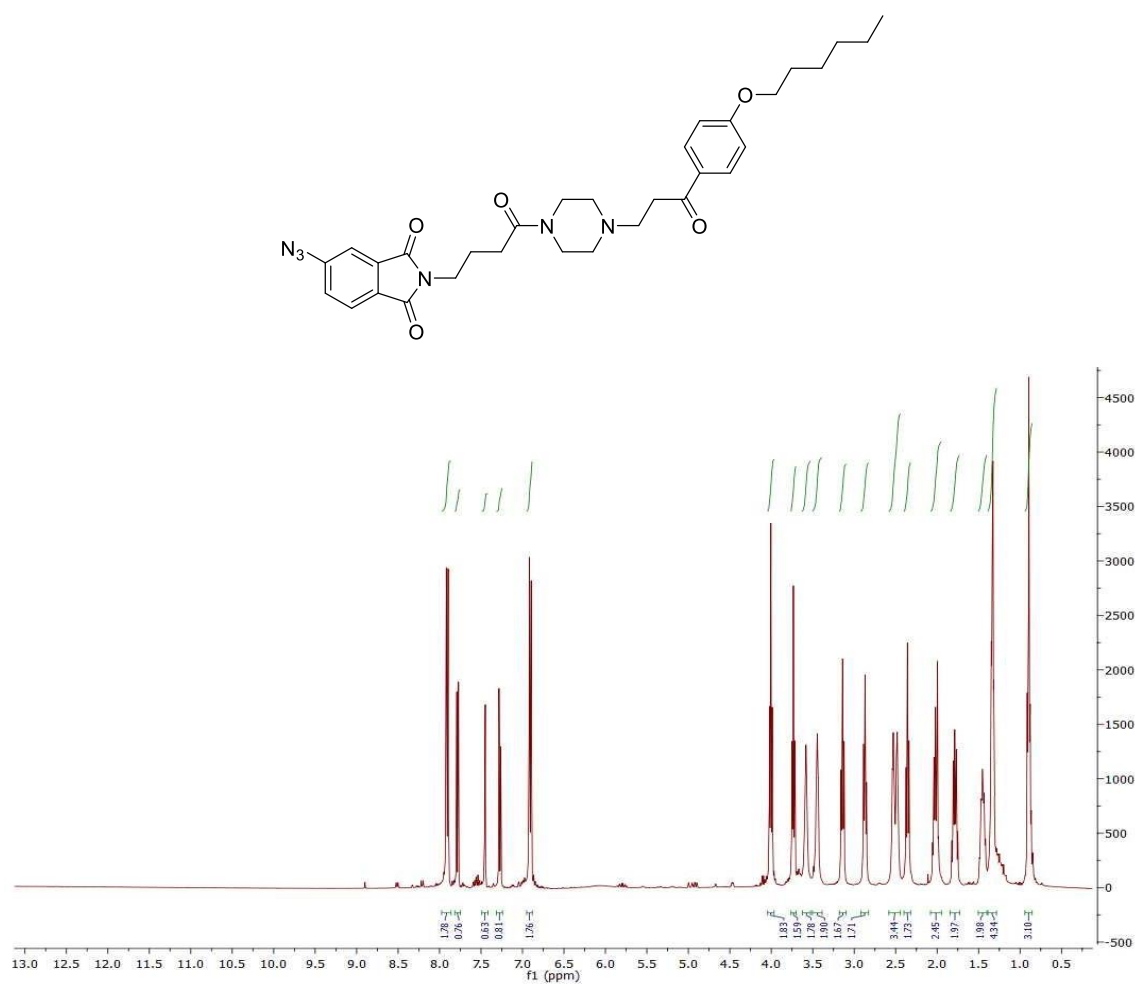
In the next future these probes will be tested on whole cells for validating their ability of fluorescently tag the biological target/targets of CC11 allowing their univocal identification.

In the following table, all the synthesized compounds are illustrated.

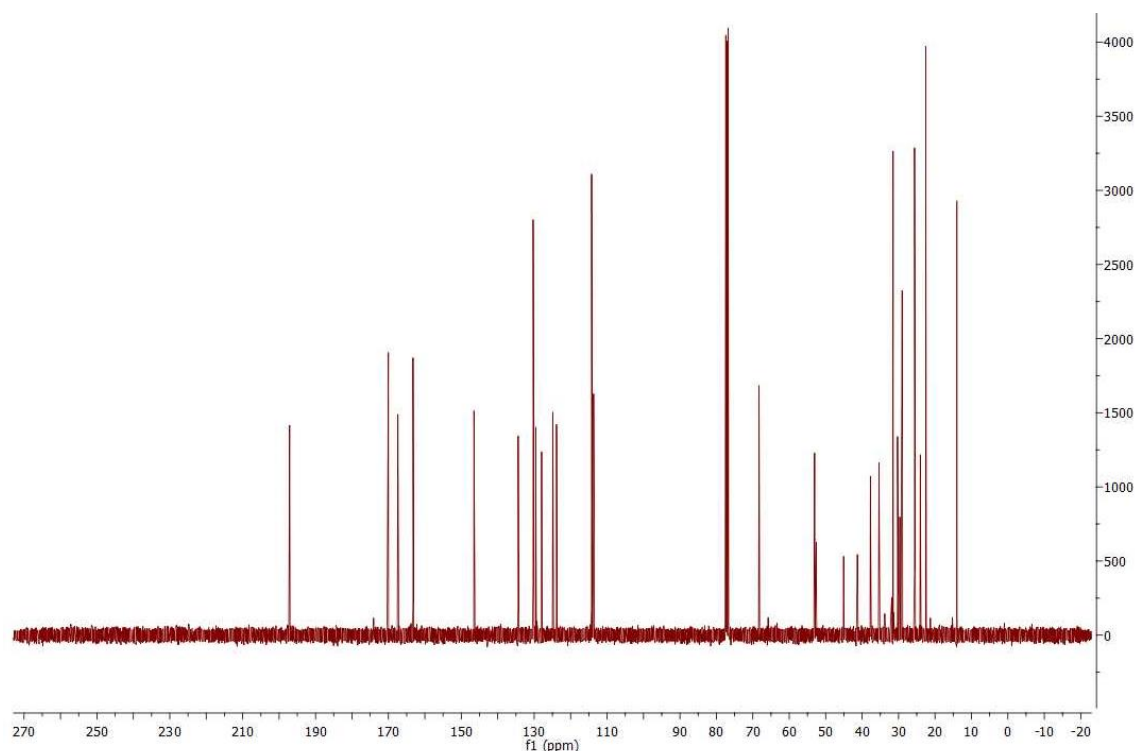
Number	Chemical structure	IUPAC
		5-azido-2-(6-(4-(3-morpholinopropanoyl)phenoxy)hexyl)isindolin-1,3-dione

		<p>2-(6-(4-(3-morpholinopropanoyl)phenoxy)hexyl)isoindolin-1,3-dione</p>
		<p>5-azido-2-(4-(4-(3-(4-(hexyloxy)phenyl)-3-oxopropyl)piperazin-1-yl)-4-oxobutyl)isoindolin-1,3-dione</p>
		<p>4-(5-azido-1,3-dioxisoindolin-2-yl)butanoic acid</p>

Example of NMR characterisation



¹H NMR (400 MHz, CDCl₃)



^{13}C NMR (101 MHz, CDCl_3)

3.1.2.3 Development of new fluorometric tools for the detection of phosphatase activity and super-resolution microscopy

The development of molecules able to restore the phosphatase activity in those cells and pathologies where it is seriously compromise, is a new research field that has aroused tremendous interest in pharmaceutical chemistry. The investigation and the development of new pharmaceutical tools have to be supported by the development of new analytical tools that allow a better understanding of the mechanisms and the effects of these new pharmacological tools.

Up to date, there is a significant lack of tools for the simple and direct detection of phosphatase activity in cells or lysates. Especially, if the selective detection of certain subclasses of phosphatases is required.

Therefore, this project aimed at the development of a new spontaneously blinking probe for the detection of ser/thr phosphatase activity in live cells and cellular lysates. The designed probe is aimed to overcome certain limitations of the currently available technologies. In particular, it could be very useful in tests that involve the isolated target enzyme, or a complex matrix represented by the whole cell-lysate and to furnish a rapid and robust protocol for performing screening of compounds. Previously developed probes lack stability and selectivity or they require a complicated method of analysis. The three main strategies to perform these screenings are Malachite Green test,^[140,141] para nitrophenylphosphate assay (*p*NPP),^[142] and ^{32}P labelled phosphopeptides.^[143]

The first method analyses the release of inorganic phosphate in the testing medium. This is a sensible technique, but it is at the same time not robust enough because it can generate false positives in the presence of other anions such as sulphates. For this reason, it can be only used with isolated enzymes and with special buffers that do not contain any traces of phosphates, sulphates or surfactants. The second method is extremely easy to use and can be adopted also for testing whole lysates. Despite this, it bears several drawbacks. First, its chemical structure resembles a tyrosine phosphate and this does not allow a fine detection of the phosphatase activity of the ser/thr phosphatases. The phosphate bond is furthermore extremely labile, due by the presence of a nitro group in the para position of the aromatic ring, which reduces the sensitivity of this probe because it can be easily degraded chemically. Indeed, the nitro substituent on the aromatic ring increases the acidity of the phenol group in para position. Consequently, the phosphoester bond is much more similar to anhydride than to an ester bond.

The third method is the most robust and most selective one. The remaining drawback is the need for particular instruments and facilities for its utilization which impairs its applicability for most laboratories.

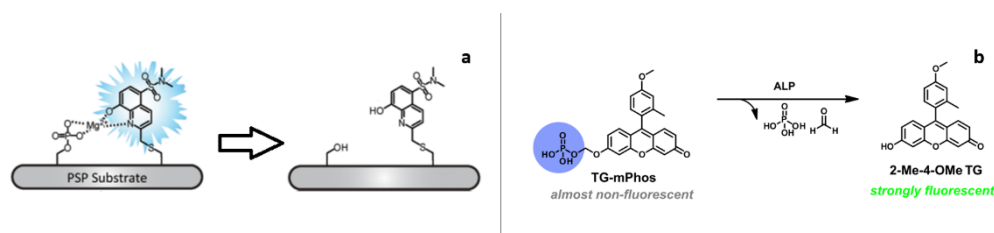


Figure 64. **a)** Phosphatase probe proposed by Beck et al.^[171] **b)** Phosphatase probe proposed by Kawaguchi et al.^[144]

Only a few probes were developed with the aim to overcome these limitations. One of the most remarkable examples is the probe developed by Beck et al.^[12] which exploits a PET (Photoinduced Electron Transfer)/CHEF (Chelation Enhanced Fluorescence) mechanism. This probe is used for the detection of the activity of PP2A in whole cell lysates after stimulation with insulin. The advantage of this probe is its selectivity, robustness and easy use, but it still presents some disadvantages. This kind of probes decreases the intensity of its emission signal in parallel with its dephosphorylation and this behaviour renders the detection of the signal and the quantification of the phosphatase activity less sensitive. Furthermore, this probe requires tight control of the cationic species present in the buffer, in particular concerning the concentration of magnesium ions. These problems lead to the development of a new kind of probes that give an enhancement in the fluorescent signal upon dephosphorylation. One example of this kind of probes is the fluorescein derivative developed by Kawaguchi et al.^[144]

Inspired by these advances, in this research project it has been set out the development of a new probe that tackles and overcome all the previously mentioned

problems and that can be used not only for functional studies but also for fluorescence microscopy to detect dephosphorylation on a subcellular level.

The new probe has to present:

- an increase in the fluorescent signal when dephosphorylated,
- phosphate groups that are similar to the substrate for native serine or threonine phosphatases,
- interesting optic properties that could be exploited for its use in super resolution microscopy. Specifically, the new probe has to allow the resolution of subcellular fractions with a resolution that is below the actual limit of resolution due by the diffraction of the light (≈ 250 nm).

The new designed molecule has to include some peculiar characteristics that should allow to resolve the spatial localisation of each single fluorescent molecule within the cell, with a precision that is far below that one allowed by the diffraction limit (super-resolution microscopy techniques). A variety of techniques has been developed with the aim to overcome this intrinsic limitation of the light diffraction and to improve resolution. The most utilized are photoactivation localization microscopy (PALM),^[145] and stochastic optical reconstruction microscopy (STORM).^[146] These two techniques rely on the use of compounds that can be interconverted between a non-fluorescent and a fluorescent state and that allow the resolution of the single molecule in the space separating them in the dimension of time. Herein, the blinking behaviour of the spontaneously blinking hydroxymethyl silicone rhodamine (HMSiR) has been exploited.^[147]

Design and synthesis of the spontaneously blinking probe

For the design of this probe, especially focusing on the characteristics that a molecule has to present for well performing in super resolution microscopy, the most promising starting scaffold seemed to be that one represented by the HMSiR developed by Urano and co-workers.^[147] This molecule presents a spontaneously blinking behaviour due to the possibility of intramolecular spirocyclization that switches the molecule from a fluorescent state to a non-fluorescent state under physiological conditions (Figure 65).

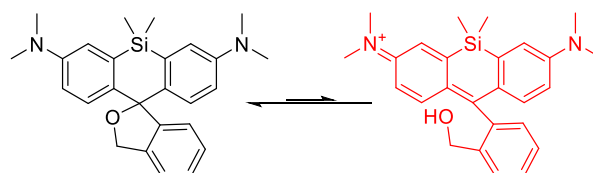


*Figure 65. Intramolecular spirocyclization of the HMSiR. The closed and **non-fluorescent** molecule is more present at physiological pH than the open and **fluorescent** form.*

The general idea was to exploit this intrinsic behavior of HMSiR for making a new probe for super resolution microscopy. The starting point was to create a HMSiR phosphorylated on the benzyl alcohol moiety. This modification leads to a new

chemical entity that is always fluorescent and when dephosphorylated by a ser/thr phosphatase, it presents an intrinsic blinking behaviour that renders it a possible probe for super resolution microscopy. The phosphorylation of the benzyl alcohol of this molecule has also the advantage that it resembles the aliphatic alcohol of a serine or threonine. The drawback of this solution is that the dephosphorylation of the probe leads to a decrease in fluorescence and this is not particularly useful for the activity tests in cell lysates. To overcome this limitation, it has been decided to develop a new molecular scaffold by coupling two different fluorophores with different λ_{ex} and λ_{em} exploiting the Förster Resonance Energy Transfer (FRET) phenomenon. With this solution, the new probe will feature increase in fluorescent signal when it is dephosphorylated and at the same time it will maintain the blinking behaviour of the HMSiR. After these considerations it seems evident that the silicon rhodamine has to be the acceptor of the FRET pair. When it is in its phosphorylated and open form, this molecule is able to quench the fluorescence emitted by the FRET donor. Instead, when the HMSiR is dephosphorylated, it is predominantly present in its closed state and this form of the molecule is no more able to absorb the fluorescence of the donor which starts to emit giving the desired signal enhancement at the λ_{em} of the donor (Figure 66). The new donor fluorophore has to present an emission spectrum that overlap as much as possible the absorbance spectrum of the HMSiR allowing the maximum efficiency of FRET. For this reason, Rhodamine 101 was chosen for its optical properties.

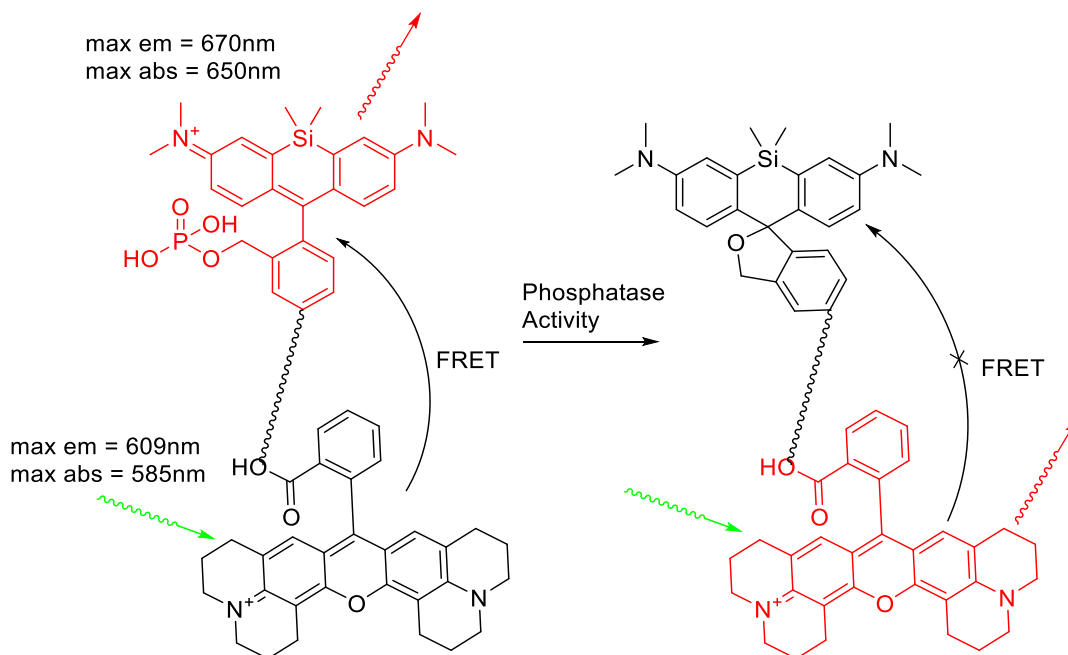


Figure 66. FRET mechanism between HMSiR and Rhodamine 101.

This configuration of fluorophores also permits the maintaining of the blinking behavior typical of the HMSiR. Indeed, in this probe the unphosphorylated state the HMSiR behaves as a blinking quencher that transforms also the Rhodamine101 into

a blinking fluorophore (Figure 67), even if this molecule is not able to blink in physiological conditions.

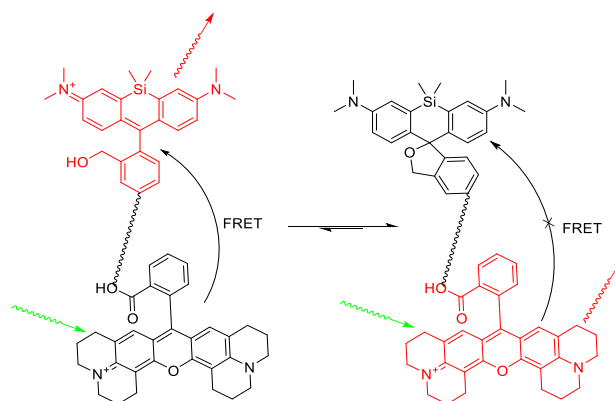


Figure 67. . Blinking behaviour of the FRET probe in the unphosphorylated state.

After this part of design, the first molecular scaffold was proposed and synthesized (compound **1**, Figure 68).

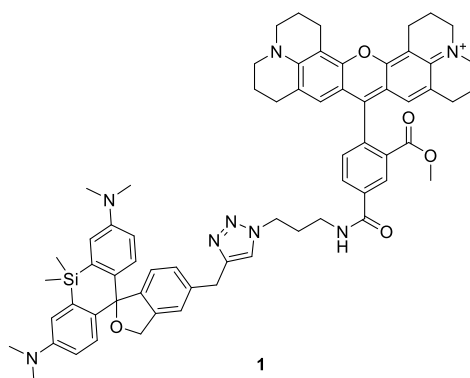


Figure 68. Chemical structure of the compound **1**.

This probe exhibits all the characteristics previously mentioned for a FRET probe. It presents in any case a drawback. The ester moiety situated in the rhodamine portion of the molecule is not particularly stable and during the last stages of the synthetic process this functional group was degraded to give the free carboxylic acid (Figure 6). The presence of the free carboxylic acid allows the lactonization of this new functional group on the xanthene core of the rhodamine portion and this does not allow to the donor of FRET to behave as a fluorescent dye because its conjugated system is altered (Figure 69).

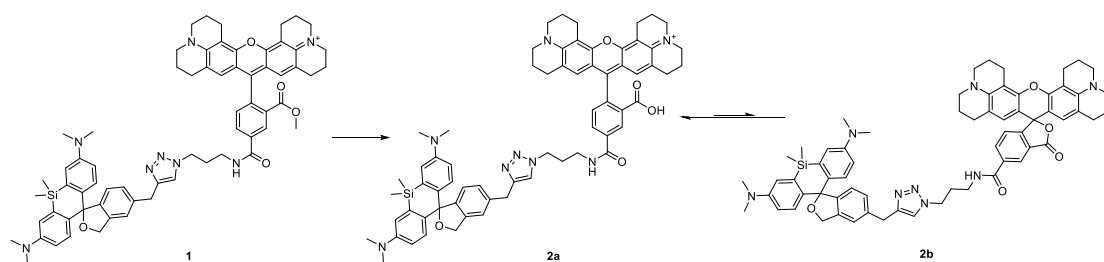


Figure 69. Degradation of the methyl ester of the rhodamine and lactonization of the free carboxylic acid. In the molecule 2b the xanthene core of the FRET donor is no more conjugated, and this does not allow the absorption and the transmission of energy of the whole system.

With the aim to overcome this limitation and for rendering easier the synthetic protocol a new FRET donor was chosen and synthesized (Figure 70).

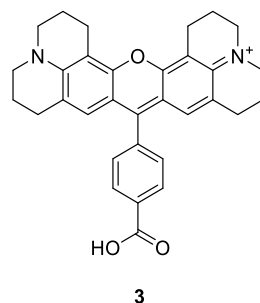
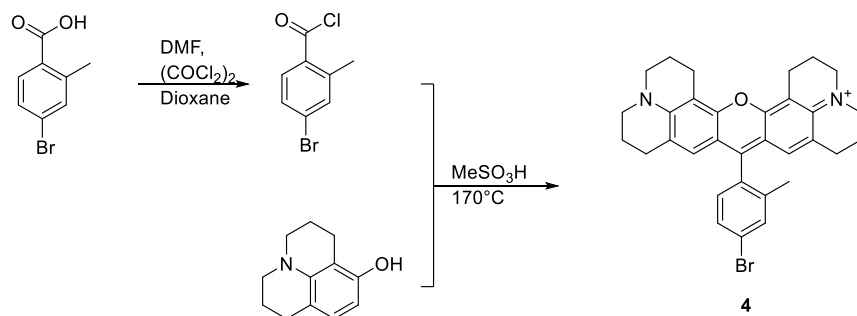


Figure 70. Chemical structure of compound 3.

Compound 3 is always fluorescent, and this is an extremely positive feature for our FRET probe. This is due to the fact that the xanthene moiety of the dye can not be affected by any functional group present on the chemical scaffold. However, also this compound has a drawback which is its very low quantum yield (8%). This is related to the absence of a group in position 3 or 5 of the lower aromatic ring. Indeed, in compound 3 the benzoic portion of the dye can easily rotate on the axis of the C-C bond resulting in a decrease of fluorescence quantum yield. For this reason, also this scaffold was abandoned and a new Rhodamine structure has been proposed and synthesized (compound 4).



Scheme 11. Synthetic scheme of compound 4.

Compound 4 has a methyl group in position 3 of the lower aromatic ring and this should improve the optic properties of this molecule. But the synthesis turned out to be extremely difficult and the yields were too low for continuing with this kind of molecular scaffold.

For this reason, it has been decided to redesign the chemical structure of the original rhodamine avoiding its lactonization and transforming it in an always fluorescent molecule (Figure 71). This was obtained by transforming the carboxylic acid of the Rhodamine101 in to an amide with a secondary amine. This new functionality is no more able to interfere with the conjugated system of the xanthene, at least in physiological conditions, and at the same time maintain the desired optical characteristics of the original molecule and this modification introduces also the desired linker that will allow the constitution of the FRET pair.

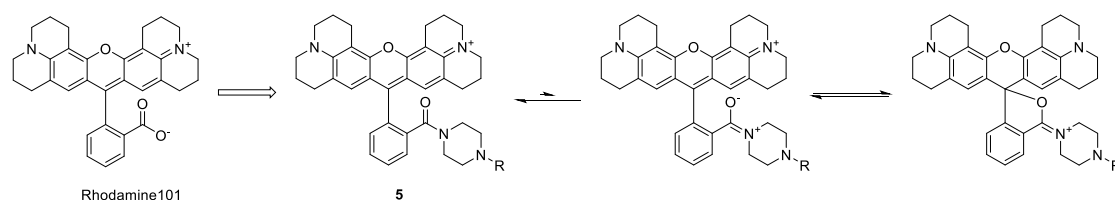
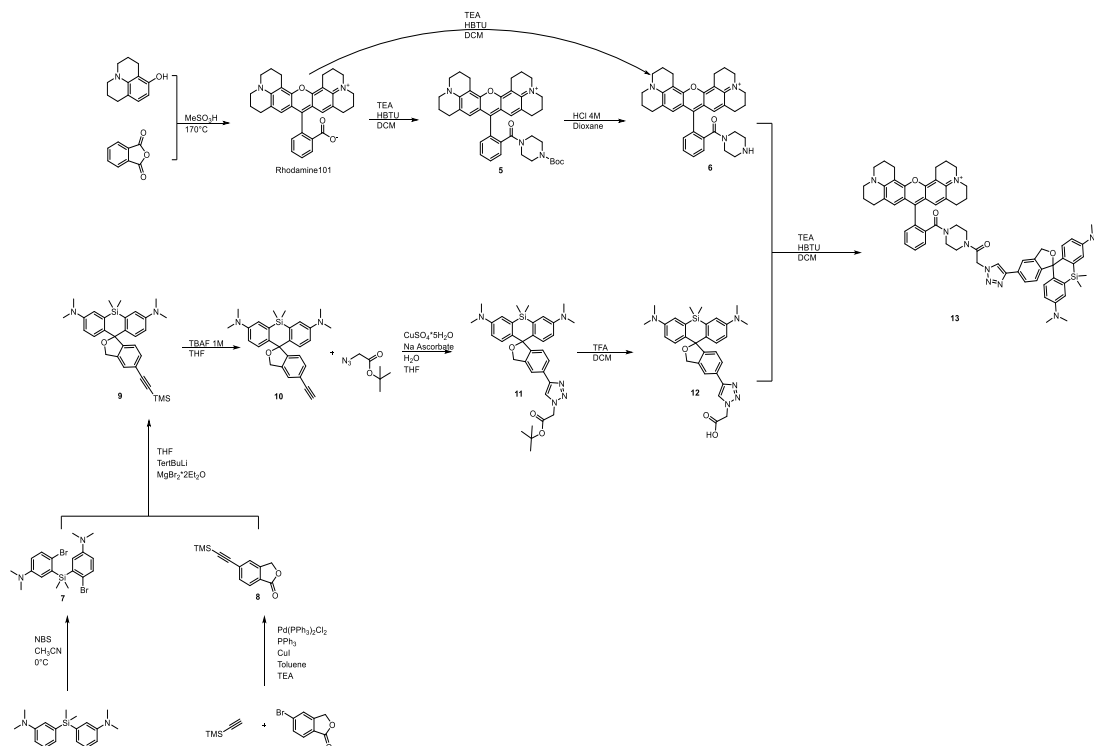


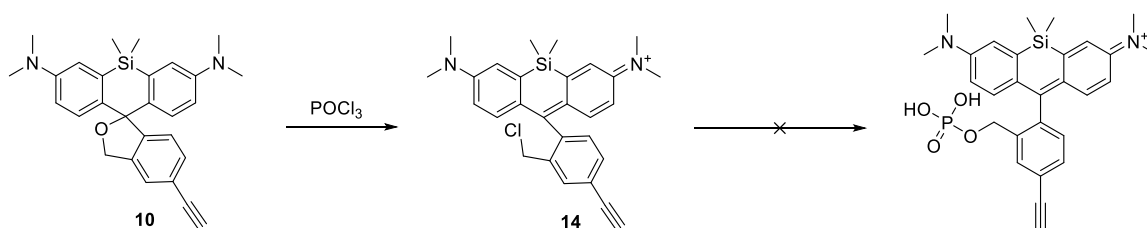
Figure 71. Modification of the chemical scaffold of Rhodamine101 in to compound 5 and possible mechanism of interference with the xanthene conjugated system which is strongly unfavoured in physiological conditions.

Compound 5 presents an optimal optical behaviour and an easy synthesis and for this reason has been adopted as the FRET donor in our probe.



Scheme 12. Synthetic scheme of the FRET probe, compound 13.

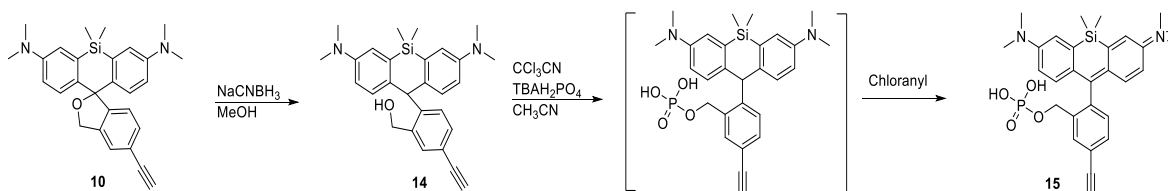
Compound **13** presents all the desired characteristics and it needs just to be phosphorylated. With the aim to find a way to phosphorylate the HMSiR moiety of the probe we used compound **10** as a model compound. Several attempts were taken using different reaction conditions and different reactants (di-tert-butyl diethylphosphoramidite, phosphorus oxychloride, pyrophosphate, trichloroacetonitrile, and tetrabutylammonium dihydrogen phosphate) without obtaining the desired compound. The problem was that all these reactions have to be performed in a basic environment and this leads to the closing of the HMSiR (Figure 2) masking the reactivity of the benzyl alcohol. To overcome this, the only feasible option was to obtain an always open structure and phosphorylate it. For this reason, as a first attempt, compound **10** has been chlorinated (Scheme 13).



Scheme 13. Attempt of synthesis of the phosphorylated HMSiR.

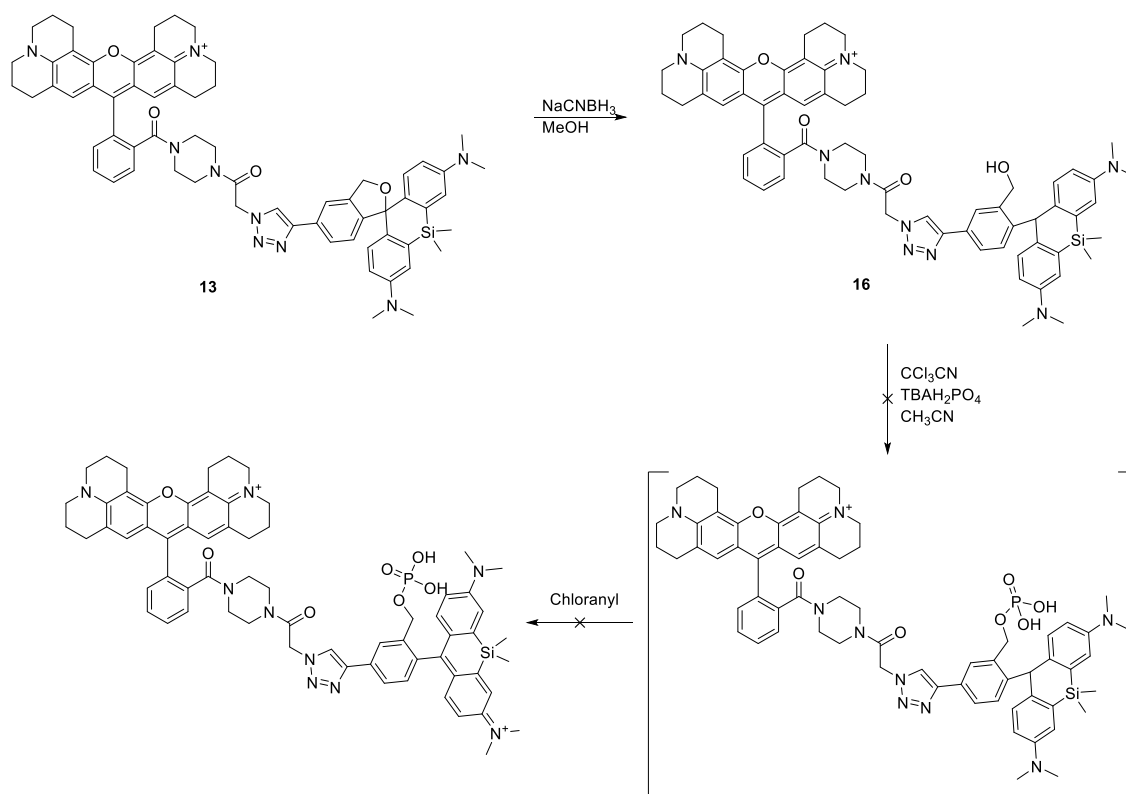
Several reactions were tried to substitute the chlorine atom with a phosphate group, without success.

Hence, another approach was adopted (Scheme 14). First, compound **10** was reduced, then phosphorylated and finally reoxidized to give compound **15**.



Scheme 14. Scheme of synthesis of compound 15.

After obtaining compound **15** with a good yield, the first attempt to obtain the final phosphorylated probe has been done following scheme 15.

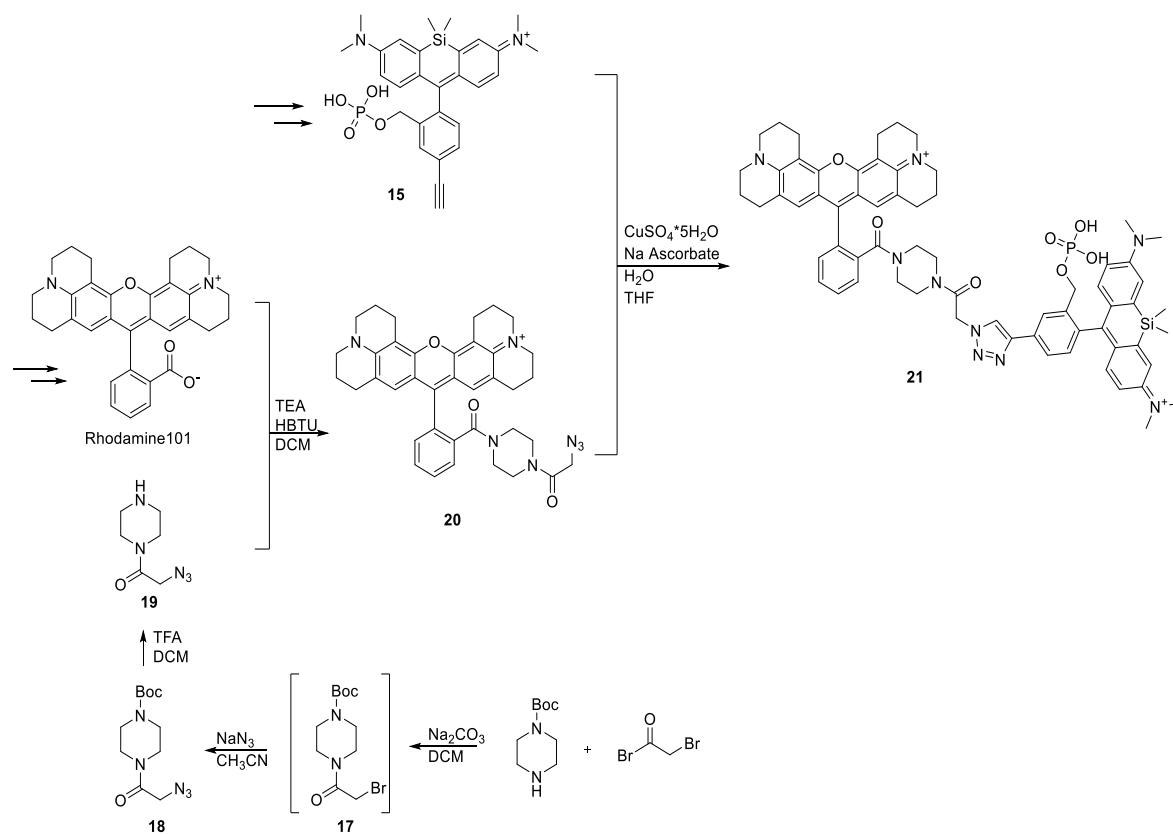


Scheme 15. Attempt of synthesis of the final FRET probe.

The phosphorylation of the reduced FRET probe remained unsuccessful (Scheme 15), probably because the chemical structure was too complex, and the conditions required for oxidation of the reduced HMSiR were too harsh. For reducing the complexity of the molecular structure, a new attempt has been tried starting from compound **12** without results.

The final desired probe structure has been obtained adopting a convergent scheme of synthesis developing a new synthetic route for making the linker between the two fluorophores (Scheme 16).

This new approach was adopted also for the synthesis of compound **13** ensuring higher yields and easier purifications of the intermediates.



Scheme 16. New scheme of synthesis of the compound **21**.

Preliminary studies on the spectroscopic behaviour of the compounds **13** and **21**

In order to validate the hypothesis that the designed molecule is able to generate a FRET phenomenon between the two fluorophores the absorption and emission spectra of the two compound **13** and **21** and of the two starting materials **15** and **20** were measured using a 96well plate reader.

As theorized in phase of design of the probe, the two starting materials present adequate photophysical properties to allow a FRET phenomenon. Compound **20** has a maximum of absorption at 589 nm and a maximum of emission at 611 nm. Compound **15** presents a maximum of absorption at 653 nm and a maximum of emission at 670 nm. As reported in Figure 9 the emission spectra of the compound **20** overlaps very well with the absorption spectra of compound **15** ensuring the optimal conditions for the occurrence of the FRET phenomenon.

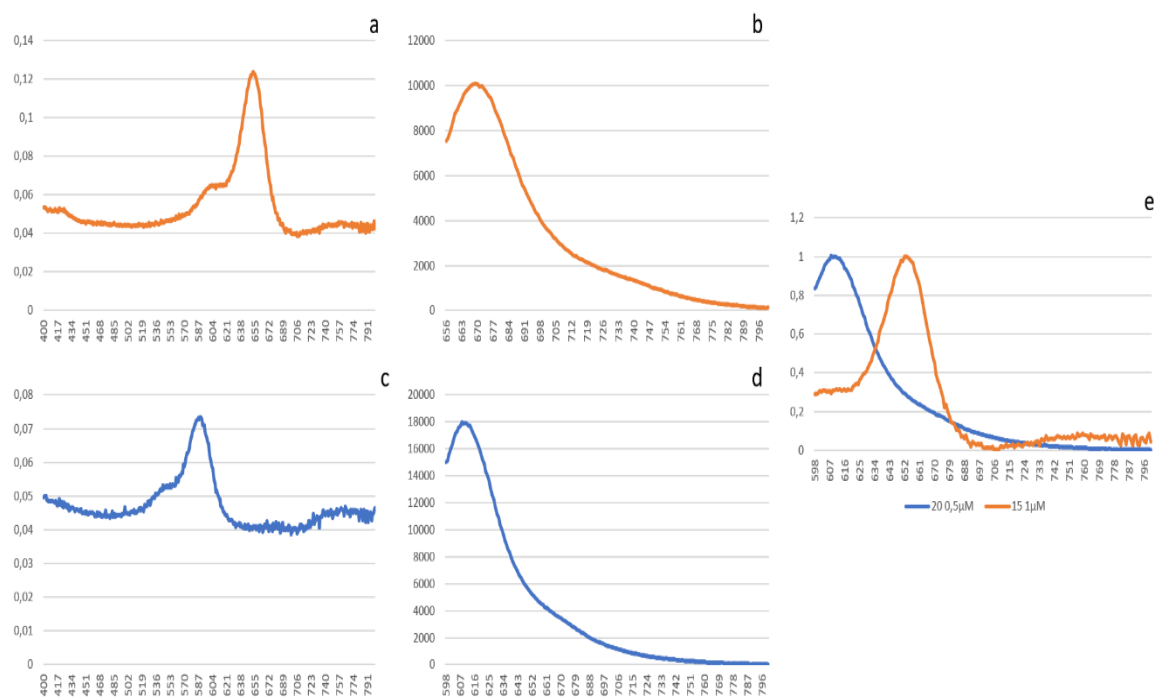


Figure 72. a) Absorbance spectrum of 15 (125 μ L, 1 μ M) in buffer TRIS-HCl 50mM, NaCl 75mM pH7.5, measured with plate reader Spark® Tecan. b) Fluorescence spectrum of 15 (125 μ L, 0.5 μ M) in buffer TRIS-HCl 50mM, NaCl 75mM pH7.5, measured with plate reader Spark® Tecan. c) Absorbance spectrum of 20 (125 μ L, 1 μ M) in buffer TRIS-HCl 50mM, NaCl 75mM pH7.5, measured with plate reader Spark® Tecan. d) Fluorescence spectrum of 20 (125 μ L, 0.5 μ M) in buffer TRIS-HCl 50mM, NaCl 75mM pH7.5, measured with plate reader Spark® Tecan. e) Superimposition of the normalised emission spectrum of 20 and the absorbing one of 15.

These hypotheses were confirmed also by the comparison of the emitting and absorbing spectra of the compounds **13** and **21**. As reported in Figure 10 when the probe is completely phosphorylated there is the appearance in the absorbance and fluorescence spectra of the typical signals that refer to the HMSiR moiety. Considering that compound **15** does not absorb at 561nm there should not be any emitting signal from this part of the chromophore. Instead, as visible in Figure 73 the emission peak of the HMSiR is present in the fluorescence spectra confirming the existence of a FRET phenomenon between the two fluorophores. Figure 10 shows another interesting feature of the compound **21**, which is its significant increase in the fluorescence. This could be due to a partial overlapping of the fluorescence spectra of the two fluorophores.

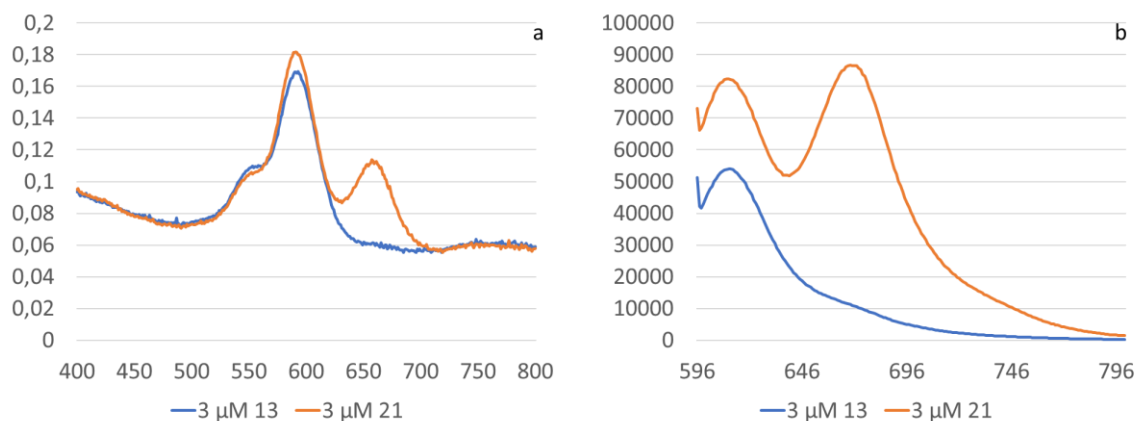


Figure 73. UV-Vis absorbance of the compounds **13** and **21** in buffer TRIS-HCl 50mM, NaCl 75mM and 50 μ g of proteins per 125 μ L of buffer, at pH 7,5. b. fluorescence spectra of the compounds **13** and **21** exciting at 561nm.

The stability of compound **21** in physiological buffer has been studied using a kinetic scanning protocol in a UV-Vis spectrophotometer, registering a new spectrum every 10 minutes for one hour at 37°C. No changes were observed, confirming its stability (Figure 74).

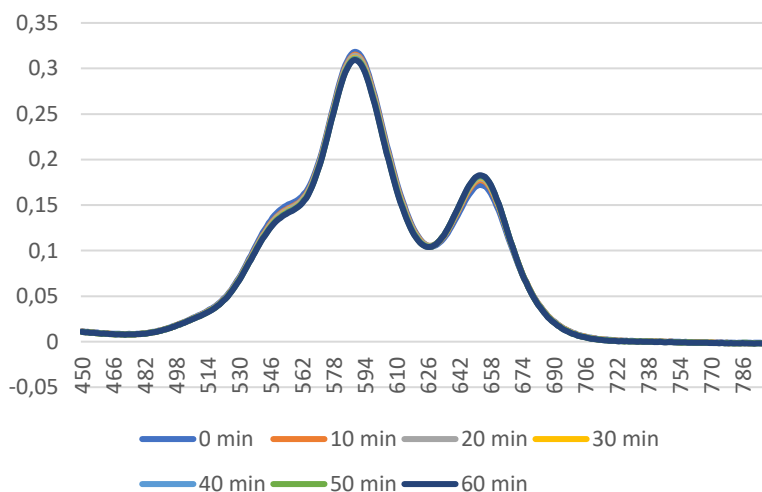


Figure 74. Stability test of compound **21** in PBS at 37°C with a concentration of 4 μ M.

With the two different compounds **21** and **13** a calibration curve was built for using it in the phosphatase activity tests with cellular lysates. The calibration curve was obtained mixing the two compounds at a fixed concentration and varying the percentage of phosphorylated compound in the mixture. The absorbance and fluorescence spectra were recorded for each point of the curve and then the ratios between the intensity at the two maxima of emission of the fluorescence spectra were plotted obtaining the calibration curve. This experiment was performed two times, using TRIS-HCl buffer or the TRIS-HCl buffer with an inactivated cell lysate. In both cases we obtained a similar result with two calibration curves almost identical.

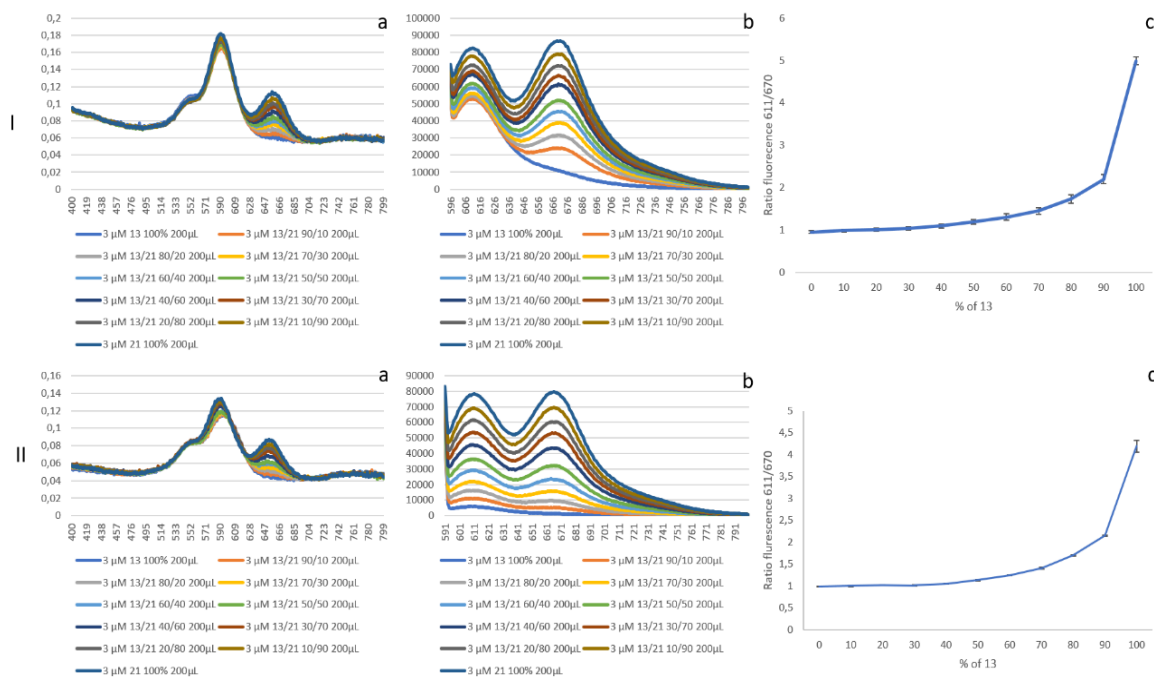


Figure 75. I. a) absorbance spectra of increasing concentrations of compound 13 in buffer TRIS-HCl 50mM, NaCl 75mM and 50 μ g of proteins per 125 μ L of buffer, at pH 7,5. b) fluorescence spectra exciting at 561nm. c) Calibration curve. II. a) absorbance spectra of increasing concentrations of compound 13 in buffer TRIS-HCl 50mM and NaCl 75mM at pH 7,5. b) fluorescence spectra exciting at 561nm. c) Calibration curve.

Figure 75 shows how compound **21**, when dephosphorylated shows a ratiometric behaviour that can be used for determining the amount of dephosphorylation during functional studies of the activity of phosphatases enzymes. The fact that the ratiometric behaviour is stable also in different buffers gives to the probe major robustness because this means that all the data obtained with this probe in different conditions of buffer or concentration of the molecule can be compared one to each other maintaining a good degree of reliability.

For better understand the stability of the signal given by this probe in different environmental conditions, compound **13** and **21** were analysed at different pH, recording the respective absorption and emission spectra.

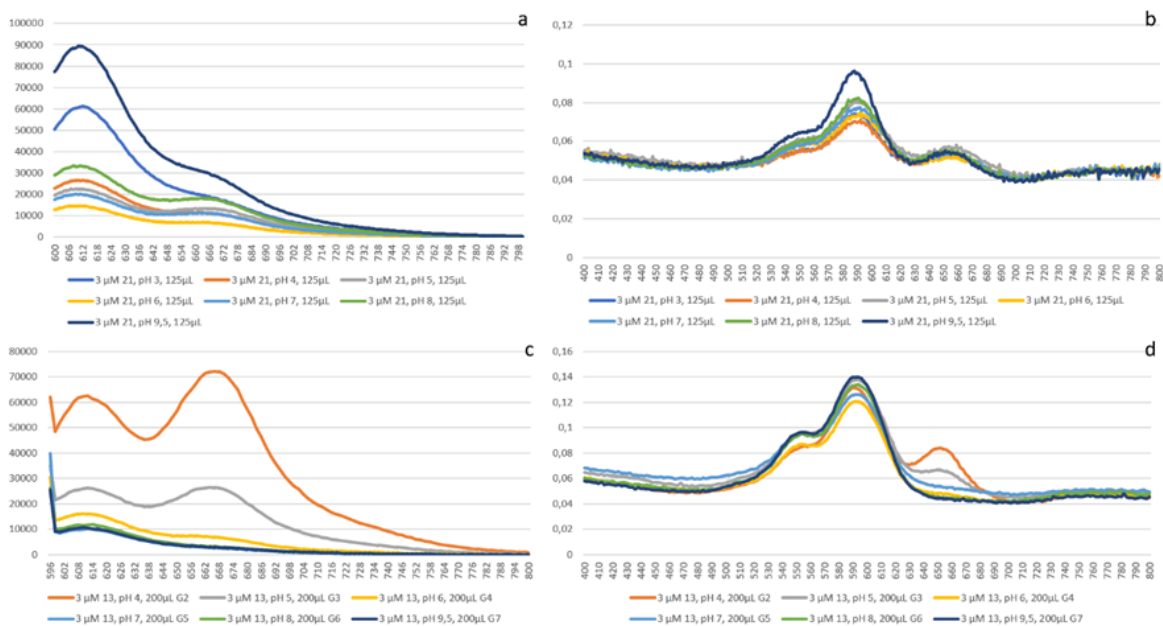


Figure 76. Fluorescence spectra, exciting at 561nm, of compound 21 (a) and compound 13 (c) at different pH. Absorbance spectra of compound 21 (b) and compound 13 (d) at different pH.

As expected, compound **13** showed a different spectroscopic behaviour in different pH values. This is correlated with the shift of the open and closed population of the HMSiR moiety of the probe. Indeed, at low pH this portion of the molecule is predominantly open, and this leads to the appearance of the absorbing peak of the silicon rhodamine in the absorbance spectra and the presence of an emission band at 670 nm that is correlated with the same phenomenon. Vice versa, at high pH, the HMSiR moiety is predominantly closed and this does not allow to see any signal deriving from this part of the molecule.

Less predictable is the trend of the compound **21**. In this molecular scaffold the two fluorophores are constantly present in an open and fluorescent form and for this reason the spectroscopic properties of this compound should not be affected by changes in the pH. Figure 13 shows that also compound **21** has a changing behaviour at different pH values. At low and high pH compound 21 seems to lose the capacity to generate the FRET phenomenon between the two fluorophores. Indeed, at pH 9.5 and at pH 3.0, in both cases the absorbance peak of the silicon rhodamine part of the molecule is still present but the fluorescent emission is strongly compromised, a symptom that the FRET mechanism does not occur anymore. For trying to find an explanation for this phenomenon, a minimization of the molecular structure of compound **21** has been performed using Avogadro as minimizing software.

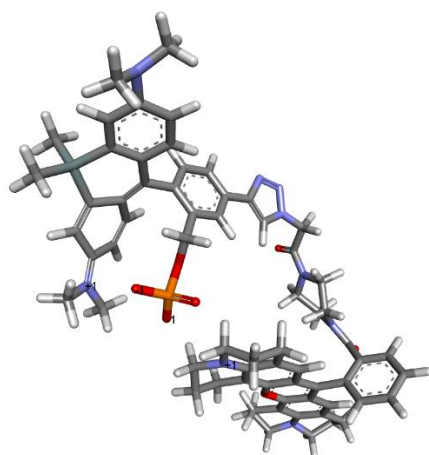


Figure 77. Minimised structure of compound 21 at pH 7.4.

The obtained structure could resemble the normal configuration of the molecule at physiological pH. In this conformation, the phosphate group coordinates the two positive charges of the two rhodamines, allowing efficient FRET. This configuration could be disturbed at low pH where the phosphate group is no more doubly negatively charged (pKa of the phosphoric acid: pKa₁=2.14; pKa₂=7.20; pKa₃=12.37. pKa of the methylphosphonic acid: pKa₁=2.12; pKa₂=7.29.). The loss of a charge could avoid that the two fluorophores are in proximity one to each other, reducing the efficacy of the FRET phenomenon (Figure 15).

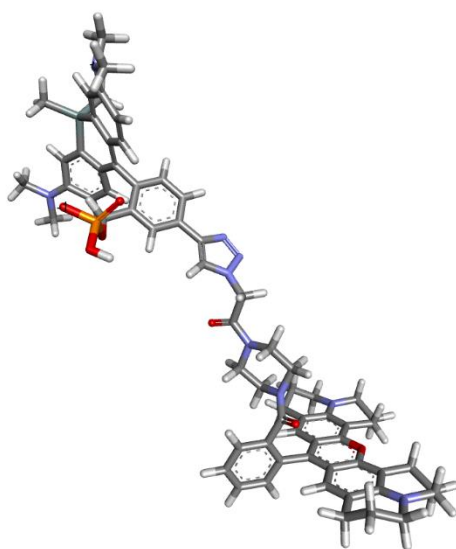


Figure 78. Minimized structure of compound 21 at pH 3.

Concerning the behaviour of this compound at higher pH it has to be considered another phenomenon, that can contribute to the final effect also at low pH, and it is the contribution of the solvent. In this case at high pH the excess of OH⁻ anions can mask the charge of the two positively charged nitrogen atoms, breaking the salt bridge that they form with the phosphate group and forcing the two fluorophores to move

away from each other reducing the effectiveness of the FRET phenomenon. The same masking effect could intervene also at low pH involving H_3O^+ cations.

Activity tests in cellular lysates and with isolated enzyme of compound 21

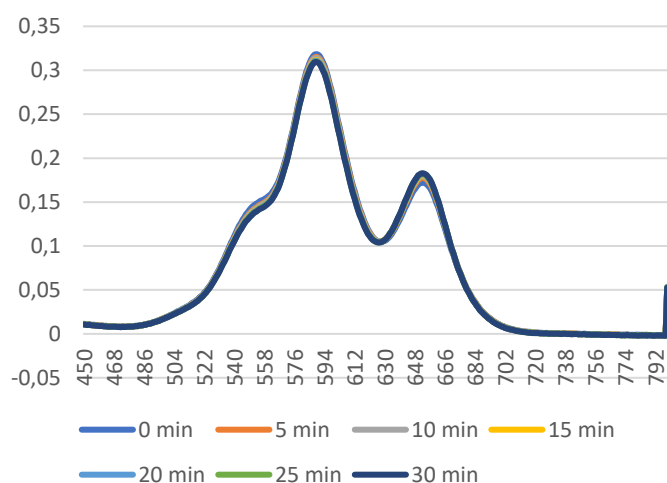


Figure 79. Dephosphorylation profile of compound 21 ($4\mu M$) in PBS at pH 7.4 and a concentration of lysate protein of $50\mu g/mL$.

With the aim to validate compound **21** as a probe for the detection of the phosphatase activity, a kinetic study was performed in a PBS buffer at pH 7.4 with the addition of an aliquot of cellular lysate, obtained from HeLa cells, at a protein concentration of $50\mu g/mL$. An adequate scanning protocol has been chosen using a UV-Vis spectrophotometer, registering a new absorbance spectrum every 5 minutes for 30 min at $37\text{ }^\circ C$. Figure 79 shows that no change intervenes in the absorbing spectrum of compound **21**, meaning that this compound seems to not be affected by the phosphatases present in the lysate.

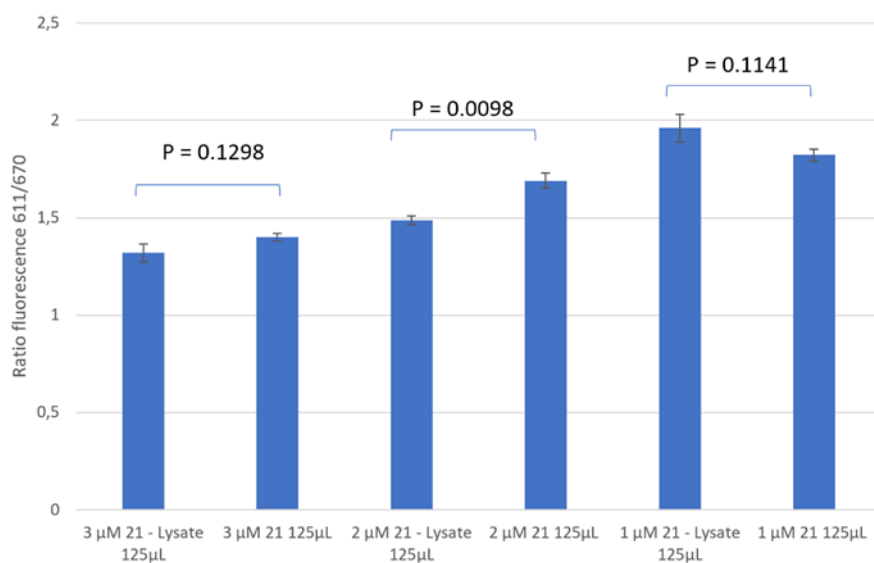


Figure 80. Ratio of fluorescence of compound 21 at different concentrations. The references standards are obtained using a solution containing TRIS-HCl 50mM, NaCl 75mM buffered at pH 7.5. The concentration of proteins in the lysate test is of $80\mu g/mL$.

Considering that the high concentration of phosphate used in the buffer could have altered the result, because this anion could have masked the active sites of all the phosphatases present in the cuvette, a new experiment has been run using a different kind of buffer and increasing the concentration of proteins. The new buffer contains TRIS-HCl 50 mM, NaCl 75 mM buffered at pH 7.5.

Figure 80 shows as compound **21**, even changing the buffer and increasing the concentration of the proteins, is not affected by the phosphatases present in the lysate. Another test has been performed using the cellular lysate increasing the concentration of the proteins to 400 $\mu\text{g}/\text{mL}$ (50 $\mu\text{g}/125\mu\text{L}$). In this case we observed a significant variation in the ratio of the fluorescence at 611 nm and 670 nm, after one hour of incubation at 37 °C (Figure 81).

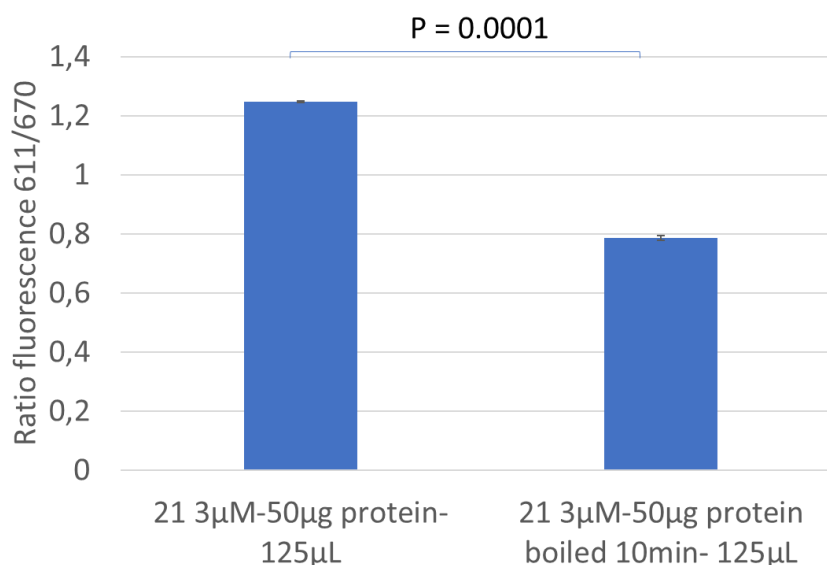


Figure 81. Activity of the lysate proteins on compound 21 after 1h of incubation at 37°C.

After these promising results compound **21** was tested with this concentration of lysate incubating it also with well-known phosphatase inhibitors. The idea of this experiments was to inhibit different classes of phosphatases and see how this perturbation of the system can affect the dephosphorylation of the probe. This should allow to identify a possible target enzyme that selectively, or at least principally, dephosphorylates this molecule. This experiment has been done using: Okadaic Acid (OA), Disodium vanadate (Na_2VO_4), 1,2-Di(cis-9-octadecenoyl)-sn-glycerol 3-phosphate sodium salt (PA).

Inhibitors	Ser/Thr Phosphatases							Tyr Phosphatases
	PPM	PPP						
		PP1	PP2A	PP4	PP6	PP2B	PP5	
Cd ²⁺	1,5 μM							
Na ₃ VO ₄								0,1 mM
OA		2-5 μM	1-2 nM	1-2 nM	1-2 nM	2-5 μM	2-5 μM	
PA		80 nM	10 μM					
Fenvalerate						1 nM		

Table 7. Principal selective inhibitors of phosphatases actually available and their selectivity through the different classes of phosphatases.

OA is a potent and selective inhibitor for PP2A, PP4 and PP6 and it acts on these targets at a concentration of 1-2 nM; at higher concentrations, 2-5 μM, this compound is able to inhibit other enzymes belonging to the family of the PPP ser/thr phosphatases.^[148] Na₃VO₄ inhibits selectively the Tyr phosphatases at a concentration of 0.1 mM acting as a competitive inhibitor in the active site of the phosphatases.^[149] PA is a selective inhibitor of the ser/thr phosphatase PP1 at 80 nM; if it is used at a concentration of 10 μM PA can act as an activator of the enzyme PP2A.^[150] All these inhibitors were previously incubated with the proteins of the lysate and then the solution of compound **21** was added. After 1 h of incubation at 37 °C the ratio between the fluorescence at 611 nm and 670 nm has been measured.

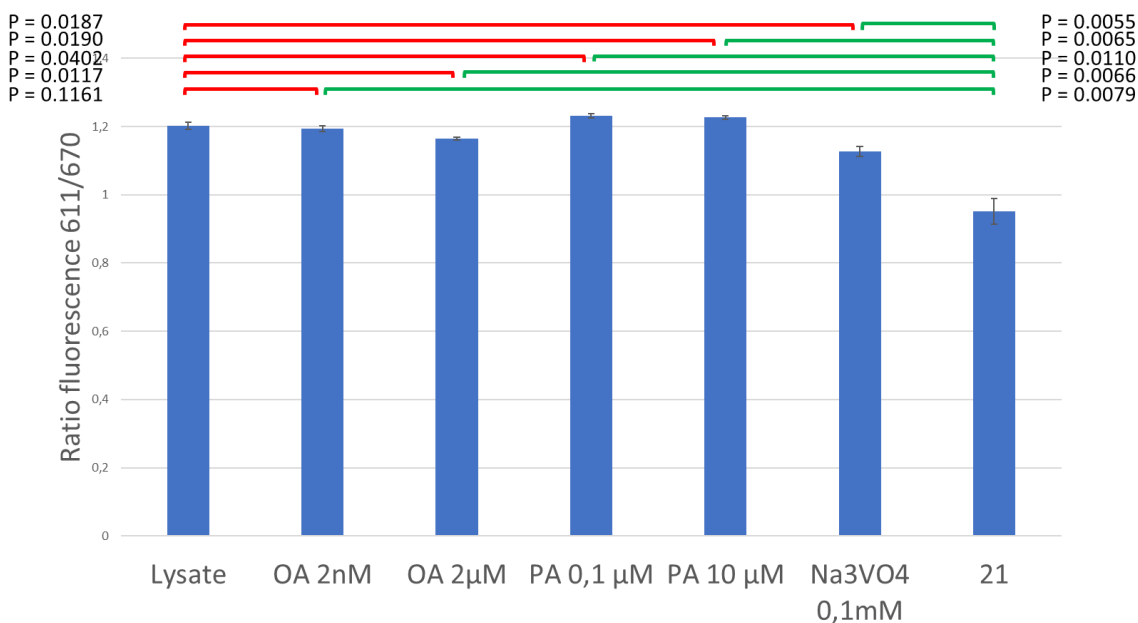


Figure 82. Inhibitions tests of the phosphatase activity. All the samples were prepared in a solution of TRIS-HCl 50mM, NaCl 75mM buffered at pH 7.5 and a concentration of proteins of 400μg/mL. Lysate refers to the sample that contains the phosphatases enzymes but no inhibitors. Sample 21 represents just the compound 21 in a buffer solution containing the

Figure 82 shows the results of these preliminary tests. All the different inhibitors seem to modify significantly the dephosphorylation of compound **21** but the magnitude of these changes is so little that it is difficult to extrapolate some useful information about the possible class of phosphatases that preferentially interacts with our probe.

Further tests were performed using an isolated enzyme. For simplicity alkaline phosphatase has been chosen.^[151] This enzyme dephosphorylates general substrates without a great selectivity and for this reason it could be considered as a good prototype for starting to test a probe. Alkaline phosphatase is able to dephosphorylate this probe if the compound and the enzyme are incubated over night at 37 °C with a TRIS-HCl buffer at pH 8. In case that the time of incubation is just 15 minutes the enzyme seems not able to alter the phosphorylation state of our compound. This could indicate that the alkaline phosphatase is not the target of compound **21** and further studies are necessary for having a better understanding of the enzymes principally involved in the dephosphorylation of the FRET probe.

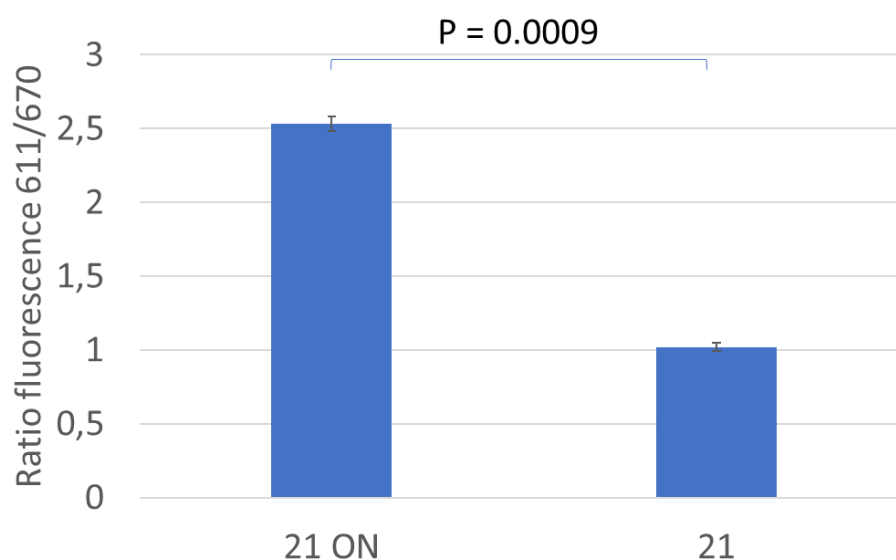


Figure 83. Ratio of the intensity of fluorescence of the two maxima of emission (611 and 670nm). Buffer TRIS-HCl 50mM, NaCl 75mM and pH 8.0. Sample 21 ON was incubated over night at 37°C. Sample 21 was incubated for 15 minutes at 37°C.

The spectroscopic behaviour of compound **21** was investigated also in presence of physiological nucleophiles like glutathione (GSH). This idea was inspired by the work of Urano and co-workers^[152] who developed a FRET probe for detecting glutathione in live-cell imaging. The probe developed by this research group has a molecular structure similar to that one adopted in this project, with an always fluorescent silicon rhodamine as FRET acceptor and a rhodamine as FRET donor. Compound **21** is effectively influenced by the presence of GSH following a linear trend as reported in figure 21.

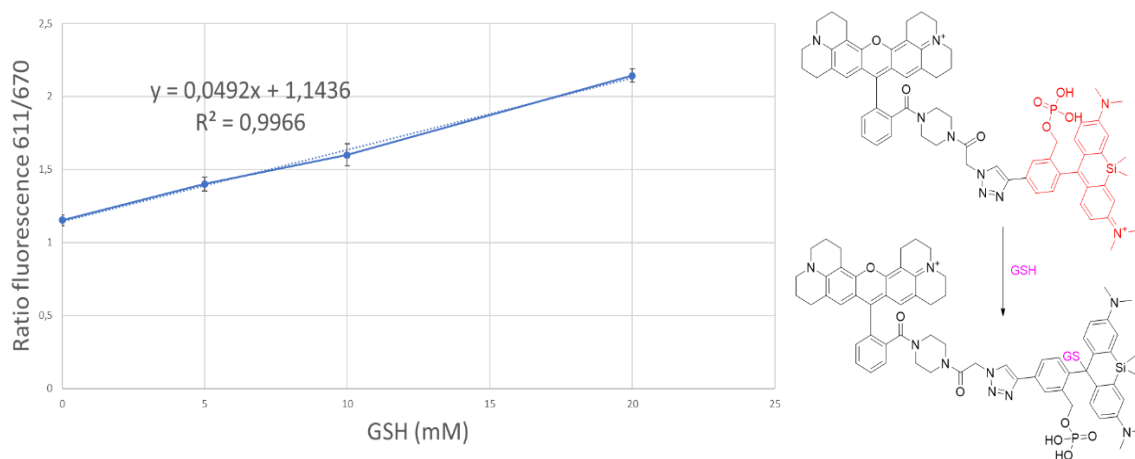


Figure 84. . Calibration curve of compound **21** ($3\mu\text{M}$) using increasing concentrations of GSH (0-20mM). Buffer TRIS-HCl 50mM, NaCl 75mM and pH 7.5. Mechanism of quenching of the HMSiR moiety with glutathione.

The ratio between the two maxima of fluorescence (611/670) can be altered by the presence of GSH because the free thiol of glutathione can insert in the xanthene system interrupting the conjugation of the aromatic structure disrupting the typical fluorescence of the HMSiR moiety as reported in Figure 84.

This result questions the possibility to use compound **21** in whole cell-lysate because there could be an interference between two different mechanisms that can alter the ratiometric signal of the probe. Nevertheless, compound **21** seems to be not really sensitive to the physiological concentration of GSH that could be present in cell-lysate. Indeed, referring to the work published by Giustarini et al.^[153], the maximum concentration of GSH that can be found in a cell line used for experiments is 91.6 nmol/mg prot (RD cells). Assuming that HeLA cells have this concentration of GSH, in the buffer used for the experiments with cellular lysate the concentration of glutathione is around $37\mu\text{M}$, not considering that GSH levels could be further lowered during preparation of lysates. This means that the read out of the experiment can be staggered of +0.0018204, that is far below the standard deviation of every measurement done. This means that compound **21** can be still considered a valid candidate for the detection of the phosphatase activity in cell lysates.

Furthermore, we investigate also the possibility that the readout of the experiments done in the presence of lysate or inactivated lysate can be altered by a CHEF phenomenon, which could enhance the fluorescence of our compound altering the ratio between the two maxima of emission. To elucidate this possible interference another experiment was performed. Compound **21** and **13** were incubated with different concentrations of MgCl_2 (20-10-5-2.5-0mM) to see if this divalent cation is able to alter the spectra of emission of the two compounds. As shown in figure 85, both the compounds are not significantly affected by the presence of the Mg^{2+} ion.

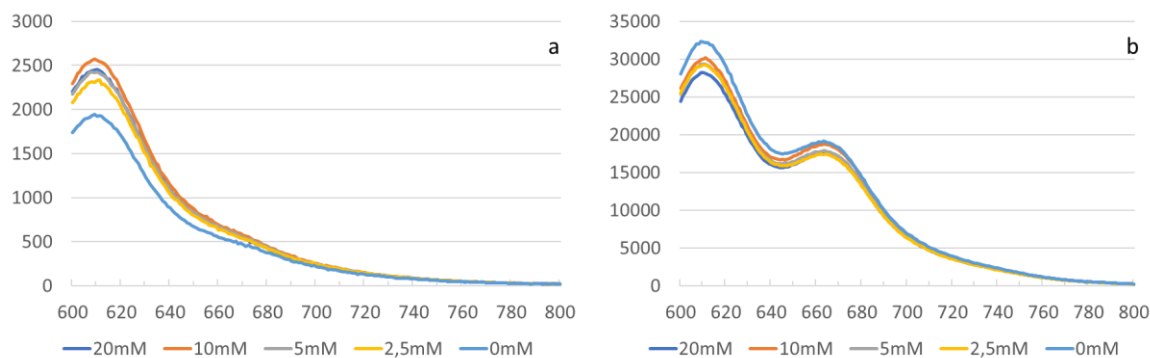


Figure 85. a) Fluorescence spectrum of compound **13** in TRIS-HCl 50mM, NaCl 75mM and pH 7.5 and increasing concentrations of MgCl₂. b) Fluorescence spectrum of compound **21** in TRIS-HCl 50mM, NaCl 75mM and pH 7.5 and increasing concentrations of MgCl₂.

Microscopy experiments

Compound **21** and compound **13** have been tested in confocal fluorescence microscopy experiments for evaluating their ability of enter within the cells and to identify their principal site of accumulation. Therefore, human cervical cancer (HeLa) cells were incubated with **21** and **13** (1 μ M) for 1 h, washed with PBS (pH 7.4) and then imaged. Fluorescence images at 561 nm excitation were then taken. Both the compounds are able to penetrate the cells and in a first approximation it is reasonable to think that both probes accumulate within organelles that resemble the typical shape of mitochondria. For a more accurate localization and validation of this hypothesis, colocalization with organelle-specific markers are required.

Single Molecule Detection experiments on PVA films have been performed with the aim to confirm the FRET and blinking behaviour of the probe. As shown in figure 9e and 9f, the plot that reports the number of photons emitted by time per each molecule of the probe confirms that the FRET donor is almost quenched by the FRET acceptor, while the latter is able to emit without any interference. This confirmed the presence of a FRET mechanism, while the blinking behaviour has been detected with other movies, not showed in this report.

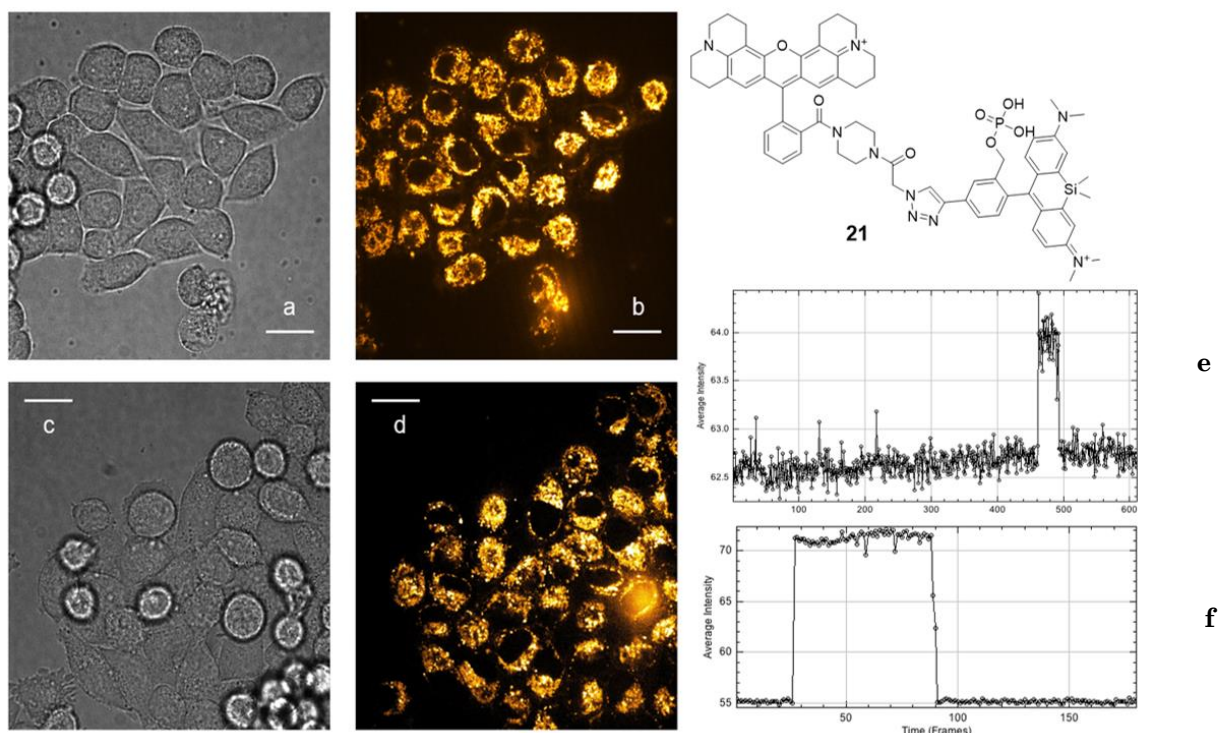


Figure 86. a) Brightfield image 13. b) 13 imaged by confocal exposure (561 nm, 200 mW, 25% power, 20 ms). c) Brightfield image 21. d) 21 imaged by confocal exposure (561 nm, 200 mW, 25% power, 100 ms). e) PVA film-Single molecule detection (Scale bars = 500 nm, Exposure time = 50 ms, Laser power (561 nm) = 50%) f) PVA film-Single molecule detection (Scale bars = 500 nm, Exposure time = 50 ms, Laser power (647 nm) = 80%).

.Outlook

Considering that compound **21** has a modest rate of dephosphorylation, probably due to the fact that the phosphate group is sterically hindered, some modifications to the chemical structure could be effective. The introduction of a self-immolative linker between the phosphate group and the HMSiR could improve the sensitivity towards phosphatases. This could help because the distance of phosphate group from the rest of the molecule would be increased which makes it more easily available for the phosphatase.

Another modification, especially interesting for live-cell microscopy is the introduction of a photoactivatable group masking the phosphate as proposed in figure 28^[154].

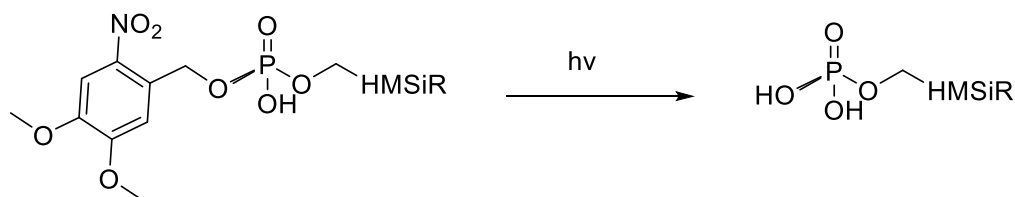


Figure 87. Photoactivatable masking of the phosphate group.

With this modification of the phosphate scaffold it will be possible to selectively and gradually release the enzyme substrate upon irradiation. This feature can be useful to detect intracellular kinetics of phosphatases.

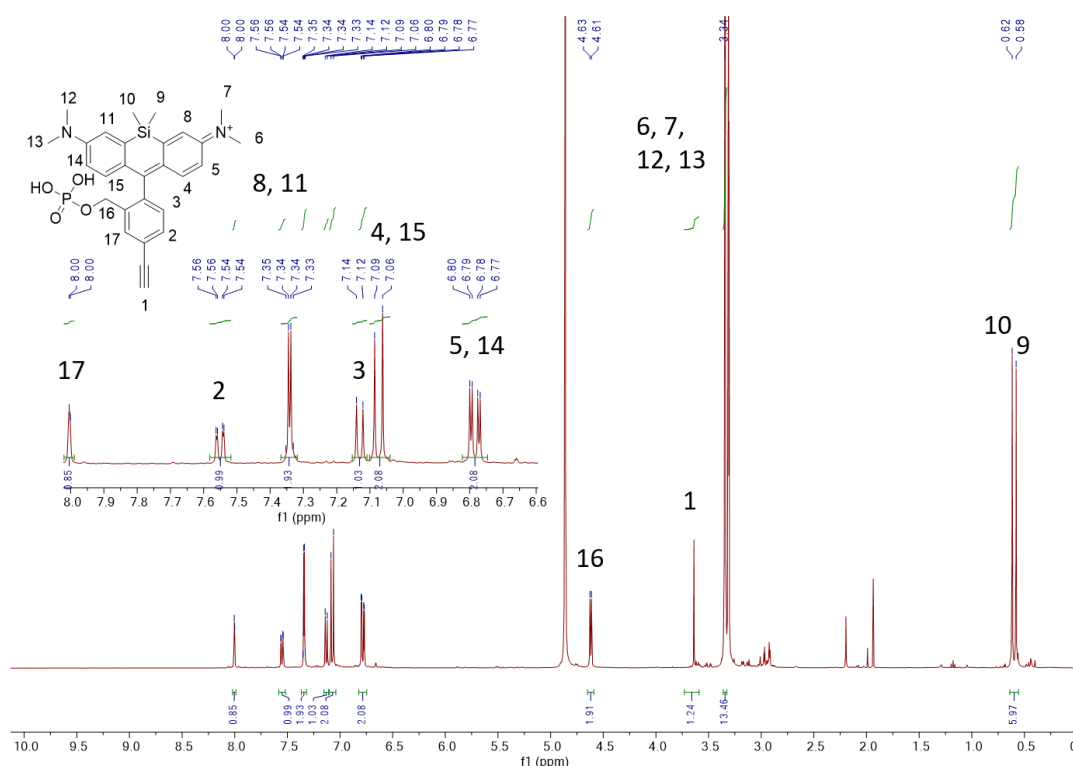
It will be interesting also to modify the molecular scaffold of the probe, introducing a targeting agent that will increase the selectivity of the compound. This will allow to discriminate between the different enzymes that are present in the lysates and this will transform the probe in a more powerful tool also for the super-resolution microscopy, allowing to track only a specific target.

Furthermore, it would be interesting to evaluate how the distance between the two fluorophores can influence the FRET efficiency. This could be done by substituting the actual spacer with a polyproline chain that has a fixed length and a higher rigidity.

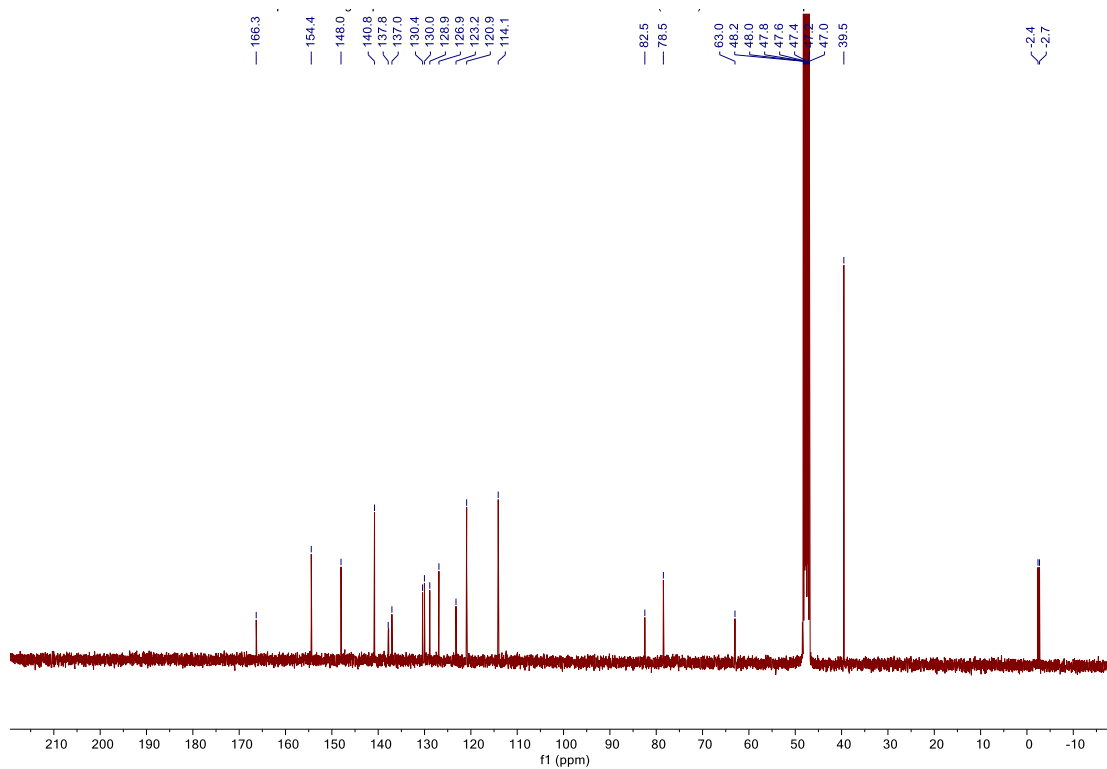
Example of NMR characterisation

Considering the complexity of the final compound, each synthon, that led to the obtainment of the desired molecule, has been fully analysed through the NMR spectroscopy performing 1D experiments (^1H , ^{13}C) but also 2D experiments (COSY, HSQC and HMBC). Successively these results have been used as referring standard for determining the following compound, till the desired one.

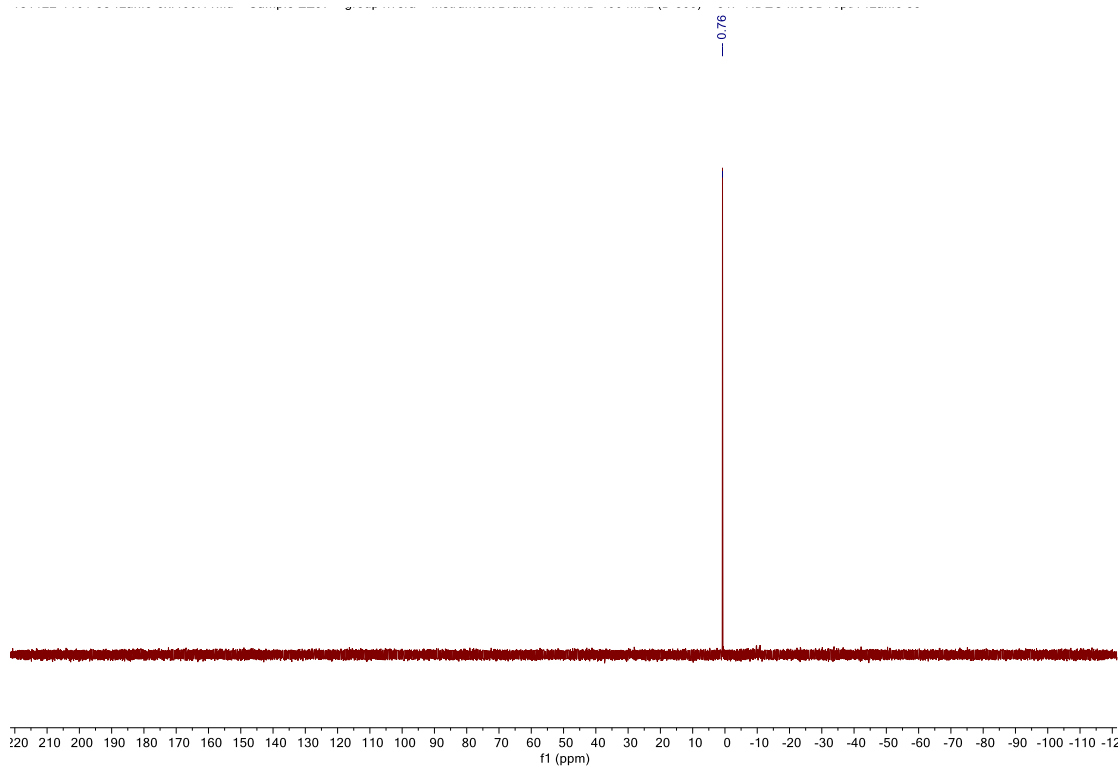
Compound 15 and the final compound have been reported as examples.



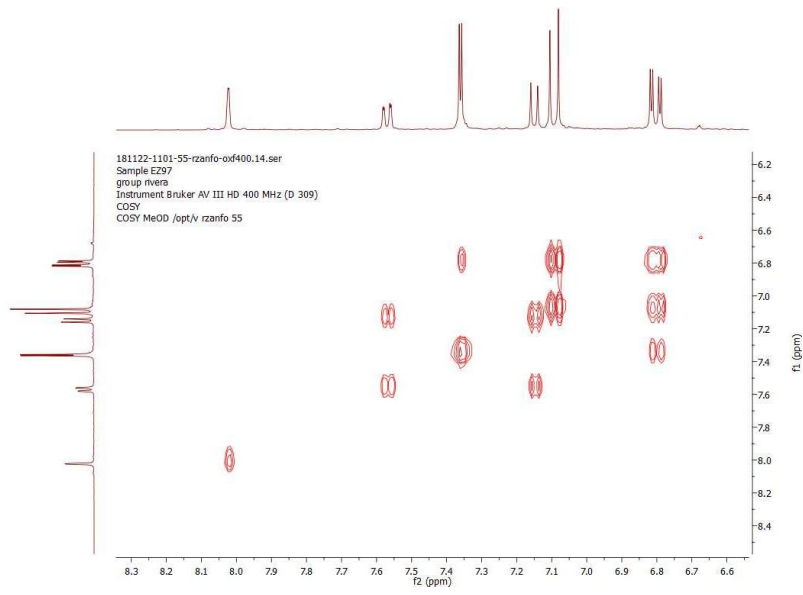
^1H NMR (MeOD, 400 MHz)



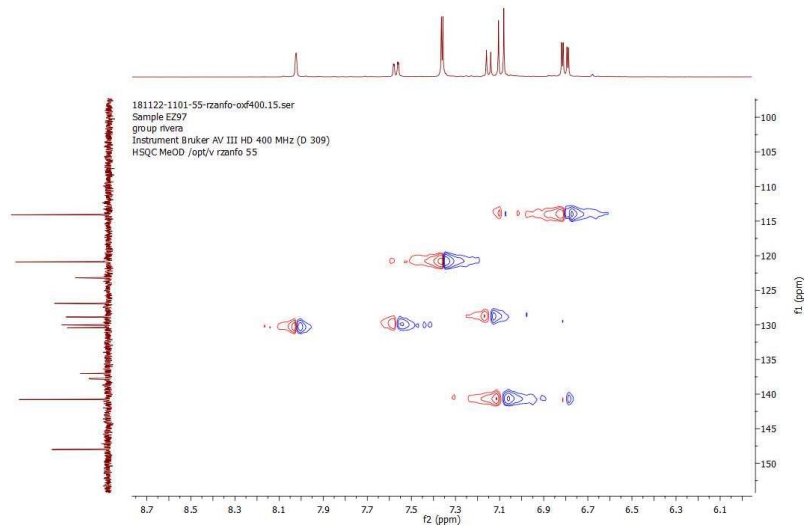
^{13}C NMR (MeOD, 100 MHz)



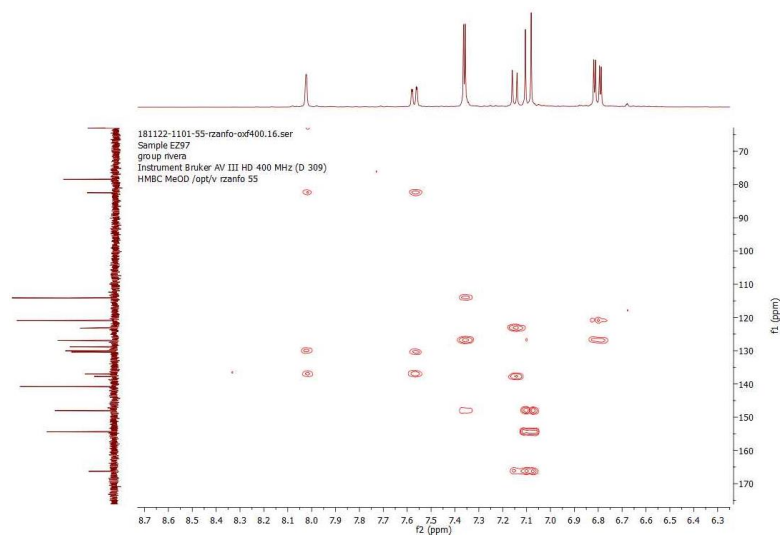
^{31}P NMR (162 MHz, MeOD)



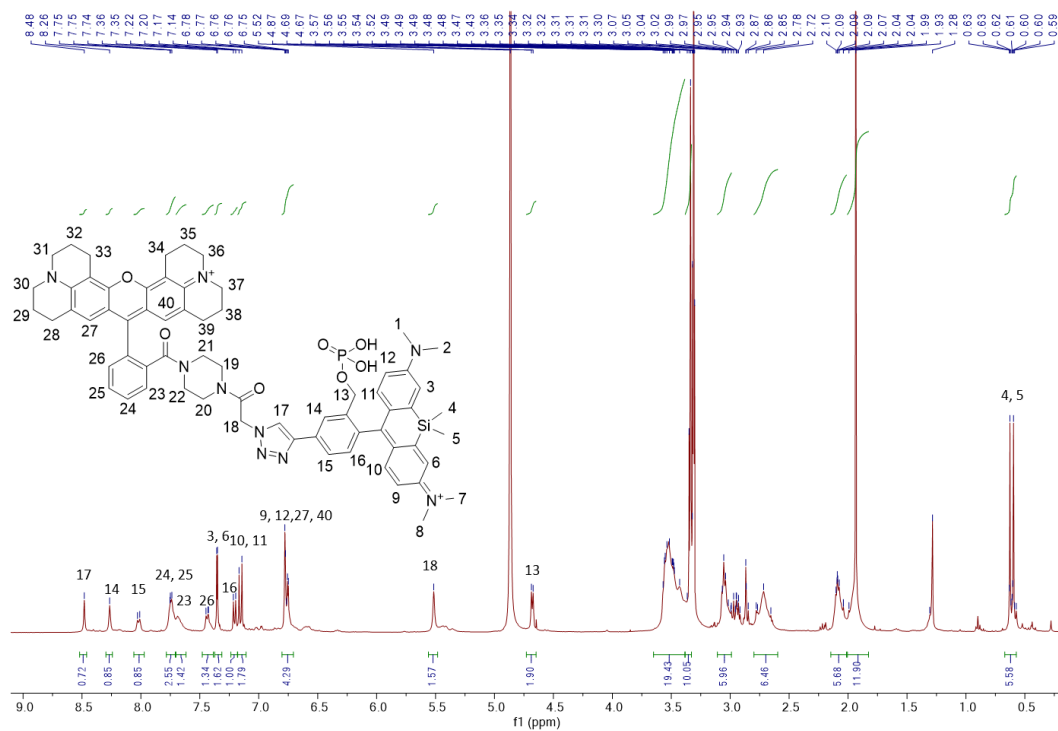
COSY NMR (MeOD, 400 MHz)



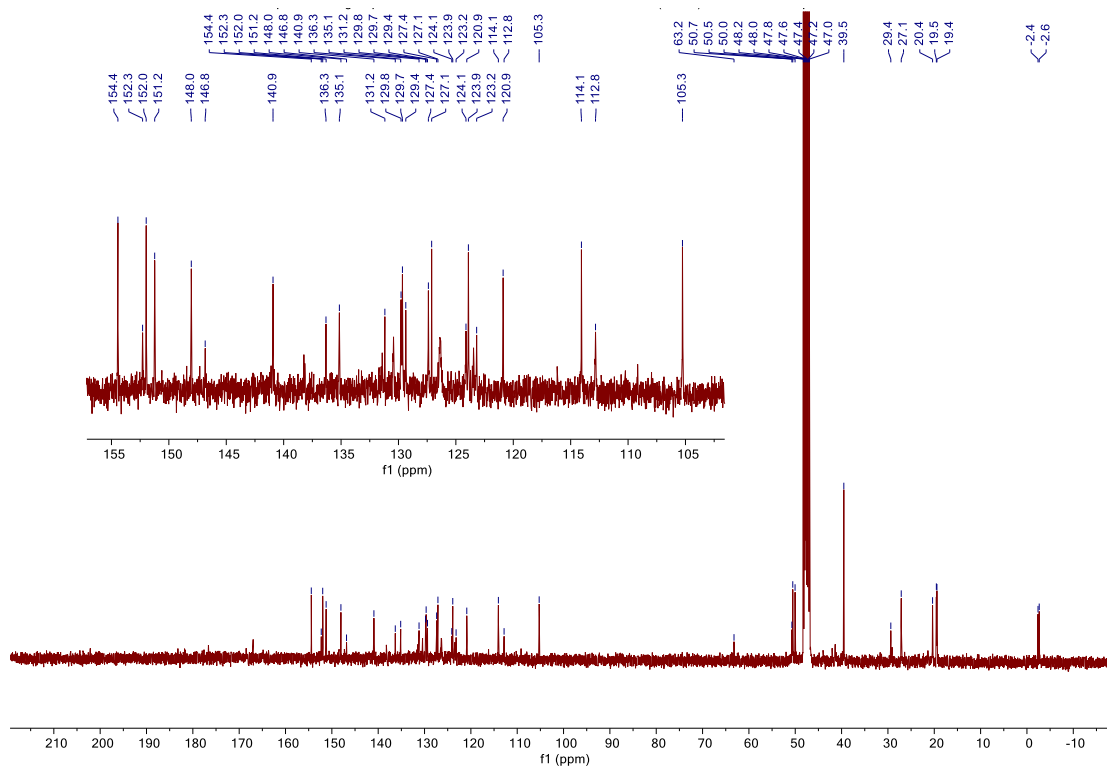
HSQC NMR (MeOD, 400 MHz)



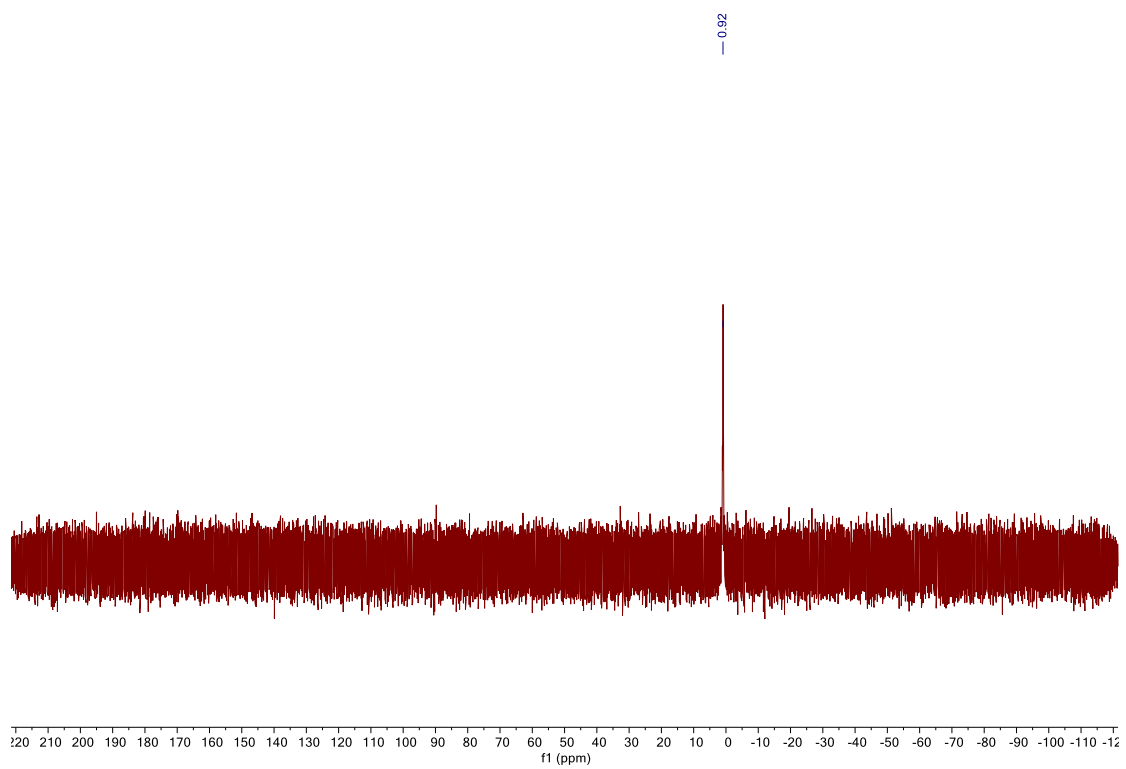
HSQC NMR (MeOD, 400 MHz)



¹H NMR (400 MHz, MeOD)



¹³C NMR (101 MHz, MeOD)



^{31}P NMR (162 MHz, MeOD)

3.2 SHP-1: Rationale and Results

Part of this PhD has been focused on the development of new molecules that are able to reconstitute the phosphatase activity of SHP-1 in leukemic cells. For developing these new chemical entities, SC-43 has been taken as model. As reported in paragraph 1.4.4, this compound has been developed by Chen and co-workers. It is a Sorafenib analogue able to reactivate SHP-1 and its potency against cancerous cells is comparable to that one of Sorafenib, but unlike its progenitor molecule, SC-43 does not present any kinase inhibitory activity. It is known that this compound interacts directly with SHP-1 but nowadays, there is no structural information available for the identification of its site of action. It has been demonstrated that the efficacy of this compound is lost if the N-SH2 domain of SHP-1 is lost. This is an extremely important information because it helps in the limitation of the research space within the structure of SHP-1. It is reasonable to think that the site of action of this class of compounds is localized within the N-SH2 domain. This sub-structure of the phosphatase presents a site for the recognition of phospho-tyrosines, a crucial modulatory domain that is the main responsible for removing N-SH2 from its autoinhibitory position. Indeed, it has been demonstrated that phosphorylated peptides that present the consensus sequence for the N-SH2 domain are able to reactivate SHP-1.[23] Merging all these notions together it seems reasonable to think that the site of action of this compound is the phospho-tyrosine binding site on the N-SH2 domain of SHP-1. This general idea has been tested, performing a blind docking with SC-43 and its analogues on the active (PDB:3PS5) and inactive (PDB: 2B3O) conformation of the phosphatase using Autodock vina as docking program. The results confirmed this hypothesis considering that the principal site of interaction diagnosed with this docking technique was exactly the theorized binding site on the active conformation. Further docking experiments have been performed focusing on the N-SH2 domain. Figure 88 illustrates the interactions generated by SC-43 with the regulatory domain, and these are principally hydrogen bonds. The proposed active site presents numerous positively charged amino acids and this feature could be exploited for developing new active molecules.

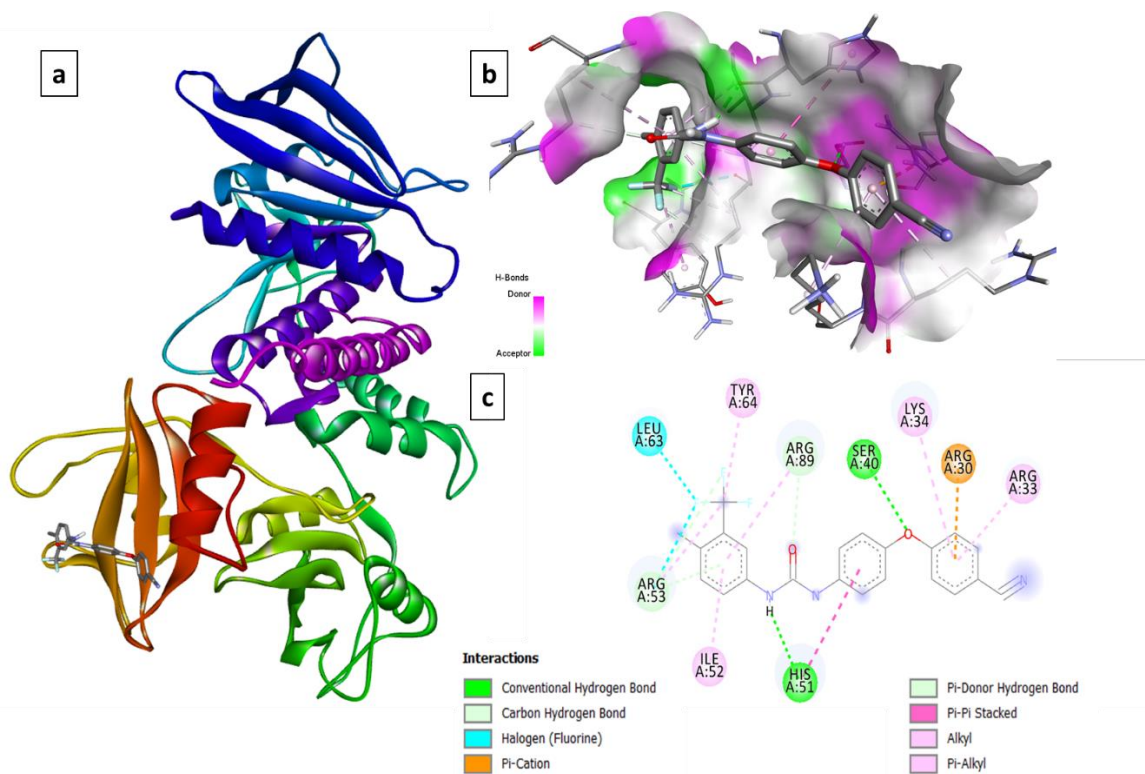


Figure 88. Proposed site of interaction of SC-43 with SHP-1 using Autodock vina. **A.** General overview of the SHP-1 structure and localization of the interacting site. **B.** SC-43 in its theorized active site. **C.** 2D plot of the generated interactions within the interacting pocket.

For this reason, several modifications of the original molecular scaffold have been proposed. The first idea has been to insert new functional carboxylic groups, that are negatively chargeable, at the two extremities of the chemical structure of SC-43: in the trifluoromethylaniline ring and on the benzonitrile portion of the molecule. The introduction of these carboxylic acids could improve the potency of the compound but could negatively affect the pharmacokinetic properties of the structure reducing its capacity of penetrating the cell membrane and consequently undermining all the gained potency. For overcoming this limitation, the analogues of the desired compounds have been synthesized with an ester moiety instead of the carboxylic one. This functional group being not charged facilitates the passage through the plasmatic membrane. This compound acts as a prodrug, a portion of the administered dose could be hydrolysed before to reach the cell, but a significant amount of the molecules will be prevalently internalised as it is. Once within the cell the ethyl ester moiety is easily hydrolysed obtaining the desired carboxylic acid derivative.

With the aim to interact with these hydrophilic amino acids another functional group has been introduced within the chemical structure: the nitro group. This functionality is extremely versatile in drug synthesis because it can form different hydrogen bonds with many hydrogen bond donors and thanks to its zwitterionic behaviour can generate weak electrostatic interactions with positively charged amino acids. For this

reason, it has been considered a valid functional group that could affect positively the potency of these new compounds.

Another idea for improving the potency of the SC-43 analogues has been the introduction in the molecular scaffold of a sulphonamide group instead of the ureido bridge. Analysing the theorised interactions generated by SC-43 with SHP-1, the ureido portion of the molecule is that one that occupies the binding site usually recognised by the phosphate group. With the aim to increase the similarity between the group that occupies this location and the phosphate group of the phosphotyrosine, the sulphonamide seemed to be the most promising one. Still focusing on the ureido bridge, another substitution has been done. Considering that the carbonyl portion of this structure is turned towards the solvent region and it explores a larger space compared to the two other nitrogen atoms, a larger substituent has been inserted instead of the oxygen atom obtaining in this way the thioureido bridge.

As previously illustrated, the docking studies evidenced the central role of the ureido portion of the SC-43 structure, which mimics the phosphate group that activates physiologically the enzyme. Considering the importance of this core domain it seems evident that so many efforts have been done with the aim to optimize the interactions generated by it with the protein, trying different solutions. One of these has been the substitution of the ureido structure with a quinazolone one. This new structure can be considered as a bio isostere of the urea because it presents a triad of heteroatoms linked together by a carbon atom hybridised in the same manner (Figure 89).

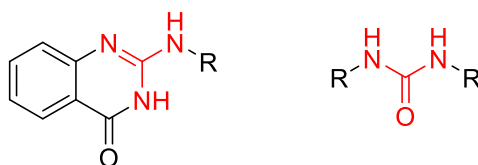
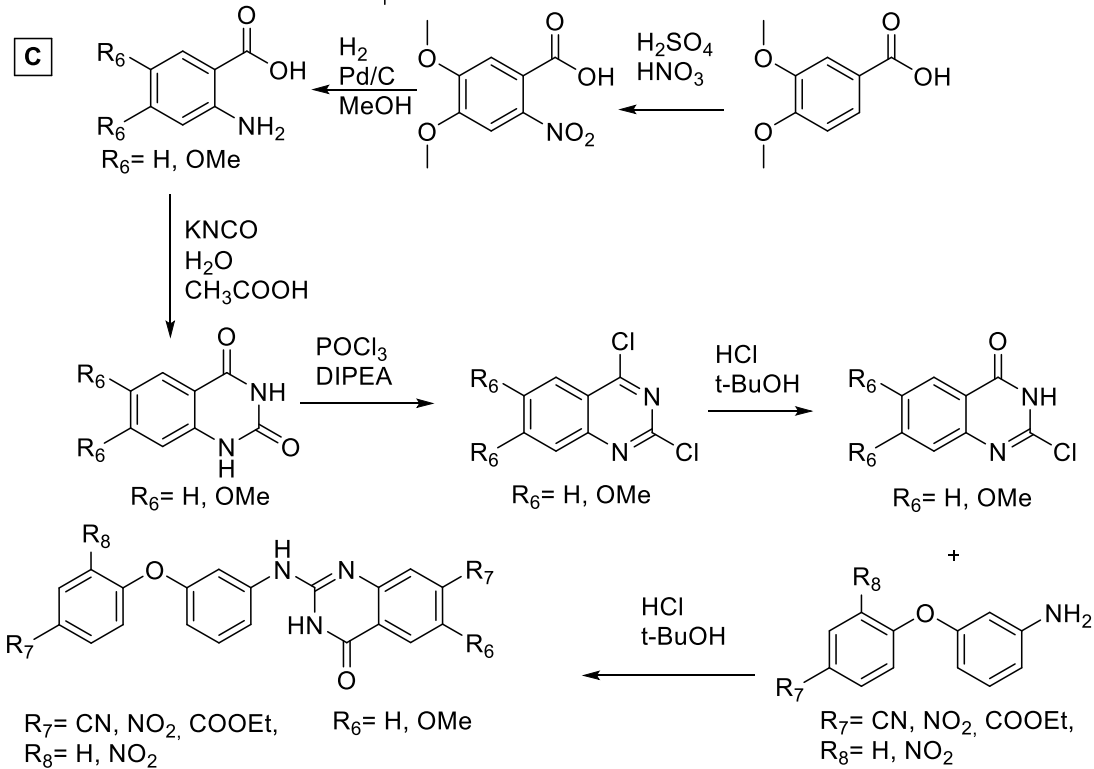
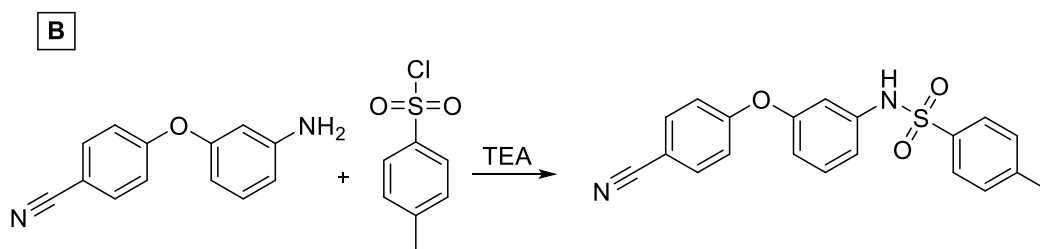
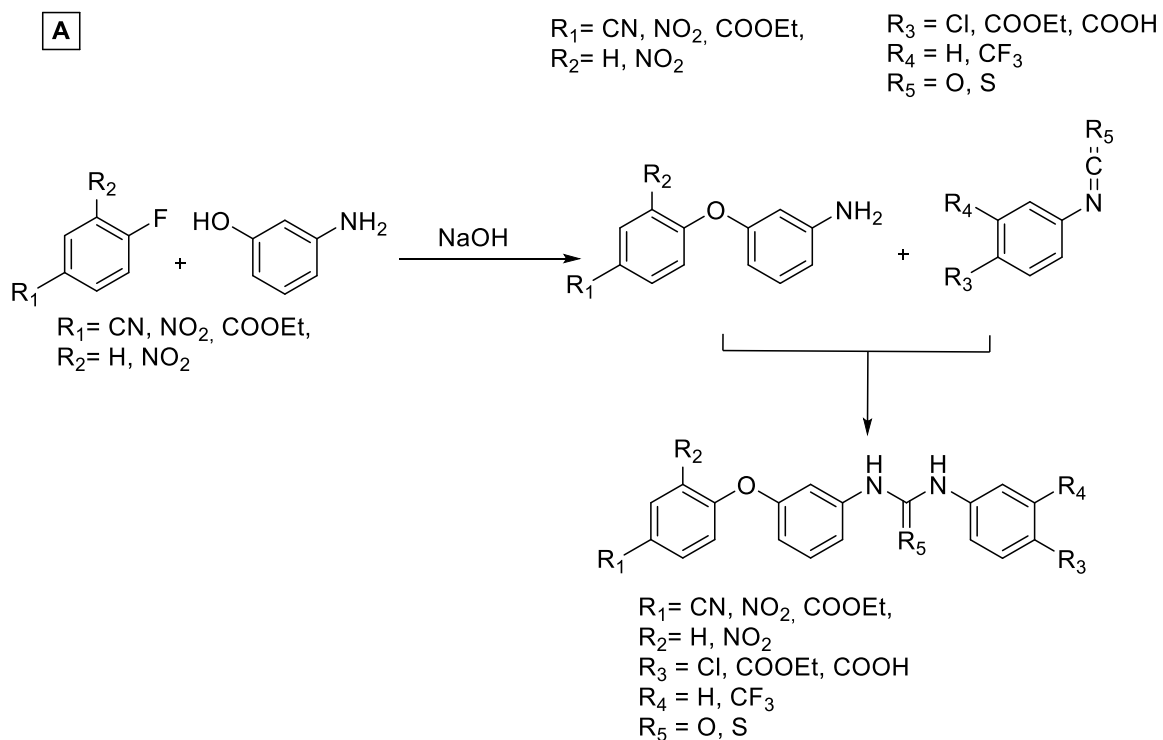


Figure 89. Structural comparison of the ureido and quinazolone groups.

Considering this possibility, several quinazolone rings have been synthesized with the aim to explore how different substituents on the bicyclic system can alter the overall potency of the final compound.

In the next page the synthetic protocol adopted for the synthesis of these SC-43 analogues will be illustrated.



Scheme 17. Synthetic pathway for the SC-43 analogues. A. Ureido derivative. B. Sulphonamide derivatives. C. Quinazolone derivatives.

The first synthetic step of the ureido derivatives of SC-43 has been a nucleophilic aromatic substitution between the meta-aminophenol and a fluorinated aromatic compound para or ortho substituted with an electron withdrawing group resulting in biphenyl amino compounds. The following reaction exploited the previously synthesized synthons and the appropriate isocyanate or isothiocyanate for the obtainment of the final ureido or thioureido structure.

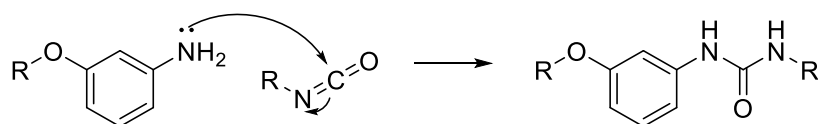


Figure 90. Mechanism of reaction of the isocyanate for the synthesis of the ureido bridge.

This synthetic pathway was slightly different compared to that one adopted by Chen and co-workers for the synthesis of SC-43, fewer passages have been required compared to the original one which was constituted of 4-5 different steps, one of which utilises the very toxic reactant phosgene.

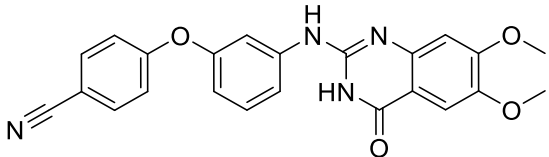
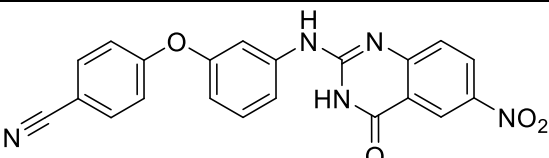
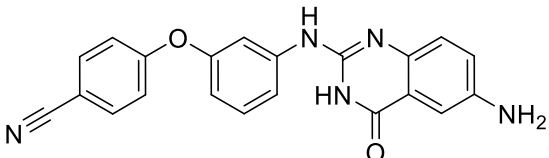
Taking in consideration the synthesis of the sulphonamide derivative, the benzonitrile biphenyl synthon, that has been synthesised for the previous category of SC-43 analogues, has been utilized as starting material. It has been reacted with tosyl chloride obtaining the desired sulphonamide. The adopted reaction for this step is a nucleophilic substitution, where the nitrogen atom of the biaryl compound acts as electrophile and the sulfonyl chloride as the nucleophile.

The last class of SC-43 analogues is constituted by the quinazolone derivatives. The synthetic protocol, for what concern the first steps till the obtainment of the 2,4-dichloroquinazoline, is identical to that one adopted for the synthesis of the TD-19-CC11 chimeric compounds. The two synthetic routes diverge after this synthon. The synthesis of the quinazolone SC-43 analogues proceeds with the introduction in position 4 of a hydroxyl group, that thanks to resonance structures generates the 2-chloro quinazolone. This step has been performed using H₂O as nucleophile and NaOH. The last step has been a nucleophilic substitution between the 2-chloro quinazolone and the biphenyl compounds synthesized for the ureido derivatives of SC-43. In this case a catalytic amount of HCl has been added for favouring the reaction.

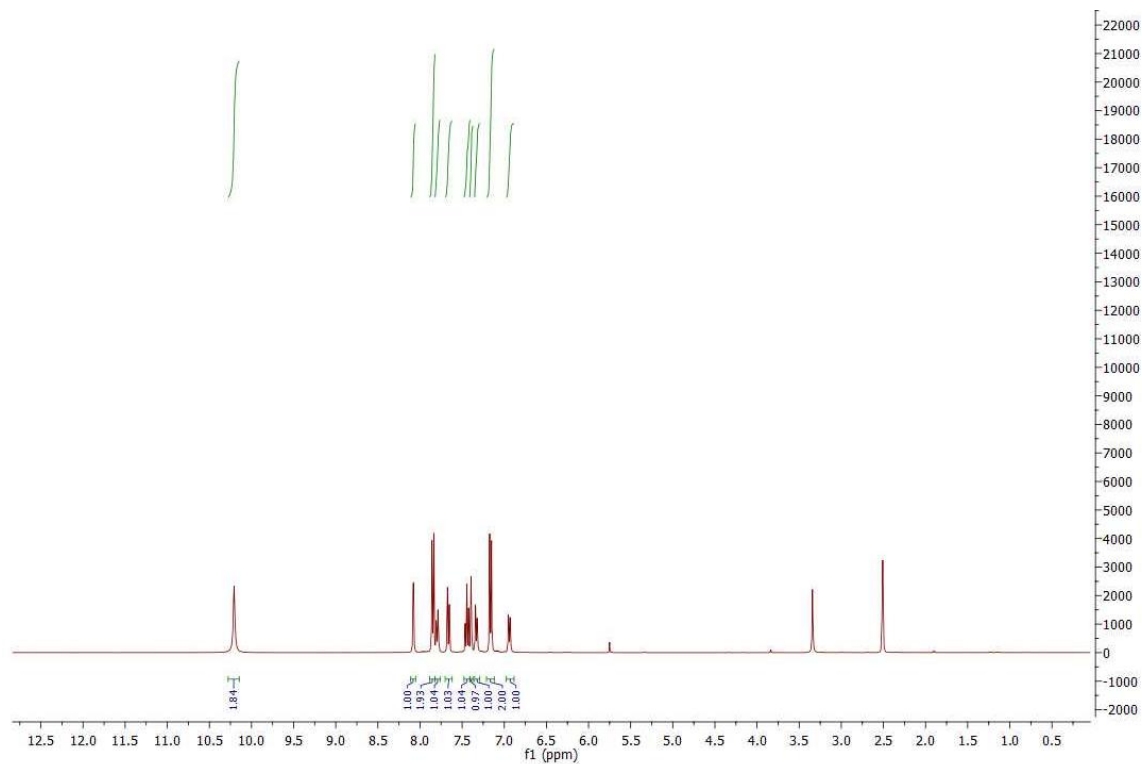
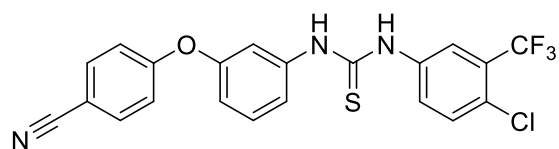
The following table summarizes all the synthesized compound.

Number	Chemical structure	IUPAC
SC-43		1-(4-chloro-3-(trifluoromethyl)phenyl)-3-(3-(4-cyanophenoxy)phenyl)urea
EZ1		1-(4-chloro-3-(trifluoromethyl)phenyl)-3-(3-(4-

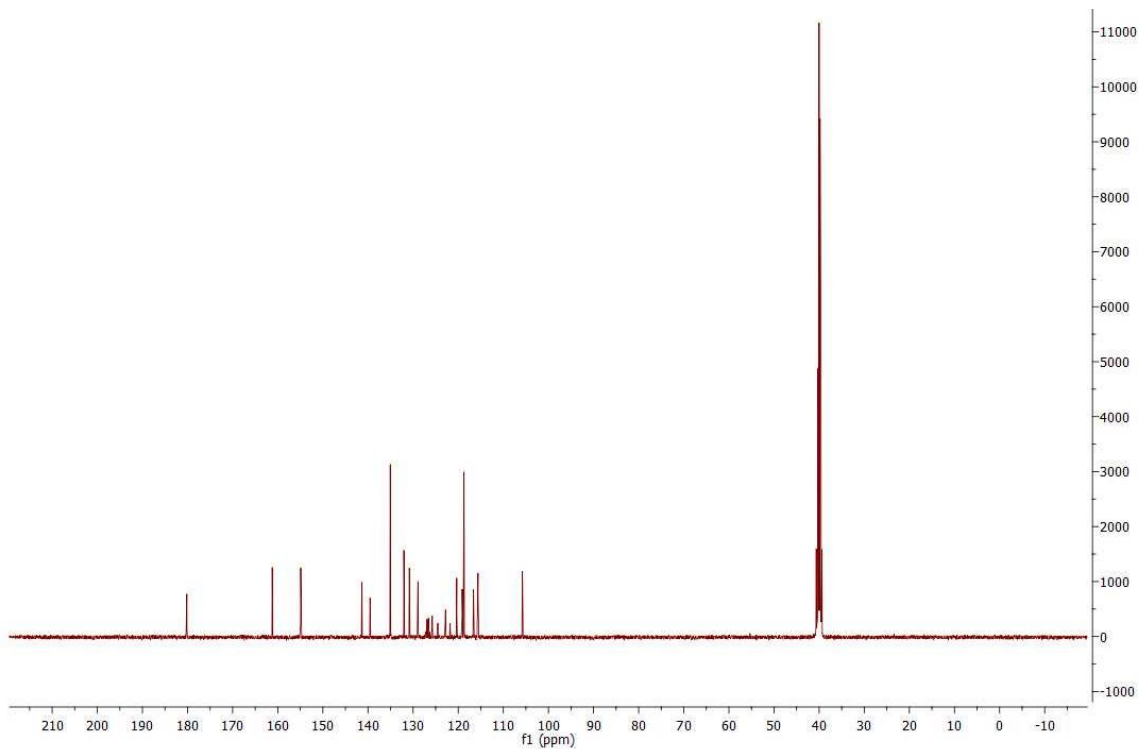
		cyanophenoxy)phenyl)thio urea
EZ2		4-(3-(3-(4-cyanophenoxy)phenyl)ureido)benzoic acid
EZ3		<i>methyl 4-(3-(3-(4-cyanophenoxy)phenyl)ureido)benzoate</i>
EZ4		N-(3-(4-cyanophenoxy)phenyl)-4-methylbenzenesulfonamide
EZ5		1-(4-chloro-3-(trifluoromethyl)phenyl)-3-(3-(4-nitrophenoxy)phenyl)urea
EZ6		ethyl 4-(3-(3-(4-chloro-3-(trifluoromethyl)phenyl)ureido)phenoxy)-3-nitrobenzoate
EZ7		2-((3-(4-nitrophenoxy)phenyl)amino)quinazolin-4(3H)-one
EZ8		ethyl 3-nitro-4-(3-((4-oxo-3,4-dihydroquinazolin-2-yl)amino)phenoxy)benzoate
EZ9		6,7-dimethoxy-2-((3-(4-nitrophenoxy)phenyl)amino)quinazolin-4(3H)-one
EZ10		ethyl 4-(3-((6,7-dimethoxy-4-oxo-3,4-dihydroquinazolin-2-yl)amino)phenoxy)-3-nitrobenzoate

EZ11		4-(3-((6,7-dimethoxy-4-oxo-3,4-dihydroquinazolin-2-yl)amino)phenoxy)benzonitrile
EZ12		4-(3-((6-nitro-4-oxo-3,4-dihydroquinazolin-2-yl)amino)phenoxy)benzonitrile
EZ13		4-(3-((6-amino-4-oxo-3,4-dihydroquinazolin-2-yl)amino)phenoxy)benzonitrile

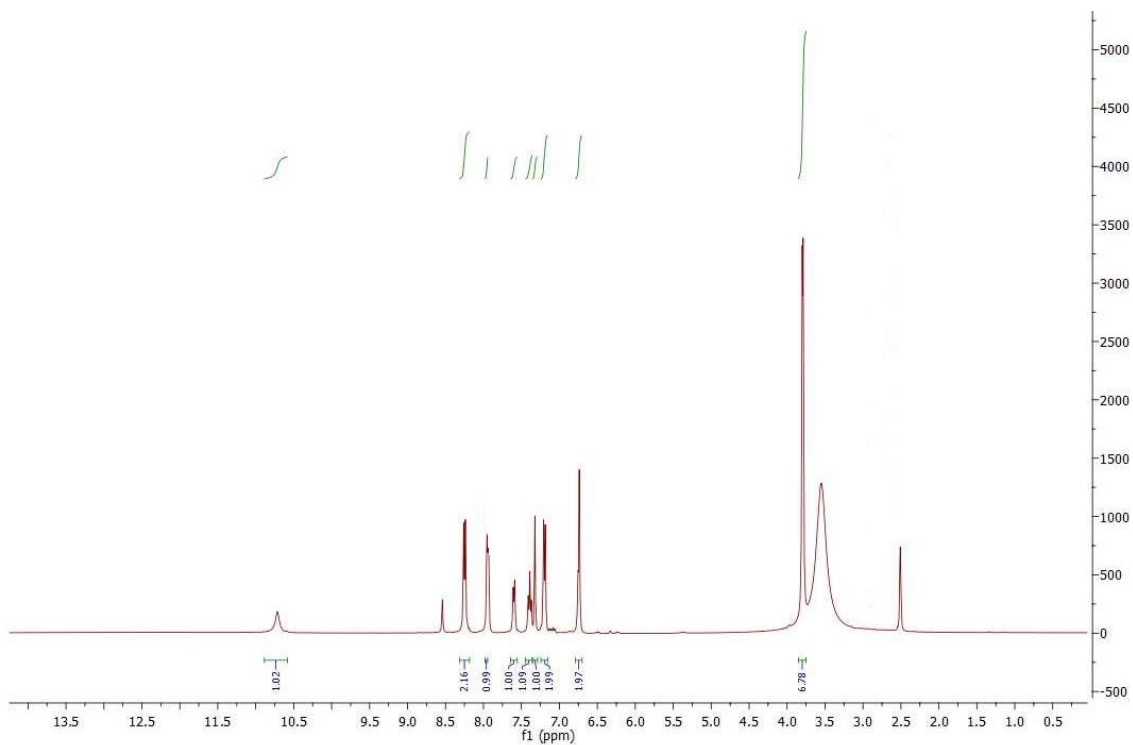
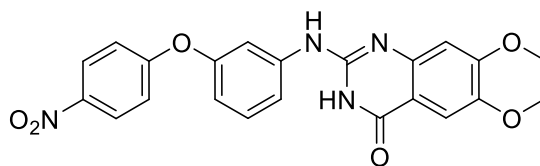
Example of NMR characterisation



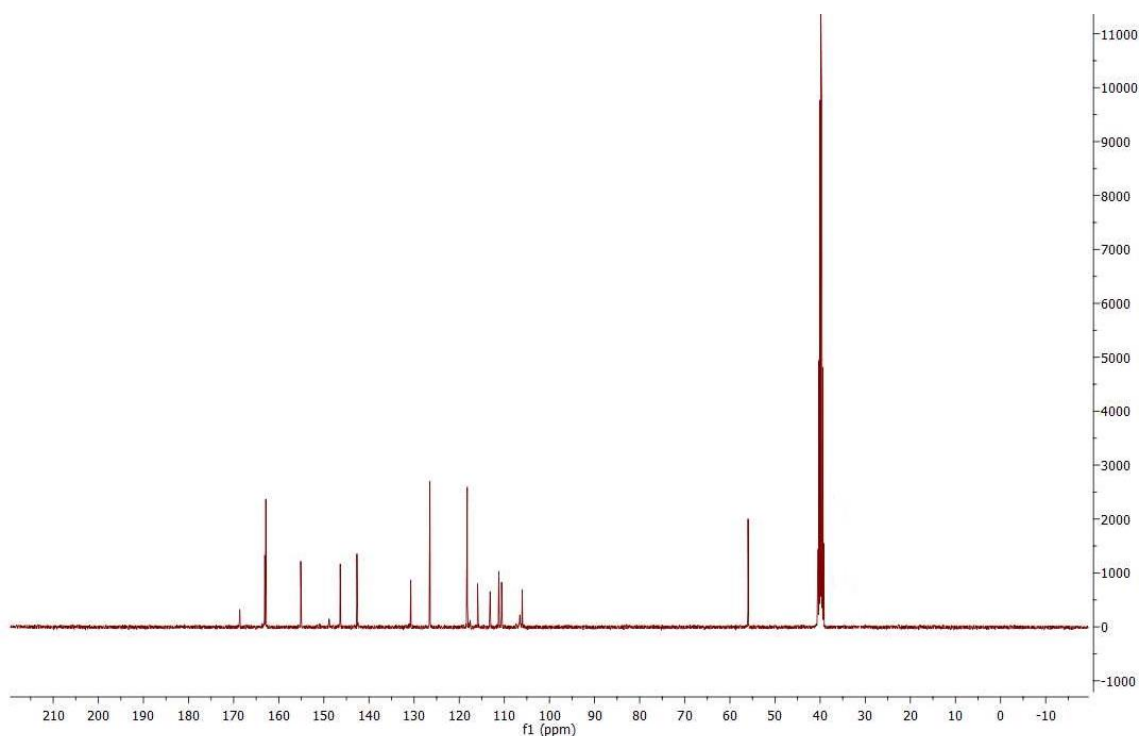
¹H NMR (400 MHz, DMSO)



¹³C NMR (101 MHz, DMSO)



¹H NMR (400 MHz, DMSO)



^{13}C NMR (101 MHz, DMSO)

The ureido derivatives of SC-43 have been tested on different cell lines at the laboratory of Prof. Brunati (biology department of the University of Padova) for validating their ability of inducing apoptosis. The cells used for these assays have been isolated from blood samples of patients affected by two different types of leukaemia: LGL and β -CLL.

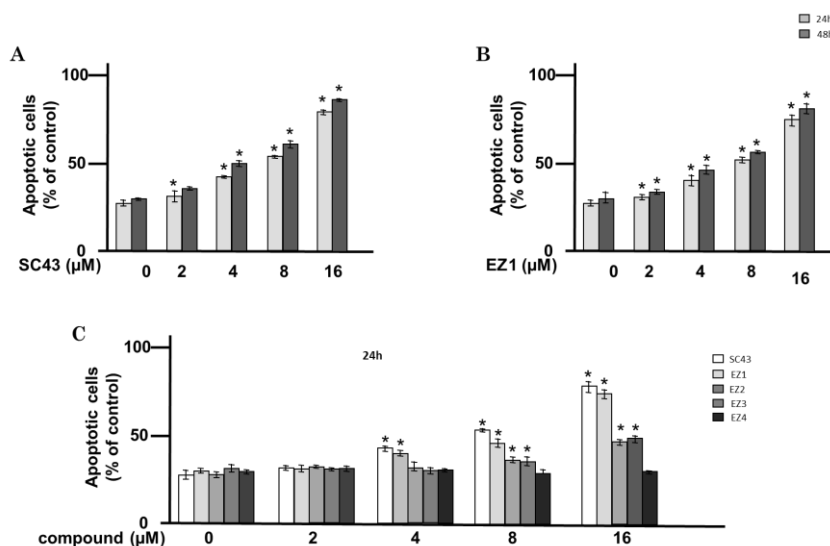


Figure 91. Results of the ureido and sulphonamide derivatives of SC-43 on LGL leukaemia cells. On the top part of the figure the percentage of apoptotic cells induced by SC-43 (A) and (B) the thioureido analogue (compound 1) at different concentrations and time exposure have been shown. Pannell C highlights the percentage of apoptotic cells induced by SC-43 and compounds 1, 2, 3, 4 at different concentrations over a period of 24h incubation.

As can be appreciated in figure 91, all the tested ureido compounds are active on LGL leukemic cells. The most active of the series, whose efficacy is comparable to that one of SC-43 is compound EZ1, which is the thioureido analogue. Contrarily to what has been supposed, the sulphonamide derivative is not effective in inducing apoptosis in LGL leukemic cells.

Other two ureido analogues of SC-43, compound EZ5 and EZ6, have been tested on β -CLL cells. As seen in figure 92, these two compounds were effective in inducing apoptosis in this kind of cancerous cells, and compound EZ5 has shown a comparable effect to that one of SC-43 at both tested doses. At the highest tested concentration both the analogues have shown an analogous potency to that one of SC-43.

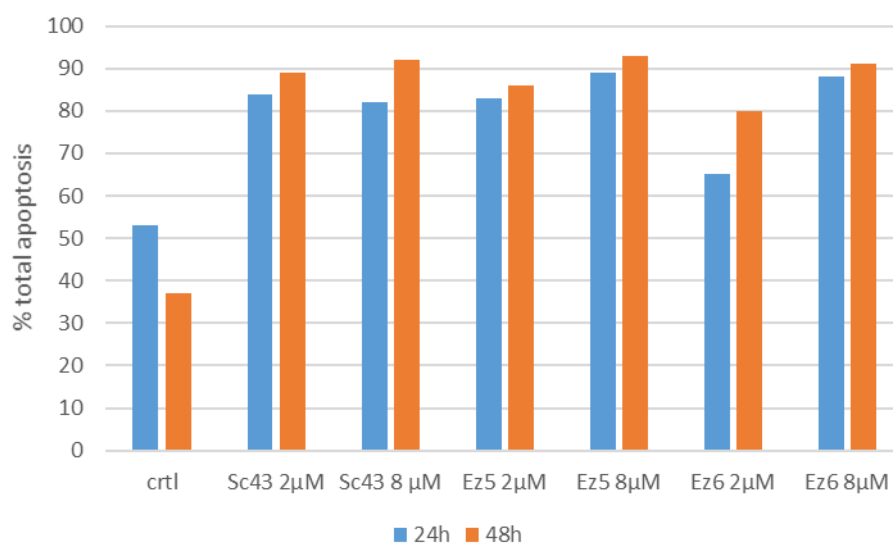


Figure 92. Percentage of apoptotic cells after an incubation period of 24h and 48h with SC-43, compound 5 and 6, at different concentrations (2 and 8 μ M).

All the tested compounds, except the sulphonamide one, have given interesting results and some of them showed a potency comparable to that one of SC-43 confirming the goodness of the postulated hypothesis. Compounds EZ1 and EZ2 have demonstrated to be able to increase the phosphatase activity of immunoprecipitated SHP-1 with radiolabelled peptides with 32 P (Data not shown) confirming that this enzyme is the target of this class of compounds. The next step will be testing the quinazolone derivatives. These compounds having a different core structure could pave the way to the development of a new class of SHP-1 activators.

3.3 CK2: Rationale and Results

The last project presented in this PhD thesis regards the development of new selective inhibitors of the serine/threonine kinase CK2. This work has been made in collaboration with Prof. Battistutta (University of Padova) and Prof. Lolli (University of Trento), who performed the structural crystallographic experiments and analysed them, and Prof. Ruzzene, that performed the *in vitro* tests. This research line started from the discovery made by Prof. Lolli and Prof. Battistutta, that demonstrated, with crystallographic data, that the well-known selective CK2 inhibitor SRPIN803 presents a molecular structure that is significantly different compared to that one proposed by its inventors Mooroka and colleagues.

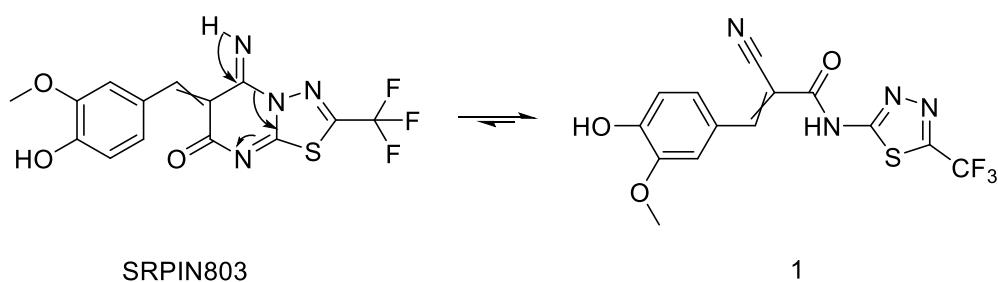


Figure 93. Chemical structure of SRPIN803 and Compound 1. They can be considered as tautomers and the tautomerization mechanism is herein reported.

Indeed, as reported in figure 93, the new compound presents a 2-cyano-2-propenamide structure where the cyano group does not cyclise with the thiadiazol ring excluding the formation of a fused bicyclic structure, as theorised for SRPIN803. For confirming that the obtained results were not due to a wrong storage protocol and consequently that the analysed compound was the product of a degradation pattern of the original stock synthesized by Mooroka and co-workers, a new batch of the molecule has been synthesized following the exact procedure reported by the Japanese research group. Also in this case the newly synthesized compound, despite it presents the same spectroscopic and analytical characteristics of the original molecule, resulted to have the same molecular structure of compound 1 and not that one of SRPIN803.

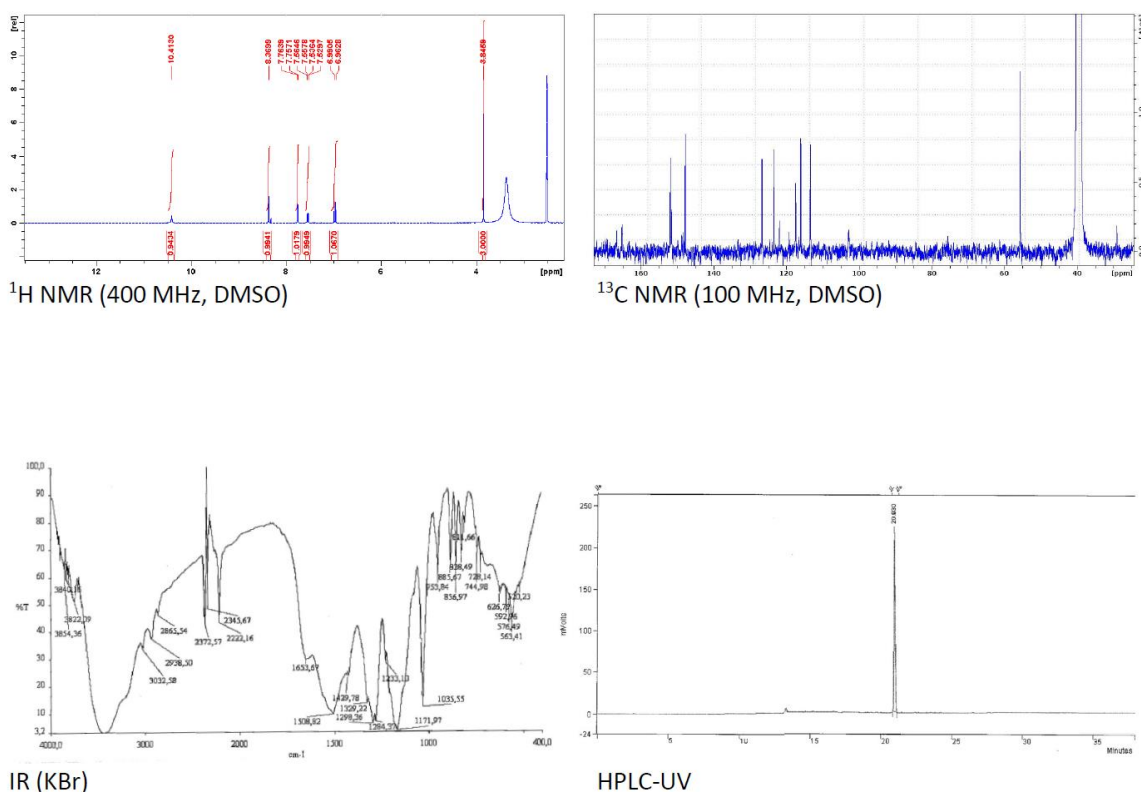


Figure 94. Spectroscopic and Chromatographic analysis of fresh compound 1.

This result highlighted the limit of the conventional methods of characterisation which are difficultly able to distinguish one tautomer from the other. Indeed, both these structures present the same ^1H , ^{13}C and mass spectra. The only significant information, that could have been useful for the discrimination between the two structure, has been obtained with the IR spectrum. Compound one presents a nitrile group ($\text{C}\equiv\text{N}$ stretching at $2260\text{-}2190\text{ cm}^{-1}$) while SRPIN803 an immine ($\text{C}=\text{N}$ stretching at $1690\text{-}1640\text{ cm}^{-1}$). These two functional groups present different wave numbers and consequently the presence of one band or the other should discriminate between the two possible structures. In this case, the IR spectrum of the compound present a peculiar band at 2222 cm^{-1} while the region between $1690\text{-}1640\text{ cm}^{-1}$ is quite occupied and this renders difficult its interpretation, but in first approximation another peak can be identified at 1653 cm^{-1} . The first signal confirms the presence of the nitrile functional group and the second one could be attributed to the $\text{C}=\text{N}$ stretching of the thiadiazol ring. All this information together confirmed further the chemical structure of the compound but not exclude one or the other.

The crystal structure of compound 1 has been obtained alone and within its active site on CK2 α . The compound was soaked into CK2 apo crystal and the crystallographic structure of the complex determined at 1.5 \AA resolution. Clear positive electron density was present in the kinase ATP pocket, not compatible with the structure of SRPIN803 (Fig. 95a) but instead corresponding to compound 1 (Figure 95b). The observed electron density did not change when only the first diffraction images were integrated, excluding a dose-dependent X-ray radiation damage.

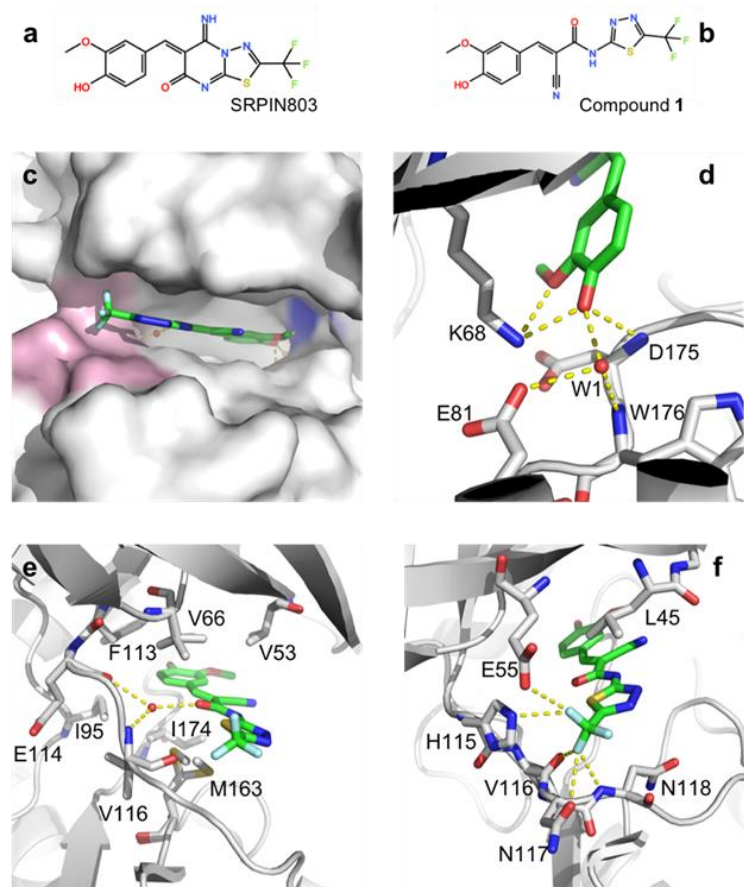


Figure 95. Binding mode of compound 1 in the CK2 ATP-pocket. a) 2D structure of SRPIN803. b) 2D structure of compound 1. c) Compound 1 inserts deeply into the pocket contacting both the basic region (blue surface) and the hinge region (pink surface). d) The guaiacol headgroup is involved in a number of polar interactions with residues in the CK2 basic region. e) The central 2-cyano-2-propenamide group is sandwiched by hydrophobic residues and contacts the hinge region through water-bridged hydrogen bonds. f) the thiadiazol ring stacks in between side chains of Leu45 and Asn118, while the trifluoromethyl end is involved in various polar interactions.

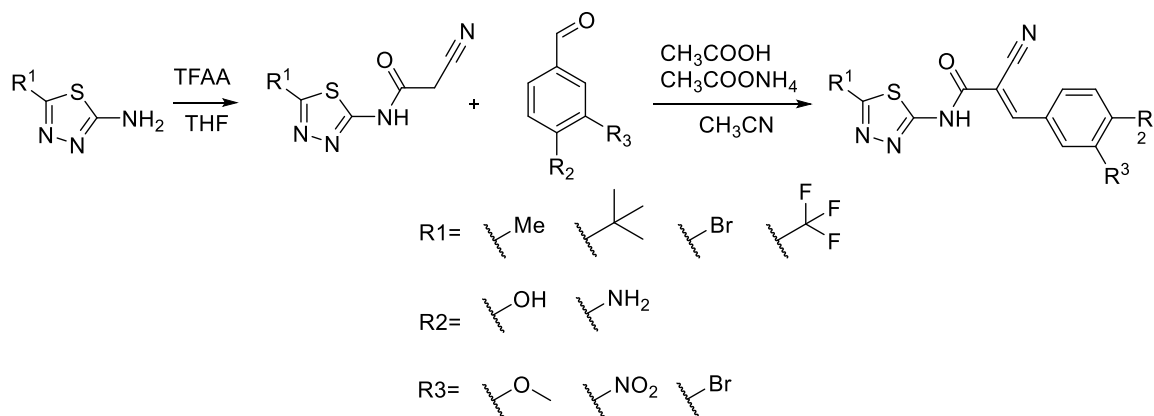
The ATP binding pocket of CK2 can roughly be divided in three areas: the basic region, where Lys 68 holds in place the ATP β -phosphate; the hinge region, on the opposite side, corresponding to the 114-120 stretch of amino acids connecting the N-terminal and C-terminal lobes of the protein; the hydrophobic area, in between the two previous regions, comprising residues Val 53, Val 66, Ile 95, Phe 113, Met 163 and Ile 174 and sandwiching the adenosine moiety of ATP.

Compound 1 is fully buried in the ATP binding pocket of CK2 α , spanning from the basic to the hinge region (Fig. 95c). The molecule is anchored to the protein through its guaiacol moiety, with both oxygen atoms tightly interacting with the positively charged ammonium tail of Lys 68 side chain. In addition, the guaiacol hydroxyl further interacts with the main chain amide of Asp 175 and with a conserved water molecule (W1) that is held in position by Trp 176 main chain amide nitrogen and Glu 81 side chain (Figure 95d). The central 2-cyano-2-propenamide region is involved in Van der Waals and hydrophobic contacts with the aforementioned apolar residues lining the cavity (Figure 95e). It also contacts the hinge region through a water-mediated

hydrogen bond between the propenamide carbonyl oxygen and Glu114 main chain oxygen and Val 116 main chain nitrogen. The nitrile group also contributes to the binding affinity through its electron-withdrawal effect, with the ultimate increase in acidity of the guaiacol hydroxyl; its pKa is estimated in 8.8 with a decrease of about 1 unit with respect to molecules with a methyl or an ethynyl group in place of the nitrile. In the local context of the CK2 basic region, the deprotonated form of the inhibitor should be, at least minimally, populated. Finally, the thiadiazol ring is sandwiched between side chains of Leu 45 and Asn 118, while the trifluoromethyl group get jammed in between the hinge region and the N-terminal lobe (Figure 95f). A number of polar interactions are established between two fluorine atoms and the protein matrix, namely with Val 116 main chain oxygen, Asn 118 main chain nitrogen and the side chains of Glu 55, Asn 117 and His 115, although poorly oriented for the establishment of hydrogen and halogen bonds. The trifluoromethyl group is placed similarly to what observed in the structure of SRPK1 in complex with the significantly different SRPIN340 inhibitor (PDB 4WUA). The observed binding mode of compound 1 in CK2 is instead completely different from the proposed docking pose of SRPIN803 in complex with the same kinase.

The analysis of the SRPIN803/Compound 1 binding mode allowed the identification of two regions that can be modified for increasing the potency of the molecular scaffold. The structures subjected to modifications are the thiadiazol core and the guaiacol ring. The propenamide spacer has been left untouched because it presents the right spacer between the two modifiable parts of the molecule and with its cyano portion is able to increase the acidity of the guaiacol group, that as will be further discussed, is a desirable feature. The thiadiazol ring has a trifluoromethyl group that is in close proximity with the solvent and it is surrounded by a big pocket that is not fully explored by this functional group. For this reason, different functionality can be introduced instead of the trifluoromethyl one with the aim to understand if this position of the molecule requires much more bulky groups or not and much more hydrophilic or not. The other region that could be modified, as already mentioned, is the guaiacol ring. This part of the molecule interacts with the basic region of the catalytic subunit of CK2 and it occupies the same space that is usually explored by the phosphate groups of ATP. All this information indicate that this region well tolerates acidic functional groups that are able to mimic the anionic phosphate.

For these reasons, several analogues of Compound 1 have been synthesized with different substituents in these two positions for validating the made hypotheses.



Scheme 18. Synthetic protocol adopted for the synthesis of the CK2 inhibitors

Concerning the synthesis of the new compounds, as first attempt the synthetic strategy proposed by Mooroka and co-workers in their paper has been adopted. Unfortunately, this protocol did not lead to the obtainment of any different compound from the original one if the thiadiazol ring does not present the trifluoromethyl group. The critical step was the formation of the amide bond between the ethyl cyanoacetate and the thiadiazol ring. This is probably due by the fact that the isolated couple of electrons, that usually gives the typical nucleophilic behaviour to an ammine, is delocalised within the thiadiazol ring decreasing the reactivity of this functional group.

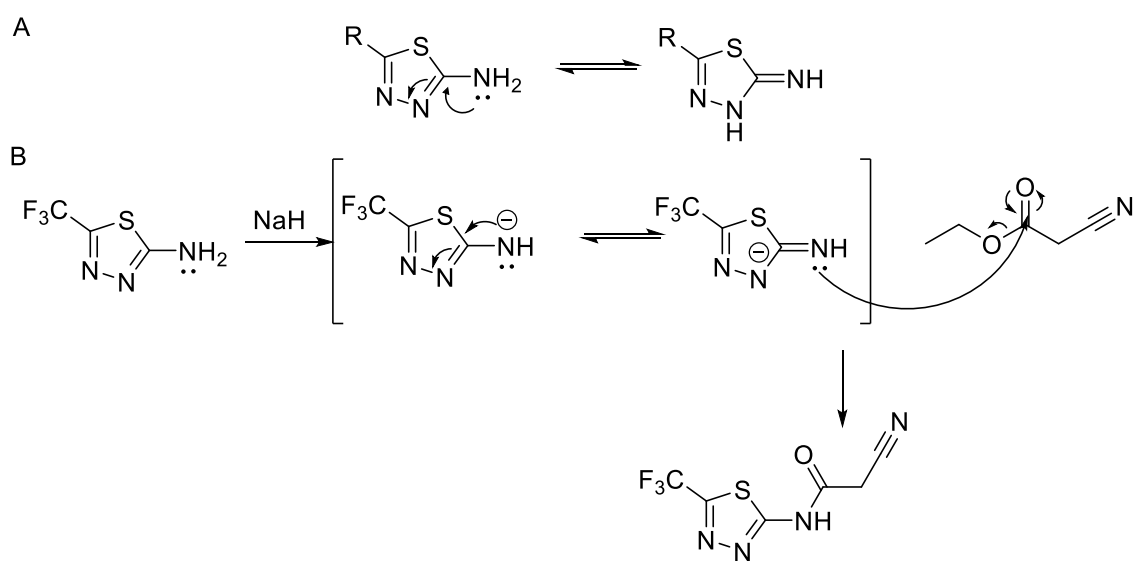


Figure 96. A. Mechanism of delocalization of the unpaired electrons of the amino group on the thiadiazol ring. B. Reaction mechanism for the formation of the amide bond in the original synthetic procedure.

In the classical procedure this problematic was bypassed by the usage of a strong base like NaH. The electronegativity of the trifluoromethyl group was able to increase the acidity of the NH₂ group that was transformed in the basic environment in a good nucleophile even in presence of the strong electronic delocalisation effect. When the electron withdrawing group is substituted with an electron donor one this solution is no more valid.

With the aim to overcome this limiting step, several changes to the original procedure have been made, from the environmental conditions (pH, solvent, temperature) to the switch of the carboxylic coupling agent. Indeed, instead of the ethyl cyanoacetate adopted in the original procedure, the cyanoacetic acid has been used and variously activated ($B(OH)_3$, HBTU, TBTU, and chlorinating agents). The only technique that allowed the formation of the amide bond with several thiadiazol ring was with the cyanoacetyl chloride, obtained freshly every time using thionyl chloride as chlorinating agent. This procedure has the great limitation that the yield of the reaction is really low. This time the major issue was the instability of the cyanoacetyl chloride. This intermediate was not stable enough and it starts to degrade immediately after its isolation and this does not facilitate also the purification of the desired amidic compound. This new problem has been solved exploiting the formation in-situ, just before the reaction, of a mixed anhydride between trifluoroacetic anhydride (TFAA) and cyanoacetic acid. TFAA has been chosen because TFA forms a less stable acylium ion compared to cyanoacetic acid, this is due to the different electron withdrawing effects of the two substituents and for the different possibility of forming stabilising resonance forms of the acylium ion. This strategy led to the obtainment of all the desired amides with high yields, short reaction time, easy workup and high purity.

As last step, for the obtainment of the final compounds, a Knoevenagel condensation has been performed between the amide synthons and the desired substituted benzaldehyde.

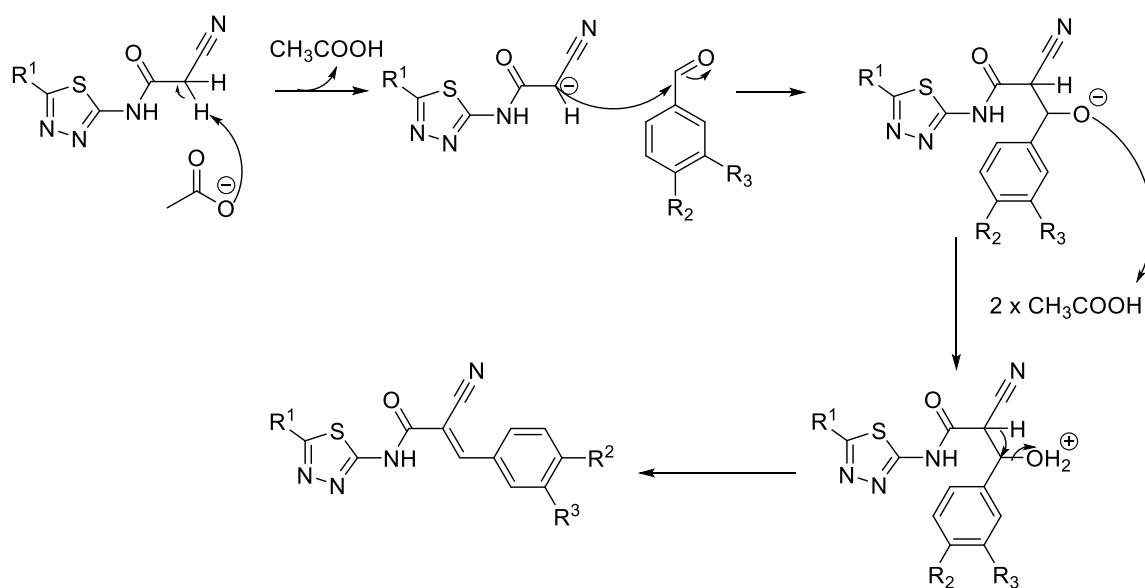
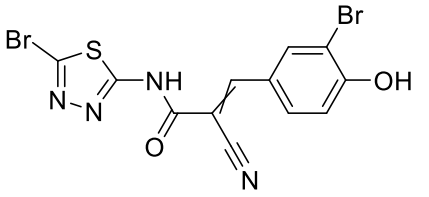
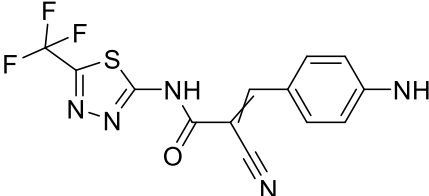
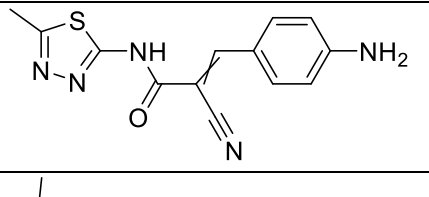
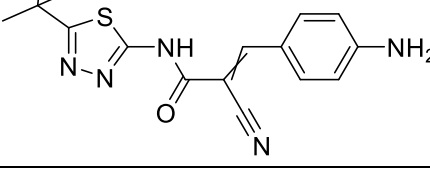


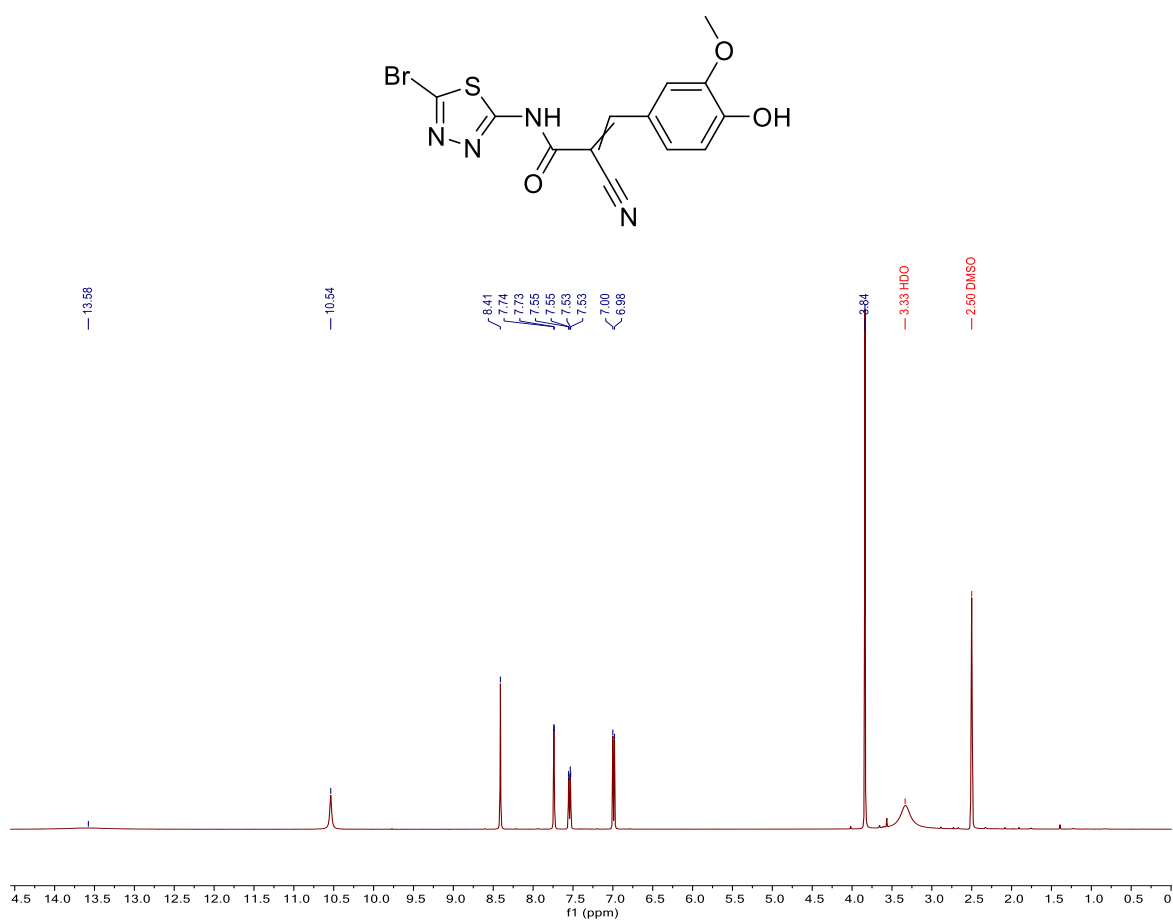
Figure 97. Mechanism of reaction of Knoevenagel condensation.

The table reported below illustrates all the synthesized compounds and their IC_{50} values on isolated CK2 α .

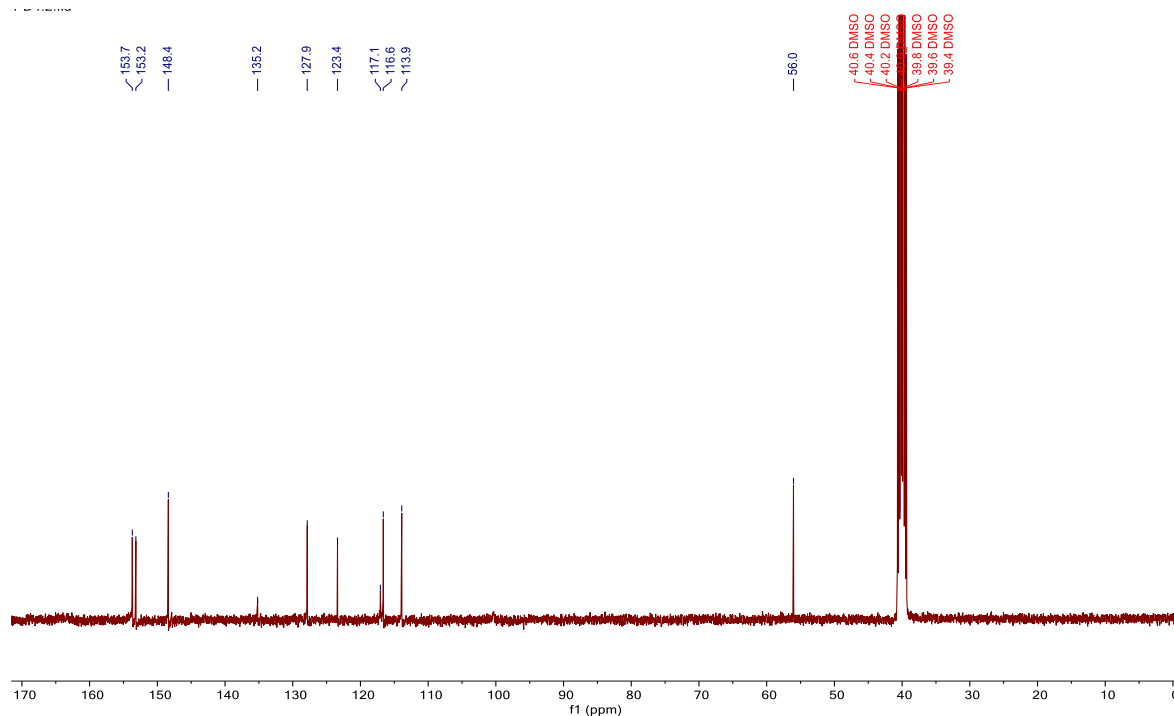
Number	Chemical structure	IC ₅₀ μM (SEM)	IUPAC
1		1.37 (0.20)	2-cyano-3-(4-hydroxy-3-methoxyphenyl)-N-(5-(trifluoromethyl)-1,3,4-thiadiazol-2-yl)acrylamide
2		0.88 (0.44)	2-cyano-3-(4-hydroxy-3-methoxyphenyl)-N-(5-methyl-1,3,4-thiadiazol-2-yl)acrylamide
3		0.36 (0.10)	N-(5-(tert-butyl)-1,3,4-thiadiazol-2-yl)-2-cyano-3-(4-hydroxy-3-methoxyphenyl)acrylamide
4		0.28 (0.09)	N-(5-bromo-1,3,4-thiadiazol-2-yl)-2-cyano-3-(4-hydroxy-3-methoxyphenyl)acrylamide
5		0.71 (0.28)	2-cyano-3-(4-hydroxy-3-nitrophenyl)-N-(5-(trifluoromethyl)-1,3,4-thiadiazol-2-yl)acrylamide
6		0.32 (0.08)	2-cyano-3-(4-hydroxy-3-nitrophenyl)-N-(5-methyl-1,3,4-thiadiazol-2-yl)acrylamide
7		0.37 (0.08)	N-(5-bromo-1,3,4-thiadiazol-2-yl)-2-cyano-3-(4-hydroxy-3-nitrophenyl)acrylamide

8		1.3 -	N-(5-bromo-1,3,4-thiadiazol-2-yl)-3-(3-bromo-4-hydroxyphenyl)-2-cyanoacrylamide
9		ND	3-(4-aminophenyl)-2-cyano-N-(5-(trifluoromethyl)-1,3,4-thiadiazol-2-yl)acrylamide
10		ND	3-(4-aminophenyl)-2-cyano-N-(5-methyl-1,3,4-thiadiazol-2-yl)acrylamide
11		ND	3-(4-aminophenyl)-N-(5-(tert-butyl)-1,3,4-thiadiazol-2-yl)-2-cyanoacrylamide

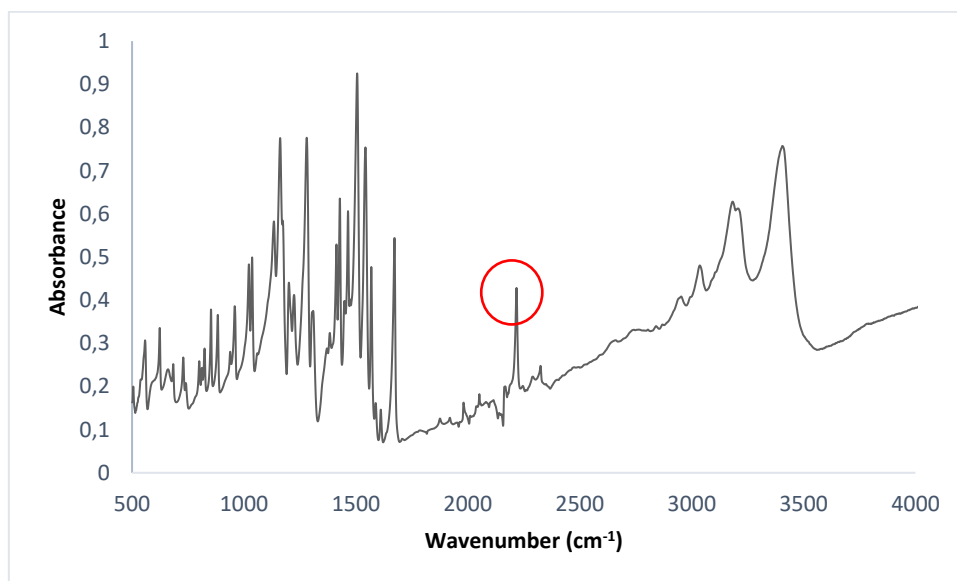
Example of NMR characterisation



¹H NMR (400 MHz, DMSO)



^{13}C NMR (101 MHz, DMSO)



IR spectrum

For each one of the synthesized compounds it has been investigated their crystallographic structure within the ATP pocket. As theorised, the structures that do not present an acidic group where it was originally positioned the guaiacol moiety are not able to penetrate within the ATP pocket and for this reason they have been discarded. All the compounds, whose crystal structure within CK2 has been determined, have been tested *in vitro* on CK2 α for assessing their activity. Analysing the crystal structure and the activity of all the active compounds a SAR has been developed.

First, compounds 2-4 were synthesized as derivatives of compound 1 with the trifluoromethyl group substituted with methyl, tert-butyl and bromine, respectively. Compound 2 is only slightly more potent than 1 while compound 3 shows a fourfold increase in inhibitor potency respect to compound 1. Compound 4 is the most potent among all tested inhibitors in this work with an $IC_{50} = 280$ nM.

The position of the guaiacol group is almost identical in compounds 1, 3 and 4 (Figure 98a) in complex with CK2 α , as determined by X-ray crystallography; all its interactions with the protein matrix are conserved. In compound 3, the bulkier tert-butyl-thiadiazole group moves significantly toward the C-terminal part of the hinge region, as compared with 1, in order to optimize the interactions with residues from both the hinge and the CK2 N-terminal lobe. The bromo-thiadiazole tail of compound 4 is closer to the hinge region with respect to compound 3, but also to compound 1 (Figure 98a); an interaction between the thiadiazole sulphur and Val 116 main chain oxygen is established. The S-O distance decreases to 3.1 Å (C_{ar} -S-O angle 127°), being 3.5 Å in the complex with compound 1. The thiadiazole sulfur acts as an electrophile due to the donation of its p_z electrons to the aromatic system and interacts with the carbonyl oxygen through σ -hole bonding. Strength of interaction increases with the number of the electron-withdrawing nitrogen atoms on the ring, so that thiadiazole is much favoured over thiazole and thiophene. Energy for the thiadiazole S-O interaction, stronger than a typical hydrogen bond, has been computed in -27 kJ/mol at the optimal distance (3 Å) and angle (156°).

On the opposite side of the molecule, the guaiacol methoxyl was then replaced by a nitro group with the aim of increasing the acidity of the ortho hydroxyl. The predicted effect is a large decrease of the pKa to a value of 5.7 with the outcome of a fully deprotonated phenolate in the basic region of the CK2 pocket. The *o*-nitrophenolic compounds 5-7 were synthesised, which included a thiadiazole ring derivatised with either a trifluoromethyl or a methyl or a bromine, respectively. Inhibitory power, with respect to compound 1, was doubled for compound 5 and the improvement was almost three times for compound 6, as compared with 2. This confirmed the favourable contribution of the *o*-nitro group for these compounds. Interestingly, this contribution is abolished in the context of the bromo-thiadiazole compounds and the *o*-nitrophenolic compound 7 performed slightly worse than the guaiacol-bearing compound 4.

The crystallographic structure of compound 7 in complex with CK2 α shows a binding mode very similar to that observed for compound 4, with a limited sliding towards the hinge region to accommodate the bulkier (with respect to the methoxyl) nitro group in the CK2 basic region (Figure 98b). The *o*-nitrophenolic group maintains all interactions observed for the guaiacol ring, with Lys 68 side chain involved in a salt bridge to the nitro group (Figure 98c). The nitro group, however, gets also close to the Asp 175 side chain. The thiadiazole sulphur is at 3.1 Å (C_{ar} -S-O angle 133°) from Val 116 carbonyl oxygen. The slight shift of compound 7 with respect to 4 causes a larger protrusion of the bromine atom toward the hinge region (Figure 98b).

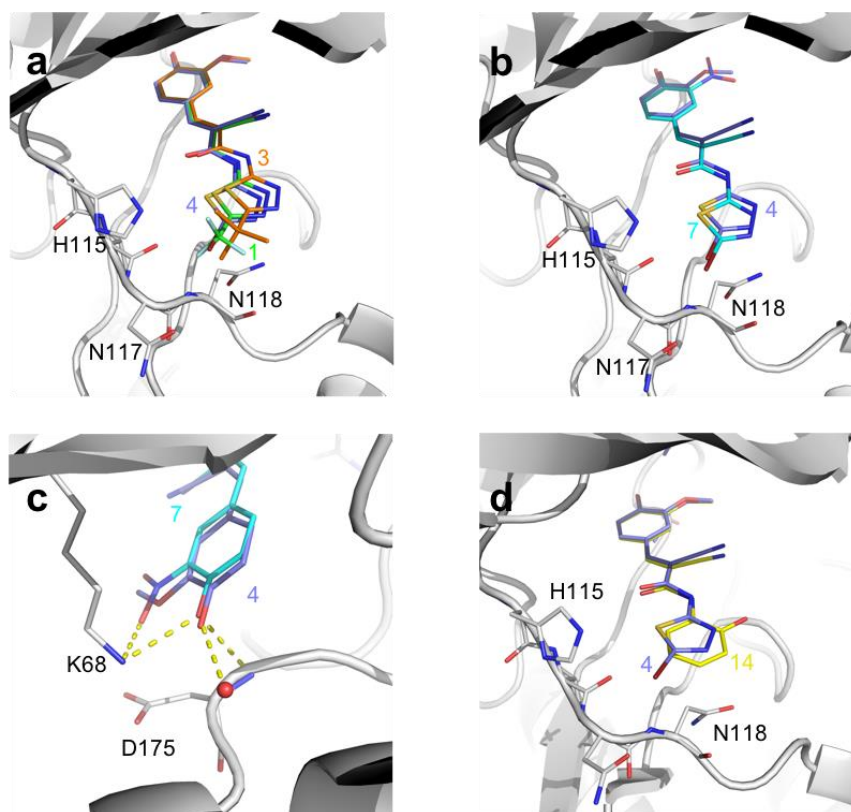


Figure 98. Comparison of binding modes for compounds 1 (green), 3 (orange), 4 (purple), 7 (cyan) and 14 (yellow). a) *Tert*-butyl-thiadiazole (3) moves away from the hinge region with respect to compound 1, bromo-thiadiazole (4) moves closer. b) The nitrophenol moiety causes the bromothiadiazoole of compound 7 to protrude more on the top of the hinge region with respect to the bromothiadiazoole of compound 4 holding a guaiacol group on the opposite side. c) The nitrophenolic headgroup of compound 7 interacts with CK2 α similarly to what observed in compound 4. d) The *o*-hydroxylbenzene ring in compound 14 exposes the phenolic oxygen to the solvent.

Compound 8 is the combination of the best hinge-contacting bromo-thiadiazole tail with a *o*-bromophenolic headgroup, with the aim of increasing the acidity of the phenolic oxygen (predicted pKa 7.2) with a small and neutral substituent. Compound 8 shows a modest IC₅₀, being significantly worse than both compounds 4 and 7.

The 2-cyano-2-propenamides here reported are the first CK2 inhibitors protruding from the active site on the top of the hinge region and in direct contact with amino acidic side chains from this region. The peculiar binding mode should define a remarkable specificity for these compounds. First, compounds 1, 4 and 7 were tested on the tetrameric CK2 $\alpha_2\beta_2$ holoenzyme by kinase assay, obtaining very similar IC₅₀s as those reported in the previous table for the α subunit. Then, the most potent compound 4 was tested on a panel of 320 kinases. Only CK2 α and its paralogue CK2 α^1 were inhibited by more than 50% when tested at 1 μ M (Figure 99).

CK2 has a flexible hinge/ α D region which can assume two different structural arrangements: an open conformation which is extremely rare among protein kinases, and a closed conformation recapitulating the correctly assembled catalytic spine (C-spine), as seen in the vast majority of the protein kinases; the binding of the compounds here reported is only compatible with the open conformation of the hinge/ α D region (Figure 100). Then, direct interactions with side chains of the hinge region, a feature not previously reported for any CK2 inhibitor only contacting main chain atoms of the same region, guarantee additional specificity.

The ability to target the CK2 open conformation has recently been exploited by the most selective CK2 inhibitor reported to date CAM4066. However, CAM4066 ($IC_{50} = 370$ nM) has a completely different binding mode and, contrary to the inhibitors reported here, targets the α D but not the hinge region (Figure 100).

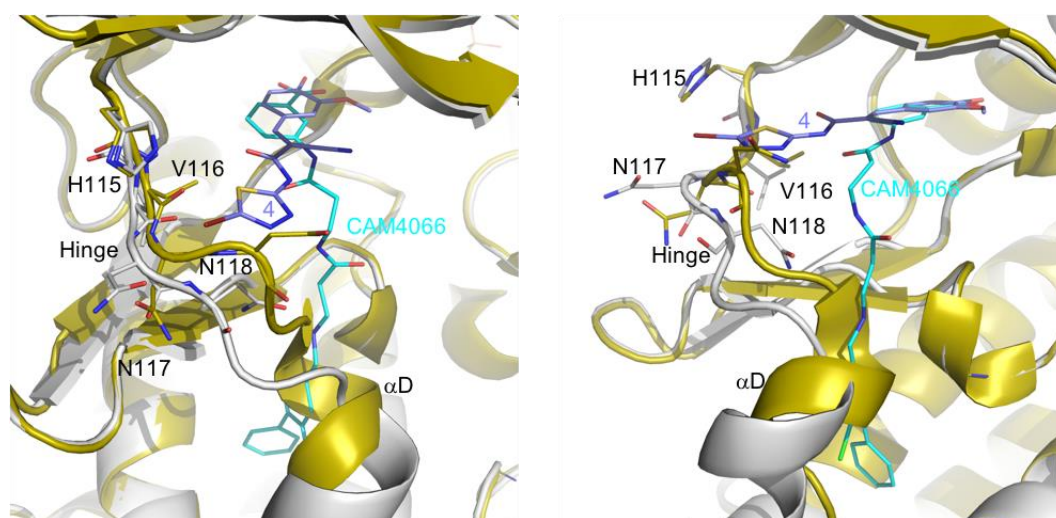


Figure 100. Comparison of binding modes for compound 4 (purple) and CAM4066 (cyan). The two different views show that both compounds are compatible with CK2 open conformation (white) but not with the closed conformation (yellow). Compound 4 discriminates the two conformations at the level of the hinge region, while CAM4066 clashes with a closed α D helix.

The most promising molecules were also analyzed for their efficacy in cells, with special focus on the best inhibitor, compound 4. We first assessed whether cells treated with the inhibitors displayed a reduced activity of endocellular CK2. This was confirmed by the analysis of the CK2-dependent Akt phospho-site, Ser 129: as shown in figure 101a, while the amount of the kinase remained intact in treated cells, the Akt phosphorylation level decreased in response to both compound 1 and compound 4. Since cell death is expected to occur in tumor cells whenever CK2 is inhibited, we measured the effect of the compounds on Jurkat cell viability. Results are shown in figure 101b, where also the effect of compound 7 is reported: all the inhibitors turned out to significantly reduce cell viability in a dose-dependent manner. The DC_{50} values (concentrations inducing 50% of cell death compared to vehicle-treated cells in 24h) indicate a very similar efficacy of compound 1 and compound 4, while compound 7 is less effective. The lower cellular activity of compound 7 can be ascribed to a reduced membrane permeability caused by the negative charge of the *o*-nitrophenolate ring.

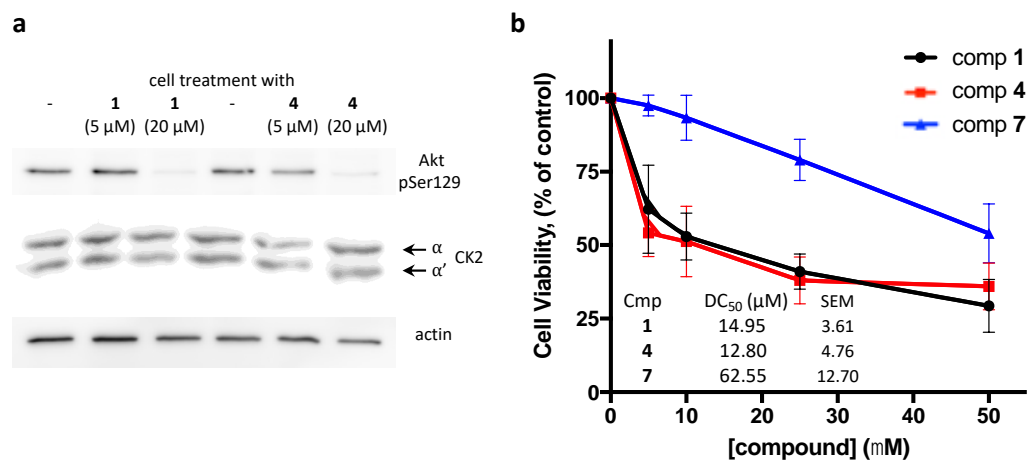


Figure 101. Effects of compounds in cells. a) Jurkat cells were treated with the indicated compounds for 16h. 20 μ g of proteins from total lysate were analysed by WB with anti phospho-Ser129 Akt antibody (upper), or an antibody recognizing both CK2 catalytic subunit α and α' (middle). 5 μ g of proteins were analysed for β -actin (lower WB), as loading control. Representative WB of three independent experiments are shown. b) Jurkat cells were treated for 24h with increasing concentrations of the indicated compounds. Cell viability was assessed by the MTT method, and it is shown as % of vehicle-treated (Control) cells. On the right, the calculated DC50 values are reported (mean values + SEM of at least four experiments).

4 CONCLUSIONS

During this PhD thesis several research fields have been explored with the aim to develop new potential anticancer agents that could overcome the actual limits of the current antitumoral strategies.

Particularly innovative and promising is the new area of the Phosphatase activators. This pharmacological approach aims to modulate the level of protein phosphorylation within the cancerous cell, inducing apoptosis and cell death. It is considered as the complementary option of the currently adopted TKIs, which modulate the same physiological equilibrium inhibiting instead the kinases. This complementarity, united to the fact that the biological targets are different compared to the TKIs, the phosphatase activators have the promising effect of overcoming the onset of TKIs resistances. Furthermore, they can be effective also in inducing apoptosis in the cancerous stem cells, which are not affected by TKIs. This due to the fact that stem cells are not in a proliferative state, a condition usually marked by upregulation of the kinases' activity, but their phosphatase activity is equally compromised. Facing with the innovativeness and the promises that this new pharmacological approach brings with it, two different targets have been investigated: PP2A and SHP-1.

For what concern PP2A during this PhD several candidates that could positively modulate PP2A, have been synthesized. Their chemical structures are heterogeneous and principally they are the result of structure optimization projects, such as in the case of Fingolimod analogues. Some of the synthesized molecules are the final outcome of merging strategies, where different molecular scaffolds have been fused together, with the aim to obtain chimeric compounds that can present contemporary the efficacy and mode of action typical of two distinct classes of compound. This is the case of the chimeric compounds ApoE-CC11, TD-19-CC11 and of the attempted TGI1002-CC11. This research project has pursued not only synthetic goals but also pharmacokinetic and pharmacodynamic ones. Indeed, a lead compound (CC11), identified in this lab by the former PhD student, has been thoroughly investigated with the scope to understand its distribution profile in mouse model. In particular, this research has demonstrated that CC11, after intraperitoneal injection, has a maximum blood concentration at 9h (1 µg/mL) and that after a chronic administration in mice, its prevalent sites of accumulation are liver, kidney and spleen. Further studies are required for identify and analyze the metabolic profile of this small molecule. Nonetheless, this is a fundamental step for proceeding in the pre-clinical development of the compound. Other efforts have been done for identifying the biological target of this class of compounds. Two different strategies have been adopted. The first one has been focused on the development of functionalized resins, to which CC11 has been grafted in different ways, for performing affinity chromatography experiments. This approach has revealed to be ineffective because the resins were not able to swell in the physiological buffer. A future perspective of this research will be the use of more hydrophilic resins that can swell in the aqueous buffers. The other approach has been based on the development of new photoactivatable fluorescent probes that can fluorescently tag the biological target/s of CC11 in experiments with live cells. Several probes have been synthesized and the preliminary tests, performed in a simple environment without protein, confirmed the ability of the probes to be photoactivate,

to covalently bind other molecules and to become fluorescent upon irradiation. All these promising results will be hopefully confirmed when the real experiments on live cells will be performed. The last followed project for PP2A has been the development of a new ratiometric probe for the detection of the phosphatase activity, even in complex matrices such as whole cell lysates. This compound has been developed with the aim to overcome all the current methods for the detection of the activity of this class of enzymes, such as robustness, easy to use, and little time consuming, for performing fast screenings of compounds, improving the productivity of the biological assays. This new fluorometric tool has been developed also with the idea to exploit it for performing super-resolution microscopy and identify the cellular localization where the phosphatases act. The preliminary results performed on cell lysates confirmed its utility and efficacy as phosphatase probe and its ratiometric behavior. Also the preliminary results obtained during microscopy imaging in cells and in single molecule imaging, confirmed the ability of the compound to penetrate within the cells and to have a blinking behavior that configures it as a good candidate for performing super-resolution microscopy.

Regarding SHP-1, new activators of this phosphatase have been synthesized taking as model a well-known SHP-1 activator: SC-43. Different analogues of this compound have been obtained and almost all the tested ones resulted active in inducing apoptosis in LGL and CLL cell lines. In particular compound EZ2 and EZ5 resulted to have a potency comparable to that one of the model compound SC-43.

The development of new phosphatase activators has not been the only topic faced during this PhD. As illustrated in the previous chapters, also a well-known serine/threonine kinase has been studied and this is CK2. CK2 is emerged as promising target for counteracting different kind of cancers because it is the main downstream effector of a myriad of proliferative pathways. The inhibition of the CK2's activity induces apoptosis prevalently in cancer cells. Considering that this kinase is involved in so many signal cascades, it is improbable that a cancer cell could overcome this block enhancing a different pathway that does not involve this kinase. For this reason, its inhibition is a considerable strategy for overcoming also the onset of TKIs resistances. During this PhD a new class of selective inhibitors of CK2 has been developed. The selectivity of this class resides in its binding mode within the ATP pocket of CK2. Crystallographic data showed that these compounds occupy all the active site and they selectively interact with the open hinge inactive conformation of the enzyme. This feature is extremely rare among tyrosine kinases and this could be the reason of the selectivity of this class of compounds. Compound 4 revealed to be the most effective molecule in *in vitro* tests on CK2 α and in Jurkat cell line. Its selectivity has been tested on a panel of 320 kinases and compound 4 was effective only on CK2 α and CK2 α^1 , defining it as a valid selective CK2 inhibitor drug candidate.

In conclusion, during this PhD several compounds have been synthesized which are able to interact and modulate three of the most appealing and innovative anticancer targets, currently studied by the scientific community. Considering their promising results, these molecules could be considered as leading structures for the development of new drugs able to modulate these important targets.

5 MATERIALS AND METHODS

5.1 ABBREVIATIONS

- Å: Angstrom/angstroms
- aa: Aminoacid/aminoacids/aminoacidic
- ACN: acetonitrile
- Akt: Protein kinase B
- AI: Autoinduction medium
- AML: Acute myeloid leukemia
- Asp: Aspartate
- B-CLL: B-cell chronic lymphocytic leukemia
- bs: Broad singlet
- °C: Celsius degrees
- Calcd: Calculated
- cAMP: Cyclic adenosin mono phosphate
- CDCl₃: Deuterated chloroform
- CIP2A: Cancerous inhibitor of PP2A
- CML: Chronic myeloid leukemia
- Concd: Concentrated
- CoSY: Correlation spectroscopy
- CV: Column volume
- δ: Delta, ppm
- d: Doublet
- D₂O: Deuterated water
- dd: Double doublet
- Da: Dalton
- DCE: 1,2-Dichloroethane
- DCM: Dichloromethane
- DMSO: Dimethylsulfoxide
- DUSP: Dual specificity phosphatase
- EB: Elution buffer
- EDTA: Ethylendiamino tetraacetic acid
- ESI: Electrospray ionization
- Et₂O: Diethylether
- EtOH: Ethanol
- Exper: Experimental
- FCP: TFIIIF-associating C-terminal domain phosphatase

- FDA: Food and drug administration
- FPLC: Fast protein liquid chromatography
- g: Gram/grams
- g: Gravity acceleration
- GPCR: G-protein coupled receptor
- h: Hour/hours
- HAD: Haloacid dehalogenase
- HEAT: Huntingtin/elongation/A subunit/TOR
- His: Histidine
- HMBC: Heteronuclear multiple bond correlation
- HRMS: High resolution mass spectrometry
- HSC: Hematopoietic stem cells
- HSQC: Heteronuclear single quantum coherence
- HTP: High throughput purification
- I2PP2A: PP2A inhibitor 2
- IMAC: Immobilized metal ion affinity chromatography
- IPTG: Isopropyl β -D-1-thiogalactopyranoside
- Jak2: Janus kinase 2
- k: Kilo
- KPSI: Kilopounds per square inch
- L: Liters
- LB: Lysogeny broth
- LCMT1: Leu-carboxyl methyltransferase
- Leu: Leucine
- μ : Micro
- m: Milli
- M: Molarity
- MALS: multi-angle light scattering
- MBP: Maltose binding protein
- MCP: Multi channel pipette
- MeOH: Methanol
- MES: 2-(N-morpholino)ethanesulfonic acid
- Met: Methionin
- m-CPBA: meta-Chloroperbenzoic acid
- MeOD: Deuterated methanol

- MeOH: Methanol
- mg: Milligrams
- MHz: Megahertz
- mL: Milliliter/milliliters
- mmol: Millimole/millimoles
- mol: Mole/moles
- MS: Multiple sclerosis
- MW: Molecular weight
- MWM: Molecular weight marker
- Ni-NTA: Ni²⁺-nitrilotriacetate
- nM: Nanomolar
- NMR: Nuclear magnetic resonance
- NOESY: Nuclear Overhauser effect spectroscopy
- NPI: Sodium chloride, phosphate, imidazole
- OA: Okadaic acid
- OD: Optical density
- o/n: Overnight
- PAGE: Polyacrylamide gel electrophoresis
- PB: Power broth
- PCR: Polymerase chain reaction
- pI: Isoelectric point
- PI3K: Phosphoinositide 3-kinase
- PK: Protein kinase
- PMSF: Phenyl methyl sulfonyl fluoride
- PP: Protein phosphatase
- PPM: Mg²⁺/Mn²⁺ dependent protein phosphatase
- ppm: Parts per million
- PPP: Phosphoprotein phosphatase
- POI: Protein of interest
- PP2A: Protein phosphatase 2A
- PTP: PhosphoTyr phosphatase
- Rf: Retention factor
- rpm: Roots per minute
- rt: Room temperature
- s: Singlet

- S1P: Sphingosine-1-phosphate
- S1PR: Sphingosine-1-phosphate receptor
- SCP: Small C-terminal domain phosphatase
- SDS: Sodium dodecyl sulfate
- SET: Suvar3-9, enhancer of zeste, trithorax
- SHP1: Src-homology 1 domain phosphatase
- SK: Sphingosine kinase
- SN2: Bimolecular nucleophilic substitution
- SV40: Simian vacuolating virus 40
- t: Triplet
- TAF-I β : Template-activating factor-I β
- TB: Terrific broth
- TBE: Tris borate EDTA
- TEA: Triethylamine
- TGF: Transforming growth factor
- TLC: Thin layer chromatography
- TOF: Time of flight
- TOR: Target of rapamycin
- Tris: Tris(hydroxymethyl)aminomethane
- Trp: Tryptophan
- Wnt: Wingless-type MMTV integration site

5.2 CONSUMABLES

Chemicals

All the chemicals were purchased by Agentcourt, Alfa-Aesar, Fluka, Sigma-Aldrich, Thermoscientific, Novagen, Qiagen or Invitrogen and used without further purifications.

Solvents

All the solvents were purchased by Sigma-Aldrich, Carlo Erba and VWR.

Deuterated solvents

All the deuterated solvents were purchased by Sigma-Aldrich and EurisoTop.

TLC plates

Analytical TLC was performed on 60F245 precoated silica gel plates (Merck); spots were visualized with UV light at 254 nm or 365 nm.

Columns for Flash chromatography

The utilized columns were SNAP cartridges 10g and 25g by Biotage.

5.3 INSTRUMENTS

Nuclear Magnetic Resonance (NMR)

NMR spectra were obtained with a NMR Bruker AVANCE III 400 MHz spectrometer and a NMR Bruker AMX 300 MHz spectrometer.

High Resolution Mass Spectrometry (HRMS)

Mass spectra were obtained with a Mariner ESI-TOF (Perceptive Biosystems Inc.) spectrometer, and with a Xevo G2-XS QToF mass spectrometer (Waters, Manchester, UK).

Flash Chromatography

A chromatographic Isolera One by Biotage unit has been used.

HPLC

A dual pump Varian Prostar with a Bio Rad UV-1806 UV/Vis detector with a XORBAX Extend-C18 4.6 x 250mm 5-Micron 80A column was used. The gradient program used consists of two phases. Phase A was a solution of 95% 0.1% trifluoroacetic acid (TFA) in H₂O and 5% acetonitrile. Phase B was composed of 95% acetonitrile and 5% of Phase A. The UV/Vis detector was set to 254nm.

Plate reader

For the experiments that necessitate of a plate reader, a Spark plate reader (Tecan) has been used.

Microwave reactor

For the microwave assisted synthesis a Discover® SP (CEM) and Biotage® Initiator+ microwave reactors have been exploited.

Microscope

The used microscope is a Nikon Eclipse Ti Light Microscope equipped with a Yokogawa spinning-disk confocal scanner unit CSU-W1-T2, two sCMOS cameras (Orca Flash 4.0 V2) and a LUDLPrecision2 stage with a piezo focus. Diode laser was used as light sources: 561nm (200mW) . All images were collected using a 100x CFI Apo TIRF (NA = 1.49) objective with oil-immersion. Emitted light was filtered using the following filters: mCherry (ET630/75) and mCherryLP (ET570LP).

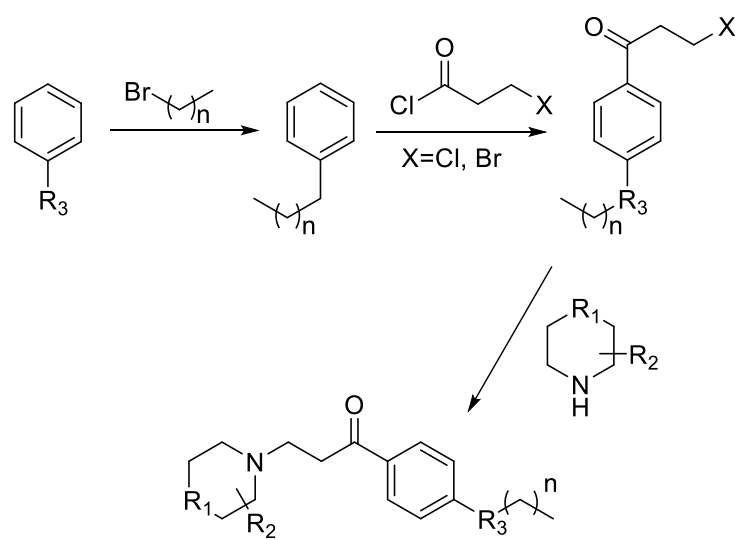
Centrifuge

For centrifuging the Eba 20 (Hettich Zentrifugen) has been used.

5.4 PP2A methods

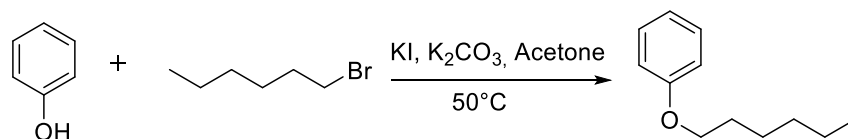
5.4.1 Synthesis of PP2A activators

5.4.1.1 Synthetic scheme of the first class of Fingolimod analogues



R₁ = O, N-Et, N-Ac, NH, N-CH₂-CH₂-OH R₃ = O, S
R₂ = Me, Et n = 5, 6

Synthesis of the phenyl ethers



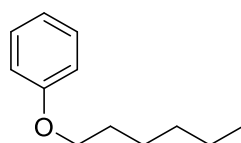
In a round bottom flask, 1-bromohexane (1.330g, 9.54 mmol, 1.180 mL) and NaI (2.144g, 14.31 mmol) were added and dissolved in 12.5 mL of acetone. The suspension was left to react for 5h under magnetic stirring at 60°C. In another round bottom flask, phenol (1.526g, 16.216 mmol) was dissolved in 12.5 mL of acetone in the presence of K₂CO₃ (3.422g, 24.80 mmol). The mixture was left under magnetic stirring at the same condition as the first round bottom flask. After 5h, the mixtures present in both flasks were combined and left to react for 24h. The progression of the reaction was monitored via TLC using a solvent system of 4:1 hexane: ethyl acetate. Once completed, the reaction mixture was filtered to remove the salts and the filtrate was evaporated. The white solid left after evaporation was dissolved in 30mL of diethyl ether and was washed with a 10% (w/v) solution of KOH (30 mL, 3x) followed by a wash of 30 mL deionized water. The organic layer was collected and dried using MgSO₄ and evaporated giving a colorless oil.

Yield: 70%

The use of 1-bromoheptane gives instead a slightly lower yield of around 60-65%.

Characterisation:

Compound 1: hexyloxybenzene



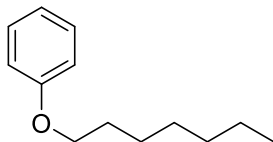
Chemical Formula: C₁₂H₁₈O

Molecular Weight: 178,2750

¹H NMR (400 MHz, CDCl₃) δ: 7.20 (m, 2H), 6.83 (m, 3H), 3.85-3.89 (t, 2H, J=7Hz) 1.71 (m, 2H), 1.2-1.5 (m, 6H) 0.83 (t, 3H, J=7Hz).

Yield: 70%

Compound 2: heptyloxybenzene



Chemical Formula: C₁₃H₂₀O

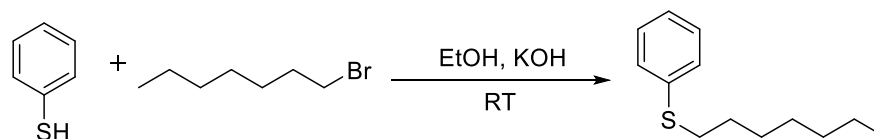
Molecular Weight: 192,3020

¹H NMR (400 MHz, CDCl₃) δ: 7.19 (m, 2H), 6.83 (m, 3H), 3.87 (t, 2H, J=7 Hz) 1.65-1.75 (m, 2H), 1.17-1.42 (m, 8H) 0.82 (t, 3H, J=7 Hz).

Yield: 65%

.

Synthesis of phenyl thioethers



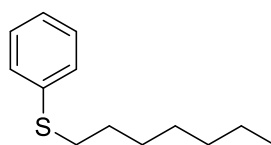
In a round bottom flask, thiophenol (1.000g, 9.07 mmol, 0.932 mL) and KOH (0.508g, 9.07 mmol) were placed under magnetic stirring at room temperature in 20 mL of ethanol. 1-bromoheptane (1.624 g, 9.07 mmol, 1.42 mL) was added dropwise. A white precipitate formed as the reaction progresses. The reaction took approximately 5h. The reaction was monitored by TLC using a solvent system of 4:1 (hexane:ethyl acetate). After completion, the reaction mixture was filtered off and washed three times with brine solution. The organic layer was isolated and dried with MgSO₄ and evaporated off the solvent to give a dense, yellow oil.

Yield: 71%

Again, the 1-bromohexane derivative will give a slightly higher yield varying around 75%.

Characterisation:

Compound 3: heptyl(phenyl)sulfane



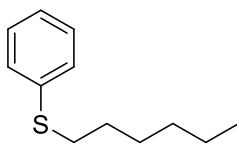
Chemical Formula: C₁₃H₂₀S

Molecular Weight: 208,3630

¹H NMR (400 MHz, CDCl₃) δ: 7.0-7.4 (m, 5H), 2.83 (t, 2H, J=7 Hz) 1.56 (m, 2H), 1.1-1.4 (m, 8H) 0.80 (t, 3H, J=8 Hz).

Yield: 71%

Compound 4: hexyl(phenyl)sulfane



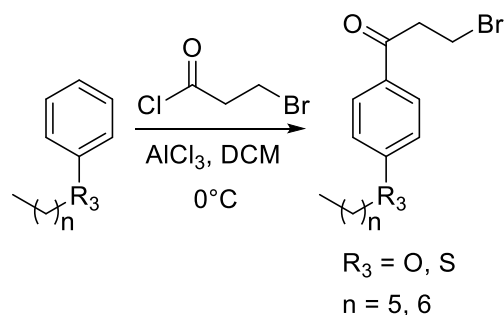
Chemical Formula: $C_{12}H_{18}S$

Molecular Weight: 194,3360

1H NMR (400 MHz, $CDCl_3$) δ : 7.0-7.4 (m, 5H), 2.83 (t, 2H, $J=7$ Hz) 1.56 (m, 2H), 1.1-1.4 (m, 6H) 0.80 (t, 3H, $J=8$ Hz).

Yield: 75%

Synthesis of the phenone synthons



For both oxygen and sulphur derivatives, the procedure is the same. The only difference is reaction time, where sulphur reacts faster than its oxygen derivative.

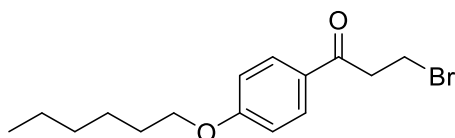
$AlCl_3$ (0.746g, 5.60 mmol) was dissolved in 16 mL of DCE in a double necked flask that was submerged in an ice bath. To this, a solution of the desired ether or thioether (2.801 mmol) and 3-bromopropanoyl chloride (1.200g, 7.00 mmol, 1.19 mL) in 9mL of DCM was added dropwise. The reaction was followed by TLC using as solvent system a mixture of 4:1 (hexane:ethyl acetate). Upon completion, the reaction mixture has been cooled in an ice bath and washed two times with 20 mL of 1M HCl solution, further 3 washes of 20 mL of 5% KOH solution and a final wash with 20 mL of deionised water have been performed. The organic layer was dried with $MgSO_4$ and evaporated off to give a slightly yellow powder.

Yield: 50-95%.

Sulphur derivatives tend to give lower yields compared to their oxygen counterparts which account for the wide variation in yields.

Characterisation:

Compound 5: 3-bromo-1-(4-(hexyloxy)phenyl)propan-1-one



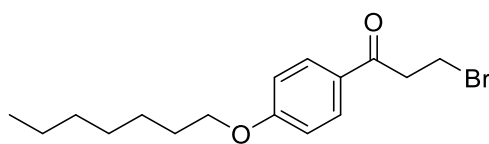
Chemical Formula: $C_{15}H_{21}BrO_2$

Molecular Weight: 313,2350

1H NMR (400 MHz, $CDCl_3$) δ : 7.94 (m, 2H), 6.95 (m, 2H) 4.04 (t, 2H, $J=7$ Hz), 3.75 (t, 2H, $J=8$ Hz) 3.55 (t, 2H, $J=7$ Hz), 1.83 (m, 2H) 1.4-1.1 (m, 6H) 0.93 (t, 3H, $J=7$ Hz).

Yield: 95%

Compound 6: 3-bromo-1-(4-(heptyloxy)phenyl)propan-1-one



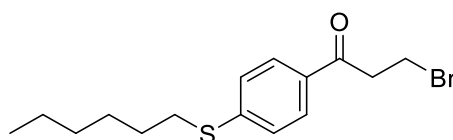
Chemical Formula: C₁₆H₂₃BrO₂

Molecular Weight: 327,2620

¹H NMR (400 MHz, CDCl₃) δ: 7.86 (d, 2H), 6.85 (d, 2H), 3.95 (t, 2H, *J*=7 Hz), 3.65 (t, 2H, *J*= 8 Hz), 3.47 (t, 2H, *J*=7 Hz), 1.74 (m, 2H), 1.2-1.4 (m, 8H) 0.82 (t, 3H, *J*=7 Hz).

Yield: 90%

Compound 7: 3-bromo-1-(4-(hexylthio)phenyl)propan-1-one



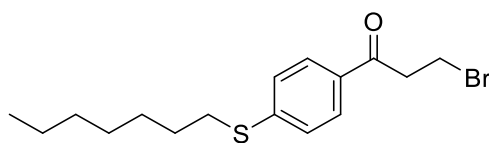
Chemical Formula: C₁₅H₂₁BrOS

Molecular Weight: 329,2960

¹H NMR (400 MHz, CDCl₃) δ: 7.86 (m, 2H), 7.32 (m, 2H), 3.75 (t, 2H, *J*=6 Hz), 3.55 (t, 2H, *J*=7 Hz) 3.01 (t, 2H, *J*=7 Hz), 1.72 (m, 2H), 1.3-1.5 (m, 6H) 0.91 (t, 3H, *J*=7 Hz).

Yield: 60%

Compound 8: 3-bromo-1-(4-(heptylthio)phenyl)propan-1-one



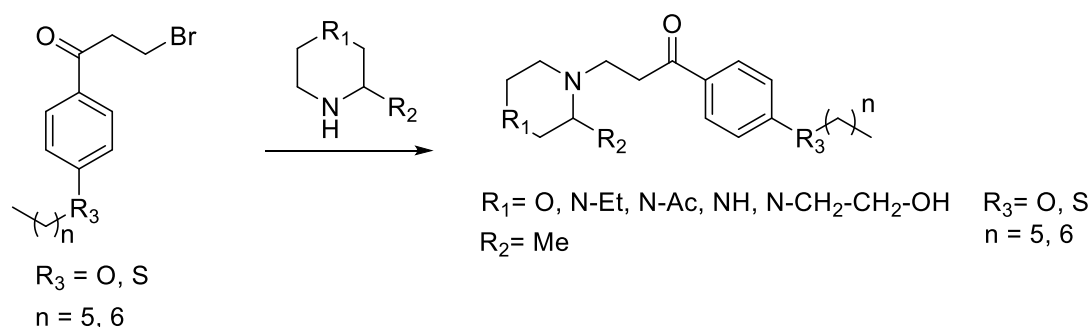
Chemical Formula: C₁₆H₂₃BrOS

Molecular Weight: 343,3230

¹H NMR (400 MHz, d₆-DMSO) δ: 7.89 (m, 2H), 7.40 (m, 2H), 3.76 (t, 2H, *J*=7 Hz), 3.63 (t, 2H, *J*=8 Hz), 3.36 (s, H₂O), 3.06 (t, 2H, *J*=6 Hz), 1.61 (m, 2H), 1.24-1.46 (m, 8H) 0.85 (t, 3H, *J*=6 Hz).

Yield: 50%

Synthesis of the final compounds belonging to the first class of Fingolimod analogues



A general procedure has been adopted for obtaining all the final compounds of this class.

One equivalent of an appropriated phenone has been dissolved in 5 mL/mmol of DCM. A solution of 2 equivalents of the desired secondary amine has been prepared in 2mL/mmol of DCM. The first solution has been slowly dropwise in the second mixture under magnetic stirring. After completion of the addition, the reaction has been checked by TLC using as elution system a mixture of DCM:MeOH 9:1. After completion of the reaction, the organic phase has been washed two times with an 10% KOH aqueous solution. The organic phase has been concentrated under reduced pressure obtaining a yellowish oil. Sometime this procedure led to the obtainment of a highly contaminated product, and for this reason another workup has been followed. The reaction mixture has been extracted with a 0.1M HCl solution two times. Subsequently the aqueous phase has been basified with Na_2CO_3 till pH 10 and then extracted with twice with 20mL of DCM, obtaining the desired compound. The crude product has been dissolved in the minimum amount of Et_2O and then precipitated as HCl salt adding a slight excess of a 2M HCl solution in Et_2O .

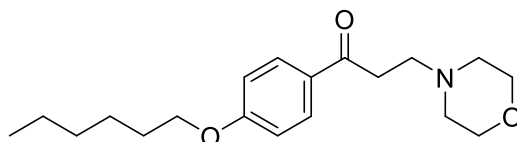
Yield: 20-80%.

The pump program for determining the purity of the compounds is reported below:

Time (mins)	Phase A%	Phase B%
0	60	40
2	60	40
12	5	95
15	5	95
16	60	40

Characterisation:

Compound FAI-01: 1-(4-(hexyloxy)phenyl)-3-morpholinopropan-1-one



Chemical Formula: C₁₉H₂₉NO₃

Molecular Weight: 319,4450

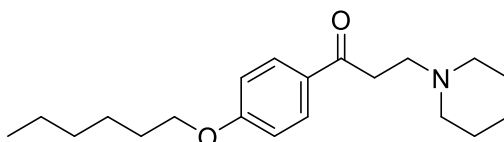
¹H NMR (400 MHz, CDCl₃) δ: 13.27 (s(br), 1H), 7.99 (d, 2H), 6.96 (d, 2H), 4.30 (m, 2H), 4.05 (t, 2H, J = 7 Hz), 4.00 (m, 2H), 3.78 (t, 2H, J = 7 Hz), 3.52 (s, 2H), 3.41 (m, 2H), 2.99 (m, 2H), 1.85 (m, 2H, J=8 Hz), 1.3-1.5 (m, 8H), 0.94 (t, 3H, J=8 Hz).

HRMS (ESI): calcd. (M+H)⁺ 320.2220, exper. 320.2237.

HPLC-UV: 98% purity (area at 254nm).

Yield: 80%

Compound FAI-02: 1-(4-(hexyloxy)phenyl)-3-(piperidin-1-yl)propan-1-one



Chemical Formula: C₂₀H₃₁NO₂

Molecular Weight: 317,4730

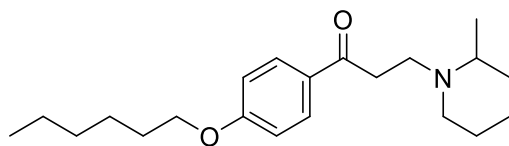
¹H NMR (400 MHz, CDCl₃) δ 11.33 (s(br), 1H), 8.01 (m, 2H), 6.96 (m, 2H), 4.05 (t, 2H, J=8 Hz), 3.82 (t, 2H, J = 8 Hz), 3.19 (m, 2H), 2.75 (m, 2H), 2.33 (m, 2H), 1.8 – 2.0 (m, 6H), 1.3-1.5 (m, 8H), 0.94 (t, 3H, J = 8 Hz).

HRMS (ESI): calcd. (M+H)⁺ 318.2427, exper. 318.2458.

HPLC-UV: 100% purity (area at 254nm).

Yield: 78%

Compound FAI-03: 1-(4-(hexyloxy)phenyl)-3-(2-methylpiperidin-1-yl)-1-one



Chemical Formula: $C_{21}H_{33}NO_2$
Molecular Weight: 331,5000

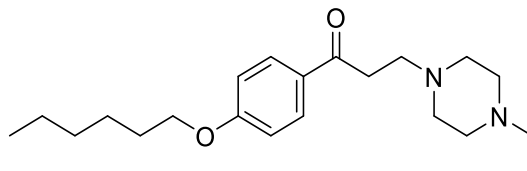
1H NMR (400 MHz, $CDCl_3$) δ 8.00 (m, 2H), 6.94 (m, 2H), 4.04 (m, 2H), 3.79 (m, 2H), 3.0 – 3.5 (m, 4H), 2.38 (m, 2H), 1.6-1.9 (m, 6H), 1.3-1.5 (m, 10H), 0.91 (m, 3H).

HRMS (ESI): calcd. (M+H)⁺ 332.2584, exper. 332.2783.

HPLC-UV: 98% purity (area at 254nm).

Yield: 71%

Compound FAI-04: 3-(4-ethylpiperazin-1-yl)-1-(4-(hexyloxy)phenyl)propan-1-one



Chemical Formula: $C_{21}H_{34}N_2O_2$
Molecular Weight: 346,5150

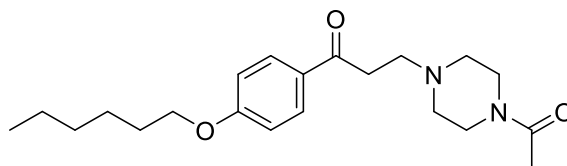
1H NMR (300 MHz, $CDCl_3$) δ 7.90 (m, 2H), 6.87 (m, 2H), 4.66 (m, 2H), 3.3-4.1 (m, 13H) 2.75 (m, 2H), 1.74 (m, 2H), 1.1 – 1.4 (m, 8H), 0.84 (t, 3H, J = 7 Hz).

HRMS (ESI): calcd. (M+H)⁺ 347.2693, exper. 347.2850.

HPLC-UV: 83% purity (area at 254nm).

Yield: 26%

Compound FAI-05: 3-(4-acetylpiperazin-1-yl)-1-(4-(hexyloxy)phenyl)propan-1-one



Chemical Formula: C₂₁H₃₂N₂O₃
Molecular Weight: 360,4980

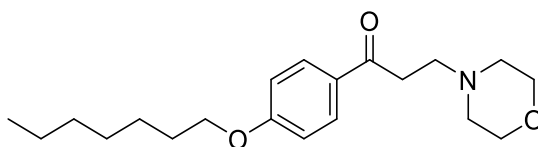
¹H NMR (400 MHz, CDCl₃) δ 7.99 (d, 2H), 6.96 (m, 2H), 4.77 (m, 1H), 4.10 (m, 2H), 4.05 (t, 2H, J = 7 Hz), 3.89 (m, 3H), 3.74 (s, 2H), 3.5-3.6 (m, 3H), 2.84 (m, 2H), 1.82 (m, 2H, J = 8 Hz), 1.2-1.5 (m, 8H) 0.94 (t, J = 7.1 Hz, 3H).

HRMS (ESI): calcd. (M+H)⁺ 361.2468, exper. 361.2413.

HPLC-UV: 95% purity (area at 254nm).

Yield: 21%

Compound FAI-06: 1-(4-(heptyloxy)phenyl)-3-morpholinopropan-1-one



Chemical Formula: C₂₀H₃₁NO₃
Molecular Weight: 333,4720

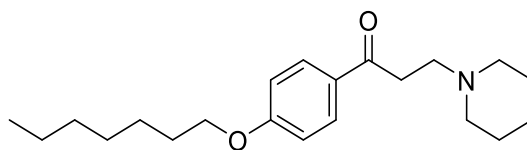
¹H NMR (400 MHz, CDCl₃) δ: 7.99 (d, 2H), 6.95 (d, 2H), 4.29 (m, 2H) 4.04 (t, 2H, J=8 Hz) 4.00 (m, 2H, J=8 Hz) 3.78 (t, 2H, J=8 Hz), 3.52 (m, 2H, J=4 Hz) 3.31 (m, 2H) 2.98 (m, 2H) 1.82 (m, 2H, J=8 Hz) 1.3-1.5 (m, 10H) 0.92 (t, 3H, J=8 Hz).

HRMS (ESI): calcd. (M+H)⁺ 334.2376, exper. 334.2456.

HPLC-UV: 95% purity (area at 254nm).

Yield: 60%

Compound FAI-07: 1-(4-(heptyloxy)phenyl)-3-(piperidin-1-yl)propan-1-one



Chemical Formula: C₂₁H₃₃NO₂

Molecular Weight: 331,5000

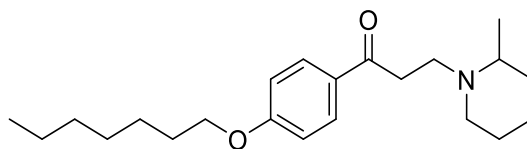
¹H NMR (400 MHz, CDCl₃) δ 11.84 (s, 1H), 8.00 (m, 2H), 6.95 (m, 2H), 4.04 (t, 2H, J = 7 Hz), 3.78 (t, 2H, J=8 Hz), 3.5-3.6 (m, 2H), 3.47 (m, 2H, J = 8 Hz), 2.72 (m, 2H), 2.29 (m, 2H), 1.7- 2.0 (m, 4H), 1.3 – 1.5 (m, 10H), 0.92 (t, 3H, J = 7 Hz).

HRMS (ESI): calcd. (M+H)⁺ 332.2584, exper. 332.2652.

HPLC-UV: 96% purity (area at 254nm).

Yield: 55%

Compound FAI-08: 1-(4-(heptyloxy)phenyl)-3-(2-methylpiperidin-1-yl)-1-one



Chemical Formula: C₂₂H₃₅NO₂

Molecular Weight: 345,5270

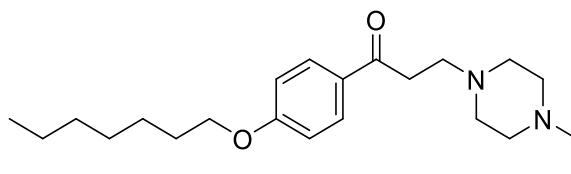
¹H NMR (300 MHz, CDCl₃) δ 11.92 (s(br), 1H) 7.92 (m, 2H), 6.86 (m, 2H), 3.95 (t, 2H, J = 7 Hz), 3.5-3.9(m, 5H) 2.8 – 3.4 (m, 3H), 2.1-2.5 (m, 2H), 1.6-1.9 (m, 6H), 1.1-1.5 (m, 10H) 0.84 (t, 3H, J = 7 Hz).

HRMS (ESI): calcd. (M+H)⁺ 346.2741, exper. 346.2680.

HPLC-UV: 100% purity (area at 254nm).

Yield: 20%

Compound FAI-09: 3-(4-ethylpiperazin-1-yl)-1-(4-(heptyloxy)phenyl)propan-1-one



Chemical Formula: C₂₂H₃₆N₂O₂
Molecular Weight: 360,5420

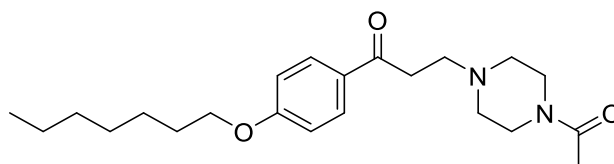
¹H NMR (300 MHz, CDCl₃) δ 7.85 (m, 2H), 6.85 (m, 2H), 3.95 (t, 2H, J = 7 Hz), 2.5-3.2 (m, 12H), 1.74 (m, 2H, J=7 Hz), 1.1-1.4 (m, 11H), 0.83 (t, 3H, J=8 Hz).

HRMS (ESI): calcd. (M+H)⁺ 361.2850, exper. 361.3160.

HPLC-UV: with a 98% purity (area at 254nm).

Yield: 34%

Compound FAI-10: 3-(4-acetylpiperazin-1-yl)-1-(4-(heptyloxy)phenyl)propan-1-one



Chemical Formula: C₂₂H₃₄N₂O₃
Molecular Weight: 374,5250

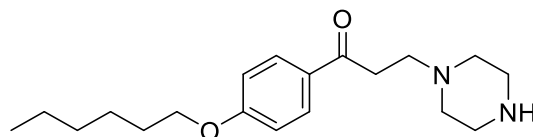
¹H NMR (300 MHz, CDCl₃) δ 12.42 (s, 1H), 7.90 (m, 2H,), 6.87 (m, 2H,), 4.67 (m, 1H), 4.08 (m, 1H), 3.96 (t, 3H, J =7 Hz), 3.4 – 3.9 (m, 10H), 2.78 (m, 2H), 1.74 (m, 2H, J=8 Hz), 1.1 – 1.4 (m, 8H), 0.83 (t, 3H, J = 7 Hz,).

HRMS (ESI): calcd. (M+H)⁺ 375.2642, exper. 375.2909.

HPLC-UV: with a 93% purity (area at 254nm).

Yield: 17%

Compound **FAI-11**: 1-(4-(hexyloxy)phenyl)-3-(piperazin-1-yl)propan-1-one



Chemical Formula: C₁₉H₃₀N₂O₂
Molecular Weight: 318,4610

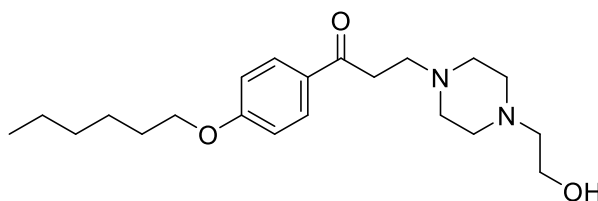
¹H NMR (300 MHz, CDCl₃) δ 7.94 – 7.87 (m, 2H), 6.91 (dt, *J* = 3.6, 2.2 Hz, 2H), 4.95 (s all, 1H), 4.01 (t, *J* = 6.6 Hz, 2H), 3.20 – 3.02 (m, 4H), 2.85 (t, *J* = 7.1, Hz, 2H), 2.50-2.70 (m, 6H), 1.87 – 1.62 (m, 2H), 1.53 – 1.40 (m, 2H), 1.40 – 1.25 (m, 4H), 0.99 – 0.75 (m, 3H).

HRMS (ESI): calcd. (M+H)⁺ 319.2380, exper. 319.2390.

HPLC-UV: with a 86% purity (area at 254nm).

Yield: 15%

Compound **FAI-12**: 1-(4-(hexyloxy)phenyl)-3-(4-(2-hydroxyethyl)piperazin-1-yl)propan-1-one



Chemical Formula: C₂₁H₃₄N₂O₃
Molecular Weight: 362,5140

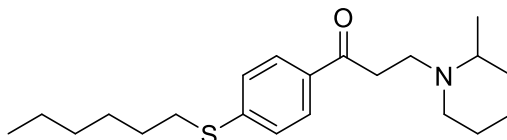
¹H NMR (400 MHz, CDCl₃) δ 7.95 – 7.89 (m, 2H), 6.95 – 6.88 (m, 2H), 4.01 (t, *J* = 6.6 Hz, 2H), 3.63 (t, *J* = 5.6 Hz 2H), 3.15 (t, *J* = 7.4 Hz, 2H), 2.87 (t, *J* = 7.4 Hz, 2H), 2.67 – 2.52 (m, 10H), 1.79 (dt, *J* = 14.5, 6.6 Hz, 2H), 1.50 – 1.40 (m, 2H), 1.34 (td, *J* = 7.0, 3.5 Hz, 4H), 0.95 – 0.87 (m, 3H).

HRMS (ESI): calcd. (M+H)⁺ 363.5215, exper. 363.5222.

HPLC-UV: with a 98% purity (area at 254nm).

Yield: 23%

Compound FAI-13: 1-(4-(hexylthio)phenyl)-3-(2-methylpiperidin-1-yl)propane-1-one



Chemical Formula: C₂₁H₃₃NOS

Molecular Weight: 347,5610

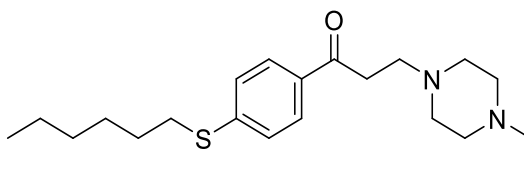
¹H NMR (300 MHz, CDCl₃) δ 7.84 (m, 2H), 7.23 (m, 2H), 3.6 – 3.9 (m, 2H), 3.3 – 3.5 (m, 3H), 2.92 (t, 2H, J=6 Hz), 2.0 – 2.4 (m, 2H), 1.7 – 1.9 (m, 3H), 1.5-1.6 (m, 4H), 1.1 – 1.5 (m, 10H), 0.83 (t, 3H, J =7 Hz).

HRMS (ESI): calcd. (M+H)⁺ 348.2356, exper. 348.2564.

HPLC-UV: 95% purity (area at 254nm).

Yield: 41%

Compound FAI-14: 3-(4-ethylpiperazin-1-yl)-1-(4-(hexylthio)phenyl)propan-1-one



Chemical Formula: C₂₁H₃₄N₂OS

Molecular Weight: 362,5760

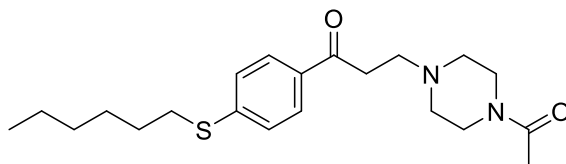
¹H NMR (300 MHz, CDCl₃) δ 13.7(s(br), 1H), 7.79 (m, 2H), 7.23(m, 2H), 3.8-4.2(m, 4H), 3.4- 3.7 (m, 6H), 3.14 (m, 2H), 2.93 (t, 3H, J= 8 Hz), 1.63 (m, 2H, J =8 Hz), 1.2 – 1.5 (m, 10H) 0.83 (t, 3H, J = 7 Hz).

HRMS (ESI): calcd. (M+H)⁺ 363.2720, exper. 363.2175.

HPLC-UV: 99% purity (area at 254nm).

Yield: 22%

Compound FAI-15: 3-(4-acetylpiperazin-1-yl)-1-(4-(hexylthio)phenyl)propan-1-one



Chemical Formula: C₂₁H₃₂N₂O₂S
Molecular Weight: 376,5590

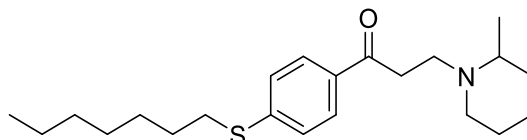
¹H NMR (300 MHz, CDCl₃) δ 12.39 (s, 1H), 7.91 (m, 2H), 7.31 (m, 2H), 4.77 (m, 1H), 3.5 – 4.2 (m, 10H), 3.26 (m, 1H), 3.02 (t, 3H, J = 8 Hz), 2.8-3.0 (m, 2H), 1.73 (m, 2H, J = 7 Hz), 1.3 – 1.5 (m, 6H), 0.92 (t, 3H, J = 7 Hz).

HRMS (ESI): calcd. (M+H)⁺ 377.2257, exper. 377.2318.

HPLC-UV: 100% purity (area at 254nm).

Yield: 70%

Compound FAI-16: 1-(4-(heptylthio)phenyl)-3-(2-methylpiperidin-1-yl)propane-1-one



Chemical Formula: C₂₂H₃₅NOS
Molecular Weight: 361,5880

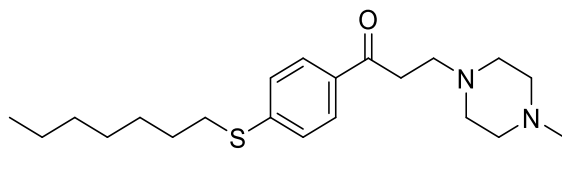
¹H NMR (400 MHz, CDCl₃) δ 12.20 (s(br), 1H), 7.93 (m, 2H), 7.31 (m, 2H), 3.6-3.9 (m, 4H), 3.54 (m, 1H), 3.25 (m, 1H), 3.01 (t, 2H, J = 8 Hz), 2.62 (m, 1H), 2.33 (m, 1H), 1.8-2.0 (m, 3H), 1.73 (m, 2H, J = 8 Hz), 1.65 (d, 2H, J = 6 Hz), 1.3 – 1.5 (m, 10H), 0.91 (t, 3H, J = 7 Hz).

HRMS (ESI): calcd. (M+H)⁺ 362.2152, exper. 362.2218.

HPLC-UV: 98% purity (area at 254nm).

Yield: 41%

Compound FAI-17: 3-(4-ethylpiperazin-1-yl)-1-(4-(heptylthio)phenyl)propan-1-one



Chemical Formula: C₂₂H₃₆N₂OS

Molecular Weight: 376,6030

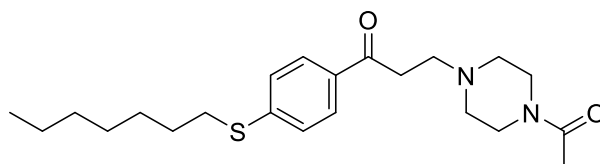
¹H NMR (400 MHz, CDCl₃) δ 7.87 (m, 2H), 7.31 (m, 2H), 3.20 – 3.13 (t, 2H, J=8 Hz), 3.00 (m, 2H, J=8 Hz), 2.87 (t, 2H, J = 7 Hz), 2.4 – 2.7 (m, 10H), 1.72 (m, 1H, J = 8 Hz), 1.4-1.5 (m, 2H), 1.2-1.4 (m, 6H), 1.12 (t, 3H, J = 7 Hz), 0.91 (t, 3H, J = 7 Hz).

HRMS (ESI): calcd. (M+H)⁺ 377.2621, exper. 377.2318.

HPLC-UV: 93% purity (area at 254nm).

Yield: 69%

Compound FAI-18: 3-(4-acetylpiperazin-1-yl)-1-(4-(heptylthio)phenyl)propan-1-one



Chemical Formula: C₂₂H₃₄N₂O₂S

Molecular Weight: 390,5860

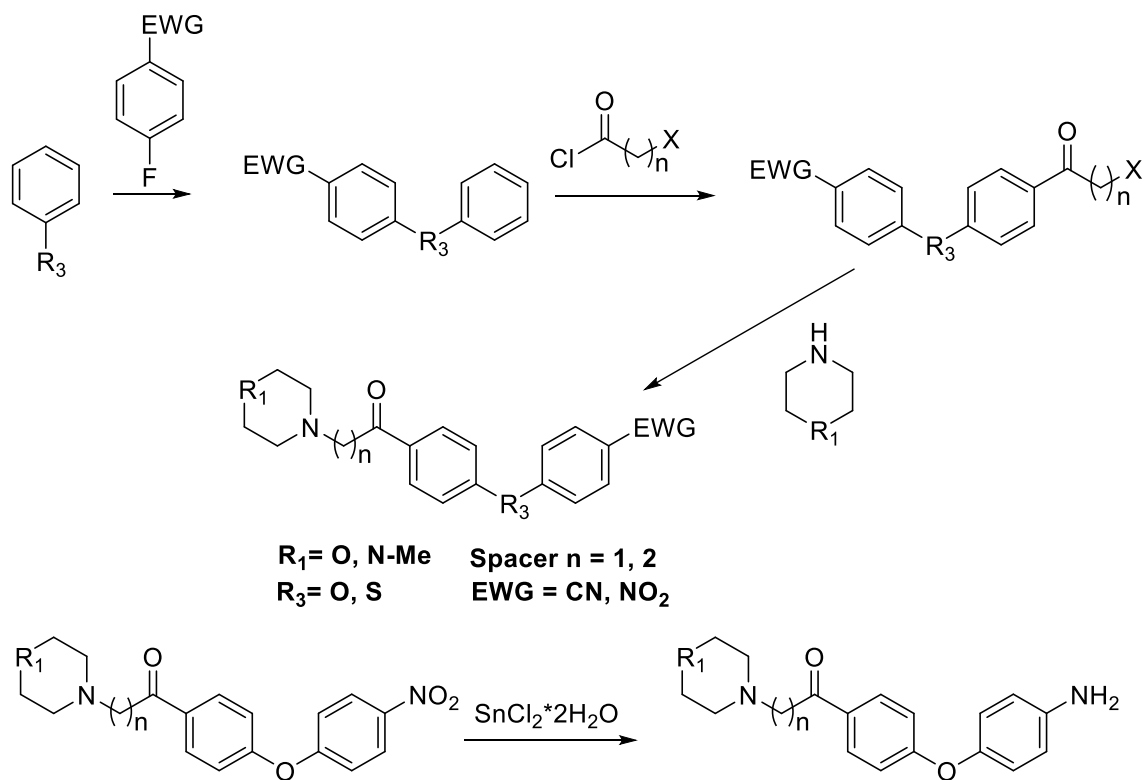
¹H NMR (400 MHz, CDCl₃) δ 12.35 (m, 1H), 7.92 (m, 2H), 7.32 (m, 2H), 4.79 (m, 1H), 4.18 (m, 1H), 4.03 (s, 1H), 3.8-4.0 (s, 3H), 3.7 – 3.8 (m, 1H), 3.59 (s, 4H), 3.27 (m, 2H), 3.02 (t, 2H, J = 8 Hz), 2.52 (m, 2H), 1.73 (m, 2H, J= 7 Hz), 1.40 (m, 8H), 0.91 (t, 3H, J = 7 Hz).

HRMS (ESI): calcd. (M+H)⁺ 391.2413, exper. 391.2728.

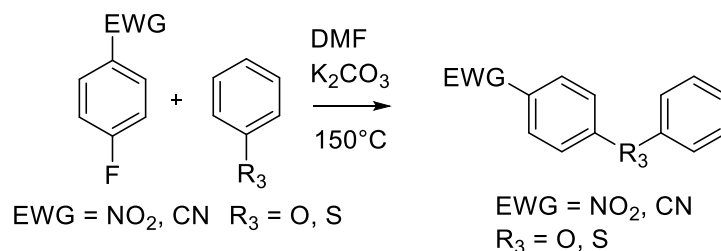
HPLC-UV: 99% purity (area at 254nm).

Yield: 20%

5.4.1.2 Synthetic scheme of the second class of Fingolimod analogues



Synthesis of the ether or thioether biphenyl rings.



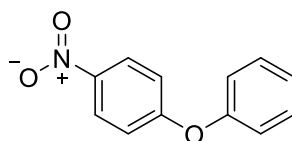
A common synthetic protocol has been adopted for the obtainment of all the biphenyl cores.

In a round bottom flask phenol (0.705 g, 7.5 mmol) and K₂CO₃ (1.382 g, 10.0 mmol) have been added and suspended in 5 mL of DMF. The mixture has been stirred at room temperature for 10 minutes and subsequently, 1-fluoro-4-nitrobenzene (0.705 g, 5 mmol) has been added. The reaction mixture has been heated under reflux for 5h. The reaction has been monitored through TLC using as elution mixture cyclohexane:EtOAc (8:2). After completion, the mixture has been cooled down at room temperature and subsequently in ice bath for few minutes, then 20mL of a saturated aqueous solution of NaHCO₃ has been added. The formed precipitate has been filtered off under vacuum and washed thoroughly with deionised water, isolating 1.025 g of final compound.

Yield: 85-96%

Characterisation:

Compound 1: 1-nitro-4-phenoxybenzene

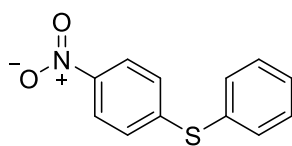


Chemical Formula: C₁₂H₉NO₃
Molecular Weight: 215,2080

¹HNMR (300MHz, CDCl₃): δ: 8.20 (2H, dt, J₁=9.32 Hz, J₂=2.22 Hz), 7.44 (2H, tt, J₁=8.32 Hz, J₂=2.5 Hz), 7.26 (1H, tt, J₁=7.14 Hz, J₂=1.21 Hz), 7.09 (2H, ddd, J₁= 8.72 Hz, J₂= 1.21 Hz, J₃=3.75 Hz), 7.01 (2H, dt, J₁=9.20 Hz, J₂=2.20 Hz).

Yield: 96%

Compound 2: (4-nitrophenyl)(phenyl)sulfane

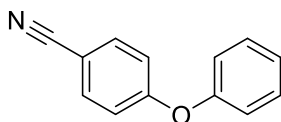


Chemical Formula: C₁₂H₉NO₂S
Molecular Weight: 231,2690

¹HNMR (300MHz, CDCl₃): δ: 8.06 (2H, dt, J₁=9.02 Hz, J₂=2.0 Hz, J₃=7.02Hz), 7.54 (2H, dd, J₁=2.5 Hz, J₂=3.6 Hz), 7.46 (3H, m), 7.18 (2H dt, J₁= 8.8 Hz, J₂= 2.0 Hz, J₃=7.02 Hz).

Yield: 90%

Compound 3: 4-phenoxybenzonitrile



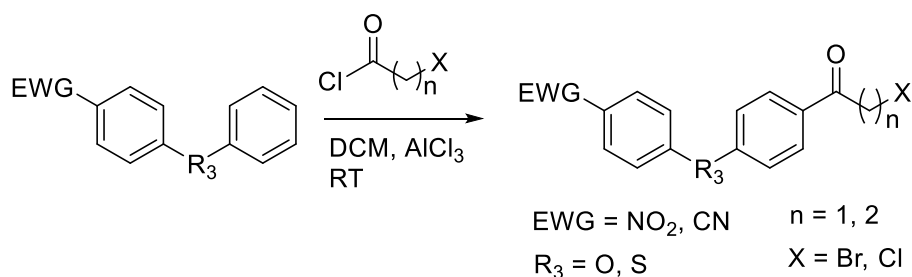
Chemical Formula: C₁₃H₉NO
Molecular Weight: 195,2210

¹HNMR (300MHz, MeOD): δ: 7.64 (2H, d, J₁=8.5Hz), 7.4 (2H, t, J₁=8.1Hz), 7.21 (1H, t, J₁=7.56Hz), 7.04 (2H, d, J₁=9.1 Hz), 7.00 (2H, d, J₁=9.1Hz).

HRMS (ESI): calcd. (M+H)⁺ 196.0757, exper. 196.0772.

Yield: 85%

Synthesis of the phenone synthons



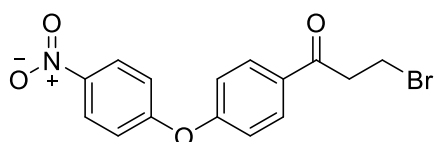
The common procedure for the obtainment of the different phenones is reported in the follow part.

In a round bottom flask AlCl₃ (0.176 g, 1.3 mmol) and 3-bromopropionyl chloride (86 μL, 0.85 mmol) have been added to 2 mL of DCM and stirred at room temperature for 30 minutes. In another flask 4-phenoxybenzonitrile (0.165 g, 0.85 mmol) has been dissolved in 1 mL of DCM. After 30 minutes the solution of the biphenyl ring has been added dropwise to the other round bottom flask. The reaction has been monitored through TLC (Ciclohexane:EtOAc, 8:2). After 4 hours the reaction was not still completed and for this reason another equivalent of AlCl₃ and 3-bromopropionyl chloride have been added to the reaction mixture. After one hour the reaction was completed. The reaction mixture has been diluted with other 10 mL of DCM and thoroughly washed with 20 mL of HCl 0,1 M, twice with deionised water and one with a saturated aqueous solution of NaHCO₃. The organic phase has been dried over MgSO₄, and finally the organic solvent has been removed through evaporation under reduced pressure obtaining a yellowish powder.

Yield: 75-99 %

Characterisation:

Compound 4: 3-bromo-1-(4-(4-nitrophenoxy)phenyl)propan-1-one



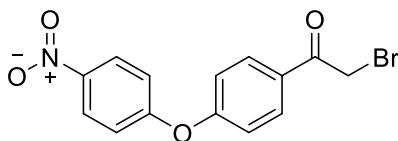
Chemical Formula: C₁₅H₁₂BrNO₄

Molecular Weight: 350,1680

¹HNMR (300MHz, CDCl₃): δ: 8.26 (2H, dt, J₁=9.0Hz, J₂=2.1 Hz), 8.02 (2H, dt, J₁=8.8 Hz, J₂=2.1 Hz), 7.14 (2H, dt, J₁=8.8Hz, J₂=2.1 Hz), 7.10 (2H, dt, J₁=9.5Hz, J₂=2.4 Hz), 3.75 (2H, t, J₁=6.87Hz), 3.57 (2H, t, J₁=6.87Hz).

Yield: 99%

Compound 5: 2-bromo-1-(4-(4-nitrophenoxy)phenyl)ethan-1-one



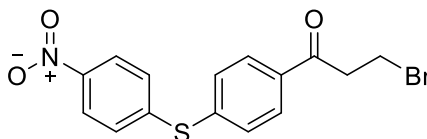
Chemical Formula: C₁₄H₁₀BrNO₄

Molecular Weight: 336,1410

¹HNMR (300MHz, CDCl₃): δ: 8.26 (2H, dt, J₁=9.2Hz, J₂=2.3Hz, J₃=7.0Hz), 8.07 (2H, dt, J₁=8.9 Hz, J₂=2.1 Hz), 7.16 (2H, dt, J₁=3.8Hz, J₂=2.1Hz), 7.13 (2H, dt, J₁=4.3Hz, J₂=2.1Hz, J₃=7.2Hz), 4.42 (2H, s).

Yield: 75%

Compound 6: 3-bromo-1-(4-((4-nitrophenyl)thio)phenyl)propan-1-one

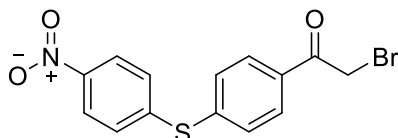


Chemical Formula: C₁₅H₁₂BrNO₃S

Molecular Weight: 366,2290

Not isolated.

Compound 7: 2-bromo-1-(4-((4-nitrophenyl)thio)phenyl)ethan-1-one

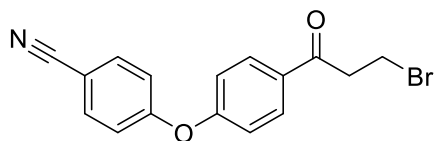


Chemical Formula: C₁₄H₁₀BrNO₃S

Molecular Weight: 352,2020

Not isolated.

Compound 8: 4-(4-(3-bromopropanoyl)phenoxy)benzonitrile



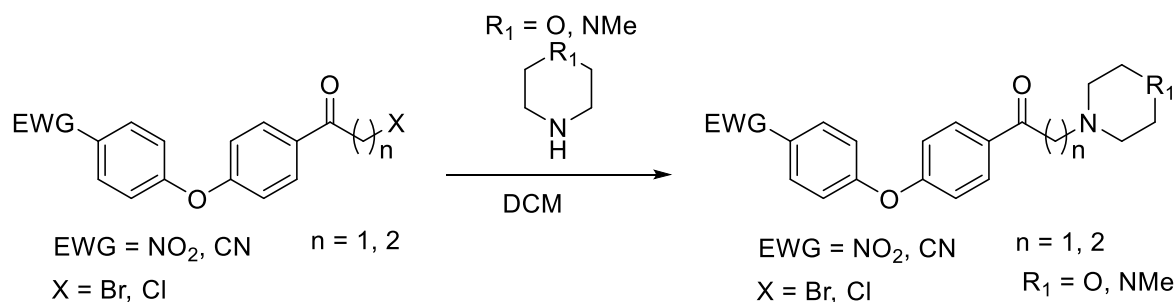
Chemical Formula: $C_{16}H_{12}BrNO_2$

Molecular Weight: 330,1810

1H NMR (300MHz, DMSO): δ : 8.08 (2H, dt, $J_1=8.9Hz$, $J_2=2.1Hz$), 7.92 (2H, dt, $J_1=8.9Hz$, $J_2=2.1Hz$), 7.26 (1H, dt, $J_1=8.9Hz$, $J_1=2.1Hz$), 7.23 (2H, dt, $J_1=8.9Hz$, $J_2=2.1Hz$), 3.78 (2H, t, $J_1=4.9Hz$), 3.69 (2H, t, $J_1=4.9Hz$)

Yield: 99%

Synthesis of the final compounds belonging to the second class of Fingolimod analogues



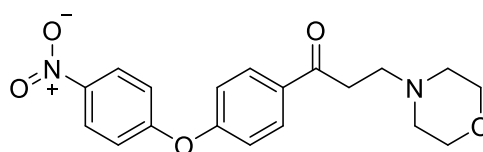
A general protocol has been adopted for the synthesis of all the final compounds.

In a round bottom flask 1 equivalent of the chosen phenone has been dissolved in 2 mL/mmol of DCM. In another round bottom flask 2 equivalents of the appropriate secondary amine have been dissolved in 5 mL/mmol of DCM. To this second solution, the first one has been added dropwise and the obtained mixture has been stirred at room temperature for 3 hours. The progression of the reaction has been controlled by TLC, using as eluting mixture cyclohexane:EtOAc (6:4). After completion of the reaction, the organic solvent has been evaporated under reduced pressure and the obtained solid has been suspended in a saturated aqueous solution of NaHCO₃. The formed precipitate has been filtered off under vacuum, obtaining the desired final compound.

Yield: 50-80 %

Characterisation:

Compound AFA-01: 3-morpholino-1-(4-(4-nitrophenoxy)phenyl)propan-1-one



Chemical Formula: C₁₉H₂₀N₂O₅

Molecular Weight: 356,3780

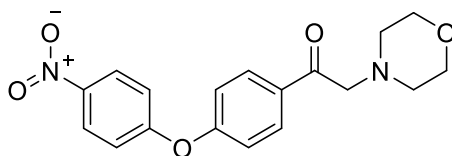
¹HNMR (300MHz, CDCl₃): δ: 8.26 (2H, dt, J₁=9.2Hz, J₂=2.1Hz), 8.05 (2H, dt, J₁=8.8Hz, J₂=1.8Hz), 7.14 (2H, dd, J₁=8.6Hz, J₂=2.0 Hz), 7.12 (2H, dd, J₁=9.1 Hz, J₂=2.0Hz), 3.86 (4H, m), 3.40 (2H, m), 3.07 (2H, m), 2.74 (4H, m).

HRMS (ESI): calcd. (M+H)⁺ 357.1445, exper. 357.1462.

HPLC-UV: 99% purity (area at 254nm).

Yield: 60%

Compound AFA-02: 2-morpholino-1-(4-(4-nitrophenoxy)phenyl)ethan-1-one



Chemical Formula: C₁₈H₁₈N₂O₅

Molecular Weight: 342,3510

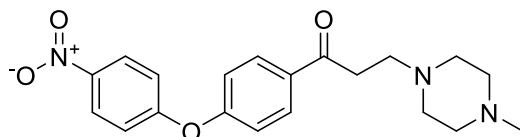
¹HNMR (300MHz, CDCl₃): δ: 8.26 (2H, dt, J₁=9.1Hz, J₂=2.0Hz), 8.10 (2H, dt, J₁=8.7Hz, J₂=1.9Hz), 7.13 (2H, dt, J₁=8.8Hz, J₂=1.8Hz), 7.11 (2H, dt, J₁=9.1 Hz, J₂=2.1Hz), 3.78 (6H, t+s, J₁=4.9Hz), 2.62 (4H, t, J₁= 4.9Hz).

HRMS (ESI): calcd. (M+H)⁺ 343.1288, exper. 343.1300.

HPLC-UV: 96% purity (area at 254nm).

Yield: 50%

Compound AFA-03: 3-(4-methylpiperazin-1-yl)-1-(4-(4-nitrophenoxy)phenyl)propan-1-one



Chemical Formula: C₂₀H₂₃N₃O₄

Molecular Weight: 369,4210

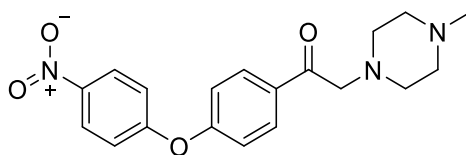
¹HNMR (300MHz, CDCl₃): δ: 8.26 (2H, dt, J₁=9.2Hz, J₂=2.1Hz), 8.03 (2H, dt, J₁=8.6 Hz, J₂=1.9Hz), 7.13 (2H, dd, J₁=8.3Hz, J₂=1.9 Hz), 7.10 (2H, dd, J₁=9.0 Hz, J₂=1.9Hz), 3.24 (2H, t, J₁=3.21Hz), 2.96 (2H, t, J₁=2.94Hz), 2.71 (8H, m), 2.42 (3H, s).

HRMS (ESI): calcd. (M+H)⁺ 370.1761, exper. 370.1763.

HPLC-UV: 95% purity (area at 254nm).

Yield: 80%

Compound AFA-04: 2-(4-methylpiperazin-1-yl)-1-(4-(4-nitrophenoxy)phenyl)ethan-1-one



Chemical Formula: C₁₉H₂₁N₃O₄
Molecular Weight: 355,3940

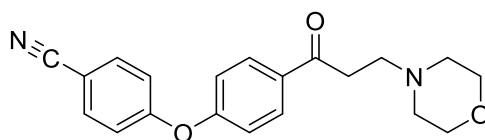
¹HNMR (300MHz, CDCl₃): δ: 8.26 (2H, dt, J₁=9.2Hz, J₂=2.1Hz, J₃=7.0 Hz), 8.07 (2H, dt, J₁=8.9 Hz, J₂=2.0Hz, J₃=6.9Hz), 7.13 (2H, dd, J₁=8.8Hz, J₂=1.9 Hz), 7.10 (2H, dd J₁=8.5 Hz, J₂=2.9Hz), 3.86 (2H, s), 2.81 (8H, m), 2.49 (3H, s)

HRMS (ESI): calcd. (M+H)⁺ 356.1605, exper. 356.1615.

HPLC-UV: 93% purity (area at 254nm).

Yield: 62%

Compound AFA-05: 4-(4-(3-morpholinopropanoyl)phenoxy)benzonitrile



Chemical Formula: C₂₀H₂₀N₂O₃
Molecular Weight: 336,3910

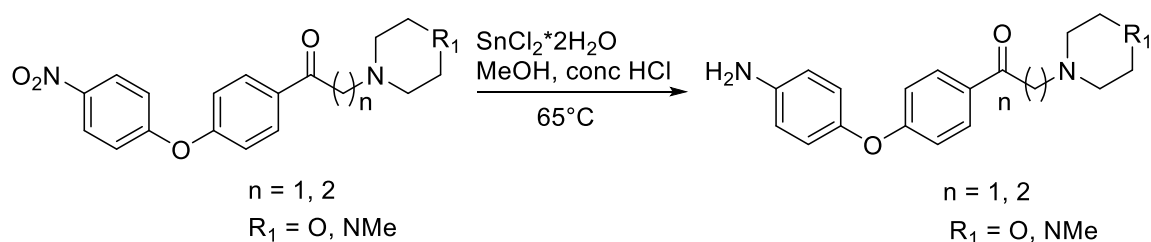
¹HNMR (300MHz, DMSO): δ: 8.08 (2H, dt, J₁=8.9Hz, J₂=2.1Hz), 7.92 (2H, dt, J₁=8.9Hz, J₂=2.1Hz), 7.26 (2H, dt, J₁=8.9Hz, J₂=2.1Hz), 7.23 (2H, dt, J₁=8.9Hz, J₂=2.1Hz), 3.86 (4H, m), 3.40 (2H, m), 3.07 (2H, m), 2.74 (4H, m).

HRMS (ESI): calcd. (M+H)⁺ 337.1547, exper. 337.1601.

HPLC-UV: 98% purity (area at 254nm).

Yield: 75%

Synthesis of the final compounds belonging to the second class of Fingolimod Analogues after reduction of the nitro group.



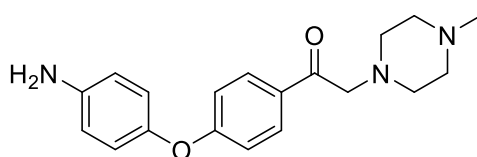
The illustrated procedure is common to all the compounds obtained through the reduction of the nitro group.

In a round bottom flask one equivalent of the compound to be reduced has been dissolved in MeOH (3mL/mmol). In another flask a solution of SnCl₂*2H₂O (4.8 equivalents) in concentrated HCl (1mL/mmol of tin chloride) has been prepared and subsequently added dropwise to the first solution, cooling during the mixture during the addition in ice bath. After the completion of the addition, the reaction mixture has been heated up at 65°C for 2 hours. The reaction has been monitored through TLC (DCM:MeOH 9:1). After completion of the reaction the mixture has been cooled down at room temperature and then 10mL/mmol of H₂O has been added and the pH adjusted to pH 9. The aqueous phase has been extracted three times with 20 mL of DCM. The organic phase has been dried on MgSO₄ and then the organic solvent has been removed under reduced pressure obtaining the final desired compound.

Yield: 40-77%

Characterisation:

Compound AFA-06: 1-(4-(4-aminophenoxy)phenyl)-2-(4-methylpiperazin-1-yl)ethan-1-one



Chemical Formula: C₁₉H₂₃N₃O₂
Molecular Weight: 325,4120

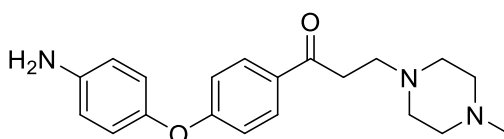
¹HNMR (300MHz, CDCl₃): δ: 7.95 (2H, dt, J₁=9.0Hz, J₂=2.0Hz), 6.92 (2H, dt, J₁=9.0Hz, J₂=2.0 Hz), 6.89 (2H, dt J₁=8.8 Hz, J₂=2.2Hz), 6.71 (2H, dt, J₁=8.8Hz, J₂=2.2 Hz), 3.77 (2H, s), 2.65 (8H, m), 2.36 (3H, s).

HRMS (ESI): calcd. (M+H)⁺ 326.1863, exper. 326.1889.

HPLC-UV: 93% purity (area at 254nm).

Yield: 45%

Compound AFA-07: 1-(4-(4-aminophenoxy)phenyl)-3-(4-methylpiperazin-1-yl)propan-1-one



Chemical Formula: C₂₀H₂₅N₃O₂

Molecular Weight: 339,4390

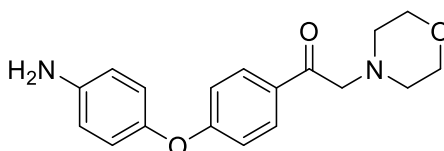
¹HNMR (300MHz, CDCl₃): δ: 7.95 (2H, dt, J₁=9.0Hz, J₂=2.0Hz), 6.92 (2H, dt, J₁=9.0Hz, J₂=2.0 Hz), 6.89 (2H, dt, J₁=8.8 Hz, J₂=2.2Hz), 6.71 (2H, dt, J₁=8.8Hz, J₂=2.2 Hz), 3.24 (2H, t, J₁=3.21Hz), 2.96 (2H, t, J₁=2.94Hz), 2.71 (8H, m), 2.42 (3H, s).

HRMS (ESI): calcd. (M+H)⁺ 340.2020, exper. 340.2020.

HPLC-UV: 90% purity (area at 254nm).

Yield: 40%

Compound AFA-08: 1-(4-(4-aminophenoxy)phenyl)-2-morpholinoethan-1-one



Chemical Formula: C₁₈H₂₀N₂O₃

Molecular Weight: 312,3690

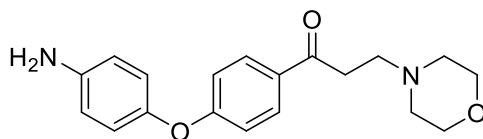
¹HNMR (300MHz, CDCl₃): δ: 7.97 (2H, dt, J₁=8.9Hz, J₂=2.1Hz), 6.93 (2H, dt, J₁=9.0Hz, J₂=2.0Hz), 6.89 (2H, dt, J₁=8.7Hz, J₂=2.1Hz), 6.70 (2H, dt, J₁=8.7 Hz, J₂=2.2Hz), 3.75 (6H, m), 2.62 (4H, m).

HRMS (ESI): calcd. (M+H)⁺ 313.1547, exper. 313.1556.

HPLC-UV: 88% purity (area at 254nm).

Yield: 60%

Compound AFA-09: 1-(4-(4-aminophenoxy)phenyl)-3-morpholinopropan-1-one



Chemical Formula: C₁₉H₂₂N₂O₃

Molecular Weight: 326,3960

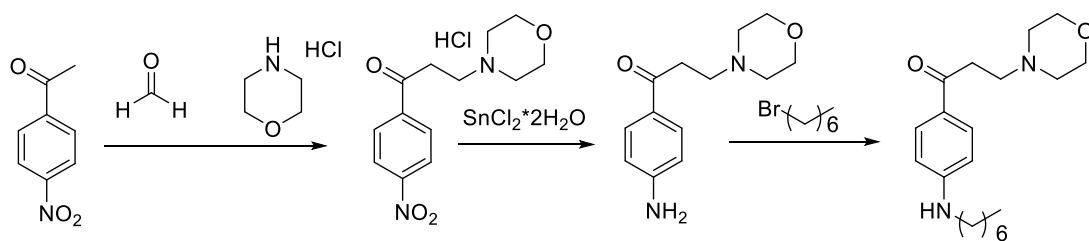
¹HNMR (300MHz, CDCl₃): δ: 7.92 (2H, dt, J₁=8.9Hz, J₂=2.0Hz), 6.94 (2H, dt, J₁=9.1Hz, J₂=2.1Hz), 6.89 (2H, dd, J₁=8.8Hz, J₂=2.2Hz), 6.72 (2H, dt J₁=8.8 Hz, J₂=2.2Hz), 3.86 (4H, m), 3.40 (2H, m), 3.07 (2H, m), 2.74 (4H, m).

HRMS (ESI): calcd. (M+H)⁺ 327.1703, exper. 327.1720.

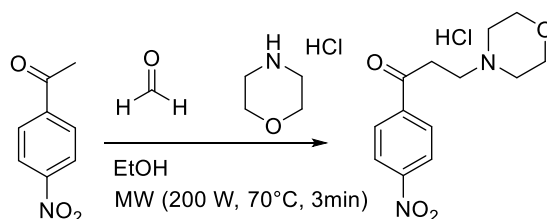
HPLC-UV: 92% purity (area at 254nm).

Yield: 77%

5.4.1.3 Synthetic scheme of the third class of Fingolimod analogues



Synthesis of the 3-morpholino-1-(4-nitrophenyl)propan-1-one

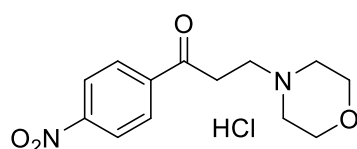


In a glass vial for microwave 4-nitroacetophenone (3.3 g, 20 mmol), paraformaldehyde (0.9 g, 30 mmol) and morpholine chlorohydrate (3.71 g, 30 mmol) have been suspended in 10 mL of EtOH. The reaction mixture has been reacted in microwave at 70 °C for 3 minutes at 200 W of power. This cycle has been repeated another time. To the obtained crude of reaction, 10 mL of acetone have been added and the mixture has been cooled in ice bath for three hours. The formed precipitate has been filtered of under vacuum obtaining 11.7 mmol of the desired intermediate.

Yield: 60%

Characterisation:

Compound 1: 3-morpholino-1-(4-nitrophenyl)propan-1-one

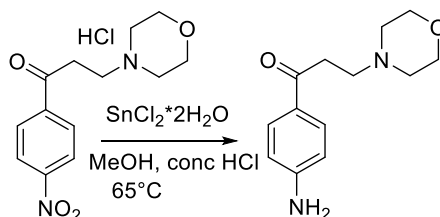


Chemical Formula: $C_{13}H_{17}ClN_2O_4$
Molecular Weight: 300,7390

^1H NMR (300MHz, DMSO): δ : 8.39 (d, 2H, $J=8.9$ Hz), 8.23 (d, 2H, $J = 8.9\text{Hz}$), 3.97 (bs, 2H), 3.81 (bs, 2H), 3.79 – 3.71 (m, 6H), 3.08 (bs, 2H).

Yield: 60%

Synthesis of the 1-(4-aminophenyl)-3-morpholinopropan-1-one

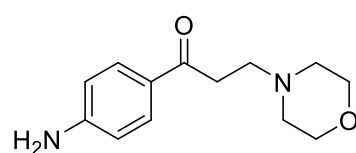


In a round bottom flask solubilize the previous synthon (1.27 g, 4.13 mmol) in 12 mL of MeOH. In another flask a fresh solution of $\text{SnCl}_2 \cdot 2\text{H}_2\text{O}$ (2.26 g, 10.0 mmol) in concentrated HCl (5 mL) has been prepared. This last solution has been added dropwise in the first one and the mixture has been heated up at reflux for 1 hour. The mixture has been cooled down to room temperature and 22 mL of H_2O have been added. The solution has been cooled in an ice bath and 20 mL of an aqueous solution of KOH 8M have been added portion wise. Finally, the pH has been adjusted to pH 9 and the aqueous phase has been extracted with three portions of EtOAc. The organic phase has been dried over MgSO_4 and the organic solvent has been removed under reduced pressure obtaining the desired final compound.

Yield: 99%

Characterisation:

Compound 2: 1-(4-aminophenyl)-3-morpholinopropan-1-one



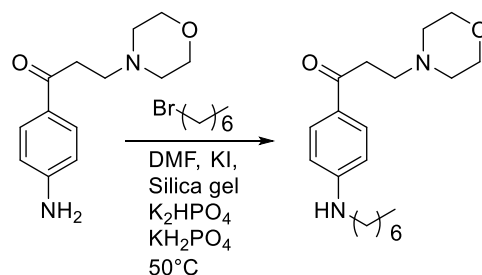
Chemical Formula: $\text{C}_{13}\text{H}_{18}\text{N}_2\text{O}_2$

Molecular Weight: 234,2990

^1H NMR (300MHz, CDCl_3): δ : 7.82 (d, 2H, $J=8.5$ Hz), 6.65 (d, 2H, $J = 8.5\text{Hz}$), 4.12 (bs, 2H), 3.74 (m, 4H), 3.12 (m, 2H), 2.86 (m, 2H), 2.55 (m, 4H).

Yield: 99%

Synthesis of the final compounds belonging to the third class of Fingolimod analogues

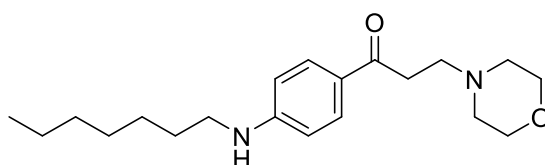


In a round bottom flask compound 2 (0.117 g, 0.5 mmol), 1-bromohexane (140 μL , 1.0 mmol), KI (0.166 mg, 1.0 mmol), KH_2PO_4 (0.068 g, 0.5 mmol), K_2HPO_4 (0.050 g, 0.25 mmol) and a little spoon of silica gel has been added in a small round bottom flask and suspended in 1 mL of DMF. The mixture has been heated up at 50°C overnight. The reaction has been monitored by TLC (DCM:MeOH, 9:1). After completion of the reaction to the mixture 10 mL of deionised H_2O have been added and the pH has been adjusted to pH 9 with an aqueous solution of NaOH 1M. The aqueous phase has been extracted three times with 10 mL of EtOAc. The combined organic phases have been dried with Na_2SO_4 and concentrated under vacuum obtaining the desired compound. The crude compound has been purified through column chromatography (DCM:MeOH, 99:1 \rightarrow 9:1) obtaining the isolated compound.

Yield: 11%.

Characterisation:

Compound FA-A1: 1-(4-(heptylamino)phenyl)-3-morpholinopropan-1-one



Chemical Formula: $\text{C}_{20}\text{H}_{32}\text{N}_2\text{O}_2$

Molecular Weight: 332,4880

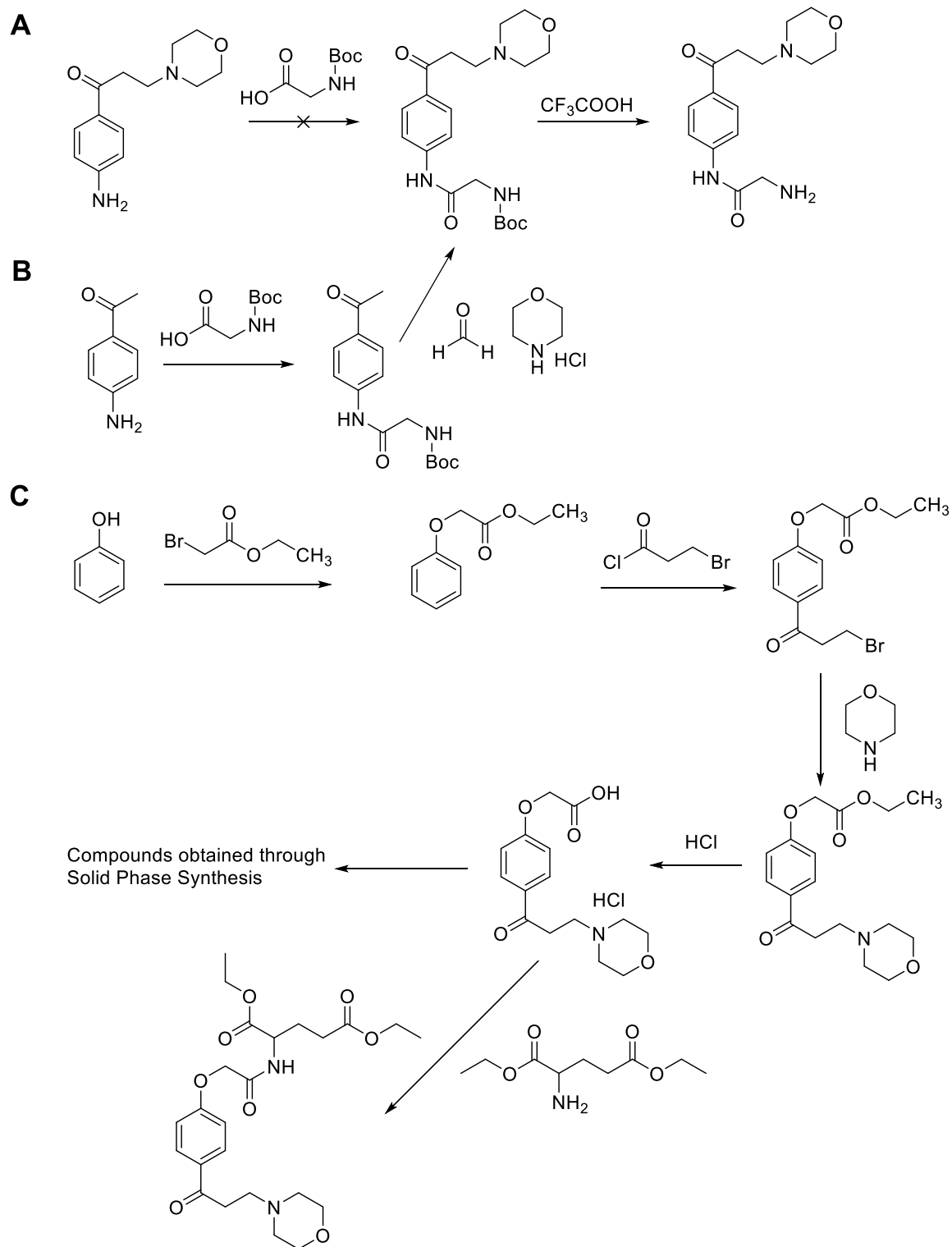
^1H NMR (400 MHz, CDCl_3) δ 7.82 (d, $J = 8.4$ Hz, 2H), 6.54 (d, $J = 8.5$ Hz, 2H), 4.26 (s, 1H), 3.77 – 3.67 (m, 4H), 3.17 (q, $J = 6.0$ Hz, 2H), 3.09 (t, $J = 7.2$ Hz, 2H), 2.84 (t, $J = 7.2$ Hz, 2H), 2.53 (s, 4H), 1.70 – 1.56 (m, 2H), 1.45 – 1.21 (m, 8H), 0.89 (t, $J = 6.5$ Hz, 3H).

HRMS (ESI): calcd. $(\text{M}+\text{H})^+$ 333.2537, exper. 333.2532.

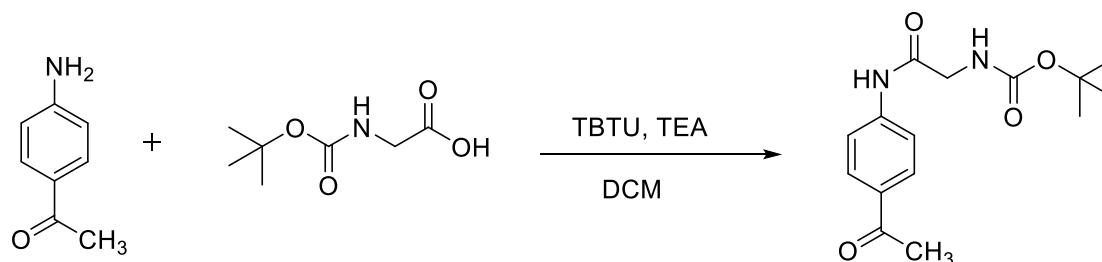
HPLC-UV: 87% purity (area at 254nm).

Yield: 11%

5.4.1.4 Synthetic scheme of the Chimeric compounds ApoE-Fingolimod analogues



Synthesis of the tert-butyl (2-((4-acetylphenyl)amino)-2-oxoethyl)carbamate

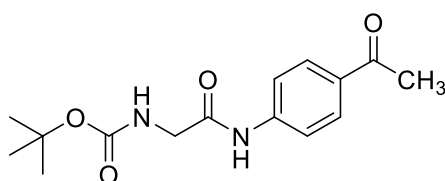


In a round bottom flask, Boc-Glycine (1.575 g, 9 mmol), TEA (1,670 mL, 12 mmol), TBTU (2.5 g, 7.80 mmol) and 4'-aminoacetophenone (0.810 g, 6 mmol) have been suspended in 9 mL of DCM. The mixture has been left at room temperature under magnetic stirring overnight. The reaction has been monitored through TLC using as eluting mixture (DCM:MeOH, 95:5). After completion of the reaction, other 20 mL of DCM were added and the organic phase has been washed two times with deionized water (20 mL), 10 mL of a saturated aqueous solution of NH_4Cl and with 10 mL of a saturated aqueous solution of NaHCO_3 . The organic phase has been dried with Na_2SO_4 , filtered and the organic solvent has been evaporated under reduced pressure obtaining the final desired compound (1.74 g, 5.95 mmol).

Yield: 99%

Characterisation:

Compound 1: tert-butyl(2-((4-acetylphenyl)amino)-2-oxoethyl)carbamate

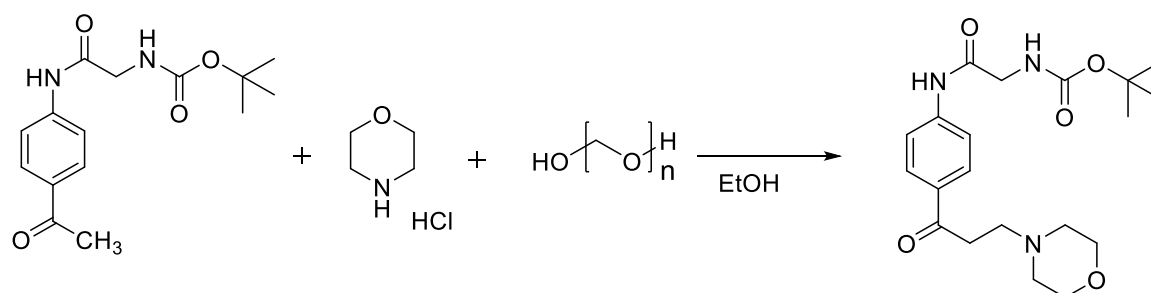


Chemical Formula: $\text{C}_{15}\text{H}_{20}\text{N}_2\text{O}_4$
Molecular Weight: 292,3350

^1H NMR (400 MHz, MeOD) δ 7.98 – 7.89 (m, 2H), 7.71 – 7.69 (m, 2H), 3.9 (s, 2H), 2.55 (s, 3 H), 1.45 (s, 9H).

Yield: 99%

Synthesis of the tert-butyl (2-((4-(3-morpholinopropanoyl)phenyl)amino)-2-oxoethyl)carbamate



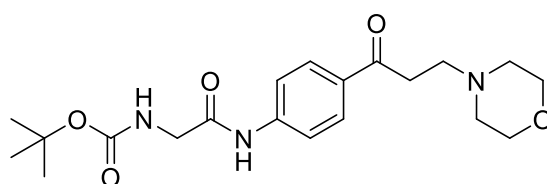
Compound 1 (1.155 g, 3.91 mmol), paraformaldehyde (0.355 g, 11.75 mmol), morpholine hydrochloride (1.455 g, 11.75 mmol) have been suspended in 2 mL of EtOH in a small round bottom flask. Under magnetic stirring the reaction has been heated up at 80 °C for 5 hours. The progression of the reaction has been monitored with TLC (n-hexane:EtOAc, 6:4). After completion of the reaction the reaction has been diluted with 20 mL of an aqueous solution of HCl 0.6 M and extracted twice with 20 mL of EtOAc. The aqueous solution has been basified with a saturated aqueous solution of NaHCO₃ till pH 8 and then extracted three times with 20 mL of EtOAc. The combined organic fractions have been thoroughly washed with an aqueous solution of NaHCO₃. The organic phase has been dried over Na₂SO₄ and the organic solvent has been evaporated off under reduced pressure obtaining compound 2 (0.886 g, 2.26 mmol).

The compound is not pure but it has been utilised directly in the following synthetic step.

Yield: 58%

Characterisation:

Compound 2: tert-butyl (2-((4-(3-morpholinopropanoyl)phenyl)amino)-2-oxoethyl)carbamate

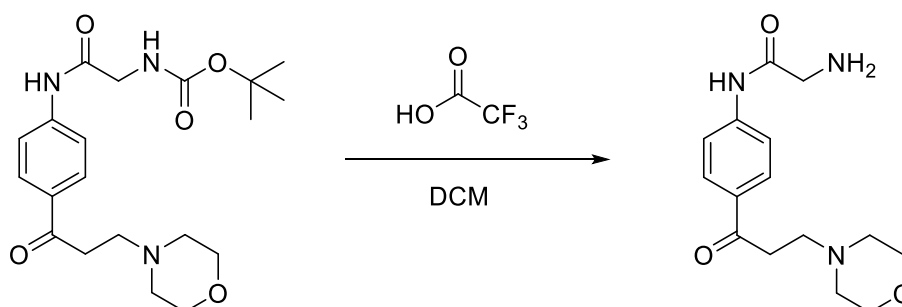


Chemical Formula: C₂₀H₂₉N₃O₅
Molecular Weight: 391,4680

¹H NMR (300 MHz, CDCl₃) δ 7.89 (d, *J* = 8.7 Hz, 2H), 7.61 (d, *J* = 8.7 Hz, 2H), 5.51 (s all, 1H), 3.95 (d, *J* = 5.9 Hz, 2H), 3.71 (m, 4H), 3.46 (s all, 1H), 3.16 (t, *J* = 7.3 Hz, 2H), 2.85 (t, *J* = 7.3 Hz, 2H), 2.55 (m, 4H), 1.45 (s, 9H).

Yield: 58%

Synthesis of the 2-amino-N-(4-(3-morpholinopropanoyl)phenyl)acetamide

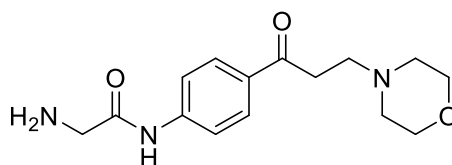


In a round bottom flask the following compounds have been added with the reported sequence: compound 2 (1.038 g, 2.65 mmol), DCM (3 mL) and TFA (3 mL, 39.20 mmol). The mixture has been left under magnetic stirring at room temperature for 3 hours. The reaction has been monitored with TLC (n-hexane/EtOAc/TEA 1.9:8:0.1). After completion of the reaction the organic solvent has been evaporated under nitrogen flux and the obtained residue has been suspended in Et₂O (10 mL) leading to the obtainment of a precipitate that was not stable at air. The precipitate and the organic phase have been combined and the solvent has been removed under reduced pressure. The viscous solid obtained after this procedure has been suspended in 40 mL of a saturated aqueous solution of NaHCO₃ and extracted three times with 40 mL of EtOAc. The combined organic fractions have been concentrated at dryness under reduced pressure and the crude compound has been purified by column chromatography on silica gel using as eluting system (DCM/MeOH/TEA 96:3.8:0.2). The final compound has been isolated as a viscous liquid and it is highly instable if exposed to the air.

Yield: 54%

Characterisation:

Compound AEFA-01: 2-amino-N-(4-(3-morpholinopropanoyl)phenyl)acetamide



Chemical Formula: C₁₅H₂₁N₃O₃

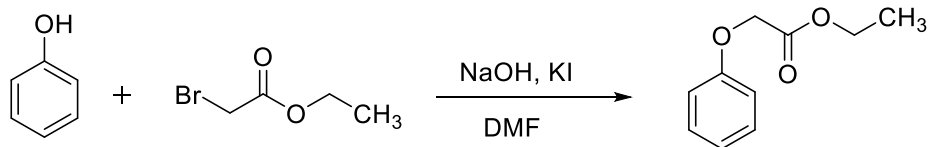
Molecular Weight: 291,3510

¹H NMR (400 MHz, MeOD) δ 8.03 – 7.96 (m, 2H), 7.74 (m, 2H), 3.95 (s, 2H), 3.86 - 3.77 (m, 2H), 3.59 (d, *J* = 6.9 Hz, 4H), 3.29 – 3.16 (m, 2H), 2.80 (s, 4H).

HRMS (ESI): calcd. (M+H)⁺ 292.1656, exper. 292.1670.

Yield: 54%

Synthesis of the ethyl 2-phenoxyacetate



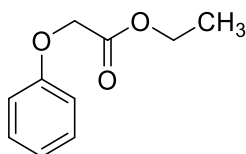
In a round bottom flask phenol (1.176 g, 12.50 mmol), NaOH (500 mg, 12.50 mmol), KI (1.660 g, 10 mmol), DMF (12 mL) and ethyl bromoacetate (1.110 mL, 10 mmol) have been added. The mixture has been heated at 80°C and left under magnetic stirring at this temperature for 5 hours monitoring its progression through TLC (n-hexane/EtOAc 8:2).

After cooling at room temperature, the reaction mixture has been diluted with 50 mL of EtOAc. The organic phase has been washed thoroughly with an aqueous solution of NaOH 2M. The organic phase has been dried over Na₂SO₄ and the organic solvent has been evaporated off under reduced pressure obtaining the desired compound as a colourless oil (1.660, 9.2 mmol).

Yield: 92%

Characterisation:

Compound 3: ethyl 2-phenoxyacetate

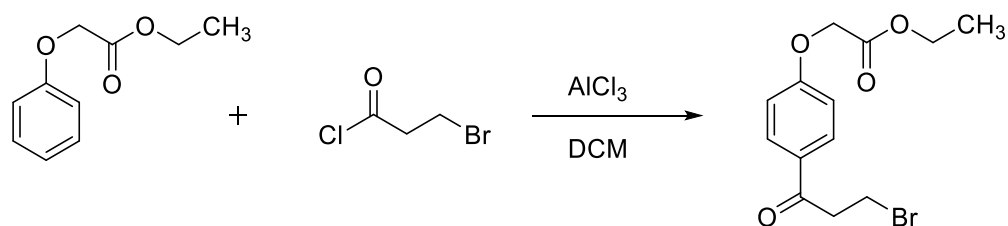


Chemical Formula: C₁₀H₁₂O₃
Molecular Weight: 180,2030

¹H NMR (300 MHz, CDCl₃) δ 7.31 – 7.20 (m, 2H), 7.01 – 6.84 (m, 3H), 4.61 – 4.54 (m, 2H), 4.29 – 4.16 (m, 2H), 1.32 – 1.19 (m, 3H).

Yield: 92%

Synthesis of the ethyl 2-(4-(3-bromopropanoyl)phenoxy)acetate

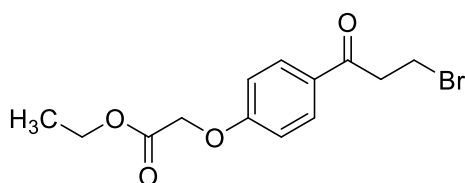


To a solution of compound 3 (1.660 g, 9.20 mmol) and DCM (10 mL), under magnetic stirring, a mixture of AlCl_3 (3.730 g, 28 mmol), DCM (20 mL) and 3-bromopropionyl chloride (2.8 mL, 28mmol) has been added dropwise. The reaction mixture has been left at room temperature for 6 hours and the progression of the reaction has been monitored by TLC (n-hexane/ EtOAc 8:2). After completion of the reaction, to the mixture ice and an aqueous solution of HCl 0.2 M (50 mL) has been added. The aqueous phase has been extracted twice with DCM (40 mL). The combined organic fractions have been thoroughly washed with an aqueous solution of NaHCO_3 (3 x 50 mL). The organic phase has been dried over Na_2SO_4 , and after that the solvent has been removed under reduced pressure obtaining the desired compound as a viscous oil (2.850 g, 9 mmol).

Yield: 98%

Characterisation:

Compound 4: ethyl 2-(4-(3-bromopropanoyl)phenoxy)acetate

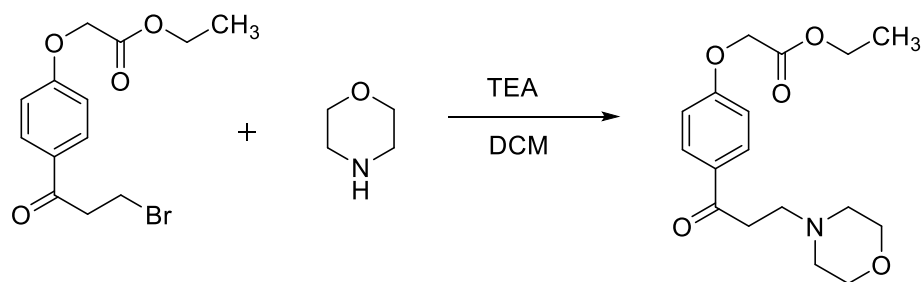


Chemical Formula: $\text{C}_{13}\text{H}_{15}\text{BrO}_4$
Molecular Weight: 315,1630

^1H NMR (300 MHz, CDCl_3) δ 8.02 – 7.94 (m, 2H), 7.04 – 6.95 (m, 2H), 4.69 (s, 2H), 4.38 – 4.21 (m, 2H), 3.65 – 3.47 (m, 4H), 1.40 – 1.27 (m, 3H).

Yield: 98%

Synthesis of the ethyl 2-(4-(3-morpholinopropanoyl)phenoxy)acetate

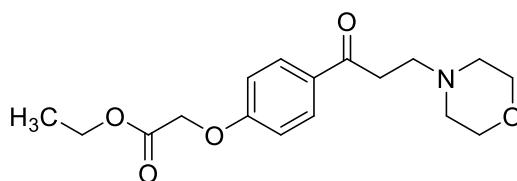


In a round bottom flask following the reported order, these reactants have been added: compound 4 (2.850 g, 9 mmol), DCM (15mL), TEA (1.250 mL, 9 mmol) and morpholine (2.2 mL, 25.20mmol). The mixture has reacted at room temperature and under magnetic stirring overnight. The progression of the reaction has been controlled through TLC (n-hexane:EtOAc, 5:5). After completion of the reaction, the organic solvent has been evaporated under reduced pressure and the obtained residue has been dissolved in 70 mL of EtOAc. The organic phase has been thoroughly washed with a saturated aqueous solution of NaHCO₃. The organic phase has been dried over Na₂SO₄ and the solvent has been removed after evaporation under reduced pressure, obtaining the desired final compound (2 g, 6.22 mmol).

Yield: 69%

Characterisation:

Compound 5: ethyl 2-(4-(3-morpholinopropanoyl)phenoxy)acetate

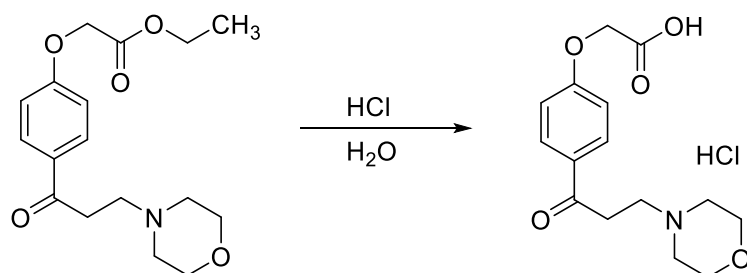


Chemical Formula: C₁₇H₂₃NO₅
Molecular Weight: 321,3730

¹H NMR (300 MHz, CDCl₃) δ 7.99 – 7.92 (m, 2H), 6.99 – 6.91 (m, 2H), 4.69 (s, 2H), 4.34 – 4.23 (m, 2H), 3.72 (dd, *J* = 6.5, 2.9Hz, 4H), 3.19 – 3.10 (t, *J* = 7.1, 2H), 2.87 – 2.78 (t, *J* = 7.1, 2H), 2.57 – 2.48 (m, 4H), 1.35 – 1.22 (m, 3H).

Yield: 69%

Synthesis of the 2-(4-(3-morpholinopropanoyl)phenoxy)acetic acid

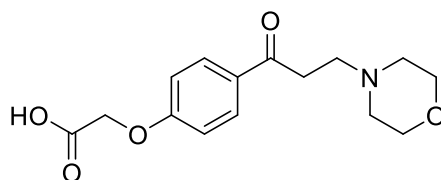


In a round bottom flask compound **5** (2.0 g, 6.22 mmol) has been dissolved in 10 mL of deionised water. 5 mL of concentrated HCl have been dropwise under magnetic stirring within the previous solution. The obtained mixture has been heated up at 100 °C for 2 hours. The reaction has been monitored through TLC (DCM/MeOH 9:1) and after the end of the reaction, the mixture has been cooled at room temperature. The solvent has been removed first under nitrogen flux and then under reduced pressure. The viscous residue obtained has been suspended in 10 mL of cold Et₂O obtaining a precipitate that has been filtered of under vacuum. The solid residue is the desired compound as HCl salt (1.6 g, 4.85 mmol).

Yield: 78%

Characterisation:

Compound AEFA-02: 2-(4-(3-morpholinopropanoyl)phenoxy)acetic acid



Chemical Formula: C₁₅H₁₉NO₅

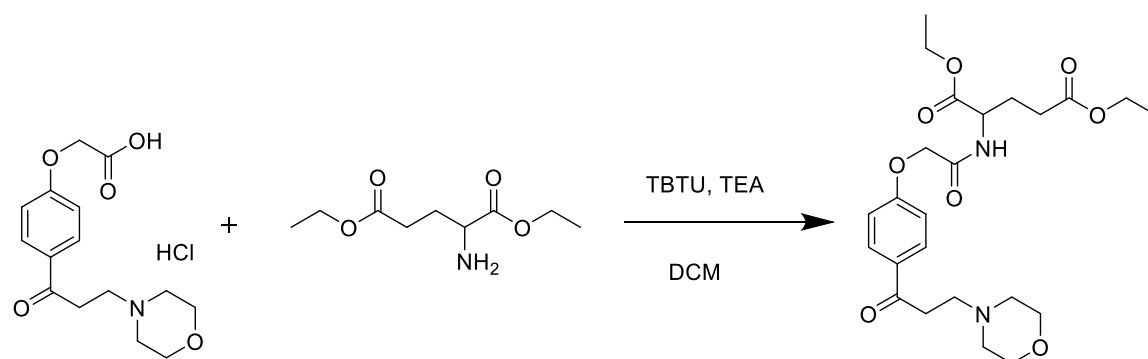
Molecular Weight: 293,3190

¹H NMR (300 MHz, CDCl₃) δ 11.19 (s, 1H), 7.98 – 7.90 (m, 2H), 6.98 – 6.90 (m, 2H), 4.68 (s, 2H), 3.71 (dd, *J* = 6.5, 2.9 Hz, 4H), 3.19 – 3.10 (t, *J* = 7.1, 2H), 2.87 – 2.78 (t, *J* = 7.1, 2H), 2.56 – 2.46 (m, 4H).

HRMS (ESI): calcd. (M+H)⁺ 294.1336, exper. 294.1351.

Yield: 78%

Synthesis of the diethyl (2-(4-(3-morpholinopropanoyl)phenoxy)acetyl)glutamate

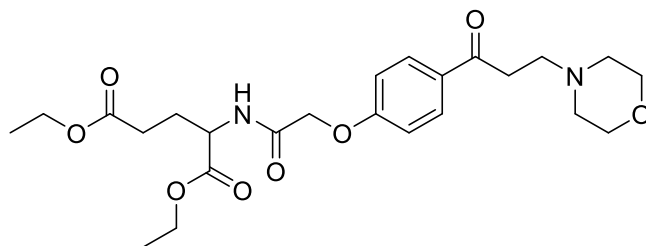


In a round bottom flask AEFA-02 (80 mg, 0.24 mmol), DCM (1 mL), TEA (68 μ L, 0.48 mmol), TBTU (78 mg, 0.24 mmol) and the L-glutamic acid diethyl ester (58 mg, 0.24 mmol) have been mixed together and left to react at room temperature for 5 hours. The progression of the reaction has been monitored through TLC using as eluting mixture (DCM:MeOH, 9:1). After completion, reaction has been dried and the solvent has been removed under nitrogen steam. The crude product has been directly purified through column chromatography on silica gel using as eluting agent a mixture of DCM and MeOH in a ratio of 95 to 5 respectively. This led to the obtainment of the final compound as a white solid (38 mg, 0.08 mmol).

Yield: 35%

Characterisation:

Compound AEFA-03: diethyl (2-(4-(3-morpholinopropanoyl)phenoxy)acetyl)glutamate



Chemical Formula: C₂₄H₃₄N₂O₈

Molecular Weight: 478,5420

¹H NMR (400 MHz, CDCl₃) δ 7.96 (d, *J* = 9.0 Hz, 2H), 7.04 – 6.98 (m, 2H), 4.67 (m, 1H), 4.56 (s, 2H), 4.24 – 4.17 (m, 2H), 4.10 (q, *J* = 7.1 Hz, 2H), 3.75 – 3.67 (m, 4H), 3.13 (t, *J* = 7.3 Hz, 2H), 2.82 (dd, *J* = 7.9, 6.8 Hz, 2H), 2.54 – 2.47 (m, 4H), 2.45 – 2.18 (m, 4H), 1.25 (dt, *J* = 20.5, 7.1 Hz, 6H).

HRMS (ESI): calcd. (M+H)⁺ 479.2388, exper. 479.2395.

HPLC-UV: 97% purity (area at 254nm).

The pump program has been the following one:

Time (mins)	Phase A%	Phase B%
0	99	1
6	99	1
12	50	50
15	50	50
16	90	10

Yield: 35%

Synthesis of the last 6 final compounds obtained through solid phase peptide synthesis

The solid phase peptide synthesis has been performed manually following the procedure herein illustrated:

PREPARATION AND SWELLING OF THE RESIN

1. 250 mg of a Fmoc-Gly-Wang resin (extent of labelling: 0.4-0.8 mmol/g loading) have been introduced in an adequate plastic support and it has been wetted with 2 mL of DCM. The resin has been gently shaken for 15 minutes for allowing its swelling. After that the solvent has been removed through filtration.
2. 1.5 mL of DMF have been added to the resin, that has been gently shaken for 1 minute and then the solvent has been removed (washing of the resin).

REMOVAL OF THE AMINO PROTECTING GROUP FROM THE LAST AMINO ACID OF THE PEPTIDE CHAIN

3. 1.5 mL of a solution of piperidine at 20% in DMF has been added to the resin. The suspension has been gently shaken for 1 minute and then the deprotecting agent has been removed.
4. Other 1.5 mL of the previous basic solution have been added to the resin. After 10 minutes of shaking the solvent has been removed.

WASHING OF THE RESIN

5. 2 mL of DMF have been added to the resin. The suspension has been shaken for 1 minute and then the solvent has been removed. This operation has been repeated other 5 times.

ACTIVATION OF THE CARBOXYLIC FUNCTION OF THE NEW AMINO ACID

6. In a glass tube the desired amino acid has been added together with TBTU (280 mg), DMF (1.5 mL) and DIPEA (260 μ L) and the mixture has been left to activate the carboxylic acid for 1 minute.

COUPLING OF THE ACTIVATED RESIDUE ON THE RESIN

7. The solution contained in the glass tube has been added to the resin and the suspension has been gently shaken for 30 minutes. Finally, the excess of the reagents has been removed through filtration.

WASHING OF THE RESIN

8. 2 mL of DMF have been added to the resin. The suspension has been shaken for 1 minute and then the solvent has been removed. This operation has been repeated other 5 times.

ELONGATION OF THE PEPTIDE CHAIN

All the procedures from 3 to 8 has to be repeated for every single amino acid that has to be introduced in the final peptide sequence, including also AEFA-02 that has been used as terminating agent.

WASHING OF THE RESIN WITH DCM

9. 2 mL of DCM have been added to the resin. The suspension has been shaken for 1 minute and then the solvent has been removed. This operation has been repeated other 5 times.

DRYING THE RESIN

10. The resin has been dried using a nitrogen flux.

REMOVAL OF THE PEPTIDE FROM THE RESIN AND REMOVAL OF ALL THE PROTECTING GROUP PRESENT ON THE SIDE CHAINS OF THE USED AMINO ACIDS

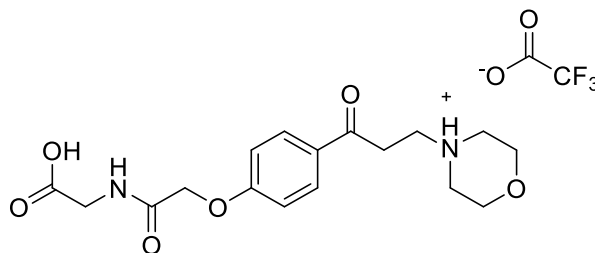
11. 2 mL of TFA/H₂O (98:2) has been added to the resin. The suspension has been gently shaken for 3 hours.
12. The resin has been removed through filtration and the filtrate has been added dropwise to 20 mL of cold Et₂O obtaining a white precipitate.
13. After 30 minutes the precipitate has been centrifuged (60000 rpm for 5 minutes).
14. The supernatant has been accurately removed and the precipitate has been washed with other 10 mL of cold Et₂O. The suspension has been centrifuged (60000 rpm for 5 minutes).
15. The supernatant has been removed and the precipitate has been completely dried under nitrogen flux obtaining the desired compounds.

CHARACTERIZATION OF THE FINAL COMPOUNDS

The final compounds have been analyzed through HPLC and HRMS for determining their identity and purity.

Characterisation:

Compound AEFA-04: 4-(3-(4-(2-((carboxymethyl)amino)-2-oxoethoxy)phenyl)-3-oxopropyl)morpholin-4-ium 2,2,2-trifluoroacetate



Chemical Formula: C₁₉H₂₃F₃N₂O₈

Molecular Weight: 464,3942

SYNTHESIS:

- 250 mg of Fmoc-Gly-Wang resin;
- 247 mg of AEFA-02.

CHARACTERISATION:

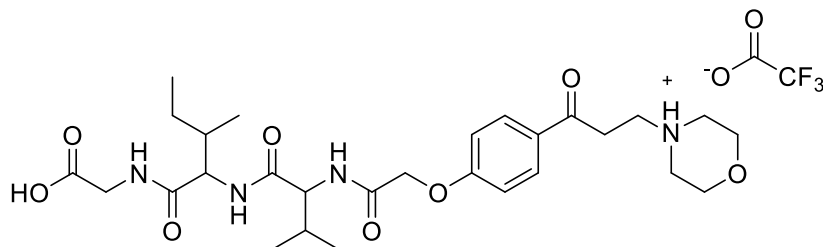
¹H NMR (300 MHz, MeOD) δ 8.09 – 8.02 (d, *J* = 9.0, 2H), 7.14 (d, *J* = 9.0 Hz, 2H), 4.89 (m, 8H), 4.69 (s, 2H), 4.01 (m, 2H), 3.59 (t, *J* = 3.1 Hz, 4H).

HRMS (ESI): calcd. (M+H)⁺ 351.1551, exper. 351.1549.

HPLC-UV: 95% purity (area at 254nm).

Yield: 60%

Compound **AEFA-05**: 4-(3-(4-(2-((1-((1-((carboxymethyl)amino)-3-methyl-1-oxopentan-2-yl)amino)-3-methyl-1-oxobutan-2-yl)amino)-2-oxoethoxy)phenyl)-3-oxopropyl)morpholin-4-ium 2,2,2-trifluoroacetate



Chemical Formula: $C_{30}H_{43}F_3N_4O_{10}$

Molecular Weight: 676,6872

SYNTHESIS:

- 250 mg of Fmoc-Gly-Wang resin;
- 266 mg of Fmoc-Ile-OH;
- 254 mg of Fmoc-Val-OH;
- 247 mg of AEFA-02.

The final compound has been purified through reverse phase flash chromatography on preloaded C18 cartridges using $(CH_3CN):(H_2O + 0.1\% TFA)$ as eluting solvents and adopting the following gradient:

Time (mins)	CH ₃ CN (%)	H ₂ O + 0.1% TFA (%)
0	0	100
10	0	100
20	50	50
22	50	50

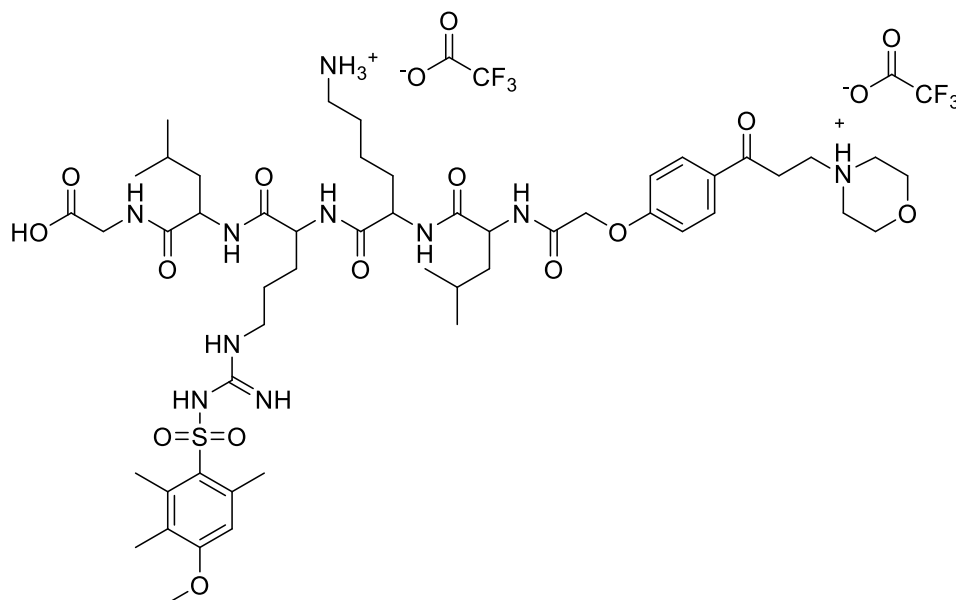
CHARACTERISATION:

HRMS (ESI): calcd. $(M+H)^+$ 562.2992, exper. 562.2303.

HPLC-UV: 99% purity (area at 254nm).

Yield: 24%

Compound AEFA-06: 4-(3-(4-((10-(4-ammonioethyl)-1-carboxy-4,13-diisobutyl-7-(3-(3-((4-methoxy-2,3,6-trimethylphenyl)sulfonyl)guanidino)propyl)-3,6,9,12,15-pentaoxo-2,5,8,11,14-pentaazahexadecan-16-yl)oxy)phenyl)-3-oxopropyl)morpholin-4-ium 2,2,2-trifluoroacetate



Chemical Formula: $C_{55}H_{82}F_6N_{10}O_{17}S$

Molecular Weight: 1301,3644

SYNTHESIS:

- 250 mg of Fmoc-Gly-Wang resin;
- 266 mg of Fmoc-Leu-OH;
- 480 mg of Fmoc-Arg(Mtr)-OH;
- 352 mg of Fmoc-Lys(Boc)-OH;
- 266 mg of Fmoc-Leu-OH;
- 247 mg of AEFA-02.

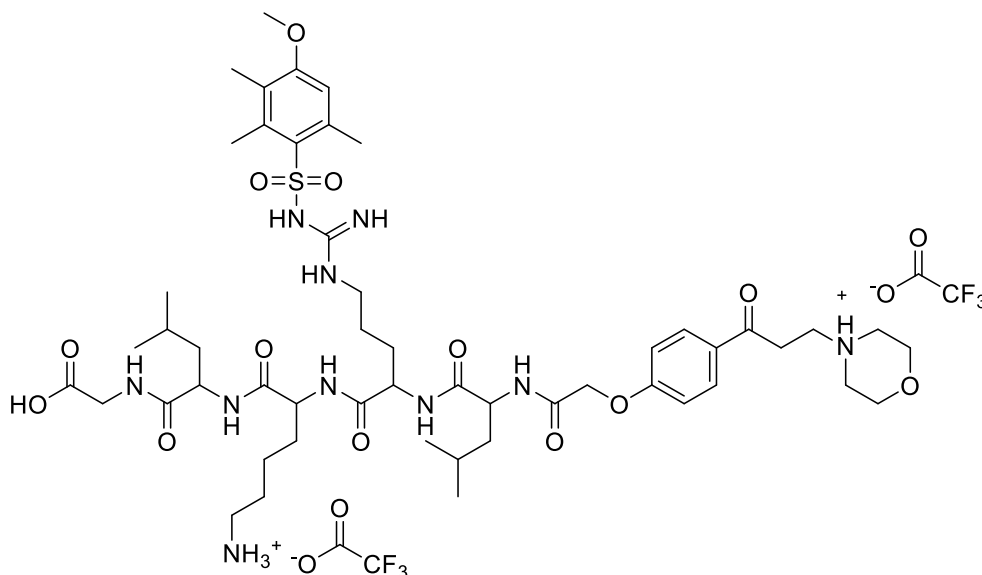
CHARACTERISATION:

HRMS (ESI): calcd. (M+H)⁺ 1073.5700, exper. 1073.5689. calcd. (M+2H)²⁺ 537.2887, exper. 537.2890.

HPLC-UV: 84% purity (area at 254nm).

Yield: 24%

Compound AEFA-07: 4-(3-(4-((7-(4-ammoniobutyl)-1-carboxy-4,13-diisobutyl-10-(3-(3-((4-methoxy-2,3,6-trimethylphenyl)sulfonyl)guanidino)propyl)-3,6,9,12,15-pentaoxo-2,5,8,11,14-pentaazahexadecan-16-yl)oxy)phenyl)-3-oxopropyl)morpholin-4-ium 2,2,2-trifluoroacetate



Chemical Formula: $C_{55}H_{82}F_6N_{10}O_{17}S$
Molecular Weight: 1301,3644

SYNTHESIS:

- 250 mg of Fmoc-Gly-Wang resin;
- 266 mg of Fmoc-Leu-OH;
- 352 mg of Fmoc-Lys(Boc)-OH;
- 480 mg of Fmoc-Arg(Mtr)-OH;
- 266 mg of Fmoc-Leu-OH;
- 247 mg of AEFA-02.

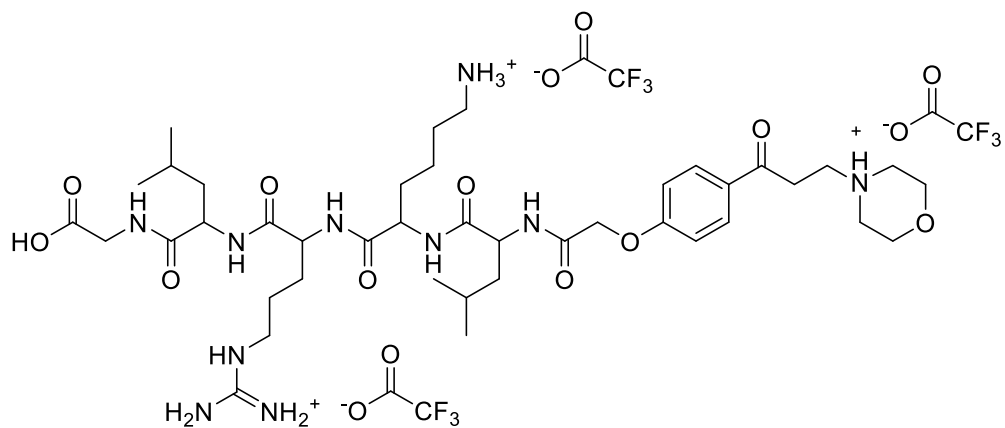
CHARACTERISATION:

HRMS (ESI): calcd. $(M+H)^+$ 1073.5700, exper. 1073.5689. calcd. $(M+2H)^{2+}$ 537.2887, exper. 537.2890.

HPLC-UV: 85% purity (area at 254nm).

Yield: 45%

Compound **AEFA-08**: 4-(3-(4-((7-(3-((amino(iminio)methyl)amino)propyl)-10-(4-ammoniobutyl)-1-carboxy-4,13-diisobutyl-3,6,9,12,15-pentaoxo-2,5,8,11,14-pentaazahexadecan-16-yl)oxy)phenyl)-3-oxopropyl)morpholin-4-ium 2,2,2-trifluoroacetate



Chemical Formula: $C_{47}H_{71}F_9N_{10}O_{16}$

Molecular Weight: 1203,1246

SYNTHESIS:

- 250 mg of Fmoc-Gly-Wang resin;
- 266 mg of Fmoc-Leu-OH;
- 480 mg of Fmoc-Arg(Mtr)-OH;
- 352 mg of Fmoc-Lys(Boc)-OH;
- 266 mg of Fmoc-Leu-OH;
- 247 mg of AEFA-02.

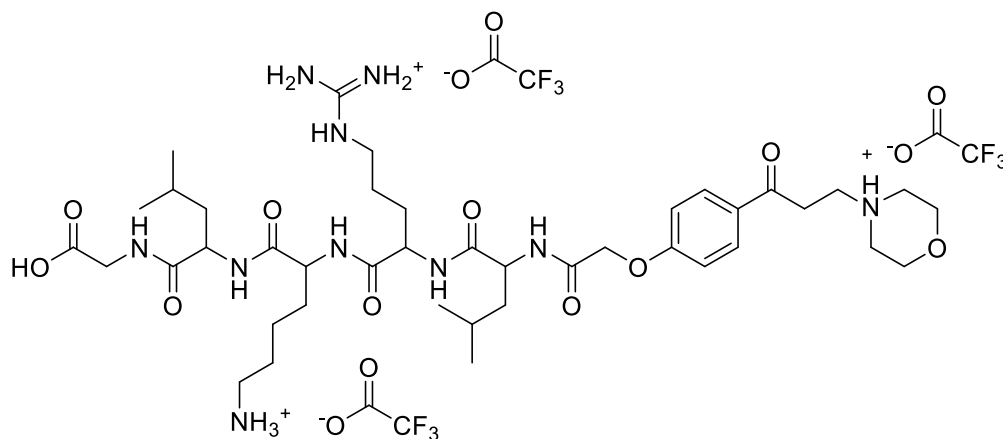
CHARACTERISATION:

HRMS (ESI): calcd. (M+H)⁺ 860.5109, exper. 860.5116. calcd. (M+2H)²⁺ 430.7591, exper. 430.7596.

HPLC-UV: 90% purity (area at 254nm).

Yield: 41%

Compound AEFA-09: 4-(3-(4-((10-(3-((amino(iminio)methyl)amino)propyl)-7-(4-ammoniobutyl)-1-carboxy-4,13-diisobutyl-3,6,9,12,15-pentaoxo-2,5,8,11,14-pentaazahexadecan-16-yl)oxy)phenyl)-3-oxopropyl)morpholin-4-ium 2,2,2-trifluoroacetate



Chemical Formula: $C_{47}H_{71}F_9N_{10}O_{16}$

Molecular Weight: 1203,1246

SYNTHESIS:

- 250 mg of Fmoc-Gly-Wang resin;
- 266 mg of Fmoc-Leu-OH;
- 352 mg of Fmoc-Lys(Boc)-OH;
- 480 mg of Fmoc-Arg(Mtr)-OH;
- 266 mg of Fmoc-Leu-OH;
- 247 mg of AEFA-02.

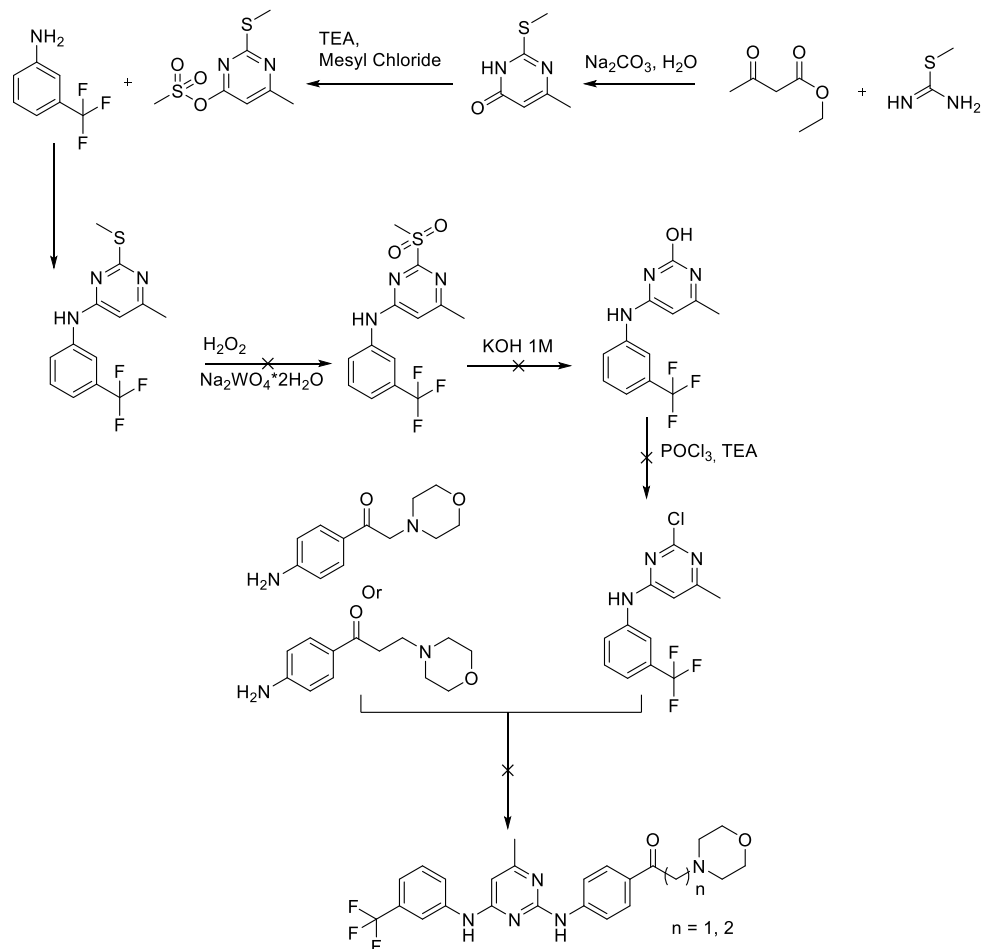
CHARACTERISATION:

HRMS (ESI): calcd. (M+H)⁺ 860.5109, exper. 860.5116. calcd. (M+2H)²⁺ 430.7591, exper. 430.7596.

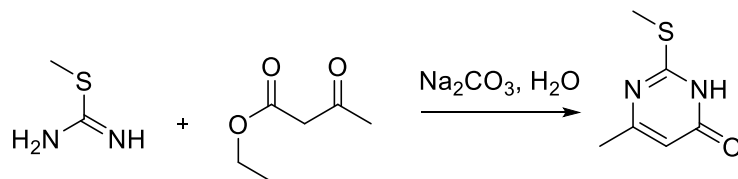
HPLC-UV: 90% purity (area at 254nm).

Yield: 44%

5.4.1.5 Synthetic scheme of the Chimeric compounds TGI1002-CC11



Synthesis of the 6-methyl-2-(methylthio)pyrimidin-4(3H)-one

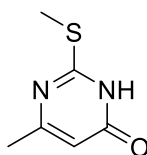


In a round bottom flask KOH (2.24 g, 40.0 mmol) has been dissolved in 15.0 mL of EtOH. In the same flask S-methylisothiourea (2.784 g, 10.0 mmol) and ethyl acetoacetate (2.53 mL, 20.0 mmol) have been added. The mixture has been heated at reflux for 3 hours, monitoring the reaction through TLC (DCM:MeOH, 95:5). At the end of the reaction the solvent has been evaporated of under reduced pressure. The crude of the reaction has been dissolved in 10 mL of water and neutralised with acetic acid. The obtained precipitate has been filtered off under vacuum and the solid has been washed with deionised water. The white solid obtained was the desired compound

Yield: 99%

Characterisation:

Compound 1: 6-methyl-2-(methylthio)pyrimidin-4(3H)-one



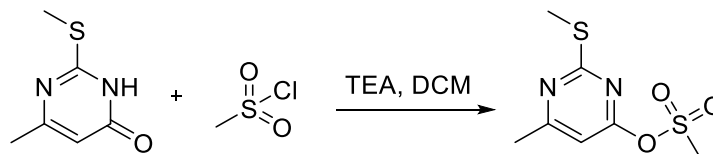
Chemical Formula: C₆H₈N₂OS

Molecular Weight: 156,2030

¹H NMR (400 MHz, DMSO) δ 5.93 (s, 1H), 2.45 (s, 3H), 2.1 (s, 3H)

Yield: 99%

Synthesis of the 6-methyl-2-(methylthio)pyrimidin-4-yl methanesulfonate

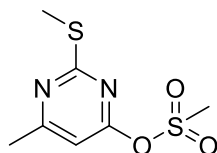


In a round bottom flask, compound 1 (0.156 g, 1.0 mmol) has been dissolved in 2 mL of DCM. To this solution TEA (152 μ L, 1.1 mmol) and mesyl chloride (85 μ L, 1.1 mmol) have been added. The reaction has been left at room temperature overnight. The organic phase has been diluted with other 10 mL of DCM and subsequently washed three times with 20 mL of a saturated aqueous solution of NaHCO₃. The organic phase has been dried over MgSO₄ and the solvent has been evaporated under reduced pressure obtaining the desired final compound.

Yield: 90%

Characterisation:

Compound 2: 6-methyl-2-(methylthio)pyrimidin-4-yl methanesulfonate



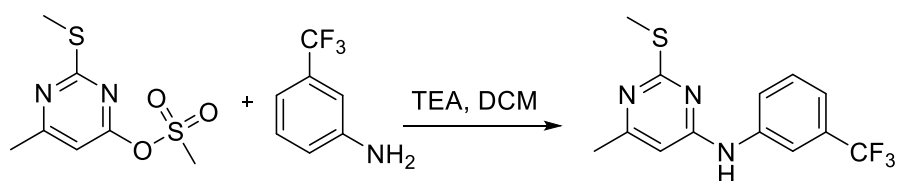
Chemical Formula: C₇H₁₀N₂O₃S₂

Molecular Weight: 234,2880

¹H NMR (400 MHz, DMSO) δ 6.61 (s, 1H), 3.56 (s, 3H), 2.59 (s, 3H), 2.51 (s, 3H)

Yield: 90%

Synthesis of the 6-methyl-2-(methylthio)-N-(3-(trifluoromethyl)phenyl)pyrimidin-4-amine

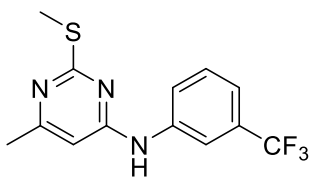


In a round bottom flask compound 2 (0.234 g, 1.0 mmol) and 3-trifluoromethyl aniline (125 μ L, 1.0 mmol) have been dissolved in 3 mL of DCM and 1mmol of TEA. The mixture has been reacted at room temperature for 4 hours. The reaction has been monitored by TLC using as eluting mixture n-hexane:EtOAc (6:4). After completion of the transformation, the organic phase has been diluted with 10 mL of DCM and washed with 10 mL of saturated solution of NaHCO_3 , and then with several washes of deionised water. The organic phase has been dried over Na_2SO_4 and then the solvent has been removed through evaporation at reduced pressure. The solid obtained was the desired compound.

Yield: 99%

Characterisation:

Compound 3: 6-methyl-2-(methylthio)-N-(3-(trifluoromethyl)phenyl)pyrimidin-4-amine

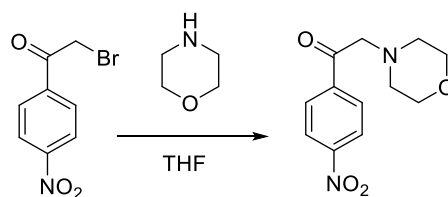


Chemical Formula: $\text{C}_{13}\text{H}_{12}\text{F}_3\text{N}_3\text{S}$
Molecular Weight: 299,3152

^1H NMR (400 MHz, DMSO) δ 10.62 (bs, 1H), 8.34 (s, 1H), 7.79 (d, $J = 8.1$ Hz, 1H), 7.61 (t, $J = 8.1$ Hz, 1H), 7.79 (d, $J = 8.1$ Hz, 1H), 6.51 (s, 1H), 2.55 (s, 3H), 2.34 (s, 3H)

Yield: 90%

Synthesis of the 2-morpholino-1-(4-nitrophenyl)ethan-1-one

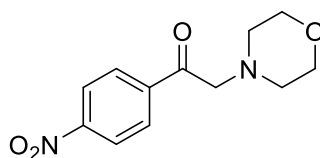


In a round bottom flask 2-bromo-1-(4-nitrophenyl)ethan-1-one (4.15 g, 16.0 mmol) and morpholine (1.41 mL, 19.2 mmol) have been dissolved in 50 mL of THF. 3.1 mL of DIPEA have been added to the reaction and the mixture has been magnetically stirred at room temperature for 3 hours. The solvent has been evaporated under reduced pressure and the solid has been suspended in 20 mL of a saturated solution of NaHCO₃, obtaining an abundant precipitate that was the desired compound.

Yield: 95%

Characterisation:

Compound 4: 2-morpholino-1-(4-nitrophenyl)ethan-1-one



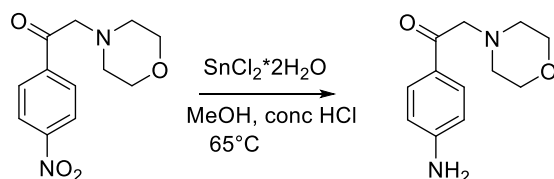
Chemical Formula: C₁₂H₁₄N₂O₄

Molecular Weight: 250,2540

¹HNMR (300MHz, DMSO): δ: 8.39 (d, 2H, J=8.9 Hz), 8.23 (d, 2H, J = 8.9Hz), 3.87 (s, 2H), 3.81 (m, 4H), 2.67 (m, 4H).

Yield: 95%

Synthesis of the 1-(4-aminophenyl)-2-morpholinoethan-1-one

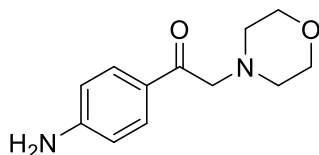


In a round bottom flask solubilize the previous synthon (1.03 g, 4.0 mmol) in 12 mL of MeOH. In another flask a fresh solution of SnCl₂·2H₂O (2.26 g, 10.0 mmol) in concentrated HCl (5 mL) has been prepared. This last solution has been added dropwise in the first one and the mixture has been heated up at reflux for 1 hour. The mixture has been cooled down to room temperature and 22 mL of H₂O have been added. The solution has been cooled in an ice bath and 20 mL of an aqueous solution of KOH 8M have been added portion wise. Finally, the pH has been adjusted to pH 9 and the aqueous phase has been extracted with three portions of EtOAc. The organic phase has been dried over MgSO₄ and the organic solvent has been removed under reduced pressure obtaining the desired final compound.

Yield: 74%

Characterisation:

Compound 5: 1-(4-aminophenyl)-2-morpholinoethan-1-one



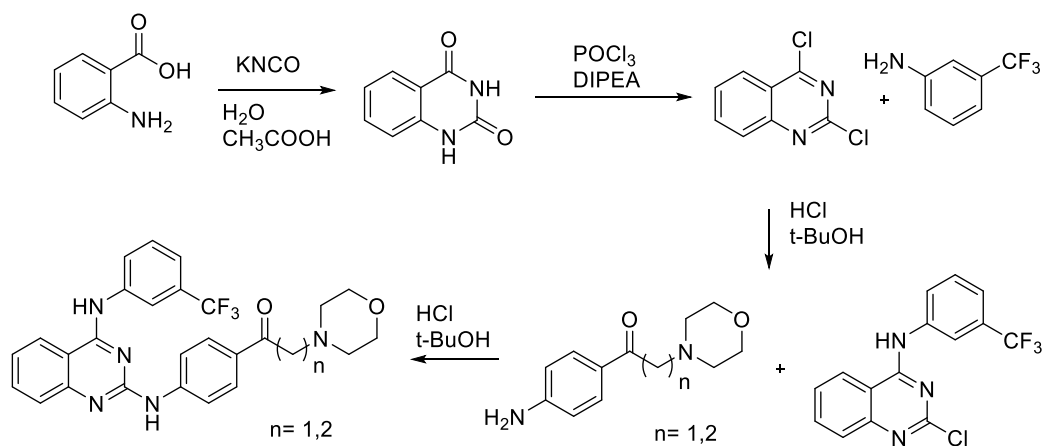
Chemical Formula: C₁₂H₁₆N₂O₂
Molecular Weight: 220,2720

¹HNMR (300MHz, CDCl₃): δ: 7.87 (d, 2H, J=8.5 Hz), 6.65 (d, 2H, J = 8.5Hz), 4.16 (bs, 2H), 3.79 (m, 4H), 3.73 (s, 2H), 2.61 (m, 4H).

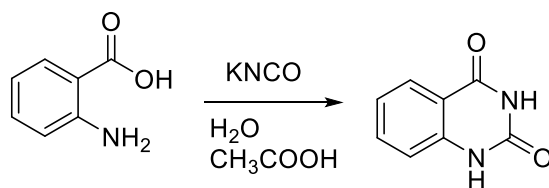
HRMS (ESI): calcd. (M+H)⁺ 221.1285, exper. 221.1341.

Yield: 74%

5.4.1.6 Synthetic scheme of the Chimeric compounds TD-19-CC11



Synthesis of the quinazoline-2,4(1H,3H)-dione

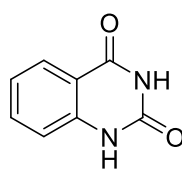


In a round bottom flask anthranilic acid (0.82 g, 6.0 mmol) has been suspended in 36 mL of deionised water. 0.7 mL of acetic acid have been added to the mixture and subsequently the flask has been heated up at 35°C for 15 minutes. After this period, a solution of potassium cyanate (1.21 g, 15.0 mmol) has been added dropwise in the reaction mixture. The reaction has been heated up for further 20 minutes at 35 °C and then it has been cooled down at room temperature. To the mixture 10.0 g of KOH have been added slowly and portion wise under continuous stirring. After the complete addition of the base, the round bottom flask has been cooled down in an ice bath and the pH of the solution has been adjusted to pH 4 with concentrated HCl. The formed precipitate has been filtered of and thoroughly washed with diluted HCl (0.1 M) obtaining the desired compound as a white powder.

Yield: 98%

Characterisation:

Compound 1: quinazoline-2,4(1H,3H)-dione



Chemical Formula: C₈H₆N₂O₂

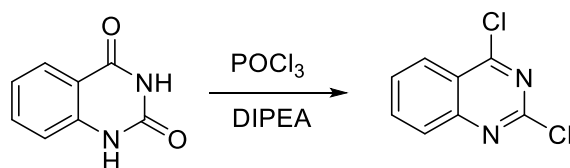
Molecular Weight: 162,1480

¹HNMR (300MHz, CDCl₃): δ: 11.26 (s, 1H), 11.18 (s, 1H), 7.89 (ddd, J₁ = 7.9 Hz, J₂ = 1.6 Hz, J₃ = 0.5 Hz, 1H), 7.64 (td, J₁ = 7.9 Hz, J₂ = 1.6 Hz, 1H), 7.18 (m, 2H).

HRMS (ESI): calcd. (M+H)⁺ 163.0502, exper. 163.0521.

Yield: 98%

Synthesis of the 2,4-dichloroquinazoline

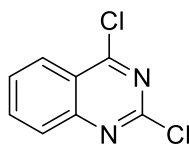


In a round bottom flask compound 1 (0.95 g, 6.0 mmol) 5 mL of POCl₃ and 2.5 mL of DIPEA have been added in the mentioned order cooling during the addition of the last two in ice bath. The mixture has been heated at 110°C for 3 hours and then it has been cooled first at room temperature and then in an ice bath. Subsequently, a mixture of water and ice has been added obtaining the formation of a thick precipitate that has been filtered of and thoroughly washed with fresh water for removing the excess of base and acid. The obtained white solid was the desired compound.

Yield: 98%

Characterisation:

Compound 2: 2,4-dichloroquinazoline



Chemical Formula: C₈H₄Cl₂N₂

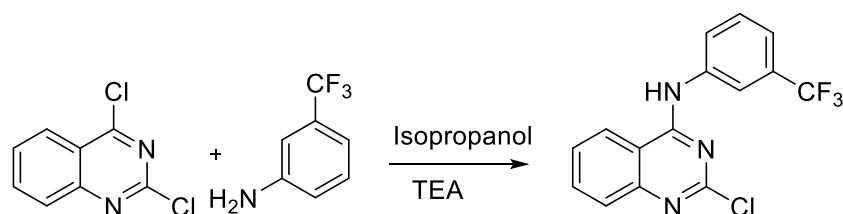
Molecular Weight: 199,0340

¹H NMR (400 MHz, DMSO) δ 8.31 (ddd, *J* = 8.4, 1.4, 0.6 Hz, 1H), 8.17 (ddd, *J* = 8.4, 7.0, 1.4 Hz, 1H), 8.04 (ddd, *J* = 8.5, 1.1, 0.7 Hz, 1H), 7.91 (ddd, *J* = 8.3, 7.0, 1.2 Hz, 1H).

HRMS (ESI): calcd. (M+H)⁺ 198.9824, exper. 198.9834.

Yield: 99%

Synthesis of the 2-chloro-N-(3-(trifluoromethyl)phenyl)quinazolin-4-amine

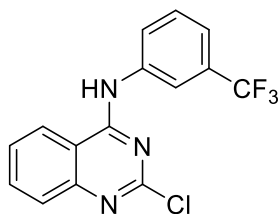


Compound 2 (0.2 g, 1.0 mmol) and 3-trifluoromethylaniline (137 μL , 1.0 mmol) have been mixed together in a round bottom flask containing 5 mL of isopropanol and 280 μL of TEA. The mixture has been heated up at 80 $^{\circ}\text{C}$ for 24 h. After completion of the reaction, the mixture has been cooled down at room temperature and 10 mL of water and 1 mL of a saturated solution of NH_4Cl have been added to the reaction mixture. The formed precipitate has been filtered off under vacuum obtaining the final compound as a white solid.

Yield: 98%

Characterisation:

Compound 3: 2-chloro-N-(3-(trifluoromethyl)phenyl)quinazolin-4-amine



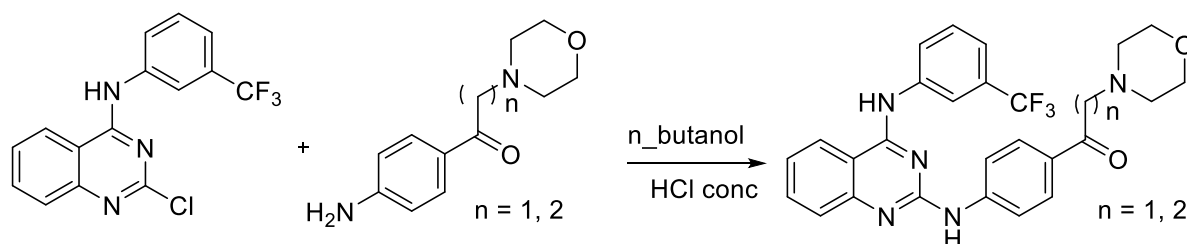
Chemical Formula: $\text{C}_{15}\text{H}_9\text{ClF}_3\text{N}_3$

Molecular Weight: 323,7032

^1H NMR (400 MHz, MeOD) δ 8.40 (ddd, $J = 8.4, 1.3, 0.5$ Hz, 1H), 8.26 (s, 1H), 8.10 (ddd, $J = 6.6, 3.3, 2.7$ Hz, 1H), 7.87 (ddd, $J = 8.4, 7.0, 1.3$ Hz, 1H), 7.71 (ddd, $J = 8.4, 1.2, 0.6$ Hz, 1H), 7.66 – 7.55 (m, 2H), 7.47 (dd, $J = 7.8, 0.7$ Hz, 1H).

Yield: 84%

Synthesis of the final compounds

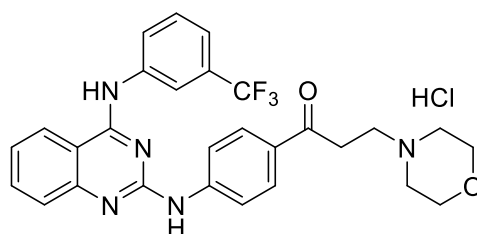


Compound 3 (50 mg, 0.15 mmol) and one of the previously synthesized p-aminoacetophenone (0.15 mmol) have been mixed in a small round bottom flask with 1 mL of n-butanol and one drop of HCl concentrated. The mixture has been heated up at 110°C for 1 hour. After the completion of the reaction, the mixture has been cooled down in an ice bath. During the cooling process a precipitate was formed. The solid has been filtered of obtaining the desired final compound.

Yield: 61-70%

Characterisation:

Compound **TDFA-01:** 3-morpholino-1-(4-((4-((3-(trifluoromethyl)phenyl)amino)quinazolin-2-yl)amino)phenyl)propan-1-one



Chemical Formula: C₂₈H₂₇ClF₃N₅O₂

Molecular Weight: 558,0022

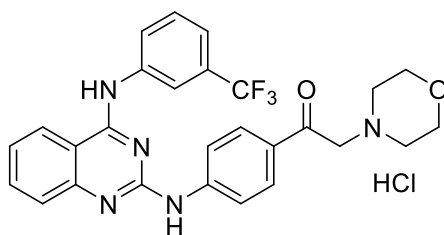
¹H NMR (400 MHz, MeOD) δ 8.49 (ddd, *J* = 8.4, 1.3, 0.5 Hz, 1H), 8.01 (m, 4H), 7.95 (m, 1H), 7.71 (m, 3H), 7.67 ((ddd, *J* = 8.4, 1.2, 0.6 Hz, 1H), 7.63 (d, *J* = 9.1 Hz, 1H), 4.10 (m, 2H), 3.87 (m, 2H), 3.61 (m, 6H), 3.28 (m, 2H).

HRMS (ESI): calcd. (M+H)⁺ 522.2111, exper. 522.2134.

HPLC-UV: 90% purity (area at 254nm).

Yield: 61%

Compound **TDFA-02:** 3-morpholino-1-(4-((4-((3-(trifluoromethyl)phenyl)amino)quinazolin-2-yl)amino)phenyl)propan-1-one



Chemical Formula: C₂₇H₂₅ClF₃N₅O₂

Molecular Weight: 543,9752

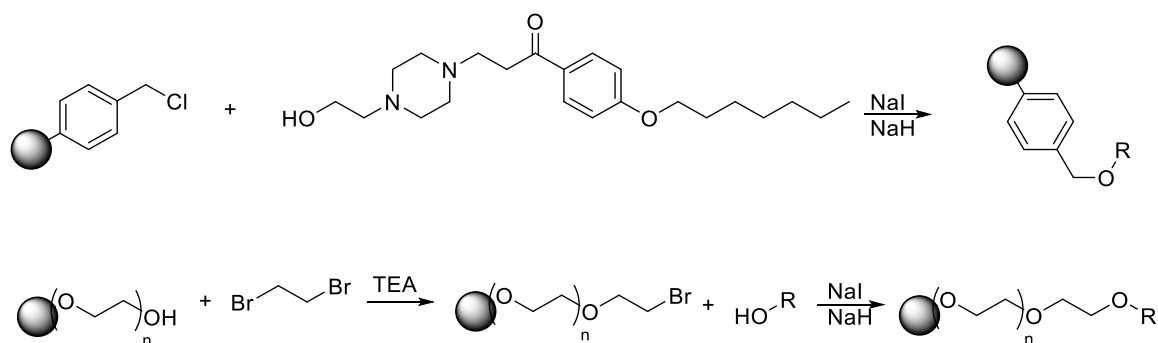
¹H NMR (400 MHz, CDCl₃) δ 8.37 (s, 1H), 8.13 (t, *J* = 9.0 Hz, 1H), 7.84 – 7.79 (m, 1H), 7.77 (ddd, *J* = 8.3, 4.7, 1.0 Hz, 2H), 7.68 – 7.63 (m, 1H), 7.61 – 7.55 (m, 1H), 7.55 – 7.50 (m, 2H), 7.46 (t, *J* = 7.9 Hz, 1H), 7.41 (d, *J* = 7.8 Hz, 1H), 7.35 (d, *J* = 7.7 Hz, 1H), 7.19 – 7.13 (m, 1H), 3.87 (dd, *J* = 5.7, 3.9 Hz, 4H), 3.81 – 3.75 (m, 6H).

HRMS (ESI): calcd. (M+H)⁺ 508.1955, exper. 508.1961.

HPLC-UV: 88% purity (area at 254nm).

Yield: 70%

5.4.2 Synthesis of the resins for affinity chromatography



Synthesis

In a round bottom flask 1.0 g of the desired resin has been suspended in 20.0 mL of DCM. The suspension has been stirred at low rpm and at room temperature for 1 hour. After that 5 mmol of the desired compound have been added to the suspension with 5.0 mmol of NaH and 5.0 mmol of NaI. The mixture has been heated up at reflux for 5 hours. After that the resin has been removed by the solvent through filtration under vacuum and then thoroughly washed with DCM, deionised water, MeOH and then DCM. The resin has been dried overnight in oven.

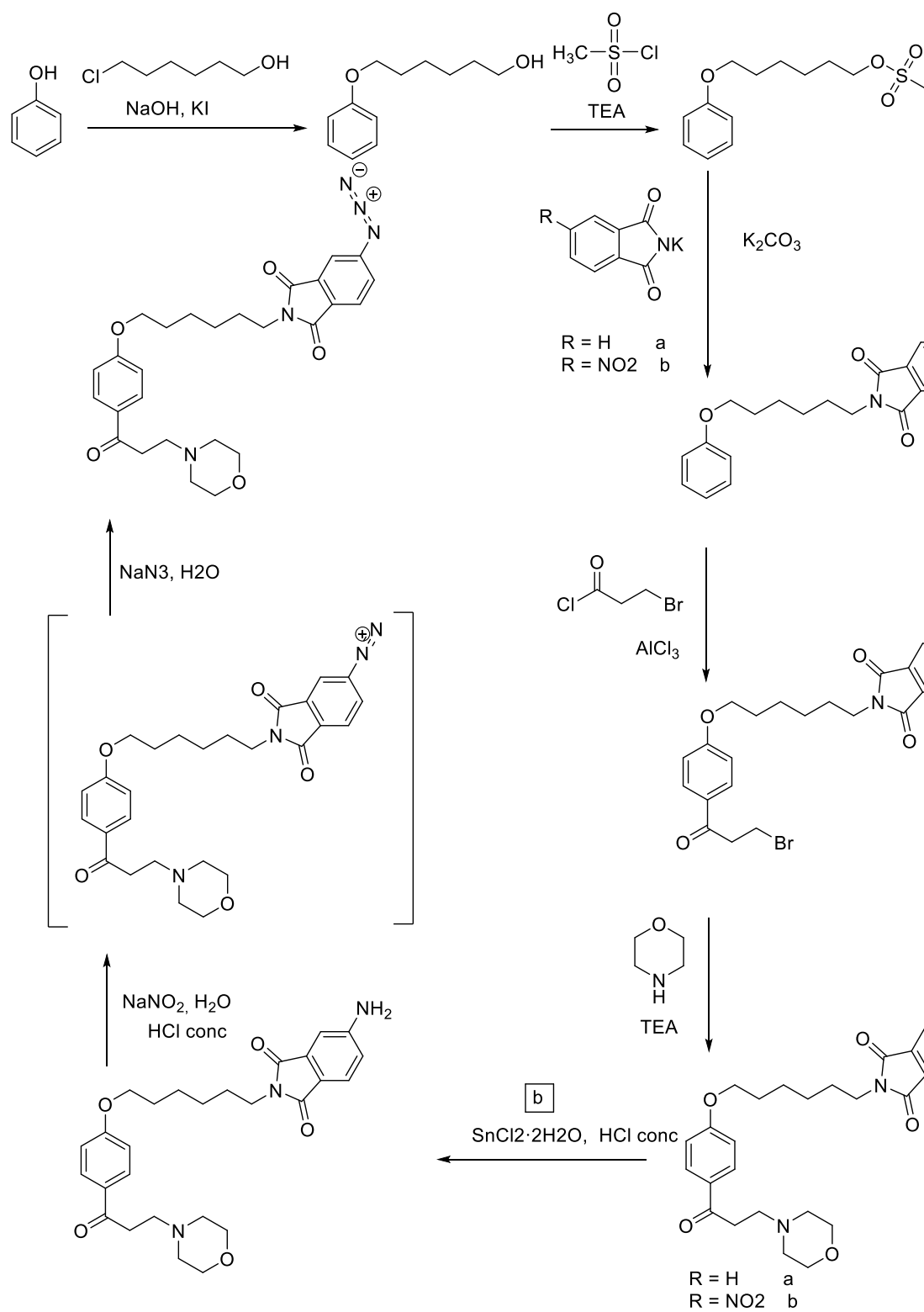
Loading determination

In a small plastic syringe for solid phase peptide synthesis, 0.25 g of the desired resin have been added. The resin has been swelled with 3 mL of THF and then, the organic solvent has been gently removed through filtration. 2 mL of a 50:50 mixture of concentrated HCl and THF have been added to the resin. The formed suspension has been left at room temperature for 10 minutes. Subsequently, the mixture has been removed and the resin has been thoroughly washed with THF, MeOH and DCM. After this a solution of TEA in DCM (1/9), has been added to the resin. The suspension has been left at room temperature for a couple of minutes and then the organic solvent has been removed through filtration and conserved in a round bottom flask. This step has been repeated other two times. The combined organic phases have been evaporated off under reduced pressure. The formed white solid (triethylammonium chloride) has been weighted and thorough the number of mmols obtained, the loading of the resin has been determined.

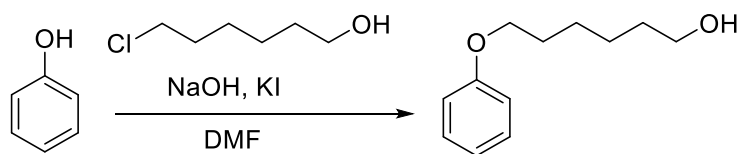
$$\text{loading of the resin} = \frac{n \text{ of mmols of triethylammonium chloride}}{2} * 4$$

5.4.3 Synthesis of the photoactivatable probes

Pathway A



Synthesis of 6-phenoxyhexan-1-ol

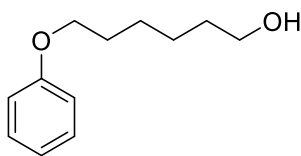


In a round bottom flask phenol (0.59 g, 6.25 mmol), NaOH (0.25 g, 6.25 mmol), KI (0.83 g, 5.0 mmol), 6-chlorohexan-1-ol (0.67 g, 5.0 mmol) have been added to 5 mL of DMF. The mixture has been heated up at 80°C and stirred at this temperature for 3 hours. The reaction has been monitored through TLC (n-hexane/EtOAc 5:5) and after its completion the mixture has been cooled down to room temperature and then added with 60 mL of DCM. The organic phase has been washed in sequence with: 40 mL of a saturated solution of NaHCO₃, 40 mL of an aqueous solution of NaOH (2M) and then with 40 mL of deionised water. After this procedure the organic phase has been dried using Na₂SO₄ and the solvent has been removed under reduced pressure obtaining a viscous oil that was the desired compound.

Yield: 99%

Characterisation:

Compound 1: 6-phenoxyhexan-1-ol

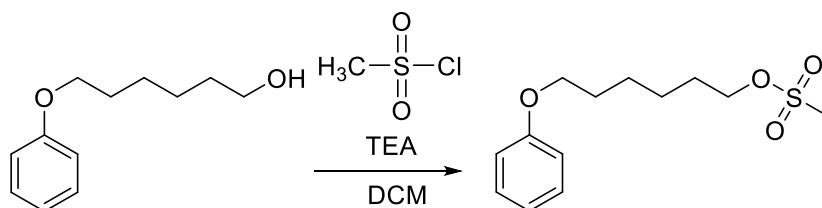


Chemical Formula: C₁₂H₁₈O₂
Molecular Weight: 194,2740

¹H NMR (300 MHz, MeOD) δ 7.28 – 7.17 (m, 2H), 6.93 – 6.82 (m, 3H), 4.89 (s, 1H), 3.91 (t, *J* = 6.4 Hz, 2H), 3.61 – 3.48 (t, *J* = 6.4 Hz, 2H), 1.81 – 1.68 (m, 2H), 1.65 – 1.32 (m, 6H).

Yield: 99%

Synthesis of 6-phenoxyhexyl methanesulfonate

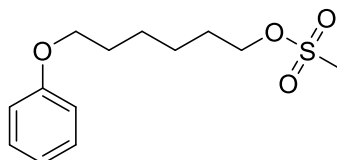


In a round bottom flask compound 1 (0.97 g, 5.0 mmol) and 1.1 mL of TEA have been added to 15.0 mL of DCM. To this solution, methanesulfonyl chloride (777 μ L, 10 mmol) has been added dropwise. The reaction mixture has been stirred at room temperature overnight and monitored by TLC using as eluting system a mixture of n-hexane/EtoAc (5:5). After completion, the reaction has been diluted with 50 mL of DCM, the so obtained organic phase has been washed with a saturated solution of NaHCO₃ (4 x 30 mL) and then it has been dried over Na₂SO₄ and then the organic solvent has been evaporated off under reduced pressure. The obtained residue is a viscous liquid.

Yield: 99%

Characterisation:

Compound 2: 6-phenoxyhexyl methanesulfonate



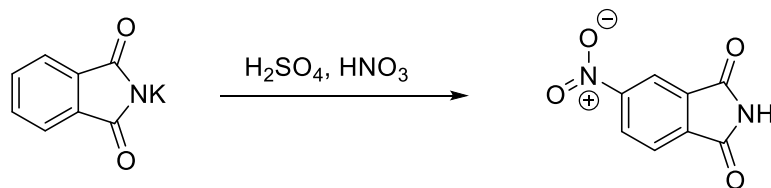
Chemical Formula: C₁₃H₂₀O₄S

Molecular Weight: 272,3590

¹H NMR (300 MHz, Acetone) δ 7.33 – 7.23 (m, 2H), 6.97 – 6.87 (m, 3H), 4.25 (t, J = 6.5 Hz, 2H), 3.99 (t, J = 6.5 Hz, 2H), 3.09 – 3.06 (s, 3H), 1.86 – 1.72 (m, 4H), 1.60 – 1.44 (m, 4H).

Yield: 99%

Synthesis of the 4-nitrophthalimide

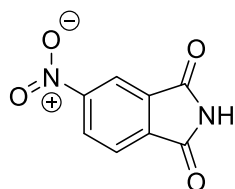


To a mixture of concentrated H₂SO₄ (15.0 mL) and HNO₃ 70% (6.0 mL) potassium phthalimide has been added under magnetic stirring and portion wise. The mixture has been reacted at room temperature overnight. After completion, the reaction mixture has been cooled in an ice bath and portionwise ice has been added. After complete melting of the ice, the aqueous phase has been extracted with 50.0 mL of EtOAc. The organic phase has been washed with 50.0 mL of a saturated solution of NaHCO₃ and then with 50.0 mL of deionised water. The organic phase has been dried over Na₂SO₄ and then the solvent has been evaporated off under reduced pressure obtaining the desired compound as a pale yellow solid.

Yield: 49%

Characterisation:

Compound 3: 4-nitrophthalimide



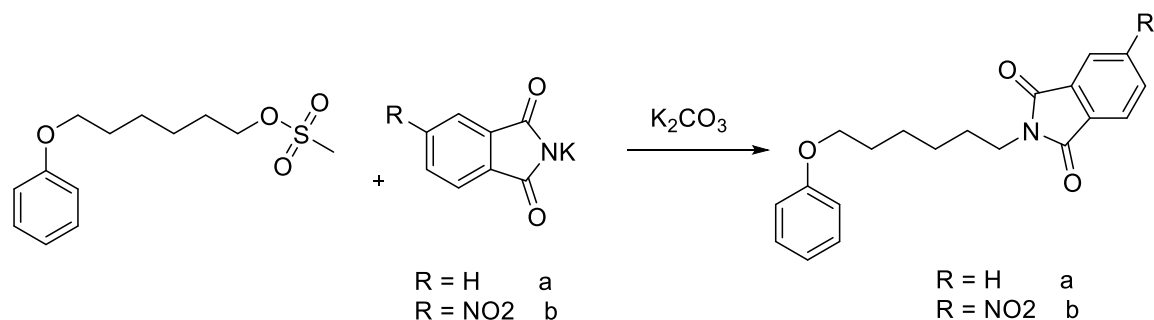
Chemical Formula: C₈H₄N₂O₄

Molecular Weight: 192,1300

¹H NMR (300 MHz, DMSO) δ 8.63 (dd, *J* = 8.2, 2.0 Hz, 1H), 8.46 (dd, *J* = 2.0, 0.6 Hz, 1H), 8.09 (dd, *J* = 8.2, 0.6 Hz, 1H), 7.84 (s all, 1H).

Yield: 49%

Synthesis of the phthalimide hexanoyl compounds

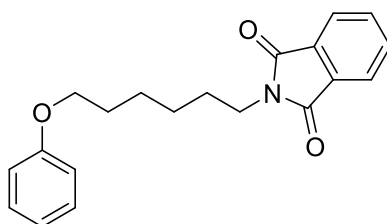


In a round bottom flask, with the following order, the desired phthalimide (3.7 mmol), K₂CO₃ (11.25 mmol), DMF (15 mL) and compound 2 (2.5 mmol) have been mixed together. The mixture has been heated up at 70°C for 3 hours and monitored by TLC (n-hexane:EtOAc, 1:1). After completion the mixture has been cooled down at room temperature and poured in a conical flask containing 25 mL of deionised water. The formed precipitate has been filtered off under vacuum. The solid residue has been purified through column chromatography on silica gel using as eluting system a mixture of n-hexane:EtOAc, starting from 7:3 ratio till 6:4. The final compound has been isolated as a waxy pale yellow solid

Yield: 54-62%

Characterisation:

Compound 4: 2-(6-phenoxyhexyl)isoindoline-1,3-dione

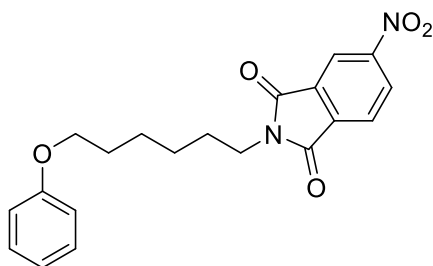


Chemical Formula: C₂₀H₂₁NO₃
Molecular Weight: 323,3920

¹H NMR (300 MHz, CDCl₃) δ 7.84 (td, *J* = 5.2, 2.1 Hz, 2H), 7.75 – 7.67 (m, 2H), 7.33 – 7.22 (m, 2H), 6.98 – 6.84 (m, 3H), 3.95 (t, *J* = 6.4 Hz, 2H), 3.71 (t, *J* = 7.2 Hz, 2H), 1.86 – 1.65 (m, 4H), 1.58 – 1.35 (m, 4H).

Yield: 62%

Compound 5: 5-nitro-2-(6-phenoxyhexyl)isoindoline-1,3-dione



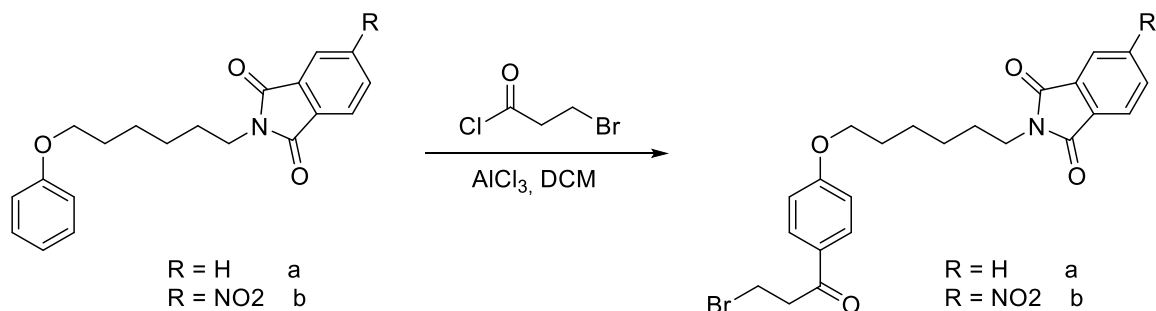
Chemical Formula: C₂₀H₂₀N₂O₅

Molecular Weight: 368,3890

¹H NMR (400 MHz, CDCl₃) δ 8.65 (dd, *J* = 2.0, 0.6 Hz, 1H), 8.59 (dd, *J* = 8.1, 2.0 Hz, 1H), 8.03 (dd, *J* = 8.1, 0.6 Hz, 1H), 7.30 – 7.23 (m, 2H), 6.95 – 6.85 (m, 3H), 3.94 (t, *J* = 6.4 Hz, 2H), 3.75 (t, *J* = 6.4 Hz, 2H), 1.83 – 1.69 (m, 4H), 1.56 – 1.39 (m, 4H).

Yield: 54%

Synthesis of compounds 6 and 7

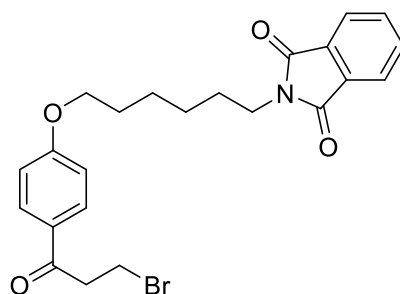


To a solution of the desired phenyl ether (Compound 4 or 5, 1.5 mmol) in DCM (10.0 mL) a solution of AlCl₃ (3.1 mmol), DCM (20 mL) and 3-bromopropionyl chloride (3.1 mmol) has been added dropwise under magnetic stirring. After complete addition of the second solution, the reaction has been left at room temperature for 2 hours. During this period it has been monitored by TLC (n-hexane/EtOAc, 8:2). Once completed the reaction has been added with ice and an aqueous solution of HCl 0.1 M (50.0 mL). The two phases have been separated through separation funnel and the aqueous one has been extracted twice with 40.0 mL of DCM. The different aliquots of organic phase have been combined together and washed three times with 50.0 mL of NaHCO₃. The organic phase has been dried over MgSO₄ and the solvent evaporated off under reduced pressure isolating the desired compound.

Yield: 77-81%

Characterisation:

Compound 6: 2-(6-(4-(3-bromopropanoyl)phenoxy)hexyl)isoindoline-1,3-dione

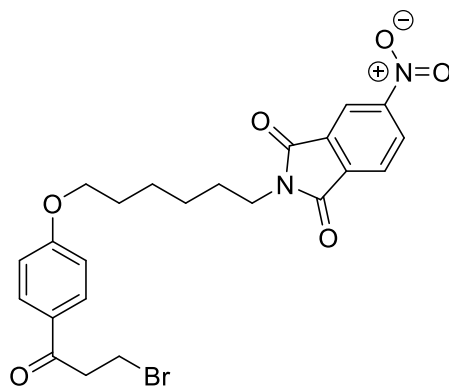


Chemical Formula: $C_{23}H_{24}BrNO_4$
Molecular Weight: 458,3520

1H NMR (400 MHz, $CDCl_3$) δ 7.98 – 7.88 (m, 2H), 7.88 – 7.81 (m, 2H), 7.76 – 7.67 (m, 2H), 6.96 – 6.89 (m, 2H), 4.03 (t, $J = 6.9$ Hz, 2H), 3.79 – 3.67 (m, 4H), 3.53 (t, $J = 7.1$ Hz, 2H), 1.89 – 1.69 (m, 4H), 1.61 – 1.40 (m, 4H).

Yield: 62%

Compound 7: 2-(6-(4-(3-bromopropanoyl)phenoxy)hexyl)-5-nitroisoindoline-1,3-dione

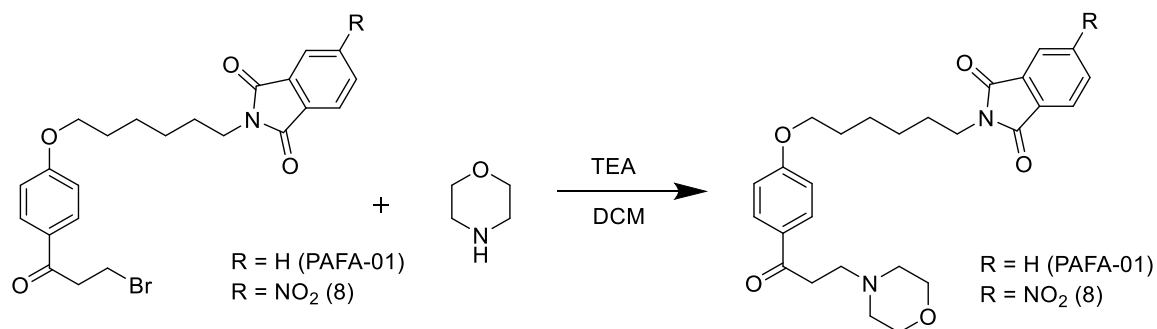


Chemical Formula: $C_{23}H_{23}BrN_2O_6$
Molecular Weight: 503,3490

It has been used directly in the following step.

Yield: 81%

Synthesis of the control compound **PAFA-01** and compound 8

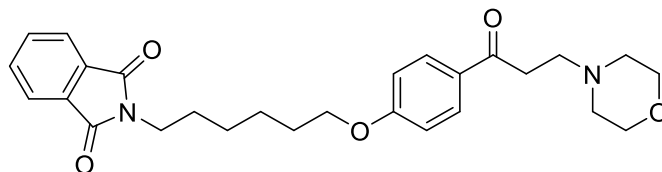


In a round bottom flask, the desired synthon (compound 6 or 7, 1.2 mmol) has been added to a solution composed by 5.0 mL of DCM and 220 μ L of TEA. To this solution, 350 μ L of morpholine (4.0 mmol) have been added under magnetic stirring. The obtained mixture has been stirred at room temperature for 2 hours, after that, the organic solvent has been evaporated off under reduced pressure. The solid residue has been suspended in a saturated solution of NaHCO₃ and the obtained precipitate has been filtered off under vacuum. The solid powder obtained was the desired in the case of compound **PAFA-01**, while for compound 8 the precipitate has been further purified by column chromatography on silica gel. The eluting mixture has been DCM:MeOH, 98:2.

Yield: 27-98%

Characterisation:

Compound PAFA-01: 2-(6-(4-(3-morpholinopropanoyl)phenoxy)hexyl)isoindoline-1,3-dione



Chemical Formula: C₂₇H₃₂N₂O₅

Molecular Weight: 464,5620

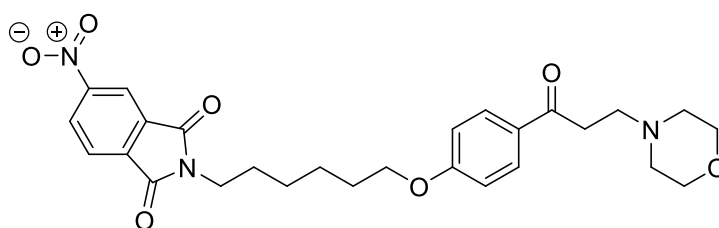
¹H NMR (400 MHz, CDCl₃) δ 7.96 – 7.87 (m, 2H), 7.82 (td, *J* = 5.4, 2.1 Hz, 2H), 7.75 – 7.65 (m, 2H), 6.95 – 6.85 (m, 2H), 4.00 (t, *J* = 6.4 Hz, 2H), 3.74 (m, 4H), 3.69 (t, *J* = 7.4 Hz, 2H), 3.16 (t, *J* = 7.3 Hz, 2H), 2.86 (t, *J* = 7.3 Hz, 2H), 2.55 (m, 4H), 1.85 – 1.65 (m, 4H), 1.56 – 1.38 (m, 4H).

HRMS (ESI): calcd. (M+H)⁺ 465.2384, exper. 465.2389.

HPLC-UV: 98% purity (area at 254nm).

Yield: 98%

Compound 8: 2-(6-(4-(3-morpholinopropanoyl)phenoxy)hexyl)-5-nitroisoindoline-1,3-dione



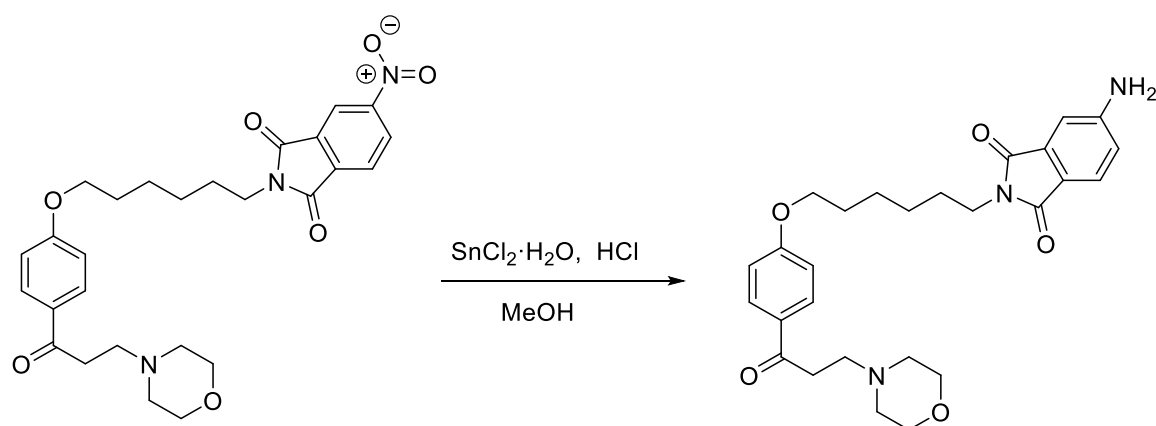
Chemical Formula: C₂₇H₃₁N₃O₇

Molecular Weight: 509,5590

¹H NMR (400 MHz, CDCl₃) δ 8.55 (dd, *J* = 2.0, 0.6 Hz, 1H), 8.51 (dd, *J* = 8.1, 2.0 Hz, 1H), 7.97 (dd, *J* = 8.1, 0.6 Hz, 1H), 7.84 (m, 2H), 6.95 – 6.85 (m, 3H), 3.94 (t, *J* = 6.4 Hz, 2H), 3.69 (t, *J* = 6.4 Hz, 2H), 3.64 (m, 4H), 3.07 (t, *J* = 7.6 Hz, 2H), 2.76 (t, *J* = 7.6 Hz, 2H), 2.46 (m, 4H), 1.83 – 1.69 (m, 4H), 1.56 – 1.39 (m, 4H).

Yield: 27%

Synthesis of 5-amino-2-(6-(4-(3-morpholinopropanoyl)phenoxy)hexyl)isoindoline-1,3-dione

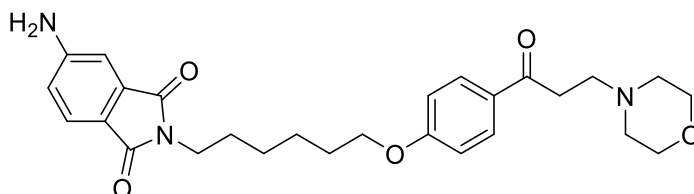


In a round bottom flask compound 8 (156 mg, 0.3 mmol) has been dissolved in 2 mL of MeOH, then a solution of SnCl₂ · 2H₂O (338 mg, 1.50 mmol) in 1.0 mL of concentrated hydrochloric acid has been added dropwise. The mixture has been heated up at 50 °C and left at this temperature for 3 hours. The progression of the reaction has been checked using TLC and as eluting mixture DCM :MeOH (95:5). The formation of the desired compound has been highlighted by the presence of a fluorescent band in yellow. After completion of the reaction the round bottom flask has been placed in an ice bath and the mixture has been added with 50.0 mL of EtOAc. The organic phase has been washed with 30 mL of a saturated solution of NaHCO₃. The organic solvent has been removed under reduced pressure and the obtained residue has been further purified by column chromatography on silica gel using as eluent a mixture of DCM:MeOH (95:5). At the end of the purification the desired compound has been isolated as a yellow fluorescent solid.

Yield: 77%

Characterisation:

Compound 9: 5-amino-2-(6-(4-(3-morpholinopropanoyl)phenoxy)hexyl)isoindoline-1,3-dione



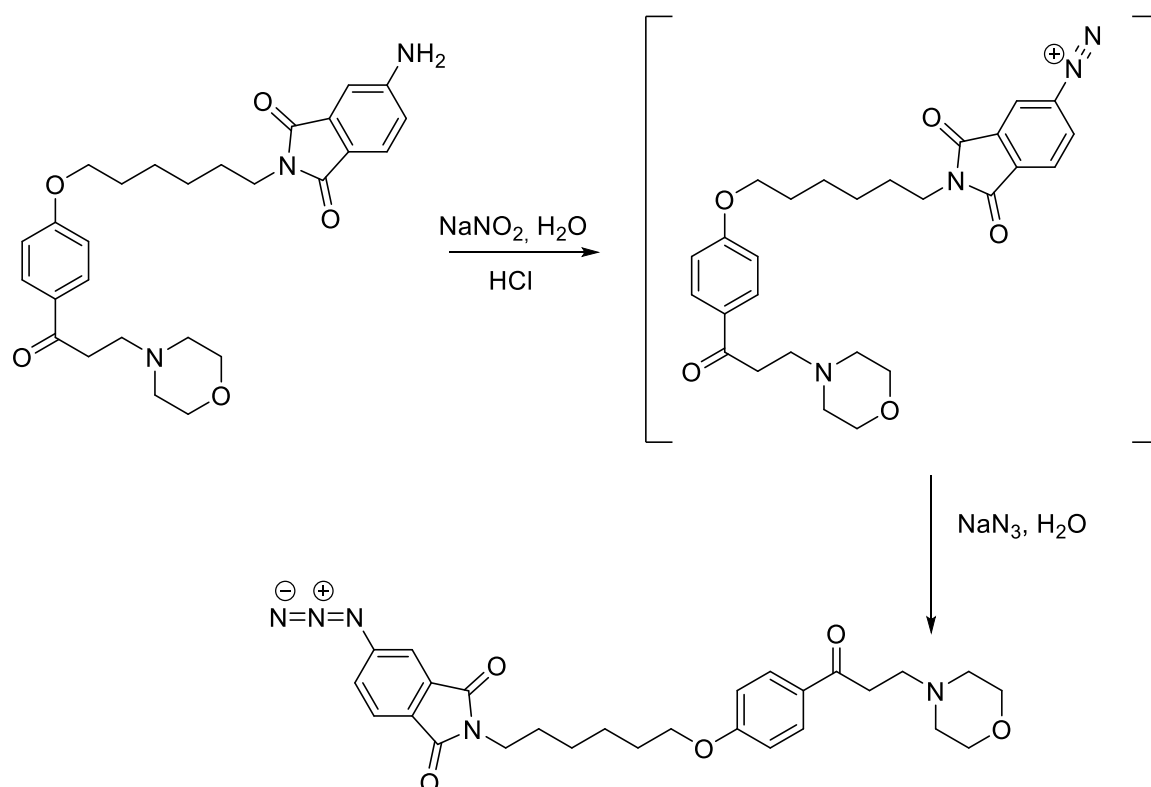
Chemical Formula: C₂₇H₃₃N₃O₅

Molecular Weight: 479,5770

¹H NMR (300 MHz, CDCl₃) δ 7.95 – 7.87 (m, 2H), 7.56 (dd, *J* = 8.1, 0.5 Hz, 1H), 7.01 (dd, *J* = 2.1, 0.4 Hz, 1H), 6.93 – 6.85 (m, 2H), 6.80 (dd, *J* = 8.1, 2.1 Hz, 1H), 4.53 (s, 2H), 3.99 (t, *J* = 6.4 Hz, 2H), 3.76 – 3.70 (m, 4H), 3.62 (t, *J* = 7.2 Hz, 2H), 3.15 (t, *J* = 7.4 Hz, 2H), 2.84 (t, *J* = 7.4 Hz, 2H), 2.59 – 2.47 (m, 4H), 1.86 – 1.61 (m, 4H), 1.57 – 1.32 (m, 4H).

Yield: 77%

Synthesis of the final compound *PAFA-02*

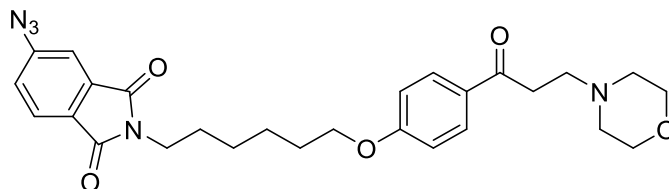


In a round bottom flask, covered with aluminium foil, compound 9 (112 mg, 0.2 mmol) it has been solubilized in a aqueous solution of HCl at 15% (1.0 mL) under magnetic stirring and at 4 °C. To this mixture, another aqueous (0.8 mL) solution of NaNO_2 (21 mg, 0.3 mmol) has been added dropwise. The resulting mixture has been maintained in ice bath and after 30 minutes it has been observed the formation of the diazonium salt intermediate. This synthon has not been isolated but the reaction proceeded directly with the following step. To the obtained mixture, a solution of NaN_3 (32 mg, 0.50 mmol) in H_2O (225 μL) has been added and the resulting solution has been reacted at room temperature for other 30 minutes. The progression of the process has been monitored through TLC ($\text{DCM}:\text{MeOH}$, 95:5) observing the disappearance of the fluorescent spot. After the completion of the reaction, 15 mL of EtOAc have been added to the mixture. The organic phase has been washed with a saturated solution of NaHCO_3 (3 x 10 mL) and subsequently it has been dried over Na_2SO_4 . The organic solvent has been evaporated off under reduced pressure obtaining the desired final compound. All the workup procedures have been performed in a dark environment reducing the risk of degrading the compound.

Yield: 43%

Characterisation:

Compound **PAFA-02:** 5-azido-2-(6-(4-(3-morpholinopropanoyl)phenoxy)hexyl)isoindoline-1,3-dione



Chemical Formula: C₂₇H₃₁N₅O₅

Molecular Weight: 505,5750

¹H NMR (300 MHz, CDCl₃) δ 7.99 – 7.85 (m, 2H), 7.78 (dd, *J* = 8.0, 0.6 Hz, 1H), 7.45 (dd, *J* = 2.0, 0.6 Hz, 1H), 7.30 – 7.24 (m, 1H), 6.92 – 6.84 (m, 2H), 3.99 (t, *J* = 6.4 Hz, 2H), 3.74 – 3.58 (m, 6H), 3.14 (t, *J* = 7.4 Hz, 2H), 2.83 (t, *J* = 7.4 Hz, 2H), 2.58 – 2.46 (m, 4H), 1.84 – 1.61 (m, 4H), 1.60 – 1.28 (m, 4H).

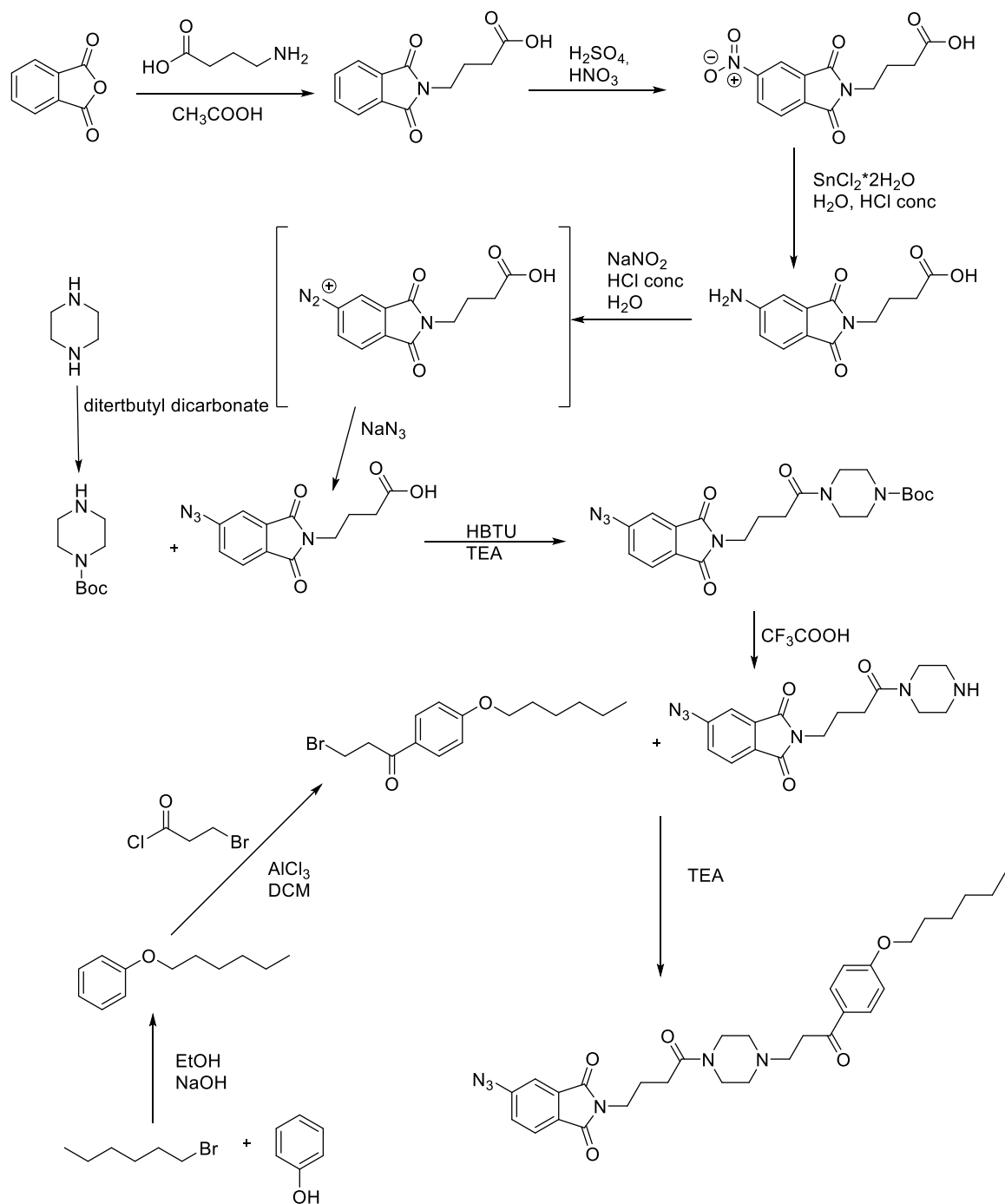
¹³C NMR (75 MHz, CDCl₃) δ 197.45, 167.68, 167.56, 163.19, 146.64, 134.48, 133.85, 130.40, 129.76, 128.05, 124.96, 123.95, 114.29, 113.78, 99.34, 68.10, 66.87, 62.83, 53.79, 53.73, 38.13, 35.51, 29.78, 28.99, 28.54, 26.61, 25.67, 22.78, 14.23, 1.11.

HRMS (ESI): calcd. (M+H)⁺ 506.2398, exper. 506.2410.

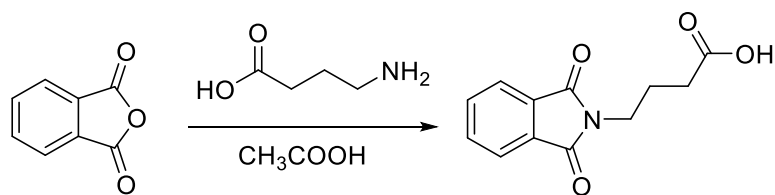
HPLC-UV: 99% purity (area at 254nm).

Yield: 43%

Pathway B



Synthesis of 4-(1,3-dioxisoindolin-2-yl)butanoic acid

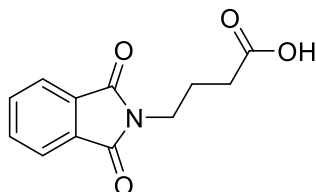


In a round bottom flask 4-aminobutirric acid (1.03 g, 10.0 mmol) and phthalic anhydride (1.48 g, 10.0 mmol) have been solubilised in 20.0 mL of acetic acid. The mixture has been heated up at reflux for 9 hours. The reaction has been monitored through TLC using a mixture of DCM:MeOH (9:1). After completion, the round bottom flask has been cooled down in an ice bath and then its content it has been slowly poured in a conical flask that contained ice and water in equal amounts (150 mL). The obtained precipitate has been filtered off under vacuum and washed with an aqueous solution of HCl (0.1 M). The desired compound has been isolated as a white powder.

Yield: 89%

Characterisation:

Compound 10: 4-(1,3-dioxisoindolin-2-yl)butanoic acid

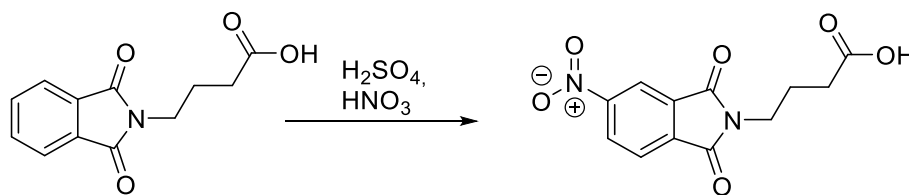


Chemical Formula: C₁₂H₁₁NO₄
Molecular Weight: 233,2230

¹H NMR (300 MHz, DMSO) δ 12.07 (s, 1H), 7.91 – 7.79 (m, 4H), 3.60 (t, *J* = 6.8 Hz, 2H), 2.27 (t, *J* = 7.2 Hz, 2H), 1.81 (p, *J* = 7.0 Hz, 2H).

Yield: 89%

Synthesis of 4-(5-nitro-1,3-dioxoisindolin-2-yl)butanoic acid

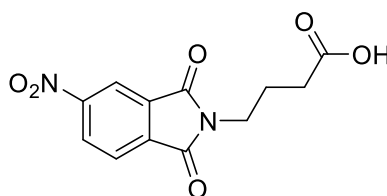


To a mixture of concentrated H_2SO_4 (10.0 mL) and HNO_3 70% (4.0 mL) compound 10 (2.1 g, 8.9 mmol) has been added under magnetic stirring and portion wise. The mixture has been reacted at room temperature for 4 hours. The progression of the reaction has been monitored using TLC (n-hexane/EtOAc, 1:1). After completion, the reaction mixture has been cooled in an ice bath and portion wise ice has been added. After complete melting of the ice, the aqueous phase has been extracted with 50.0 mL of EtOAc. The organic phase has been dried over Na_2SO_4 and then the solvent has been evaporated off under reduced pressure. The yellow solid has been crystallized using a mixture of H_2O :EtOH (2:1) obtaining the desired compound as a pale yellow solid.

Yield: 70%

Characterisation:

Compound 11: 4-(5-nitro-1,3-dioxoisindolin-2-yl)butanoic acid

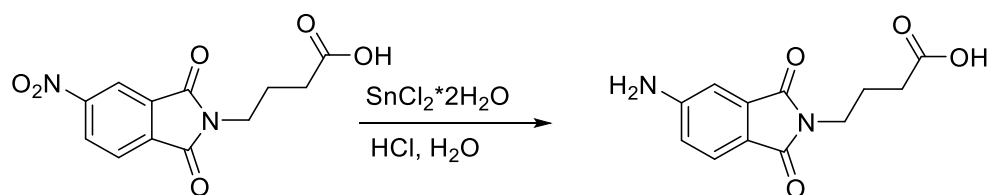


Chemical Formula: $\text{C}_{12}\text{H}_{10}\text{N}_2\text{O}_6$
Molecular Weight: 278,2200

^1H NMR (400 MHz, DMSO) δ 12.05 (s, 1H), 8.62 (dd, J = 8.1, 2.0 Hz, 1H), 8.48 (dd, J = 2.0, 0.5 Hz, 1H), 8.11 (dd, J = 8.2, 0.6 Hz, 1H), 3.66 (t, J = 6.8 Hz, 2H), 2.30 (t, J = 7.2 Hz, 2H), 1.84 (p, J = 7.0 Hz, 2H).

Yield: 70%

Synthesis of 4-(5-amino-1,3-dioxisoindolin-2-yl)butanoic acid

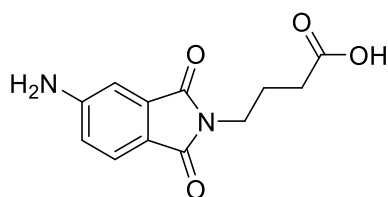


In a round bottom flask compound 11 (1.4 g, 5.0 mmol) has been suspended in 15.0 mL of H_2O , then a solution of $\text{SnCl}_2 \cdot 2\text{H}_2\text{O}$ (5.1 g, 22.5 mmol) in 10.0 mL of concentrated hydrochloric acid has been added dropwise. The mixture has been heated up at 50°C and left at this temperature for 3 hours. The progression of the reaction has been checked using TLC and as eluting mixture DCM :MeOH (95:5). The formation of the desired compound has been highlighted by the presence of a fluorescent band in yellow. After completion of the reaction the round bottom flask has been placed in an ice bath and the pH of the solution has been adjusted to 5 with a basic solution of NaOH 2 M. To the aqueous phase has been extracted with 50.0 mL of EtOAc. The organic phase has been washed with 30 mL of a saturated solution of NaHCO_3 . The organic solvent has been removed under reduced pressure and the obtained residue has been further purified by crystallisation using toluene as solvent. At the end of the purification the desired compound has been isolated as a pale yellow fluorescent solid.

Yield: 80%

Characterisation:

Compound 12: 4-(5-amino-1,3-dioxisoindolin-2-yl)butanoic acid

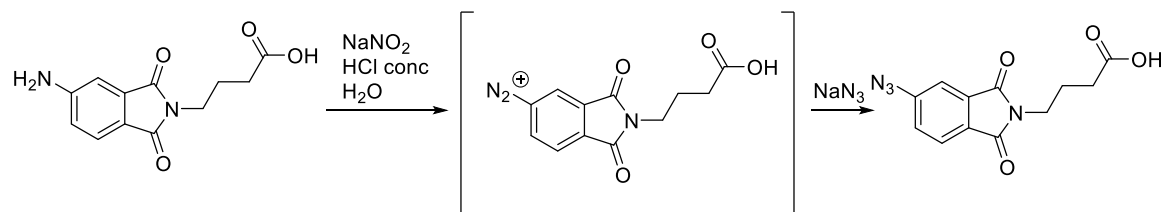


Chemical Formula: $\text{C}_{12}\text{H}_{12}\text{N}_2\text{O}_4$
Molecular Weight: 248,2380

^1H NMR (400 MHz, CDCl_3) δ 7.57 (d, $J = 8.1$ Hz, 1H), 7.04 (d, $J = 2.0$ Hz, 1H), 6.82 (dd, $J = 8.1, 2.1$ Hz, 1H), 4.54 (s, 2H), 3.68 (t, $J = 6.9$ Hz, 2H), 2.37 (t, $J = 7.5$ Hz, 2H), 1.99 (p, $J = 7.1$ Hz, 2H).

Yield: 80%

Synthesis of 4-(5-azido-1,3-dioxisoindolin-2-yl)butanoic acid

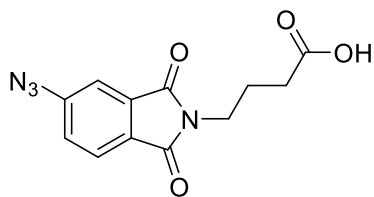


In a round bottom flask, covered with aluminium foil, compound 12 (0.74 g, 3.0 mmol) it has been suspended in a aqueous solution of HCl at 15% (5.0 mL) under magnetic stirring and at 4 °C. To this mixture, another aqueous (2.4 mL) solution of NaNO₂ (231 mg, 3.3 mmol) has been added dropwise. The resulting mixture has been maintained in ice bath and after 30 minutes it has been observed the formation of the diazonium salt intermediate. This synthon has not been isolated but the reaction proceeded directly with the following step. To the obtained mixture, a solution of NaN₃ (352 mg, 5.5 mmol) in H₂O (2.0 mL) has been added and the resulting solution has been reacted at room temperature for other 30 minutes. The progression of the process has been monitored through TLC (DCM:MeOH, 95:5) observing the disappearance of the fluorescent spot. After the completion of the reaction, 15 mL of EtOAc have been added to the mixture. The organic phase has been washed with an aqueous solution of HCl 0.1 M and subsequently it has been dried over Na₂SO₄. The organic solvent has been evaporated off under reduced pressure obtaining the desired final compound. All the workup procedures have been performed in a dark environment reducing the risk of degrading the compound.

Yield: 80%

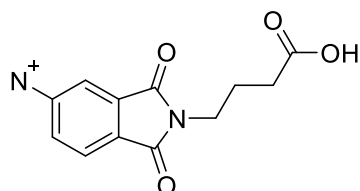
Characterisation:

Compound 13: 4-(5-azido-1,3-dioxisoindolin-2-yl)butanoic acid



Chemical Formula: C₁₂H₁₀N₄O₄
Molecular Weight: 274,2360

¹H NMR (400 MHz, DMSO) δ 12.04 (s, 1H), 7.86 (dd, *J* = 8.0, 0.6 Hz, 1H), 7.54 (dd, *J* = 2.0, 0.6 Hz, 1H), 7.49 (dd, *J* = 8.0, 2.1 Hz, 1H), 3.60 (t, *J* = 6.8 Hz, 2H), 2.26 (t, *J* = 7.2 Hz, 2H), 1.92 – 1.74 (m, 2H).

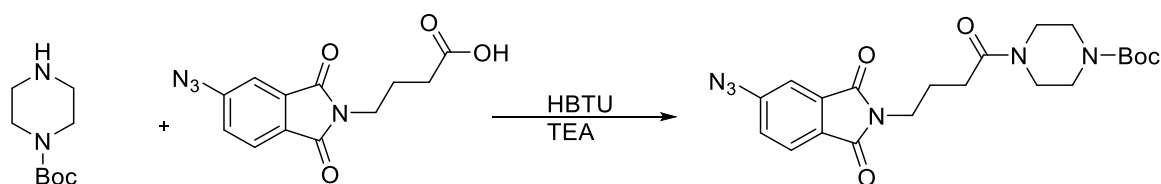


HRMS (ESI): calcd. (M-N₂)⁺ 246.0635, exper. 246.1781.

HPLC-UV: 99% purity (area at 254nm).

Yield: 65%

Synthesis of tert-butyl 4-(4-(5-azido-1,3-dioxisoindolin-2-yl)butanoyl)piperazine-1-carboxylate



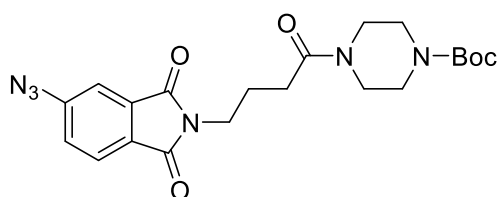
For this reaction boc-piperazine has been prepared freshly following the procedure reported in literature.

In a round bottom flask boc-piperazine (0.21 g, 1.1 mmol) and compound 13 (0.27 g, 1.0 mmol) has been solubilised in 3 mL of DCM. To this solution 144 μ L of TEA and HBTU (0.41 g, 1.1 mmol) have been added. The obtained mixture has been reacted at room temperature for 3 hours. The Progression of the reaction has been monitored through TLC using as eluent a mixture 4:6 of n-hexane-EtOAc. After completion of the reaction the organic phase has been diluted with other 10.0 mL of DCM and subsequently washed twice with 20.0 mL of an saturated aqueous solution of NaHCO_3 . The organic phase has been dried over MgSO_4 and then the solvent removed by evaporation at reduced pressure. The final compound is a white solid. As in the previous case all the operations have been made in a dark fume hood for preventing the photoreaction of the desired compound.

Yield: 99%

Characterisation:

Compound 14: tert-butyl 4-(4-(5-azido-1,3-dioxisoindolin-2-yl)butanoyl)piperazine-1-carboxylate



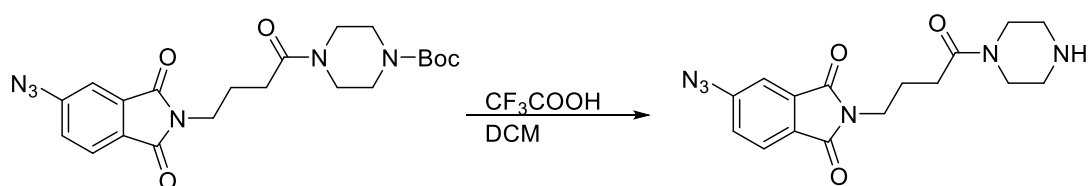
Chemical Formula: $\text{C}_{21}\text{H}_{26}\text{N}_6\text{O}_5$

Molecular Weight: 442,4760

^1H NMR (400 MHz, CDCl_3) δ 7.83 (dd, $J = 8.0, 0.6$ Hz, 1H), 7.50 (dd, $J = 2.0, 0.6$ Hz, 1H), 7.31 (dd, $J = 8.0, 2.0$ Hz, 1H), 3.78 (t, $J = 6.6$ Hz, 2H), 3.60 – 3.53 (m, 2H), 3.45 (s, 2H), 3.41 (t, $J = 5.3$ Hz, 4H), 2.40 (t, $J = 7.2$ Hz, 2H), 2.07 (p, $J = 6.9$ Hz, 2H), 1.49 (s, 9H).

Yield: 99%

Synthesis of 5-azido-2-(4-oxo-4-(piperazin-1-yl)butyl)isoindoline-1,3-dione

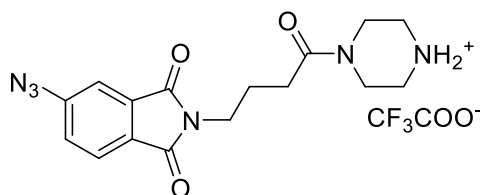


In a small round bottom flask compound 14 (0.44 g, 1.0 mmol) has been solubilised in 3.0 mL of a mixture composed by CF₃COOH/DCM (1:2.5). the solution has been magnetically stirred at room temperature for 1 hour and then the organic solvents have been removed fluxing within the round bottom flask nitrogen gas. The final compound has been isolated as trifluoroacetate salt.

Yield: 99%

Characterisation:

Compound 15: 5-azido-2-(4-oxo-4-(piperazin-1-yl)butyl)isoindoline-1,3-dione



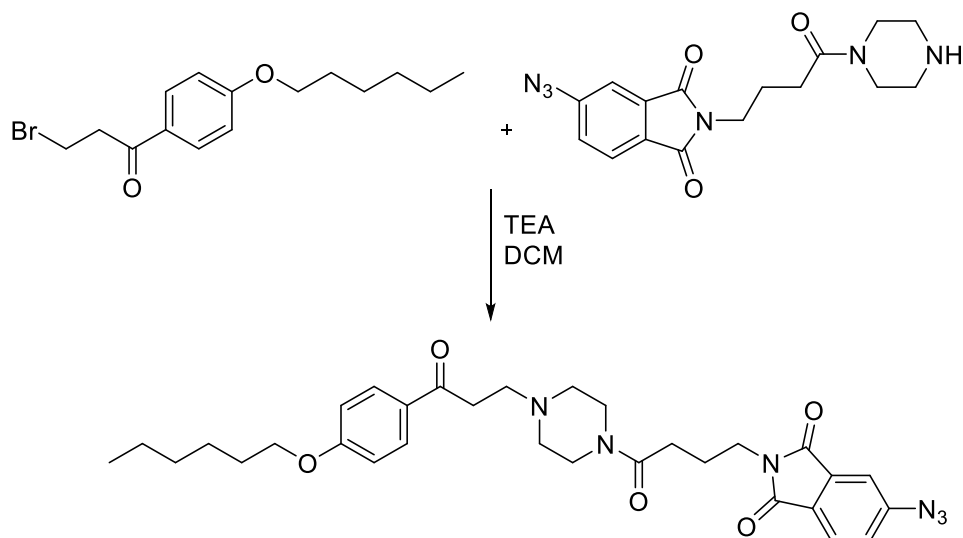
Chemical Formula: C₁₈H₁₉F₃N₆O₅

Molecular Weight: 456,3822

¹H NMR (400 MHz, DMSO) δ 8.83 (bs, 1H), 7.86 (dd, *J* = 7.9, 0.7 Hz, 1H), 7.53 (dd, *J* = 2.0, 0.7 Hz, 1H), 7.51 (dd, *J* = 7.9, 2.1 Hz, 1H), 3.60 (dd, *J* = 8.7, 4.7 Hz, 6H), 3.10 (s, 2H), 3.04 (s, 2H) 2.41 (t, *J* = 7.1 Hz, 2H), 1.85 (p, *J* = 6.8 Hz, 2H).

Yield: 99%

Synthesis of the final compound PAFA-03



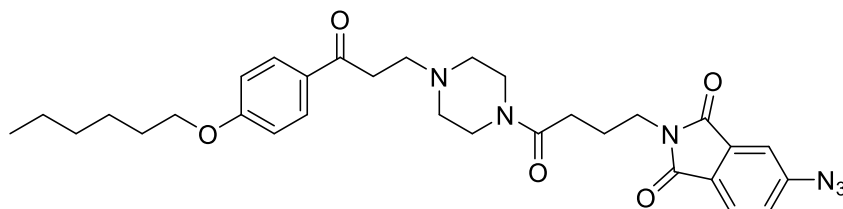
3-bromo-1-(4-(hexyloxy)phenyl)propan-1-one has been prepared following the same procedures reported in the paragraph 5.4.1.1.

Compound 15 (0.2 g, 0.4 mmol) has been dissolved in 1.0 mL of DCM added with 80 μ L of TEA. To this mixture, a solution of 3-bromo-1-(4-(hexyloxy)phenyl)propan-1-one (0.14 g, 0.4 mmol) in 1.0 mL of DCM has been added dropwise. The solution has been left under magnetic stirring and at room temperature for 4 hours. For monitoring the evolution of the reaction several TLC have been made using DCM:MeOH (95:5) as eluting mixture. After completion of the reaction, the organic phase has been diluted with 10 mL of DCM and then washed twice with 10.0 mL of deionised water. The organic phase has been dried using Na_2SO_4 and then the solvent has been evaporated off under reduced pressure. The remaining residue has been further purified through column chromatography on silica gel using as eluting mixture DCM:MeOH (95:5). The final compound has been isolated as a yellow solid.

Yield: 50%

Characterisation:

Compound PAFA-03: 5-azido-2-(4-(4-(3-(4-(hexyloxy)phenyl)-3-oxopropyl)piperazin-1-yl)-4-oxobutyl)isoindoline-1,3-dione



Chemical Formula: C₃₁H₃₈N₆O₅

Molecular Weight: 574,6820

¹H NMR (400 MHz, CDCl₃) δ 7.91 (d, *J* = 8.9 Hz, 2H), 7.78 (d, *J* = 8.0 Hz, 1H), 7.45 (d, *J* = 2.0 Hz, 1H), 7.27 (dd, *J* = 8.1, 2.1 Hz, 1H), 6.91 (d, *J* = 8.9 Hz, 2H), 4.00 (t, *J* = 6.6 Hz, 2H), 3.73 (t, *J* = 6.7 Hz, 2H), 3.58 (s, 2H), 3.44 (s, 2H), 3.14 (t, *J* = 7.2 Hz, 2H), 2.87 (t, *J* = 7.2 Hz, 2H), 2.53 (s, 2H), 2.48 (s, 2H), 2.36 (t, *J* = 7.3 Hz, 2H), 2.07 – 1.95 (m, 2H), 1.85 – 1.73 (m, 2H), 1.51 – 1.40 (m, 2H), 1.33 (td, *J* = 7.0, 3.5 Hz, 4H), 0.90 (t, *J* = 7.0 Hz, 3H).

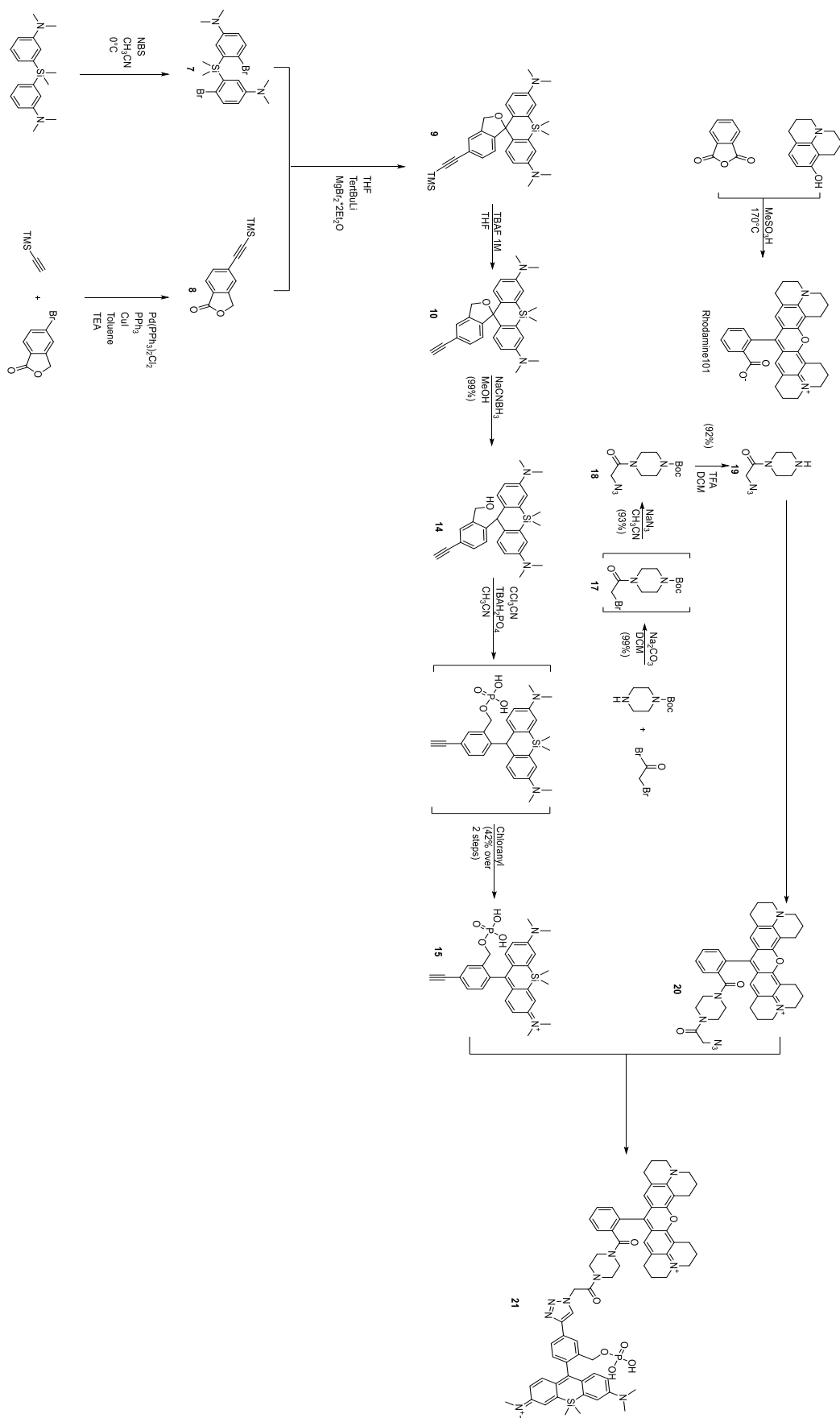
¹³C NMR (101 MHz, CDCl₃) δ 197.11, 170.00, 167.50, 167.40, 163.25, 146.53, 134.38, 130.29, 129.58, 127.96, 124.86, 123.86, 114.24, 113.68, 68.28, 53.12, 53.03, 52.61, 45.09, 41.31, 37.74, 35.38, 31.51, 31.49, 31.48, 30.28, 29.66, 29.02, 25.62, 25.61, 24.04, 22.54, 14.00, 13.99.

HRMS (ESI): calcd. (M+H)⁺ 575.2976, exper. 575.3001.

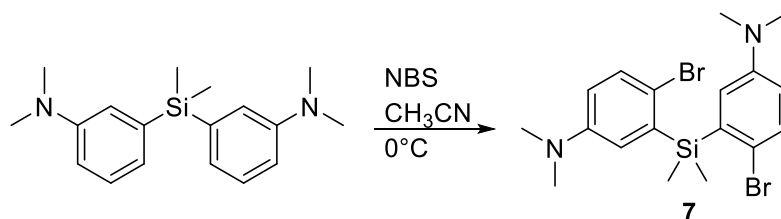
HPLC-UV: 99% purity (area at 254nm).

Yield: 50%

5.4.4 Synthesis of the fluorescent FRET probes



Synthesis of 3,3'-(dimethylsilanediyl)bis(4-bromo-N,N-dimethylaniline)

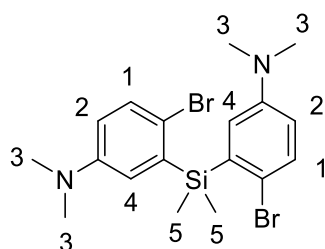


In a flame-dried Schlenk flask 3,3'-(dimethylsilanediyl)bis(N,N-dimethylaniline) (3.68 g, 12.32 mmol) was dissolved in dry CH₃CN (83 mL) and the solution was cooled at 0°C. NBS (4.61 g, 25.88 mmol) was added to the cold solution over a period of 5 minutes. The mixture has been stirred at 0°C for 80 minutes. After full conversion of the starting material 100 mL of CH₂Cl₂ were added to the solution. The organic phase has been washed with 150 mL of a saturated aqueous solution of NaHCO₃. The aqueous phase was extracted two times with 60 mL of CH₂Cl₂. All the organic phases were collected together and evaporated under reduced pressure. The solid residue has been dissolved in 30 mL of CH₂Cl₂. The organic phase was extracted three times with 50 mL of an aqueous solution of HCl 1M. The aqueous solutions were collected together and to this 6.5 g of NaOH are gradually added. The obtained suspension has been cooled down in an ice bath for 1 hour. The formed precipitate has been filtered of and washed with cold water and hexane obtaining the desired compound **7** as a fine white powder (3.6 g, 65%).

Yield: 65%

Characterisation:

Compound 7: 3,3'-(dimethylsilanediyl)bis(4-bromo-N,N-dimethylaniline)



Chemical Formula: C₁₈H₂₄Br₂N₂Si
Molecular Weight: 456,2970

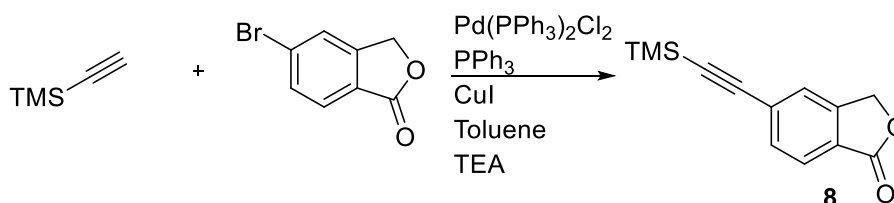
¹H NMR (300 MHz, CDCl₃) δ = 0.76 (s, 6H, H₅), 2.88 (s, 12H, H₃), 6.60 (dd, *J* = 8.8, 3.2 Hz, 2H, H₂), 6.84 (d, *J* = 3.2 Hz, 2H, H₄), 7.35 (d, *J* = 8.7 Hz, 2H, H₁) ppm.

¹³C NMR (101 MHz, CDCl₃) δ -0.90, 40.58, 76.72, 77.04, 77.36, 115.27, 116.82, 121.80, 132.99, 138.75, 148.92 ppm.

HRMS (ESI) calcd for [C₁₈H₂₅Br₂N₂Si]⁺: 455.0148, found 455.0130.

Yield: 65%

Synthesis of 5-((trimethylsilyl)ethynyl)isobenzofuran-1(3H)-one

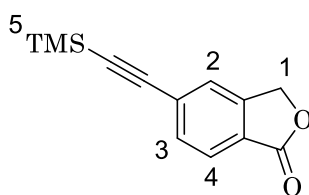


In a flame-dried Schlenk flask 5-bromoisobenzofuran-1(3H)-one (1.5 g, 7.04 mmol), Pd(PPh₃)₂Cl₂ (89 mg, 0.13 mmol), PPh₃ (203 mg, 0.77 mmol) and CuI (94 mg, 0.49 mmol) were added to 9.5 mL of Toluene under N₂ atmosphere. 1.26 mL of TEA were added to the mixture. Finally, ethynyltrimethylsilane (1.58 mL, 7.04 mmol) was added to the mixture. The reaction mixture has been stirred at 80°C for 3 hours. After 50 mL of CH₂Cl₂ were added to the reaction and the obtained precipitate has been filtered out two times filtering on celite. 50 mL of pentane were added to the filtrate and the mixture was sonicated for 15 minutes. The solution was cooled down at -20°C for 1 hour and then the formed precipitate was filtered off. The liquid fraction has been evaporated off under reduced pressure and the crude product has been purified by flash column chromatography (SiO₂; Hexane/EtOAc 98:2 to Hexane/EtOAc 85:15) to give a yellow powder (1.03 g, 63%).

Yield: 63%

Characterisation:

Compound 8: 5-((trimethylsilyl)ethynyl)isobenzofuran-1(3H)-one



Chemical Formula: C₁₃H₁₄O₂Si

Molecular Weight: 230,3380

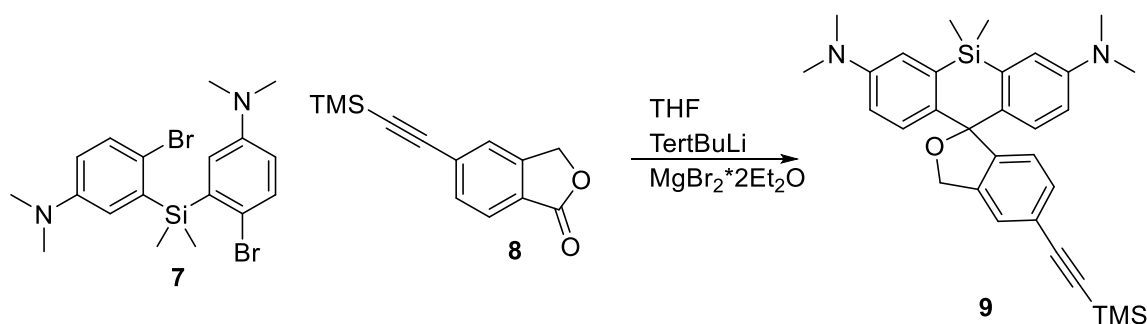
¹H NMR (300 MHz, CDCl₃) δ = 0.27 (s, 9H, H5), 5.29 (s, 2H, H1), 7.53 – 7.63 (overlapped signals, 2H, H3, H2), 7.85 (d, *J* = 7.9 Hz, 1H, H4) ppm.

¹³C NMR (126 MHz, CDCl₃) δ = -0.47, -0.24, -0.02, 69.27, 76.77, 77.03, 77.28, 99.05, 103.39, 125.22, 125.38, 125.60, 129.20, 132.81, 146.40, 170.33 ppm.

HRMS (ESI) calcd for [C₁₃H₁₅O₂Si]⁺: 231.0836, found: 231.0837.

Yield: 63%

Synthesis of N3,N3,N7,N7,5,5-hexamethyl-5'-((trimethylsilyl)ethynyl)-3'H,5H-spiro[dibenzo[b,e]siline-10,1'-isobenzofuran]-3,7-diamine

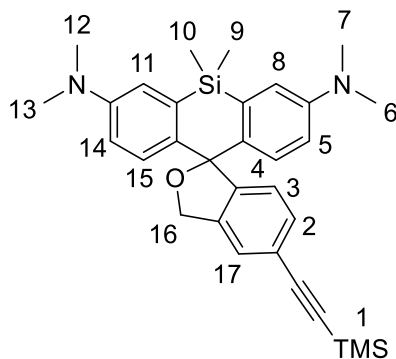


In a flame-dried Schlenk flask **7** (780 mg, 1.71 mmol) was dissolved in 10 mL of dry THF. The solution has been cooled down at -78°C and tert-butyllithium (4.43 mL, 7.5 mmol) was added dropwise over a period of 15 minutes. The solution turned to yellow. The mixture has been stirred at -78°C for 20 minutes and then warmed up to -15°C . In a flame-dried flask a solution of MgBr₂·Et₂O (970 mg, 3.8 mmol) in 18 mL of dry THF was prepared under N₂ atmosphere, sonicating. This solution was added dropwise to the reaction mixture. The solution turned to orange and it was stirred at -15°C for 15 minutes. A solution of **8** (668 mg, 2.9 mmol) in 10 mL of dry THF was added to the reaction mixture over a period of 15 minutes and the whole reaction was gradually warmed up to room temperature. The mixture was stirred for another 90 minutes. 9 mL of a saturated aqueous solution of NH₄Cl and 15 mL of brine were added to the reaction and then extracted three times with 60 mL of EtOAc. The collected organic phases were dried over MgSO₄ and the volatiles were removed under reduced pressure. The crude product has been purified by flash column chromatography (SiO₂; Hexane/EtOAc 95:5 to Hexane/EtOAc 80:20) to give a yellow powder that by NMR contains 1:1 of **9** and **8** (460 mg, 36%). The mixture has been used directly in the next step without any further purifications.

Yield: 36%

Characterisation:

Compound 9: N3,N3,N7,N7,5,5-hexamethyl-5'-((trimethylsilyl)ethynyl)-3'H,5'H-spiro[dibenzo[b,e]siline-10,1'-isobenzofuran]-3,7-diamine

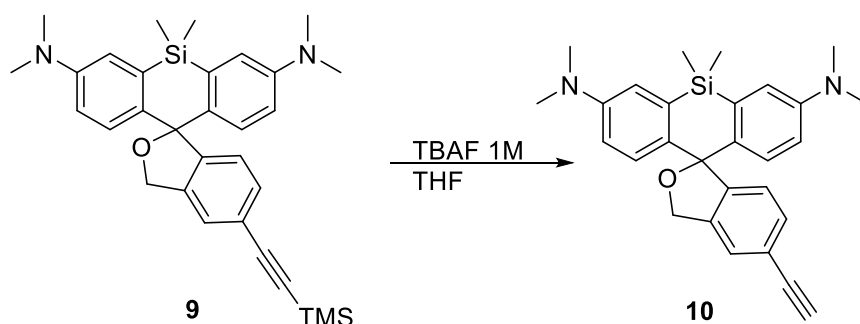


Chemical Formula: $C_{31}H_{38}N_2OSi_2$
Molecular Weight: 510,8280

1H NMR (300 MHz, $CDCl_3$) δ = 0.27 (s, 9H, H1), 0.53 (s, 3H, H9), 0.60 (s, 3H, H10), 2.95 (s, 12H, H6-H7-H12-H13), 5.16 (s, 2H, H16), 6.59 (dd, J = 8.9, 2.9 Hz, 2H, H5-H14), 6.90 (d, J = 8.8 Hz, 2H, H4-H15), 6.97 (d, J = 2.9 Hz, 2H, H8-H11), 7.00 (d, J = 7.9 Hz, 1H, H3), 7.31 – 7.42 (m, 1H, H2), 7.42 – 7.46 (m, 1H, H17) ppm.

Yield: 36%

Synthesis of 5'-ethynyl-N3,N3,N7,N7,5,5-hexamethyl-3'H,5H-spiro[dibenzo[b,e]siline-10,1'-isobenzofuran]-3,7-diamine

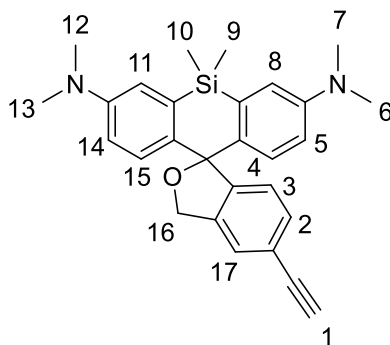


The contaminated mixture **9-8** (460 mg, 0.62 mmol) was dissolved in 2.5 mL of THF. 1.9 mL of a 1 M solution of TBAF in THF were added dropwise. The mixture was stirred at room temperature for 30 minutes. 20 mL of H₂O were added for quenching the reaction and the two-phase mixture has been stirred at room temperature for 15 minutes. 10 mL of a 1 M HCl aqueous solution were added and the aqueous phase was washed with 30 mL of EtOAc. The organic phase was extracted five times with 30 mL of HCl 0.3 M. The collected aqueous phases were slowly basified adding 12 mL of a solution of NaOH 6 M. The aqueous phase was extracted three times with 30 mL of EtOAc. The organic phase was dried with Mg₂SO₄ and then the volatiles were evaporated off under reduced pressure. **10** was obtained as a cream solid (250 mg, 92%).

Yield: 92%

Characterisation:

Compound 10: 5'-ethynyl-N3,N3,N7,N7,5,5-hexamethyl-3'H,5H-spiro[dibenzo[b,e]siline-10,1'-isobenzofuran]-3,7-diamine



Chemical Formula: $C_{28}H_{30}N_2OSi$
Molecular Weight: 438,6460

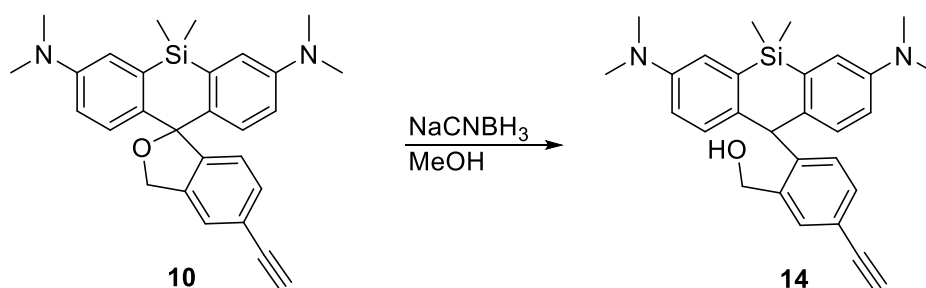
1H NMR (300 MHz, $CDCl_3$) δ = 0.57 (s, 3H, H9), 0.64 (s, 3H, H10), 2.98 (s, 12H, H6-H7-H12-H13), 3.10 (s, 1H, H1), 5.24 (s, 2H, H16), 6.64 (dd, J = 8.9, 2.9 Hz, 2H, H14), 6.93 – 7.08 (m, 5H, H4-H15-H8-H11-H3), 7.37 – 7.45 (m, 1H, H2), 7.47 (dt, J = 1.6, 0.8 Hz, 1H, H17).

^{13}C NMR (101 MHz, $CDCl_3$) δ = -1.24, 0.56, 40.56, 40.84, 71.93, 76.70, 76.96, 77.01, 77.33, 83.71, 113.85, 116.80, 120.93, 124.56, 124.93, 128.54, 131.46, 135.55, 137.88, 140.05, 147.16, 148.70 ppm.

HRMS (ESI) calcd for $[C_{28}H_{31}N_2OSi]^+$: 439,2200, found: 439,2201.

Yield: 92%

Synthesis of (2-(3,7-bis(dimethylamino)-5,5-dimethyl-5,10-dihydrodibenzo[b,e]silin-10-yl)-5-ethynylphenyl)methanol

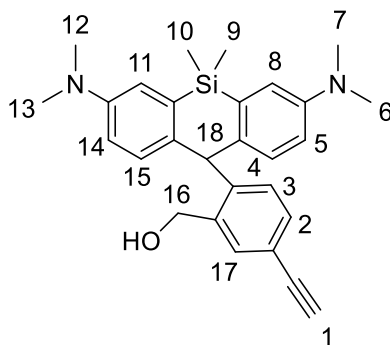


10 (350 mg, 0.8 mmol) was dissolved in 5 mL of CH₃OH. 150 μL of a 4 M HCl solution in Dioxane were added to the methanolic suspension and vigorously stirred till complete solubilization of **10**. NaCNBH₃ (420 mg, 6.72 mmol) was added to the reaction. The mixture was stirred at room temperature for 1 hour till complete disappearance of the blue coloration. The reaction was quenched adding 30 mL of CH₂Cl₂ and the organic phase was washed with 15 mL of a saturated solution of NaHCO₃ and then with 15 mL of brine. The organic phase was dried over Mg₂SO₄ and then the volatiles were removed under reduced pressure. The obtained white solid was used without further purifications. Yield (350 mg, 99%).

Yield: 99%

Characterisation:

Compound 14: (2-(3,7-bis(dimethylamino)-5,5-dimethyl-5,10-dihydrodibenzo[b,e]silin-10-yl)-5-ethynylphenyl)methanol



Chemical Formula: C₂₈H₃₂N₂OSi

Molecular Weight: 440,6620

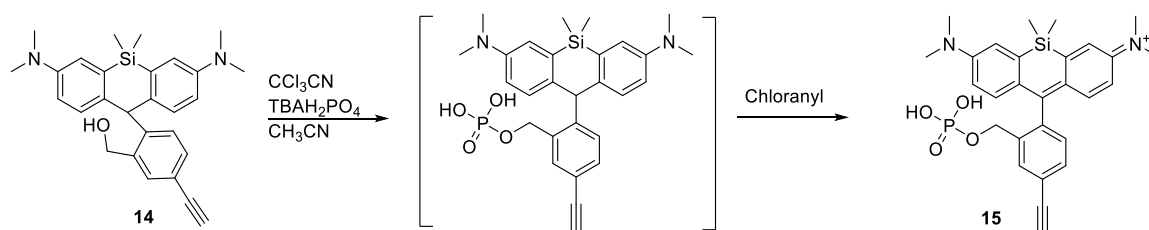
¹H NMR (400 MHz, CDCl₃) δ = 0.43 (s, 3H, H9), 0.61 (s, 3H, H10), 2.94 (s, 12H, H6-H7-H12-H13), 3.04 (s, 1H, H1), 4.44 (s, 2H, H16), 5.54 (s, 1H, H18), 6.64 (dd, *J* = 8.8, 2.9 Hz, 2H, H5-H14), 6.87 (d, *J* = 8.8 Hz, 2H, H4-H15), 6.94 (d, *J* = 2.9 Hz, 2H, H8-H11), 7.21 (d, *J* = 7.8 Hz, 1H, H3), 7.38 (dd, *J* = 7.9, 1.7 Hz, 1H, H2), 7.58 (d, *J* = 1.8 Hz, 1H, H17) ppm.

¹³C NMR (101 MHz, CDCl₃) δ = -1.10, -0.11, 40.59, 50.01, 62.69, 67.11, 76.71, 76.88, 77.03, 77.35, 83.66, 114.51, 116.38, 120.23, 130.14, 131.48, 131.69, 133.63, 133.78, 136.07, 138.63, 146.66, 148.11 ppm.

HRMS (ESI) calcd for [C₂₈H₃₃N₂OSi]⁺: 441,2357, found: 441,2353.

Yield: 99%

Synthesis of N-(7-(dimethylamino)-10-(4-ethynyl-2-((phosphonoxy)methyl)phenyl)-5,5-dimethyldibenzo[b,e]silin-3(5H)-ylidene)-N-methylmethanaminium

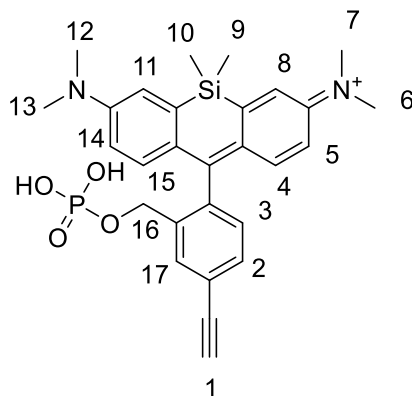


In a flame-dried double neck round bottom flask **14** (320 mg, 0.73 mmol) was solubilized in 6.5 mL of dry CH_3CN . 175 μL of trichloroacetonitrile were added to the reaction. A solution of flame-dried tetrabutylammonium dihydrogen phosphate (496 mg, 1.46 mmol) in 15 mL of dry CH_3CN was added to the reaction and stirred at room temperature for 2 hours. 254 μL of DIPEA were added and then the reaction was stirred at room temperature for 2 hours. Chloranil (360 mg, 1.46 mmol) was added to the reaction and the mixture was stirred at room temperature for 2 hours. The suspension of the reaction has been evaporated of under reduced pressure. The residue was dissolved in 50 mL of CH_3OH and directly adsorbed on celite. The organic solvent was evaporated under reduced pressure and the solid residue was purified by reverse phase flash column chromatography (C_{18} ; aq NH_4OH (1%)/ CH_3CN 100:0 for 20 minutes and then to aq NH_4OH (1%)/ CH_3CN 0:100). **15** was obtained as a blue solid. Yield (160 mg, 42%).

Yield: 42%

Characterisation:

Compound **15**: N-(7-(dimethylamino)-10-(4-ethynyl-2-((phosphonooxy)methyl)phenyl)-5,5-dimethyldibenzo[b,e]silin-3(5H)-ylidene)-N-methylmethanaminium



Chemical Formula: $C_{28}H_{32}N_2O_4PSi^+$

Molecular Weight: 519,6322

1H NMR (400 MHz, CD_3OD) δ = 0.58 (s, 3H, H9), 0.62 (s, 3H, 10H), 3.34 (s, 12H, H6-H7-H12-H13), 3.64 (s, 1H, H1), 4.62 (d, J = 5.8 Hz, 2H, H16), 6.78 (dd, J = 9.7, 2.9 Hz, 2H, H5-H14), 7.07 (d, J = 9.6 Hz, 2H, H4-H15), 7.13 (d, J = 7.8 Hz, 1H, H3), 7.34 (d, J = 2.8 Hz, 2H, H8-H11), 7.55 (dd, J = 7.8, 1.7 Hz, 1H, H2), 8.00 (d, J = 1.4 Hz, 1H 17) ppm.

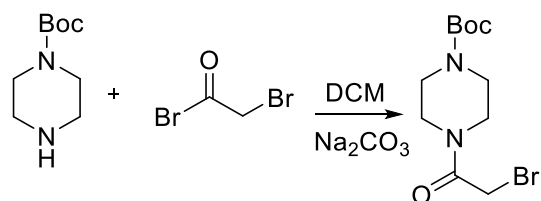
^{13}C NMR (101 MHz, CD_3OD) δ = -2.71, -2.39, 39.52, 46.96, 47.17, 47.39, 47.60, 47.81, 48.02, 48.24, 63.01, 78.46, 82.46, 114.10, 120.91, 123.21, 126.90, 128.87, 130.02, 130.42, 137.04, 137.84, 140.79, 148.02, 154.44, 166.32 ppm.

^{31}P NMR (162 MHz, CD_3OD) δ 0.76 ppm.

HRMS (ESI) calcd for $[C_{28}H_{32}N_2O_4PSi]^+$: 519,1863, found: 519,1869.

Yield: 42%

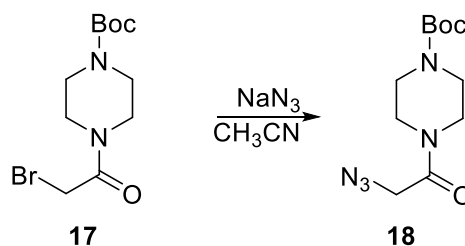
Synthesis of tert-butyl 4-(2-bromoacetyl)piperazine-1-carboxylate (17)



Tert-butyl piperazine-1-carboxylate (745 mg, 4.0 mmol) was dissolved in 4 mL of CH₂Cl₂ and then 636 mg of Na₂CO₃ (6 mmol) were added. The suspension was cooled to 0°C and then 2-bromoacetyl bromide (524 μL, 6 mmol) was added to the reaction. The mixture was warm up at room temperature and stirred for 2 hours. 20 mL of CH₂Cl₂ were added to the reaction. The organic phase was washed in sequence with 10 mL of a saturated solution of NaHCO₃, 10 mL of HCl 1M and 10 mL of brine. The organic phase was dried over Mg₂SO₄ and the solvent was evaporated off under reduced pressure. **17** was obtained as a viscous liquid and it was used in the next step without further purifications. (1.23 g, 99%).

Yield: 99%

Synthesis of tert-butyl 4-(2-azidoacetyl)piperazine-1-carboxylate

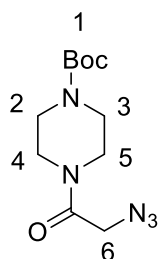


17 (1.2 g, 4 mmol) was dissolved in 20 mL of CH_3CN and then sodium azide (650 mg, 10 mmol) was added. The reaction was heated up at 90°C for 1,5 hour and then the solvent was evaporated off under reduced pressure. 15 mL of a saturated solution of NaHCO_3 were added to the solid and then the aqueous phase was extracted two times with 20 mL of CH_2Cl_2 . The organic phase was dried over MgSO_4 and evaporated off giving **18** as a white solid. Yield (1.0 g, 93%).

Yield: 93%

Characterisation:

Compound **18**: tert-butyl 4-(2-azidoacetyl)piperazine-1-carboxylate



Chemical Formula: $\text{C}_{11}\text{H}_{19}\text{N}_5\text{O}_3$

Molecular Weight: 269,3050

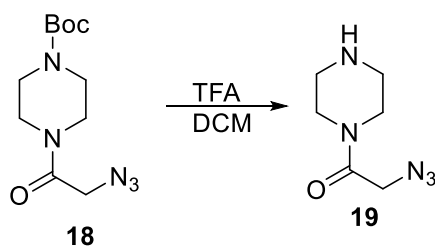
^1H NMR (400 MHz, CDCl_3) δ = 1.46 (s, 9H, H1), 3.35 (dd, J = 6.6, 3.9 Hz, 2H, H5), 3.44 (q, J = 5.1 Hz, 4H, H2 and H3), 3.61 (t, J = 5.3 Hz, 2H, H4), 3.94 (s, 2H, H6) ppm.

^{13}C NMR (101 MHz, CDCl_3) δ = 28.35, 41.86, 44.99, 50.79, 76.73, 77.05, 77.37, 80.56, 154.43, 165.81 ppm.

IR: characteristic band at 2090 cm^{-1}

Yield: 93%

Synthesis of 2-azido-1-(piperazin-1-yl)ethan-1-one

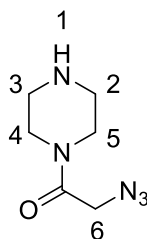


18 (1.0 g, 3.7 mmol) was dissolved in 3 mL of CH_2Cl_2 and 2 mL of TFA. The solution was stirred at room temperature for 1 hour. The solvents were removed under reduced pressure and the sticky residue obtained was dissolved in 5 mL of CH_3OH and then 1 mL of a solution of HCl 4M in dioxane was added. The mixture was evaporated off under reduced pressure. This step was repeated other two times since the obtainment of a nice white powder that is the HCl salt of **18**. Yield (700 mg, 92%).

Yield: 92%

Characterisation:

Compound **19**: 2-azido-1-(piperazin-1-yl)ethan-1-one



Chemical Formula: $\text{C}_6\text{H}_{11}\text{N}_5\text{O}$

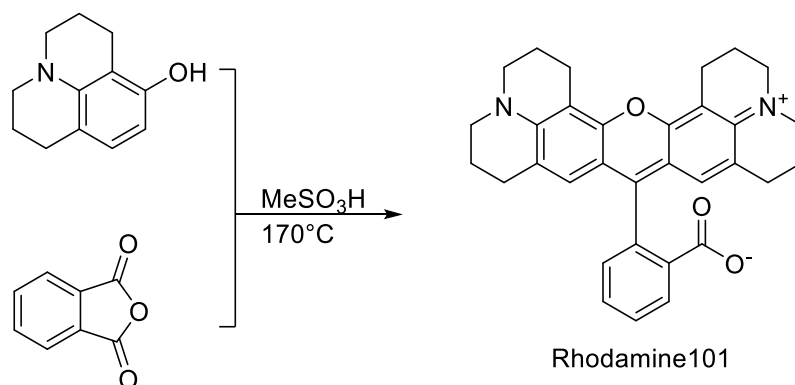
Molecular Weight: 169,1880

^1H NMR (400 MHz, CD_3OD) δ = 3.27 (m, J = 5.1 Hz, 4H), 3.71 (t, J = 5.4 Hz, 2H), 3.86 (dd, J = 7.9, 3.8 Hz, 2H), 4.18 (s, 2H) ppm.

^{13}C NMR (101 MHz, CD_3OD) δ = 38.39, 41.42, 42.89, 50.06, 167.24 ppm.

Yield: 92%

Synthesis of 2-(2,3,6,7,12,13,16,17-octahydro-1H,5H,11H,15H-pyrido[3,2,1-ij]quinolino[1',9':6,7,8]chromeno[2,3-f]quinolin-4-ium-9-yl)benzoate (Rhodamine 101)

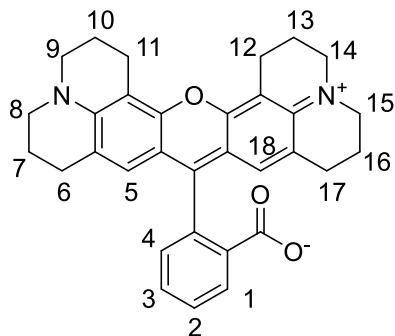


2,3,6,7-tetrahydro-1H,5H-pyrido[3,2,1-ij]quinolin-8-ol (161 mg, 0.85 mmol) and isobenzofuran-1,3-dione (50 mg, 0.34 mmol) were dissolved in 500 μL of $\text{CH}_3\text{SO}_3\text{H}$ in a Microwave vial. The suspension was heated at 175°C in microwave for 30 minutes and then at 170°C for 2 hours. In an ice bath, the reaction mixture was poured in 10 mL of H_2O and then 00 mL of CH_2Cl_2 were added. The organic phase was washed with two times 15 mL of HCl 1M and two times with 20 mL of brine. The organic phase was dried with MgSO_4 and evaporated off under reduced pressure. The crude product has been purified by flash column chromatography (SiO_2 ; $\text{CH}_2\text{Cl}_2/\text{CH}_3\text{OH}$ 100:0 to $\text{CH}_2\text{Cl}_2/\text{CH}_3\text{OH}$ 90:10) to give a purple powder (43 mg, 27%).

Yield: 27%

Characterisation:

Compound Rhodamine 101: 2-(2,3,6,7,12,13,16,17-octahydro-1H,5H,11H,15H-pyrido[3,2,1-ij]quinolizino[1',9':6,7,8]chromeno[2,3-f]quinolin-4-ium-9-yl)benzoate



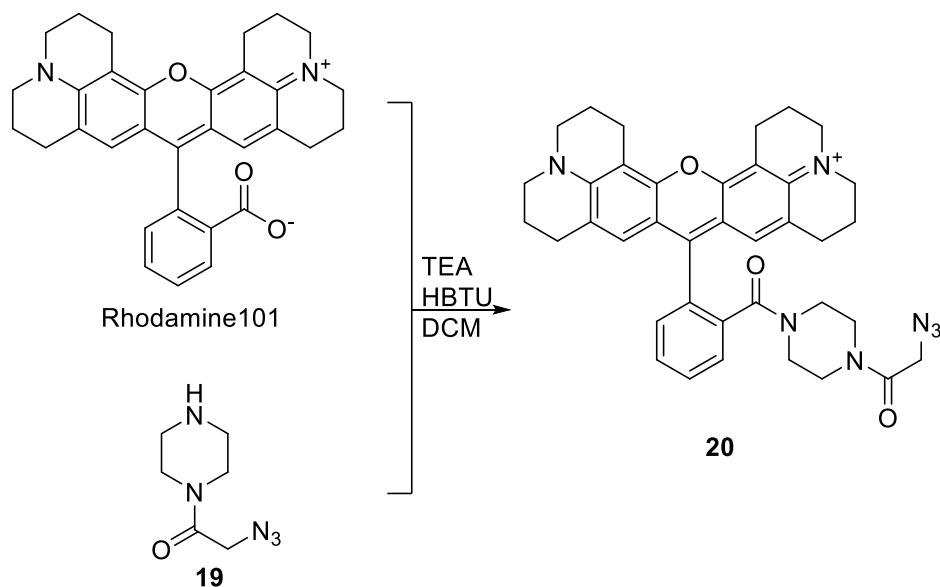
^1H NMR (400 MHz, CD_3OD) δ = 1.94 (m, 4H, H10-H7), 2.10 (m, 4H, H13-H16), 2.68 (ddt, J = 7.3, 3.4, 1.8 Hz, 4H, H6-H11), 3.08 (dd, J = 7.1, 5.7 Hz, 4H, H17-H12), 3.48 (t, J = 5.7 Hz, 4H, H8-H9), 3.54 (t, J = 5.7 Hz, 4H, H14-H15), 6.69 (s, 2H, H5-H17), 7.24 – 7.30 (m, 1H, H4), 7.66 – 7.75 (overlapped signals, 2H, H2-H3), 8.18 – 8.23 (m, 1H, H1) ppm.

^{13}C NMR (101 MHz, CD_3OD) δ = 20.96, 21.01, 21.85, 28.57, 51.33, 51.80, 106.38, 114.30, 125.01, 127.42, 130.80, 131.33, 146.74, 152.33, 153.61 ppm.

HRMS (ESI) calcd for $[\text{C}_{32}\text{H}_{31}\text{N}_2\text{O}_3]^+$: 491,2329, found: 491,2331.

Yield: 27%

Synthesis of Precursor 20

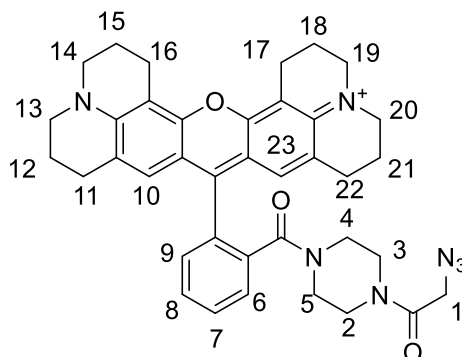


Rhodamine101 (200 mg, 0.41mmol) was solubilized in 5 mL of CH₂Cl₂ and then **19** (85 mg, 0.41 mmol) and 171 μ L of TEA (1.23 mmol) were added. Under vigorous stirring HBTU (187 mg, 0.5 mmol) was added. The reaction was stirred at RT for 1 hour then the solvent was evaporated under reduced pressure. 7 mL of H₂O were added to the solid residue. The obtained precipitate was filtered and then washed with other 7 mL of H₂O and two times with 7 mL of Et₂O. The residue was purified by flash column chromatography (SiO₂; CH₂Cl₂/CH₃OH 100:0 to CH₂Cl₂/CH₃OH 80:20) to give a purple powder (143 mg, 52%).

Yield: 52%

Characterisation:

Compound 20



Chemical Formula: $C_{38}H_{40}N_7O_3^+$

Molecular Weight: 642,7835

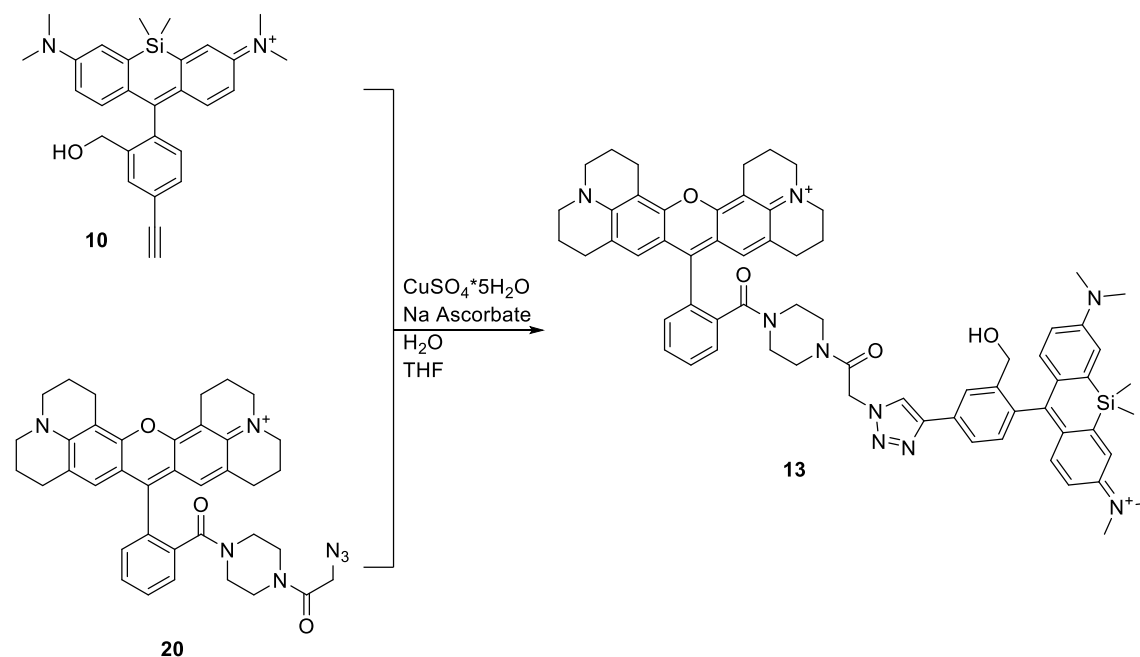
1H NMR (400 MHz, CD_3OD) δ = 1.96 (dtd, J = 11.5, 6.6, 3.1 Hz, 4H, H12-H15), 2.04 – 2.14 (m, 4H, H18-H11), 2.68 – 2.77 (m, 4H, H11-H16), 3.06 (t, J = 6.4 Hz, 4H, H22-H17), 3.40 (s, 8H, H2-H3-H4-H5), 3.54 (dt, J = 13.4, 5.7 Hz, 8H, H13-H14-H19-H20), 4.04 (s, 2H, H1), 6.76 (s, 2H, H10-H23), 7.39 – 7.47 (m, 1H, H9), 7.62 – 7.68 (m, 1H, H6), 7.70 – 7.78 (m, 2H, H7-H8) ppm.

^{13}C NMR (101 MHz, CD_3OD) δ = 19.41, 19.52, 20.36, 27.11, 46.96, 47.18, 47.39, 47.60, 47.81, 48.03, 48.24, 50.02, 50.17, 50.51, 105.26, 112.83, 123.88, 127.34, 129.60, 129.74, 130.42, 131.41, 135.11, 151.23, 151.97, 152.29 ppm.

HRMS (ESI) calcd for $[C_{38}H_{40}N_7O_3]^+$: 642,3187, found: 642,3189.

Yield: 52%

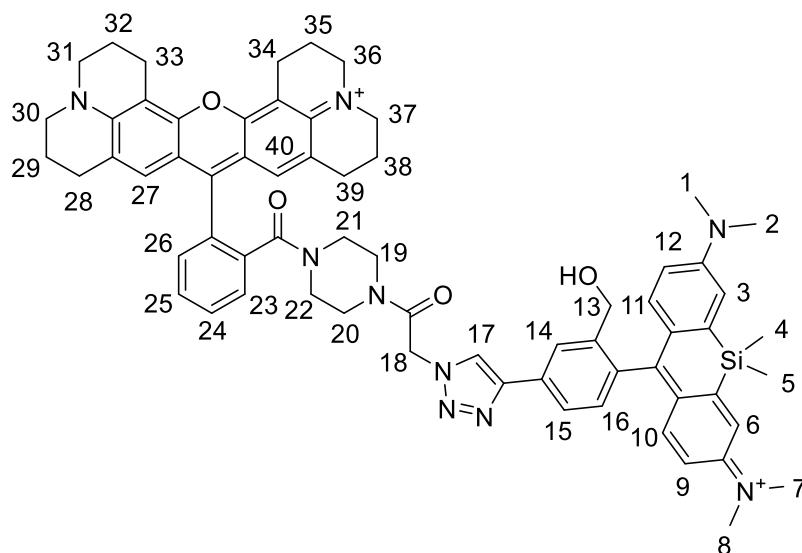
Synthesis of Precursor 13



10 (20 mg, 0.046 mmol) and **20** (31 mg, 0.046 mmol) were dissolved in 1.8 mL of THF. 11.5 mg of $\text{CuSO}_4 \cdot 5\text{H}_2\text{O}$ (0.046 mmol) were dissolved in 1.0 mL of H_2O and then 18.2 mg of Na ascorbate (0.092 mmol) were added forming a yellow milky suspension. The aqueous suspension was added to the THF solution. The mixture was stirred at room temperature for 2 hours. The reaction mixture was evaporated off under reduced pressure. The solid residue was dispersed in a saturated solution of NaHCO_3 and the precipitate was filtered and washed with cold Et_2O . The solid residue was dissolved in CH_3OH and then the solution has been adsorbed on celite and purified by reverse phase flash chromatography (C_{18} ; $\text{H}_2\text{O}/\text{CH}_3\text{CN}$ 90:20 to $\text{H}_2\text{O}/\text{CH}_3\text{CN}$ 0:100). Compound **13** was obtained as a purple solid. Yield (23 mg, 53%).

Characterisation:

Compound **13**



Chemical Formula: C₆₆H₇₁N₉O₄Si²⁺

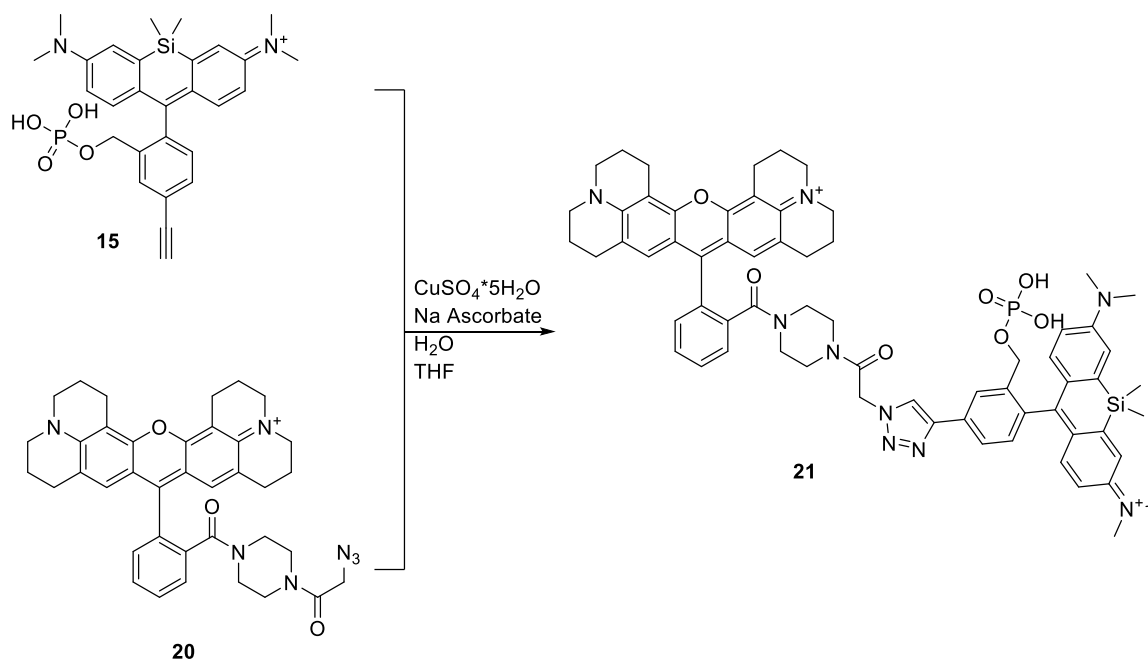
Molecular Weight: 1082,4369

¹H NMR (500 MHz, CD₃OD) δ = 0.63 (overlapped signals, 6H, H4-H5), 2.00 (d, J = 11.6 Hz, 4H, H32-H29), 2.13 (p, J = 6.2 Hz, 4H, H35-H38), 2.74 (d, J = 18.3 Hz, 4H, H33-H28), 3.09 (t, J = 6.4 Hz, 4H, H34-H39), 3.37 (s, 12H, H1-H2-H7-H8), 3.44 – 3.64 (overlapped signals, 16H, H19-H20-H21-H22-H30-H31-H36-H37), 4.39 (s, 2H, H18), 5.56 (s, 2H, H13), 6.76 – 6.83 (m, 4H, H27-H40-H12-H9), 7.19 (d, J = 9.6 Hz, 2H, H10-H11), 7.25 (d, J = 7.8 Hz, 1H, H16), 7.39 (d, J = 2.8 Hz, 2H, H3-H6), 7.48 (s, 1H, H26), 7.71 (s, 1H, H23), 7.78 (s, 2H, H24-H25), 7.95 (d, J = 7.9 Hz, 1H, H15), 8.23 (s, 1H, H14), 8.41 (s, 1H, H17).

¹³C NMR (126 MHz, CD₃OD) δ = -2.73, -2.47, 19.44, 19.54, 20.38, 27.14, 39.50, 47.09, 47.26, 47.43, 47.54, 47.60, 47.71, 47.77, 47.88, 47.94, 48.05, 48.11, 48.22, 50.04, 50.53, 50.67, 60.91, 105.27, 113.81, 120.81, 123.18, 123.91, 127.22, 127.35, 129.63, 129.81, 141.03, 148.05, 151.25, 152.01, 154.42 ppm.

HRMS (ESI/maldi) calcd for [C₆₆H₇₀N₉O₄Si]⁺: 1080,5315, found: 1080,5316.

Synthesis of Probe 21

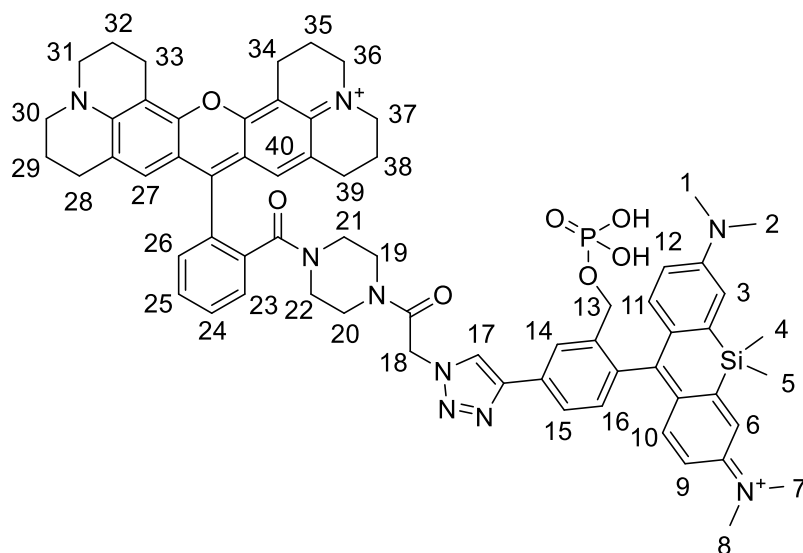


15 (10 mg, 0.019 mmol) and **20** (13 mg, 0.019 mmol) were dissolved in 900 μL of THF. 5 mg of $\text{CuSO}_4 \cdot 5\text{H}_2\text{O}$ (0.019 mmol) were dissolved in 500 μL of H_2O and then 7.6 mg of Na ascorbate (0.039 mmol) were added forming a yellow milky suspension. The aqueous suspension was added to the THF solution. The mixture was stirred at room temperature for 2 hours. The reaction mixture was evaporated off under reduced pressure. The solid residue was dissolved in CH_3OH and then the solution has been adsorbed on celite and purified by reverse phase flash chromatography (C_{18} ; aqNH₄OH (1%)/ CH_3CN 100:0 for 20 minutes and then to aqNH₄OH (1%)/ CH_3CN 0:100). Compound **21** was obtained as a blue solid. Yield (13 mg, 57%).

Yield: 57%

Characterisation:

Probe 21



Chemical Formula: $C_{66}H_{72}N_9O_7PSi^{2+}$

Molecular Weight: 1162,4157

1H NMR (400 MHz, CD_3OD) δ = 0.57 – 0.67 (m, 6H H4-H5), 1.93 (s, 10H), 2.01 – 2.15 (m, 4H), 2.75 (d, J = 24.9 Hz, 4H), 3.04 (q, J = 8.9, 7.0 Hz, 4H), 3.34 (d, J = 4.9 Hz, 6H), 3.38 – 3.65 (m, 16H), 4.68 (d, J = 5.8 Hz, 2H, H13), 5.52 (s, 2H, H18), 6.71 – 6.80 (m, 4H, H9-H12-H27-H40), 7.16 (d, J = 9.7 Hz, 2H, H11-H10), 7.21 (d, J = 7.8 Hz, 1H, H16), 7.35 (d, J = 2.8 Hz, 2H, H3-H6), 7.39 – 7.48 (m, 1H, H26), 7.69 (s, 1H, H23), 7.71 – 7.78 (m, 2H, H24-H25), 8.02 (d, J = 7.9 Hz, 1H, H15), 8.26 (s, 1H, H14), 8.48 (s, 1H, H17).

^{13}C NMR (101 MHz, CD_3OD) δ = -2.65, -2.39, 19.43, 19.55, 20.37, 27.13, 29.38, 39.52, 46.96, 47.18, 47.39, 47.60, 47.82, 48.03, 48.24, 50.04, 50.53, 50.73, 63.22, 105.26, 112.83, 114.06, 120.88, 123.19, 123.91, 124.12, 127.11, 127.39, 129.36, 129.65, 129.78, 131.18, 135.15, 136.31, 140.93, 146.84, 148.05, 151.24, 151.97, 152.29, 154.44 ppm.

^{31}P NMR (162 MHz, CD_3OD) δ 0.92.

HRMS (ESI) calcd for $[C_{66}H_{72}N_9O_7PSi]^{2+}$: 580,7525, found: 580,7530.

Yield: 57%

5.4.5 Biological experiments

5.4.5.1 Pharmacokinetic profiling of CC11

Estimation of the CC11's concentration in the blood

The experimental protocol adopted has been extrapolated by different approaches found in literature for compounds chemically analogues to CC11.^[95,155–159]

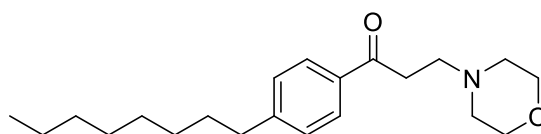
Each blood sample (50 µl) has been extracted with a mixture of solvents: 0,5 ml of Et₂O and 0,5 ml of CH₂Cl₂. The mixture has been shaken at room temperature for 1 hour. After that, from each sample the organic phase was separated and transferred in another Eppendorf. The so obtained samples were evaporated under nitrogen flux. The dry extract has been dissolved with 100 µl of a mixture of DI water (50%) and acetonitrile (50%) and spiked with a solution of internal standard (5 µL of a solution 50'000 ppb). After that the sample has been analysed through LC/MS using a Xevo G2-XS QToF mass spectrometer (Waters, Manchester, UK).

Before to start with the real experiment, a preliminary experiment has been done with the aim to determine the percentage of recovery obtainable with this kind of protocol. For this experiment an uncontaminated blood sample was taken and then spiked with a standard solution of CC11, reaching a total concentration of the analyte within the sample of 0,5 µg/ml. The percentage of recovery was estimated to be 60%.

Estimation of the body distribution of CC11 after chronic administration

This experiment has been performed injecting daily two couples of mice with two different doses of compound for a week. One couple was treated with a high dose (H, 40 mg/Kg) of the molecule and the other one with a low dose (L, 20 mg/Kg). After one week of treatment the mice were sacrificed and biological samples were collected, in particular of: blood, kidneys, brain, liver, heart and spleen. The blood was treated following the previous procedure. All the other samples were treated in a different way. They were suspended in 5 mL of acetonitrile and then homogenised with appropriate rotating blades and then refrigerates at 4°C for 1h. After that the samples have been centrifuged at 6'000 G for 7 minutes. The supernatant was spiked with a known quantity of internal standard before to perform the analysis (5 µL of a solution 50'000 ppb). All the samples were analysed with an LC/MS technique like that one used for the analysis of blood (Xevo G2-XS QToF mass spectrometer).

Internal Standard



Chemical Formula: C₂₁H₃₃NO₂

Molecular Weight: 331,5000

5.4.5.2 Spectroscopic behaviour of the photoactivatable probes

Photoactivation in phosphate buffer

A solution of compound **13** (100 μM) has been prepared in phosphate buffer at pH 7.4. The UV-Vis absorption spectrum has been measured in triplicate from 200 nm to 800 nm (instrument: Cary 60, version: 2.0). The fluorescence spectrum has been measured for the same solution from 400 nm to 800 nm, exciting the sample at 384 nm (instrument: Cary eclipse). Subsequently, the solution has been irradiated with a TLC lamp at 365 nm for 1 hour and then the UV-Vis and fluorescence spectra have been acquired again.

Photolabeling of nucleophiles

A 100 μM solution of compound **13** has been prepared in PBS. Lysine hydrochloride has been added to the solution reaching a final concentration of 10 mM. The mixture has been irradiated for 20 min with a TLC lamp at 365 nm and then a sample of the irradiated solution and of the non irradiated one have been analysed through mass spectrometry, using a Xevo G2-XS QToF mass spectrometer (Waters, Manchester, UK). The exact maxes have been calculated using Chem Draw software.

5.4.5.3 Biological experiments with the FRET fluorescent probe

Cell Culture

HeLa cells were cultured in Dulbecco's Modified Eagle Medium (DMEM) supplemented with fetal bovine serum (FBS, 10%) and penicillin-streptomycin (0.1%) at 37 °C in a 95% humidity atmosphere under 5% CO₂ environment. The cells were grown to 90% confluence and seeded onto Nunc™ Lab-Tek™ II chambered cover glass plates 48 h prior to imaging experiments. Before imaging, the growth medium was removed and the attached HeLa cells were washed with PBS (0.5 mL). Cells were subsequently incubated for the indicated time with 0.3 mL of complete growth medium containing the fluorescent probe.

Lysate preparation

HeLa cells were cultured in Dulbecco's Modified Eagle Medium (DMEM) supplemented with fetal bovine serum (FBS, 10%) and penicillin-streptomycin (0.1%) at 37 °C in a 95% humidity atmosphere under 5% CO₂ environment. The cells were grown to 90% confluence in a 75mL, washed twice with PBS and then detached using Trypsin. The cells were diluted with 9mL of complete medium and all the clusters of cells dissociated. The cells were counted using EVE automated cell counter (NanoEnTek). The cell suspension was centrifuged at 4°C, at 450 x g for 3 minutes. The supernatant was discarded. The cells were resuspended in cold PBS and centrifuged again at 450 x g for 3 minutes and then the supernatant was discarded. The cells were treated using CytoBuster (Merck Millipore) lysis buffer and adding 1.5µL of protease inhibitor cocktail for mammalian cells (Sigma: P834) per 10⁶ cells. After 5 minutes of incubation and mixing at room temperature the suspension has been centrifuged for 10min at 16,000 x g and then the supernatant transferred to new Eppendorf tubes and stored at -80°C. The amount of proteins was estimated using the BCA assay.

Optical spectroscopic methods

Stock solutions of **13**, **15**, **20** and **21** in DMSO were prepared at concentrations in the range 1 mM and stored at -20 °C in 0.1 mL aliquots and thawed immediately before each experiment. Spectroscopic measurements were conducted in TRIS buffer (TRIS-HCl 50mM, NaCl 75mM and pH 7.5). UV-visible spectra were acquired employing a Perkin Elmer Lambda 20 spectrometer using quartz cuvettes from Starna (10 mm path length). Fluorescence spectra were acquired using a Spark plate reader (Tecan). All measurements were conducted at room temperature or at 37°C for kinetic experiments. For stability tests a new absorbance spectrum was acquired every 10 minutes covering a period of 60 minutes. For dephosphorylation kinetics a new absorbance spectrum was acquired every 5 minutes covering a period of 30 minutes.

96-well plate assay with cellular lysate:

Stock solution of **21** in (CH₃)₂SO was prepared at concentration of 1 mM and stored at -20 °C. Stock solutions of cellular lysates were prepared following the above mentioned protocol and stored at -20°C. Stock solutions were thawed immediately before each experiment. A solution with the desired concentration of protein was prepared diluting the concentrated lysate in buffer (TRIS-HCl 50mM, NaCl 75mM and pH 7.5). To 1mL of each prepared solution 3μL of the 1mM stock solution of **21** were added reaching the final concentration of 3μM. Three 125 μL aliquots of each solution were filled into the wells of a 96-well plate. The plate was incubated from 15 minutes to overnight at 37°C and then analyzed using a Spark plate reader (Tecan) measuring the absorbance and fluorescence spectra.

Calibration curve for the detection of the percentage of dephosphorylation in buffer

Stock solutions of **13** and **21** in (CH₃)₂SO were prepared at concentration of 1 mM and stored at -20 °C. Stock solutions were thawed immediately before each experiment. A solution of each compound was prepared with a final concentration of 3μM in buffer (TRIS-HCl 50mM, NaCl 75mM and pH 7.5). Eleven different wells of a 96-well plate were used for the calibration curve covering from 100% of **13** to 100% of **21** increasing for each well the 10% of the adding compound. The final volume of each well was 200μL. For the intermediate concentrations every solution was added following the following equation $\mu\text{L}_{\text{added}} = (\% \text{ of compound} * 2)$. Each point of the calibration curve has been repeated in triplicates. The plate was incubated from 15 minutes to overnight at 25°C and then analyzed using a Spark plate reader (Tecan) measuring the absorbance and fluorescence spectra.

Calibration curve for the detection of the percentage of dephosphorylation in deactivated lysate

2mL of a cellular lysate have been boiled for 10 minutes maintaining the volume constant with DI-water. The obtained deactivated lysate has been centrifuged for 2 minutes in mini star bench centrifuge of VWR. The supernatant has been removed and used without further manipulations. The same volume of lysate that was necessary for reach a concentration of 400μg/mL of proteins has been added to 7 mL of TRIS buffer. The obtained solution has been split in two parts. 10,5μL of **21** were added to 3,5mL of the previously prepared solution. 10,5μL of **13** were added to 3,5mL of the previously prepared solution. The two prepared solutions were used for the obtainment of the calibration curve following the same protocol used in the other calibration curve.

96-well plate assay with cellular lysate and phosphatase inhibitors

Stock solutions of OA in (CH₃)₂SO were prepared at concentration of 200μM and 200nM and stored at -20 °C. Stock solutions of PA in (CH₃)₂SO were prepared at concentration of 1mM and 10μM and stored at -20 °C. Stock solution of Na₃VO₄ in TRIS buffer was prepared at concentration of 100mM and stored at -20 °C. Stock solutions were thawed immediately before each experiment. A solution with a protein's concentration of 400μg/mL was prepared diluting the concentrated lysate in buffer (TRIS-HCl 50mM, NaCl 75mM and pH 7.5). To 0.495mL of the prepared solution 5μL of stock solution of phosphatase inhibitor were added reaching the desired concentration of inhibitor. This procedure was repeated for each inhibitor and for each desired concentration. All the solutions were incubated at 25°C for 10 minutes. Three 125 μL aliquots of each solution were filled into the wells of a 96-well plate. The plate was incubated from 60 minutes at 37°C and then analyzed using a Spark plate reader (Tecan) measuring the absorbance and fluorescence spectra.

96-well plate assay with GSH

Stocks solutions of GSH in TRIS-HCl 50mM, NaCl 75mM and pH 7.5 buffer were prepared at a concentration of 20mM, 10mM, 5mM. To 1mL of each solution 3μL of **21** (1mM) have been added. All the solutions were incubated for 10min at 25°C and then analyzed using a Spark plate reader (Tecan) measuring the absorbance and fluorescence spectra.

96-well plate assay with MgCl₂

Stocks solutions of MgCl₂ in TRIS-HCl 50mM, NaCl 75mM and pH 7.5 buffer were prepared at a concentration of 20mM, 10mM, 5mM. To 1mL of each solution 3μL of **13** or **21** (1mM) have been added. All the solutions were incubated for 10min at 25°C and then analyzed using a Spark plate reader (Tecan) measuring the absorbance and fluorescence spectra.

Single molecule detection on PVA films

For performing single molecule detection at the fluorescence microscopy, the lids for the experiments have to be extremely cleaned. For doing this a rigid protocol has been adopted:

1. Remove lids and immerse products in ddH₂O in an appropriately sized beaker.
2. Sonicate for 10 minutes.
3. Decant the ddH₂O completely.
4. Add 1 M HCl.
5. Sonicate for 10 minutes.

6. Decant the HCl completely and wash twice with ddH₂O. Decant the ddH₂O completely.
7. Add iso-propanol (100%).
8. Sonicate for 10 minutes.
9. Aspirate the iso-propanol completely. Make sure that all products are completely dry. Wash twice with ddH₂O and aspirate the ddH₂O completely.
10. Add ethanol (100%).
11. Sonicate for 10 minutes.
12. Aspirate the ethanol completely. Make sure that all products are completely dry. Wash twice with ddH₂O.
13. Sonicate in ddH₂O for 10 min.
14. Decant ddH₂O and blow dry carefully with canned air or clean nitrogen gas.

A polyvinyl alcohol solution (0.1%) solution was prepared in PBS (pH = 7.4). Preparation method A: 400 mL of PVA (1%) were added to each well and left to evaporate at 50 °C overnight. Before imaging, 400 mL of a solution containing the compound (1 nM) at the desired pH was added, incubated for 5 min, washed thoroughly with the same buffer, and imaged with using a perfect focus system (PFS) for SMLM. Preparation method B: 20 mL of PVA (1%) solution containing the desired compound (1 nM) were added to each well and left to evaporate at 50 °C overnight. Before imaging, 200 mL the appropriate buffer at pH (5 or 7.4) was added, washed, and imaged using the PFS setting for SMLM. Both preparation methods gave comparable results

Fluorescence Microscopy

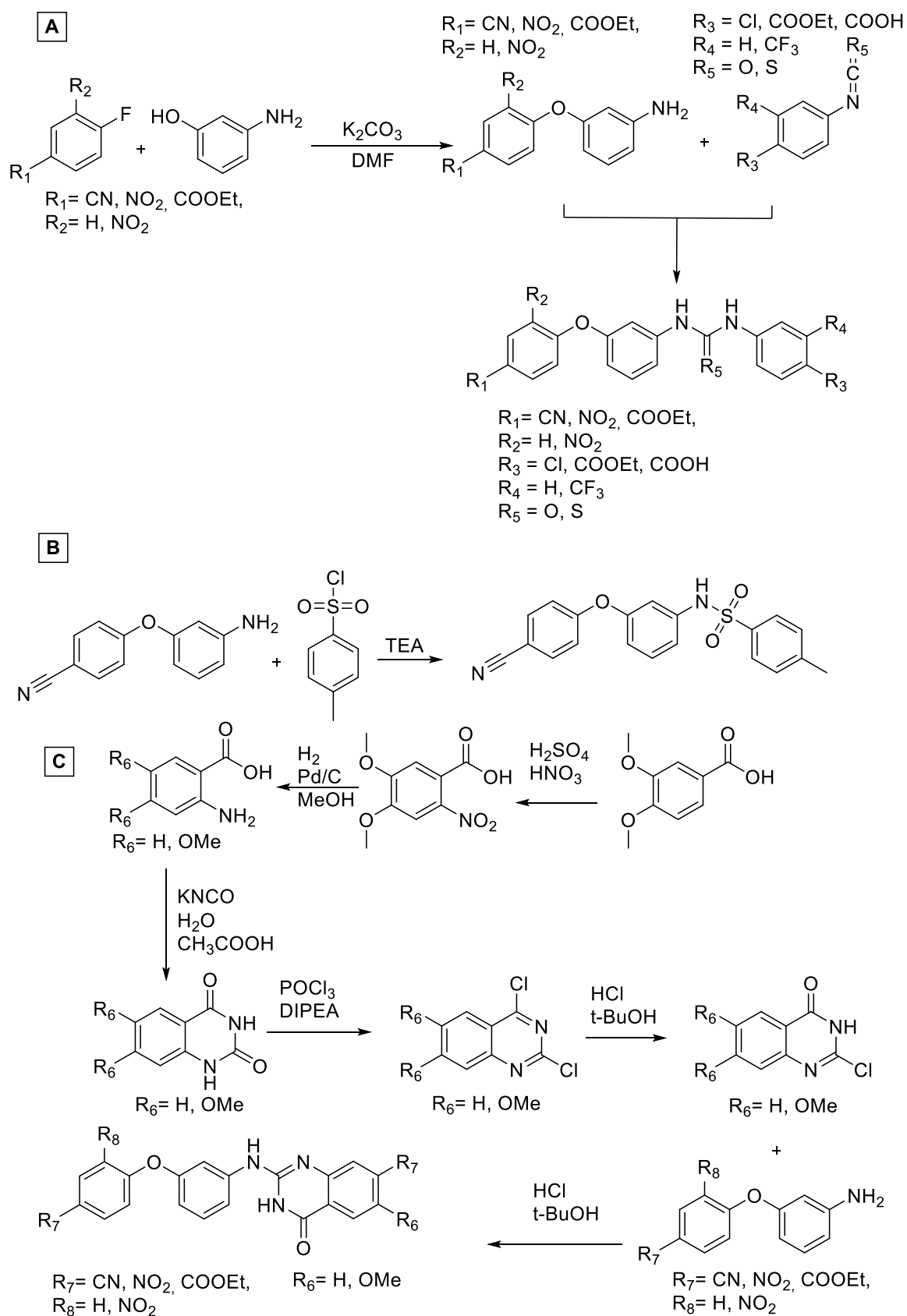
Fluorescence images of cells were taken using a Nikon Eclipse Ti Light Microscope equipped with a Yokogawa spinning-disk confocal scanner unit CSU-W1-T2, two sCMOS cameras (Orca Flash 4.0 V2) and a LUDLPrecision2 stage with a piezo focus. Diode laser was used as light sources: 561nm (200mW) . All images were collected using a 100x CFI Apo TIRF (NA = 1.49) objective with oil-immersion. Emitted light was filtered using the following filters: mCherry (ET630/75) and mCherryLP (ET570LP). The microscope was operated using VisiVIEW (Metamorph) software. For the fluorescence microscopy all the cells were incubated with the fluorescent probe for 1 hour and then they were washed with PBS (0.5 mL). To the Cells were subsequently added 0.3 mL of imaging medium (Fluorobrite©, Thermo Fisher Scientific).

Images

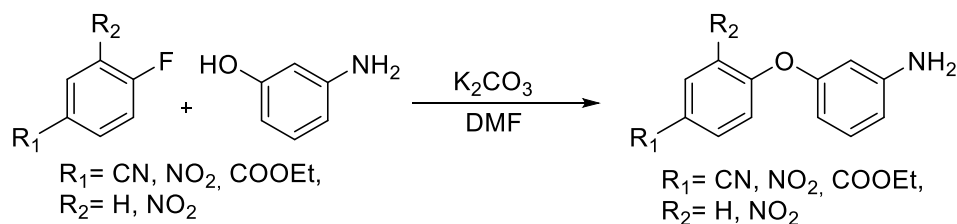
Images obtained from fluorescence microscopy were edited using Fiji (ImageJ 1.5d, NIH).

5.5 SHP-1 methods

5.5.1 Synthesis of SC-43 analogues



Synthesis of the biphenyl synthons



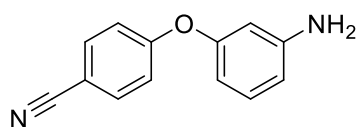
The illustrated procedure has been adopted for all the synthesized biphenyl compound.

In a round bottom flask the desired fluorinated phenyl ring (1.0 equivalents) is dissolved in 0.7 mL/mmol of DMF. To this mixture, 1.0 equivalents of *m*-aminophenol and 1.0 equivalent of potassium carbonate have been added. The mixture has been heated up at 90°C for 3 hours. The progression of the reaction has been monitored by TLC (n-hexane:EtOAc, 1:1). After completion the mixture has been cooled down in an ice bath and 10.0 mL of deionised water have been added. The formed precipitate has been filtered off under vacuum and washed with water. The white powder was the desired intermediates.

Yields: 85-97%

Characterisation:

Compound 1: 4-(3-aminophenoxy)benzonitrile



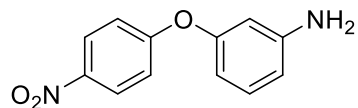
Chemical Formula: $\text{C}_{13}\text{H}_{10}\text{N}_2\text{O}$

Molecular Weight: 210,2360

^1H NMR (300 MHz, DMSO) δ 7.86 – 7.76 (m, 2H), 7.07 (ddd, $J = 6.2, 4.5, 2.1$ Hz, 3H), 6.44 (ddd, $J = 8.1, 2.1, 0.9$ Hz, 1H), 6.26 (t, $J = 2.2$ Hz, 1H), 6.21 (ddd, $J = 7.9, 2.3, 0.9$ Hz, 1H), 5.35 (bs, 2H).

Yield: 91%

Compound 2: 3-(4-nitrophenoxy)aniline



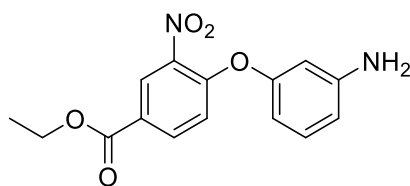
Chemical Formula: C₁₂H₁₀N₂O₃

Molecular Weight: 230,2230

¹H NMR (400 MHz, CDCl₃) δ 8.23 – 8.16 (m, 2H), 7.19 (t, *J* = 8.0 Hz, 1H), 7.08 – 7.00 (m, 2H), 6.57 (ddd, *J* = 8.1, 2.2, 0.8 Hz, 1H), 6.46 (ddd, *J* = 8.0, 2.3, 0.8 Hz, 1H), 6.41 (t, *J* = 2.2 Hz, 1H), 3.84 (bs, 2H).

Yield: 97%

Compound 3: ethyl 4-(3-aminophenoxy)-3-nitrobenzoate



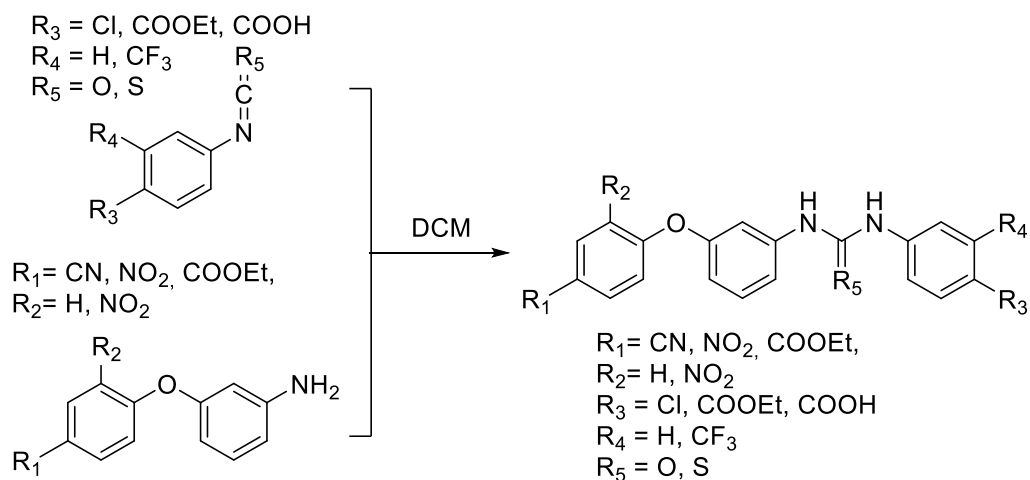
Chemical Formula: C₁₅H₁₄N₂O₅

Molecular Weight: 302,2860

¹H NMR (400 MHz, CDCl₃) δ 8.59 (s, 1H), 8.12 (d, *J* = 8.6 Hz, 1H), 7.18 (t, *J* = 8.0 Hz, 1H), 7.04 (d, *J* = 8.8 Hz, 1H), 6.57 (d, *J* = 7.8 Hz, 1H), 6.51 – 6.40 (m, 3H), 4.41 (q, *J* = 7.0 Hz, 2H), 1.42 (t, *J* = 7.1 Hz, 3H).

Yield: 85%

Synthesis of the final compounds with an ureido or thioureido function



The illustrated protocol has been adopted for the synthesis of all the final compounds that present an ureido or thioureido group.

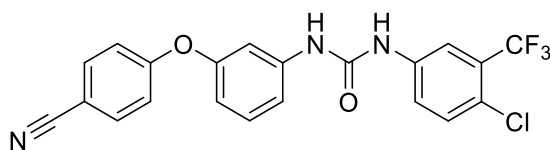
In a well dried round bottom flask and under nitrogen atmosphere, the desired biphenyl compound (1.0 equivalents) has been dissolved in DCM (6 mL/mmol) and then the chosen isocyanate or isothiocyanate has been added (1.0 equivalents). The mixture has been stirred at room temperature for 6 hours. The progression of the reaction has been monitored by TLC (DCM:MeOH, 99:1). After the consumption of the two reagents, the organic solvent has been evaporated off under reduced pressure and the obtained residue has been suspended in 2.0 mL of an aqueous solution of HCl (9%). The precipitate has been filtered off under vacuum. The obtained white solid is the desired compound. In some cases, a further purification was necessary and in these cases a column chromatography on silica gel has been adopted, choosing for each compound the adequate eluting system.

Yield: 30-80%

For what concern compound EZ2, it has been obtained by acidic hydrolysis of the methyl ester derivative in HCl 1M at reflux for 1 hour.

Characterisation:

Final compound **SC-43:** 1-(4-chloro-3-(trifluoromethyl)phenyl)-3-(3-(4-cyanophenoxy)phenyl)urea



Chemical Formula: $C_{21}H_{13}ClF_3N_3O_2$

Molecular Weight: 431,7992

1H NMR (400MHz, $CDCl_3$): δ 9.17 (s,1H), 8.94 (s,1H), 8.10 (s,1H), 7.81 (d, 2H, $J = 6.8$), 7.63e7.59 (m, 2H), 7.54 (d, 2H, $J = 7.2$ Hz), 7.10 (d, 2H, $J = 6.8$ Hz), 7.05 (d, 2H, $J = 7.2$ Hz).

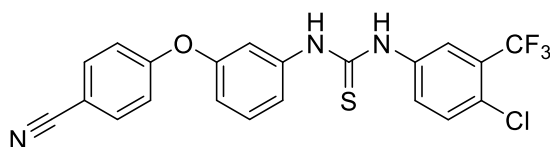
^{13}C NMR (100 MHz, MeOD): δ 163.7, 163.6, 154.8, 151.4, 151.2, 140.1, 137.7, 137.4, 135.3, 132.9, 129.7, 129.4, 129.1, 128.8, 128.3, 125.6, 125.5, 125.4, 124.2, 122.9, 122.4, 122.3, 122.1, 120.2, 119.7, 118.8, 118.7, 118.6, 118.6, 106.5, 106.4;

HRMS (ESI): calcd. (M+H)⁺ 432.0721, exper. 432.0741.

HPLC-UV: 99% purity (area at 254nm).

Yield: 70%

Final compound **EZ1:** 1-(4-chloro-3-(trifluoromethyl)phenyl)-3-(3-(4-cyanophenoxy)phenyl)thiourea



Chemical Formula: $C_{21}H_{13}ClF_3N_3OS$

Molecular Weight: 447,8602

1H NMR (400 MHz, DMSO) δ 10.21 (s, 2H), 8.08 (d, $J = 2.3$ Hz, 1H), 7.85 (d, $J = 8.8$ Hz, 2H), 7.80 (dd, $J = 8.7, 2.3$ Hz, 1H), 7.66 (d, $J = 8.7$ Hz, 1H), 7.44 (t, $J = 8.1$ Hz, 1H), 7.39 (d, $J = 1.9$ Hz, 1H), 7.33 (d, $J = 8.0$ Hz, 1H), 7.16 (d, $J = 8.8$ Hz, 2H), 6.94 (dd, $J = 8.0, 1.7$ Hz, 1H).

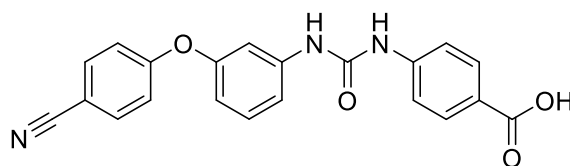
^{13}C NMR (101 MHz, DMSO) δ 180.15, 161.23, 154.91, 141.34, 139.54, 135.06, 132.04, 130.83, 128.92, 126.90, 126.59, 125.75, 124.52, 122.87, 122.81, 121.81, 120.32, 119.12, 118.72, 116.63, 115.61, 105.78.

HRMS (ESI): calcd. (M+H)⁺ 452.0493, exper. 452.0514.

HPLC-UV: 99% purity (area at 254nm).

Yield: 30%

Final compound EZ2: 4-(3-(3-(4-cyanophenoxy)phenyl)ureido)benzoic acid



Chemical Formula: C₂₁H₁₅N₃O₄

Molecular Weight: 373,3680

¹H NMR (400 MHz, DMSO) δ 9.31 (d, *J* = 30.8 Hz, 2H), 7.90 (t, *J* = 9.0 Hz, 4H), 7.61 (t, *J* = 7.7 Hz, 2H), 7.47 (s, 1H), 7.46 – 7.39 (m, 1H), 7.28 (d, *J* = 8.3 Hz, 1H), 7.18 (d, *J* = 8.7 Hz, 2H), 6.81 (d, *J* = 7.9 Hz, 1H).

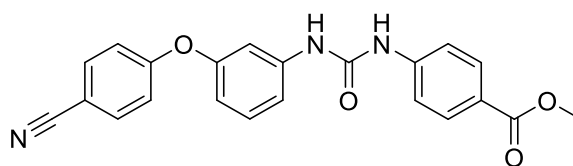
¹³C NMR (101 MHz, DMSO) δ 167.50, 161.45, 155.37, 152.64, 144.22, 144.13, 141.81, 135.09, 130.99, 124.26, 119.20, 118.66, 117.85, 117.77, 115.27, 113.97, 110.13, 105.59.

HRMS (ESI): calcd. (M+H)⁺ 374.3755, exper. 374.3772.

HPLC-UV: 92% purity (area at 254nm).

Yield: 32%

Final compound EZ3: methyl 4-(3-(3-(4-cyanophenoxy)phenyl)ureido)benzoate



Chemical Formula: C₂₂H₁₇N₃O₄

Molecular Weight: 387,3950

¹H NMR (400 MHz, DMSO) δ 9.20 (s, 1H), 9.08 (s, 1H), 7.86 (dd, *J* = 11.1, 8.8 Hz, 4H), 7.58 (d, *J* = 8.7 Hz, 2H), 7.43 (d, *J* = 1.9 Hz, 1H), 7.37 (t, *J* = 8.1 Hz, 1H), 7.24 (d, *J* = 8.1 Hz, 1H), 7.14 (d, *J* = 8.7 Hz, 2H), 6.77 (dd, *J* = 8.0, 1.8 Hz, 1H), 3.81 (s, 3H).

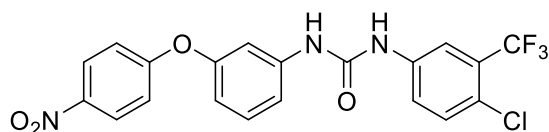
¹³C NMR (101 MHz, DMSO) δ 166.37, 161.44, 155.39, 152.55, 144.63, 141.79, 135.09, 131.00, 130.84, 123.27, 123.09, 119.18, 118.68, 118.02, 117.91, 115.34, 113.99, 110.22, 105.64, 52.23.

HRMS (ESI): calcd. (M+H)⁺ 388.1292, exper. 388.1305.

HPLC-UV: 96% purity (area at 254nm).

Yield: 50%

Final compound **EZ5:** 1-(4-chloro-3-(trifluoromethyl)phenyl)-3-(3-(4-nitrophenoxy)phenyl)urea



Chemical Formula: $C_{20}H_{13}ClF_3N_3O_4$

Molecular Weight: 451,7862

1H NMR (400 MHz, DMSO) δ 9.95 (s, 2H), 8.30 – 8.20 (m, 2H), 8.07 (d, $J = 2.4$ Hz, 1H), 7.67 (dd, $J = 8.8, 2.3$ Hz, 1H), 7.55 (d, $J = 8.8$ Hz, 1H), 7.46 (t, $J = 2.0$ Hz, 1H), 7.34 (dt, $J = 8.4, 4.8$ Hz, 2H), 7.18 – 7.09 (m, 2H), 6.77 (dd, $J = 4.5, 3.3$ Hz, 1H).

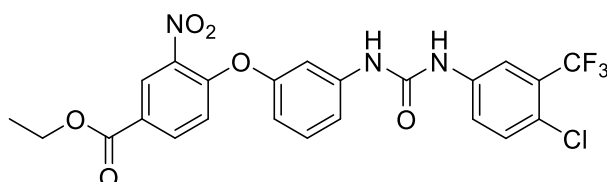
^{13}C NMR (101 MHz, DMSO) δ 163.30, 155.05, 153.07, 142.69, 142.18, 139.98, 132.33, 130.98, 127.26, 126.96, 126.62, 124.62, 123.48, 122.62, 121.91, 117.80, 117.21, 115.77, 114.08, 110.60.

HRMS (ESI): calcd. (M+H)⁺ 452.0619, exper. 452.0624.

HPLC-UV: 97% purity (area at 254nm).

Yield: 80%

Final compound **EZ6:** ethyl 4-(3-(3-(4-chloro-3-(trifluoromethyl)phenyl)ureido)phenoxy)-3-nitrobenzoate



Chemical Formula: $C_{23}H_{17}ClF_3N_3O_6$

Molecular Weight: 523,8492

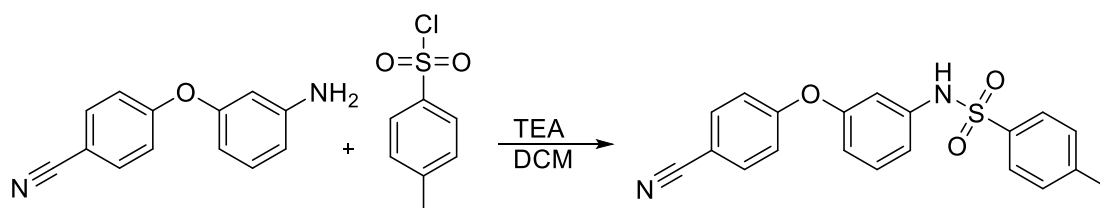
1H NMR (400 MHz, $CDCl_3$) δ 8.52 (d, $J = 2.1$ Hz, 1H), 8.07 (dd, $J = 8.8, 2.2$ Hz, 2H), 8.00 (s, 1H), 7.61 (d, $J = 2.5$ Hz, 1H), 7.32 (dd, $J = 8.7, 2.5$ Hz, 1H), 7.29 – 7.27 (m, 1H), 7.24 (d, $J = 8.7$ Hz, 1H), 7.20 (t, $J = 8.2$ Hz, 1H), 6.94 (d, $J = 8.8$ Hz, 2H), 6.71 – 6.65 (m, 1H), 4.39 (q, $J = 7.1$ Hz, 2H), 1.40 (t, $J = 7.1$ Hz, 3H).

HRMS (ESI): calcd. (M+H)⁺ 524.0831, exper. 524.0847.

HPLC-UV: 98% purity (area at 254nm).

Yield: 65%

Synthesis of the final compound **EZ4**

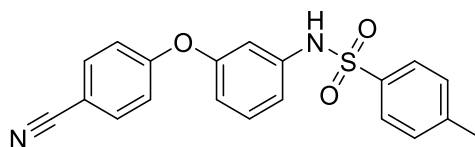


Compound 1 (0.10 g, 0.5 mmol) has been solubilised in 3.0 mL of DCM. To this solution, first 70 μ L of TEA have been added and subsequently tosyl chloride (0.1 g, 0.5 mmol) has been introduced in the reaction mixture. The solution has been heated up at reflux for 3 hours. After completion of the reaction the organic solvent has been removed under reduced pressure. The obtained solid has been suspended in 4 mL of a saturated solution of NaHCO_3 . The obtained precipitate has been filtered off under vacuum and washed with deionised water. The obtained white powder is the desired compound.

Yield: 50%

Characterisation:

Final compound **EZ4**: N-(3-(4-cyanophenoxy)phenyl)-4-methylbenzenesulfonamide



Chemical Formula: $\text{C}_{20}\text{H}_{16}\text{N}_2\text{O}_3\text{S}$

Molecular Weight: 364,4190

^1H NMR (400 MHz, DMSO) δ 10.41 (s, 1H), 7.88 – 7.78 (m, 2H), 7.62 (d, $J = 8.3$ Hz, 2H), 7.37 (d, $J = 8.0$ Hz, 2H), 7.34 – 7.26 (t, $J = 8.2$ Hz, 1H), 7.03 – 6.94 (m, 3H), 6.82 – 6.74 (m, 2H), 2.36 (s, 3H).

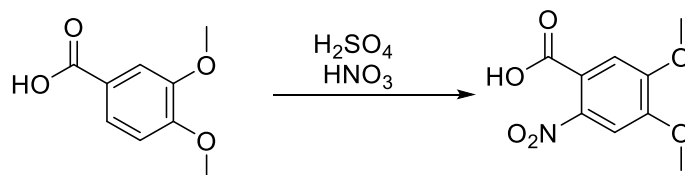
^{13}C NMR (101 MHz, DMSO) δ 161.02, 155.46, 143.91, 140.43, 136.88, 135.09, 131.48, 130.22, 127.16, 119.10, 118.72, 116.68, 115.58, 111.38, 105.91, 21.42.

HRMS (ESI): calcd. (M+H)⁺ 365.0954, exper. 365.0960.

HPLC-UV: 99% purity (area at 254nm).

Yield: 50%

Synthesis of the 4,5-dimethoxy-2-nitrobenzoic acid

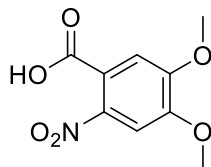


Veratric acid (5.0 g, 27.5 mmol) has been added to a mixture of acetic acid (10.0 mL) and concentrated nitric acid (5.0 mL). The solution has been heated up at 60°C for 40 minutes. Then the mixture has been cooled down in an ice bath and 30 mL of deionised water have been added. The obtained precipitate has been filtered off under vacuum and washed with deionised water. This led to the obtainment of the desired compound as a pale yellow solid.

Yield: 90%

Characterisation:

Compound 4: 4,5-dimethoxy-2-nitrobenzoic acid



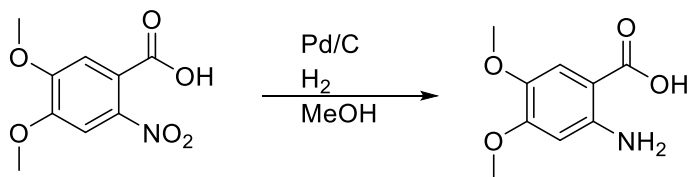
Chemical Formula: C₉H₉NO₆

Molecular Weight: 227,1720

¹H NMR (400 MHz, CDCl₃) δ 7.39 (s, 2H), 7.22 (s, 2H), 3.99 (s, 6H), 3.98 (s, 7H).

Yield: 90%

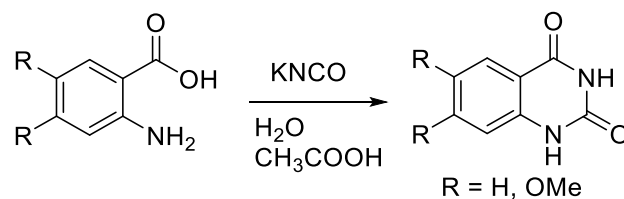
Synthesis of the 2-amino-4,5-dimethoxybenzoic acid (5)



Compound 4 (5.6 g, 25.0 mmol) has been solubilised in 40 mL of MeOH under inert atmosphere. To the solution 540 mg of Pd/C have been added slowly and then the atmosphere within the round bottom flask has been saturated of H₂. The mixture has been stirred at room temperature overnight. The suspension has been filtered on a celite bed and then the liquid phase has been evaporated of under reduced pressure obtaining the desired compound that has been used directly in the following step without further purifications.

Yield: 99%

Synthesis of the quinazolindione cores



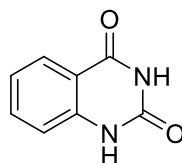
The illustrated protocol has been adopted for the synthesis of all the quinazolindione synthons.

In a round bottom flask anthranilic acid (0.82 g, 6.0 mmol) has been suspended in 36 mL of deionised water. 0.7 mL of acetic acid have been added to the mixture and subsequently the flask has been heated up at 35°C for 15 minutes. After this period, a solution of potassium cyanate (1.21 g, 15.0 mmol) has been added dropwise in the reaction mixture. The reaction has been heated up for further 20 minutes at 35 °C and then it has been cooled down at room temperature. To the mixture 10.0 g of KOH have been added slowly and portion wise under continuous stirring. After the complete addition of the base, the round bottom flask has been cooled down in an ice bath and the pH of the solution has been adjusted to pH 4 with concentrated HCl. The formed precipitate has been filtered of and thoroughly washed with diluted HCl (0.1 M) obtaining the desired compound as a white powder.

Yield: 98%

Characterisation:

Compound 6: quinazoline-2,4(1H,3H)-dione

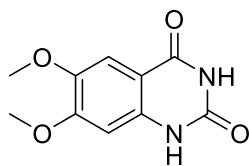


Chemical Formula: $C_8H_6N_2O_2$
Molecular Weight: 162,1480

1H NMR (300MHz, $CDCl_3$): δ : 11.26 (s, 1H), 11.18 (s, 1H), 7.89 (ddd, $J_1 = 7.9$ Hz, $J_2 = 1.6$ Hz, $J_3 = 0.5$ Hz, 1H), 7.64 (td, $J_1 = 7.9$ Hz, $J_2 = 1.6$ Hz, 1H), 7.18 (m, 2H).

Yield: 98%

Compound 7: 6,7-dimethoxyquinazoline-2,4(1H,3H)-dione



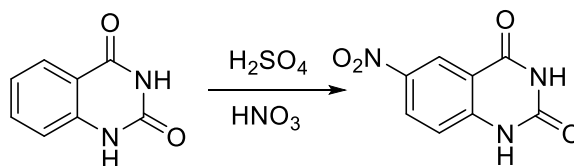
Chemical Formula: C₁₀H₁₀N₂O₄

Molecular Weight: 222,2000

This compound was not pure but after several attempts it resulted to be much more effective and simple to purify it in the following step.

Yield: -

Synthesis of the 6-nitroquinazoline-2,4(1H,3H)-dione

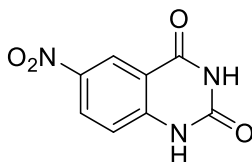


In a round bottom flask compound 6 (0.5 g, 3.0 mmol) has been added to a mixture of concentrated HNO₃ (2 mL) and concentrated H₂SO₄ (3 mL). The mixture has been stirred at room temperature for 30 minutes and then it has been slowly poured in a conical flask containing ice and water in equal quantities. The obtained precipitate has been filtered off under vacuum and washed with deionised water. The obtained solid has been further purified through column chromatography on silica gel (n-heane:EtOAc, 1:1). The resulting pale-yellow compound was the desired synthon.

Yield: 20%

Characterisation:

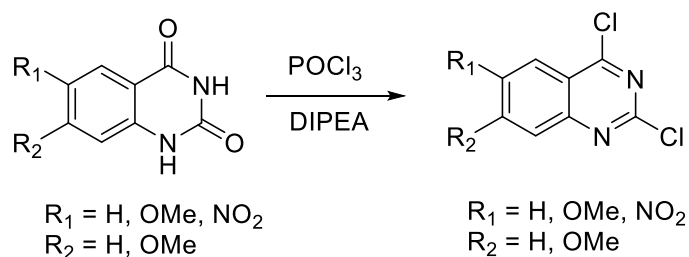
Compound 8: 6-nitroquinazoline-2,4(1H,3H)-dione



¹H NMR (400 MHz, DMSO) δ 8.59 (d, *J* = 2.7 Hz, 1H), 8.42 (ddd, *J* = 9.0, 2.7, 0.5 Hz, 1H), 7.38 – 7.24 (m, 1H).

Yield: 20%

Synthesis of the dichloroquinazoline synthons



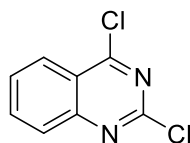
The reported procedure has been exploited for the obtainment of all the dichloroquinazolines used in this project.

In a round bottom flask the desired quinazolinone core (6 equivalents), 5 mL of POCl_3 and 2.5 mL of DIPEA have been mixed in the mentioned order cooling during the addition of the last two in ice bath the glassware. The mixture has been heated at 110°C for 3 hours and then it has been cooled first at room temperature and then in an ice bath. Subsequently, a mixture of water and ice has been added obtaining the formation of a thick precipitate that has been filtered off and thoroughly washed with fresh water for removing the excess of base and acid. The obtained white solid was the desired compound.

Yield: 30-98%

Characterisation:

Compound 9: 2,4-dichloroquinazoline

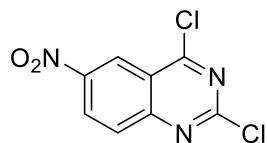


Chemical Formula: $\text{C}_8\text{H}_4\text{Cl}_2\text{N}_2$
Molecular Weight: 199,0340

^1H NMR (400 MHz, DMSO) δ 8.31 (ddd, $J = 8.4, 1.4, 0.6$ Hz, 1H), 8.17 (ddd, $J = 8.4, 7.0, 1.4$ Hz, 1H), 8.04 (ddd, $J = 8.5, 1.1, 0.7$ Hz, 1H), 7.91 (ddd, $J = 8.3, 7.0, 1.2$ Hz, 1H).

Yield: 98%

Compound 10: 2,4-dichloro-6-nitroquinazoline



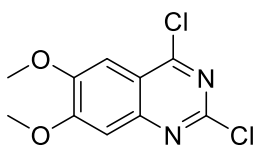
Chemical Formula: $C_8H_3Cl_2N_3O_2$

Molecular Weight: 244,0310

1H NMR (300 MHz, DMSO) δ 8.75 (dd, $J = 2.7, 0.4$ Hz, 1H), 8.57 (dd, $J = 9.0, 2.7$ Hz, 1H), 7.81 (dd, $J = 9.0, 0.4$ Hz, 1H).

Yield: 30%

Compound 11: 2,4-dichloro-6,7-dimethoxyquinazoline



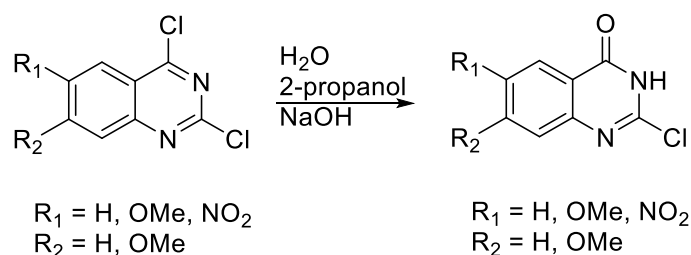
Chemical Formula: $C_{10}H_8Cl_2N_2O_2$

Molecular Weight: 259,0860

1H NMR (300 MHz, DMSO) δ 7.47 (s, 1H), 7.40 (s, 1H), 4.02 (s, 3H), 4.01 (s, 3H).

Yield: 19% over 4 steps from veratric acid

Synthesis of the chloroquinazolin-4(3H)-one synthons



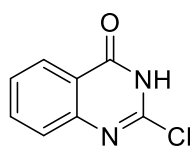
The reported procedure has been exploited for the obtainment of all the chloroquinazolin-4(3H)one used in this project.

In a round bottom flask the desired dichloroquinazoline core (1 equivalent) has been suspended in a mixture composed by 13.0 mL of H₂O, 13.0 mL of isopropanol and 532 mg of NaOH. The suspension has been heated up at 80°C for 4 hours. The progression of the reaction has been monitored by TLC (n-hexane:EtOAc, 1:1). After completion the mixture has been cooled down to room temperature and 1.2 mL of concentrated hydrochloric acid have been added dropwise obtaining the formation of a precipitate. The solid has been filtered off under vacuum and washed with deionised water. The obtained powder was the desired compound.

Yield: 70-92%

Characterisation:

Compound 12: 2-chloroquinazolin-4(3H)-one



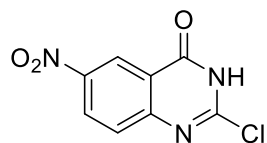
Chemical Formula: C₈H₅ClN₂O

Molecular Weight: 180,5910

¹H NMR (400 MHz, DMSO) δ 8.09 (d, *J* = 7.3 Hz, 1H), 7.84 (t, *J* = 7.6 Hz, 1H), 7.61 (d, *J* = 8.0 Hz, 1H), 7.55 (t, *J* = 7.5 Hz, 1H).

Yield: 74%

Compound 13: 2-chloro-6-nitroquinazolin-4(3H)-one



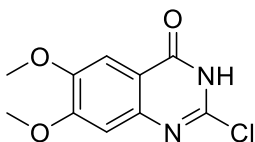
Chemical Formula: $C_8H_4ClN_3O_3$

Molecular Weight: 225,5880

1H NMR (400 MHz, $CDCl_3$): 9.07 (s, 1H), 8.56 (d, $J=8.9$ Hz, 1H), 7.78 (d, $J=8.8$ Hz, 1H).

Yield: 70%

Compound 14: 2-chloro-6,7-dimethoxyquinazolin-4(3H)-one



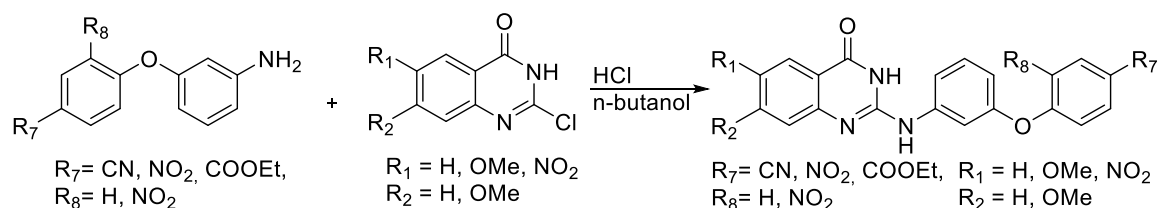
Chemical Formula: $C_{10}H_9ClN_2O_3$

Molecular Weight: 240,6430

1H NMR (400 MHz, DMSO) δ 13.09 (s, 1H), 7.41 (s, 1H), 7.12 (s, 1H), 3.90 (s, 3H), 3.88 (s, 3H).

Yield: 92%

Synthesis of the final compounds with a quinazolinone core



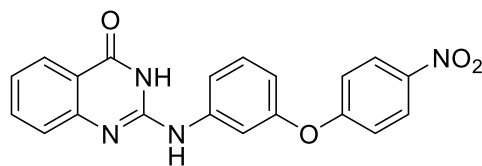
The reported procedure has been exploited for the obtainment of all the final compounds with a quinazolinone core.

The desired chloroquinazolinone core (1 equivalent) and aminobiphenyl (1 equivalent) have been suspended in 4.0 mL/mmol of n-butanol in a small vial with screw cap. 100 μ L/mmol of concentrated HCl have been added to the mixture. The vial has been closed and heat up at 90°C for 1 hour. The progression of the reaction has been monitored by TLC (n-hexane:EtOAc, 6:4). After completion of the reaction, the mixture has been cooled down to room temperature. The solvent has been removed under nitrogen flux. To the solid residue, 2.0 mL/mmol of a saturated solution of NaHCO₃ have been added and the formed precipitate has been filtered off under vacuum, obtaining the desired final compound.

Yield: 68-99%

Characterisation:

Compound EZ7: 2-((3-(4-nitrophenoxy)phenyl)amino)quinazolin-4(3H)-one



Chemical Formula: C₂₀H₁₄N₄O₄

Molecular Weight: 374,3560

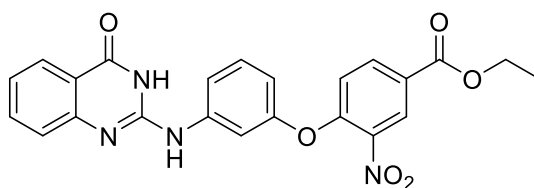
¹H NMR (300 MHz, DMSO) δ 9.25 (bs, 1H), 8.35 – 8.25 (m, 2H), 7.97 (dd, $J = 7.9, 1.1$ Hz, 1H), 7.80 (s, 1H), 7.68 – 7.60 (m, 1H), 7.49 – 7.44 (m, 2H), 7.34 – 7.20 (m, 4H), 6.88 (m, 1H).

HRMS (ESI): calcd. (M+H)⁺ 375.1088, exper. 375.1092.

HPLC-UV: 96% purity (area at 254nm).

Yield: 86%

Compound **EZ8:** ethyl 3-nitro-4-(3-((4-oxo-3,4-dihydroquinazolin-2-yl)amino)phenoxy)benzoate



Chemical Formula: C₂₃H₁₈N₄O₆
Molecular Weight: 446,4190

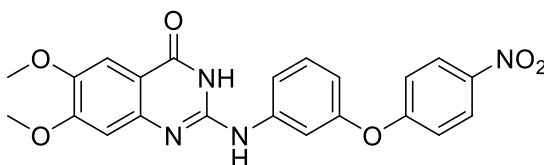
¹H NMR (300 MHz, DMSO) δ 9.05 (s, 1H), 8.57 (d, *J* = 2.1 Hz, 1H), 8.24 (dd, *J* = 8.8, 2.2 Hz, 1H), 7.96 (dd, *J* = 8.1, 1.5 Hz, 1H), 7.85 (s, 1H), 7.67 – 7.58 (m, 1H), 7.44 (dd, *J* = 4.8, 2.1 Hz, 2H), 7.31 (d, *J* = 8.8 Hz, 1H), 7.28 – 7.20 (m, 2H), 6.88 (dt, *J* = 6.8, 2.4 Hz, 1H), 4.37 (q, *J* = 7.1 Hz, 2H), 1.34 (t, *J* = 7.1 Hz, 3H).

HRMS (ESI): calcd. (M+H)⁺ 447.1299, exper. 447.1312.

HPLC-UV: 99% purity (area at 254nm).

Yield: 99%

Compound **EZ9:** 6,7-dimethoxy-2-((3-(4-nitrophenoxy)phenyl)amino)quinazolin-4(3H)-one



Chemical Formula: C₂₂H₁₈N₄O₆
Molecular Weight: 434,4080

¹H NMR (400 MHz, DMSO) δ 10.71 (s, 1H), 8.25 (d, *J* = 8.8 Hz, 2H), 7.95 (s, 1H), 7.60 (d, *J* = 7.9 Hz, 1H), 7.39 (t, *J* = 8.0 Hz, 1H), 7.32 (s, 1H), 7.20 (d, *J* = 8.8 Hz, 2H), 6.75 (d, *J* = 6.3 Hz, 2H), 3.80 (s, 3H), 3.79 (s, 3H).

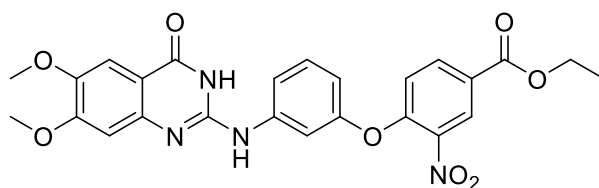
¹³C NMR (101 MHz, DMSO) δ 168.33, 162.79, 154.82, 154.70, 148.51, 146.07, 142.36, 142.17, 130.41, 126.18, 117.90, 115.59, 112.84, 110.91, 110.30, 106.25, 105.71, 55.66.

HRMS (ESI): calcd. (M+H)⁺ 435.1299, exper. 435.1313.

HPLC-UV: 98% purity (area at 254nm).

Yield: 94%

Compound EZ10: ethyl 4-(3-((6,7-dimethoxy-4-oxo-3,4-dihydroquinazolin-2-yl)amino)phenoxy)-3-nitrobenzoate



Chemical Formula: C₂₅H₂₂N₄O₈

Molecular Weight: 506,4710

¹H NMR (400 MHz, DMSO) δ 9.16 (s, 1H), 8.48 (s, 1H), 8.14 (d, *J* = 8.6 Hz, 1H), 7.94 (s, 1H), 7.39 (d, *J* = 3.9 Hz, 2H), 7.31 – 7.20 (m, 2H), 6.79 (d, *J* = 3.6 Hz, 1H), 6.71 (s, 1H), 4.31 (q, *J* = 7.0 Hz, 2H), 3.78 (s, 3H), 3.77 (s, 3H), 1.31 (t, *J* = 7.0 Hz, 3H).

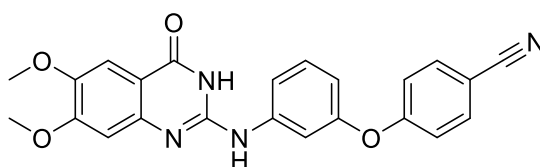
¹³C NMR (101 MHz, DMSO) δ 163.70, 154.99, 154.78, 153.35, 146.29, 141.42, 140.29, 135.18, 130.54, 126.70, 124.93, 120.47, 115.67, 112.63, 110.84, 109.62, 106.39, 105.58, 61.59, 55.62, 14.11.

HRMS (ESI): calcd. (M+H)⁺ 507.1510, exper. 507.1531.

HPLC-UV: 99% purity (area at 254nm).

Yield: 95%

Compound EZ11: 4-(3-((6,7-dimethoxy-4-oxo-3,4-dihydroquinazolin-2-yl)amino)phenoxy)benzonitrile



Chemical Formula: C₂₃H₁₈N₄O₄

Molecular Weight: 414,4210

¹H NMR (400 MHz, DMSO) δ 8.51 (s, 1H), 7.88 (d, *J* = 8.4 Hz, 2H), 7.73 (s, 1H), 7.49 – 7.34 (m, 2H), 7.31 (s, 1H), 7.22 (d, *J* = 8.4 Hz, 2H), 6.85 (d, *J* = 7.3 Hz, 1H), 6.77 (s, 1H), 3.86 (s, 3H), 3.81 (s, 3H).

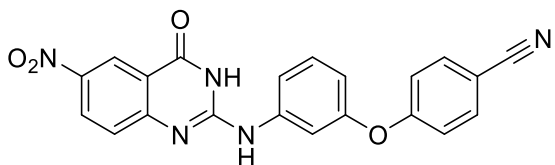
¹³C NMR (101 MHz, DMSO) δ 160.68, 160.53, 155.32, 154.92, 147.26, 146.49, 134.63, 130.69, 118.82, 118.72, 110.29, 105.75, 105.44, 55.85, 55.66.

HRMS (ESI): calcd. (M+H)⁺ 415.1401, exper. 415.1427.

HPLC-UV: 97% purity (area at 254nm).

Yield: 68%

Compound EZ12: 4-(3-((6-nitro-4-oxo-3,4-dihydroquinazolin-2-yl)amino)phenoxy)benzonitrile



Chemical Formula: C₂₁H₁₃N₅O₄

Molecular Weight: 399,3660

¹H NMR (400 MHz, DMSO) δ 11.42 (s, 1H), 9.40 (s, 1H), 8.67 (d, *J* = 2.6 Hz, 1H), 8.37 (dd, *J* = 9.0, 2.7 Hz, 1H), 7.90 (d, *J* = 8.7 Hz, 2H), 7.73 (s, 1H), 7.46 (d, *J* = 5.9 Hz, 2H), 7.39 (d, *J* = 9.0 Hz, 1H), 7.21 (d, *J* = 8.7 Hz, 2H), 6.93 – 6.83 (m, 1H).

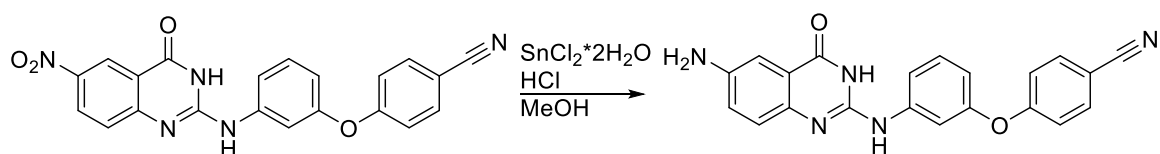
¹³C NMR (101 MHz, DMSO) δ 161.18, 155.53, 142.50, 140.43, 138.81, 135.16, 131.06, 128.99, 122.79, 119.12, 118.44, 117.05, 115.04, 112.11, 105.94.

HRMS (ESI): calcd. (M+H)⁺ 400.1040, exper. 400.1053.

HPLC-UV: 96% purity (area at 254nm).

Yield: 90%

Synthesis of the final compound **EZ13**

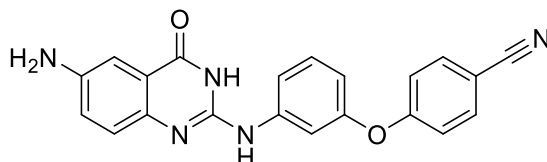


In a round bottom flask solubilize EZ12 (0.2 g, 0.5 mmol) in 2 mL of MeOH. In another flask a fresh solution of $\text{SnCl}_2 \cdot 2\text{H}_2\text{O}$ (0.56 g, 2.5 mmol) in concentrated HCl (1 mL) has been prepared. This last solution has been added dropwise in the first one and the mixture has been heated up at reflux for 1 hour. The mixture has been cooled down to room temperature and 5 mL of H_2O have been added. The pH of the solution has been adjusted to a value of 6 using an aqueous solution of NaOH 1M. The formed precipitate has been filtered off under vacuum and washed with deionised water obtaining the desired final compound.

Yield: 74%

Characterisation:

Compound **EZ13**: 4-(3-((6-amino-4-oxo-3,4-dihydroquinazolin-2-yl)amino)phenoxy)benzonitrile



Chemical Formula: $\text{C}_{21}\text{H}_{15}\text{N}_5\text{O}_2$
Molecular Weight: 369,3840

^1H NMR (300 MHz, MeOD) δ 8.05 (m, 1H), 7.78 (d, $J = 9.0$ Hz, 2H), 7.72 (dd, $J = 9.0$, 2.6 Hz, 1H), 7.60 (m, 2H), 7.49 – 7.43 (m, 1H), 7.40 (m, 1H), 7.22 (d, $J = 9.0$ Hz, 2H), 7.15 (t, $J = 7.1$ Hz, 1H).

^{13}C NMR (101 MHz, DMSO) δ 161.26, 155.63, 148.62, 140.71, 135.15, 131.12, 119.12, 105.87.

HRMS (ESI): calcd. $(\text{M}+\text{H})^+$ 370.1299, exper. 400.1315.

HPLC-UV: 95% purity (area at 254nm).

Yield: 74%

5.5.2 Biological experiments

Isolation of lymphocytes from the peripheral blood

Lymphocytes have been isolated from the peripheral blood of patients affected by B-CLL and LGLL. The biological samples were obtained through a venous heparinised blood sample, stratified on Ficoll/hypaque (F/H). Considering the high leucocyte count, a dilution of the blood sample has been made using a physiological solution, with a ratio of 1:6, shaking gently the sample before and during the F/H separation. The sample has been centrifuged at 900 G for 20 minutes at 20°C. The cells located on the upper part of the F/H layer have been collected and subsequently washed twice with a physiological solution and centrifuged at 400 G for 10 minutes. After resuspension of the formed pellet in an adequate buffer solution, the cells have been counted through Burker chamber.

Cell cultures of B-CLL and LGLL

The isolated lymphocytes have been aliquoted and suspended in complete terrain constituted by RPMI 1640 and FBS 10% with a concentration of 10×10^6 cells/mL for what concern the B-LLC and 2×10^6 cells/mL for the LGLL. After the addition of the desired compounds, the cells have been incubated at 37°C in humidified atmosphere containing a 5% level of CO₂. Several aliquots have been sampled at different incubation times for evaluating the apoptosis.

Electrophoresis on polyacrylamide gel in SDS (SDS-PAGE)

The cell lysates have been boiled 5 minutes with β-mercaptoethanol and SDS (1.25 ml 1 M Tris-HCl (pH 6.8), 4.0 ml 10% (w/v) SDS, 2.0 ml glycerol, 0.5 ml 0.5 M EDTA, 4 mg bromophenol blue, 0.2 ml β-mercaptoethanol (14.3 M), bring the volume to 10 ml with ddH₂O). The polyacrylamide gel has been prepared following the Laemmli method. The electrophoretic apparatus is a Mighty small-se 250 (Hoefer scientific instruments). The running buffer was constituted by: Tris 50mM, glycine 0.38M ed SDS 3.4mM. The separation last for 1.5 hours at 40 mA/gel.

Western blotting and antibody revelation

The different cell lysates have been subjected to electrophoretic separation. The obtained gels have been putted to direct contact with a nitrocellulose membrane and sandwiched between two papers of Whatman 3MM Chr. Through electric current (350 mA for 2.5 hours) the protein spots have been transferred to the nitrocellulose membrane. For this step a buffer constituted by Tris 25mM, glycine 192mM, methanol 20%, SDS 0.1% at pH 8.0 has been used. After the electro-transferring, the membrane has been saturated for 1 hour using buffer A (Tris/HCl 50mM pH7.5, NaCl 150 mM, BSA 3%). The following step has been the incubation overnight at 4°C, or for 2.5 hours

at room temperature, with a primary antibody diluted in buffer B (Tris/HCl 50mM pH7.5, NaCl 150mM, BSA 1%, NaN₃ 0.02% and Tween 0.1%). Three washes of 5 minutes each using buffer C (Tween 0.1%, Tris 50mM pH7.5 and NaCl 150mM) have been made. The membrane has been incubated for 30 minutes with a secondary antibody conjugated with the horseradish peroxidase in buffer: Tris/HCl 50mM pH7.5, NaCl 150mM and BSA 1%. Three more washes with buffer C have been made. The fluorescence revelation has been done with the ECL system (Enhanced ChemiLuminescence). The membrane has been treated with luminol and coumaric acid, opportunely dissolved in a Tris/HCl buffer 0.1M at pH 8.1. Above the sample a photographic plate has been impressed and subsequently processed.

Evaluation of the apoptosis through cytofluorimetry

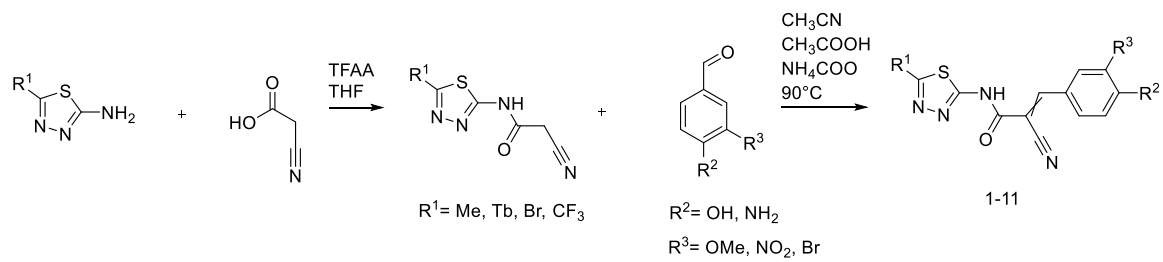
The apoptosis' degree has been evaluated using the *Annexin V Apoptosis Detection Kit*. After the different treatments with the different SC-43 analogues, aliquots of the various biological sample have been taken (500x10³ cells). The cells have been washed and then incubated for 10 minutes in the dark and room temperature with 100 µL of binding buffer (that contains Ca²⁺), 5 µL of AnnexinV-FITC and 10 µL of propidium iodide at a final concentration of 1 µg/mL. After the incubation, other 100 µL of binding buffer have been added and then the cells have been analysed through flux cytofluorometer FACScan. For each sample 20'000 measurements have been acquired and the number of apoptotic cells has been expressed as % of cells positives to the AnnexinV over the totality of the analysed (software FacsDiva). For differentiating the various apoptotic cells from the others, the following antibodies have been used: AnnexinV-FITC, anti-CD5 PE-Cy5 and anti-CD19 APC.

5.5.3 Docking studies

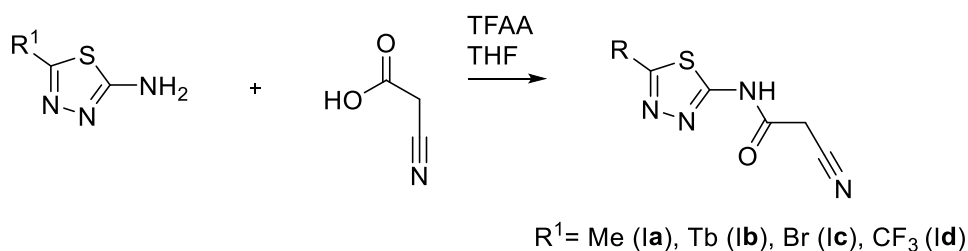
All the compounds used for these computational studies have been drawn with ChemDraw and then minimized with Avogadro.^[160] For the process of minimization, the appropriate hydrogen atoms were added to all the drawn compounds, considering an environmental pH of 7.4. All the structures have been minimized using the MMFF94 forcefield. For what concerns the choice of the enzymatic crystal structure used for the docking assays, both the active and inactive conformation have been used for the docking studies (active: PDB: 3PS5, inactive: PDB: 2B3O). The PDB structures were optimized for the docking studies. All the hydrogens were added considering a pH of 7.4. After the preparation of the PDB files of SHP-1 and of the small molecules, a rough massive screening has been performed with all the SC-43 analogues synthesized by Chen and co-workers, using the software PyRx (<https://pyrx.sourceforge.io/>). In this first part of the virtual screening, both the two crystal structures of SHP-1 have been used. The whole surface area of the enzyme was used for the docking process (*blind docking*). An average of the energies of interactions (Kcal/mol) obtained with the two different PDB structures have been calculated. The active conformation resulted to be more promising and the majority of the tested compounds interact principally with the N-SH2. SC-43 has been chosen as a model and it has been used for refining the docking pose. A further set of docking experiments has been performed using 3PS5 and SC-43 as a model and Autodock Vina^[161] as docking software. Firstly, another blind docking has been performed on the whole enzyme surface and then focusing on just the N-SH2 domain. The obtained complexes were analyzed using BIOVIA Discovery Studio and the relative 2D interaction plots were obtained with the same software.^[162]

5.6 CK2 methods

5.6.1 Synthesis of the SRPIN803 analogues



General synthesis of the compounds **Ia**, **Ib**, **Ic**, **Id**.

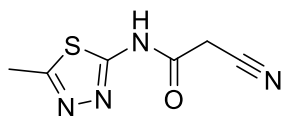


Trifluoroacetic anhydride (1eq) and 1.1 equivalents of cyanoacetic acid were added in a round bottom flask. Suddenly THF (1mL per mmol) was added and finally 1 equivalent of the thiadiazole reactant was introduced within the reaction mixture. The reaction was stirred at room temperature and the completeness of the reaction was checked by TLC (EtOAc/Hexane 6/4). If the reaction was not completed, a mixture of 1:1 trifluoroacetic anhydride and cyanoacetic acid in THF was added. After completion of the reaction 3mL of H₂O per mmol were added and then the reaction was basified to pH 8 with NaHCO₃. In case of precipitate it was filtered off and dried, otherwise the aqueous phase was extracted with EtOAc three times. The organic phase was dried with magnesium sulphate and then it was concentrate under reduced pressure till the obtainment of a cream solid.

Yield: 85-91%

Characterisation:

Compound **Ia**: 2-cyano-N-(5-methyl-1,3,4-thiadiazol-2-yl)acetamide



Chemical Formula: C₆H₆N₄OS

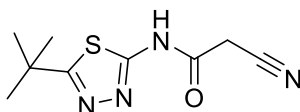
Molecular Weight: 182,2010

¹H NMR (400 MHz, DMSO-*d*₆) δ 2.62 (s, 3H), 4.07 (s, 2H).

HRMS (ESI) found 182.0263, calc. 182.0262.

Yield: 85%.

Compound Ib: N-(5-(tert-butyl)-1,3,4-thiadiazol-2-yl)-2-cyanoacetamide



Chemical Formula: C₉H₁₂N₄OS

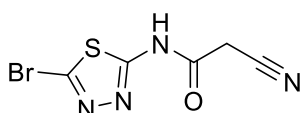
Molecular Weight: 224,2820

¹H NMR (400 MHz, DMSO-*d*₆) δ 1.41 (s, 9H), 4.07 (s, 2H).

HRMS (ESI) found 224.0735, calc. 224.0732.

Yield: 87%.

Compound Ic: N-(5-bromo-1,3,4-thiadiazol-2-yl)-2-cyanoacetamide



Chemical Formula: C₅H₃BrN₄OS

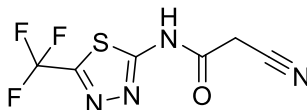
Molecular Weight: 247,0700

¹H NMR (400 MHz, DMSO-*d*₆) δ 4.07 (s, 2H).

HRMS (ESI) found 245.9213, calc. 245.9211.

Yield: 90%.

Compound Id: 2-cyano-N-(5-(trifluoromethyl)-1,3,4-thiadiazol-2-yl)acetamide



Chemical Formula: C₆H₃F₃N₄OS

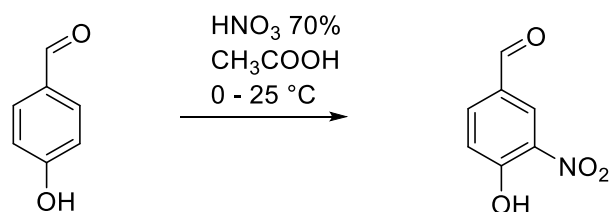
Molecular Weight: 236,1722

¹H NMR (400 MHz, DMSO-*d*₆) δ 4.07 (s, 2H).

HRMS (ESI) found 235.9978, calc. 235.9980.

Yield: 91%.

Synthesis of 4-hydroxy-3-nitrobenzaldehyde^[163]



A round bottom flask containing 4-hydroxybenzaldehyde (610mg, 5mmol) in 1mL of acetic acid was cooled down in an ice bath, avoiding the complete freezing of the solution. 0.45mL of HNO_3 (70%) were dropwise in the solution and then the mixture was warmed up to room temperature. The reaction was stirred at room temperature for 1 hour. The obtained precipitate was filtered off it was washed with hexane.

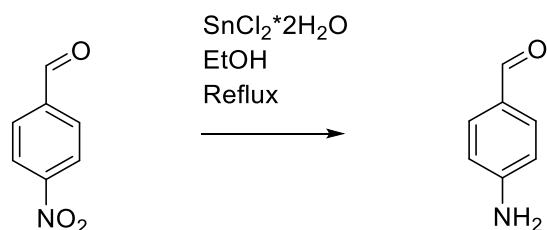
Yield: 46%.

Characterisation:

^1H NMR (400 MHz, $\text{DMSO}-d_6$) δ 7.26 (d, $J = 8.4$ Hz, 1H), 8.01 (dd, $J = 8.4, 2.1$ Hz, 1H), 8.44 (d, $J = 2.1$ Hz, 1H), 9.88 (s, 1H).

HRMS (ESI) found 167.0217, calc. 167.0219.

Synthesis of 4-aminobenzaldehyde^[164]



In a round bottom flask, ethanol (15 mL), then 4-nitrobenzaldehyde (756 mg, 5 mmol) and tin(II) chloride (5,640 mg, 25 mmol) were added. The reaction was allowed to stir under reflux at 70°C for 1 hour. 15 g of ice was stirred into the mixture and the pH was adjusted to pH 8/9. The mixture was filtered under vacuum and the solid extracted with ethyl acetate (3x50 mL). All of the organic phases were combined and evaporated under reduced pressure to give the product as an orange solid.

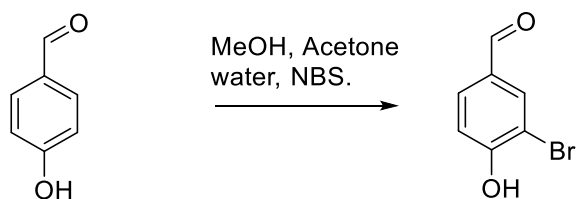
Yield: 63 %.

Characterisation:

^1H NMR (400MHz, CDCl_3): δ 4.25 (bs, 2 H), 6.71 - 6.69 (d, 2 H), 7.71 - 7.69 (d, 2 H), 9.76 (s, 1 H).

HRMS (ESI) found 121.0530, calc. 121.0528.

Synthesis of 3-bromo-4-hydroxybenzaldehyde



To a solution of 4-hydroxybenzaldehyde (610mg, 5mmol) in methanol (10mL), acetone (20mL) and water (5mL), 5 mmol of NBS (880mg) were added. The mixture has been stirred at room temperature for 1 hour and then all the solvents were evaporated under reduced pressure. The solid residue has been sonicated in water (15mL) for 10min. After that, the obtained precipitated was filtered off and discarded. The aqueous solution has been extracted with EtOAc 3 times. All the organic phases were collected together, dried with magnesium sulphate and evaporate of under reduced pressure giving a white solid.

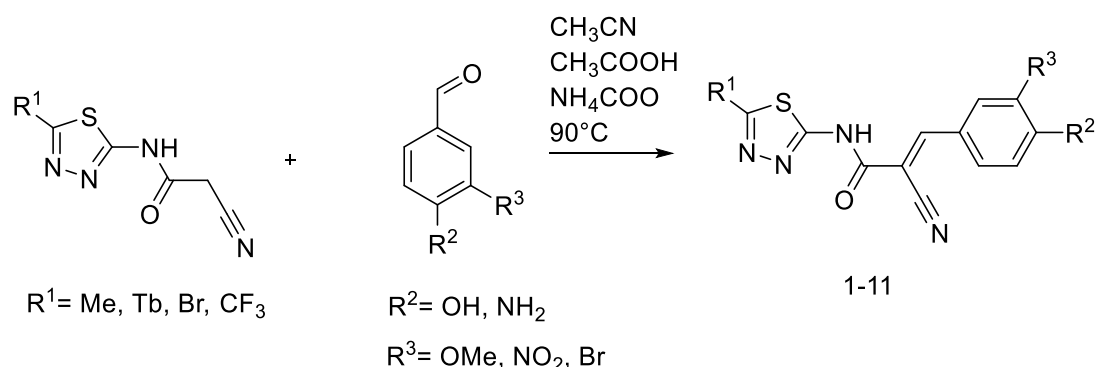
Yield: 54%.

Characterisation:

^1H NMR (400 MHz, DMSO- d_6) δ 7.10 (d, J = 8.4 Hz, 1H), 7.75 (dd, J = 8.4, 2.0 Hz, 1H), 8.02 (d, J = 2.0 Hz, 1H), 9.77 (s, 1H), 11.50 (s, 1H).

HRMS (ESI) found 199.9472, calc. 199.9473.

General synthesis of the final compounds 1-11

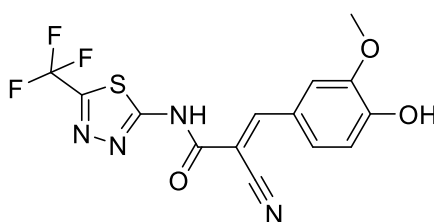


In a round bottom flask the thiadiazole moiety (1 equivalent) have been dissolved in 5mL of CH₃CN and then 1 equivalent of aldehyde was added. 0.8 equivalents of acetic acid and 1 equivalent of NH₄CH₃COO were added to the reaction mixture. The solution has been warmed up to 90°C for three hours and the progression of the reaction was checked by TLC (DCM/MeOH 95:5). When the reaction was completed a mixture of 50:50 H₂O and a saturated aqueous solution of NH₄Cl were added. The precipitate was filtered, washed with fresh water and dried in the oven ON. If the precipitate is not formed, the aqueous phase was extracted with EtOAc three times. The organic phase was dried with magnesium sulphate and then it was concentrated under reduced pressure till the obtainment of a yellow or orange solid.

Yield: 75-90%

Characterisation:

Compound 1 (SRPIN803): 2-cyano-3-(4-hydroxy-3-methoxyphenyl)-N-(5-(trifluoromethyl)-1,3,4-thiadiazol-2-yl)acrylamide



Chemical Formula: C₁₄H₉F₃N₄O₃S
Molecular Weight: 370,3062

¹H NMR (400 MHz, DMSO-*d*₆) δ 3.84 (s, 3H), 6.98 (d, *J* = 8.3 Hz, 1H), 7.53 (dd, *J* = 8.4, 2.1 Hz, 1H), 7.76 (d, *J* = 2.2 Hz, 1H), 8.36 (s, 1H), 10.41 (s, 1H).

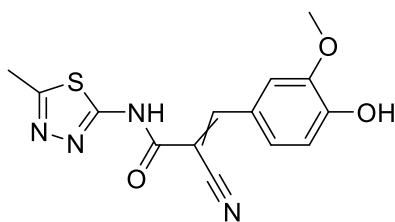
¹³C NMR (101 MHz, DMSO) δ 56.03, 113.87, 116.51, 117.85, 123.68, 127.35, 148.31, 152.65, 152.88.

HRMS (ESI): calcd. (M+H)⁺ 371.0420, exper. 371.0437.

HPLC-UV: 98% purity (area at 254nm).

Yield: 87%.

Compound 2: 2-cyano-3-(4-hydroxy-3-methoxyphenyl)-N-(5-methyl-1,3,4-thiadiazol-2-yl)acrylamide



Chemical Formula: C₁₄H₁₂N₄O₃S
Molecular Weight: 316,3350

¹H NMR (400 MHz, DMSO-*d*₆) δ 2.59 (s, 3H), 3.84 (s, 3H), 7.01 (d, *J* = 8.3 Hz, 1H), 7.54 (dd, *J* = 8.4, 2.1 Hz, 1H), 7.76 (d, *J* = 2.2 Hz, 1H), 8.36 (s, 1H), 10.49 (s, 1H).

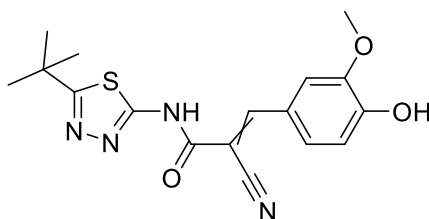
¹³C NMR (101 MHz, DMSO) δ 15.84, 56.03, 113.87, 116.51, 117.85, 123.68, 127.35, 148.31, 152.65, 152.88.

HRMS (ESI) found 317.0703, calc. 317.0721.

HPLC-UV: 98% purity (area at 254nm).

Yield: 87%.

Compound 3: N-(5-(tert-butyl)-1,3,4-thiadiazol-2-yl)-2-cyano-3-(4-hydroxy-3-methoxyphenyl)acrylamide



Chemical Formula: C₁₇H₁₈N₄O₃S
Molecular Weight: 358,4160

¹H NMR (400 MHz, DMSO-*d*₆) δ 1.39 (s, 9H), 3.85 (s, 3H), 6.97 (d, *J* = 8.3 Hz, 1H), 7.54 (dd, *J* = 8.4, 2.1 Hz, 1H), 7.74 (d, *J* = 2.1 Hz, 1H), 8.31 (s, 1H).

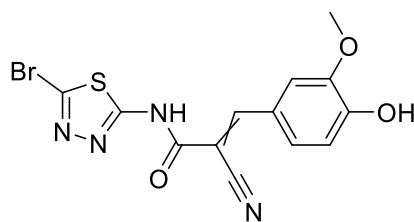
¹³C NMR (101 MHz, DMSO) δ 29.35, 29.55, 29.57, 29.75, 35.61, 56.03, 113.87, 116.51, 117.85, 123.68, 127.35, 148.31, 152.65, 152.88.

HRMS (ESI): calcd. (M+H)⁺ 359.1172, exper. 359.1184.

HPLC-UV: 99% purity (area at 254nm).

Yield: 75%.

Compound 4: N-(5-bromo-1,3,4-thiadiazol-2-yl)-2-cyano-3-(4-hydroxy-3-methoxyphenyl)acrylamide



Chemical Formula: C₁₃H₉BrN₄O₃S
Molecular Weight: 381,2040

¹H NMR (400 MHz, DMSO-*d*₆) δ 3.84 (s, 3H), 6.99 (d, *J* = 8.3 Hz, 1H), 7.54 (dd, *J* = 8.4, 2.1 Hz, 1H), 7.74 (d, *J* = 2.1 Hz, 1H), 8.41 (s, 1H), 10.54 (s, 1H), 13.58 (s, 1H).

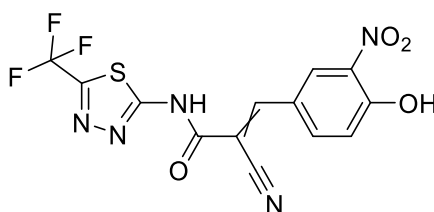
¹³C NMR (101 MHz, DMSO) δ 56.00, 106, 113.90, 116.62, 117.05, 123.39, 127.86, 135.19, 148.37, 153.17, 153.70.

HRMS (ESI): calcd. (M+H)⁺ 380.9651, exper. 380.9678.

HPLC-UV: 99% purity (area at 254nm).

Yield: 78%.

Compound 5: 2-cyano-3-(4-hydroxy-3-nitrophenyl)-N-(5-(trifluoromethyl)-1,3,4-thiadiazol-2-yl)acrylamide



Chemical Formula: C₁₃H₆F₃N₅O₄S
Molecular Weight: 385,2772

¹H NMR (400 MHz, MeOD) δ 7.23 (d, *J* = 8.8 Hz, 1H), 8.26 (dd, *J* = 9.0, 2.5 Hz, 1H), 8.34 (s, 1H), 8.75 (d, *J* = 2.5 Hz, 1H).

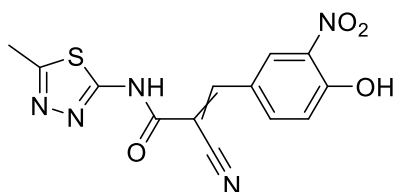
¹³C NMR (101 MHz, MeOD) δ 117.23, 129.87, 136.87, 138.29, 138.29, 150.77, 166.74.

HRMS (ESI): calcd. (M+H)⁺ 386.0165, exper. 386.0169.

HPLC-UV: 99% purity (area at 254nm).

Yield: 85%.

Compound 6: 2-cyano-3-(4-hydroxy-3-nitrophenyl)-N-(5-methyl-1,3,4-thiadiazol-2-yl)acrylamide



Chemical Formula: C₁₃H₉N₅O₄S

Molecular Weight: 331,3060

¹H NMR (400 MHz, MeOD) δ 2.62 (s, 3H), 6.76 (d, *J* = 9.2 Hz, 1H), 8.03 (dd, *J* = 9.3, 2.6 Hz, 1H), 8.15 (s, 1H), 8.54 (d, *J* = 2.6 Hz, 1H).

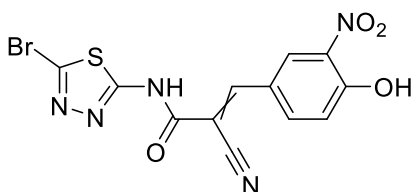
¹³C NMR (101 MHz, MeOD) δ 15.36, 117.09, 127.50, 136.08, 139.62, 170.82.

HRMS (ESI): calcd. (M+H)⁺ 375.0448, exper. 375.0456.

HPLC-UV: 97% purity (area at 254nm).

Yield: 90%.

Compound 7: N-(5-bromo-1,3,4-thiadiazol-2-yl)-2-cyano-3-(4-hydroxy-3-nitrophenyl)acrylamide



Chemical Formula: C₁₂H₆BrN₅O₄S

Molecular Weight: 396,1750

¹H NMR (400 MHz, DMSO-*d*₆) δ 7.06 (d, *J* = 8.9 Hz, 1H and bs, 1H), 8.07 (dd, *J* = 9.0, 2.4 Hz, 1H), 8.22 (s, 1H), 8.53 (d, *J* = 2.4 Hz, 1H).

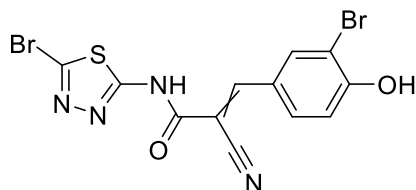
¹³C NMR (101 MHz, DMSO) δ 118.31, 120.96, 122.41, 129.55, 132.38, 135.91, 138.00, 148.22, 159.26, 165.81, 168.94.

HRMS (ESI): calcd. (M+H)⁺ 395.9397, exper. 395.9420.

HPLC-UV: 98% purity (area at 254nm).

Yield: 80%.

Compound 8: N-(5-bromo-1,3,4-thiadiazol-2-yl)-3-(3-bromo-4-hydroxyphenyl)-2-cyanoacrylamide



Chemical Formula: C₁₂H₆Br₂N₄O₂S

Molecular Weight: 430,0740

¹H NMR (400 MHz, DMSO-*d*₆) δ 7.11 (d, *J* = 8.5 Hz, 1H), 7.88 (dd, *J* = 8.5, 2.1 Hz, 1H), 8.21 (s, 1H), 8.24 (d, *J* = 2.1 Hz, 1H).

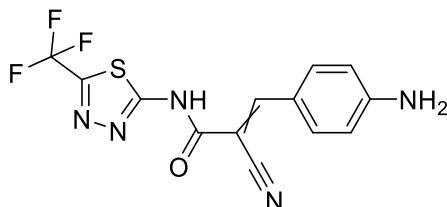
¹³C NMR (101 MHz, DMSO) δ 105.76, 110.61, 117.23, 117.62, 125.20, 130.07, 132.45, 133.21, 135.63, 149.61, 158.57, 160.20, 165.33, 172.50, 179.89.

HRMS (ESI): calcd. (M+H)⁺ 428.8651, exper. 428.8651.

HPLC-UV: 97% purity (area at 254nm).

Yield: 88%.

Compound 9: 3-(4-aminophenyl)-2-cyano-N-(5-(trifluoromethyl)-1,3,4-thiadiazol-2-yl)acrylamide



Chemical Formula: C₁₃H₈F₃N₅OS

Molecular Weight: 339,2962

¹H NMR (400 MHz, MeOD) δ 6.62 (d, *J* = 8.4 Hz, 2H), 7.79 (d, *J* = 8.5 Hz, 2H), 8.11 (s, 1H).

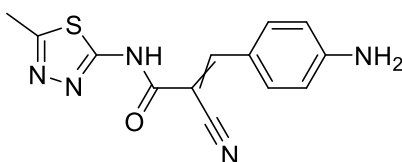
¹³C NMR (101 MHz, MeOD) δ 114.78, 120.98, 135.58.

HRMS (ESI): calcd. (M+H)⁺ 340.0474, exper. 340.0495.

HPLC-UV: 98% purity (area at 254nm).

Yield: 90%.

Compound 10: 3-(4-aminophenyl)-2-cyano-N-(5-methyl-1,3,4-thiadiazol-2-yl)acrylamide



Chemical Formula: C₁₃H₁₁N₅OS

Molecular Weight: 285,3250

¹H NMR (400 MHz, DMSO-*d*₆) δ 6.27 (s, 2H), 6.65 (d, *J* = 8.3 Hz, 2H), 7.75 (d, *J* = 8.3 Hz, 2H), 8.04 (s, 1H).

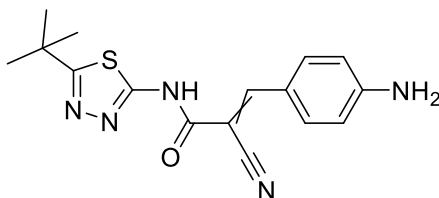
¹³C NMR (101 MHz, DMSO) δ 15.87, 21.55, 102.00, 113.99, 116.16, 119.65, 120.11, 124.67, 133.36, 149.92, 153.66, 157.04, 163.51, 166.37, 167.31, 172.56.

HRMS (ESI): calcd. (M+H)⁺ 286.0757, exper. 286.0781.

HPLC-UV: 97% purity (area at 254nm).

Yield: 86%.

Compound 11: 3-(4-aminophenyl)-N-(5-(tert-butyl)-1,3,4-thiadiazol-2-yl)-2-cyanoacrylamide



Chemical Formula: C₁₆H₁₇N₅OS

Molecular Weight: 327,4060

¹H NMR (400 MHz, DMSO-*d*₆) δ 6.34 (bs, 2H), 6.66 (s, 2H), 7.79 (s, 2H), 8.09 (s, 1H).

¹³C NMR (101 MHz, MeOD) δ 29.35, 29.55, 29.57, 29.75, 35.61, 60.13, 94.96, 113.36, 113.56, 113.76, 117.26, 119.73, 134.29, 153.48, 154.99.

HRMS (ESI): calcd. (M+H)⁺ 328.1227, exper. 328.1238.

HPLC-UV: 99% purity (area at 254nm).

Yield: 90%.

5.6.2 Crystallographic and biological assays on SRPIN803 derivatives

Protein production

The expression of human CK2 α and β subunits was induced in *E. coli* BL21-DE3 with 0,5 mM IPTG for 4 hours at 30 °C. CK2 α pellet mixed with an equal amount of pellet expressing β subunit was resuspended in buffer A (50 mM Tris-HCl pH 8.5 and 7 mM 2-Mercaptoethanol). After sonication and centrifugation, the supernatant was adjusted at the salt concentration of 0,4 M NaCl and loaded on Heparin-Sepharose (5 mL, GE Healthcare). The column was eluted with a linear gradient from 0.4 to 1 M NaCl in buffer A. Holoenzyme $\alpha_2\beta_2$ was purified to homogeneity by size-exclusion chromatography on Superdex 200 (26/60, GE Healthcare) in buffer A + 0,5 M NaCl. The fractions containing the purified holoenzyme were pooled and dialyzed for 4 hours against 25 mM Tris-HCl pH 7,5 and 50% glycerol and stored at -80 °C. The same protocol was applied to purify CK2 α used in activity assays.

CK2 α for crystallization purposes was produced as previously reported [29]. Briefly, after expression in *E. coli* BL21-DE3, human CK2 α (aa. 1-336) was purified by sequential affinity, anion exchange and size-exclusion chromatography (HiTrap Heparin, MonoQ and Superdex 75). Protein was concentrated to 10 mg/mL and frozen in liquid nitrogen.

Crystallization and structure solution

Crystals of apo CK2 and binding of inhibitors in its ATP pocket were obtained as previously described.^[132] Briefly, CK2 crystals were first obtained by vapor diffusion sitting drop and then soaked in the cryoprotective solution containing 5 mM inhibitor in 1% DMSO. Diffraction data were collected at the Elettra Synchrotron Light Source (Trieste, Italy), XRD1 beamLine and at the ESRF (Grenoble, France), beamLines ID30-A1 and ID30-A3. Data were processed with XDS^[165] and AimLess^[166]; structures were solved by molecular replacement with Phaser^[167] using PDB 4KWP^[132] as a search model. Initial models were refined alternating cycles of automatic refinement with Phenix^[168] and manual model building with COOT.^[169]

In vitro CK2 activity assay

Recombinant α CK2 (20–50 ng) was incubated with 0.1 mM synthetic peptide substrate RRRADDSDDDDD (CK2-tide) in a phosphorylation buffer containing 50 mM Tris-HCl pH 7.5, 10 mM MgCl₂, 20 μ M [γ -³³P]ATP (1000–2000 cpm/pmol), in a final volume of 30 μ L, with increasing concentrations of each inhibitor. Controls were performed in the absence of any inhibitor, but with the addition of the solvent DMSO (3%, v/v), which was ineffective on CK2 activity. Reactions were performed at 30 °C for 10 minutes and stopped by sample absorption on phospho-cellulose papers. Papers were washed three times with 75 mM phosphoric acid and counted in a scintillation counter (Perkin Elmer). The same protocol was applied for the activity of recombinant

α 2 β 2 CK2, except for the addition of 0.1 M NaCl in the phosphorylation assay. Results were analysed by GraphPad Prism 7.0a software, for the calculation of the IC₅₀ (concentrations inducing 50% inhibition).

Kinase panel

The activity of compound 4 was tested at 1 μ M in duplicate on a 320 protein kinases panel at ProQinase GmbH (Freiburg – Germany, <https://www.proqinase.com>). The final DMSO concentration in all reaction cocktails was 1 %. A radiometric protein kinase assay (33PanQinase® Activity Assay) was used for measuring the kinase activities.^[170]

Cell culture, treatments and lysis

Jurkat cells (human T lymphoblastoid cell line) were cultured in an atmosphere containing 5% CO₂, maintained in RPMI 1640 medium (Sigma), supplemented with 10% (v/v) fetal calf serum (FCS), 2mM L-glutamine, 100U/mL penicillin, and 100mg/mL streptomycin. Cell treatments with inhibitors were performed in the culture medium, but with 1% (v/v) FCS. Control cells were treated with equal amounts of the inhibitor solvent (DMSO), which never exceeded 1% (v/v). For lysate preparation, cells were lysed as described in ^[131]. Protein concentration was determined by the Bradford method.

Cell viability assay

Cell viability was detected by means of MTT (3-(4,5-dimethylthiazol-2-yl)-3,5-diphenyltriazolium bromide) reagent: cells (10⁵ cells/100 μ L) were incubated for 24h in a 96-well plate under the indicated conditions. 1 h before the end of the incubation, 10 μ L of MTT solution (5 mg/mL in phosphate buffered saline) were added to each well. Incubations were stopped by addition of 20 μ L of lysis solution at pH 4.7, as described elsewhere [37]. Plates were read for OD at λ 590 nm, in a Titertek Multiskan Plus plate reader (Flow Laboratories). Calculation of the DC₅₀ values (concentrations inducing 50% cell death in 24h) were performed by analysing the results with GraphPad Prism 7.0a software.

Endocellular CK2 activity assay

Endocellular CK2 activity was evaluated by assessing the phosphorylation state of the CK2 substrate Akt phosphor-Ser129 (Abcam) as in [38]. For this purpose, equal amounts of proteins from treated cells were loaded on 11% SDS-PAGE, blotted on Immobilon-P membranes (Millipore), processed in Western blot (WB), and detected by chemiluminescence. Endocellular CK2 amount was assessed by WB with an antibody recognizing the two catalytic isoforms α and α' (Biorad Laboratories). β -actin antibody,

used for normalization, was from Sigma. Quantitation of the signal was obtained by chemiluminescence detection on a Kodak Image Station 440MMPRO and analysis with the Kodak 1DImage software.

6 INDEX OF THE FIGURES

Figures

FIGURE 1. CATALYTIC MECHANISMS OF DIFFERENT CLASSES OF PHOSPHATASES. A. FCP/SCP CLASS. WITHIN THE ACTIVE SITE A SINGLE ION OF Mg^{2+} IS PRESENT. IT IS COORDINATE BY THE DxDx(T/V) MOTIF AND TOGETHER EXERT THE PHOSPHATSE ACTIVITY. B. PPP AND PPM CLASSES. TWO DIVALENT CATAIONS ARE COORDINATED WITHIN THE ACTIVE SITE TO MEDIATE THE PHOSPHATE TRANSFER WITHOUT FORMING AN INTERMEDIATE. C. PTPS, WHICH ARE METAL-INDEPENDENT CYS- BASED PHOSPHATASES, AN ACTIVE SITE CYSTEINE SERVES AS THE NUCLEOPHILE WHICH ATTACKS THE PHOSPHATE GROUP, FORMING A PHOSPHO-CYSTEINYL INTERMEDIATE.	8
FIGURE 2. HETEROTRIMERIC STRUCTURE OF PP2A [PDB: 2IAE]. THE CATALYTIC SUBUNIT IS REPORTED IN YELLOW , THE REGULATORY ONE IS COLOURED IN RED AND THE SCAFFOLD SUBUNIT IN BLUE	9
FIGURE 3. A. CRYSTAL STRUCTURE [PDB: 3FGA] OF THE CATALYTIC SUBUNIT, ISOFORM A, THE RED CIRCLE HIGHLIGHTS THE ACTIVE SITE. B. MOLAR RATIO OF METAL ION SPECIES VS PP2A _C IN PORCINE BRAIN.	11
FIGURE 4. CRYSTAL STRUCTURE [PDB: 2IAE] OF THE STRUCTURAL SUBUNIT, ISOFORM A. .	12
FIGURE 5. CRYSTAL STRUCTURE OF THE CATALYTIC SUBUNIT OF PP2A (YELLOW) AND LCMT-1 (ORANGE) [PDB: 3P71]	15
FIGURE 6. CRYSTAL STRUCTURE OF THE CORE ENZYME PP2A (CATALYTIC SUBUNIT IN YELLOW AND SCAFFOLD IN BLUE) AND PME-1 IN GREEN [PDB: 3C5W].	16
FIGURE 7. A. CRYSTAL STRUCTURE OF PTPA (RED) AND THE CORE STRUCTURE OF PP2A (CATALYTIC SUBUNIT IN YELLOW AND SCAFFOLD SUBUNIT IN BLUE) [PDB: 4LAC]. B. A CLOSE-UP VIEW OF THE COMBINED ATP-BINDING POCKET OF THE PP2A-PTPA COMPLEX BOUND TO ATPtS. RESIDUES FROM PTPA AND PP2AC ARE IN BALL-AND-STICK AND CYLINDER, AND COLORED MAGENTA AND CYAN, RESPECTIVELY. ATPtS IS SHOWN IN CYLINDER AND COLORED BY ATOM TYPE. CATALYTIC METAL IONS ARE INDICATED BY RED SPHERES. THE BLACK DASHED LINES INDICATE H-BONDS. C. ILLUSTRATION OF DUAL OCTAHEDRAL METAL ION CHELATION AT THE PP2AC ACTIVE SITE BY ATP γ PHOSPHATE AND SIX METAL ION-CHELATING RESIDUES WITH PROPOSED MECHANISM OF ATP HYDROLYSIS.	17
FIGURE 8. CRYSTAL STRUCTURE OF THE N-TERMINAL REGION OF CIP2A [PDB: 5UFL].....	18
FIGURE 9. CRYSTAL STRUCTURE OF SET PROTEIN, MONOMER EDITED WITH SWISS-MODEL FROM THE PDB 2E50.....	19

FIGURE 10. SCHEMATIC REPRESENTATION OF THE PP2A'S NETWORK OF PATHWAYS. THE FIGURE SHOWS THE MANY LEVELS AT WHICH PP2A AFFECTS THE NORMAL PHYSIOLOGY OF CELLS.	20
FIGURE 11. SCHEMATIC REPRESENTATION OF THE CELL CYCLE.....	20
FIGURE 12. MOLECULAR SCAFFOLD OF THE PRINCIPAL PP2A INHIBITORS.....	26
FIGURE 13. MOLECULAR STRUCTURE OF TWO CANTHARIDIN DERIVATIVES: LB100 AND LB102.	26
FIGURE 14. CHEMICAL STRUCTURE OF PERPHENAZINE AND LEAD COMPOUND BELONGING TO SMAPS CATEGORY.....	28
FIGURE 15. CHEMICAL STRUCTURE OF THE COMPOUNDS ACTIVE ON CIP2A.....	29
FIGURE 16. MECHANISM OF ACTION OF FTY720 AND MOLECULAR SCAFFOLD OF ONE OF THE NON PHOSPHORYLABLE DERIVATIVES SYNTHETIZED IN OUR LABORATORY.	30
FIGURE 17. MODEL OF FTY720 BOUND SET RESULTED FROM NMR-BASED ANALYSIS.	31
FIGURE 18. SEQUENCE OF THE PRINCIPAL APOE MIMETICS AND CHEMICAL STRUCTURE OF TGI1002.....	31
FIGURE 19. CHEMICAL STRUCTURE OF EHT.....	32
FIGURE 20. CHEMICAL STRUCTURE OF DIFFERENT PP2A ACTIVATORS.	33
FIGURE 21. CRYSTAL STRUCTURE OF THE FULL LENGTH SHP-1 IN ITS ACTIVE CONFORMATION _[PDB: 3PS5] . THE CATALYTIC DOMAIN IS HIGHLIGHTED IN BLUE , IN GREEN THE C-SH2 AND IN RED THE N-SH2.....	36
FIGURE 22. CRYSTAL STRUCTURE OF SHP-1 IN ITS INHIBITED CONFORMATION _[PDB: 2B30] . THE CATALYTIC DOMAIN IS HIGHLIGHTED IN BLUE , IN GREEN THE C-SH2 AND IN RED THE N-SH2.	38
FIGURE 23. STRUCTURAL COMPARISONS OF SHP-1 WITH THE TAIL-TRUNCATED SHP-1 AND SHP-2. A: STRUCTURAL COMPARISON OF SHP-1 (GREEN) WITH TAIL-TRUNCATED SHP-1 (BLUE) AND SHP-2 (RED). THE YELLOW DASHED CIRCLE SHOWS THE POSITION OF THE ACTIVE SITE. THE Nb4-Nb5 HAIRPIN LOOPS ARE COLOURED MAGENTA. THE Nb4-Nb5 LOOP IN SHP-1 IS QUOTED BECAUSE WE USE THIS NAME FROM TAIL-TRUNCATED SHP-1 REGARDLESS OF THE DIFFERENCES BETWEEN THEIR SECONDARY STRUCTURES. THE N-SH2 DOMAINS OF THE TAIL-TRUNCATED SHP-1 AND SHP-2 ARE LOCATED ON THE LEFT SIDE OF THE PTP DOMAIN BUT SHIFTED TO THE RIGHT SIDE IN THE CURRENT SHP-1 STRUCTURE, RESULTING IN THE EXPOSURE OF THE ACTIVE SITE. B: THE CONFORMATIONAL CHANGE BETWEEN THE C-SH2 DOMAINS IN SHP-1 (GREEN) AND TAIL-TRUNCATED SHP-1 (BLUE) STRUCTURES. THE C-SH2 DOMAIN OF THE INTACT PROTEIN IS ROTATED ANTICLOCKWISE BY ABOUT 110°	

RELATIVE TO THE TRUNCATED PROTEIN AS REVEALED FROM THE SUPERPOSITION OF THEIR PTP DOMAINS.	39
FIGURE 24. SCHEMATIC REPRESENTATION OF THE C-TERMINAL TAIL OF THE TWO SHP-1 PRINCIPAL ISOFORMS.	40
FIGURE 25. CHEMICAL STRUCTURE OF THE TWO PRINCIPAL SHP-1 INHIBITORS.	44
FIGURE 26. CHEMICAL STRUCTURE OF THE PRINCIPAL SHP-1 AGONISTS.	44
FIGURE 27. CRYSTAL STRUCTURE OF THE TETRAMERIC FORM OF CK2 _[PDB: 1JWH] . THE CATALYTIC DOMAINS ARE REPRESENTED IN RED WHILE THE REGULATORY ONES ARE SHOWN IN BLUE	47
FIGURE 28. CRYSTAL STRUCTURE OF THE CK2A SUBUNIT IN THE PRESENCE OF AN ATP MIMICKING MOLECULE _[PDB: 1JWH]	48
FIGURE 29. CRYSTAL STRUCTURE OF THE DIMER CONSTITUTED BY TWO REGULATORY SUBUNITS _[PDB: 1JWH]	50
FIGURE 30. SCHEMATIC REPRESENTATION OF THE KEY REGULATION REGIONS WITHIN THE AMINOACIDIC SEQUENCE OF CK2B.	51
FIGURE 31. CHEMICAL STRUCTURE OF THE COMPOUNDS PRESENTED IN THIS PARAGRAPH.	54
FIGURE 32. COMPARISON OF THE TWO CHEMICAL STRUCTURES OF FINGOLIMOD AND THE LEAD COMPOUND THAT HAS BEEN USED AS A MODEL FOR THE SYNTHESIS OF THE NEW ANALOGUES AND FOR ALL THE OTHER STUDIES.	63
FIGURE 33. PHARMACOPHORIC STRUCTURE OF THE FINGOLIMOD ANALOGUES SYNTHETIZED DURING THIS PHD.	64
FIGURE 34. ORTHO-PARA ORIENTATION IN PHENYL-ETHERS.	67
FIGURE 35. MECHANISM OF REACTION OF THE NUCLEOPHILIC AROMATIC REACTION. FOR COMMODITY IT HAS BEEN USED A NEGATIVELY CHARGED NUCLEOPHILE, BUT THE SAME MECHANISM IS FOLLOWED BY A NON CHARGED NUCLEOPHILE.	71
FIGURE 36. REACTION MECHANISM OF FRIES REARRANGEMENT. A SIMILAR MECHANISM IS ADOPTED ALSO IN CASE OF THE USE OF STRONG ACIDS.	76
FIGURE 37. REACTION MECHANISM OF THE FRIES REARRANGEMENT UNDER UV IRRADIATION.	76
FIGURE 38. CHEMICAL STRUCTURE OF THE MIXED ANHYDRIDES FORMED DURING THE REACTION.	77
FIGURE 39. REACTION MECHANISM OF THE MANNICH REACTION.	77
FIGURE 40. DELOCALIZATION MECHANISM OF THE UNPAIRED ELECTRONS OF THE NITROGEN ATOM.	78

FIGURE 41. SUPPOSED DEGRADATION MECHANISM OF THE ISOLATED COMPOUND.....	79
FIGURE 42. GENERAL MOLECULAR SCAFFOLD OF THE NEW CHIMERIC COMPOUNDS. ...	80
FIGURE 43. SYNTHETIC PROTOCOL ADOPTED FOR THE SYNTHESIS OF THE CHIMERIC APOE/FINGOLIMOD ANALOGUES.	81
FIGURE 44. REACTION MECHANISM OF THE TBTU MEDIATED AMIDE COUPLING.	83
FIGURE 45. REPRESENTATIVE SCHEME OF THE SYNTHETIC PATHWAY ADOPTED DURING THE SOLID PHASE PEPTIDE SYNTHESIS.	85
FIGURE 46. CHEMICAL STRUCTURE OF THE FMOC-GLYCINE WANG RESIN AND OF ALL THE PROTECTING GROUPS USED DURING THE SOLID PHASE SYNTHESIS.	86
FIGURE 47. PHARMACOPHORIC ANALYSIS OF THE MOLECULAR SCAFFOLDS OF CC11 AND TGI1002. WITH A RED CIRCLE THE HYDROPHOBIC PORTION OF THE TWO MOLECULES IS HIGHLIGHTED WHILE THE BASIC AND POLAR MOIETY IS UNDERLINED WITH A BLUE BOX. THE KEY DETERMINANTS OF THE STRUCTURE THAT ARE CONSERVED ALSO IN THE CHIMERIC MOLECULE ARE EVIDENCED WITH DIFFERENT COLOURS.	91
FIGURE 48. REACTION MECHANISM FOR THE OBTAINMENT OF THE PYRIMIDONE RING.	92
FIGURE 49. REACTION MECHANISMS FOR THE SYNTHESIS OF 2-(METHYLTHIO)PYRIMIDIN- 4-YL METHANESULFONATE AND 2-(METHYLTHIO)-N-(3- (TRIFLUOROMETHYL)PHENYL)PYRIMIDIN-4-AMINE.	93
FIGURE 50. PROPOSED MECHANISM FOR THE ENHANCING OF THE PYRIMIDINE'S ELECTROPHILIC CHARACTER MEDIATED BY THE CATALYTIC HCL.	94
FIGURE 51. PHARMACOPHORIC ANALYSIS OF THE MOLECULAR SCAFFOLDS OF CC11 AND TD-19. WITH A RED CIRCLE THE HYDROPHOBIC PORTION OF THE TWO MOLECULES IS HIGHLIGHTED WHILE THE BASIC AND POLAR MOIETY OF CC11 IS UNDERLINED WITH A BLUE BOX. THE KEY DETERMINANTS OF THE STRUCTURE THAT ARE CONSERVED ALSO IN THE CHIMERIC MOLECULE ARE EVIDENCED WITH DIFFERENT COLOURS...	95
FIGURE 52. REACTION MECHANISM FOR NITRATION OF VERATRIC ACID.	97
FIGURE 53. REACTION MECHANISM FOR THE SYNTHESIS OF THE QUINAZOLINE-2,4-DIONE CORE.....	97
FIGURE 54. BLOOD SAMPLE ADDED WITH 5 μ L OF 50000 PPB SOLUTION OF CC11 ANALYSED THROUGH LC/MS. THE LOWER PART IS THE M/Z RATIO OF CC11, THE MIDDLE ONE IS THE TIC LC-MS CHROMATOGRAM AND THE UPPER ONE THE ISOLATED PEAK OF CC11.....	101
FIGURE 55. BLOOD CONCENTRATION OF CC11 FROM 0 TO 48 HOURS AFTER ADMINISTRATION (ALL THE SHOWN DATA ARE THE AVERAGE VALUE OF THE THREE EXPERIMENTS).....	102

FIGURE 56. MASS SPECTRUM OF THE ANALYTE IN PLASTIC VIALS.....	103
FIGURE 57. MASS SPECTRUM OF THE ANALYTE IN GLASS VIALS.....	104
FIGURE 58. MOLECULAR STRUCTURE OF THE FLUORESCENT PHOTOACTIVATABLE SYNTHON.....	108
FIGURE 59. MECHANISM OF PHOTOACTIVATION OF THE AZIDO PHTHALIMIDE PORTION AND OF FLUORESCENCE OF THE PHOTOACTIVATED COMPOUND.	109
FIGURE 60. MECHANISM OF REACTION OF THE AZIDO PHTHALIMIDE PORTION.....	112
FIGURE 61. MECHANISM OF REACTION FOR THE SYNTHESIS OF THE 4-(1,3- DIOXISOINDOLIN-2-YL)BUTANOIC ACID.....	114
FIGURE 62. UV-VIS AND FLUORESCENCE SPECTRA OF THE OF THE AZIDO PHTHALIMIDE SYNTHON BEFORE AND AFTER ONE HOUR OF IRRADIATION AT 365 NM IN A PBS BUFFER SOLUTION AT A CONCENTRATION OF 100 μ M. A AND C ARE RESPECTIVELY THE UV-VIS AND FLUORESCENCE SPECTRA OF THE COMPOUND AFTER IRRADIATION. B AND D ARE RESPECTIVELY THE UV-VIS AND FLUORESCENCE SPECTRA OF THE COMPOUND BEFORE IRRADIATION.	116
FIGURE 63. MASS SPECTRA OF THE NON IRRADIATED (A) AND IRRADIATED (B) SAMPLES. THE MOLECULAR STRUCTURE OF THE PRINCIPAL PEAKS OF THE TWO SPECTRA ARE REPORTED.....	117
FIGURE 64. A) PHOSPHATASE PROBE PROPOSED BY BECK ET AL. ^[171] B) PHOSPHATASE PROBE PROPOSED BY KAWAGUCHI ET AL. ^[144]	120
FIGURE 65. INTRAMOLECULAR SPYROCICLIZATION OF THE HMSiR. THE CLOSED AND NON-FLUORESCENT MOLECULE IS MORE PRESENT AT PHYSIOLOGICAL pH THAN THE OPEN AND FLUORESCENT FORM.	121
FIGURE 66. FRET MECHANISM BETWEEN HMSiR AND RHODAMINE 101.....	122
FIGURE 67. . BLINKING BEHAVIOUR OF THE FRET PROBE IN THE UNPHOSPHORYLATED STATE.	123
FIGURE 68. CHEMICAL STRUCTURE OF THE COMPOUND 1.	123
FIGURE 69. DEGRADATION OF THE METHYL ESTER OF THE RHODAMINE AND LACTONIZATION OF THE FREE CARBOXYLIC ACID. IN THE MOLECULE 2B THE XANTHENE CORE OF THE FRET DONOR IS NO MORE CONJUGATED, AND THIS DOES NOT ALLOW THE ABSORPTION AND THE TRANSMISSION OF ENERGY OF THE WHOLE SYSTEM.....	124
FIGURE 70. CHEMICAL STRUCTURE OF COMPOUND 3.....	124
FIGURE 71. MODIFICATION OF THE CHEMICAL SCAFFOLD OF RHODAMINE101 IN TO COMPOUND 5 AND POSSIBLE MECHANISM OF INTERFERENCE WITH THE XANTHENE	

CONJUGATED SYSTEM WHICH IS STRONGLY UNFAVOURED IN PHYSIOLOGICAL CONDITIONS.	125
FIGURE 72. A) ABSORBANCE SPECTRUM OF 15 (125 μ L, 1 μ M) IN BUFFER TRIS-HCL 50MM, NA ₂ CO ₃ 75MM PH7.5, MEASURED WITH PLATE READER SPARK® TECAN. B) FLUORESCENCE SPECTRUM OF 15 (125 μ L, 0.5 μ M) IN BUFFER TRIS-HCL 50MM, NA ₂ CO ₃ 75MM PH7.5, MEASURED WITH PLATE READER SPARK® TECAN. C) ABSORBANCE SPECTRUM OF 20 (125 μ L, 1 μ M) IN BUFFER TRIS-HCL 50MM, NA ₂ CO ₃ 75MM PH7.5, MEASURED WITH PLATE READER SPARK® TECAN. D) FLUORESCENCE SPECTRUM OF 20 (125 μ L, 0.5 μ M) IN BUFFER TRIS-HCL 50MM, NA ₂ CO ₃ 75MM PH7.5, MEASURED WITH PLATE READER SPARK® TECAN. E) SUPERIMPOSITION OF THE NORMALISED EMISSION SPECTRUM OF 20 AND THE ABSORBING ONE OF 15.....	129
FIGURE 73. UV-VIS ABSORBANCE OF THE COMPOUNDS 13 AND 21 IN BUFFER TRIS-HCL 50MM, NA ₂ CO ₃ 75MM AND 50 μ G OF PROTEINS PER 125 μ L OF BUFFER, AT PH 7,5. B. FLUORESCENCE SPECTRA OF THE COMPOUNDS 13 AND 21 EXCITING AT 561NM...	130
FIGURE 74. STABILITY TEST OF COMPOUND 21 IN PBS AT 37°C WITH A CONCENTRATION OF 4 μ M.	130
FIGURE 75. I. A) ABSORBANCE SPECTRA OF INCREASING CONCENTRATIONS OF COMPOUND 13 IN BUFFER TRIS-HCL 50MM, NA ₂ CO ₃ 75MM AND 50 μ G OF PROTEINS PER 125 μ L OF BUFFER, AT PH 7,5. B) FLUORESCENCE SPECTRA EXCITING AT 561NM. C) CALIBRATION CURVE. II. A) ABSORBANCE SPECTRA OF INCREASING CONCENTRATIONS OF COMPOUND 13 IN BUFFER TRIS-HCL 50MM AND NA ₂ CO ₃ 75MM AT PH 7,5. B) FLUORESCENCE SPECTRA EXCITING AT 561NM. C) CALIBRATION CURVE.	131
FIGURE 76. FLUORESCENCE SPECTRA, EXCITING AT 561NM, OF COMPOUND 21 (A) AND COMPOUND 13 (C) AT DIFFERENT PH. ABSORBANCE SPECTRA OF COMPOUND 21 (B) AND COMPOUND 13 (D) AT DIFFERENT PH.	132
FIGURE 77. MINIMISED STRUCTURE OF COMPOUND 21 AT PH 7.4.	133
FIGURE 78. MINIMIZED STRUCTURE OF COMPOUND 21 AT PH 3.	133
FIGURE 79. DEPHOSPHORYLATION PROFILE OF COMPOUND 21 (4 μ M) IN PBS AT PH 7.4 AND A CONCENTRATION OF LYSATE PROTEIN OF 50 μ G/ML.	134
FIGURE 80. RATIO OF FLUORESCENCE OF COMPOUND 21 AT DIFFERENT CONCENTRATIONS. THE REFERENCES STANDARDS ARE OBTAINED USING A SOLUTION CONTAINING TRIS-HCL 50MM, NA ₂ CO ₃ 75MM BUFFERED AT PH 7.5. THE CONCENTRATION OF PROTEINS IN THE LYSATE TEST IS OF 80 μ G/ML.....	134

FIGURE 81. ACTIVITY OF THE LYSATE PROTEINS ON COMPOUND 21 AFTER 1H OF INCUBATION AT 37°C.....	135
FIGURE 82. INHIBITIONS TESTS OF THE PHOSPHATASE ACTIVITY. ALL THE SAMPLES WERE PREPARED IN A SOLUTION OF TRIS-HCL 50MM, NAACL 75MM BUFFERED AT PH 7.5 AND A CONCENTRATION OF PROTEINS OF 400µG/ML. LYSATE REFERS TO THE SAMPLE THAT CONTAINS THE PHOSPHATASES ENZYMES BUT NO INHIBITORS. SAMPLE 21 REPRESENTS JUST THE COMPOUND 21 IN A BUFFER SOLUTION CONTAINING THE INACTIVATED LYSATE.	136
FIGURE 83. RATIO OF THE INTENSITY OF FLUORESCENCE OF THE TWO MAXIMA OF EMISSION (611 AND 670NM). BUFFER TRIS-HCL 50MM, NAACL 75MM AND PH 8.0. SAMPLE 21 ON WAS INCUBATED OVER NIGHT AT 37°C. SAMPLE 21 WAS INCUBATED FOR 15 MINUTES AT 37°C.....	137
FIGURE 84. . CALIBRATION CURVE OF COMPOUND 21 (3µM) USING INCREASING CONCENTRATIONS OF GSH (0-20MM). BUFFER TRIS-HCL 50MM, NAACL 75MM AND PH 7.5. MECHANISM OF QUENCHING OF THE HMSiR MOIETY WITH GLUTATHIONE.	138
FIGURE 85. A) FLUORESCENCE SPECTRUM OF COMPOUND 13 IN TRIS-HCL 50MM, NAACL 75MM AND PH 7.5 AND INCREASING CONCENTRATIONS OF MgCl2. B) FLUORESCENCE SPECTRUM OF COMPOUND 21 IN TRIS-HCL 50MM, NAACL 75MM AND PH 7.5 AND INCREASING CONCENTRATIONS OF MgCl2.	139
FIGURE 86. A) BRIGHTFIELD IMAGE 13. B) 13 IMAGED BY CONFOCAL EXPOSURE (561 NM, 200 mW, 25% POWER, 20 MS). C) BRIGHTFIELD IMAGE 21. D) 21 IMAGED BY CONFOCAL EXPOSURE (561 NM, 200 mW, 25% POWER, 100 MS). E) PVA FILM-SINGLE MOLECULE DETECTION (SCALE BARS = 500 NM, EXPOSURE TIME = 50 MS, LASER POWER (561 NM) = 50%) F) PVA FILM-SINGLE MOLECULE DETECTION (SCALE BARS = 500 NM, EXPOSURE TIME = 50 MS, LASER POWER (647 NM) = 80%).....	140
FIGURE 87. PHOTOACTIVABLE MASKING OF THE PHOSPHATE GROUP.	140
FIGURE 88. PROPOSED SITE OF INTERACTION OF SC-43 WITH SHP-1 SING AUTODOCK VINA. A. GENERAL OVERVIEW OF THE SHP-1 STRUCTURE AND LOCALIZATION OF THE INTERACTING SITE. B. SC-43 IN ITS THEORIZED ACTIVE SITE. C. 2D PLOT OF THE GENERATED INTERACTIONS WITHIN THE INTERACTING POCKET.....	148
FIGURE 89. STRUCTURAL COMPARISON OF THE UREIDO AND QUINAZOLONE GROUPS.	149
FIGURE 90. MECHANISM OF REACTION OF THE ISOCYANATE FOR THE SYNTHESIS OF THE UREIDO BRIDGE.	151

FIGURE 91. RESULTS OF THE UREIDO AND SULPHONAMIDE DERIVATIVES OF SC-43 ON LGL LEUKAEMIA CELLS. ON THE TOP PART OF THE FIGURE THE PERCENTAGE OF APOPTOTIC CELLS INDUCED BY SC-43 (A) AND (B) THE THIOUREIDO ANALOGUE (COMPOUND 1) AT DIFFERENT CONCENTRATIONS AND TIME EXPOSURE HAVE BEEN SHOWN. PANNELL C HIGHLIGHTS THE PERCENTAGE OF APOPTOTIC CELLS INDUCED BY SC-43 AND COMPOUNDS 1, 2, 3, 4 AT DIFFERENT CONCENTRATIONS OVER A PERIOD OF 24H INCUBATION.....	155
FIGURE 92. PERCENTAGE OF APOPTOTIC CELLS AFTER AN INCUBATION PERIOD OF 24H AND 48H WITH SC-43, COMPOUND 5 AND 6, AT DIFFERENT CONCENTRATIONS (2 AND 8 μ M).	156
FIGURE 93. CHEMICAL STRUCTURE OF SRPIN803 AND COMPOUND 1. THEY CAN BE CONSIDERED AS TAUTOMERS AND THE TAUTOMERIZATION MECHANISM IS HEREIN REPORTED.	157
FIGURE 94. SPECTROSCOPIC AND CHROMATOGRAPHIC ANALYSIS OF FRESH COMPOUND 1.	158
FIGURE 95. BINDING MODE OF COMPOUND 1 IN THE CK2 ATP-POCKET. A) 2D STRUCTURE OF SRPIN803. B) 2D STRUCTURE OF COMPOUND 1. C) COMPOUND 1 INSERTS DEEPLY INTO THE POCKET CONTACTING BOTH THE BASIC REGION (BLUE SURFACE) AND THE HINGE REGION (PINK SURFACE). D) THE GUAIACOL HEADGROUP IS INVOLVED IN A NUMBER OF POLAR INTERACTIONS WITH RESIDUES IN THE CK2 BASIC REGION. E) THE CENTRAL 2-CYANO-2-PROPENAMIDE GROUP IS SANDWICHED BY HYDROPHOBIC RESIDUES AND CONTACTS THE HINGE REGION THROUGH WATER-BRIDGED HYDROGEN BONDS. F) THE THIADIAZOL RING STACKS IN BETWEEN SIDE CHAINS OF LEU45 AND ASN118, WHILE THE TRIFLUOROMETHYL END IS INVOLVED IN VARIOUS POLAR INTERACTIONS.....	159
FIGURE 96. A. MECHANISM OF DELOCALIZATION OF THE UNPAIRED ELECTRONS OF THE AMINO GROUP ON THE THIADIAZOL RING. B. REACTION MECHANISM FOR THE FORMATION OF THE AMIDE BOND IN THE ORIGINAL SYNTHETIC PROCEDURE.	161
FIGURE 97. MECHANISM OF REACTION OF KNOEVENAGEL CONDENSATION.	162
FIGURE 98. COMPARISON OF BINDING MODES FOR COMPOUNDS 1 (GREEN), 3 (ORANGE), 4 (PURPLE), 7 (CYAN) AND 14 (YELLOW). A) TERT-BUTYL-THIADIAZOLE (3) MOVES AWAY FROM THE HINGE REGION WITH RESPECT TO COMPOUND 1, BROMO-THIADIAZOLE (4) MOVES CLOSER. B) THE NITROPHENOL MOIETY CAUSES THE BROMOTHIADIAZOLE OF COMPOUND 7 TO PROTRUDE MORE ON THE TOP OF THE HINGE REGION WITH RESPECT TO THE BROMOTHIADIAZOLE OF COMPOUND 4 HOLDING A GUAIACOL GROUP ON THE	

OPPOSITE SIDE. C) THE NITROPHENOLIC HEADGROUP OF COMPOUND 7 INTERACTS WITH CK2□ SIMILARLY TO WHAT OBSERVED IN COMPOUND 4. D) THE O-HYDROXYLBENZENE RING IN COMPOUND 14 EXPOSES THE PHENOLIC OXYGEN TO THE SOLVENT.....	167
FIGURE 99. RESULTS OF THE RADIOMETRIC PROTEIN KINASE ASSAY (³³ PANQINASE® ACTIVITY ASSAY).....	168
FIGURE 100. COMPARISON OF BINDING MODES FOR COMPOUND 4 (PURPLE) AND CAM4066 (CYAN). THE TWO DIFFERENT VIEWS SHOW THAT BOTH COMPOUNDS ARE COMPATIBLE WITH CK2 OPEN CONFORMATION (WHITE) BUT NOT WITH THE CLOSED CONFORMATION (YELLOW). COMPOUND 4 DISCRIMINATES THE TWO CONFORMATIONS AT THE LEVEL OF THE HINGE REGION, WHILE CAM4066 CLASHES WITH A CLOSED AD HELIX.....	169
FIGURE 101. EFFECTS OF COMPOUNDS IN CELLS. A) JURKAT CELLS WERE TREATED WITH THE INDICATED COMPOUNDS FOR 16H. 20 μG OF PROTEINS FROM TOTAL LYSATE WERE ANALYSED BY WB WITH ANTI PHOSPHO-SER129 AKT ANTIBODY (UPPER), OR AN ANTIBODY RECOGNIZING BOTH CK2 CATALYTIC SUBUNIT A AND A' (MIDDLE). 5 μG OF PROTEINS WERE ANALYSED FOR B-ACTIN (LOWER WB), AS LOADING CONTROL. REPRESENTATIVE WB OF THREE INDEPENDENT EXPERIMENTS ARE SHOWN. B) JURKAT CELLS WERE TREATED FOR 24H WITH INCREASING CONCENTRATIONS OF THE INDICATED COMPOUNDS. CELL VIABILITY WAS ASSESSED BY THE MTT METHOD, AND IT IS SHOWN AS % OF VEHICLE-TREATED (CONTROL) CELLS. ON THE RIGHT, THE CALCULATED DC50 VALUES ARE REPORTED (MEAN VALUES + SEM OF AT LEAST FOUR EXPERIMENTS).....	170

Schemes

SCHEME 1. SYNTHETIC PATHWAY ADOPTED FOR THE SYNTHESIS OF THIS FIRST CLASS OF PP2A ACTIVATORS.....	65
SCHEME 2. SCHEME OF ACTIVATION OF THE ACYL-HALIDE AND THE FORMATION OF THE REACTIVE SPECIES ACYLIUM ION.	66
SCHEME 3. SYNTHETIC PATHWAY OF THE BIARILIC FINGOLIMOD ANALOGUES.....	71
SCHEME 4. OPTIMIZATION PROCESS OF THE SYNTHETIC PROTOCOL FOR THE OBTAINMENT OF A COMPOUND WITH A NITROGEN ATOM IN POSITION R ₃	74
SCHEME 5. ATTEMPT OF SYNTHESIS OF TGI1002-CC11 CHIMERIC COMPOUNDS.....	91
SCHEME 6. SYNTHESIS OF 1-(4-AMINOPHENYL)-2-MORPHOLINOETHAN-1-ONE SYNTHON.	92

SCHEME 7. SYNTHETIC PATHWAY FOR THE OBTAINMENT OF THE DESIRED TD-19-CC11 CHIMERIC COMPOUNDS. THE SYNTHESIS OF THE HYDROXYMETHYL ETHER ANALOGUES HAS BEEN STOPPED AT THE LEVEL OF THE 1,4-DICHLOROQUINAZOLINE SYNTHON.....	96
SCHEME 8. SYNTHESIS OF THE DIFFERENT RESINS.....	106
SCHEME 9. SYNTHETIC ROUTE FOR THE SYNTHESIS OF PHOTOACTIVATABLE PROBES FUNCTIONALISED ON THE ALKYL CHAIN.....	111
SCHEME 10. SYNTHETIC ROUTE FOR THE SYNTHESIS OF PHOTOACTIVATABLE PROBES FUNCTIONALISED ON THE POLAR HEAD.	113
SCHEME 11. SYNTHETIC SCHEME OF COMPOUND 4.	124
SCHEME 12. SYNTHETIC SCHEME OF THE FRET PROBE, COMPOUND 13.	125
SCHEME 13. ATTEMPT OF SYNTHESIS OF THE PHOSPHORYLATED HMSiR.....	126
SCHEME 14. SCHEME OF SYNTHESIS OF COMPOUND 15.....	126
SCHEME 15. ATTEMPT OF SYNTHESIS OF THE FINAL FRET PROBE.....	127
SCHEME 16. NEW SCHEME OF SYNTHESIS OF THE COMPOUND 21.....	128
SCHEME 17. SYNTHETIC PATHAWY FOR THE SC-43 ANALOGUES. A. UREIDO DERIVATIVE. B. SULPHONAMIDE DERIVATIVES. C. QUNIAZOLONE DERIVATIVES.	150
SCHEME 18. SYNTHETIC PROTOCOL ADOPTED FOR THE SYNTHESIS OF THE CK2 INHIBITORS.....	161

Tables

TABLE 1. DIFFERENT ISOFORMS THAT CONSTITUTE EACH SUBUNIT. ^[18]	10
TABLE 2. CORRELATIONS BETWEEN ALTERATIONS IN PP2A SUBUNITS OR ITS BINDING PROTEINS AND DIFFERENT TYPES OF PATHOLOGIES.	22
TABLE 3. INHIBITION OF PROTEIN PHOSPHATASE 1 AND 2A.	25
TABLE 4. COMPARISON AMONG HALIDES AS LEAVING GROUPS.	66
TABLE 5. CONCENTRATION OF CC11 IN SEVERAL ORGANS AND IN THE BLOOD. THE CONCENTRATION IN THE BLOOD IS EXPRESSED IN $\mu\text{G}/\text{ML}$ AND THE CONCENTRATION OF THE ANALYTE IN THE ORGANS IS REPORTED IN μG OF CC11 VERSUS MG OF TISSUE ANALYSED	102
TABLE 6. COMPARISON BETWEEN PLASTIC VIALS AND GLASS VIALS IN THE MAINTAINING OF THE CONCENTRATION.....	103
TABLE 7. PRINCIPAL SELECTIVE INHIBITORS OF PHOSPHATASES ACTUALLY AVAILABLE AND THEIR SELECTIVITY THROUGH THE DIFFERENT CLASSES OF PHOSPHATASES.	136

7 REFERENCES

- [1] Y. Sharma, A. Ahmad, S. Bashir, A. Elahi, F. Khan, *Futur. Oncol.* **2016**, *12*, 1287–1298.
- [2] M. K. Paul, A. K. Mukhopadhyay, *Int. J. Med. Sci.* **2004**, *1*, 101–115.
- [3] P. P. Ruvolo, *BBA Clin.* **2016**, *6*, 87–99.
- [4] S. Mazhar, S. E. Taylor, J. Sangodkar, G. Narla, *Biochim. Biophys. Acta - Mol. Cell Res.* **2019**, *1866*, 51–63.
- [5] M. Nakada, D. Kita, T. Watanabe, Y. Hayashi, J. I. Hamada, *Brain Tumor Pathol.* **2014**, *31*, 198–207.
- [6] A. J. Lamontanara, E. B. Gencer, O. Kuzyk, O. Hantschel, *Biochim. Biophys. Acta - Proteins Proteomics* **2013**, *1834*, 1449–1459.
- [7] H. Bruzzoni-Giovanelli, V. Alezra, N. Wolff, C. Z. Dong, P. Tuffery, A. Rebollo, *Drug Discov. Today* **2018**, *23*, 272–285.
- [8] Y. Shi, *Cell* **2009**, *139*, 468–484.
- [9] H. Fujiki, E. Sueoka, T. Watanabe, M. Suganuma, *J. Cancer Res. Clin. Oncol.* **2018**, *144*, 2339–2349.
- [10] D. Perrotti, P. Neviani, *Lancet Oncol.* **2013**, *14*, 38–46.
- [11] G. Narla, J. Sangodkar, C. B. Ryder, *Cell. Mol. Life Sci.* **2018**, *75*, 2695–2718.
- [12] R. Baskaran, B. K. Velmurugan, *Life Sci.* **2018**, *210*, 40–46.
- [13] M. Moura, C. Conde, *Biomolecules* **2019**, *9*, 1–54.
- [14] Y. Xu, Y. Xing, Y. Chen, Y. Chao, Z. Lin, E. Fan, J. W. Yu, S. Strack, P. D. Jeffrey, Y. Shi, *Cell* **2006**, *127*, 1239–1251.
- [15] C. M. O'Connor, A. Perl, D. Leonard, J. Sangodkar, G. Narla, *Int. J. Biochem. Cell Biol.* **2018**, *96*, 182–193.
- [16] A. Alonso, J. Sasin, N. Bottini, I. Friedberg, I. Friedberg, A. Osterman, A. Godzik, T. Hunter, J. Dixon, T. Mustelin, et al., *Cell* **2004**, *117*, 699–711.
- [17] M. Zhang, S. D. Yogesha, J. E. Mayfield, G. N. Gill, *FEBS J.* **2013**, *280*, 4739–4760.
- [18] D. Perrotti, P. Neviani, *Lancet Oncol.* **2013**, *14*, e229–e238.
- [19] A. Bononi, C. Agnoletto, E. De Marchi, S. Marchi, S. Patergnani, M. Bonora, C. Giorgi, S. Missiroli, F. Poletti, A. Rimessi, et al., *Enzym. Res* **2011**, *2011*, 329098.
- [20] J. T. Metz, E. F. Johnson, N. B. Soni, P. J. Merta, L. Kifle, P. J. Hajduk, *Nat. Chem. Biol.* **2011**, *7*, 7–9.
- [21] R. R. Jr, *Pharmacol. Res.* **2015**, *100*, 1–23.
- [22] W. Wang, L. Liu, X. Song, Y. Mo, C. Komma, H. D. Bellamy, Z. J. Zhao, G. W. Zhou, *J. Cell. Biochem.* **2011**, *112*, 2062–2071.
- [23] A. W. Poole, M. L. Jones, *Cell. Signal.* **2005**, *17*, 1323–1332.

- [24] N. Wlodarchak, Y. Xing, N. Wlodarchak, Y. Xing, *Crit. Rev. Biochem. Mol. Biol.* **2017**, *9238*, DOI 10.3109/10409238.2016.1143913.
- [25] V. Kolupaeva, *Biochim. Biophys. Acta - Mol. Cell Res.* **2019**, *1866*, 83–89.
- [26] W. C. M. Dempke, P. Uciechowski, K. Fenchel, T. Chevassut, *Oncol.* **2018**, *95*, 257–269.
- [27] Z. A. Knight, H. Lin, K. M. Shokat, *Nat. Rev. Cancer* **2010**, *10*.
- [28] D. Fabbro, S. W. Cowan-Jacob, H. Moebitz, *Br. J. Pharmacol.* **2015**, *172*, 2675–2700.
- [29] J. Sangodkar, C. C. Farrington, K. McClinch, M. D. Galsky, D. B. Kastrinsky, G. Narla, *FEBS J.* **2016**, *283*, DOI 10.1111/febs.13573.
- [30] S. Gross, R. Rahal, N. Stransky, C. Lengauer, K. P. Hoeflic, *J. Clin. Invest.* **2015**, *125*, 1780–1789.
- [31] P. W. Manley, S. W. Cowan-Jacob, E. Buchdunger, D. Fabbro, G. Fendrich, P. Furet, T. Meyer, J. Zimmermann, *Eur. J. Cancer* **2002**, *38*, *Supple*, S19–S27.
- [32] V. Pavan, *DESIGN , SYNTHESIS AND BIOCHEMICAL CHARACTERIZATION OF FINGOLIMOD ANALOGS FOR TARGETING PP2A*, **2016**.
- [33] A. J. Rabalski, L. Gyenis, D. W. Litchfield, *Clin. Cancer Res.* **2016**, *22*, 2840–2847.
- [34] T. G. Cross, D. Scheel-Toellner, N. V. Henriquez, E. Deacon, M. Salmon, J. M. Lord, *Exp. Cell Res.* **2000**, *256*, 34–41.
- [35] D. Bixby, M. Talpaz, *Hematology Am. Soc. Hematol. Educ. Program* **2009**, 461–476.
- [36] P. W. Manley, N. J. Stief, in *BC Med. J.*, Springer International Publishing, **2011**, pp. 404–408.
- [37] M. Lindauer, A. Hochhaus, *Small Molecules in Oncology*, **2014**.
- [38] H. M. Kantarjian, M. Talpaz, F. Giles, S. O. Brien, J. Cortes, *Ann. Intern. Med.* **2006**, 913–924.
- [39] J. Cao, K. Barrett, R. M. Fine, C. Gritzen, J. Hood, J. Kang, D. Lohse, C. C. Mak, A. Mcpherson, G. Noronha, et al., **2006**, 92121.
- [40] D. R. Camidge, W. Pao, L. V. Sequist, *Nat. Rev. Clin. Oncol.* **2014**, *11*, 473–481.
- [41] N. S. Gray, D. Fabbro, *Discovery of Allosteric Bcr – Abl Inhibitors from Phenotypic Screen to Clinical Candidate*, Elsevier Inc., **2014**.
- [42] V. V. Padma, *BioMedicine* **2015**, *5*, 1–6.
- [43] T. L. Holyoake, D. Vetrie, *bloodjournal* **2017**, *129*, 1595–1607.
- [44] Y. Chen, L. Fu, *Acta Pharm. Sin. B* **2011**, *1*, 197–207.
- [45] B. N. Rexer, J. A. Engelman, C. L. Arteaga, *Cell Cycle* **2009**, *8*, 18–22.
- [46] H. Than, C. Chuah, S. T. Ong, in *Mol. Pathog. Treat. Chronic Myelogenous*

- Leuk.* (Ed.: M. Kizaki), Springer Japan, **2016**, pp. 167–182.
- [47] S. A. Rosenzweig, *Biochem. Pharmacol.* **2012**, *83*, 1041–1048.
- [48] L. Huang, L. Fu, *Acta Pharm. Sin. B* **2015**, *5*, 390–401.
- [49] M. Khateb, N. Ruimi, H. Khamisie, Y. Najajreh, A. Mian, A. Metodieva, M. Ruthardt, J. Mahajna, *BMC Cancer* **2012**, *12*, 1.
- [50] S. Tabarestani, A. Movafagh, *Iran J Cancer Prev* **2016**, *9*, e3961.
- [51] M. M. J. Chua, C. E. Ortega, A. Sheikh, M. Lee, H. Abdul-rassoul, K. L. Hartshorn, I. Dominguez, **2017**, 20–22.
- [52] D. W. Litchfield, *Biochem. J.* **2003**, *369*, 1–15.
- [53] J. H. Trembley, Z. Chen, G. Unger, J. Slaton, B. T. Kren, C. Van Waes, K. Ahmed, *BioFactors* **2010**, *36*, 187–195.
- [54] S. Reynhout, V. Janssens, *Biochim. Biophys. Acta - Mol. Cell Res.* **2019**, *1866*, 31–50.
- [55] V. Janssens, J. Goris, *Biochem. J.* **2001**, *353*, 417–439.
- [56] G. Moorhead, Ed. , *Protein Phosphatase Protocols*, Humana Press, Totowa, NJ, **2008**.
- [57] P. Seshacharyulu, P. Pandey, K. Datta, S. K. Batra, *Cancer Lett.* **2013**, *335*, 9–18.
- [58] E. Tibaldi, M. A. Pagano, F. Frezzato, V. Trimarco, M. Facco, G. Zagotto, G. Ribaud, V. Pavan, L. Bordin, A. Visentin, et al., *Haematologica* **2017**, *102*, 1401–1412.
- [59] U. S. Cho, W. Xu, *Nature* **2007**, *445*, 53–57.
- [60] D. Haesen, W. Sents, K. Lemaire, Y. Hoorne, V. Janssens, *Front. Oncol.* **2014**, *4*, 1–11.
- [61] C. Low, E. M. Quistgaard, M. Kovermann, M. Anandapadamanaban, J. Balbach, P. Nordlund, *Biol. Chem.* **2014**, *395*, 881–889.
- [62] F. Guo, V. Stanevich, N. Wlodarchak, R. Sengupta, L. Jiang, K. a Satyshur, Y. Xing, *Cell Res.* **2014**, *24*, 190–203.
- [63] M. Martin, R. Kettmann, F. Dequiedt, *Biotechnol. Agron. Soc. Env.* **2010**, *14*, 243–252.
- [64] J. Wang, J. Okkeri, K. Pavic, Z. Wang, O. Kauko, T. Halonen, G. Sarek, P. M. Ojala, Z. Rao, W. Xu, et al., *EMBO Rep.* **2017**, *18*, 437–450.
- [65] L. Martin, X. Latypova, C. M. Wilson, A. Magnaudeix, M. L. Perrin, F. Terro, *Ageing Res. Rev.* **2013**, *12*, 39–49.
- [66] P. De, J. Carlson, B. Leyland-Jones, N. Dey, *Oncotarget* **2014**, *5*, 4581–4602.
- [67] R. Lajarín-Cuesta, R. L. Arribas, C. De Los Rios, *Expert Opin. Ther. Pat.* **2016**, *26*, 389–407.
- [68] S. R. Stauffer, *ACS Chem. Neurosci.* **2011**, *2*, 450–70.

- [69] T. M. Fyles, C. C. Leznoff, *Can. J. Chem.* **1976**, *54*, 935–942.
- [70] W. Chen, Z. Wang, C. Jiang, Y. Ding, *Gastroenterol Res Pr.* **2013**, *2013*, 675429.
- [71] M. L. Tsai, N. Cronin, S. Djordjevic, *Acta Crystallogr. Sect. D Biol. Crystallogr.* **2011**, *67*, 14–24.
- [72] E. Ogris, X. Du, K. C. Nelson, E. K. Mak, X. X. Yu, W. S. Lane, D. C. Pallas, *J. Biol. Chem.* **1999**, *274*, 14382–14391.
- [73] R. M. De Palma, S. R. Parnham, Y. Li, J. J. Oaks, Y. K. Peterson, Z. M. Szulc, B. M. Roth, Y. Xing, B. Ogretmen, *FASEB J.* **2019**, *33*, 7647–7666.
- [74] Y. Luo, Y. J. Nie, H. R. Shi, Z. F. Ni, Q. Wang, J. Z. Wang, G. P. Liu, *Biochim. Biophys. Acta - Mol. Cell Res.* **2013**, *1833*, 1235–1243.
- [75] C. Y. Liu, F. S. Hsieh, P. Y. Chu, W. C. Tsai, C. T. Huang, Y. Bin Yu, T. T. Huang, P. S. Ko, M. H. Hung, W. L. Wang, et al., *Br. J. Haematol.* **2017**, *177*, 726–740.
- [76] A. Khanna, J. E. Pimanda, J. Westermarck, *Cancer Res.* **2013**, *73*, 6548–6553.
- [77] A. Khanna, J. E. Pimanda, *Int. J. Cancer* **2016**, *138*, 525–532.
- [78] J. Oaks, B. Ogretmen, *Front. Oncol.* **2014**, *4*, 388.
- [79] A. Mukhopadhyay, S. A. Saddoughi, P. Song, I. Sultan, S. Ponnusamy, C. E. Senkal, C. F. Snook, H. K. Arnold, R. C. Sears, Y. A. Hannun, et al., *FASEB J.* **2009**, *23*, 751–763.
- [80] S. Wang, W. Xie, D. Wang, Z. Peng, Y. Zheng, N. Liu, W. Dai, Y. Wang, Z. Wang, Y. Yang, et al., *Oncotarget* **2015**, *6*, 12128–12140.
- [81] S. Muto, M. Senda, Y. Akai, L. Sato, T. Suzuki, R. Nagai, T. Senda, M. Horikoshi, *Proc. Natl. Acad. Sci. U. S. A.* **2007**, *104*, 4285–4290.
- [82] L. Yin, Y. Zeng, Y. Xiao, Y. Chen, H. Shen, J. Dong, *Cell Death Dis.* **2019**, *10*, DOI 10.1038/s41419-019-1621-2.
- [83] M. Wu, G. Yu, T. Yan, D. Ke, Q. Wang, R. Liu, J. Z. Wang, B. Zhang, D. Chen, X. Wang, *Neurobiol. Aging* **2018**, *69*, 38–47.
- [84] A. Agarwal, R. J. MacKenzie, R. Pippa, C. A. Eide, J. Oddo, J. W. Tyner, R. Sears, M. P. Vitek, M. D. Odero, D. J. Christensen, et al., *Clin. Cancer Res.* **2014**, *20*, 2092–2103.
- [85] A. A. Sablina, M. Hector, N. Colpaert, W. C. Hahn, *Cancer Res.* **2010**, *70*, 10474–10484.
- [86] B. M. D'Arcy, M. R. Swingle, C. M. Papke, K. A. Abney, E. S. Bouska, A. Prakash, R. E. Honkanen, *Mol. Cancer Ther.* **2019**, *18*, 556–566.
- [87] D. B. Kastrinsky, J. Sangodkar, N. Zaware, S. Izadmehr, N. S. Dhawan, G. Narla, M. Ohlmeyer, *Bioorganic Med. Chem.* **2015**, *23*, 6528–6534.
- [88] A. Gutierrez, A. T. Look, J. C. Aster, A. Gutierrez, L. Pan, R. W. J. Groen, F. Baleyrier, A. Kentsis, S. Poglio, B. Uzan, et al., *J. Clin. Invest.* **2014**, *124*, 644–655.

- [89] T.-T. Chao, C.-Y. Wang, C.-C. Lai, Y.-L. Chen, Y.-T. Tsai, P.-T. Chen, H.-I. Lin, Y.-C. T. Huang, C.-W. Shiau, C.-J. Yu, et al., *J. Pharmacol. Exp. Ther.* **2014**, *351*, 352–358.
- [90] S. N. Patmanathan, L. F. Yap, P. G. Murray, I. C. Paterson, *J. Cell. Mol. Med.* **2015**, *19*, 2329–2340.
- [91] N. J. Pyne, A. El Buri, D. R. Adams, S. Pyne, *Adv. Biol. Regul.* **2018**, *68*, 97–106.
- [92] S. A. Saddoughi, S. Gencer, Y. K. Peterson, K. E. Ward, A. Mukhopadhyay, J. Oaks, J. Bielawski, Z. M. Szulc, R. J. Thomas, S. P. Selvam, et al., *EMBO Mol. Med.* **2013**, *5*, DOI 10.1002/emmm.201201283.
- [93] Y. Nagahara, S. Enosawa, M. Ikekita, S. Suzuki, T. Shinomiya, *Immunopharmacology* **2000**, *48*, 75–85.
- [94] J. Chun, H. Hartung, *Clin Neuropharmacol* **2010**, *33*, 91–101.
- [95] C. A. Foster, L. M. Howard, A. Schweitzer, E. Persohn, P. C. Hiestand, B. Balatoni, R. Reuschel, C. Beerli, M. Schwartz, A. Billich, *J. Pharmacol. Exp. Ther.* **2007**, *323*, 469–476.
- [96] T. Lee, H. S. Moon, S. W. Kim, J. Shrestha, S. M. Shin, J. Y. Lee, S. Kim, E. Y. Park, D. J. Baek, *Chem. Pharm. Bull.* **2018**, *66*, 1015–1018.
- [97] J. Yang, L. Liu, D. He, X. Song, X. Liang, Z. J. Zhao, G. W. Zhou, *J. Biol. Chem.* **2003**, *278*, 6516–6520.
- [98] C. Wu, M. Sun, L. Liu, G. W. Zhou, *Gene* **2003**, *306*, 1–12.
- [99] C. Y. Liu, T. T. Huang, P. Y. Chu, C. T. Huang, C. H. Lee, W. L. Wang, K. Y. Lau, W. C. Tsai, T. I. Chao, J. C. Su, et al., *Exp. Mol. Med.* **2017**, *49*, DOI 10.1038/emmm.2017.114.
- [100] C. Liu, J. Su, T. Huang, P. Chu, C. Huang, **2017**, 1–14.
- [101] T. L. Yi, J. L. Cleveland, J. N. Ihle, *Mol. Cell. Biol.* **1992**, *12*, 836–846.
- [102] J. Huang, K. Chen, **2013**, 190–201.
- [103] J. Yang, Z. Cheng, T. Niu, X. Liang, Z. J. Zhao, G. W. Zhou, *J. Biol. Chem.* **2000**, *275*, 4066–4071.
- [104] C. T. Hua, J. R. Gamble, M. A. Vadas, D. E. Jackson, *J. Biol. Chem.* **1998**, *273*, 28332–28340.
- [105] D. Imhof, A. S. Wavreille, A. May, M. Zacharias, S. Tridandapani, D. Pei, *J. Biol. Chem.* **2006**, *281*, 20271–20282.
- [106] M. J. Park, R. Sheng, A. Silkov, D. J. Jung, Z. G. Wang, Y. Xin, H. Kim, P. Thiagarajan-Rosenkranz, S. Song, Y. Yoon, et al., *Mol. Cell* **2016**, *62*, 7–20.
- [107] C. L. Abram, C. A. Lowell, *J. Leukoc. Biol.* **2017**, *102*, 657–675.
- [108] K. Chen, H. Chen, C. Shiau, **2013**, DOI 10.1111/j.1476-5381.2012.02212.x.
- [109] Y. Mittal, Y. Pavlova, M. Garcia-Marcos, P. Ghosh, *J. Biol. Chem.* **2011**, *286*, 32404–32415.
- [110] N. R. D. Paling, M. J. Welham, *Biochem. J.* **2002**, *368*, 885–894.

- [111] D. Xu, C. K. Qu, *Front. Biosci.* **2008**, *13*, 4925–4932.
- [112] J. C. Su, C. H. Chang, S. H. Wu, C. W. Shiau, *J. Enzyme Inhib. Med. Chem.* **2018**, *33*, 1248–1255.
- [113] T. T. Huang, J. C. Su, C. Y. Liu, C. W. Shiau, K. F. Chen, *Int. J. Mol. Sci.* **2017**, *18*, 8–11.
- [114] K. Chen, W. Tai, C. Hsu, J. Huang, C. Liu, P. Chen, *Eur. J. Med. Chem.* **2012**, *55*, 220–227.
- [115] C. C. Delibrias, J. E. Floettmann, M. Rowe, D. T. Fearon, *J. Exp. Med.* **1997**, *186*, 1575–1583.
- [116] M. K. Pathak, T. Yi, *J. Immunol.* **2001**, *167*, 3391–3397.
- [117] S. Kundu, K. Fan, M. Cao, D. J. Lindner, Z. J. Zhao, E. Borden, T. Yi, *J. Immunol.* **2010**, *184*, 6529–6536.
- [118] K. Chen, W. Tai, J. Huang, C. Hsu, W. Chen, *Eur. J. Med. Chem.* **2011**, *46*, 2845–2851.
- [119] T. Chao, W. Tai, M. Hung, M. Tsai, M. Chen, **2016**, *371*, 205–213.
- [120] W. Tai, C. Shiau, Y. Li, Y. Chen, P. Chu, J. Huang, **n.d.**, *1*, 27–36.
- [121] F. Buontempo, J. A. McCubrey, E. Orsini, M. Ruzzene, A. Cappellini, A. Lonetti, C. Evangelisti, F. Chiarini, C. Evangelisti, J. T. Barata, et al., *Leukemia* **2018**, *32*, 1–10.
- [122] F. Meggio, L. A. Pinna, *FASEB J.* **2003**, *17*, 349–368.
- [123] J. Raaf, O. G. Issinger, K. Niefind, *J. Mol. Biol.* **2009**, *386*, 1212–1221.
- [124] N. Bischoff, B. Olsen, J. Raaf, M. Bretner, O. G. Issinger, K. Niefind, *J. Mol. Biol.* **2011**, *407*, 1–12.
- [125] K. Niefind, B. Guerra, I. Ermakowa, O. G. Issinger, *EMBO J.* **2001**, *20*, 5320–5331.
- [126] L. Chantalat, D. Leroy, O. Filhol, A. Nueda, M. J. Benitez, E. M. Chambaz, C. Cochet, O. Dideberg, *EMBO J.* **1999**, *18*, 2930–2940.
- [127] M. K. Homma, Y. Homma, *Mol. Cell. Biochem.* **2005**, *274*, 47–52.
- [128] M. K. Homma, Y. Homma, *Mol. Cell. Biochem.* **2008**, *316*, 49–55.
- [129] B. BOLDYREFF, P. JAMES, W. STAUDENMANN, O. -G ISSINGER, *Eur. J. Biochem.* **1993**, *218*, 515–521.
- [130] D. W. Litchfield, D. G. Bosc, E. Slominski, *BBA - Mol. Cell Res.* **1995**, *1269*, 69–78.
- [131] S. Zanin, C. Borgo, C. Girardi, S. E. O'Brien, Y. Miyata, L. A. Pinna, A. Donella-Deana, M. Ruzzene, *PLoS One* **2012**, *7*, DOI 10.1371/journal.pone.0049193.
- [132] G. Cozza, C. Girardi, A. Ranchio, G. Lolli, S. Sarno, A. Orzeszko, Z. Kazimierzczuk, R. Battistutta, M. Ruzzene, L. A. Pinna, *Cell. Mol. Life Sci.* **2014**, *71*, 3173–3185.

- [133] S. Morooka, M. Hoshina, I. Kii, T. Okabe, H. Kojima, N. Inoue, Y. Okuno, M. Denawa, S. Yoshida, J. Fukuhara, et al., **2015**, 316–325.
- [134] S. Ferrini, F. Ponticelli, M. Taddei, *Org. Lett.* **2007**, *9*, 69–72.
- [135] K. T. Koshy, H. Mitchner, *J. Pharm. Sci.* **1964**, *53*, 1381–1385.
- [136] D. S. Hage, J. a Anguizola, C. Bi, R. Li, R. Matsuda, E. Pfaunmiller, J. Vargas, X. Zheng, *J. Pharm. Biomed. Anal.* **2012**, *69*, 93–105.
- [137] R. Lazny, M. Michalak, *Synlett* **2002**, 1931–1934.
- [138] K. Chiba, M. Asanuma, M. Ishikawa, Y. Hashimoto, K. Dodo, M. Sodeoka, T. Yamaguchi, **2017**, *7*, 8751–8754.
- [139] R. A. Abramovitch, E. P. Kyba, F. V. Scriven, *J. or* **1971**, *36*, 3796–3803.
- [140] Cayman Chemical, *Malachite Green Phosphate Detection Kit*, **n.d.**
- [141] R&D Systems, *Malachite Green Phosphate Detection Kit*, **n.d.**
- [142] New England BioLabs, *P-Nitrophenyl Phosphate (PNPP)*, **n.d.**
- [143] D. G. Hardie, *Protein Phosphorylation*, Oxford University Press, New York, **1999**.
- [144] M. Kawaguchi, K. Hanaoka, T. Komatsu, T. Terai, T. Nagano, *Bioorganic Med. Chem. Lett.* **2011**, *21*, 5088–5091.
- [145] E. Betzig, G. H. Patterson, R. Sougrat, O. W. Lindwasser, S. Olenych, J. S. Bonifacino, M. W. Davidson, J. Lippincott-schwartz, H. F. Hess, **2006**, *x*, 1642–1646.
- [146] M. J. Rust, M. Bates, X. W. Zhuang, *Nat Methods* **2006**, *3*, 793–795.
- [147] S. Uno, M. Kamiya, T. Yoshihara, K. Sugawara, K. Okabe, M. C. Tarhan, H. Fujita, T. Funatsu, Y. Okada, S. Tobita, et al., *Nat. Chem.* **2014**, *6*, 681–689.
- [148] H. Ishihara, B. L. Martin, D. L. Brautigan, H. Karaki, H. Ozaki, Y. Kato, N. Fusetani, S. Watabe, K. Hashimoto, D. Uemura, et al., *Biochem. Biophys. Res. Commun.* **1989**, *159*, 871–877.
- [149] S. J. Enna, D. B. Bylund, *Methods Enzymol.* **1991**, *201*, 477–482.
- [150] K. Kishikawa, C. E. Chalfant, D. K. Perry, A. Bielawska, Y. A. Hannun, *J. Biol. Chem.* **1999**, *274*, 21335–21341.
- [151] U. Sharma, D. Pal, R. Prasad, *Indian J. Clin. Biochem.* **2014**, *29*, 269–278.
- [152] K. Umezawa, M. Yoshida, M. Kamiya, T. Yamasoba, Y. Urano, *Nat. Chem.* **2017**, *9*, 279–286.
- [153] D. Giustarini, F. Galvagni, A. Tesei, A. Farolfi, M. Zanoni, S. Pignatta, A. Milzani, I. M. Marone, I. Dalle-Donne, R. Nassini, et al., *Free Radic. Biol. Med.* **2015**, *89*, 972–981.
- [154] I. A. Yudushkin, A. Schleifenbaum, A. Kinkhabwala, B. G. Neel, C. Schultz, P. I. H. Bastiaens, *Science (80-.)*. **2007**, *315*, 115–119.
- [155] J. O. Enoru, B. Yang, S. Krishnamachari, E. Villanueva, W. DeMaio, A. Watanyar, R. Chinnasamy, J. B. Arterburn, R. G. Perez, *PLoS One* **2016**, *11*,

- 1–22.
- [156] M. L. Reyzer, Y. Hsieh, K. Ng, W. A. Korfmacher, R. M. Caprioli, *J. Mass Spectrom.* **2003**, *38*, 1081–1092.
- [157] N. Snelder, B. A. Ploeger, O. Luttringer, D. R. Stanski, M. Danhof, *Biotech Week* **2014**, 290.
- [158] M. Fridén, F. Bergström, H. Wan, M. Rehngren, G. Ahlin, M. Hammarlund-Udenaes, U. Bredberg, *Drug Metab. Dispos.* **2011**, *39*, 353–362.
- [159] M. Mirzaian, P. Wisse, M. J. Ferraz, A. R. A. Marques, T. L. Gabriel, C. P. A. A. van Roomen, R. Ottenhoff, M. van Eijk, J. D. C. Codée, G. A. van der Marel, et al., *Clin. Chim. Acta* **2016**, *459*, 36–44.
- [160] M. D. Hanwell, D. E. Curtis, D. C. Lonie, T. Vandermeersch, E. Zurek, G. R. Hutchinson, *J. Cheminform.* **2012**, *4*, 1–17.
- [161] O. Trott, A. J. Olson, *J. Comput. Chem.* **2009**, 455–461.
- [162] Dassault Systemes, **2015**.
- [163] N. R. Wadhwa, N. C. Hughes, J. A. Hachem, G. Mezei, **2016**, 11430–11440.
- [164] D. Steinhilber, H. Stark, A. P. Lill, B. R. Carmen, B. Hofmann, **2015**, *89*, DOI 10.1016/j.ejmech.2014.10.054.
- [165] W. Kabsch, *Acta Crystallogr. Sect. D* **2010**, *66*, 125–132.
- [166] P. R. Evans, G. N. Murshudov, *Acta Crystallogr. Sect. D Biol. Crystallogr.* **2013**, *69*, 1204–1214.
- [167] A. J. McCoy, R. W. Grosse-Kunstleve, P. D. Adams, M. D. Winn, L. C. Storoni, R. J. Read, *J. Appl. Crystallogr.* **2007**, *40*, 658–674.
- [168] P. D. Adams, P. V. Afonine, G. Bunkóczi, V. B. Chen, I. W. Davis, N. Echols, J. J. Headd, L. W. Hung, G. J. Kapral, R. W. Grosse-Kunstleve, et al., *Acta Crystallogr. Sect. D Biol. Crystallogr.* **2010**, *66*, 213–221.
- [169] P. Emsley, B. Lohkamp, W. G. Scott, K. Cowtan, *Acta Crystallogr. Sect. D Biol. Crystallogr.* **2010**, *66*, 486–501.
- [170] R. Horbert, B. Pinchuk, E. Johannes, J. Schlosser, D. Schmidt, D. Cappel, F. Totzke, C. Schächtele, C. Peifer, *J. Med. Chem.* **2015**, *58*, 170–182.
- [171] J. R. Beck, T. Truong, C. I. Stains, *ACS Chem. Biol.* **2016**, *11*, 3284–3288.